ENGINEERING RESEARCH INSTITUTE
UNIVERSITY OF MICHIGAN
ANN ARBOR

A LARGE-SIGNAL ANALYSIS OF THE TRAVELING-WAVE AMPLIFIER

Technical Report No. 19
Electron Tube Laboratory
Department of Electrical Engineering

By

Joseph E. Rowe

Approved by: W. G. Dow
G. Hok

Project 2112

NAVY DEPARTMENT BUREAU OF SHIPS
ELECTRONICS DIVISION
CONTRACT No. NObsr-63114
INDEX No. NE-071417

Submitted in partial fulfillment of the requirements for the Degree
of Doctor of Philosophy in the University of Michigan

April, 1955

ABSTRACT

It is the purpose of this dissertation to derive the large-signal traveling-wave amplifier equations, to outline a method by which these equations may be solved on a high-speed digital computer, and to present the resulting equations in such form that the information will lead to a fuller understanding of the physical phenomena involved in the high-level operation of the traveling-wave amplifier.

Equations are derived describing the large-signal operation of the traveling-wave amplifier, including the effects of a-c space charge and attenuation along the helical slow-wave structure. The equations constitute a system of nonlinear partial-differential-integral equations and are valid for all values of the parameters which are encountered in typical high-power traveling-wave amplifiers. The parameters which appear in the equations are the relative injection velocity b, the gain parameter C, the large-signal space-charge parameters K and B, the loss parameter d, and the input-signal level A_o.

The working equations were programmed for and solved on the Michigan Digital Automatic Computer, MIDAC, located at the University of Michigan's Willow Run Research Center. The r-f voltage amplitude A(y), the phase lag of the r-f wave relative to the electron stream $\theta(y)$, the electron phase $\phi(y,\phi_o)$, and the velocity deviation $2Cu(y,\phi_o)$ were computed for several values of C, K, and b at B = 1, A_o = 0.0225, and d = 0. Zero-space-charge solutions are presented for C = 0.05, 0.1, and 0.2 with b as the parameter in order to determine the value of b which gives the maximum saturation gain and the optimum tube length. For C = 0.1 similar solutions are obtained for two values of the space-charge parameter K, 1.61 and 3.42. Then the input-signal level A_o is varied for a fixed C, K, and b.

In addition, the effect of attenuation along the helix is determined by obtaining solutions for several values of the loss parameter d, namely 0.1, 0.25, 1.0, and 2.0, with fixed injection velocity and then the effect of attenuation in lowering the optimum injection velocity is shown through solutions for several values of b at d = 2.0. Finally, the effect on the saturation gain of the placement of the loss is studied: solutions are given for loss beginning at approximately 2, 3, and 4 wavelengths respectively from the input.

The results of these various solutions are presented in graphical form and are very useful for designing and predicting the performance of large-signal traveling-wave amplifiers.

PREFACE

The first chapter of this dissertation contains general material on the traveling-wave amplifier, background information on the small-signal analysis, and a discussion of why this approach is not suitable to be extended to describe the large-signal operation of the traveling-wave amplifier. In Chapter II and Appendices A and B the working equations describing the operation of the large-signal traveling-wave amplifier are derived. The boundary conditions are also discussed in Chapter II, and Appendix C presents an outline of the method used to obtain the roots of the small-signal equations needed to evaluate these boundary conditions.

In Chapter III the working equations are programmed for solution on MIDAC and a discussion of the characteristics of MIDAC is presented. An experimental analysis of the presence of errors in the solutions and of the stability of the working equations relative to the propagation of errors is also discussed in detail, and a flow diagram for the solution of these equations on MIDAC is presented. Appendix D contains the programs and operating instructions for the solutions.

In Chapter IV the results are presented in graphical form and discussed. In Chapters V and VI these results are analyzed further and interpretive curves are presented for use in the design of large-signal traveling-wave amplifiers and also in predicting the performance of these tubes. A suggested program for future work is also outlined in Chapter VI.

The author wishes to express his appreciation to the members of his committee for their assistance, and especially to Professors W. G. Dow and Gunnar Hok, who devoted considerable time and offered valuable suggestions during the course of the work. The Mathematics Group at the Willow Run Research Center, in particular Messrs. R. T. Dames and L. Razgunas, rendered invaluable assistance in the programming and running of the problem on MIDAC. Appreciation is also due to Miss Priscilla Woodhead for her excellent work in preparing the many figures.

The research on which this dissertation is based was supported by funds from the U.S. Navy Bureau of Ships under Contract NObsr 63114 and the U.S. Signal Corps under Contract DA 36-039 sc-52654.

TABLE OF CONTENTS

TABLE OF CONTENTS (cont.)

LIST OF FIGURES

LIST OF FIGURES (cont.)

LIST OF FIGURES (cont.)

LIST OF FIGURES (cont.)

LIST OF FIGURES (cont.)

LIST OF FIGURES (cont.)

LIST OF FIGURES (concl.)

CHAPTER I. INTRODUCTION

1.1 Statement of the Problem

The traveling-wave amplifier is an important and useful tube; its high gain and inherently large bandwidth compare favorably with the characteristics of other microwave devices. A detailed understanding of its behavior under various conditions is needed, however, if the tube is to be used with maximum effectiveness.

Equations describing the behavior of an idealized traveling-wave amplifier transmitting small signals have been derived and studied extensively by Pierce[8], Kompfner[5,6,7], and others[2]. These equations for the small-signal case can be linearized by application of a few reasonable assumptions and hence are amenable to solution by straightforward methods. The large-signal case, however, has not been studied in any great detail up to the present time, largely due to the complexity of the equations involved and to the lack of adequate mathematical techniques for solving them.

Since high-speed digital computers now afford a means by which complex systems of mathematical equations of the type encountered in the large-signal case may reasonably be handled, it has seemed worthwhile, in terms of both time and expense, to undertake an analysis of the operation of the traveling-wave amplifier at high output levels.

It is therefore the purpose of this dissertation to derive the equations describing the large-signal operation of a traveling-wave amplifier, to outline a method by which these equations may be solved on a high-speed digital computer, and to present the resulting calculations in such form

that the information will lead to a fuller understanding of the physical phenomena involved in the high-level operation of the traveling-wave amplifier and assist in the construction of tubes that more closely realize a given set of specifications.

1.2 History of the Problem

1.2.1 General Description of the Traveling-Wave Amplifier. The essential parts of a traveling-wave amplifier, as shown in Fig. 1-1, are (1) the electron gun, which produces an electron stream*; (2) the slow-wave structure, in this case a helix, which supports the propagation of a slow electromagnetic wave with a longitudinal electric field; and (3) an electron collector. Figure 1-2 is a picture of a helix-type traveling-wave amplifier showing the helix and electron gun structure. The phase velocity of the radio-frequency wave as it travels longitudinally along the helix is of the order of one-tenth the velocity of light; the phase velocity variation with frequency for a typical helix is shown in Fig. 1-3.

An r-f signal is applied to the helix, at the same point as the electron stream enters the helix, by means of a waveguide and an antenna or by a coaxial line. This signal appears, amplified, at the output end of the helix and is removed from the helix by similar means. The bandwidth of the transducers used to couple the signal into and out of the helix limits the overall bandwidth of the device, since unfortunately transducers have not yet been built which can utilize the full electronic bandwidth of

*In this dissertation a differentiation is made between the words "beam" and "stream". "Beam" is used to apply to the gross movement of electrons; i.e., when Eulerian mechanics are applicable, hence only in the small-signal theory. The term "stream", on the other hand, is used where the electrons must be considered as individual particles (Lagrangian mechanics) as in the large-signal theory.

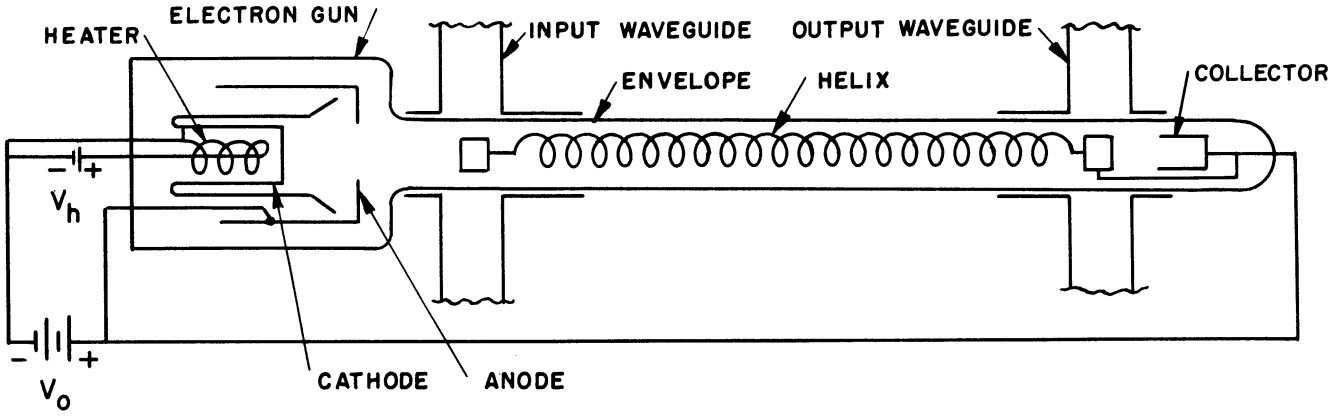

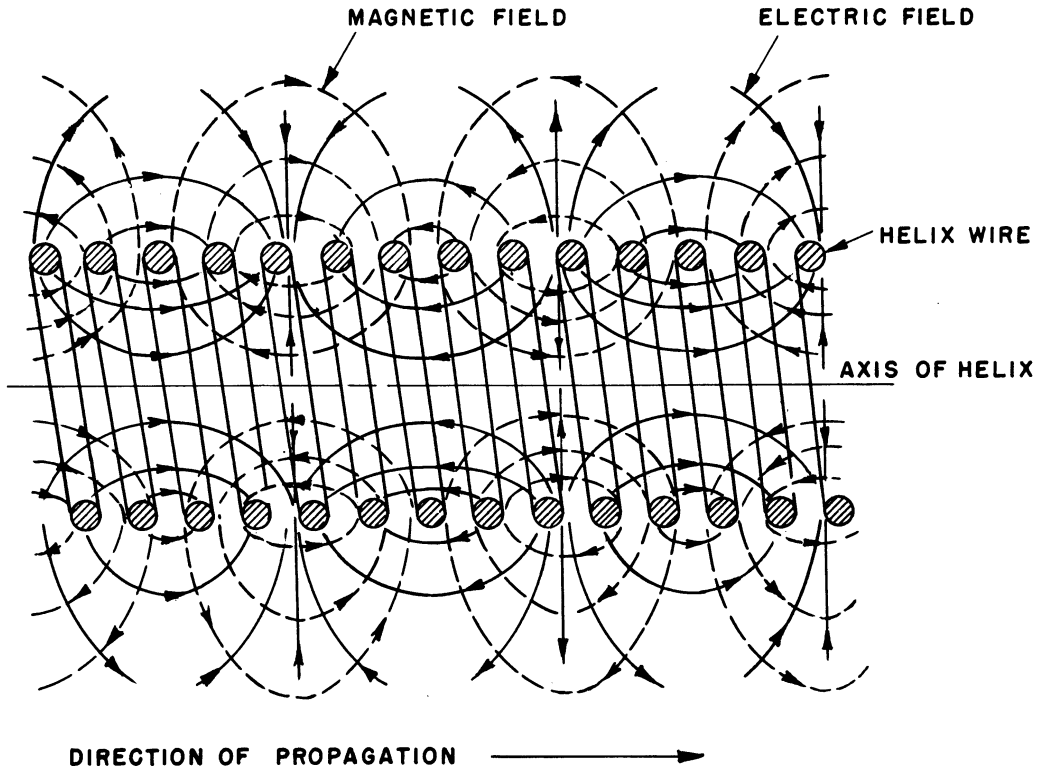

FIG. 1-1 SCHEMATIC DIAGRAM OF A TYPICAL TRAVELING-WAVE AMPLIFIER AND A SKETCH OF THE ELECTRIC AND MAGNETIC FIELD DISTRIBUTION ABOUT THE HELIX

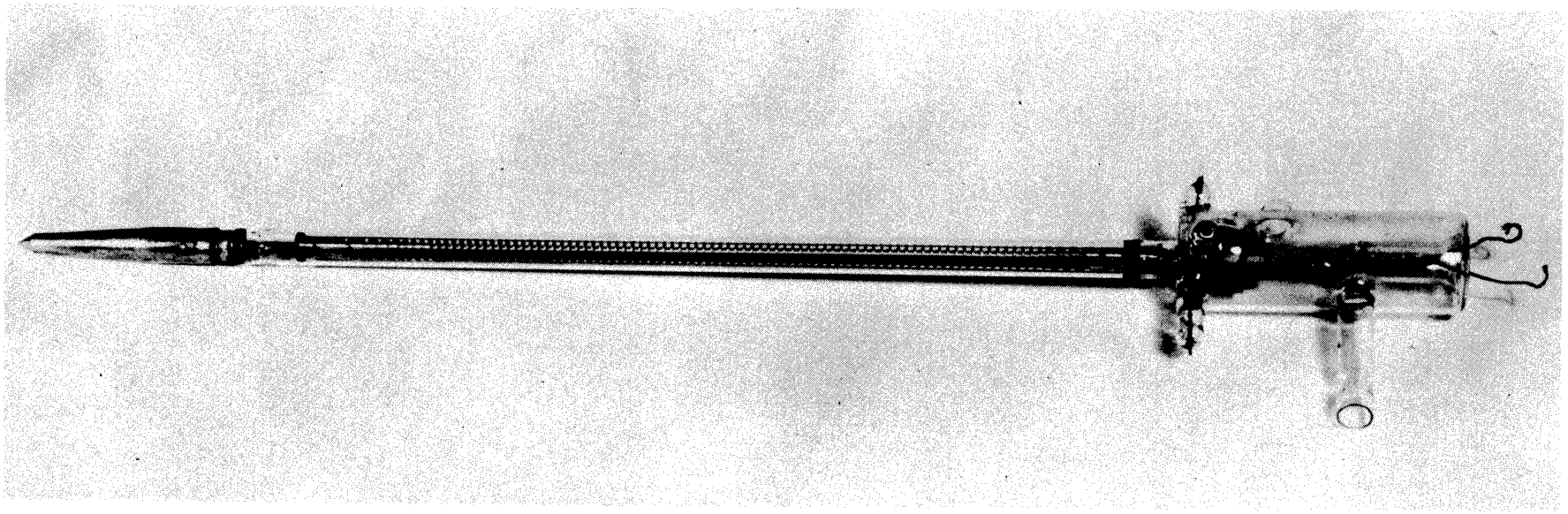

FIG. 1-2

A HELIX-TYPE TRAVELING-WAVE AMPLIFIER

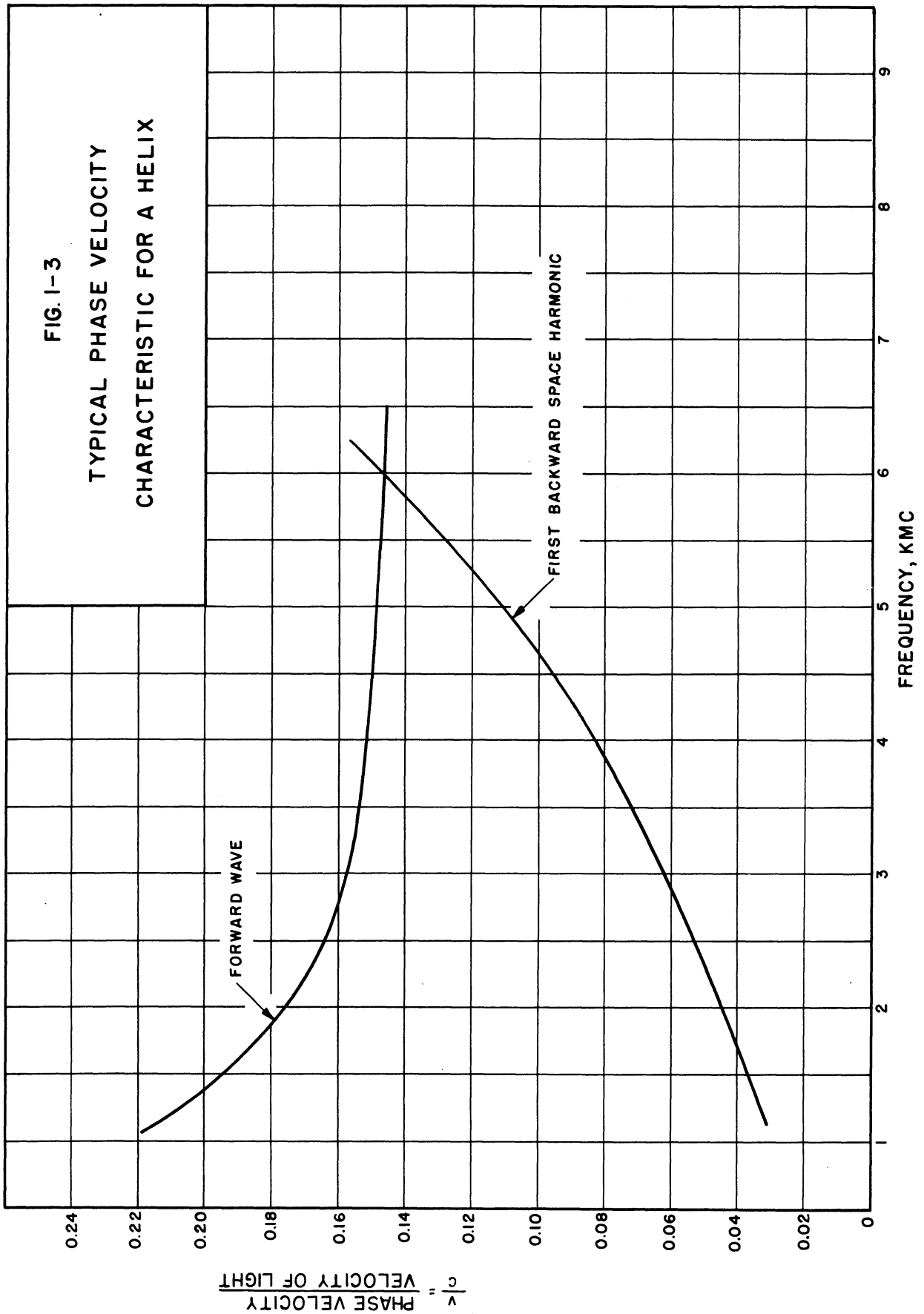
FIG. 1-3
TYPICAL PHASE VELOCITY
CHARACTERISTIC FOR A HELIX
FORWARD WAVE
FIRST BACKWARD SPACE HARMONIC
FREQUENCY, KMC
PHASE VELOCITY / VELOCITY OF LIGHT = v/c
0.24
0.22
0.20
0.18
0.16
0.14
0.12
0.10
0.08
0.06
0.04
0.02
0
1
2
3
4
5
6
7
8
9

the traveling-wave amplifier. Typically, the overall bandwidth of a traveling-wave amplifier operating at 3000 mcs, with coaxial-line-to-waveguide transducers, for example, may be as high as 30 percent.

In addition, a longitudinal magnetic focusing field of several hundred gauss must be provided to confine the electron stream so that it will pass completely through the helix. Either electromagnets or permanent magnets may be used for this purpose. Recently the technique of periodic focusing has been applied to traveling-wave amplifiers, reducing the weight of the focusing magnets by a factor of approximately 10.

For the analysis of the operation of the traveling-wave amplifier it is necessary to consider only the slow-wave structure and the electron stream.

1.2.2 Brief Description of Amplifier Operation. The operation of the traveling-wave amplifier described in the previous section depends on the interaction of the r-f wave propagating along the helix with the electron stream traveling along the axis of the helix at a velocity approximately, but not exactly, equal to the axial phase velocity of the r-f wave.

The longitudinal electric field in the stream due to the r-f wave on the helix exerts forces which velocity-modulate the stream, resulting in current-amplitude modulation. Since as many electrons are accelerated as are retarded, no energy is transferred from the wave to the stream in this process. This current modulation induces a longitudinal r-f current in the helix, which increases the amplitude of the r-f wave on the helix. The phase of the induced r-f wave is such that more electrons are retarded than are accelerated and hence the electron stream on the average loses energy, which accounts for the increase in the amplitude of the r-f wave.

This cycle of operation is repeated many times along the length of the helix. The phase velocity of the complete wave resulting from this repeated interaction between the initial wave and the electron stream will be lower than that of the initial wave because each wave which the bunched electron stream induces onto the helix will lag its predecessor. Hence it is easily seen that interaction can occur even when the phase velocity of the wave is equal to the velocity of the electron stream, although this is not in general the condition for optimum gain.

Thus, electrons injected at approximately the same velocity as the wave will produce a net increase in the amplitude of the wave. However, the amplitude of the r-f wave will not increase indefinitely, since the nonlinearities of an actual tube set an upper limit to the final amplitude. In short, there is a saturation power output for a particular device, regardless of further increase in power input.

1.2.3 Small-Signal Analyses. The small-signal theory as outlined by Pierce[8] leads to a simple analysis of the operation of the traveling-wave amplifier. In this analysis properties of various types of slow-wave structures are first discussed in detail. Then simplified equations describing the overall behavior of the traveling-wave amplifier are introduced and solved. Rather thorough discussions of overall gain, insertion loss of the helix, a-c space-charge effects, noise figure, and power output are included.

The small-signal analysis is limited chiefly by the assumption that the a-c velocity of the electrons is small compared to their average velocity, so that the nonlinear terms in the equations may be neglected and a wave-type solution obtained. It is also assumed that all the electrons in the same cross section of the stream are acted on by the same electric

field, which is a reasonable approximation if the stream is small compared to the size of the helix or if an annular electron stream is used. Further, it is assumed that a strong magnetic focussing field is used and transverse motion may therefore be neglected.

The small-signal analysis of Kompfner[5,6,7], although obtained by a considerably more complicated procedure, is essentially the same as Pierce's and arrives at the same conclusions but employs the same assumptions and hence suffers from the same limitations.

The field theory of traveling-wave tubes derived by Chu and Jackson[2] is a more elegant and rigorous treatment of the problem than Pierce's network-and-beam theory, but it leads to more complicated expressions which are not so useful to the engineer designing a traveling-wave amplifier. It is interesting to note, however, that the two analyses are in quite good agreement.

1.2.4 Need for Large-Signal Analysis. In view of the many applications for a traveling-wave amplifier operating at high output levels, it seems desirable to study the large-signal equations governing its behavior in detail. Of particular interest are the variations of gain and phase shift at high output levels for different values of such parameters as space charge, electron injection velocity, loss along the helical transmission line, and the gain parameter. Also of interest are the effects of space charge and loss along the helical transmission line on the saturation gain and power output. The overall objective, of course, is to learn how to design a traveling-wave amplifier to operate at high power levels with maximum efficiency.

1.2.5 Previous Large-Signal Analyses. Partial large-signal theories of the traveling-wave amplifier have been presented by Brillouin[11] and by

Nordsieck[12] and a more complete theory has recently been presented by Poulter.[13]

Brillouin's analysis treats the large-signal case as an extension of the small-signal theory, using the hydrodynamical equation of continuity (Eulerian mechanics) as opposed to a particle-dynamics treatment (Lagrangian mechanics) where individual electron trajectories are followed. The fluid-dynamics treatment of the electron stream is clearly inadequate when overtaking of electrons, i.e., electrons with different starting times appearing at a point together, causes crossing of electron flight lines. This problem is discussed more fully in Section 1.3. In addition, Brillouin's analysis neglects the effect of loss along the helical transmission line and the effects of the space-charge-induced r-f fields.

The large-signal analysis of Nordsieck also neglects the effects of space-charge r-f fields and circuit loss. Furthermore, the equations are valid only for small (i.e., small compared to 0.1) values of the gain parameter C. But in traveling-wave amplifiers operating at high output levels, where the d-c stream currents encountered may be of the order of hundreds of milliamperes or even amperes, the effects of the space-charge-induced r-f fields may not with impunity be neglected. Furthermore the gain parameter in these large-signal devices may be of the order of 0.3 or 0.4 and hence ought not to be neglected.

The work reported in this dissertation follows similar lines to those of Nordsieck's analysis, but it takes into consideration the effects of the space-charge-induced r-f fields, loss along the helical transmission line, and large values of the gain parameter.

Another approach to the large-signal theory has been presented by Poulter[13] of Stanford University. His method is quite similar to Kompfner's

treatment of the small-signal problem in that he considers a unit of charge in the stream which excites both forward-traveling and backward-traveling energy on the helix; then the solution for the field on the helix is written as a convolution integral. The resulting system of equations has been solved for two non-space-charge cases, b = 1.5 and b = 2.2 at C = 0.2 and QC = 0, giving answers very close to those obtained for these cases in this dissertation. One disadvantage of his method is that it is difficult to interpret physically some of the intermediate steps and also the final working equations. In addition, the equations do not lend themselves to solution by numerical methods as readily as those derived here.

Very recently additional large-signal calculations for the traveling-wave amplifier have been presented by Tien, Walker, and Wolontis[14]. Nordsieck's equations were used for this work with a space-charge term added. The space-charge field was evaluated by considering an infinite array of unit-space-charge discs separated by a distance z and replacing the helix by a conducting cylinder of the same radius. This method of evaluating the space-charge field gives essentially the same results as those obtained for the space charge in this dissertation. However, the assumptions made in the Tien analysis are the same as those made by Nordsieck. The maximum value of the gain parameter C for which these results apply is approximately 0.02 and hence this theory, like Nordsieck's, does not include high-efficiency conditions. Also, the large values of the space-charge parameter QC investigated by Tien are not consistent with practical tubes, since the maximum applicable C is approximately 0.02. No solutions are included in the Tien work for the relative injection velocity b that gives maximum saturation gain and efficiency as a function of QC.

1.3 Extension of the Eulerian Approach

The objections to extending the Eulerian approach to the large-signal case should perhaps be examined in more detail.

Using the basic assumptions of Pierce's small-signal analysis, the continuity equation, Newton's force law, and the circuit equations are written in differential form for a helical transmission line composed of series inductance and shunt capacitance. For the sake of simplicity, the series loss along the line will be neglected and the equivalent circuit shown in Fig. 1-4, in which the distributed inductance and capacitance are chosen to match the phase velocity and field strength of the field acting on the electrons, will be used in the following development.

From this simplified model*,

$$\frac{\partial \rho}{\partial t} + \rho \frac{\partial v}{\partial z} + v \frac{\partial \rho}{\partial z} = 0, \tag{1-1}$$

$$\frac{\partial v}{\partial t} + v \frac{\partial v}{\partial z} - \eta \xi \frac{\partial V_h}{\partial z} = 0, \tag{1-2}$$

$$\frac{\partial V_h}{\partial z} + \frac{Z_o}{v_o} \frac{\partial I_h}{\partial z} = 0, \tag{1-3}$$

and

$$\frac{\partial I_h}{\partial z} + \frac{1}{Z_o v_o} \frac{\partial V_h}{\partial t} - \xi \frac{\partial \rho}{\partial t} = 0, \tag{1-4}$$

where η = q/m, the ratio of charge to mass for the electron, coulombs/kg;

$Z_o = \sqrt{L_h/C_h}$, the characteristic impedance of a lossless helix, ohms;

$v_o = 1/\sqrt{L_h C_h}$, the undisturbed axial phase velocity of the r-f wave along the helix, m/sec;

*Symbols are defined where they are first introduced in the report. In addition, a list of symbols is given at the end of the text.

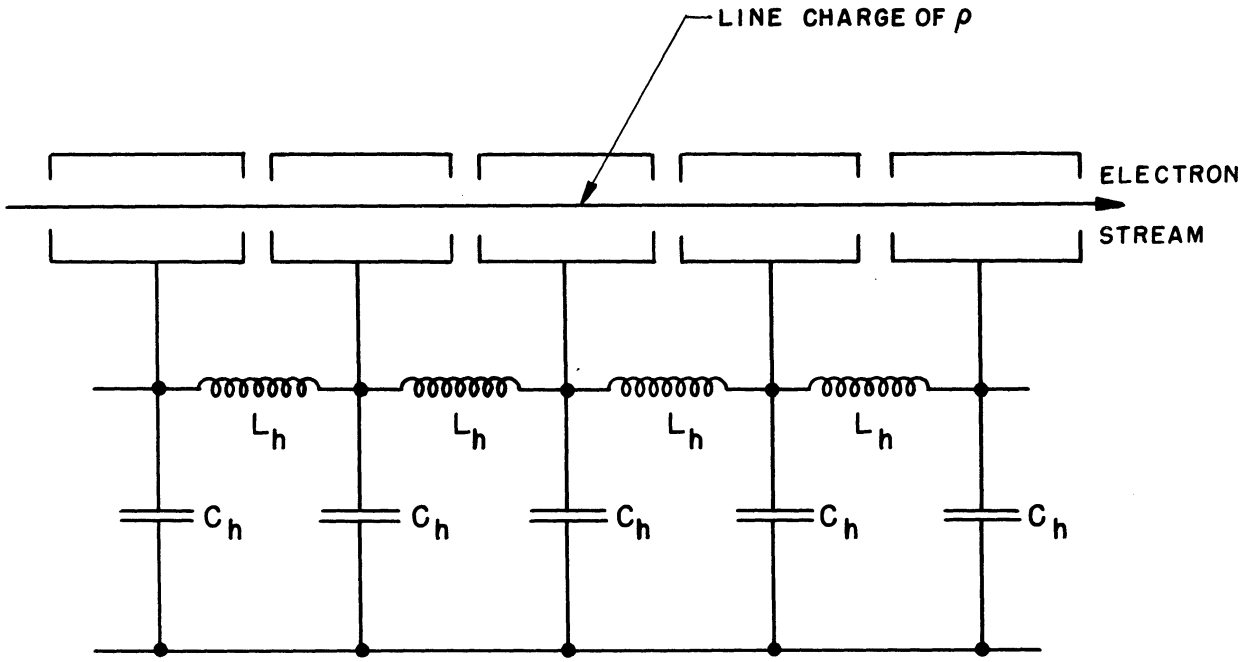

FIG. 1-4

EQUIVALENT CIRCUIT OF A TRAVELING-WAVE TUBE ASSUMING A LOSSLESS HELIX

L_h AND C_h ARE THE EQUIVALENT SERIES INDUCTANCE AND SHUNT CAPACITANCE PER UNIT LENGTH.

$v(z,t)$ = the axial velocity of the r-f wave along the helix, m/sec;

C_h = the distributed shunt capacitance per unit length, farads/m;

L_h = the distributed series inductance per unit length, henries/m;

ξ = the beam-to-circuit coupling coefficient;

$\rho(z,t)$ = the a-c space-charge density per unit length, coulombs/m;

$V_h(z,t)$ = the r-f potential along the helix, volts;

$I_h(z,t)$ = the longitudinal r-f helix current, amp;

and I_h, V_h, v, and ρ are dependent variables, functions of both the independent variables z and t.

In order to put the above equations in dimensionless form, all the variables are normalized with respect to v_o, the undisturbed phase velocity of the helix. Writing the equations in terms of these new normalized variables yields

$$\frac{\partial\bar{\rho}}{\partial\bar{t}} + \bar{\rho}\frac{\partial\bar{v}}{\partial\bar{z}} + \bar{v}\frac{\partial\bar{\rho}}{\partial\bar{z}} = 0, \tag{1-5}$$

$$\frac{\partial\bar{v}}{\partial\bar{t}} + \bar{v}\frac{\partial\bar{v}}{\partial\bar{z}} - \frac{\partial\bar{V}_h}{\partial\bar{z}} = 0, \tag{1-6}$$

$$\frac{\partial\bar{V}_h}{\partial\bar{z}} + \frac{\partial\bar{I}_h}{\partial\bar{t}} = 0, \tag{1-7}$$

and

$$\frac{\partial\bar{I}_h}{\partial\bar{z}} + \frac{\partial\bar{V}_h}{\partial\bar{t}} - \frac{\partial\bar{\rho}}{\partial\bar{t}} = 0, \tag{1-8}$$

where $\bar{\rho} = \rho/\rho_o = \eta\xi^2 Z_o/v_o$,

$\bar{v} = v/v_o$,

$$\bar{V}_h = V_h/e_o = \eta\xi V_h/v_o^2 \text{ , and}$$

$$\bar{I}_h = I_h/i_o = \eta\xi Z_o I_h/v_o^2 \text{ .}$$

It will be noticed that Eqs. 1-5 and 1-6 are nonlinear, whereas Eqs. 1-7 and 1-8 (the circuit equations) are linear.

To obtain the small-signal equations, Eqs. 1-5 and 1-6 are linearized by writing the velocity v and space-charge density ρ as the sum of their d-c and a-c components and then neglecting the squares and products of the a-c quantities in combining Eqs. 1-5 and 1-6. The resultant expression is then combined with Eqs. 1-7 and 1-8 to give a single fourth-degree differential equation in the r-f helix potential V_h. The solution of this equation is of the familiar exponential type.

The next step would of course be application of the boundary conditions at the input and output ends of the tube. However, since the equations presented in this section are not those ultimately to be solved, discussion of the boundary conditions will be omitted.

This approach yields valid results for the small-signal case, but difficulties arise when large signals are considered. Since the equations are based on the hydrodynamical equation of continuity, Eqs. 1-5, 1-6, 1-7, and 1-8 are valid only until the electron flight lines cross. This crossing of electron flight lines is due to overtaking of electrons, i.e., electrons that entered the tube at different times appearing at a point simultaneously. Overtaking of electrons by other electrons results in the velocity v, appearing in the above equations, becoming a multi-valued function of the independent variable z.

This overtaking of electrons does unfortunately occur in a large-signal traveling-wave amplifier considerably before the point of saturation

is reached. The exact point in any particular tube at which overtaking begins to occur depends on such factors as the gain parameter, the space-charge density, the amplitude of the r-f wave initially impressed on the helix, and the relative injection velocity. Therefore these equations cannot be used for the large-signal case.

Additional equations may be written to take this difficulty into account, but the number of equations to be solved soon becomes enormous as the number of electron-flight-line crossings increases. The number of these crossings will be seen to approach infinity as saturation is neared and the electrons, becoming trapped, oscillate back and forth in the regions of minimum potential.

Therefore it seems desirable to reformulate the problem in terms of new variables so as to eliminate the difficulty introduced by the crossing of electron flight lines. The new independent variables to be used are entrance phase, i.e., the phase at which the electron enters the helix relative to the r-f wave at the input, and position along the tube. Thus the Eulerian approach is replaced by a Lagrangian treatment, which greatly simplifies the large-signal problem. The resulting equations are a system of second-order nonlinear partial-differential-integral equations. A detailed discussion of these new independent variables is presented in Chapter II.

CHAPTER II. THEORETICAL EQUATIONS FOR THE LARGE-SIGNAL ANALYSIS

2.1 Derivation of the Theoretical Equations

It is anticipated that a large-signal study of the traveling-wave amplifier will yield information relating the various design parameters of any tube to the saturation power output and maximum obtainable efficiency. For this investigation the large-signal traveling-wave amplifier equations have therefore been derived, on the basis of Nordsieck's[12] work but taking into account the influence of the a-c space-charge fields and circuit loss in the form of series loss along the helix. Also, the equations are valid for large values of the gain parameter C. The MKS rationalized system of units is used throughout the derivation.

The general transmission-line equation, including the series loss, is derived in Appendix A as*

$$\frac{\partial^2 \bar{V}(z,t)}{\partial t^2} - v_o^2 \frac{\partial^2 \bar{V}(z,t)}{\partial z^2} + 2\omega C d \frac{\partial \bar{V}(z,t)}{\partial t} = v_o Z_o \frac{\partial^2 \bar{\rho}(z,t)}{\partial t^2} + 2\omega C d Z_o v_o \frac{\partial \bar{\rho}(z,t)}{\partial t}, \quad (2\text{-}1)$$

where $-\frac{\partial \bar{V}(z,t)}{\partial z}$ = the longitudinal radio-frequency electric-field intensity, due to the circuit, at the electron stream, volts/m;

z = distance measured along the tube, m;

$\bar{\rho}(z,t)$ = the linear space-charge density of the electron stream, coulombs/m;

*The bars over the dependent variables do not represent normalization as in Chapter I but serve only to differentiate the voltage and space-charge density as functions of z and t from the same quantities as necessarily different functions of y and ϕ.

$v_o = \frac{1}{\sqrt{LC}}$ = the undisturbed phase velocity of the line, m/sec;

$Z_o = \sqrt{L/C}$ = the characteristic impedance of the lossless line, ohms;

C = the gain parameter defined by $C^3 = |\eta| ZI_o/2u_o^2$;*

I_o = the d-c stream current, amp;

$u_o = \sqrt{2\eta V_o}$, the d-c stream velocity, m/sec;

V_o = the d-c stream voltage, volts;

η = q/m, the charge-to-mass ratio for the electron, coulombs/kg;

ω = angular frequency of the wave impressed on the helix, radians/sec;

$d = \ell/20(2\pi)(\log e)(C) = 0.01836\ \ell/C$, the loss factor;[8] and

ℓ = the series loss expressed in db per undisturbed wavelength along the helix.

The actual field along a helix is composed of an infinite number of components orthogonal to one another. The phase velocities of the space-harmonic fields, however, are lower than that of the fundamental field, and the electron stream will interact appreciably only with the fundamental field, since in a typical traveling-wave amplifier the electron stream is approximately in synchronism with the phase velocity of the fundamental field. Consequently, the space-harmonic fields on a helix serve to carry power along the helix but do not contribute to the gain of the amplifier. Tien[10] has calculated the impedance parameter for a tape helix model surrounded by

*The impedance used in evaluating the gain parameter in the large-signal theory is that which the electron stream sees, not necessarily Z_o. In the linear theory C is developed on the basis that the beam grazes the helix; however, in the large-signal theory when the ratio of helix diameter to stream diameter is not 1 the impedance Z_o must be replaced by $Z = \xi^2 Z_o$ where ξ is the stream-to-circuit coupling coefficient defined on page 13.

a dielectric medium, and found that the results predicted by the theory agree quite well with measurements on several tubes. He reports that the presence of the space-harmonic fields lowers the actual helix impedance.

Hence, even though the space-charge density $\bar{\rho}(z,t)$ in Eq. 2-1 will be exceedingly rich in harmonics of the impressed frequency of the r-f wave, the longitudinal r-f voltage along the helix will be approximately all at the fundamental frequency since the helix impedance is very small for harmonics of the fundamental frequency. Thus the assumption that all but the fundamental frequency component of space-charge density may be neglected in determining the helix voltage $\bar{V}(z,t)$ in the transmission-line equation is not an appreciable limitation to the theory.

On the basis of this assumption we may represent the r-f voltage along the helix $\bar{V}(z,t)$ in terms of two slowly varying functions of z, an amplitude and a phase, as shown in Eq. 2-12.

The fields due to the longitudinal flow of energy on the helix and the field due to space charge are linearly superimposed to write the Newton equation of motion for an electron in a traveling-wave amplifier as

$$\frac{d^2z}{dt^2} = -|\eta|\left(\frac{\partial\bar{V}(z,t)}{\partial z} + \frac{\partial\bar{V}_s(z,t)}{\partial z}\right), \qquad (2\text{-}2)$$

where $\partial\bar{V}_s(z,t)/\partial z = -\bar{E}_s(z,t)$ = the space-charge field intensity, volts/m. The electron trajectories which are solutions of Eq. 2-2 will have the form

$$z = F(z_o,t) \quad , \qquad (2\text{-}3)$$

where z_o = the position of an electron at time t = 0. Equation 2-3 may of course be inverted and solved for z_o in terms of z and t as follows*:

*It should be noted that the function G(z,t) is not unique since z_o is a multi-valued function of z.

$$z_o = G(z,t) \quad . \tag{2-4}$$

The electrons enter the helix at z = 0 but may be considered to originate at $z = z_o$ at t = 0, and each particular electron n has its own entrance position z_{o_n} as shown in Fig. 2-1.

The solutions of Eq. 2-2 represented by Eq. 2-3 may be related to the space-charge density $\bar{\rho}(z,t)$ by remembering that conservation of charge requires the charge $\bar{\rho}_o dz_o$ entering the tube unmodulated at the input, due to all electrons whose initial positions lie between z_o and $z_o + dz_o$, to equal the charge $\bar{\rho}dz$ at some later position z. This requirement is expressed mathematically as

$$\bar{\rho}(z,t)dz = \bar{\rho}(z,t)\left|\frac{\partial z}{\partial z_o}\right| dz_o = \bar{\rho}(z_o,0)dz_o \quad . \tag{2-5}$$

The space-charge density in the stream entering the tube may be related to the stream current and voltage by

$$\bar{\rho}(z_o,0) = \frac{I_o}{u_o} \quad . \tag{2-6}$$

Hence the desired relationship may be obtained using Eqs. 2-4, 2-5, and 2-6:

$$\bar{\rho}(z,t) = \frac{I_o}{u_o}\left|\frac{\partial z_o}{\partial z}\right| \quad . \tag{2-7}$$

Considerably before saturation is reached, the electrons begin to overtake one another; i.e., electrons starting at different initial times appear simultaneously at the same point. When this occurs, z_o is no longer a single-valued function of z and Eq. 2-7 must be modified by replacing the quantity $(\partial z_o/\partial z)\big|_t$ by the sum of its values for all branches of the multi-valued

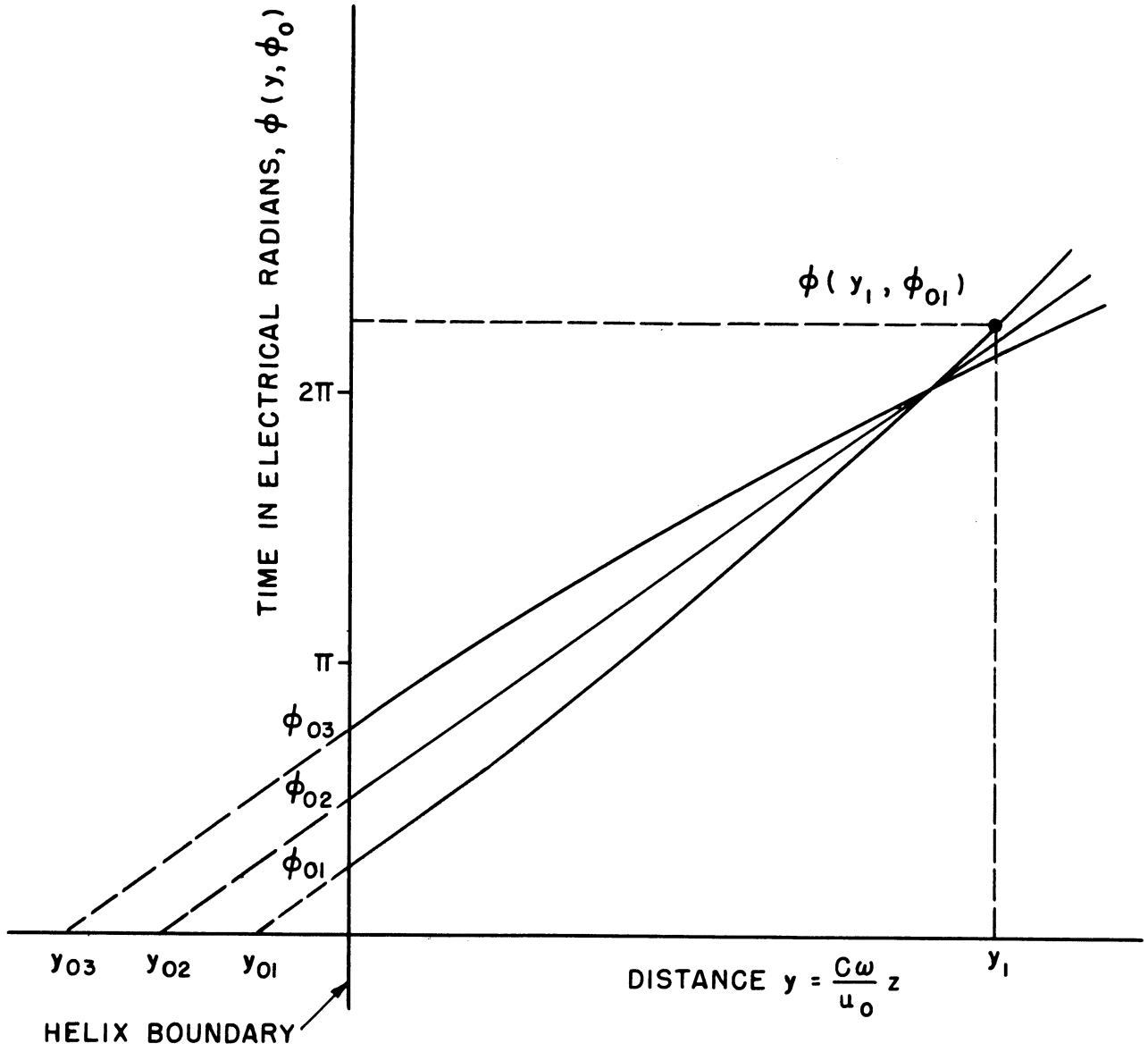

FIG. 2–1 DISTANCE–TIME DIAGRAM FOR ELECTRONS ENTERING THE HELIX REGION, INDICATING STARTING TIME AND ENTRANCE TIME FOR EACH ELECTRON. ALSO THE MULTIVALUEDNESS OF z_0 OR y_0 AS A FUNCTION OF z OR y IS SHOWN WHEN OVERTAKING OCCURS. DISTANCE MAY BE MEASURED IN UNITS OF z OR y.

function z_o. The calculations are therefore made in terms of z_o as the independent variable, since z is a single-valued function of z_o.

In order to simplify the calculations and put the equations in a form applicable to all traveling-wave amplifiers, whatever the frequency range, new variables are introduced. The new variables defined are usually normalized with respect to some constant velocity occurring in the problem; in the case of the traveling-wave amplifier either the stream velocity u_o or the undisturbed phase velocity of the helix v_o would be suitable. The definition of new variables amounts to changing to a coordinate system riding with the undisturbed phase velocity v_o or with the stream velocity u_o, the advantage being that the dependent variables vary more slowly with time and distance in these coordinate systems.

The choice of which velocity to use is somewhat arbitrary, but it is believed that the numerical calculations will be simpler if the variables are normalized with respect to the initial stream velocity. The alternate set of equations is presented in Section 2.2.

The normalized independent variables are therefore defined as follows:*

$$y \triangleq \frac{C\omega z}{u_o} = \frac{2\pi C}{\lambda_s} z \tag{2-8}$$

and

$$\phi_o \triangleq \frac{\omega z_o}{u_o} = \omega t_o \quad , \tag{2-9}$$

where $\lambda_s = u_o/f$, the stream wavelength in meters. Physically, y is proportional to the position along the tube in stream wavelengths. ϕ_o, the entrance phase, relative to the r-f wave at the input, of an electron in

*The symbol $\triangleq$ means that the left-hand side of the equation is by definition equal to the right-hand side.

radians, may be thought of as a "tag" for a particular electron entering the helix region*. In fact, ϕ_o is a time standard in radians of the frequency of the input voltage. Thus in this Lagrangian formulation of the problem, particular electrons are followed through the interaction region rather than considering the electron stream as a "fluid". Introducing the new variable y into Eqs. 2-1 and 2-2 gives

$$\frac{\partial^2 V(y,t)}{\partial t^2} - C^2\omega^2\left(\frac{v_o}{u_o}\right)^2 \frac{\partial^2 V(y,t)}{\partial y^2} + 2\omega C d \frac{\partial V(y,t)}{\partial t}$$

$$= v_o Z_o \frac{\partial^2 \rho(y,t)}{\partial t^2} + 2\omega C d v_o Z_o \frac{\partial \rho(y,t)}{\partial t} \qquad (2\text{-}10)$$

$$\frac{d^2 y}{dt^2} = -|\eta| \left[\left(\frac{C\omega}{u_o}\right)^2 \frac{\partial V(y,t)}{\partial y} - \frac{C\omega}{u_o} E_s(y,t)\right]. \qquad (2\text{-}11)$$

In the large-signal equations the space-charge density $\rho(y,t)$, which is a fluid constant, is interpreted as the electron charge q_e times the number density of electrons N_e.

In accordance with the discussion following Eq. 2-1 the following dependent variables are defined:

$$\bar{V}(z,t) = V(y,\phi) \triangleq \mathrm{Re}\left[\frac{Z_o I_o}{C} A(y) e^{-j\phi}\right]. \qquad (2\text{-}12)$$

Equation 2-12 serves to define A(y), the normalized voltage amplitude of the r-f wave along the helix, and $\phi(y,\phi_o)$, the phase of the fundamental-frequency r-f wave in the circuit relative to the phase of the wave at the input to the helix. A particular value of y not only defines a phase plane

*Also, as may be seen in Fig. 2-1, ϕ_o is in a sense a transit angle for a particular electron traveling from the point z_{on} to the helix boundary at z = 0.

of the r-f wave but also serves as the axial coordinate of one or more electrons; similarly $\phi(y,\phi_o)$ can be used in a second sense as the phase of the displacement component of an electron at y that entered the helix at the moment ϕ_o relative to the r-f wave. It is easily seen that the new time variable $\phi(y,\phi_o)$ in Eq. 2-13 is based on a coordinate system which moves with the initial stream velocity u_o.

The following additional reduced dependent variables are defined:

$$\theta(z) \triangleq \omega\left(\frac{z}{u_o} - t\right) - \phi(z,t) \tag{2-13}$$

and

$$u_t(y,\phi_o) = \frac{dz}{dt} \triangleq u_o\,[1 + 2Cu(y,\phi_o)] \quad . \tag{2-14}$$

Equation 2-13 defines $\theta(z)$, the phase lag across the amplifier, at any point y, in radians. In particular, $\theta(z)$ is the r-f phase angle (or lag) in radians of the wave on the helix relative to a hypothetical traveling wave whose phase velocity is the initial stream velocity u_o. Equation 2-14, an expression for the total velocity of an electron, defines $2Cu_o u(y,\phi_o)$, the velocity deviation of an electron relative to the initial d-c stream velocity. Since u is a function of ϕ_o, the entrance phase of an electron, the velocity of an electron at any point y can be calculated. $u(y,\phi_o)$ is a dimensionless large-signal velocity parameter.

Solving Eq. 2-13 for z and converting to the new independent variable y gives

$$y = C\,[\phi(y,\phi_o) + \theta(y) + \omega t] \quad . \tag{2-15}$$

Equation 2-14 written in terms of y is

$$\frac{dy}{dt} = C\omega\,[1 + 2Cu(y,\phi_o)] \quad . \tag{2-16}$$

Taking the time derivative of Eq. 2-15 and equating the result to Eq. 2-16 gives

$$\left[\frac{\delta\phi}{\delta y}\frac{dy}{dt} + \frac{d\theta(y)}{dy}\frac{dy}{dt} + \omega\right] = [\omega + 2\omega C u(y,\phi_o)] \quad . \tag{2-17}$$

Partial differentiation with respect to y and t is represented by $\partial/\partial y$ and $\partial/\partial t$, and partial differentiation with respect to ϕ_o and y is represented by $\delta/\delta\phi_o$ and $\delta/\delta y$ in the equations of this section. Obviously, $\partial/\partial y = \delta/\delta y$ and $\partial/\partial t = (1/\omega)(\delta/\delta\phi_o)$. Equation 2-17 may be simplified and written as

$$\frac{\delta\phi(y,\phi_o)}{\delta y} + \frac{d\theta(y)}{dy} = \frac{2u(y,\phi_o)}{1 + 2Cu(y,\phi_o)} \quad . \tag{2-18}$$

Equation 2-18 is the first of the working equations, relating the dependent variables $\phi(y,\phi_o)$, $\theta(y)$, and $u(y,\phi_o)$.

In terms of the new dependent variables, Eq. 2-10 may be rewritten with the space-charge density $\rho(y,t)$ replaced by its fundamental-frequency component ρ_1, in keeping with the previous discussion:

$$-C\left(\frac{\omega v_o}{u_o}\right)^2 Z_o I_o \left\{\left[\frac{d^2A(y)}{dy^2} - A(y)\left\{\left(\frac{1}{C} - \frac{d\theta(y)}{dy}\right)^2 - \left(\frac{u_o}{v_o C}\right)^2\right\}\right]\cos\phi(y,\phi_o)\right.$$

$$\left. + \left[\left(\frac{1}{C} - \frac{d\theta(y)}{dy}\right)\left(-2\frac{dA(y)}{dy}\right) + A(y)\frac{d^2\theta(y)}{dy^2} - \frac{2d}{C}\left(\frac{u_o}{v_o}\right)^2 A(y)\right]\sin\phi(y,\phi_o)\right\}$$

$$= v_o Z_o \frac{\partial^2\rho_1}{\partial t^2} + 2\omega C d\, v_o Z_o \frac{\partial\rho_1}{\partial t} \quad . \tag{2-19}$$

Upon substitution from Eq. 2-12 for $\partial V/\partial y$, the force equation, 2-2, becomes

$$\frac{dv}{dt} = \frac{d^2y}{dt^2} = -|\eta| \left\{ \frac{Z_o I_o \omega}{u_o} \left[\frac{dA(y)}{dy} \cos \phi(y,\phi_o) - A(y) \sin \phi(y,\phi_o) \left(\frac{1}{C} - \frac{d\theta(y)}{dy} \right) \right] - E_s(y,\phi) \right\} . \quad (2\text{-}20)$$

From Eq. 2-16,

$$\frac{dv}{dt} = \frac{\delta v}{\delta y} \frac{dy}{dt} = 2Cu_o \frac{\delta u}{\delta y} \frac{dy}{dt} = 2C^2 u_o \omega \left[1 + 2Cu(y,\phi_o)\right] \frac{\delta u(y,\phi_o)}{\delta y} . \quad (2\text{-}21)$$

The next step is to equate Eqs. 2-20 and 2-21 and simplify:

$$\frac{\delta u(y,\phi_o)}{\delta y} \left[1 + 2Cu(y,\phi_o)\right] = A(y) \left[1 - C \frac{d\theta(y)}{dy} \right] \sin \phi(y,\phi_o) - C \frac{dA(y)}{dy} \cos \phi(y,\phi_o) + \frac{u_o C}{\omega Z_o I_o} E_s(y,\phi) . \quad (2\text{-}22)$$

In terms of the newly defined variables Eq. 2-7, expressing the conservation of charge, may be written as

$$\rho(y,\phi) = \frac{I_o}{u_o} \left| \frac{\partial \phi_o}{\partial \phi} \right| \frac{1}{1 + 2Cu(y,\phi_o)} . \quad (2\text{-}23)$$

Next, $\rho(y,\phi)$ is expanded in a Fourier series in the time variable $\phi(y,\phi_o)$. This operation introduces no additional assumptions in the analysis.

$$\rho(y,\phi) = \sum_{n=1}^{\infty} \frac{\sin n\phi}{\pi} \int_0^{2\pi} \rho \sin n\phi \, d\phi_o + \sum_{n=1}^{\infty} \frac{\cos n\phi}{\pi} \int_0^{2\pi} \rho \cos n\phi \, d\phi_o . \quad (2\text{-}24)$$

Substituting Eq. 2-24 into Eq. 2-23 gives

$$\rho(y,\phi) = \mathrm{Re}\left\{\frac{I_o}{u_o\pi}\sum_{n=1}^{\infty} e^{-jn\phi}\left[\int_0^{2\pi}\frac{\cos n\phi(y,\phi_o')d\phi_o'}{1+2Cu(y,\phi_o')} + j\int_0^{2\pi}\frac{\sin n\phi(y,\phi_o')d\phi_o'}{1+2Cu(y,\phi_o')}\right]\right\}. \quad (2\text{-}25)$$

(In Eq. 2-25 the prime denotes the variable of integration.)

In terms of the new variables the first and second time derivatives of the fundamental component of space-charge density, ρ_1 of Eq. 2-19, may be expressed as follows:

$$\frac{\partial\rho_1}{\partial t} = \frac{\partial\rho_1}{\partial\phi}\frac{\partial\phi}{\partial t}, \quad (2\text{-}26)$$

$$\frac{\partial^2\rho_1}{\partial t^2} = \frac{\partial\rho_1}{\partial\phi}\frac{\partial^2\phi}{\partial t^2} + \left(\frac{\partial\phi}{\partial t}\right)^2\frac{\partial^2\rho_1}{\partial\phi^2}, \quad (2\text{-}27)$$

and

$$\rho_1 = \rho_{1c}\cos\phi + \rho_{1s}\sin\phi. \quad (2\text{-}28)$$

If Eqs. 2-26, 2-27, and 2-28 are substituted into the right-hand side of Eq. 2-19 with the aid of Eq. 2-25, the resulting expression may be written as two equations simply by equating the coefficients of sin ϕ and of cos ϕ on each side of the equation. This is a valid procedure because the coefficients are independent of ϕ and the sine and cosine functions are orthogonal. In the two equations thus obtained, the constants are written in terms of the parameters previously defined and the additional parameter

$$b \triangleq \frac{u_o - v_o}{Cv_o}, \quad (2\text{-}29)$$

where b = a relative injection velocity parameter. Thus

$$\frac{d^2A(y)}{dy^2} - A(y)\left[\left(\frac{1}{C} - \frac{d\theta(y)}{dy}\right)^2 - \frac{(1+Cb)^2}{C^2}\right]$$

$$= \frac{1+Cb}{\pi C}\left[\int_0^{2\pi} \frac{\cos \phi(y,\phi_o')\, d\phi_o'}{1 + 2Cu(y,\phi_o')} + 2Cd\int_0^{2\pi} \frac{\sin \phi(y,\phi_o')\, d\phi_o'}{1 + 2Cu(y,\phi_o')}\right] \quad (2\text{-}30)$$

and

$$A(y)\left[\frac{d^2\theta(y)}{dy^2} - \frac{2d}{C}(1+Cb)^2\right] + 2\frac{dA(y)}{dy}\left(\frac{d\theta(y)}{dy} - \frac{1}{C}\right)$$

$$= \frac{1+Cb}{\pi C}\left[\int_0^{2\pi} \frac{\sin \phi(y,\phi_o')\, d\phi_o'}{1 + 2Cu(y,\phi_o')} - 2Cd\int_0^{2\pi} \frac{\cos \phi(y,\phi_o')\, d\phi_o'}{1 + 2Cu(y,\phi_o')}\right]. \quad (2\text{-}31)$$

Finally, the expression for the space-charge field E_s (derived in Appendix B),

$$E_s(y,\phi) = -\frac{2\omega u_o}{|\eta|(1+Cb)}\left(\frac{\omega_p}{\omega}\right)^2 \int_0^{2\pi} \frac{F(\phi-\phi')\, d\phi_o'}{1 + 2Cu(y,\phi_o')}, \quad (2\text{-}32)$$

is substituted into the force equation, Eq. 2-22, to obtain the last of the working equations:

$$\frac{\delta u(y,\phi_o)}{\delta y}[1 + 2Cu(y,\phi_o)] = A(y)\left[1 - C\frac{d\theta(y)}{dy}\right]\sin \phi(y,\phi_o)$$

$$- C\frac{dA(y)}{dy}\cos \phi(y,\phi_o) - \frac{1}{1+Cb}\left(\frac{\omega_p}{\omega C}\right)^2 \int_0^{2\pi} \frac{F(\phi-\phi')\, d\phi_o'}{1 + 2Cu(y,\phi_o')}. \quad (2\text{-}33)$$

To summarize, the four equations 2-18, 2-30, 2-31, and 2-33 are the final working equations which will be solved for the dependent variables $A(y)$, $\theta(y)$, $u(y,\phi_o)$, and $\phi(y,\phi_o)$ subject to the boundary conditions discussed

in Section 2.4. This system of second-order nonlinear partial-differential-integral equations is valid for a wide range of the parameters C, d, b, ω_q/ω, and A_o (the normalized amplitude of the r-f signal impressed on the helix at the input) and is limited only by the assumptions mentioned in their derivation:

1. The electrons will interact appreciably only with the fundamental field and hence all but the fundamental component of space-charge density may be neglected in determining the helix voltage.

2. There is no initial thermal velocity distribution in the electron stream.

3. The electric field is constant across the electron stream.

4. The radio-frequency wave impressed on the helix bunches the stream in such a manner that the space-charge density is constant in amplitude (i.e., has no radial variation) and varies sinusoidally with axial distance. (In calculating the space-charge forces it is assumed that the growth constant of the growing space-charge wave is small compared to unity.)

5. The relationships may be described using nonrelativistic mechanics; i.e., the squares of the ratios of the stream velocity u_o and the wave velocity v to the velocity of light are small compared to unity, and hence the motion of the electrons is sufficiently slow that the formulas of electrostatics are valid.

6. The electron stream is in a strong axial d-c magnetic field (rectilinear flow), so that the electrons are constrained to follow linear paths. Consequently there is considered to be no transverse motion and the stream boundary is smooth.

7. A sufficient quantity of positive ions is present to neutralize the average space charge.

Assumptions 3 and 4 are considered to be the chief limitations to the theory as presented here.

For the small-signal theory one parameter, namely QC, is sufficient to specify the space charge; but in the large-signal theory it is necessary, for any given ratio of helix diameter to stream diameter, to specify two

parameters, a space range of effectiveness and an amplitude. The range parameter used is $\beta b'$, shown in Fig. B-6. The space-charge weighting function $F(\phi-\phi')$ drops off more rapidly for smaller values of $\beta b'$ than for the larger values, and thus $\beta b'$ determines the range over which the space-charge forces are effective. The coefficient $(\omega_p/\omega C)^2$ of the space-charge field term in the force equation, Eq. 2-33, would seem to be a better choice for the amplitude parameter of the large-signal case than the QC appropriate to the linear theory. The relationship between $(\omega_p/\omega C)^2$ and QC is discussed in Appendix B.

In the small-signal theory the current is essentially all at the fundamental frequency; hence QC need be evaluated only for the fundamental component of current. Correspondingly in the large-signal theory the reduction factor R_n of Fig. B-3 must necessarily, then, be evaluated only for the fundamental component of space charge (i.e., n = 1), even though the harmonic content of the stream current is high.

The recommended space-charge parameters for the large-signal analysis are therefore $\beta b'$ and $(\omega_p/\omega C)^2$, which might be more briefly represented as

$$K = \left(\frac{\omega_p}{\omega C}\right)^2$$

and

$$B = \beta b' \quad .$$

For the purpose of calculation a mathematical model will be used in which the helix-stream interaction region of the traveling-wave amplifier is considered to be infinite in length and the helix is thus terminated in its characteristic impedance Z_o. Hence the effect of reflections due to a mismatch at the output end is not considered, and the collector and helix d-c potentials are taken as equal. The small-signal conditions, corresponding

to the three waves, are applied at the input: a voltage is applied to the helix at y = 0, and the equations are integrated stepwise until a maximum occurs in the amplitude of the normalized r-f voltage A(y). The amplitude of the r-f signal initially impressed on the helix, A_o, is usually taken as 0.0225, which is approximately 30 db below CI_oV_o. However, solutions are also obtained for other values of A_o to provide data for a plot of power output vs. power input.

In applying the results of these computations, therefore, to any existing finite-length traveling-wave amplifier, it must be assumed that there are no reflections at the input or output (which may be due to a mismatch in the coupling networks or to a discontinuity in the acceleration if the helix and the collector are operated at different d-c potentials), and that the interaction region is sufficiently long for small-signal conditions to prevail at the input.

2.2 Relation to Nordsieck's Equations

The general working equations derived in the preceding section may be reduced to Nordsieck's[12] "large-signal" equations,

$$\frac{\delta\phi(y,\phi_o)}{\delta y} + \frac{d\theta(y)}{dy} = 2u(y,\phi_o) , \tag{2-34}$$

$$\frac{\delta u(y,\phi_o)}{\delta y} = A(y) \sin \phi(y,\phi_o) , \tag{2-35}$$

$$\frac{dA(y)}{dy} = -\frac{1}{2\pi} \int_0^{2\pi} \sin \phi(y,\phi_o)\, d\phi_o , \tag{2-36}$$

and

$$\frac{d\theta(y)}{dy} + b = \frac{1}{2\pi A(y)} \int_0^{2\pi} \cos \phi(y,\phi_o)\, d\phi_o , \tag{2-37}$$

by the application of the appropriate assumptions. The necessary assumptions are (1) that the gain parameter C, a measure of stream-to-circuit coupling, is small compared to 1, i.e., $C \ll 1$; (2) that the a-c velocity term $2Cu_o u(y,\phi_o)$ is a small fraction of the average velocity u_o; and (3) that terms involving second space derivatives of $A(y)$ and $\theta(y)$ and products of the first space derivatives may be neglected.

Nordsieck's equations are not valid for a C greater than about 0.02 or 0.03, which is much smaller than the C values of typical large-signal traveling-wave amplifiers. In addition, the assumptions listed above are valid only when the a-c quantities in the stream are small. Since efficiency is proportional to C, Nordsieck's theory does not cover high-efficiency operation and hence describes a transition region between that to which Pierce's[8] small-signal equations apply and that to which the large-signal equations derived in Section 2.1 may be applied.

2.3 Derivation of Alternate Theoretical Equations

As pointed out on page 21, there is an alternate possibility of defining new dependent variables relative to the undisturbed velocity of the wave, v_o, so that the coordinate system moves with the velocity v_o rather than traveling with the initial stream velocity u_o. It is felt that the equations which result are sufficiently different and interesting to warrant presenting them here, although the mathematical manipulations involved are quite similar to those in Section 2.1.

The general transmission-line equation, the force equation, and the conservation of charge relationship derived in Section 2.1 are repeated here for ease of reference:

$$\frac{\partial^2 \bar{V}(z,t)}{\partial t^2} - v_o^2 \frac{\partial^2 \bar{V}(z,t)}{\partial z^2} + 2\omega C d \frac{\partial \bar{V}(z,t)}{\partial t}$$

$$= v_o Z_o \frac{\partial^2 \bar{\rho}(z,t)}{\partial t^2} + 2\omega C d v_o Z_o \frac{\partial \bar{\rho}(z,t)}{\partial t} \qquad (2\text{-}1)$$

$$\frac{d^2 z}{dt^2} = - |\eta| \left(\frac{\partial \bar{V}(z,t)}{\partial z} + \frac{\partial \bar{V}_s(z,t)}{\partial z} \right) \qquad (2\text{-}2)$$

$$\bar{\rho}(z,t) = \frac{I_o}{u_o} \left| \frac{\partial z_o}{\partial z} \right| \quad . \qquad (2\text{-}7)$$

The new normalized independent variables to be used are defined as

$$y \triangleq \frac{C\omega z}{v_o} = \frac{2\pi C}{\lambda_g} z \qquad (2\text{-}38)$$

and

$$\phi_o \triangleq \frac{\omega z_o}{u_o} = \omega t_o \quad , \qquad (2\text{-}39)$$

where $\lambda_g = v_o/f$, the undisturbed helix wavelength in meters. Thus y is now proportional to the position along the tube in undisturbed helix wavelengths.

Introducing these new variables into Eqs. 2-1 and 2-2 yields

$$\frac{\partial^2 V(y,t)}{\partial t^2} - C^2\omega^2 \frac{\partial^2 V(y,t)}{\partial y^2} + 2\omega C d \frac{\partial V(y,t)}{\partial t}$$

$$= v_o Z_o \frac{\partial^2 \rho(y,t)}{\partial t^2} + 2\omega C d v_o Z_o \frac{\partial \rho(y,t)}{\partial t} \qquad (2\text{-}40)$$

and

$$\frac{d^2 y}{dt^2} = - |\eta| \left[\left(\frac{C\omega}{v_o} \right)^2 \frac{\partial V(y,t)}{\partial y} - \frac{C\omega}{v_o} E_s(y,t) \right] \quad . \qquad (2\text{-}41)$$

Next the dependent variables

$$\Phi(z,t) \triangleq \omega \left(\frac{z}{v_o} - t\right) \tag{2-42}$$

and

$$v_t(y,\phi_o) = \frac{dz}{dt} \triangleq v_o \left[1 + C\, v(y,\phi_o)\right] \tag{2-43}$$

are defined. Equation 2-42 transfers the problem to a coordinate system moving with the undisturbed velocity of the wave v_o, while Eq. 2-43 expresses the velocity deviation of an electron $Cv(y,\phi_o)$ relative to the undisturbed phase velocity of the wave. In addition, a normalized r-f voltage is defined in terms of its vector components $a_1(y)$ and $a_2(y)$ as follows:

$$\overline{V}(z,t) = V(y,\phi_o) \triangleq \frac{Z_o I_o}{4C} \left[a_1(y) \cos \Phi(y,\phi_o) - a_2(y) \sin \Phi(y,\phi_o)\right] . \tag{2-44}$$

Solving Eq. 2-42 for z and converting to the new independent variable y gives

$$y = C \left[\Phi(y,\phi_o) + \omega t\right] . \tag{2-45}$$

Equation 2-43, written in terms of y, is

$$\frac{dy}{dt} = C\omega \left[1 + Cv(y,\phi_o)\right] . \tag{2-46}$$

Taking the time derivative of Eq. 2-45, equating the result to Eq. 2-46, and simplifying yields

$$\frac{\delta\Phi(y,\phi_o)}{\delta y} = \frac{v(y,\phi_o)}{1 + Cv(y,\phi_o)} . \tag{2-47}$$

Equation 2-47, relating the dependent variables $\Phi(y,\phi_o)$ and $v(y,\phi_o)$, is the first of the alternate working equations.

In terms of the new dependent variables, Eq. 2-44 may be written with the space-charge density $\rho(y,t)$ replaced by its fundamental-frequency component ρ_1, as discussed in Section 2.1:

$$Z_o I_o \omega^2 \left\{ \left[-C \frac{d^2 a_1(y)}{dy^2} + 2 \frac{da_2(y)}{dy} + 2da_2(y) \right] \cos \Phi(y,\phi_o) \right.$$
$$\left. + \left[C \frac{d^2 a_2(y)}{dy^2} + 2 \frac{da_1(y)}{dy} + 2\, da_1(y) \right] \sin \Phi(y,\phi_o) \right\}$$
$$= v_o Z_o \frac{\partial^2 \rho_1}{\partial t^2} + 2\omega C dv_o Z_o \frac{\partial \rho_1}{\partial t} . \quad (2\text{-}48)$$

When $\partial V/\partial y$ is written in terms of the new variables, the force equation, 2-2, becomes

$$\frac{dv}{dt} = \frac{d^2 z}{dt^2} = - |\eta| \left\{ \frac{Z_o I_o \omega}{4 v_o} \left[\left(\frac{da_1(y)}{dy} - \frac{a_2(y)}{C} \right) \cos \Phi(y,\phi_o) \right. \right.$$
$$\left. \left. - \left(\frac{da_2(y)}{dy} + \frac{a_1(y)}{C} \right) \sin \Phi(y,\phi_o) - E_s(y,\phi) \right] \right\} . \quad (2\text{-}49)$$

Also, from Eq. 2-46,

$$\frac{dv}{dt} = \frac{\delta v}{\delta y} \frac{dy}{dt} = C v_o \frac{\delta v(y,\phi_o)}{\delta y} \frac{dy}{dt} = C^2 \omega v_o [1 + C v(y,\phi_o)] \frac{\delta v(y,\phi_o)}{\delta y} . \quad (2\text{-}50)$$

Equating Eqs. 2-49 and 2-50 and simplifying yields the second working equation:

$$\frac{\delta v(y,\phi_o)}{\delta y} [1 + C v(y,\phi_o)]^2 = C(1+Cb)^2 \left[\left(a_2(y) - C \frac{da_1(y)}{dy} \right) \cos \Phi(y,\phi_o) \right.$$
$$\left. + \left(a_1(y) + C \frac{da_2(y)}{dy} \right) \sin \Phi(y,\phi_o) - \frac{4 v_o C}{\omega Z_o I_o} E_s(y,\phi) \right] . \quad (2\text{-}51)$$

In terms of the newly defined variables Eq. 2-7, expressing the conservation of charge, may be written as

$$\rho(y,\Phi) = \frac{I_o}{v_o}\left|\frac{\partial \phi_o}{\partial \phi}\right| \frac{1}{1 + Cv(y,\phi_o)} \quad . \tag{2-52}$$

Next $\rho(y,\Phi)$ is expanded in a Fourier series in the time variable Φ:

$$\rho(y,\Phi) = \sum_{n=1}^{\infty} \frac{\sin n\Phi}{\pi} \int_0^{2\pi} \rho \sin n\Phi \, d\phi_o + \sum_{n=1}^{\infty} \frac{\cos n\Phi}{\pi} \int_0^{2\pi} \rho \cos n\Phi \, d\phi_o \quad . \tag{2-53}$$

Substituting Eq. 2-53 into 2-52 gives

$$\rho(y,\Phi) = \mathrm{Re}\left\{\frac{I_o}{v_o \pi} \sum_{n=1}^{\infty} e^{-jn\Phi}\left[\int_0^{2\pi} \frac{\cos n\Phi(y,\phi_o')d\phi_o'}{1 + Cv(y,\phi_o')} + j\int_0^{2\pi} \frac{\sin n\Phi(y,\phi_o')d\phi_o'}{1 + Cv(y,\phi_o')}\right]\right\}. \tag{2-54}$$

The next step is to substitute Eqs. 2-26, 2-27, 2-28, and 2-54 into Eq. 2-48. The resulting expression may be written as two equations simply by equating the coefficients of sin Φ and of cos Φ on each side of the equation, since the coefficients are independent of Φ and the sine and cosine functions are orthogonal:

$$\frac{C}{2}\frac{d^2a_1(y)}{dy^2} - \frac{da_2(y)}{dy} - da_2(y) = \frac{2}{\pi}\left[\int_0^{2\pi} \frac{\cos n\Phi(y,\phi_o')\, d\phi_o'}{1 + Cv(y,\phi_o')} + 2Cd\int_0^{2\pi} \frac{\sin n\Phi(y,\phi_o')\, d\phi_o'}{1 + Cv(y,\phi_o')}\right] \tag{2-55}$$

$$\frac{C}{2}\frac{d^2a_2(y)}{dy^2} + \frac{da_1(y)}{dy} + da_1(y) = -\frac{2}{\pi}\left[\int_0^{2\pi} \frac{\sin n\Phi(y,\phi_o')\, d\phi_o'}{1 + Cv(y,\phi_o')} - 2Cd \int_0^{2\pi} \frac{\cos n\Phi(y,\phi_o')\, d\phi_o'}{1 + Cv(y,\phi_o')}\right]. \quad (2\text{-}56)$$

Finally, the expression for the space-charge field E_s, derived in Appendix B,

$$E_s(y,\phi) = -\frac{2\omega u_o}{|\eta|(1 + Cb)}\left(\frac{\omega_p}{\omega}\right)^2 \int_0^{2\pi} \frac{F(\Phi-\Phi')\, d\phi_o'}{1 + Cv(y,\phi_o')}, \quad (2\text{-}31)$$

is substituted into the force equation, Eq. 2-51, to obtain the last working equation:

$$\frac{\delta v(y,\phi_o)}{\delta y}[1 + Cv(y,\phi_o)]^2 = C(1 + Cb)^2\left[\left(a_2(y) - C\frac{da_1(y)}{dy}\right)\cos\Phi(y,\phi_o) + \left(a_1(y) + C\frac{da_2(y)}{dy}\right)\sin\Phi(y,\phi_o) + \frac{4}{(1+Cb)^2}\left(\frac{\omega_p}{\omega C}\right)^2 \int_0^{2\pi} \frac{F(\Phi-\Phi')\, d\phi_o'}{1 + Cv(y,\phi_o')}\right]. \quad (2\text{-}57)$$

Equations 2-47, 2-55, 2-56, and 2-57 are the working equations in terms of the alternate coordinate system. The range of validity of these equations and the underlying assumptions are the same as those for the equations presented in Section 2.1.

The dependent variables $a_1(y)$ and $a_2(y)$ of Section 2.2 are related to the dependent variables $A(y)$ and $\theta(y)$ by the equations

$$A(y) = \frac{1}{4}\sqrt{a_1^2(y) + a_2^2(y)} \tag{2-58}$$

and

$$\tan [-\theta(y) - by] = \frac{a_2(y)}{a_1(y)} \quad . \tag{2-59}$$

Equations 2-47, 2-55, 2-56, and 2-57 reduce to Nordsieck's[12] so-called "large C" equations if a-c space charge and series loss are neglected except for terms involving the second space derivative of the variables $a_1(y)$ and $a_2(y)$, which clearly should not be neglected especially in the regions of rapidly changing slope, e.g., near the maximum value of $A(y)$.

The large-signal equations of Section 2.1 have been selected for numerical analysis because it is believed that the equations of Section 2.2 would require more time to evaluate, since in the latter case a square root and an arctangent would have to be evaluated to find the r-f voltage amplitude and the phase lag across the tube at each step in the integration procedure. This is a consequence of the manner in which $A(y)$ was defined (i.e., in terms of its vector components) and not the fact that a coordinate system moving with the velocity v_o was selected.

2.4 Boundary Conditions

In Section 2.1 it was assumed that the r-f wave on the helix is of a single frequency. Hence the r-f voltage on the helix was defined by two slowly varying functions of distance, an amplitude and a phase, which mathematically assures the termination of the helix in its characteristic impedance. It was also assumed that the collector and helix are at the same d-c potential (i.e., there is no discontinuity in acceleration), and

in the Fourier analysis of the space-charge density only forward-traveling waves, not reflections, are considered.

The three boundary conditions at the input, the amplitude and phase of the impressed voltage and the continuity of the electron velocity, are satisfied by linear superposition of the three waves of the small-signal solution. The initial values of the dependent variables $A(y)$, $\theta(y)$, $\phi(y,\phi_o)$, and $u(y,\phi_o)$ can therefore be obtained from the small-signal conditions.

The normalized amplitude of the r-f signal $A(y)$ is by definition A_o, which is usually assigned a value approximately 30 db below CI_oV_o, or 0.0225. The phase lag $\theta(y)$ is of course initially zero. Since the electron stream enters the helix unmodulated, the velocity deviation $u(y,\phi_o)$ is initially zero for all electrons.

The instantaneous phase $\phi(y,\phi_o)$ at $y = 0$ is equal to the initial phase ϕ_o, which is chosen to be $2\pi j/m$ where $j = 0,1,\ldots,m$ and m is the number of equally spaced electrons followed through the integration procedure. Since the storage space required in the computer and the computation time increase several fold with each twofold increase in the number of electrons, it is desirable to use as few electrons as possible. The word electron is used here to mean not an individual particle but rather a finite amount of charge distributed over a finite cross-sectional area that enters the helix region at a phase ϕ_o relative to the r-f wave at $y = 0$. This concept is discussed further in interpreting the infinite peaks in the current-density curves of Section 4.6. It was found that 16 electrons are too few for this work, but 32 electrons are sufficient to insure the smoothness of the functions and this value has therefore been used in the computations reported in Chapter III. A more detailed discussion of the influence of the number of electrons on the solutions is presented in Section 3.5.1.

Mathematically the initial values of the dependent variables may be stated as follows:

$$A(0) = A_o = 0.0225 \text{ (for most runs)}$$

$$\theta(0) = 0$$

$$\phi_j(0,\phi_o) = \phi_{oj} = \frac{2\pi j}{32}, \quad \text{where } j = 0,1,2,\ldots,32$$

and

$$u_j(0,\phi_o) = 0 \text{ for all electrons.}$$

At the output of the helix the boundary conditions are satisfied implicitly if the ratio of voltage to current on the helix is equal to the characteristic impedance Z_o and the velocity is continuous. The derivatives of the functions $A(y)$ and $\theta(y)$ with respect to y at $y = 0$ are determined by the small-signal conditions at the input.

The desired derivatives are obtained from the small-signal solutions in the following manner. Since the small-signal solutions are written as summations of three linearly independent, exponentially varying waves, the voltage on the helix near the input may be written as the sum of three components, for the three waves, each varying with distance and time in a manner described by the expression

$$e^{j\omega t - \Gamma z} = e^{j\omega t}\, e^{-j\beta_e(1 - \beta_i C)z}\, e^{\beta_e \alpha_i C z}, \qquad (2\text{-}60)$$

where α_i and β_i are the growth and phase constants respectively of the individual wave. In terms of the new distance variable y, the right-hand side of Eq. 2-60 is written as

$$e^{-jy/C + j(\alpha_i + j\beta_i)y + j\omega t}. \qquad (2\text{-}61)$$

If $j\theta(y)$ is added and subtracted from the exponent, this expression may be written in terms of the new phase variable $\phi(y,\phi_o)$ as

$$e^{(\alpha_i + j\beta_i)\, y \,-\, j\,\phi \,-\, j\,\theta(y)} \quad . \tag{2-62}$$

Hence, the voltage on the helix may be written as

$$\mathrm{Re}\left[A(y)\; e^{-j\phi}\right] \;=\; \sum_{i=1}^{3} A_i e^{\delta_i y \,-\, j[\phi+\theta(y)]} \quad . \tag{2-63}$$

Cancelling $e^{-j\phi}$ and multiplying through by $e^{j\theta(y)}$ in Eq. 2-63 yields

$$A(y)\; e^{j\theta(y)} \;=\; \sum_{i=1}^{3} A_i\; e^{\delta_i y} \quad , \tag{2-64}$$

where

$$\delta_i \;=\; \alpha_i \;+\; j\beta_i \quad .$$

Taking the derivative with respect to y in Eq. 2-64 and evaluating at y = 0 gives

$$A'(y)\,\Big|_{y=0} + j\; A_o\; \theta'(y)\,\Big|_{y=0} \;=\; \sum_{i=1}^{3} A_i \delta_i \quad . \tag{2-65}$$

Equation 2-65 may be separated into its real and imaginary parts to obtain explicit expressions for the derivatives of A(y) and $\theta(y)$ at the input:

$$A'(y)\,\Big|_{y=0} \;=\; \mathrm{Re}\left[A_o \sum_{i=1}^{3} \frac{A_i}{A_o}\,\delta_i\right] \tag{2-66}$$

and

$$\theta'(y)\,\Big|_{y=0} \;=\; \mathrm{Im}\left[\sum_{i=1}^{3} \frac{A_i}{A_o}\,\delta_i\right] \tag{2-67}$$

Pierce's[8] small-signal analysis may be used to write the total voltage (including the space-charge component) in terms of both the a-c velocity and the convection current as given by the equations

$$A = \frac{-u_o\,(j\beta_e - \Gamma)}{\eta\,\Gamma}\,v \qquad (2\text{-}68)$$

and

$$A = \frac{2V_o\,(j\beta_e - \Gamma)^2}{j\,I_o\,\beta_e\,\Gamma}\,i \quad . \qquad (2\text{-}69)$$

The quantity $-\Gamma$ may be defined as

$$-\Gamma = -j\beta_e + \beta_e C\delta \quad , \qquad (2\text{-}70)$$

which when substituted into Eqs. 2-68 and 2-69 gives the following expressions for the voltage on the line in terms of the a-c velocity, the convection current, and the propagation constant δ for each wave:

$$A = \frac{-2V_o\,C^2\delta^2}{I_o}\,i \qquad (2\text{-}71)$$

and

$$A = \frac{u_o}{\eta}\left(\frac{C^2\delta^2 + jC\delta}{1 + C^2\delta^2}\right)v \quad . \qquad (2\text{-}72)$$

Since δ is usually of the order of unity and C is small compared to 1, the terms involving $C^2\delta^2$ may be neglected, even for C as large as 0.1, and Eq. 2-72 may be simplified to

$$A = \frac{ju_oC\delta}{\eta}\,v \quad . \qquad (2\text{-}73)$$

Hence at z = 0 the following relations apply:

$$A_o = \sum_{i=1}^{3} A_i \quad , \tag{2-74}$$

$$\sum_{i=1}^{3} \frac{A_i}{\delta_i^2} = \frac{-2V_oC^2}{I_o} i = 0 \quad , \tag{2-75}$$

and

$$\sum_{i=1}^{3} \frac{A_i}{\delta_i} = \frac{ju_oC}{\eta} v = 0 \quad . \tag{2-76}$$

Since the electron stream enters the interaction region unmodulated, the a-c velocity and convection current may be taken as zero at the input; i.e., $i = v = 0$ at $z = 0$. Hence the normalized voltage amplitudes for each wave needed to evaluate $A'(y)\Big|_{y=0}$ and $\theta'(y)\Big|_{y=0}$ in Eqs. 2-66 and 2-67 may be calculated from the various δ_i's for the particular solution to be studied.

The α_i's and β_i's used here as growth and phase constants correspond to the x's and y's of Pierce's[8] small-signal analysis. The values of the α_i's and β_i's for various values of QC, C, and b when the loss factor d is zero were obtained as indicated in Appendix C. For values of d other than zero, an extensive tabulation of the x's and y's for a wide range of QC, C, and b has been given by Brewer and Birdsall[1].

Since, as noted previously, the stream is unmodulated when it enters the interaction region, the stream initially (at $y = 0$) has no convection current and therefore cannot act on the circuit. Hence for zero loss on the helix the voltage initially does not change in amplitude. If the loss parameter d is not zero, the initial change in voltage amplitude is determined by d. The value of $\theta'(y)$ at $y = 0$ constitutes an apparent phase constant β_a of the composite wave at the input.

CHAPTER III. SOLUTION OF THE THEORETICAL EQUATIONS ON MIDAC

3.1 Introduction

Since the working equations derived in Section 2.1 form a nonlinear system of partial-differential-integral equations in two independent variables, they are not readily amenable to an analytical solution. The alternative, a numerical solution, is practical only with the aid of a high-speed electronic computer.

The equations could be solved on an analogue computer, but a large amount of complex equipment would be needed. Since an analogue computer has only one independent variable (time), it would be necessary to scan each of the two independent variables in a specific manner on the time scale, which would require considerable storage space and many complex switching circuits.[15]

Since a large-scale high-speed digital computer was considered preferable and the Michigan Digital Automatic Computer (MIDAC), located at the University of Michigan's Willow Run Research Center, was available, the equations were solved on this machine.

3.2 Brief Description of MIDAC

3.2.1 General Characteristics. The Michigan Digital Automatic Computer is a high-speed electronic computer of considerable versatility. It uses the binary number system, in which the two digits "0" and "1" correspond to the absence and presence, respectively, of an electronic pulse in the machine. An input translation program can be used to convert decimal numbers automatically to the binary number system.

MIDAC operates sequentially on the digits of a "word", which consists of a sign and 44 binary digits. Such a word may convey operational instructions or it may represent a number of 44 binary digits, equivalent to approximately 13 decimal digits. Storage elements provide space for 512 words of both types in a high-speed acoustic memory and 6144 additional words in a slower-speed magnetic-drum memory.

Instructions may be stored in any desired portion of the memory; they are of the "three-address" type, using two operand locations and a result location. Since numbers are stored in the same type of memory elements and are handled in the same way as the instruction words, instructions may be modified on the basis of results as computation progresses. This ability to make "decisions" in the course of a program is an important property of MIDAC.

Since the computer can operate only on numbers with an absolute value less than 1, programs must be designed either with a fixed binary point and a scaling factor selected to keep the results below 1, or with an automatic scaling factor or "floating" binary point.

Figure 3-1 is an overall view of the MIDAC components, which are discussed in detail in the following paragraphs.

3.2.2 Input Photoelectric Tape Reader. The problem to be solved is first programmed and the resulting instructions and numbers, in the hexadecimal system, are transferred to a paper tape with six levels of punched holes. The information is presented to the machine by a high-speed Photoelectric Paper Tape Reader, shown in Fig. 3-2, at a speed of 200 characters/second. Light shining through the holes strikes photoelectric cells which translate it into electronic pulses. These pulses are stored in the memory in accordance with the prepared program.

FIG. 3-1 MICHIGAN DIGITAL AUTOMATIC COMPUTER INSTALLATION

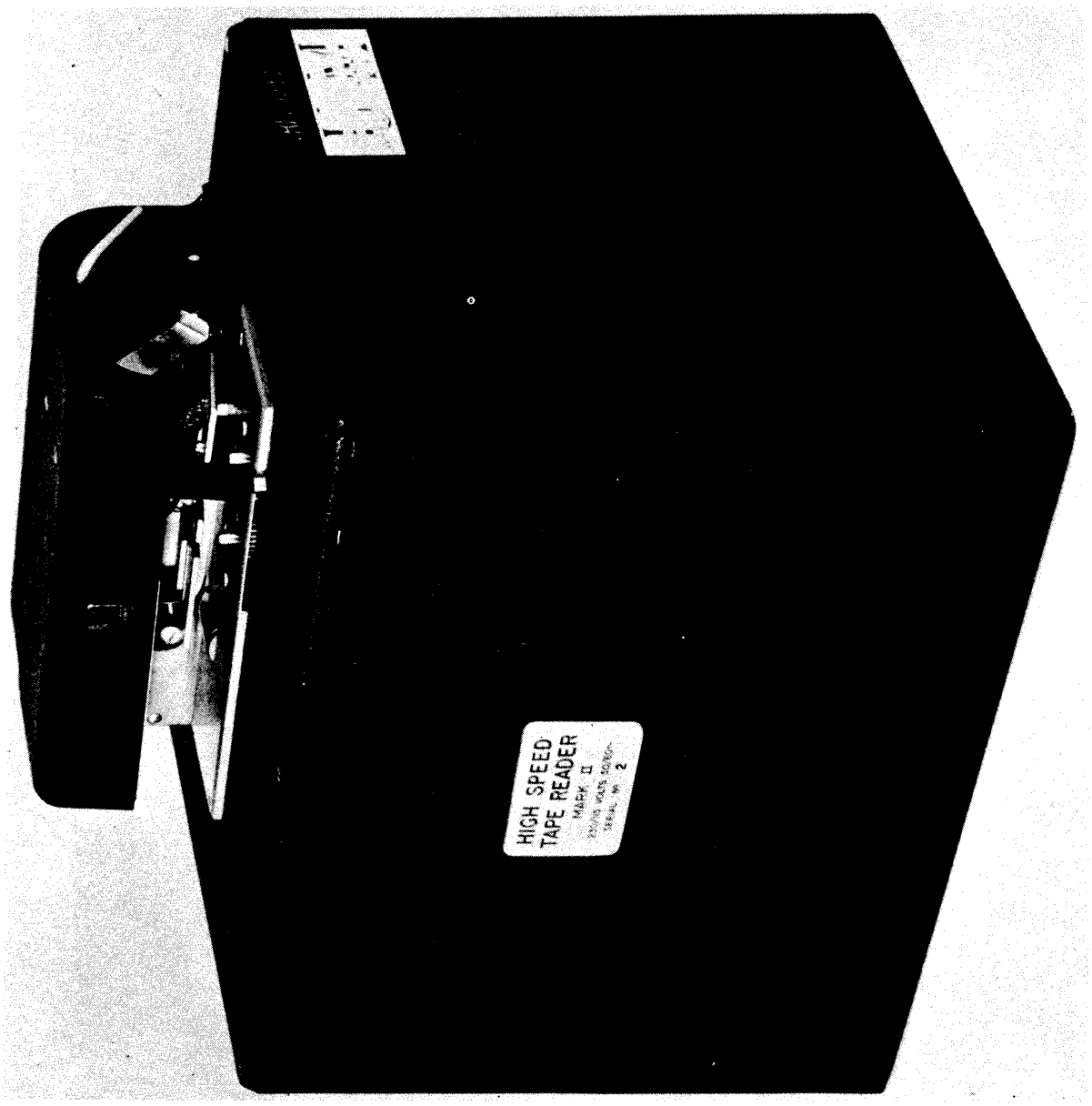

FIG. 3-2 INPUT PHOTOELECTRIC TAPE READER

3.2.3 Control and Arithmetic Units. The control unit of Fig. 3-3 superintends the entire operation, calling in instructions from the memory, analyzing them, and sending each individual portion to the arithmetic unit, also shown in Fig. 3-3, in proper sequence. The arithmetic unit performs the actual addition, subtraction, multiplication, and division and sends the results back to storage. Computation times, including access to the acoustic memory, are listed below for the various operations.

Operation	Time, microseconds	
	Minimum	Maximum
Addition	192	1536
Subtraction	192	1536
Multiplication	2304	3168
Division	2304	3168
Comparison	192	1200
Number conversion	768	1776

Larger operations, such as making "decisions" on the basis of the results, are handled by the control unit.

3.2.4 Storage Units. The primary storage unit is the high-speed acoustic memory, shown in Fig. 3-4, which has a capacity of 512 words stored in the form of sound pulses in a column of mercury. These pulses must be recirculated constantly if the memory is to retain its information; hence, the acoustic memory is not a permanent memory unit. Its access time averages 192 microseconds, with a maximum of 384 microseconds.

Additional storage for some 6144 words is available on a magnetic-drum memory, shown in Fig. 3-5, which holds the information as magnetization of one polarity or another on the surface of a cylindrical drum coated with iron oxide. The magnetized "spots" on the drum retain their information

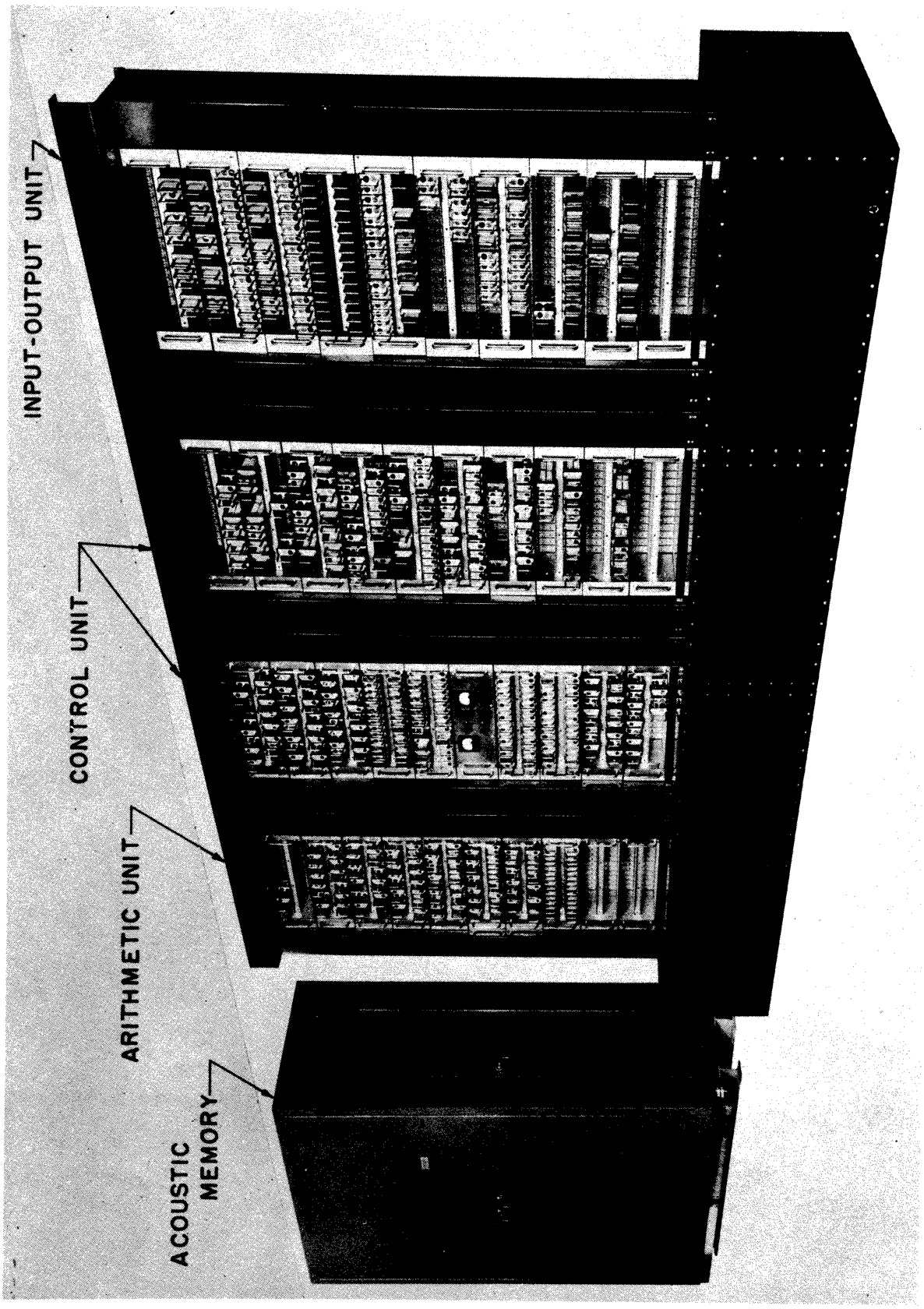

FIG. 3-3 FUNCTIONAL COMPONENTS OF MIDAC

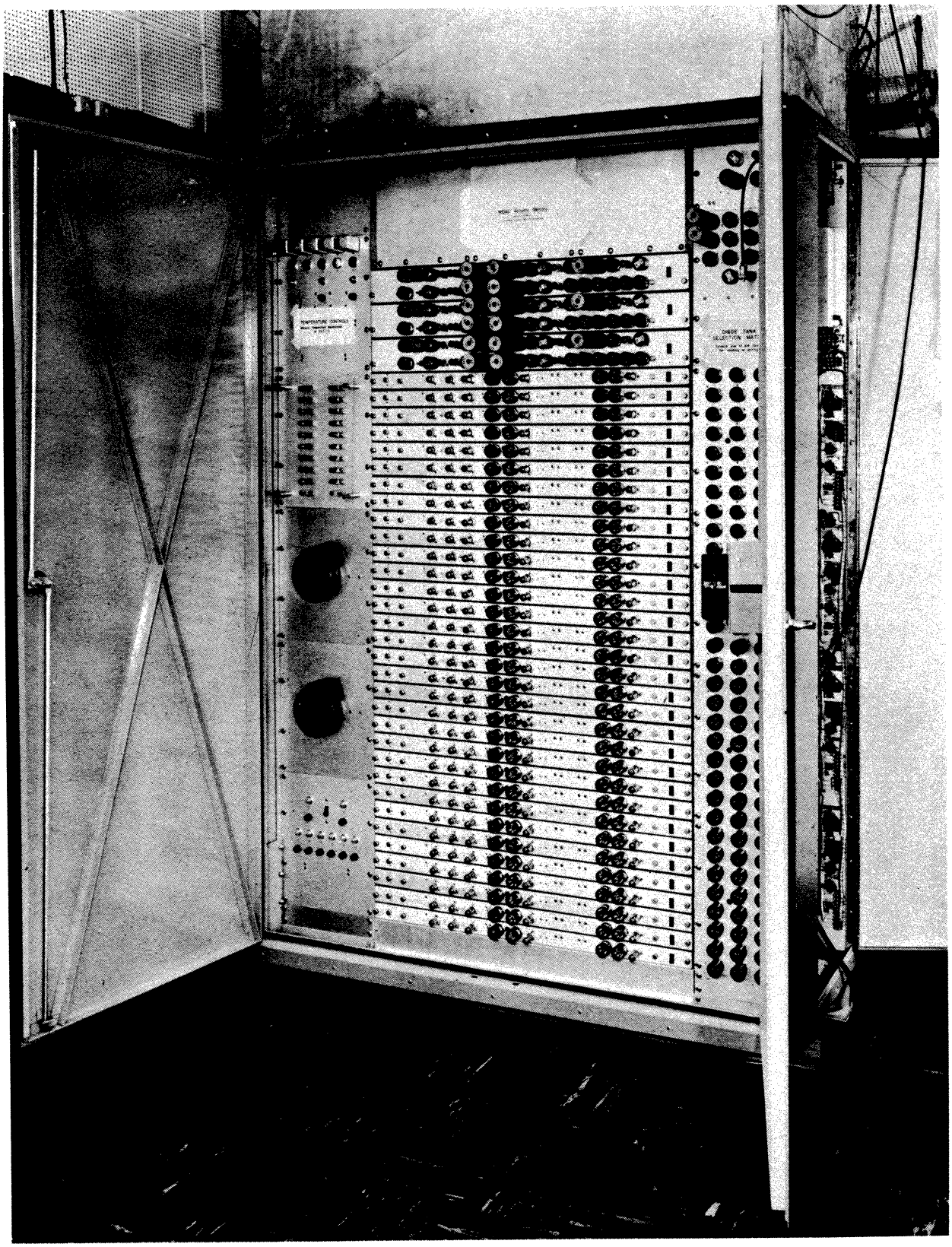

FIG. 3-4 MIDAC HIGH-SPEED ACOUSTIC MEMORY

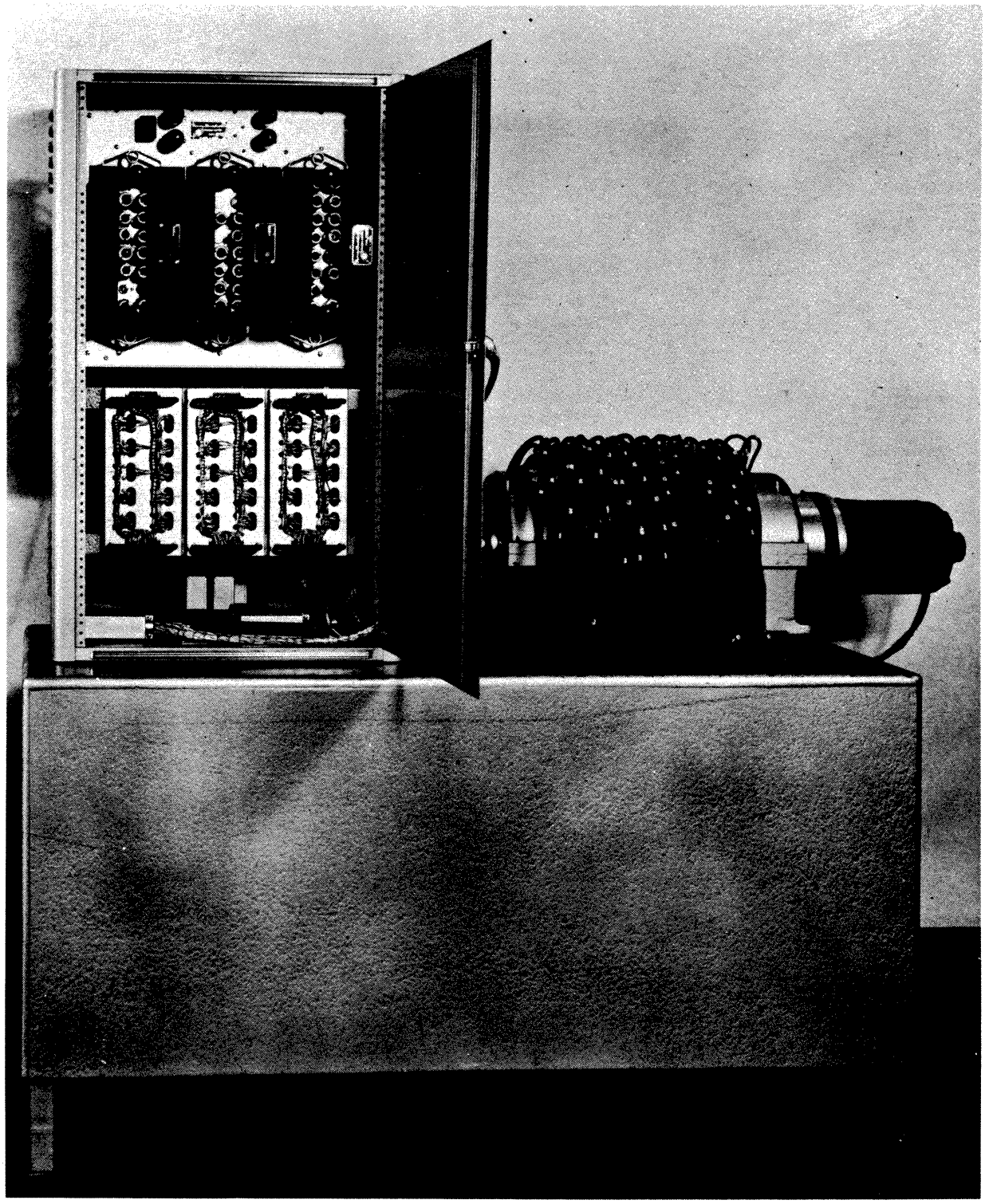

FIG. 3-5 MIDAC LOW-SPEED MAGNETIC DRUM MEMORY

indefinitely, even when the power is turned off, unless disturbed by new magnetization; hence the drum is a permanent memory unit. This memory has an average access time of 9 milliseconds and a maximum of 17 milliseconds.

Information can be shifted between the two memories by the control unit.

3.2.5 Output Flexowriter. The computational results are printed on paper at a rate of 10 characters/second by an automatic typewriter actuated by sequences of electronic pulses from the acoustic memory.

3.3 Transformation of the Differential Equations into Difference Form

To solve the working equations for a given set of parameters and initial conditions, electron trajectories are followed from the input boundary, and integration is carried out along the tube in y, using 32 points in ϕ_o (corresponding to 32 representative electrons) as indicated in Fig. 3-6. The effect of the number of electrons is discussed in detail in Section 3.5.1. To facilitate this process the working equations are transformed into difference equations.

For this purpose first-order difference formulas are obtained using the first two terms of a Taylor series expansion of a function about a point. The general Taylor series expansion of the function f(x) about the point a may be written as

$$f(x) = f(a) + f'(a)\,(x-a) + \frac{f''(a)}{2!}\,(x-a)^2 + \ldots + \frac{f^{(n-1)}(a)}{(n-1)!}\,(x-a)^{n-1} + \ldots \qquad (3\text{-}1)$$

Using the first two terms of this series expansion, expressions for the dependent variables A(y), $\Theta(y)$, $\phi(y,\phi_o)$, and $u(y,\phi_o)$ at the (i+1)st row may

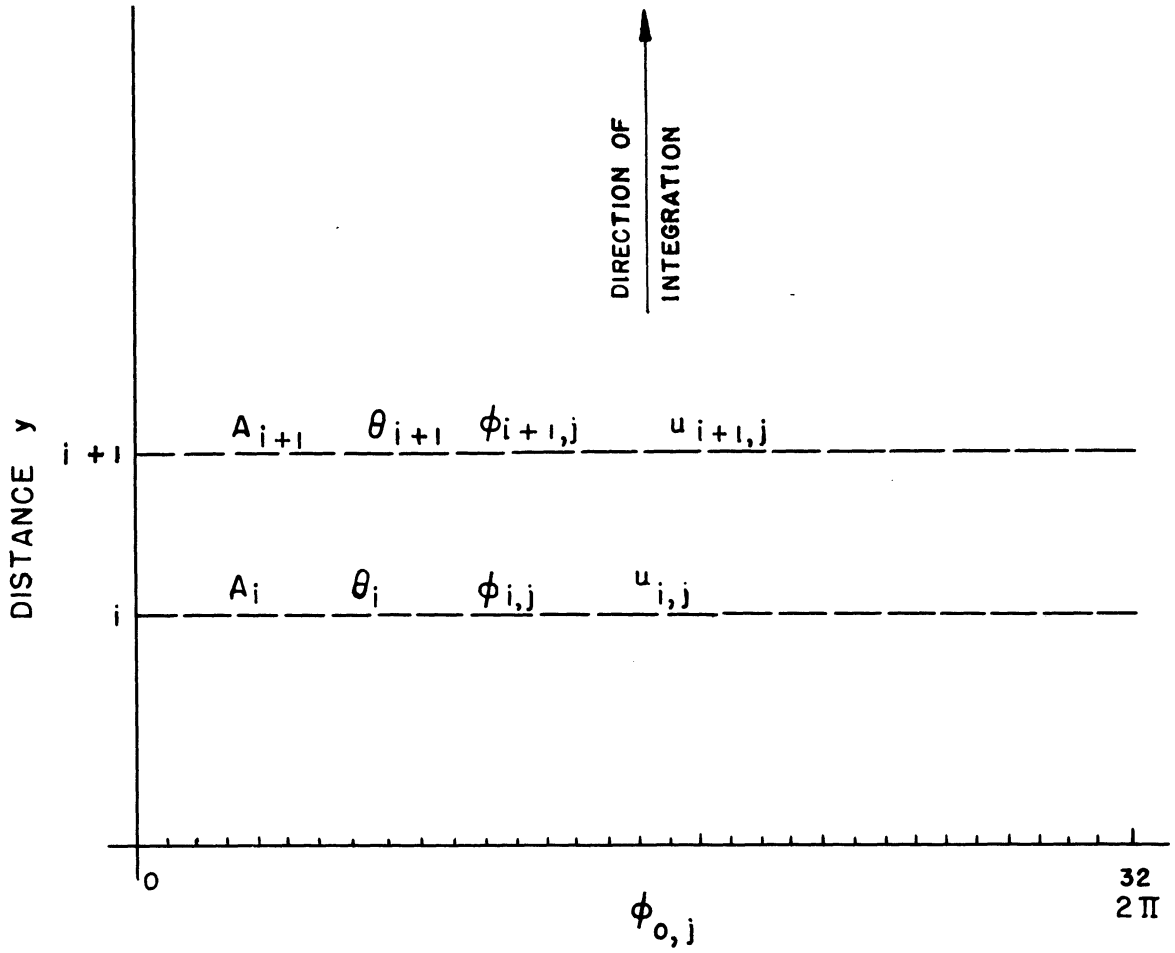

FIG. 3-6

INTEGRATION DIAGRAM USED IN THE NUMERICAL SOLUTION OF THE WORKING EQUATIONS

be written in terms of their values at the ith row and their first derivatives with respect to y at the ith row, as follows:

$$A_{i+1} = A_i + \Delta y\, A_i' \quad , \tag{3-2}$$

$$\Theta_{i+1} = \Theta_i + \Delta y\, \Theta_i' \quad , \tag{3-3}$$

$$\phi_{i+1,j} = \phi_{ij} + \Delta y\, \phi_{ij}' \quad , \tag{3-4}$$

and

$$u_{i+1,j} = u_{ij} + \Delta y\, u_{ij}' \quad , \tag{3-5}$$

where Δy = the increment of integration in y.

In terms of the dependent variables' second derivatives with respect to y at the ith row, the equations for the (i+1)st row are

$$A_{i+1} = 2\, A_i - A_{i-1} + (\Delta y)^2\, A_i'' \tag{3-6}$$

and

$$\Theta_{i+1} = 2\, \Theta_i - \Theta_{i-1} + (\Delta y)^2\, \Theta_i'' \quad . \tag{3-7}$$

The corresponding expressions for $\phi(y,\phi_o)$ and $u(y,\phi_o)$ are not written because their second derivatives do not occur in the working equations.

Higher-order difference formulas such as the classic Runge-Kutta fourth-order process, which uses more terms of the Taylor series, would give more accurate results but would also increase the storage space and computation time required. It was found that considerable accuracy can be obtained using first-order difference equations if the integration increment Δy is selected carefully. A detailed discussion of this point is included in Section 3.5 on sources of error in the numerical integration.

Using Eqs. 3-2, 3-3, 3-4, and 3-5, the working equations, Eqs. 2-18, 2-30, 2-31, and 2-33, are written as

$$\phi(y_{i+1},\phi_{oj}) - \phi(y_i,\phi_{oj}) + \theta(y_{i+1}) - \theta(y_i) = \frac{2\Delta y u(y_i,\phi_{oj})}{1 + 2Cu(y_i,\phi_{oj})} , \qquad (3\text{-}8)$$

$$A(y_{i-1}) + A(y_{i+1}) - 2A(y_i) - A(y_i)\left[\left(\frac{1}{C} - \frac{\theta(y_{i+1})-\theta(y_i)}{\Delta y}\right)^2 - \frac{(1+Cb)^2}{C^2}\right](\Delta y)^2$$

$$= \frac{(\Delta y)^2(1+Cb)}{\pi C}\left[\int_0^{2\pi} \frac{\cos\phi(y_i,\phi'_{oj})d\phi'_{oj}}{1 + 2Cu(y_i,\phi'_{oj})} + 2Cd\int_0^{2\pi} \frac{\sin\phi(y_i,\phi'_{oj})d\phi'_{oj}}{1 + 2Cu(y_i,\phi'_{oj})}\right] , \qquad (3\text{-}9)$$

$$A(y_i)\left[\theta(y_{i-1}) + \theta(y_{i+1}) - 2\theta(y_i) - \frac{2d(\Delta y)^2}{C}(1+Cb)^2\right]$$

$$+ 2[A(y_{i+1}) - A(y_i)]\left[\theta(y_{i+1}) - \theta(y_i) - \frac{\Delta y}{C}\right]$$

$$= \frac{(\Delta y)^2(1+Cb)}{\pi C}\left[\int_0^{2\pi} \frac{\sin\phi(y_i,\phi'_{oj})d\phi'_{oj}}{1 + 2Cu(y_i,\phi'_{oj})} - 2Cd\int_0^{2\pi} \frac{\cos\phi(y_i,\phi'_{oj})d\phi'_{oj}}{1 + 2Cu(y_i,\phi'_{oj})}\right] , \qquad (3\text{-}10)$$

and

$$[u(y_{i+1},\phi_{oj}) - u(y_i,\phi_{oj})]\,[1 + 2Cu(y_i,\phi_{oj})]$$

$$= A(y_i)\left\{\Delta y - C[\theta(y_{i+1}) - \theta(y_i)]\right\}\sin\phi(y_i,\phi_{oj})$$

$$- C[A(y_{i+1})-A(y_i)]\cos\phi(y_i,\phi_{oj}) - \frac{\Delta y}{1+Cb}\left(\frac{\omega_p}{\omega C}\right)^2\int_0^{2\pi} \frac{F(\phi-\phi')d\phi'_o}{1 + 2Cu(y_i,\phi'_{oj})} . \qquad (3\text{-}11)$$

The next step is to solve Eq. 3-9 for $A(y_{i+1})$. Let

$$\bigwedge = \frac{(\Delta y)^2(1+Cb)}{\pi C}\left[\int_0^{2\pi}\frac{\cos\phi(y_i,\phi'_{oj})d\phi'_{oj}}{1+2Cu(y_i,\phi'_{oj})} + 2Cd\int_0^{2\pi}\frac{\sin\phi(y_i,\phi'_{oj})d\phi'_{oj}}{1+2Cu(y_i,\phi'_{oj})}\right]. \quad (3\text{-}12)$$

Solving Eq. 3-12 for $A(y_{i+1})$ and simplifying gives

$$A(y_{i+1}) = \bigwedge - A(y_{i-1}) + A(y_i)\left[\theta^2(y_{i+1}) - 2\left\{\theta(y_i) + \frac{\Delta y}{C}\right\}\theta(y_{i+1}) + \theta^2(y_i) + \frac{2\Delta y}{C}\theta(y_i) - \frac{(\Delta y)^2 b(2+Cb)}{C} + 2\right]. \quad (3\text{-}13)$$

The quantity

$$\prod = \bigwedge - A(y_{i-1}) + A(y_i)\left[\theta^2(y_i) + \frac{2\Delta y}{C}\theta(y_i) - \frac{(\Delta y)^2 b(2+Cb)}{C} + 2\right] \quad (3\text{-}14)$$

is then defined and substituted into Eq. 3-13 to give

$$A(y_{i+1}) = A(y_i)\theta^2(y_{i+1}) - 2A(y_i)\left[\theta(y_i) + \frac{\Delta y}{C}\right]\theta(y_{i+1}) + \prod. \quad (3\text{-}15)$$

Next the quantities

$$\Upsilon = \frac{(\Delta y)^2(1+Cb)}{\pi C}\left[\int_0^{2\pi}\frac{\sin\phi(y_i,\phi'_{oj})d\phi'_{oj}}{1+2Cu(y_i,\phi'_{oj})} - 2Cd\int_0^{2\pi}\frac{\cos\phi(y_i,\phi'_{oj})d\phi'_{oj}}{1+2Cu(y_i,\phi'_{oj})}\right] \quad (3\text{-}16)$$

and

$$\Psi = A(y_i)\left[\theta(y_{i-1}) + \frac{2\Delta y}{C} - \frac{2d(\Delta y)^2}{C}(1+Cb)^2\right] \quad (3\text{-}17)$$

are defined, whereupon Eq. 3-10 can be written as

$$A(y_i)\theta(y_{i+1}) - 2A(y_{i+1})\left[\theta(y_{i+1}) - \theta(y_i) - \frac{\Delta y}{C}\right] - \Psi + \Upsilon = 0. \quad (3\text{-}18)$$

Finally, the expression for $A(y_{i+1})$ in Eq. 3-15 is substituted into Eq. 3-18 to give, after simplification,

$$2A(y_i)\,\theta^3(y_{i+1}) - 6A(y_i)\left[\theta(y_i) + \frac{\Delta y}{C}\right]\theta^2(y_{i+1})$$

$$+\left\{2\prod + A(y_i)\left[4\left\{\theta(y_i) + \frac{\Delta y}{C}\right\}^2 - 1\right]\right\}\theta(y_{i+1}) + \Psi - 2\prod\left[\theta(y_i) + \frac{\Delta y}{C}\right] = \Upsilon \quad (3\text{-}19)$$

The three equations 3-8, 3-11, and 3-19 represent the difference form of the working equations derived in Section 2.1.

These three equations can of course be derived symbolically from the original working equations. At the (i+1)st level the working equations are written in terms of their values at the ith level symbolically as follows:

$$\phi + \theta = C_1 \quad , \quad (3\text{-}20)$$

$$A - \theta^2 + \theta = C_2 \quad , \quad (3\text{-}21)$$

$$\theta + 2A\dot{\theta} = C_3 \quad , \quad (3\text{-}22)$$

and

$$u + \theta = C_4 \quad , \quad (3\text{-}23)$$

where C_1, C_2, C_3, and C_4 represent the right-hand sides of the equations, which have constant values for any particular row in the integration procedure. Solving Eq. 3-21 for A and substituting into Eq. 3-22 gives

$$2\theta^3 - 2\theta^2 + (1 + 2C_2)\theta = C_3 \quad . \quad (3\text{-}24)$$

Equations 3-20, 3-23, and 3-24 are equivalent symbolically to Eqs. 3-8, 3-11, and 3-19.

3.4 Details of the Computing Process

Figure 3-7 is a flow diagram for the numerical solution of Eqs. 3-8, 3-11, and 3-19. Most of the computation involves straightforward addition, subtraction, multiplication, and division. However, some of the steps, such as the evaluation of the integrals, the solution of a cubic equation to find the new value of Θ at the (i+1)st row, and the numerical evaluation of the space-charge-field weighting function, warrant a somewhat detailed discussion.

3.4.1 Numerical Evaluation of Integrals. For the evaluation of the integrals in Eqs. 3-12 and 3-16, 32 electrons are carried through the integration procedure. As mentioned in Section 2.3, it is believed that consideration of 32 electrons will give results which are not markedly different from those which would be obtained if a larger number of electrons were considered. This point is taken up in more detail in Section 3.5.1.

Therefore the functions under the integral signs are evaluated over the interval from 0 to 2π for 32 equally spaced values of ϕ_{oj}. However, the equations employ integral signs rather than summation signs; the answers are desired not to the 32-point problem but to the continuous problem. The integrals are evaluated from the 32 equally spaced values of each function between 0 and 2π using the familiar Simpson Rule[37], which may be stated as follows:

If y_0, y_1, y_2, ... are the values of $y = f(x)$ at equally spaced points x_0, x_1, x_2, ... with interval h, then

$$\int_{x_0}^{x_{2m}} y\,dx = \frac{h}{3}\left(y_0 + 4y_1 + 2y_2 + 4y_3 + 2y_4 + 4y_5 + \ldots 4y_{2m-1} + y_{2m}\right) - \frac{m y^{(4)} h^5}{90} \quad , \qquad (3\text{-}25)$$

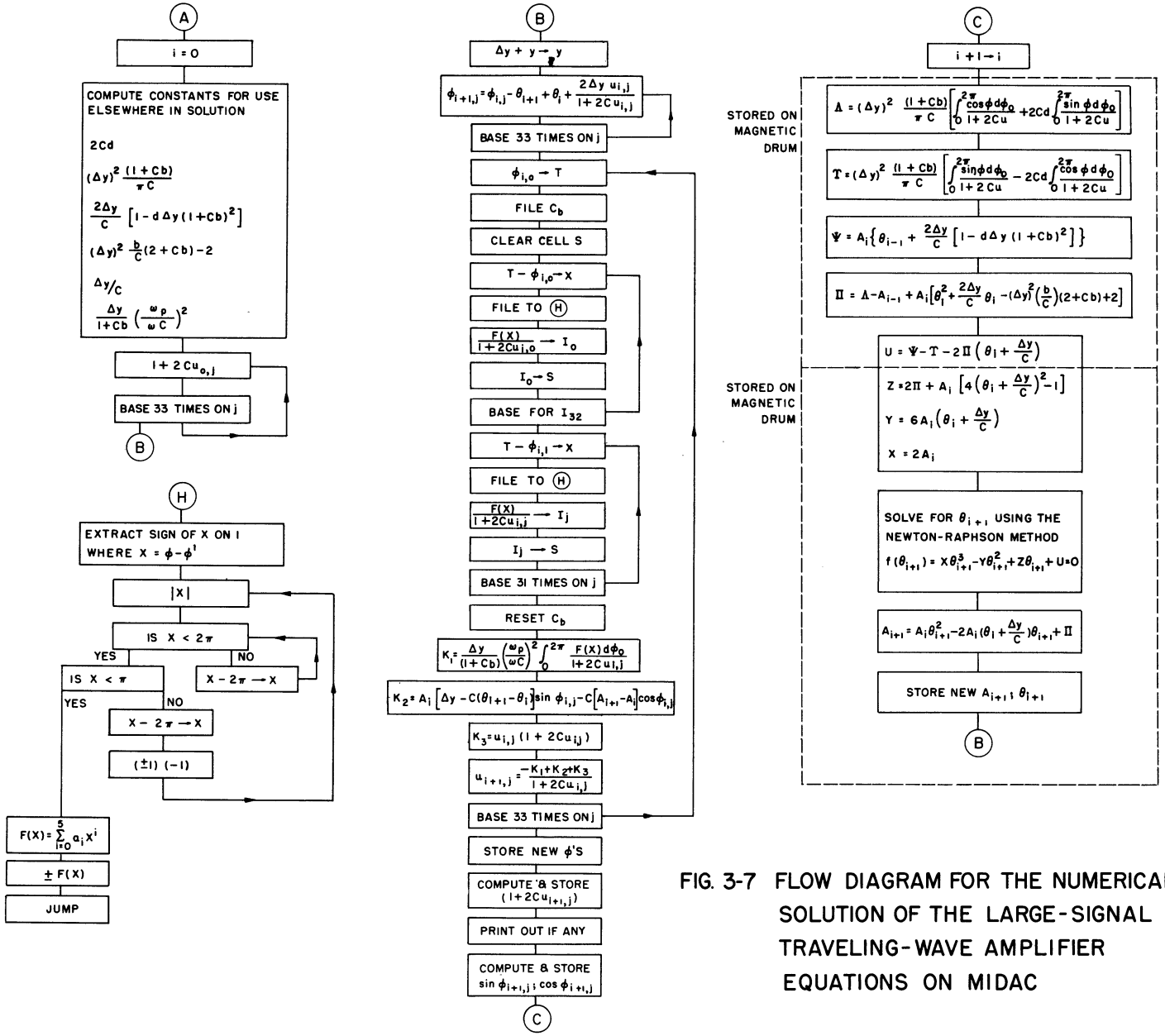

FIG. 3-7 FLOW DIAGRAM FOR THE NUMERICAL SOLUTION OF THE LARGE-SIGNAL TRAVELING-WAVE AMPLIFIER EQUATIONS ON MIDAC

where h = the interval in x and $y^{(4)}$ = the value of the fourth derivative at some point between x_o and x_{2m}.

Simpson's Rule is simple in form and quite accurate. It does have the disadvantage that it can be applied only to an even number of intervals, but that requirement causes no difficulty in this problem. The accuracy of Simpson's Rule for the evaluation of these integrals may be estimated by evaluating the remainder term, $my^{(4)}h^5/90$, of Eq. 3-25. The increment h is $\pi/16$ here, and the value of the fourth derivative is taken as unity. Thus the error in applying Simpson's Rule to this problem will amount to less than 10^{-5}.

The evaluation of the integral of the space-charge weighting function $F(\phi-\phi')$ is discussed in Section 3.4.3.

3.4.2 Newton-Raphson Iterative Process. As indicated in the flow diagram, Fig. 3-7, it is necessary to solve for the real root of a cubic at each level of the integration procedure in order to find the phase lag $\theta(y)$. A general second-order iterative process called the Newton-Raphson Process is used for this purpose.

The solution of $f(x) = 0$ is to be found at a point not in the neighborhood of a maximum or minimum of $f(x)$:

$$x_{K+1} = x_K - \frac{f(x_K)}{f'(x_K)} \quad . \tag{3-26}$$

In terms of $\theta(y)$, Eq. 3-26 becomes

$$\theta_{i+1}^{(K)} = \theta_i^{(K)} - \frac{f(\theta_i^{(K)})}{f'(\theta_i^{(K)})} \quad , \tag{3-27}$$

where $f(\theta_i) = X\theta_i^3 - Y\theta_i^2 + Z\theta_i + U$.

As shown in Fig. 3-8, this process may be interpreted geometrically as linear interpolation along the tangent to the curve at $\theta^{(K)}$.

In order to find the solution by this procedure, it is necessary to guess at the root for the first iteration. The value of $\theta(y)$ at the preceding row is used for this first guess, and the process is carried on until the second term of Eq. 3-27 is less than 2^{-26}.

3.4.3 Numerical Evaluation of the Space-Charge Weighting Function. The space-charge-field weighting function $F(\phi-\phi')$, derived in Appendix B, is

$$F(\phi-\phi') = \sum_{n=1}^{\infty} \frac{\sin n(\phi-\phi')}{2\pi n} R_n^2 \quad . \tag{B-22}$$

Since $(1-R_n)$ varies exponentially with $n\beta b'$, $\ln(1-R_n)$ vs. $n\beta b'$ will be a straight line. Thus Eq. B-22 may be written as

$$F(\phi-\phi') = \sum_{n=1}^{\infty} \frac{\sin n(\phi-\phi')}{2\pi n} \left[1 - e^{-n\beta b' f(a'/b')}\right]^2 \quad , \tag{3-28}$$

where $f(a'/b')$ = the slope of $\ln(1-R_n)$ vs. $n\beta b'$. For $a'/b' = 2$, this slope is approximately unity.

Since the series represented by the first term of Eq. 3-28 is not uniformly convergent as $(\phi-\phi')$ approaches zero, the point of discontinuity, it would be necessary to sum an infinite number of terms in order to avoid the familiar Gibbs phenomenon encountered in Fourier series: at $(\phi-\phi') = 0$, the summation required is of an infinite number of zeros, which is undefined. This last difficulty is cleared up if the first term is written as

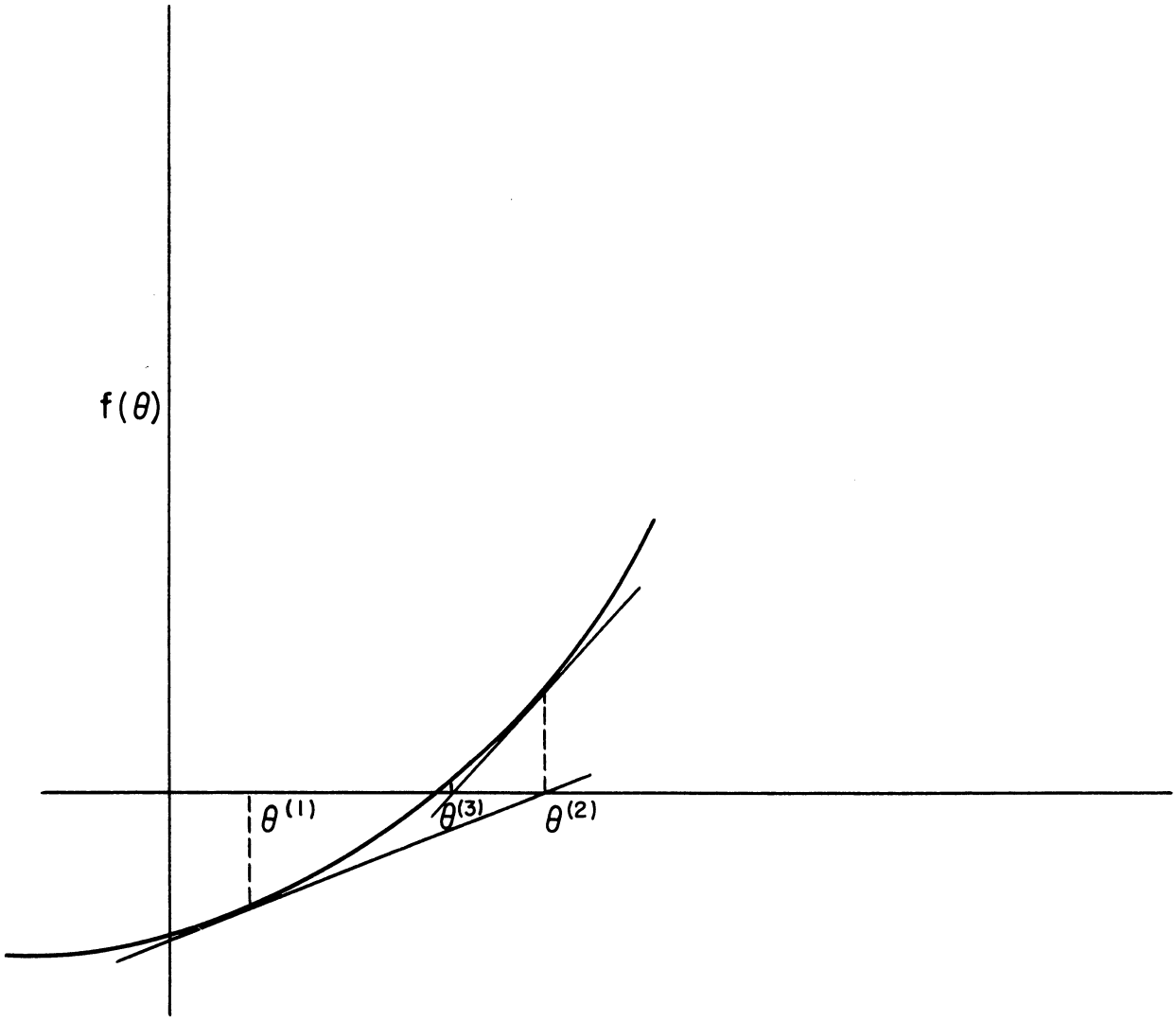

FIG. 3-8 GEOMETRICAL INTERPRETATION OF THE NEWTON-RAPHSON PROCESS FOR THE SOLUTION OF $f(\theta) = 0$

$$F(\phi-\phi') = \lim_{N\to\infty} \sum_{n=1}^{N} \frac{\sin n(\phi-\phi')}{2\pi n} , \qquad (3\text{-}29)$$

which clearly has a finite limit as $(\phi-\phi')$ approaches zero. Thus it is desirable to write Eq. 3-28 in closed form.

Consider the following general term of Eq. 3-28:

$$\sum_{n=1}^{\infty} \frac{\sin n(\phi-\phi')}{n} e^{-n\alpha} \quad \text{for } \alpha > 0 \qquad . \qquad (3\text{-}30)$$

Replacing $\sin n(\phi-\phi')$ by its exponential form, Eq. 3-30 may be written as

$$\sum_{n=1}^{\infty} \frac{\sin n(\phi-\phi')}{n} e^{-n\alpha} = \frac{1}{2i} \sum_{n=1}^{\infty} \frac{1}{n} \left[e^{-n[\alpha-i(\phi-\phi')]} - e^{-n[\alpha+i(\phi-\phi')]} \right] . \qquad (3\text{-}31)$$

The relation

$$\sum_{n=1}^{\infty} \frac{Z^n}{n} = \ln \frac{1}{1-Z} \quad \text{for } |Z| < 1 \qquad , \qquad (3\text{-}32)$$

where Z may be complex and the locus of $|Z| = 1$ is called the circle of convergence, may be used to rewrite Eq. 3-31 as

$$\sum_{n=1}^{\infty} \frac{\sin n(\phi-\phi')}{n} e^{-n\alpha} = \frac{1}{2i} \ln \frac{1 - e^{-[\alpha+i(\phi-\phi')]}}{1 - e^{-[\alpha-i(\phi-\phi')]}} \qquad . \qquad (3\text{-}33)$$

Writing the exponentials of Eq. 3-33 in terms of their real and imaginary parts gives

$$\sum_{n=1}^{\infty} \frac{\sin n(\phi-\phi')}{n} e^{-n\alpha} = \frac{1}{2i} \ln \frac{[e^{\alpha} - \cos(\phi-\phi')] + i \sin(\phi-\phi')}{[e^{\alpha} - \cos(\phi-\phi')] - i \sin(\phi-\phi')} \qquad . \qquad (3\text{-}34)$$

Since the logarithm of a complex number is given by

$$\ln Z = \ln(x + iy) = \ln \sqrt{x^2 + y^2} + i \tan^{-1} \frac{y}{x} , \qquad (3\text{-}35)$$

Eq. 3-34 can be simplified to

$$\sum_{n=1}^{\infty} \frac{\sin n(\phi-\phi')}{n} e^{-n\alpha} = \tan^{-1} \frac{\sin (\phi-\phi')}{e^{\alpha} - \cos (\phi-\phi')} . \qquad (3\text{-}36)$$

It is easily seen that this expression is also valid when $\alpha = 0$, i.e., on the circle of convergence.

Applying the form of Eq. 3-36 to Eq. 3-28 gives

$$F(\phi-\phi') = \frac{1}{2\pi} \left[\tan^{-1} \frac{\sin (\phi-\phi')}{1 - \cos (\phi-\phi')} - 2 \tan^{-1} \frac{\sin (\phi-\phi')}{e^{\beta b' f(a'/b')} - \cos (\phi-\phi')} + \tan^{-1} \frac{\sin (\phi-\phi')}{e^{2\beta b' f(a'/b')} - \cos (\phi-\phi')} \right] . \qquad (3\text{-}37)$$

Since, if $0 < (\phi-\phi') < 2\pi$,

$$\tan^{-1} \frac{\sin (\phi-\phi')}{1 - \cos (\phi-\phi')} = \frac{\pi - (\phi-\phi')}{2} , \qquad (3\text{-}38)$$

an alternate form of Eq. 3-37 is

$$F(\phi-\phi') = \frac{1}{2\pi} \left[\frac{\pi - (\phi-\phi')}{2} - 2 \tan^{-1} \frac{\sin (\phi-\phi')}{e^{\beta b' f(a'/b')} - \cos (\phi-\phi')} + \tan^{-1} \frac{\sin (\phi-\phi')}{e^{2\beta b' f(a'/b')} - \cos (\phi-\phi')} \right] . \qquad (3\text{-}39)$$

Equation 3-39 is presented in graphical form in Fig. B-6.

In order to shorten the computation time, the function $F(\phi-\phi')$ is approximated by a polynomial in $\phi-\phi'$ for each of five values of the parameter $\beta b'$ where $f(a'/b') = 1$. The following expression is seen to satisfy the end conditions:

$$F(x) = \frac{[1 + f(x)\, x]\,(16 - x)}{64} \quad , \tag{3-40}$$

where $f(x)$ = a polynomial in x and

$$x \equiv \phi-\phi' \ .$$

By the method of least squares[39] it is found that for each value of the parameter $\beta b'$ a cubic,

$$f(x) = A + Bx + Cx^2 + Dx^3 \quad , \tag{3-41}$$

can be found which will satisfy the accuracy requirements of the problem. Hence Eq. 3-40 may be written as

$$F(x) = \frac{1}{64}\,(16 - x)(1 + Ax + Bx^2 + Cx^3 + Dx^4) \ . \tag{3-42}$$

Evaluating the coefficients in Eq. 3-42 gives the following polynomials for $\beta b' = 0.5, 0.75, 1.0, 1.5,$ and 2.0 respectively:

$$F(x) = 0.25 - 0.54288x + 0.48836x^2 - 0.21903x^3 + 0.048302x^4 - 0.0041769x^5 \tag{3-43}$$

$$F(x) = 0.25 - 0.34891x + 0.17590x^2 - 0.026466x^3 - 0.0044749x^4 + 0.0019788x^5 \tag{3-44}$$

$$F(x) = 0.25 - 0.25227x + 0.063644x^2 + 0.023688x^3 - 0.014493x^4 + 0.0019333x^5 \tag{3-45}$$

$$F(x) = 0.25 - 0.16432x + 0.0064676x^2 + 0.027203x^3 - 0.010045x^4 + 0.0011026x^5 \qquad (3\text{-}46)$$

$$F(x) = 0.25 - 0.12640x - 0.00091601x^2 + 0.015709x^3 - 0.0048276x^4 + 0.00045523x^5 \; . \qquad (3\text{-}47)$$

The integral of the space-charge weighting function is evaluated using the Trapezoidal Rule, which can be stated as:

If $y_0, y_1, y_2, \ldots$ are the values of $y = f(x)$ at equally spaced points $x_0, x_1, x_2, \ldots$ with interval h, then

$$\int_{x_0}^{x_m} y \, dx = h\left(\frac{1}{2} y_0 + y_1 + y_2 + \ldots + y_{m-1} + \frac{1}{2} y_m\right) - \frac{my''h^3}{12} \; . \qquad (3\text{-}48)$$

The Trapezoidal Rule is not as accurate as Simpson's Rule, as may be seen by comparing the remainder terms of Eqs. 3-25 and 3-48, but the difference was considered to be more than offset in this case by the lessening of storage capacity and computation time required.

3.5 Experimental Study of Computation Errors

In order for the numerical results of this work to be applied intelligently to the analysis and design of traveling-wave amplifiers, it is necessary to consider the accuracy of the solutions. This section will discuss only the accuracy of the solutions to the differential equations; the exactness with which the equations describe the physical phenomena occurring in the tube and the physical limitations of their application are considered in Chapter II as the working equations are derived.

As yet no theory has been advanced for error analysis on solutions of nonlinear partial-differential-integral equations. The possibility of making an analytical study of error in a nonlinear system for application to this problem was explored but proved to be so complex that an experimental approach was chosen instead. An experimental investigation was therefore made into the presence of errors in the dependent variables $A(y)$ and $\Theta(y)$ and the question of stability of the solution.

It should be noted here that the experimental error analysis described below has been carried out for the special case where the space-charge field E_s is zero in order to shorten the computation time required. Although the space-charge force is of course not zero in the general problem, it is believed that the errors involved are of the same type and order of magnitude as those encountered in the special case considered.

3.5.1 Effect of the Number of Electrons Considered. The number of electrons which must be followed through the computations was determined by running the same solution for different numbers of electrons and examining the magnitude of the error resulting from use of the smaller number. It was established in this way that for the solutions where the space-charge parameter QC is taken as zero, consideration of 32 electrons is sufficient for the accuracy desired since non-space-charge solutions are insensitive to the number of electrons followed above that number.

However, when the space-charge term is not zero the accuracy of the solutions is highly dependent on the number of electrons followed. The difficulty arises in the evaluation of the space-charge weighting function $F(\phi-\phi')$. (The function $F(\phi-\phi')$ vs. $\phi-\phi'$ measures the space-charge force between each electron and its neighbors.) This function, as seen in Fig. B-6, is an odd periodic function and consequently has a discontinuity

at $2\pi n$ for $n = 0,1,2,\ldots$; therefore the accuracy of the integration of $F(\phi-\phi')/[1 + 2Cu(y,\phi_o)]$ over the period 2π is determined by the number of values of $\phi-\phi'$ between 0 and 2π considered. This number of points is in turn determined by the number of electrons considered.

Inaccuracies in evaluating the space-charge weighting function are reflected immediately in determination of the a-c velocity term at the (i+1)st row, as shown in the following equation taken from the flow diagram of Fig. 3-7:

$$u_{i+1,j} = \frac{-K_1 + K_2 + K_3}{1 + 2Cu_{ij}} \quad , \tag{3-49}$$

where

$$K_1 = \frac{\Delta y}{1 + Cb}\left(\frac{\omega_p}{\omega C}\right)^2 \int_0^{2\pi} \frac{F(\phi-\phi')\, d\phi_o}{1 + 2Cu(y,\phi_o)} \quad .$$

The terms K_2 and K_3 are related to the force on the electron due to the field on the helix, while K_1 is due to the space-charge force. Clearly these two forces act in opposite directions. If the space-charge force is small compared to the other force on the electron, i.e., if K_1 is small compared to $K_2 + K_3$, then an error in evaluating K_1 will have only a small effect on the new a-c electron velocities. However, if the space-charge force is of the same order of magnitude as the helix-field force, then an error in K_1 will have a pronounced effect on the new a-c velocities.

A study of this effect has shown that for $QC \leq 0.25$ the difference in the solutions when 32 electrons and a larger number are used is not appreciable. For values of QC around 0.5, however, it is necessary to use at least 64 electrons and for $QC \geq 1.0$ an even greater number of electrons should be followed. The difference between solutions for 32 and 64 electrons

for a particular case is shown in Figs. 3-9 and 3-10. The two solutions are compared on a percentage basis in Figs. 3-11 and 3-12.

The dependent variables $\phi(y,\phi_o)$ and $u(y,\phi_o)$ are more sensitive to the number of electrons considered than the variables $A(y)$ and $\Theta(y)$, which is fortunate since only qualitative information is needed on $\phi(y,\phi_o)$ and $u(y,\phi_o)$ while more exact, quantitative information is needed about $A(y)$ and $\Theta(y)$.

3.5.2 Truncation Error. The differential equations were solved using a difference-equation approximation of the first order. That is, only the first two terms of the Taylor series expansion were used, which means that the first term neglected was of relative order $(\Delta y)^2$. This difference-equation approximation amounts to replacing the function by a straight line drawn tangent to the function over the interval Δy. Hence, if the interval taken is too large, the first-order difference equation is a relatively poor approximation to the function over that interval. The resulting error is known as the truncation error.

Truncation error can be lessened by either of two means. First, higher-order differences may be taken into account; i.e., more terms in the Taylor series expansion may be included. Considerably more machine storage space is required, however, when higher-order difference equations are used, and the computation time is usually extended also. The alternative is to decrease the interval Δy to the point where the straight-line approximation to the function is quite accurate. Unfortunately, this procedure leads, in the limit, to round-off error, which is discussed in the following section. A compromise value of Δy must therefore be selected to yield a minimum in the combined effect of the two types of error.

As can be seen in Figs. 3-13 and 3-14, solutions for intervals greater than 0.025 differed markedly from those for $\Delta y = 0.025$ in any region where

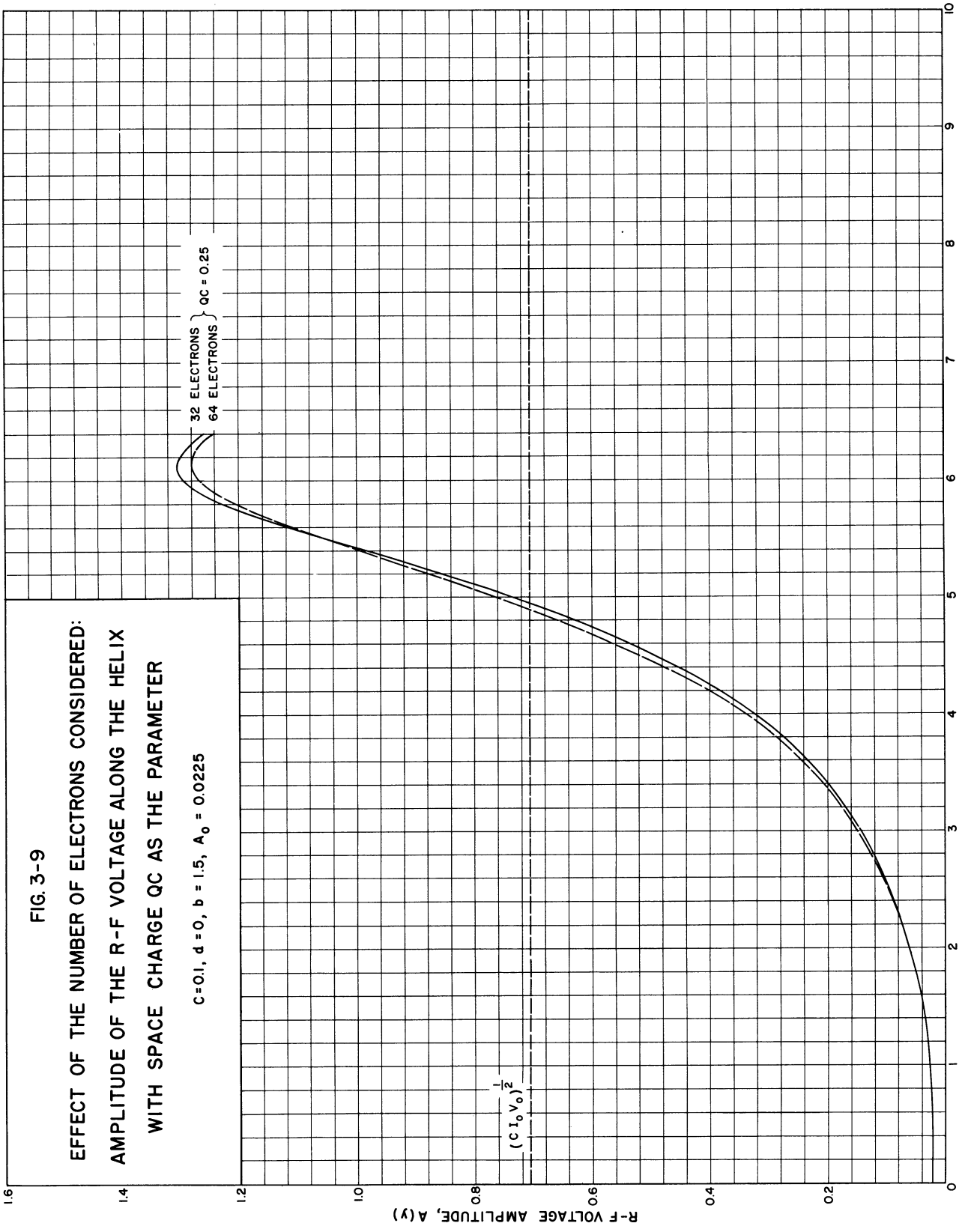
FIG. 3-9
EFFECT OF THE NUMBER OF ELECTRONS CONSIDERED:
AMPLITUDE OF THE R-F VOLTAGE ALONG THE HELIX
WITH SPACE CHARGE QC AS THE PARAMETER
C=0.1, d=0, b=1.5, A_0 = 0.0225
32 ELECTRONS
64 ELECTRONS
QC = 0.25
$(C I_0 V_0)^{\frac{1}{2}}$
R-F VOLTAGE AMPLITUDE, A(y)
y
0
0.2
0.4
0.6
0.8
1.0
1.2
1.4
1.6
1
2
3
4
5
6
7
8
9
10

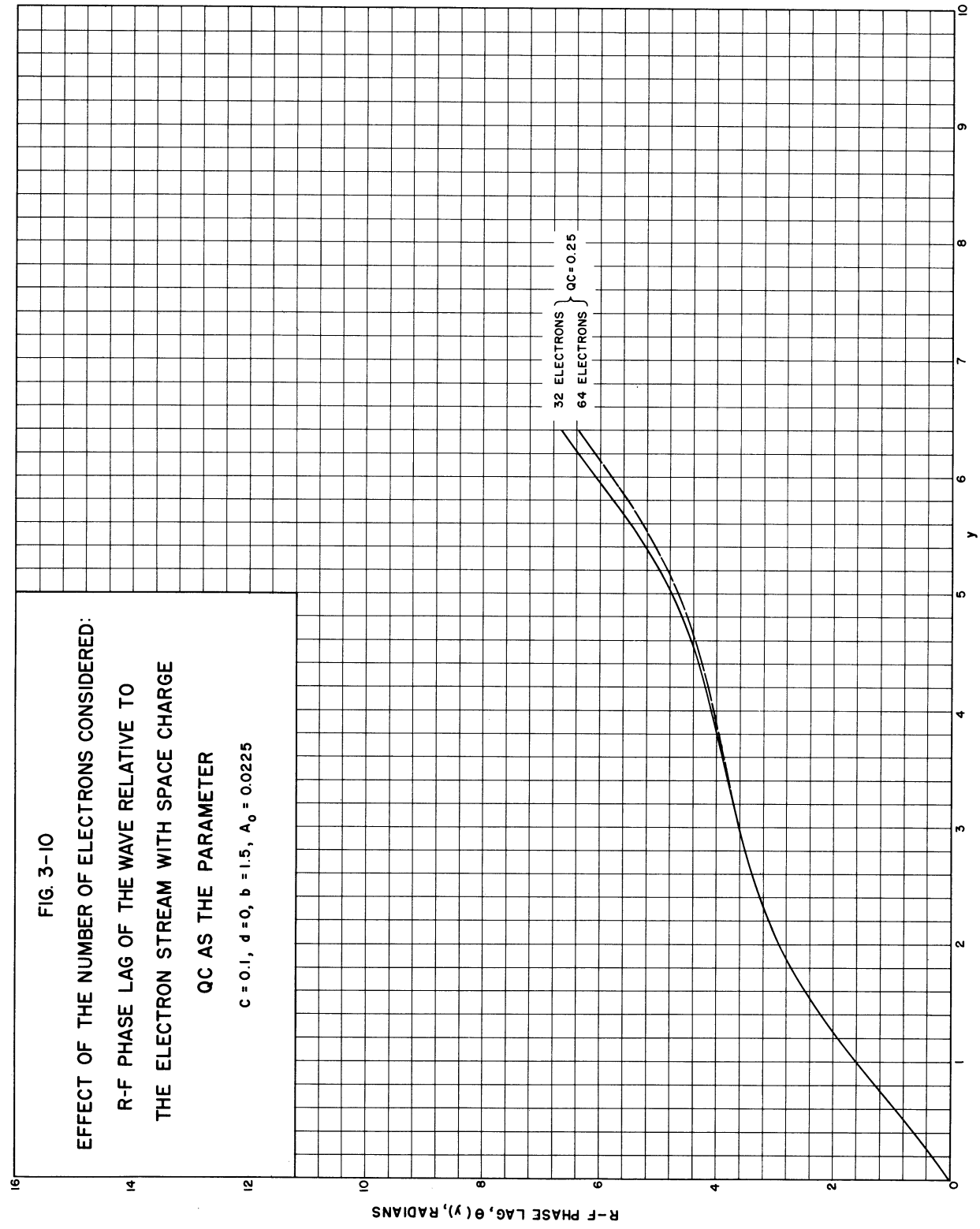

FIG. 3-10

EFFECT OF THE NUMBER OF ELECTRONS CONSIDERED:

R-F PHASE LAG OF THE WAVE RELATIVE TO

THE ELECTRON STREAM WITH SPACE CHARGE

QC AS THE PARAMETER

$C = 0.1,\ d = 0,\ b = 1.5,\ A_0 = 0.0225$

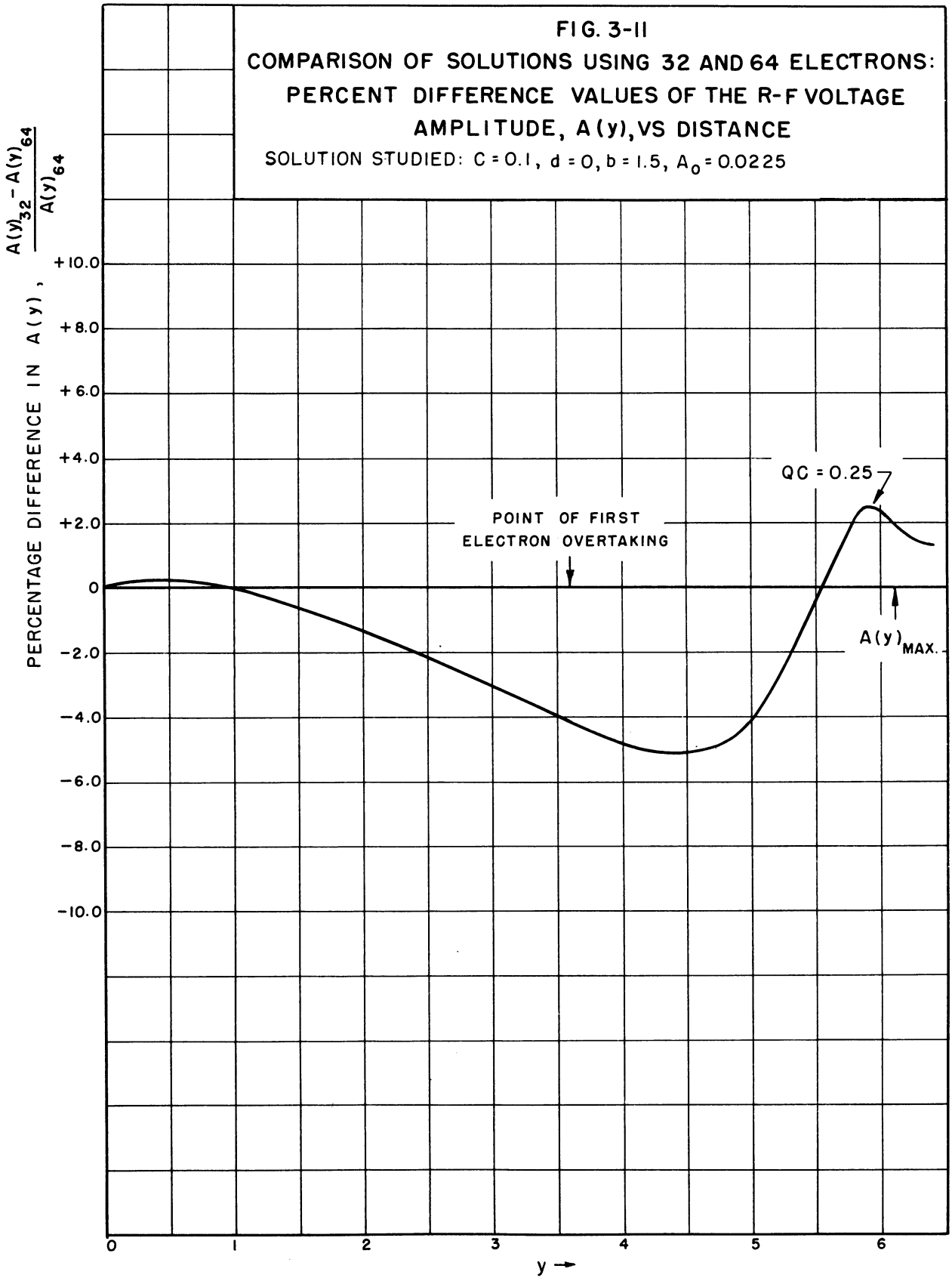
FIG. 3-11
COMPARISON OF SOLUTIONS USING 32 AND 64 ELECTRONS:
PERCENT DIFFERENCE VALUES OF THE R-F VOLTAGE
AMPLITUDE, A(y), VS DISTANCE
SOLUTION STUDIED: C = 0.1, d = 0, b = 1.5, A_0 = 0.0225
PERCENTAGE DIFFERENCE IN A(y), $\frac{A(y)_{32} - A(y)_{64}}{A(y)_{64}}$
+10.0
+8.0
+6.0
+4.0
+2.0
0
-2.0
-4.0
-6.0
-8.0
-10.0
QC = 0.25
POINT OF FIRST
ELECTRON OVERTAKING
$A(y)_{MAX.}$
0
1
2
3
4
5
6
y →

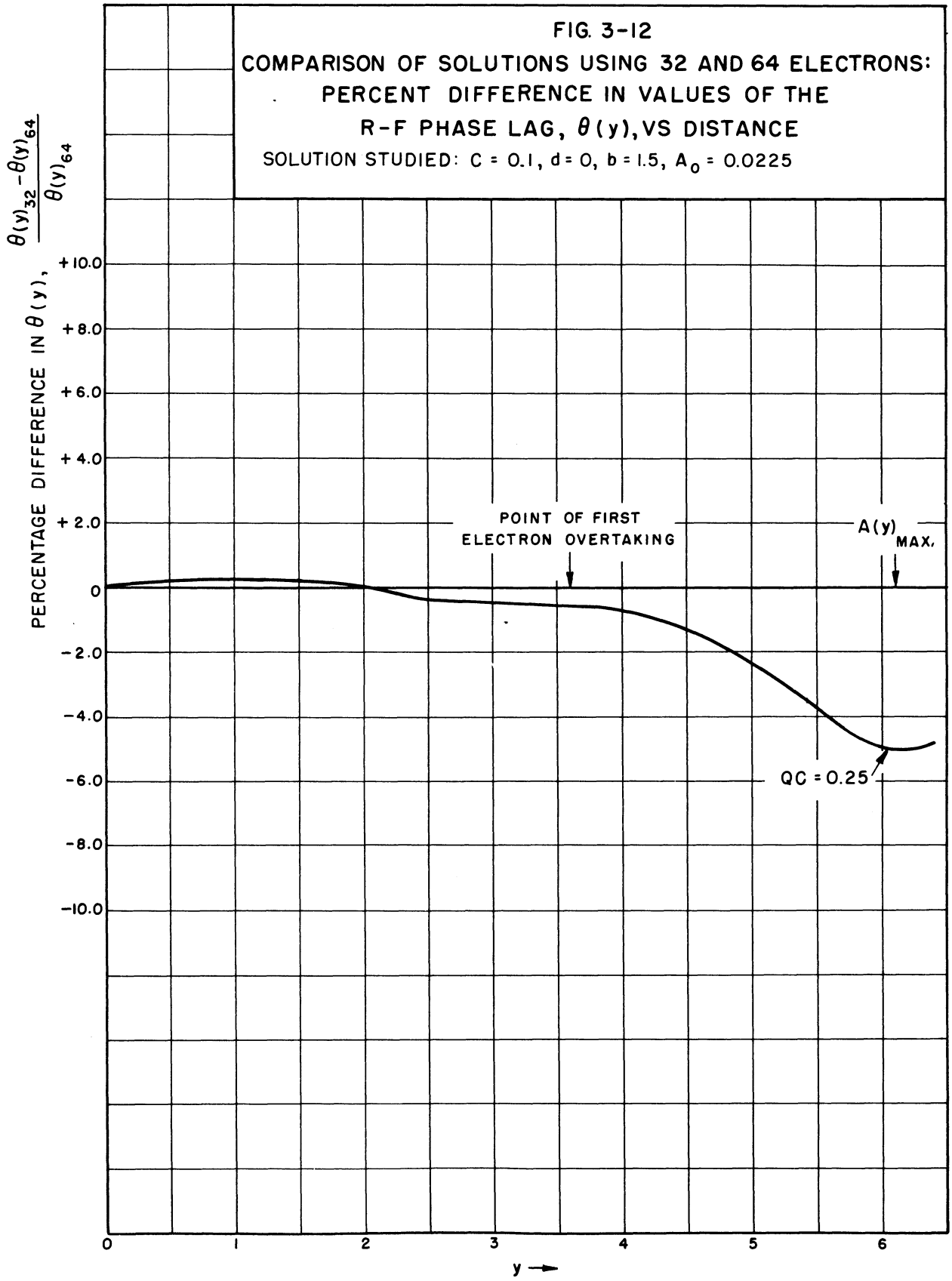
FIG. 3-12
COMPARISON OF SOLUTIONS USING 32 AND 64 ELECTRONS:
PERCENT DIFFERENCE IN VALUES OF THE
R-F PHASE LAG, θ(y), VS DISTANCE
SOLUTION STUDIED: C = 0.1, d = 0, b = 1.5, A0 = 0.0225
PERCENTAGE DIFFERENCE IN θ(y), (θ(y)32 − θ(y)64) / θ(y)64
+10.0
+8.0
+6.0
+4.0
+2.0
0
-2.0
-4.0
-6.0
-8.0
-10.0
POINT OF FIRST ELECTRON OVERTAKING
A(y) MAX.
QC = 0.25
0
1
2
3
4
5
6
y →

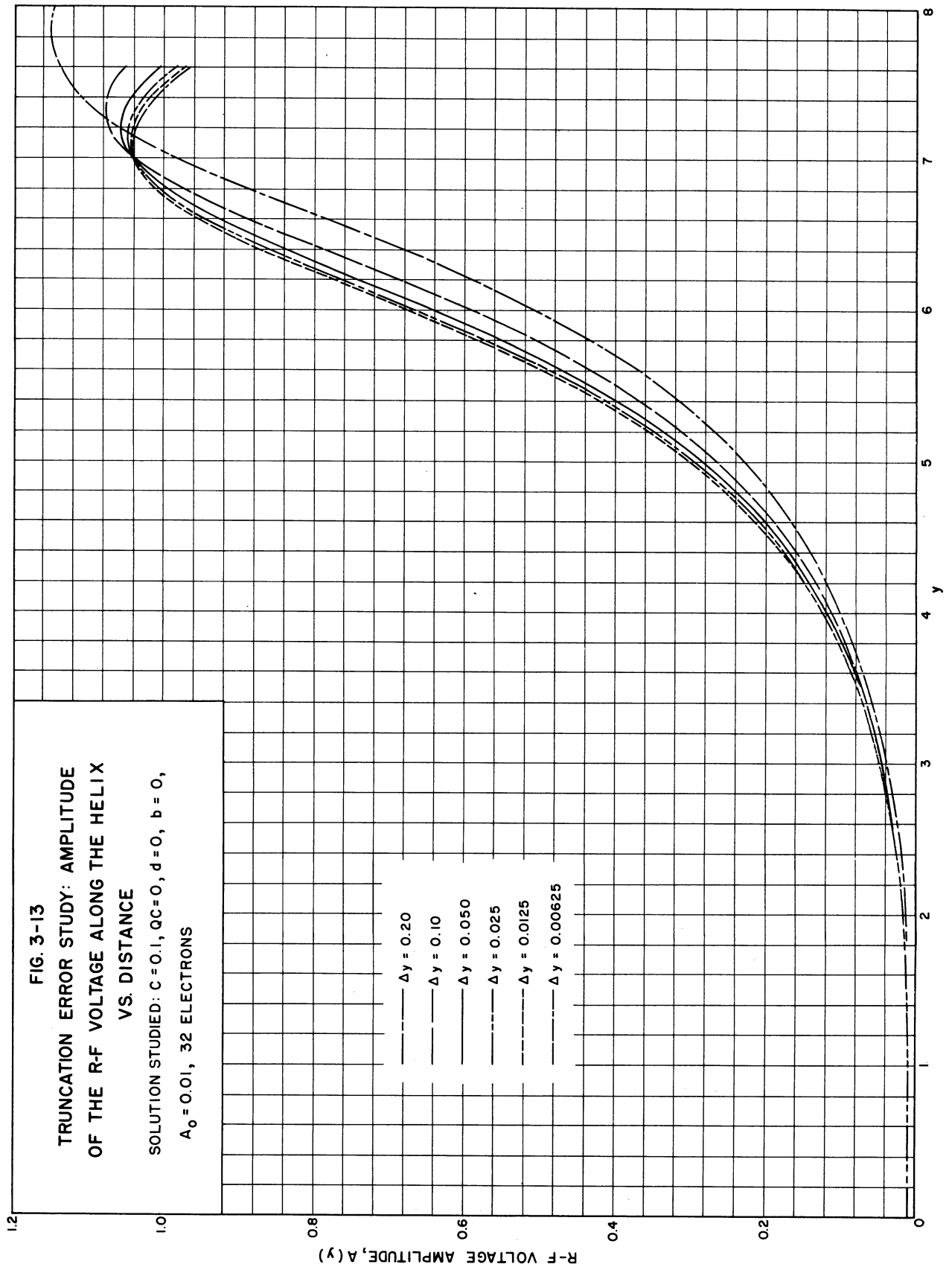

FIG. 3-13
TRUNCATION ERROR STUDY: AMPLITUDE OF THE R-F VOLTAGE ALONG THE HELIX VS. DISTANCE
SOLUTION STUDIED: C = 0.1, QC = 0, d = 0, b = 0, A_0 = 0.01, 32 ELECTRONS

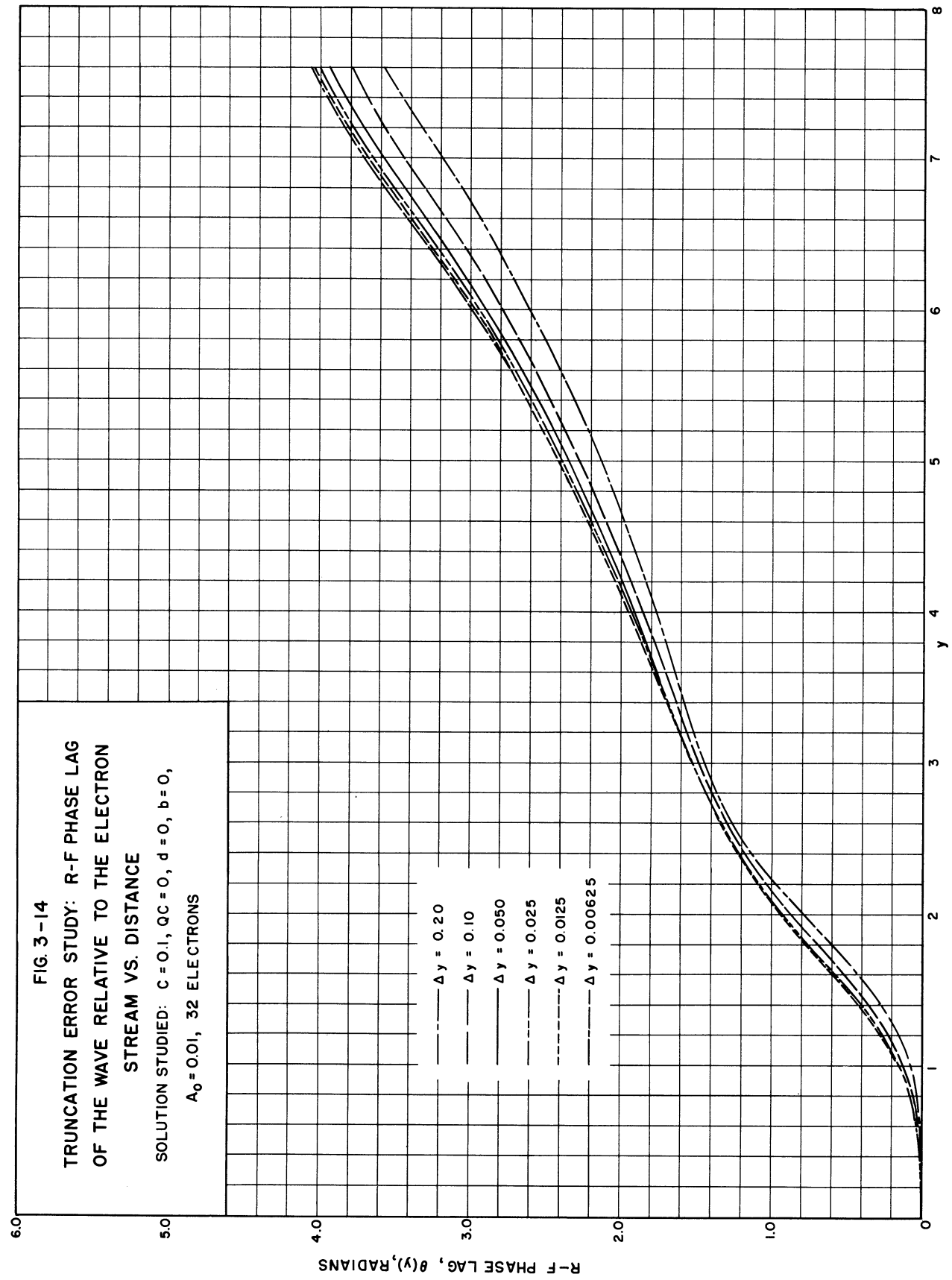
FIG. 3-14
TRUNCATION ERROR STUDY: R-F PHASE LAG OF THE WAVE RELATIVE TO THE ELECTRON STREAM VS. DISTANCE
SOLUTION STUDIED: C = 0.1, QC = 0, d = 0, b = 0, A_0 = 0.01, 32 ELECTRONS
Δy = 0.20
Δy = 0.10
Δy = 0.050
Δy = 0.025
Δy = 0.0125
Δy = 0.00625
R-F PHASE LAG, θ(y), RADIANS
y
0
1.0
2.0
3.0
4.0
5.0
6.0
1
2
3
4
5
6
7
8

the second derivatives of the function were of comparable magnitude to the function and its first derivative; whereas with intervals smaller than 0.025, down to $\Delta y = 0.00625$, there is little difference from the solutions for $\Delta y = 0.025$. Thus, $\Delta y = 0.025$ seems to be the upper limit of the region in which truncation error is insignificant in this problem.

3.5.3 Round-off Error. Round-off error occurs when the machine register is not large enough to store a number to the required number of significant figures, or when the shifting necessary to combine numbers in an iteration process results in moving a round-off originally beyond the point of interest into a significant place. As numbers are shifted to the left, the numbers used to start the next iteration are accurate to fewer significant figures, and thus the error increases in proportion to the number of iterations carried out.

Round-off error could be minimized by using double-precision arithmetic. However, this has the disadvantage of requiring twice as much machine storage space, so that it is more practical to control the round-off error by choosing Δy sufficiently large (thus requiring sufficiently few iterations) to obtain the accuracy required. The limitation on Δy mentioned in Section 3.5.2 must of course be kept in mind.

Solutions to the difference equations were therefore obtained using successively smaller increments in y, down to $\Delta y = 0.00625$. No appreciable difference between the solutions for $\Delta y = 0.00625$ and those for $\Delta y = 0.025$ was found out to five or six decimal places, from which it was concluded that round-off error is not present in the solutions to the accuracy desired. It was felt that continuing to decrease the integration interval in order to find the value of Δy at which the round-off error is so great that it completely dominates the solution (i.e., affects the first significant figure)

would require so much computation time on the machine as to make this approach highly impractical.

A different type of test was used to find out something about the amount of round-off error present in the solutions for $\Delta y = 0.025$. The method was to determine the sensitivity of the solutions to an error introduced in the 44th bit of the machine, which corresponds approximately to the 13th decimal place in a number.

The machine normally runs, and this problem was run, using rounded multiplication; i.e., the last digit for which there is room in the register is increased by 1 if the following decimal digit is equal to or greater than 5. Rounded multiplication in general produces some products which are greater and some which are smaller in absolute magnitude than the true values It is for this reason that the rounded multiplication order is used since it is assumed that working with both too large and too small numbers will tend to reduce the overall round-off error. When the unrounded multiplication order is used, the products formed must be either less than or equal to the true product in absolute magnitude. It should be noted that division and shifting have the same round-off effect as unrounded multiplication, while addition and subtraction are theoretically exact if the operands are exact.

The propagation of round-off error was therefore examined by running a solution using the rounded multiplication order and then running the same solution with the same Δy using the unrounded multiplication order. Since multiplication of two 44-bit numbers by these two different methods will result in differing 44th binary digits an average of half the time and since a deviation in the 44th bit of an intermediate number is necessarily shifted to a more significant place as iterations are carried out, an error may be expected to propagate and show up in the solutions if enough iterations occur after the difference appears.

When intermediate numbers in a program are small or are scaled so that they are represented by only a few significant binary digits, it is quite obvious that round-off is of greater importance; i.e., a change in the last binary bit of a small number produces a larger relative round-off error than in a large number. Even in problems where the magnitudes of intermediate numbers are unknown initially it is often possible to rescale these numbers on the basis of trial solutions in order to retain more significance. However, it is not always possible to avoid small numbers by rescaling, as in the case of a number obtained by addition of small numbers or subtraction of nearly equal numbers.

For example, in the problem which is the subject of this thesis the first derivatives are replaced by the approximation

$$\frac{dx}{dy} = \frac{x_{i+1} - x_i}{\Delta y} \quad ,$$

in which it is clear that if Δy is small $x_{i+1} - x_i$ will be a small number. Hence when this number is used in forming a product the round-off error will become increasingly significant with decreasing Δy. In addition, the smaller Δy is the greater will be the number of iterations required to go a unit distance along the y axis, and this increased number of arithmetic operations will increase the frequency of round-off error. Thus it would be expected that some lower bound B on Δy exists such that for $\Delta y < B$ round-off error will completely dominate the problem and give diverging results.

Some intuitive insight into the phenomenon of round-off error may be gained by comparing the solutions obtained by using rounded and unrounded multiplications. When the differences in corresponding solutions are slight it may be concluded that the problem is not sensitive to errors in

the 44th bit, if the program involves sufficient multiplication to insure reasonably frequent introduction of errors.

When, on the other hand, corresponding ordinates of two solutions using rounded and unrounded multiplications differ in the jth significant figure, the accuracy of the results to j significant figures is certainly questionable since if changes in the rounding procedure can produce diverging results it is reasonable to assume that the true solution differs from the exact solution in at least the jth significant figure. Thus we have bounded the round-off error in a greater-than-or-equal-to sense.

Solutions for $A(y)$ and $\theta(y)$ using both rounded and unrounded multiplication were obtained for $\Delta y = 0.025$, 0.00625, and 0.003125. The solutions differed by approximately one unit in the seventh decimal place for $\Delta y = 0.025$ while the difference showed up in the fourth and fifth decimal places for $\Delta y = 0.00625$ and in the second decimal place for $\Delta y = 0.003125$. The results of this investigation are presented graphically in Fig. 3-15.

3.5.4 Selection of the Integration Interval. Two factors were considered in the selection of the integration increment Δy to be used for the solutions: the degree of accuracy desired and the computation time required. Obviously the larger the value of Δy the better from the standpoint of minimizing the computation time. As pointed out in Sections 3.5.2 and 3.5.3, accuracy considerations suggest a small value to minimize truncation error and a large value to minimize round-off error. The two types of error are independent of one another; what is desired is the smallest rms error.

The value selected for Δy was 0.025. Computation can be carried out in a reasonable time with this interval, truncation error is insignificant at this level, and round-off error appears in approximately the seventh

FIG. 3-15

ROUND-OFF ERROR STUDY: FIRST SIGNIFICANT FIGURE AFFECTED IN $\theta(y)$ WHEN ROUNDED MULTIPLICATIONS ARE REPLACED BY UNROUNDED MULTIPLICATIONS VS. INTEGRATION INCREMENT

SOLUTION STUDIED: C = 0.1, QC = 0, d = 0, b = 0, A_0 = 0.01

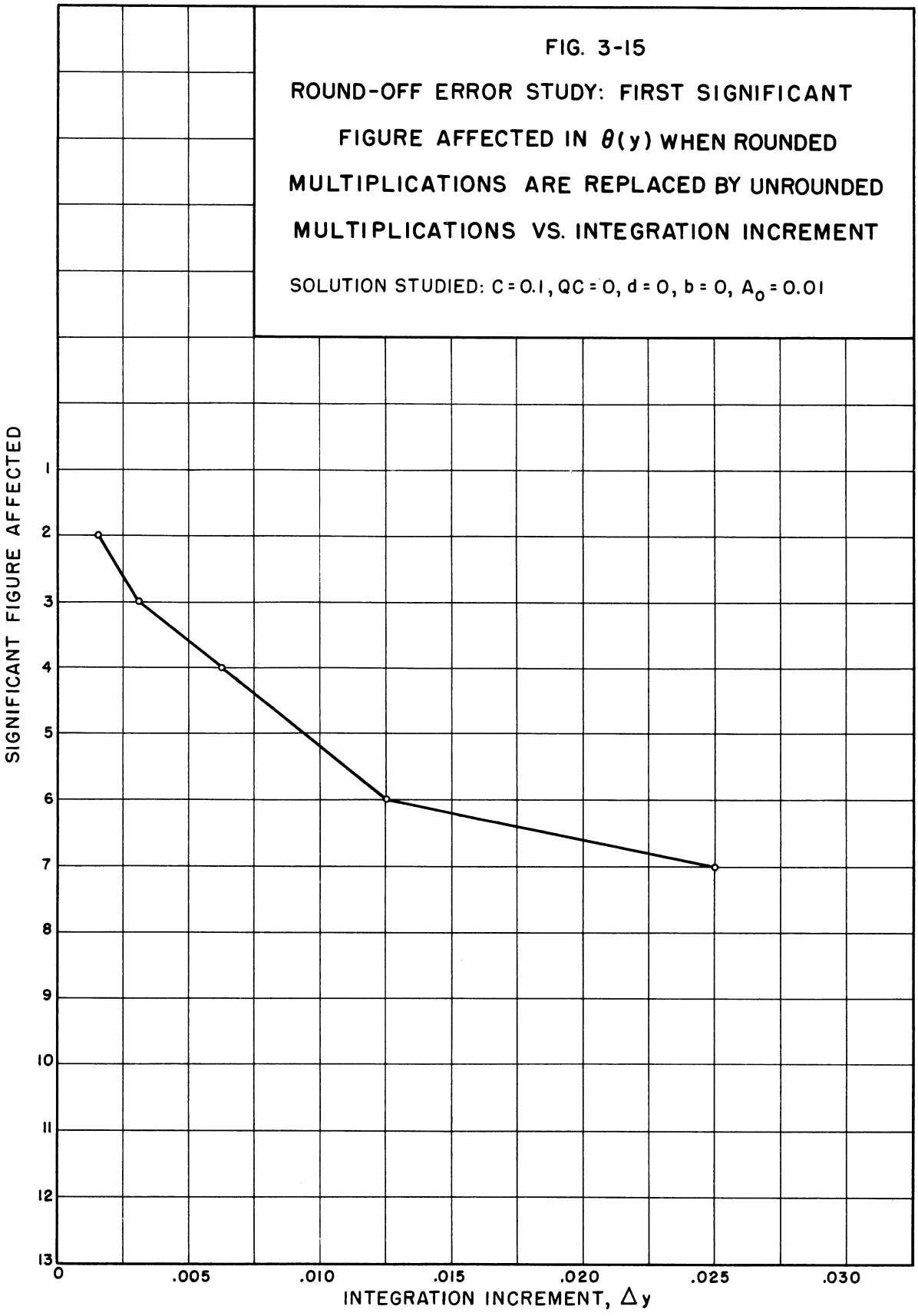

decimal place for the required iterations, so that the results are believed to be accurate to approximately six decimal places.

3.5.5 Stability of the Solution. If the solution of a differential equation is stable with respect to the propagation of errors, then an error introduced into one of the dependent variables at some point in the iteration procedure will result in a solution which either is parallel to the exact solution or converges to the exact solution. If the solution is unstable with respect to error propagation, then a solution containing an error will tend to diverge from the exact solution. In Fig. 3-16, line AB represents the exact solution; solutions 1, 2, and 6 are seen to be unstable; and solutions 3, 4, and 5 are considered stable.

In order to test the stability of the solutions of this work relative to errors in the dependent variables, errors of 5, 10, and 15 percent were introduced in A(y) at several values of y (for example, at y = 3, 4, and 6) and the solution carried forward. A similar test was conducted on $\theta(y)$. In all cases the resulting solutions proved to be parallel to the solution into which no error had been introduced. It was therefore concluded that this type of solution is stable with respect to the propagation of errors.

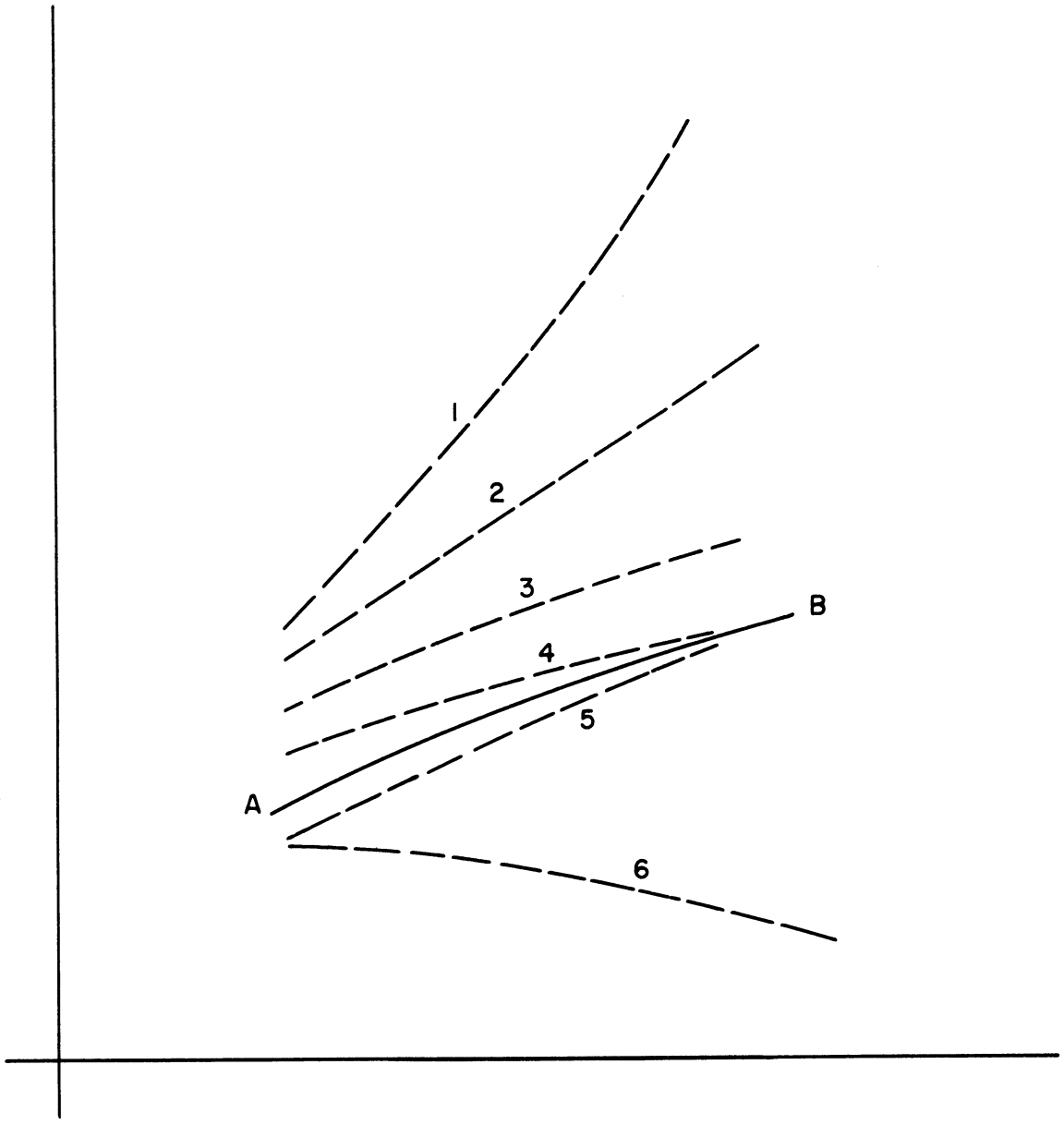

FIG. 3-16 PROPAGATION OF ERRORS: STABLE AND UNSTABLE SOLUTIONS OF A DIFFERENTIAL EQUATION.

CHAPTER IV. GRAPHICAL PRESENTATION OF RESULTS

Solutions of the general large-signal equations derived in Chapter II may be obtained for a wide range of the parameters introduced there. For convenience the normalized variables, in addition to the parameters necessary for a particular solution, are listed below. The normalized variables are:

$y = \frac{C\omega}{u_o} z = \frac{2\pi C}{\lambda_s} z$, distance measured from the input to the helix;

$\phi_o = \frac{\omega z_o}{u_o} = \omega t_o$, entrance phase of an electron relative to the r-f wave at the input, radians;

$|A(y)| = \frac{C}{I_o Z_o} |V(y,\phi_o)|$, normalized amplitude of the r-f wave on the helix;

$\theta(y) = y/C - \omega t - \phi(y,\phi_o)$, the r-f phase angle (or lag) of the wave on the helix relative to a hypothetical traveling wave whose phase velocity is the initial stream velocity u_o, radians;

$\phi(y,\phi_o)$ = the phase of an electron relative to the r-f wave at a particular y plane, radians;

$2Cu(y,\phi_o)$ = the normalized velocity deviation of an electron at a particular y plane, defined by $u_t(y,\phi_o) = u_o[1 + 2Cu(y,\phi_o)]$; and

$u_t(y,\phi_o) = u_o[1 + 2Cu(y,\phi_o)]$, the total velocity of an electron at a particular y plane, m/sec.

The parameters which must be prescribed for a particular solution are:

C = the gain parameter defined by $C^3 = |\eta| ZI_o/2u_o^2$;

$QC = \frac{1}{4C^2} \left(\frac{\omega_q/\omega}{1 + \omega_q/\omega} \right)^2$, small-signal space-charge parameter*;

*The solutions were actually carried out for values of the large-signal space-charge parameters K and B discussed in Section 2.4. However, since QC is more familiar to workers in the field the curves were plotted in terms of QC. Equivalent values of K and QC may be computed from Fig. B-4.

$B = \beta b'$ = the large-signal space-charge range parameter, radians;

$b = \frac{u_o - v_o}{Cv_o}$, the relative injection velocity;

$d = \ell/20(2\pi)(\log e)(C) = 0.01836\ \ell/C$, the loss factor;

ℓ = the series loss expressed in db per undisturbed wavelength along the helix;

$A_o = A(0)$ = the input-signal level, usually taken to be 30 db below CI_oV_o; and

a'/b' = the ratio of mean helix diameter to stream diameter.

The range of parameters to be investigated was selected so that the results would apply to high-power traveling-wave amplifiers in general, whatever their frequency range.

As stated earlier, the object of this investigation was to study the high-level operation of the traveling-wave amplifier, and in particular how the various parameters listed above affect the saturation power output and efficiency of the amplifier. Clearly this objective requires determination of the optimum injection velocity (i.e., that value of b which gives maximum saturation gain) for each value of C and QC. In general, the b for maximum saturation gain will be greater than that for maximum small-signal gain.

In order to determine the injection velocity for maximum saturation gain at various values of C and QC, the input-signal level A_o was fixed for these calculations. The value selected was approximately 30 db below C times the stream power I_oV_o, or precisely $A_o = 0.0225$, which insures that the operation is initially linear and the boundary conditions may be calculated as indicated in Section 2.4.

In addition, for all the calculations the ratio of helix to stream diameter a'/b' is taken as 2 and the space-charge range parameter $\beta b'$ has the

typical value of 1. Except in the loss studies presented in Section 4.8, the loss factor d was considered to be zero.

Since the effect of space charge is of particular interest, solutions were obtained both with the space-charge parameter QC taken as 0 and for two other values of QC, namely 0.125 and 0.25. (For the values of a'/b' and $\beta b'$ used, the corresponding values of $(\omega_p/\omega C)^2$ are 1.61 and 3.42 respectively.) The non-space-charge solutions were carried out for three values of the gain parameter C, 0.05, 0.1, and 0.2, which are considered to be representative of large-signal tubes in general. The value C = 0.1 was selected for the space-charge calculations as being nearest the C values most frequently encountered.

The results of the computations carried out on the Michigan Digital Automatic Computer are presented and discussed in the following sections of this chapter. The curves are presented in historical order; i.e., the curves plotted directly from the data taken from the computer are presented first and are followed by cross plots of the data. The flight-line diagrams, which are perhaps the most useful curves from the standpoint of understanding the physical phenomena involved in a large-signal traveling-wave amplifier, are presented in Section 4.5.

4.1 R-F Voltage and Power along the Helix

The r-f voltage amplitude A(y) is plotted vs. the tube length both in units of y and in units of the stream wavelength λ_s (the latter is denoted by N_s) for a number of values of b in Figs. 4-1 through 4-5. One of the values of b selected for each set of calculations was that value which gives maximum small-signal gain, i.e., that b for which the growth constant x_1 of the slow-and-growing wave is a maximum. As was expected, in each case the

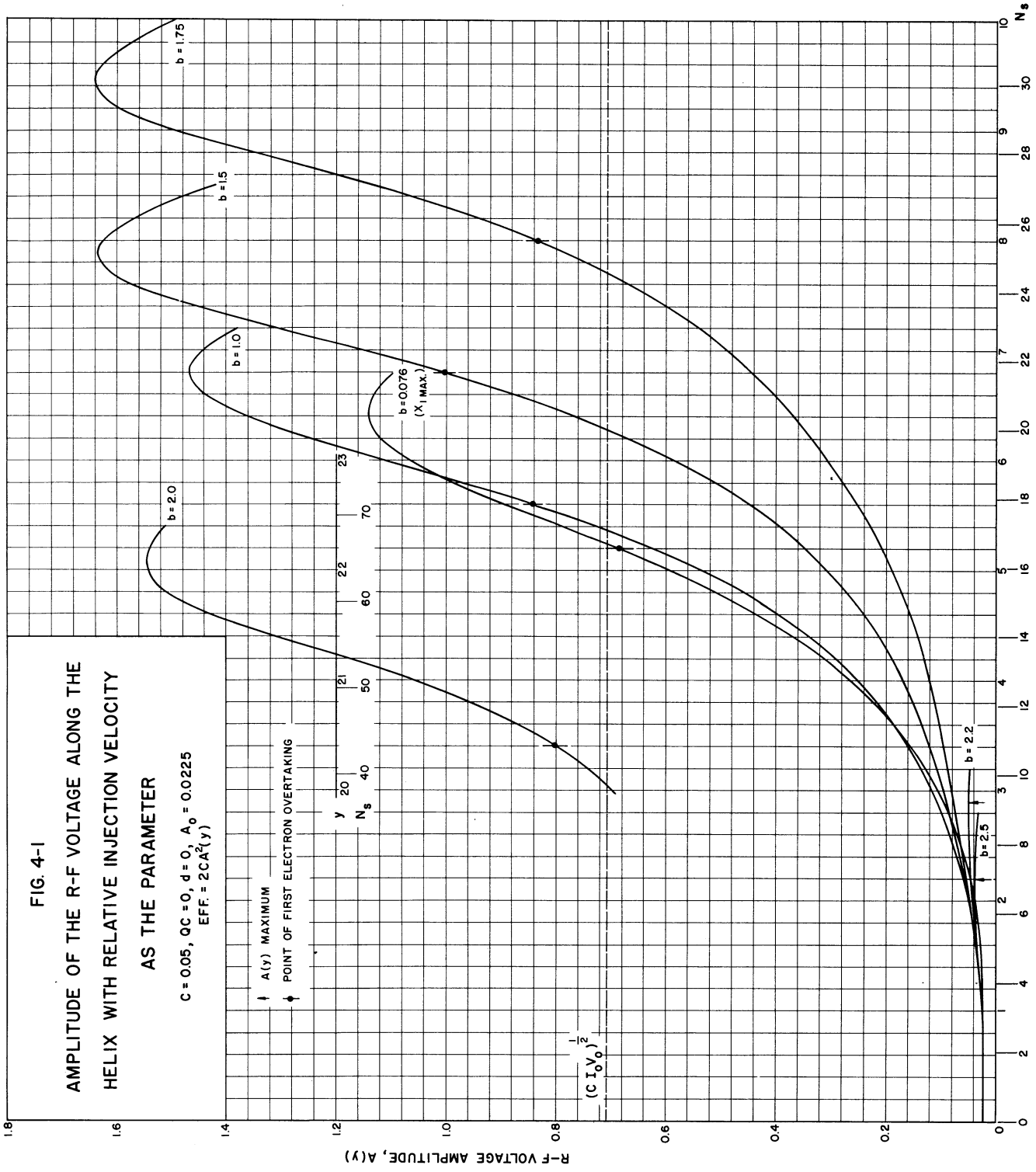
FIG. 4-1
AMPLITUDE OF THE R-F VOLTAGE ALONG THE HELIX WITH RELATIVE INJECTION VELOCITY AS THE PARAMETER
C = 0.05, QC = 0, d = 0, A_0 = 0.0225
EFF. = $2CA^2(y)$
A(y) MAXIMUM
POINT OF FIRST ELECTRON OVERTAKING
b = 2.0
b = 1.75
b = 1.5
b = 1.0
b = 0.076 ($X_{1\,MAX.}$)
b = 2.2
b = 2.5
y
N_s
R-F VOLTAGE AMPLITUDE, A(y)
$(C\,I_0V_0)^{\frac{1}{2}}$

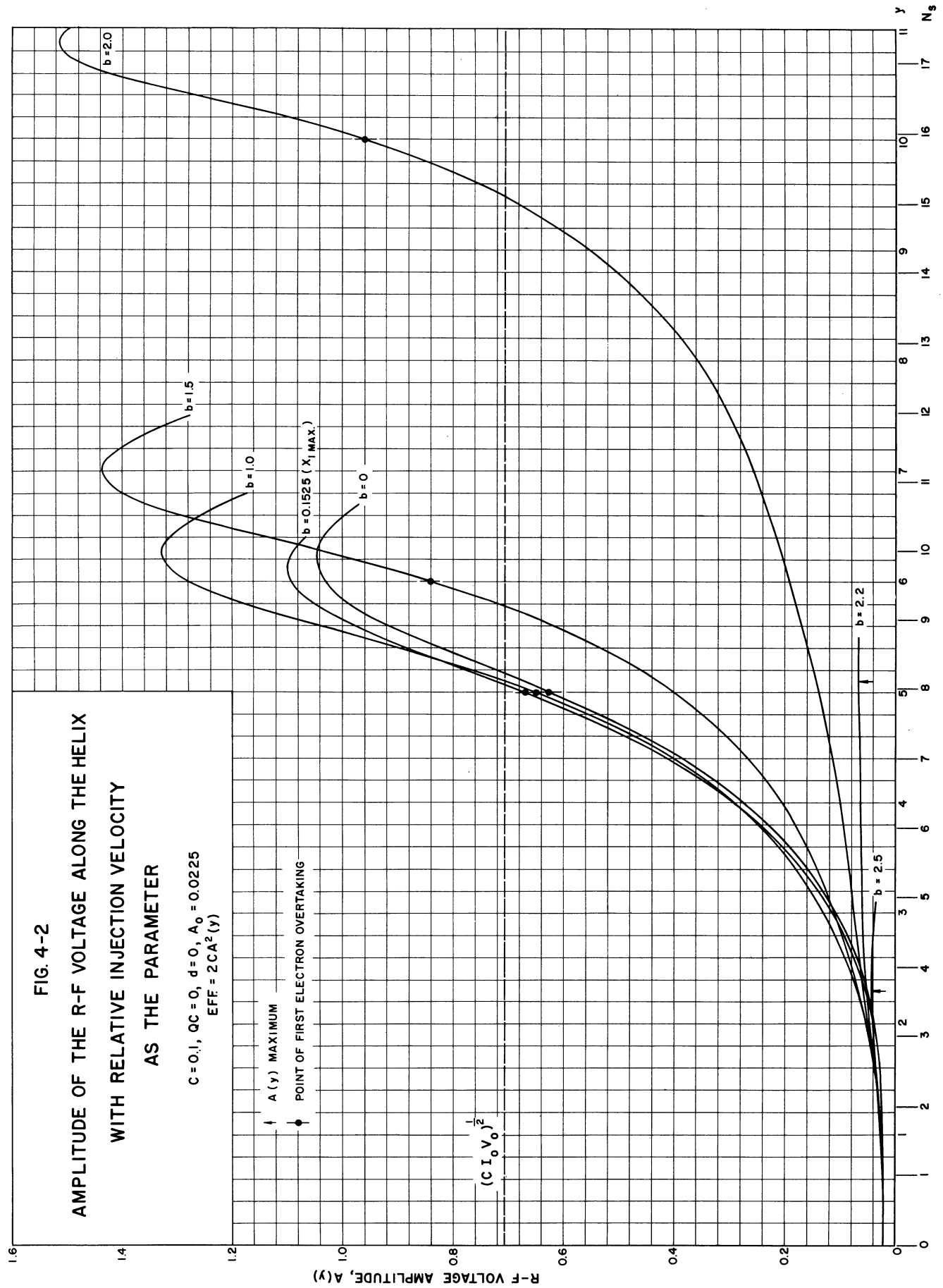
FIG. 4-2
AMPLITUDE OF THE R-F VOLTAGE ALONG THE HELIX
WITH RELATIVE INJECTION VELOCITY
AS THE PARAMETER
C = 0.1, QC = 0, d = 0, A_0 = 0.0225
EFF. = $2CA^2(y)$
A(y) MAXIMUM
POINT OF FIRST ELECTRON OVERTAKING
$(C I_o V_o)^{\frac{1}{2}}$
b = 2.0
b = 1.5
b = 1.0
b = 0.1525 (X_1 MAX.)
b = 0
b = 2.2
b = 2.5
R-F VOLTAGE AMPLITUDE, A(y)
y
N_s

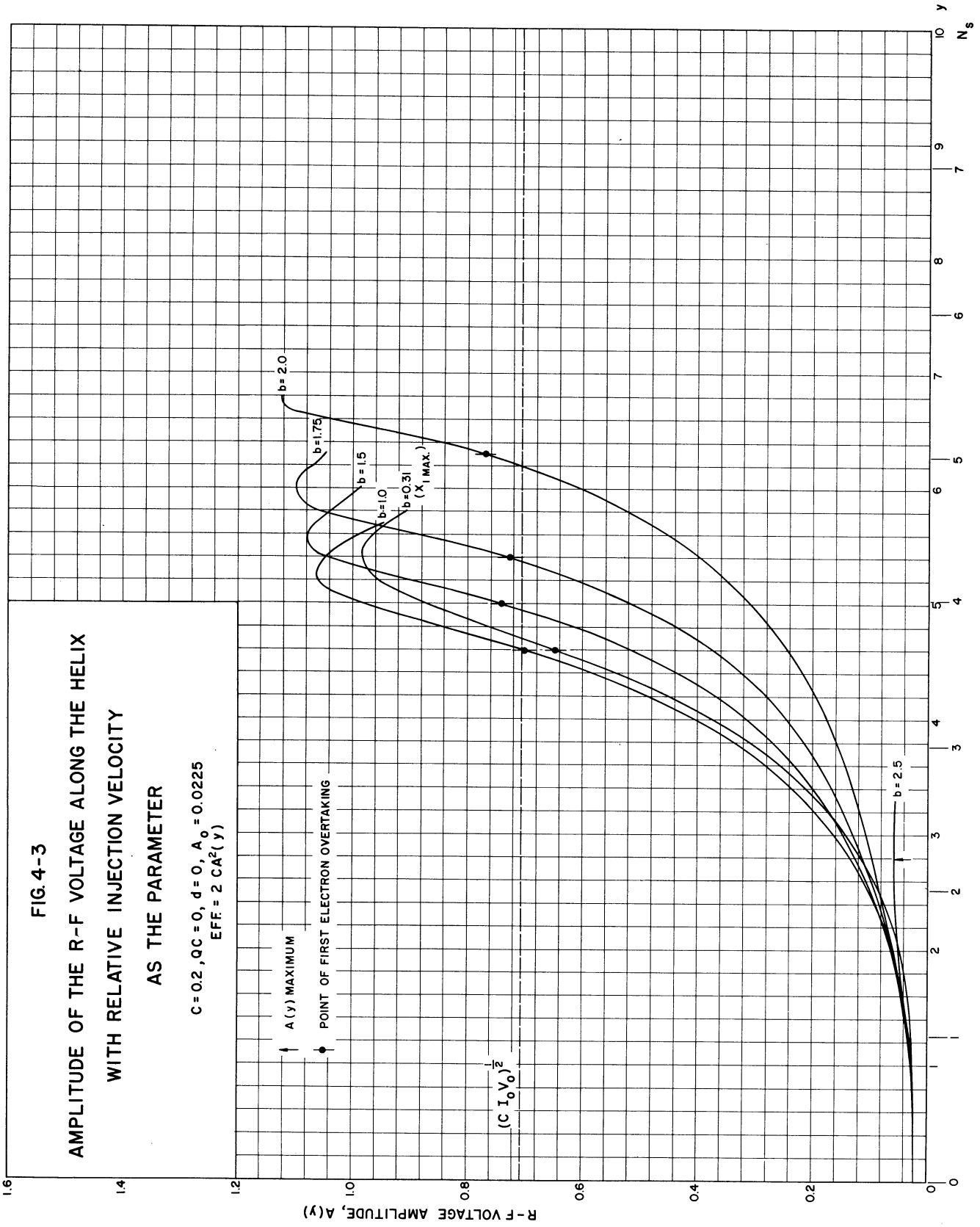

FIG. 4-3

AMPLITUDE OF THE R-F VOLTAGE ALONG THE HELIX WITH RELATIVE INJECTION VELOCITY AS THE PARAMETER

C = 0.2, QC = 0, d = 0, A_o = 0.0225
EFF. = 2 $CA^2(y)$

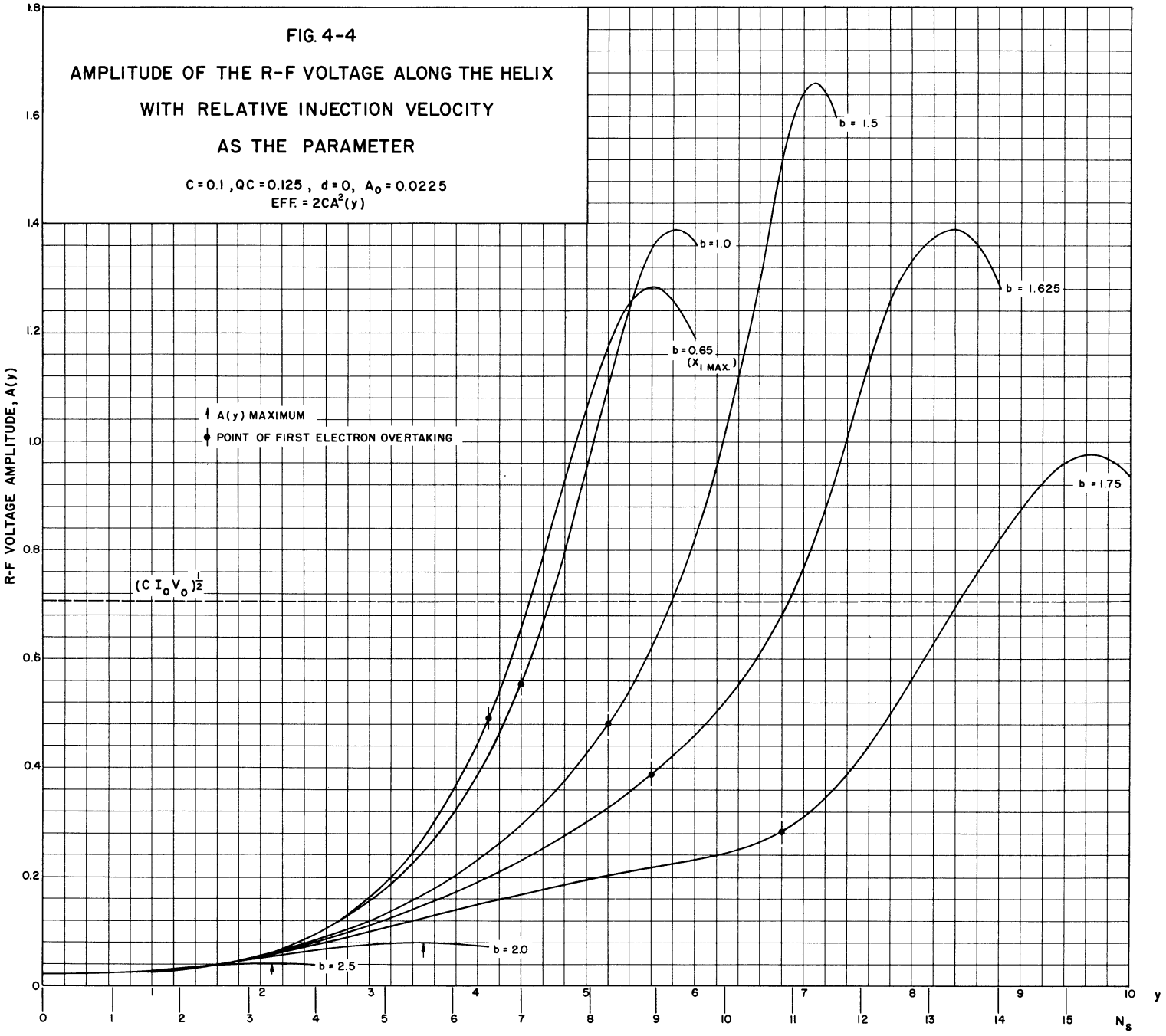
FIG. 4-4
AMPLITUDE OF THE R-F VOLTAGE ALONG THE HELIX
WITH RELATIVE INJECTION VELOCITY
AS THE PARAMETER
C = 0.1 , QC = 0.125 , d = 0, A_0 = 0.0225
EFF. = $2CA^2(y)$
R-F VOLTAGE AMPLITUDE, A(y)
A(y) MAXIMUM
POINT OF FIRST ELECTRON OVERTAKING
$(C I_0 V_0)^{\frac{1}{2}}$
b = 1.5
b = 1.0
b = 0.65
($X_{1\ MAX.}$)
b = 1.625
b = 1.75
b = 2.0
b = 2.5
y
N_s

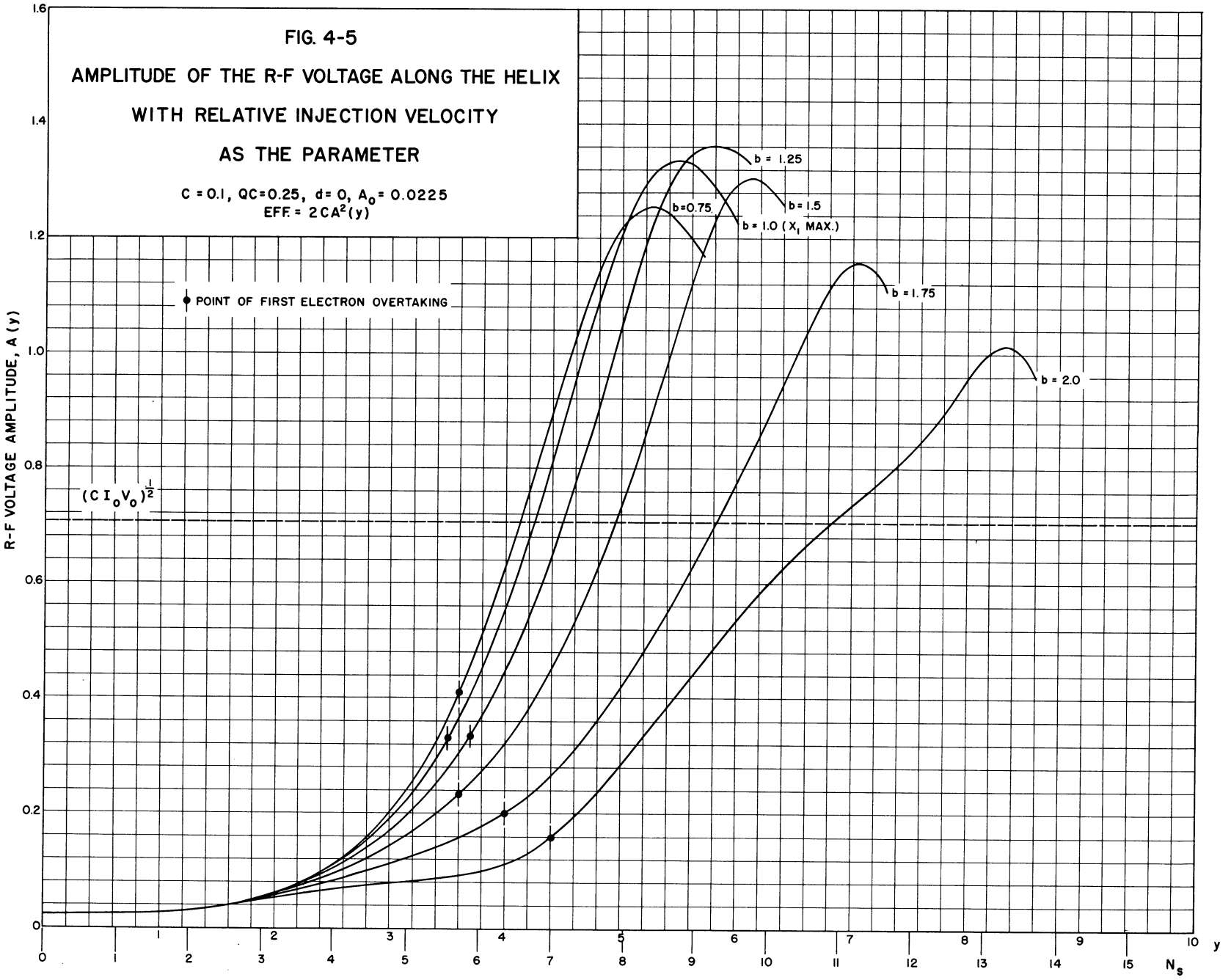
FIG. 4-5
AMPLITUDE OF THE R-F VOLTAGE ALONG THE HELIX
WITH RELATIVE INJECTION VELOCITY
AS THE PARAMETER
C = 0.1, QC=0.25, d= 0, A0= 0.0225
EFF. = 2CA²(y)
R-F VOLTAGE AMPLITUDE, A (y)
POINT OF FIRST ELECTRON OVERTAKING
(C I0V0)^½
b = 1.25
b=0.75
b = 1.5
b = 1.0 (X1 MAX.)
b = 1.75
b = 2.0
y
Ns

value of b for maximum saturation gain turns out to be greater than that for maximum small-signal gain.

On each of the curves it will be noticed that the saturation tube length is largest for that b which gives maximum saturation gain, which is also to be expected since the low-level gain is in general less as b is increased.

The point of first electron overtaking is noted on each of the graphs. From the flight-line diagrams presented in Section 4.5 it can be seen that this point along the tube at which electrons first overtake one another is in general dependent on all the parameters and occurs well into the nonlinear region.

The first maximum of the r-f voltage amplitude is also marked on the curves when it cannot be located quickly by inspection. It can be seen from the working equations that if the solutions are carried beyond this first maximum the amplitude will drop to a minimum and then rise to a peak again. Since the later maxima are in general lower than the first maximum, the solutions were not computed beyond that point.

In Fig. 4-1, for C = 0.05 and QC = 0, the b = 2.0 curve is plotted only for the region near saturation because the tube is quite long, some 65 stream wavelengths, for this case. It should be noted that the value of b for this curve is greater than that for which maximum saturation gain is obtained. Hence the interaction is less and the signal level on the helix builds up slowly with distance.

Figure 4-2, for C = 0.1 and QC = 0, includes a solution for b = 0 (i.e., $u_o = v_o$) in order to show that gain may also be obtained when the wave and the electron stream are initially in synchronism. Clearly this is not an optimum value of b.

In Fig. 4-3, for C = 0.2 and QC = 0, the b = 2.0 curve has not been carried beyond saturation. Computation was suspended at this point because at saturation one electron has very nearly stopped; i.e., its total velocity as given by

$$u_t(y,\phi_o) = u_o[1 + 2Cu(y,\phi_o)] \qquad (2\text{-}14)$$

is approaching zero. One electron has in fact dropped back one period in time, as may be seen in the velocity-deviation curve of Fig. 4-37. The electron-velocity curves of Sections 4.4.1 and 4.4.2 show the approach of $2Cu(y,\phi_o)$ to -1 for the case where C = 0.2; i.e., $u(y,\phi_o)$ approaches -2.5. Integration must be stopped when this condition is approached, since several terms in the working equations are divided by the quantity $[1 + 2Cu(y,\phi_o)]$. The resultant large a-c velocities are a result of the "strongness of coupling" between the stream and the circuit as C becomes significant compared to 1. This situation illustrates the great inaccuracy introduced by neglecting the space-charge forces when C is large. Consideration of the space charge prevents this condition from arising and in general reduces the velocity deviation.

The r-f power level along the helix is of considerable interest also because on a plot of power level vs. distance along the tube the point of departure of the signal from the small-signal value is clearly recognizable. The small-signal power output is a straight-line function of the input power; hence the deviation from a straight line drawn tangent to the power-level curve near the input is a measure of the nonlinearities present.

The power along the lossless helix is given by

$$P = \left[\frac{\overline{V}^2(z,t)}{Z_o}\right]_{avg.} = 2CI_oV_oA^2(y) \quad . \qquad (4\text{-}1)$$

The power-level curves for the solutions of Figs. 4-1 through 4-5 are presented in Figs. 4-6 through 4-10. The power level is plotted in db relative to the input signal, which is taken to be 30 db below CI_oV_o. The CI_oV_o level is marked for reference on each figure.

4.2 Phase Angle of the Wave Relative to the Electron Stream

As pointed out in Section 2.1, $\theta(y)$ is the r-f phase angle (or lag) between the actual wave on the helix and a hypothetical traveling wave whose phase velocity is the initial electron velocity u_o. In Figs. 4-11 through 4-15 the r-f phase lag is plotted vs. distance along the helix, for the same parameter values as the Section 4.1 solutions. In all cases $\theta(y)$ increases negatively with distance and also with the relative injection velocit

In the small-signal region sufficiently far removed from the input so that only the slow-and-growing wave is present, $\theta(y)$ vs. y is a straight line with slope equal to β_1, the phase constant of the slow-and-growing wave. In this region where the solutions are of exponential form and the slow-and-growing wave of the small-signal theory predominates, the phase velocity of the wave is given by

$$v = u_o(1 + C\beta_1) \quad . \qquad (4\text{-}2)$$

However, in the large-signal region where the variation of the dependent variables with time and distance can no longer be expressed in the familiar exponential form, the wave picture developed with the linear theory loses much of its significance and consequently its usefulness.

Nevertheless, some information on the wave velocity may be obtained from these phase curves. At any point y along the tube the phase velocity of the helix wave is given by

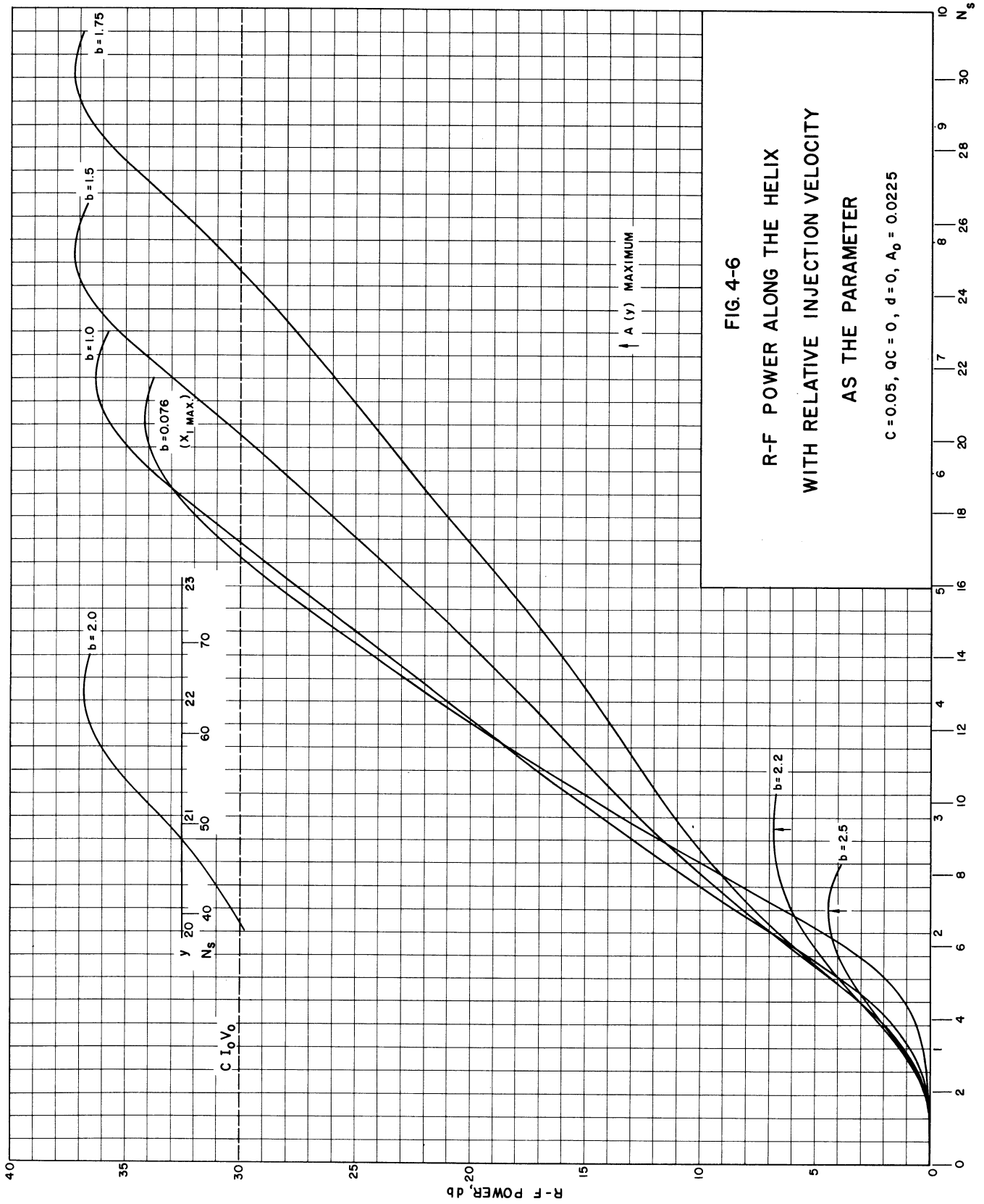
FIG. 4-6
R-F POWER ALONG THE HELIX
WITH RELATIVE INJECTION VELOCITY
AS THE PARAMETER
C=0.05, QC = 0, d = 0, A_0 = 0.0225
R-F POWER, db
y
N_s
$C I_0 V_0$
A (y) MAXIMUM
b=1.75
b=1.5
b=1.0
b=0.076
(X_1 MAX.)
b=2.0
b=2.2
b=2.5

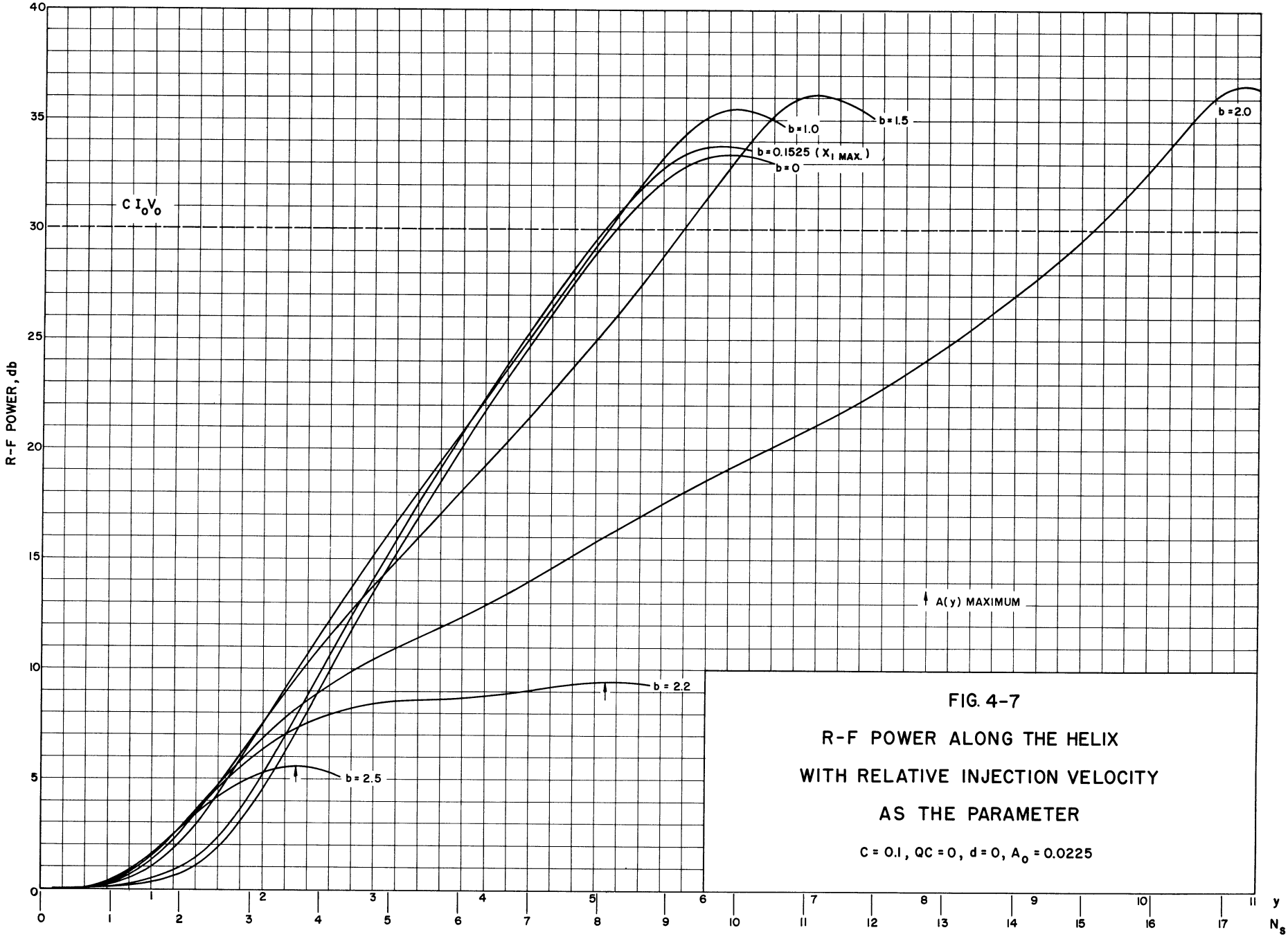

FIG. 4-7

R-F POWER ALONG THE HELIX

WITH RELATIVE INJECTION VELOCITY

AS THE PARAMETER

C = 0.1, QC = 0, d = 0, A_0 = 0.0225

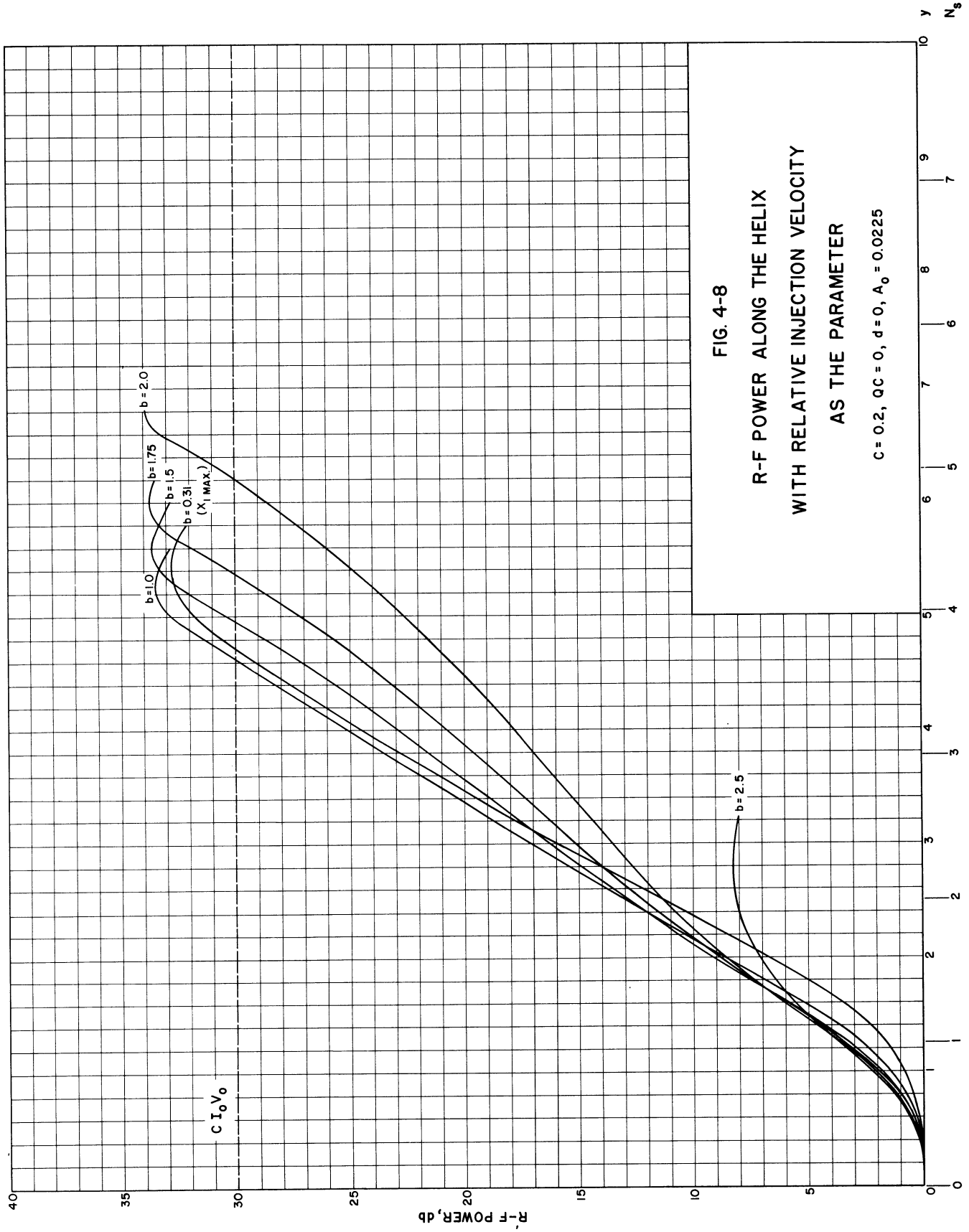

FIG. 4-8

R-F POWER ALONG THE HELIX

WITH RELATIVE INJECTION VELOCITY

AS THE PARAMETER

$C = 0.2,\ QC = 0,\ d = 0,\ A_o = 0.0225$

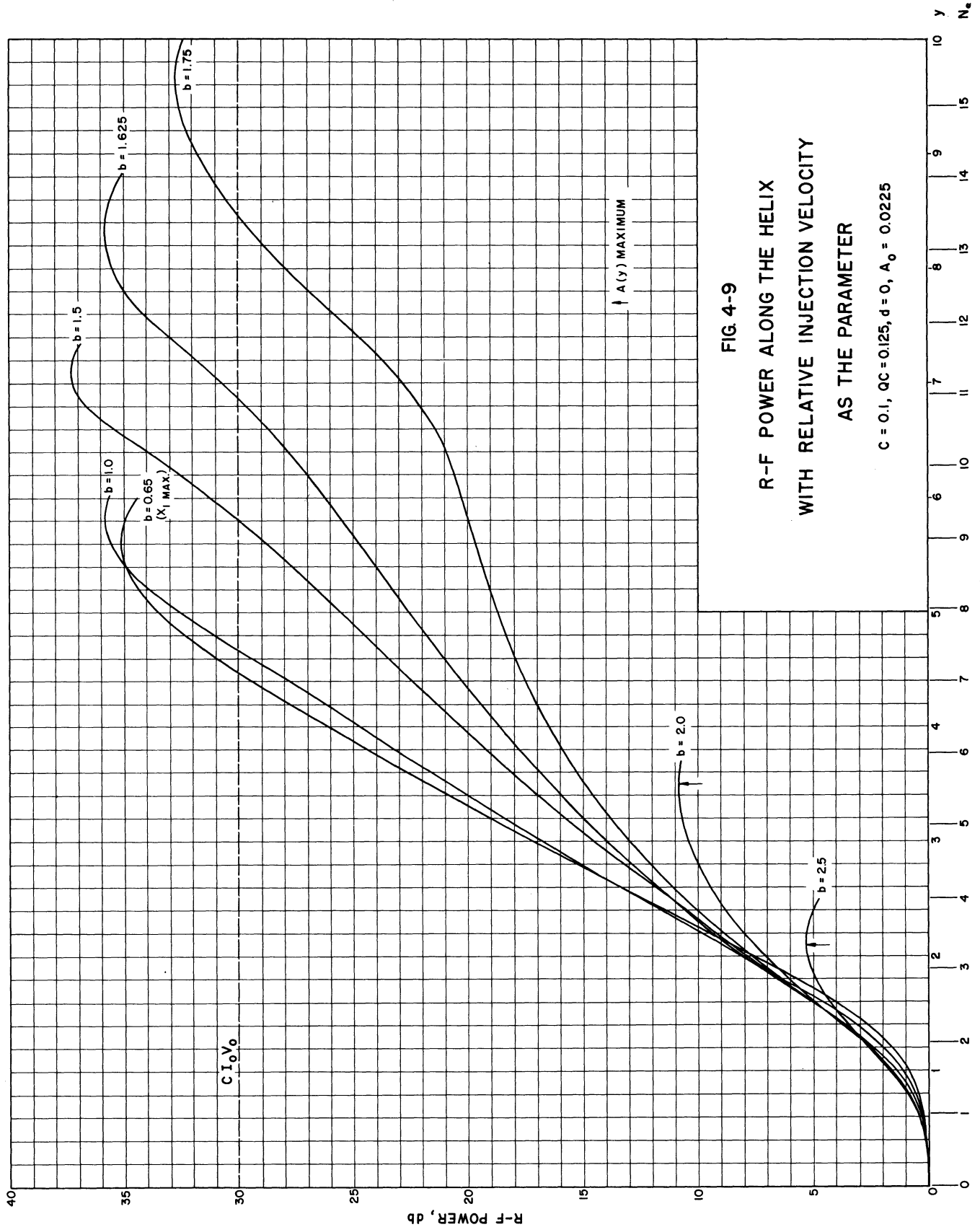

FIG. 4-9

R-F POWER ALONG THE HELIX

WITH RELATIVE INJECTION VELOCITY

AS THE PARAMETER

C = 0.1, QC = 0.125, d = 0, A_0 = 0.0225

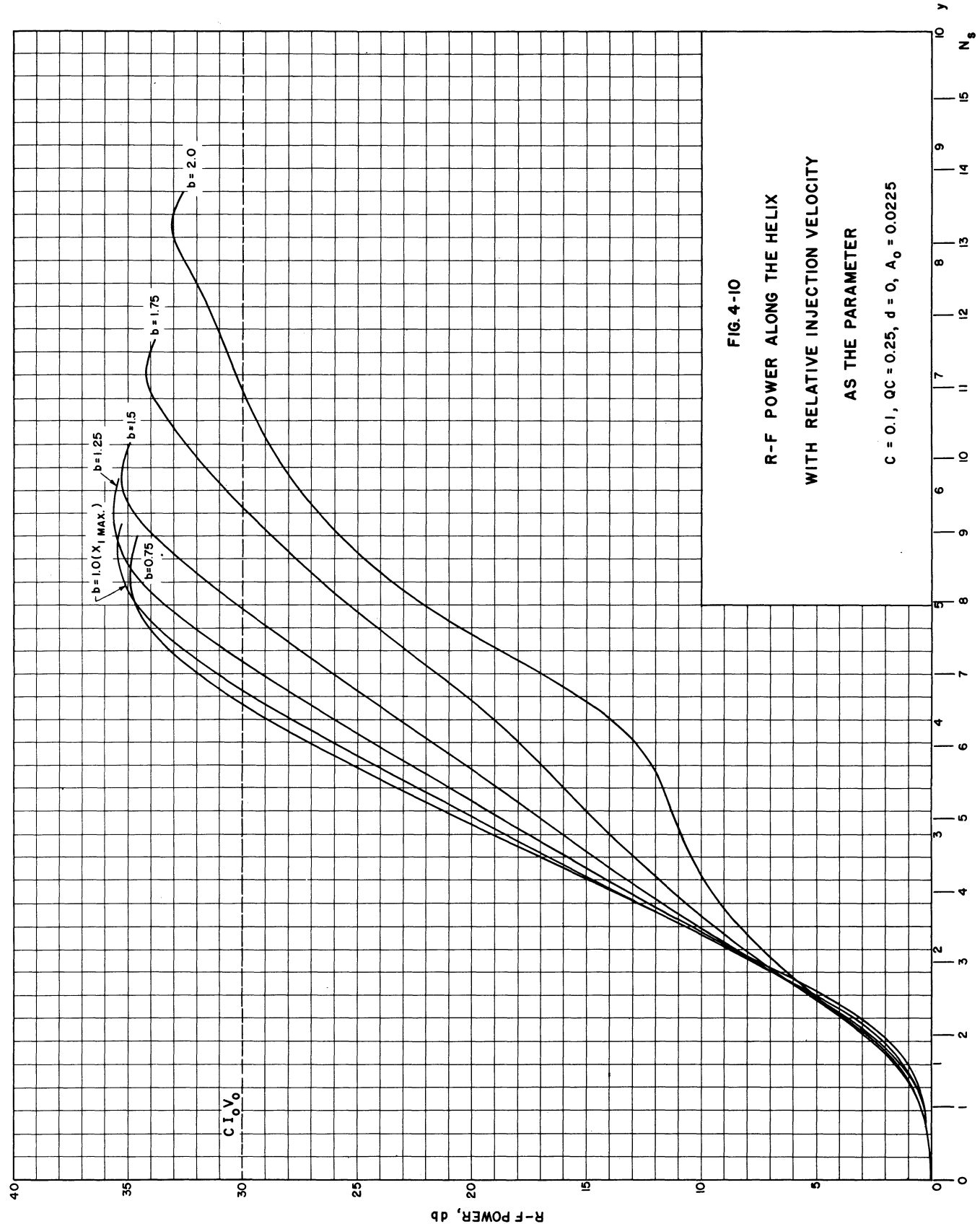

FIG. 4-10

R-F POWER ALONG THE HELIX

WITH RELATIVE INJECTION VELOCITY

AS THE PARAMETER

C = 0.1, QC = 0.25, d = 0, A_o = 0.0225

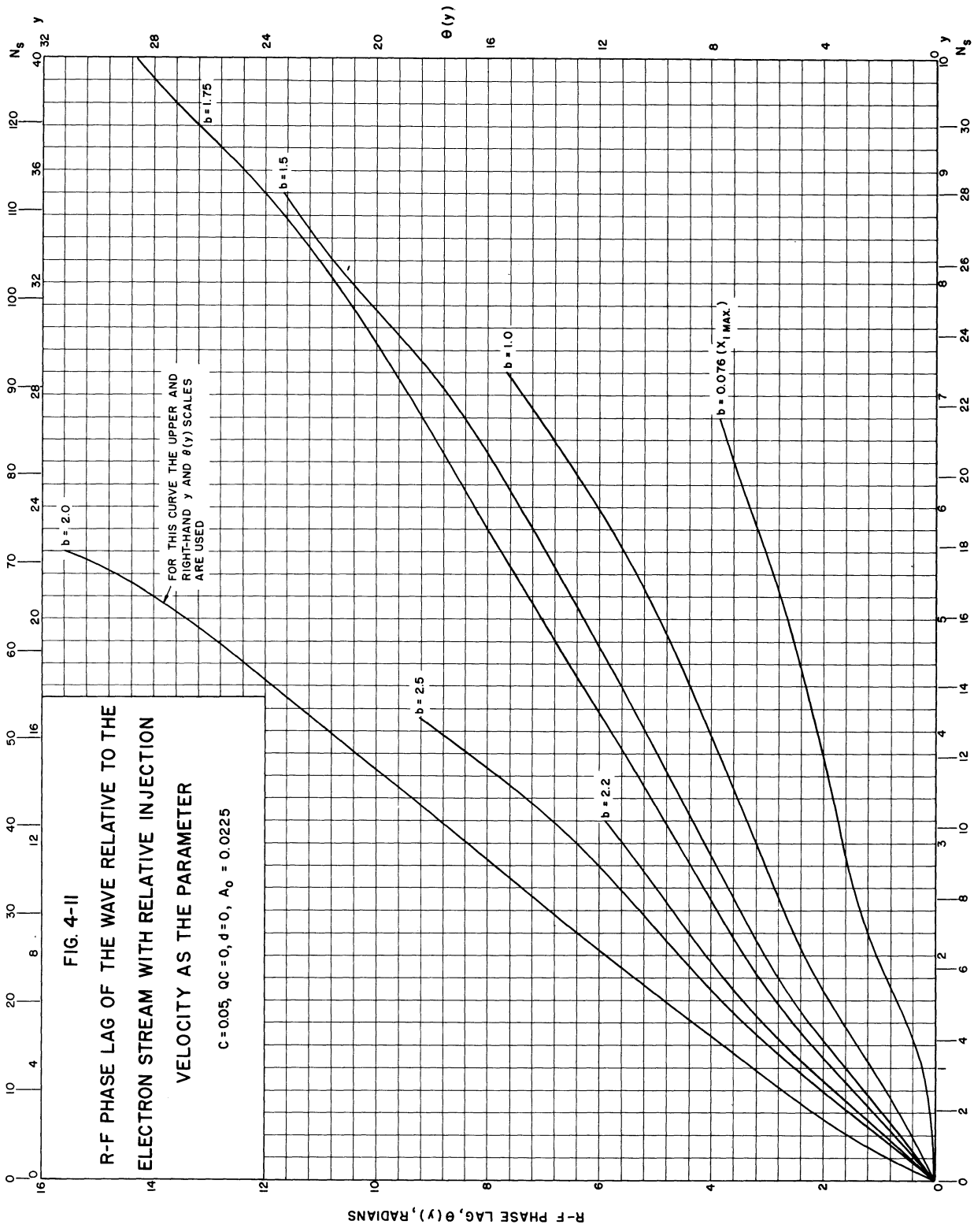

FIG. 4-11

R-F PHASE LAG OF THE WAVE RELATIVE TO THE ELECTRON STREAM WITH RELATIVE INJECTION VELOCITY AS THE PARAMETER

C=0.05, QC=0, d=0, A_0 = 0.0225

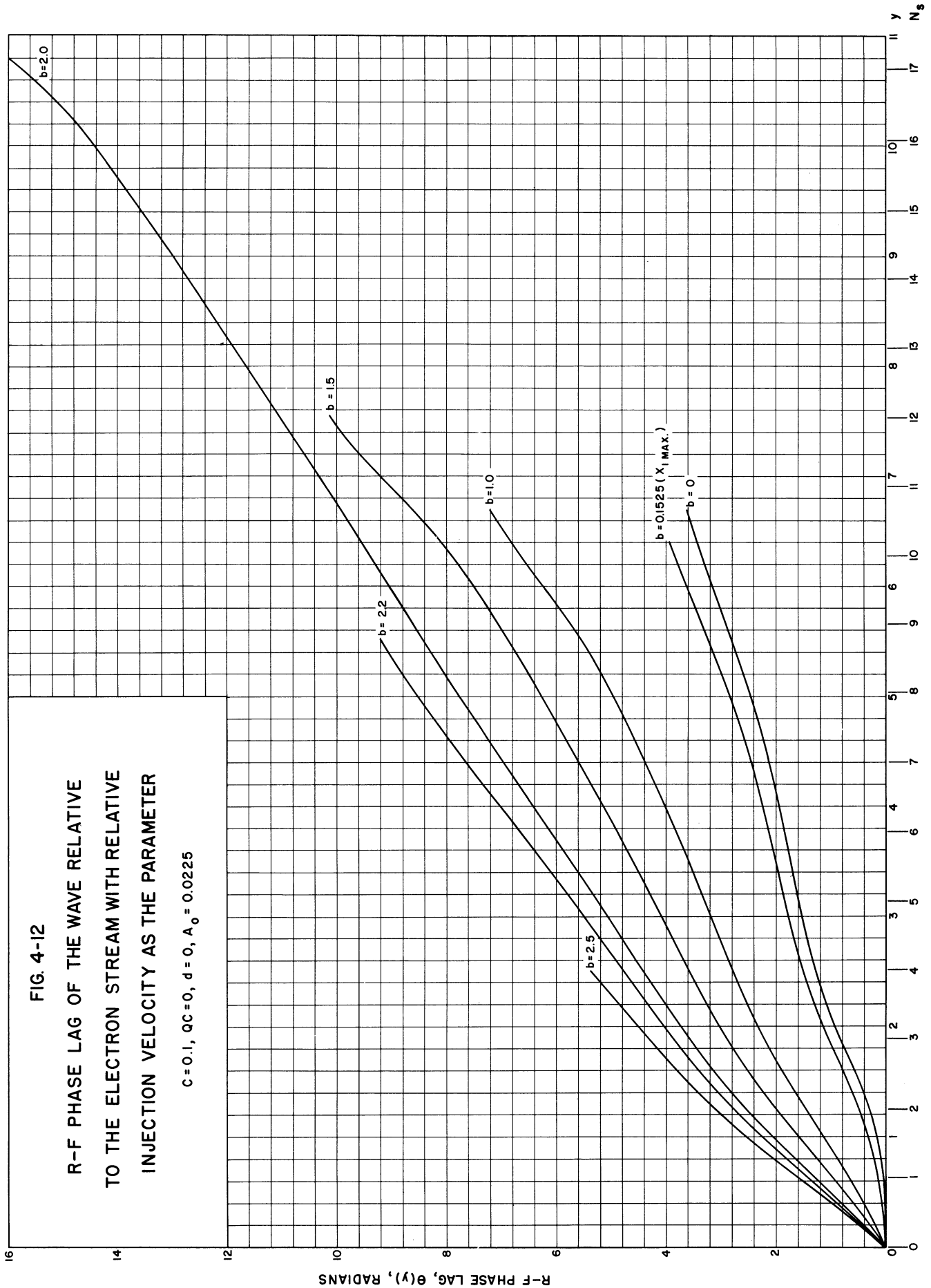

FIG. 4-12

R-F PHASE LAG OF THE WAVE RELATIVE TO THE ELECTRON STREAM WITH RELATIVE INJECTION VELOCITY AS THE PARAMETER

C = 0.1, QC = 0, d = 0, A_0 = 0.0225

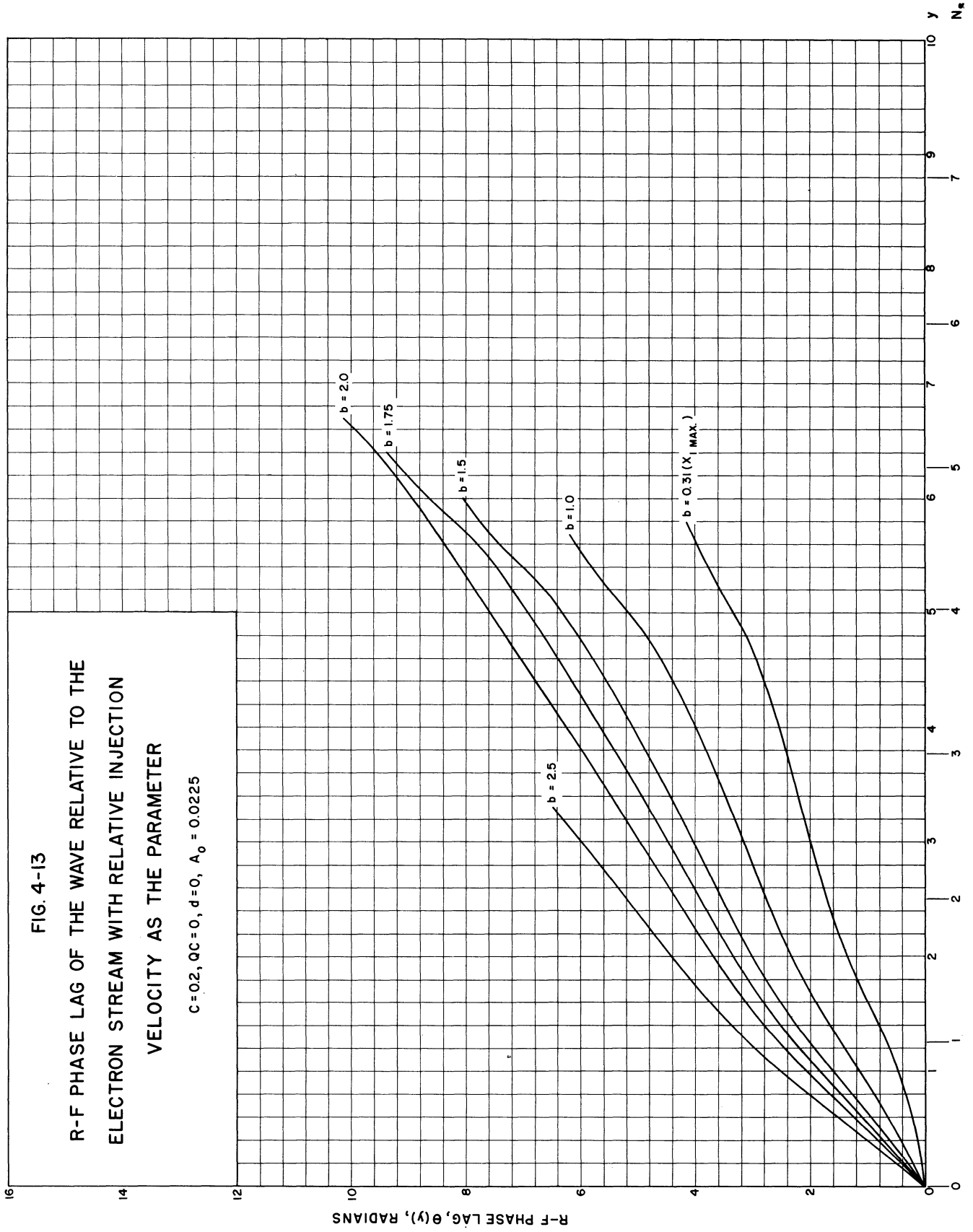
FIG. 4-13
R-F PHASE LAG OF THE WAVE RELATIVE TO THE ELECTRON STREAM WITH RELATIVE INJECTION VELOCITY AS THE PARAMETER
C=0.2, QC=0, d=0, A_0 = 0.0225
b = 2.0
b = 1.75
b = 1.5
b = 1.0
b = 0.31(X MAX.)
b = 2.5
R-F PHASE LAG, θ(y), RADIANS
y
N_s

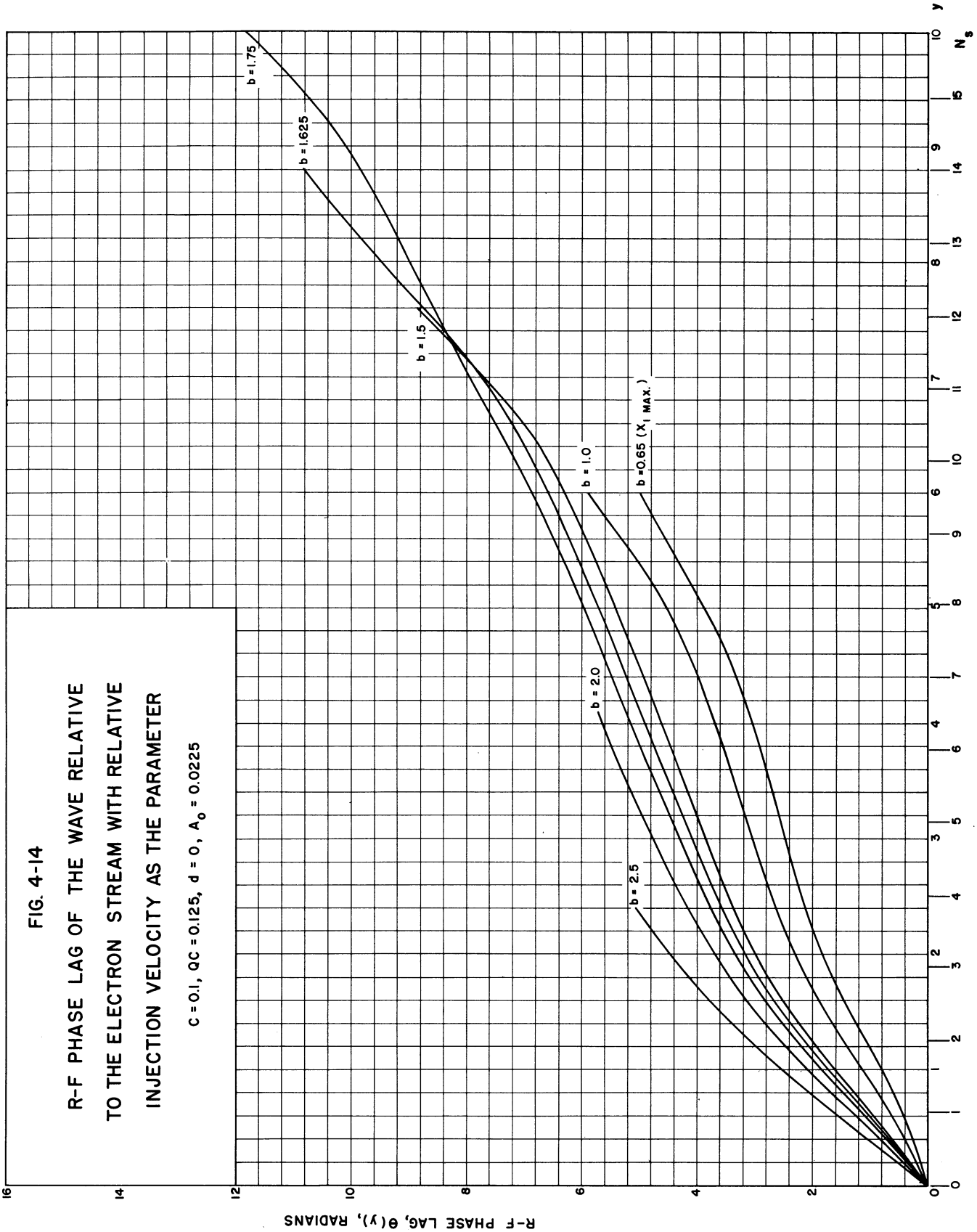

FIG. 4-14

R-F PHASE LAG OF THE WAVE RELATIVE TO THE ELECTRON STREAM WITH RELATIVE INJECTION VELOCITY AS THE PARAMETER

C = 0.1, QC = 0.125, d = 0, A_0 = 0.0225

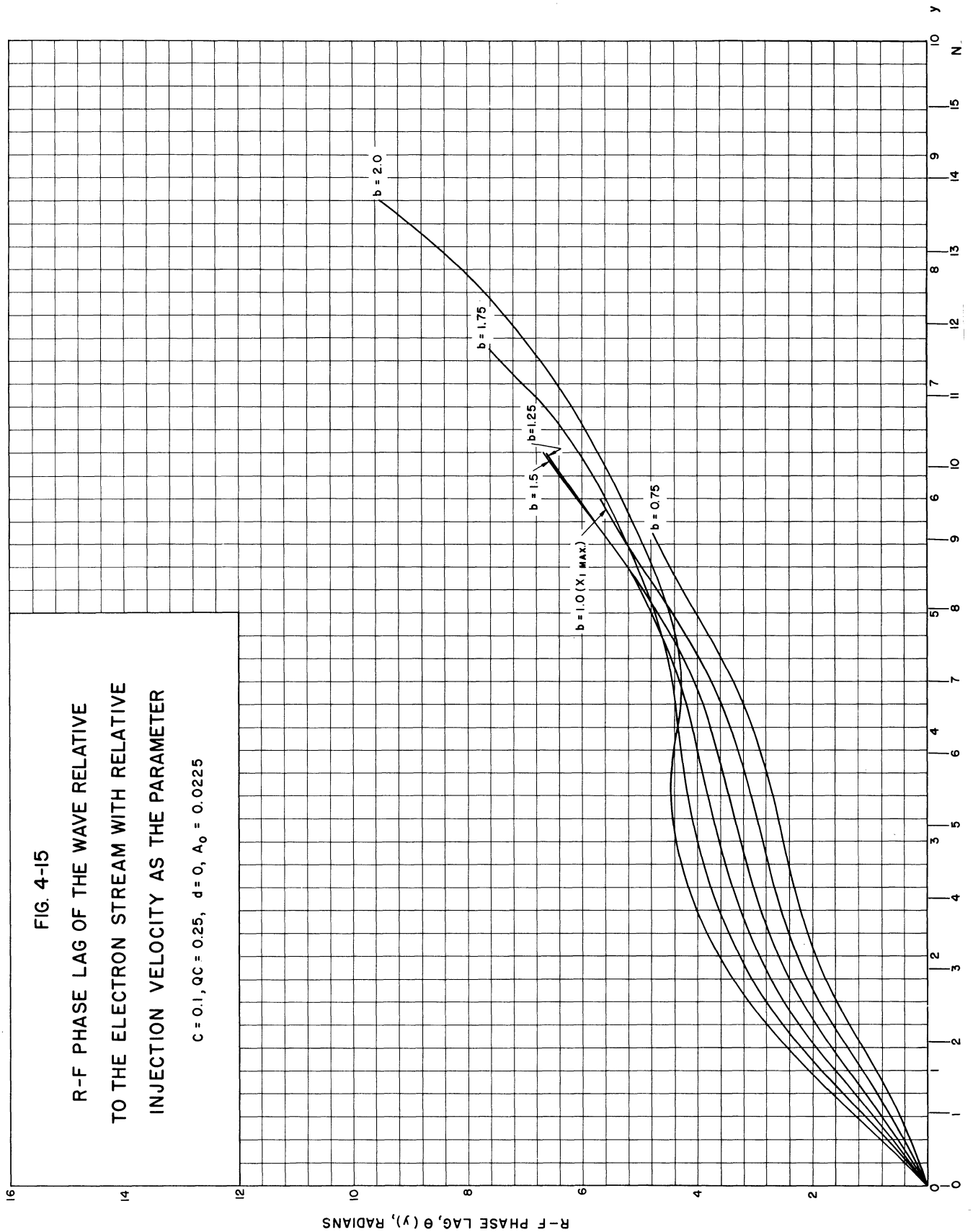

FIG. 4-15

R-F PHASE LAG OF THE WAVE RELATIVE TO THE ELECTRON STREAM WITH RELATIVE INJECTION VELOCITY AS THE PARAMETER

$C = 0.1, QC = 0.25, d = 0, A_0 = 0.0225$

$$v = u_o + v_{pr} = \frac{\omega}{\beta_e + \theta'(y)} \quad . \qquad (4\text{-}3)$$

Hence the phase velocity v_{pr} relative to the stream velocity u_o is

$$v_{pr} = \frac{-u_o\theta'(y)}{\beta_e + \theta'(y)} \quad . \qquad (4\text{-}4)$$

Hence when $\theta'(y)$ is zero as at $y = 3.5$ and 4.4 on the $b = 2.0$ curve of Fig. 4-15, the phase velocity of the wave is equal to u_o. This is the only solution obtained in which this condition occurred, and it should be noted that the b for this case is greater than that for maximum saturation gain. In these regions where the slope of the $\theta(y)$ vs. y curve is zero, the phase velocity of the wave has increased to u_o, since v_{pr} is zero, and as might be expected the interaction between wave and stream accordingly decreases and a low-level saturation is nearly reached, as indicated in the plot of power level vs. distance for this case in Fig. 4-10.

4.3 Electron Phase vs. Initial Phase

Considerable information on the bunching of the electrons in the stream may be obtained from a plot of the dependent variable $\phi(y,\phi_o)$ vs. ϕ_o. The information contained in these curves is the same as that in the flight-line diagrams of Section 4-5 but is plotted in a different manner. $\phi(y,\phi_{oj})$ is the phase of a particular electron relative to the r-f wave on the helix and hence is proportional to the time a particular electron (which entered at a time ϕ_o relative to the r-f wave) arrives at some point y along the tube. Thus the ϕ plots show a distribution of the electrons in time (in electrical radians) for a constant y, and the distribution in y for constant t is the same.

The $\phi(y,\phi_o)$ vs. ϕ_o data could be plotted for all the cases presented in Figs. 4-1 through 4-5, but since the various curves are of a similar nature, a few will serve to indicate the pattern and trends. Graphs of electron phase vs. initial phase are therefore presented as Figs. 4-16 through 4-23 for (1) at QC = 0, the two values of b which are considered to be most significant, namely the b for which the small-signal gain is a maximum at the particular C and QC involved and that value of b for which the saturation gain is a maximum, and (2) at QC = 0.125 and 0.25, only for the b that gives maximum small-signal gain.

Note that only electrons whose initial phases are within the interval 0 to 2π need be considered, since electrons of the same phase or phases which differ by an integral multiple of 2π are acted upon by the same fields and hence move in the same way. Instead of the curves beginning at the origin as is customary for periodic functions, the data have been plotted in the computed sequence. A feature of this system is that a particular electron may be followed through the tube simply by selecting a value of ϕ_o and remaining on that vertical line. The parameter is taken as distance from the input, and for each value of y the r-f signal level on the helix is given in db referenced to the saturation level. Negative values of db indicate power levels below saturation, while positive values indicate that saturation has been passed and the power has decreased by the amount given.

The phenomenon of electron overtaking is depicted in these ϕ vs. ϕ_o curves by regions of zero or negative slope. When this occurs it is evident that ϕ_o is a multi-valued function of ϕ.

In the space-charge cases, some curves had to be faired through the indicated points. The deviations of these points from the smooth curve are due to the inaccuracy involved in evaluating the space-charge weighting function $F(\phi-\phi')$ as indicated in Section 3.5.1.

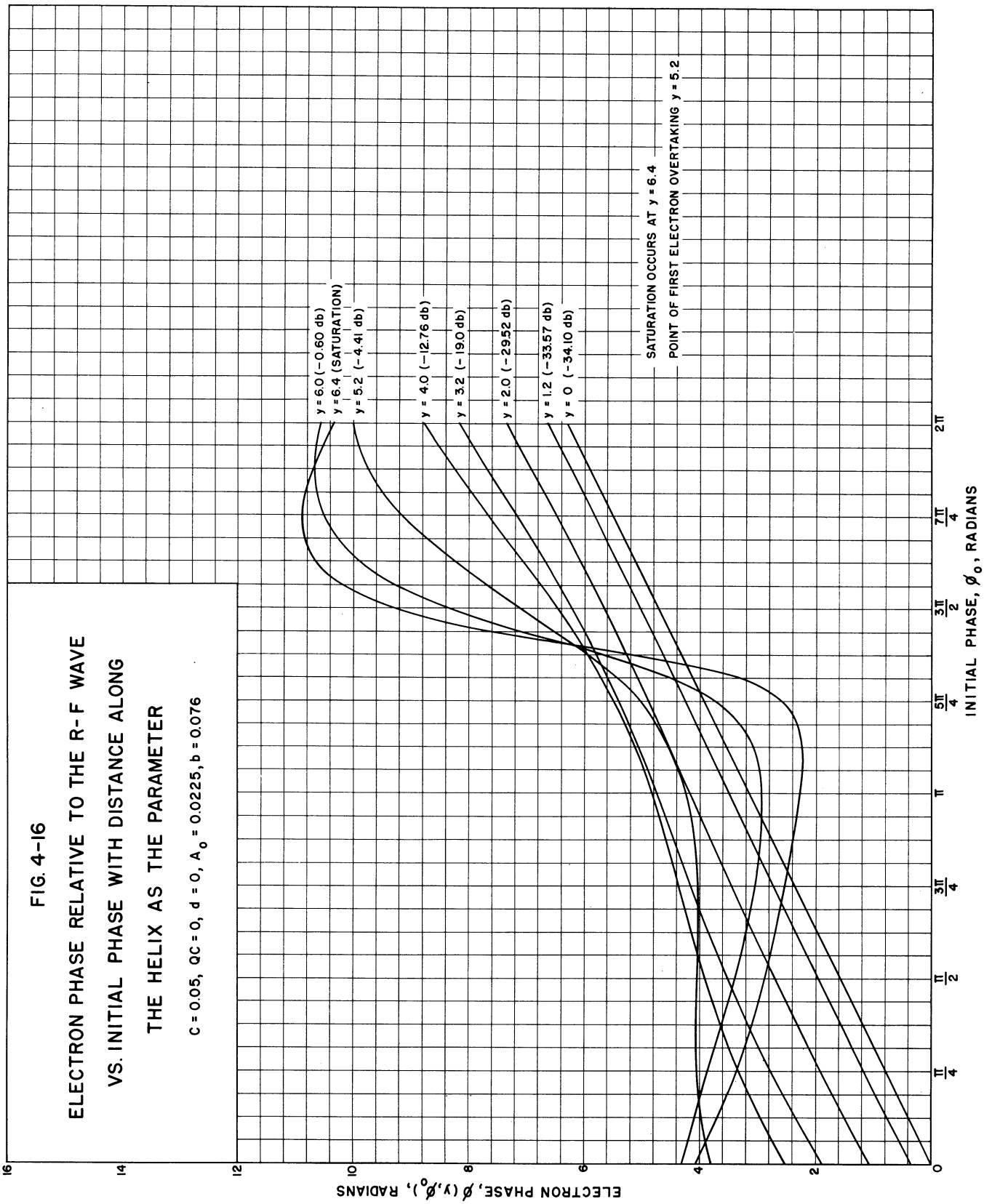

FIG. 4-16

ELECTRON PHASE RELATIVE TO THE R-F WAVE VS. INITIAL PHASE WITH DISTANCE ALONG THE HELIX AS THE PARAMETER

C = 0.05, QC = 0, d = 0, A_o = 0.0225, b = 0.076

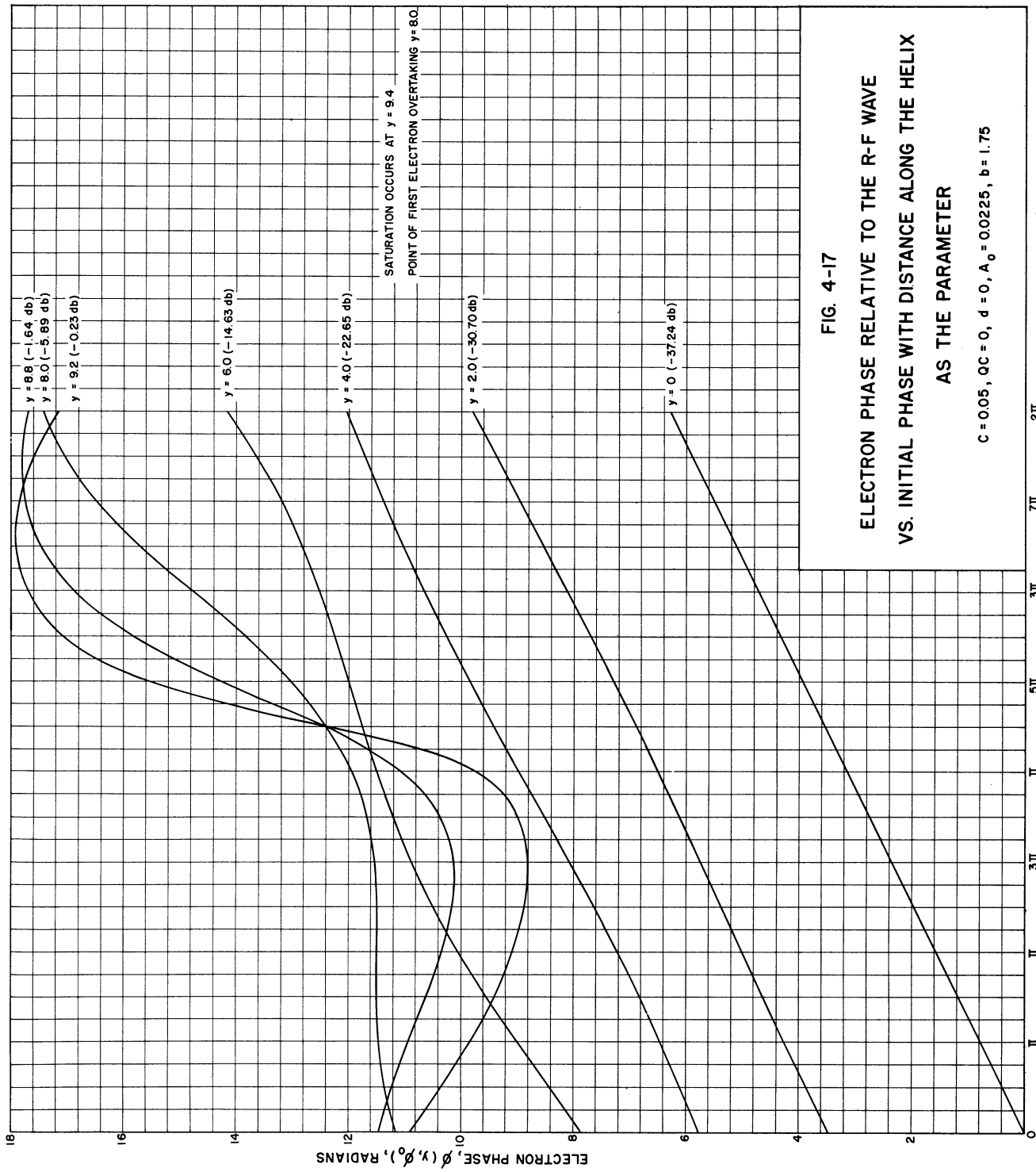

FIG. 4-17

ELECTRON PHASE RELATIVE TO THE R-F WAVE VS. INITIAL PHASE WITH DISTANCE ALONG THE HELIX AS THE PARAMETER

C = 0.05, QC = 0, d = 0, A_o = 0.0225, b = 1.75

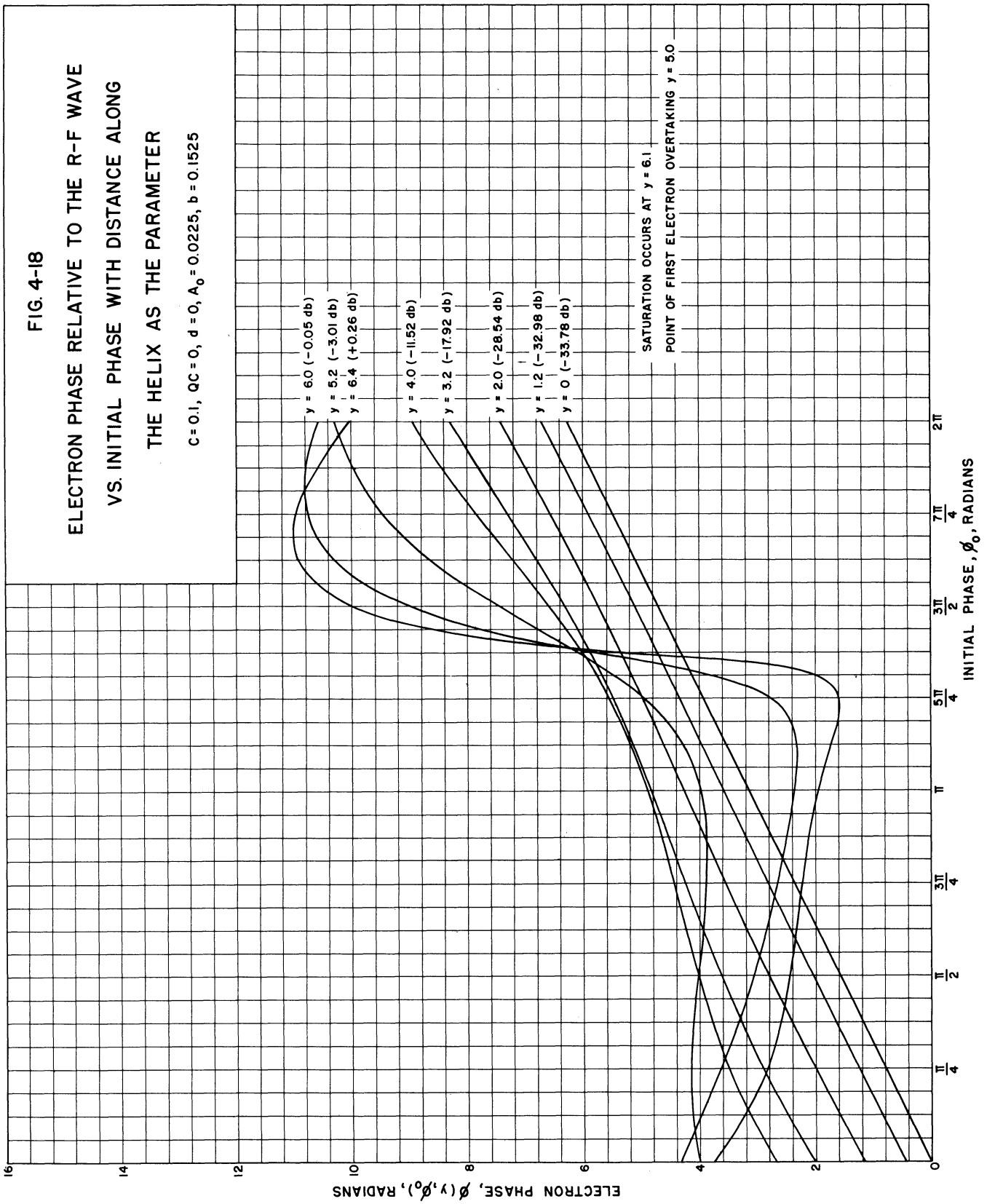
FIG. 4-18
ELECTRON PHASE RELATIVE TO THE R-F WAVE
VS. INITIAL PHASE WITH DISTANCE ALONG
THE HELIX AS THE PARAMETER
C = 0.1, QC = 0, d = 0, A_0 = 0.0225, b = 0.1525
y = 6.0 (−0.05 db)
y = 5.2 (−3.01 db)
y = 6.4 (+0.26 db)
y = 4.0 (−11.52 db)
y = 3.2 (−17.92 db)
y = 2.0 (−28.54 db)
y = 1.2 (−32.98 db)
y = 0 (−33.78 db)
SATURATION OCCURS AT y = 6.1
POINT OF FIRST ELECTRON OVERTAKING y = 5.0
ELECTRON PHASE, ∅(y,∅o), RADIANS
INITIAL PHASE, ∅o, RADIANS

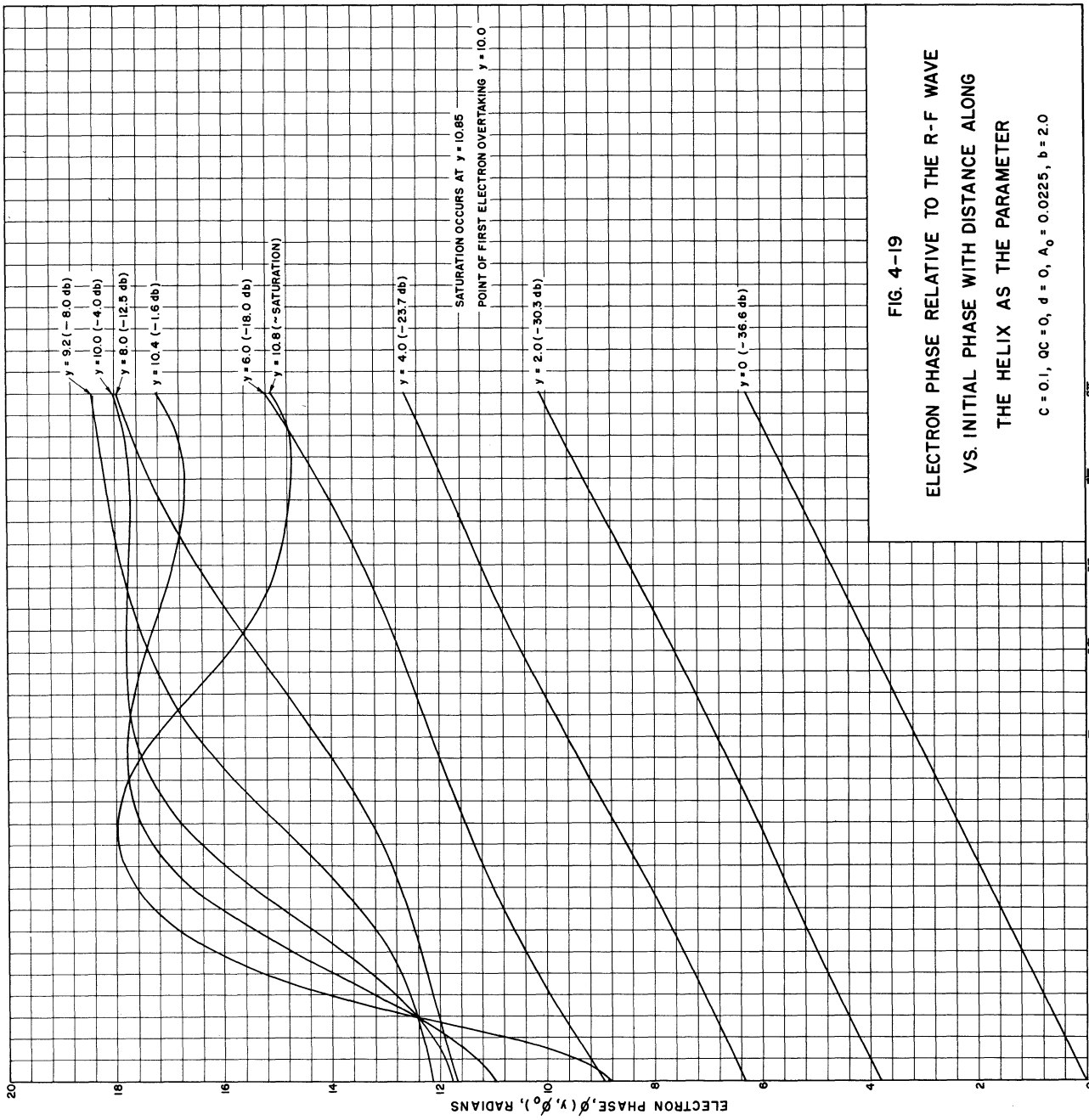

FIG. 4-19

ELECTRON PHASE RELATIVE TO THE R-F WAVE VS. INITIAL PHASE WITH DISTANCE ALONG THE HELIX AS THE PARAMETER

C = 0.1, QC = 0, d = 0, A_0 = 0.0225, b = 2.0

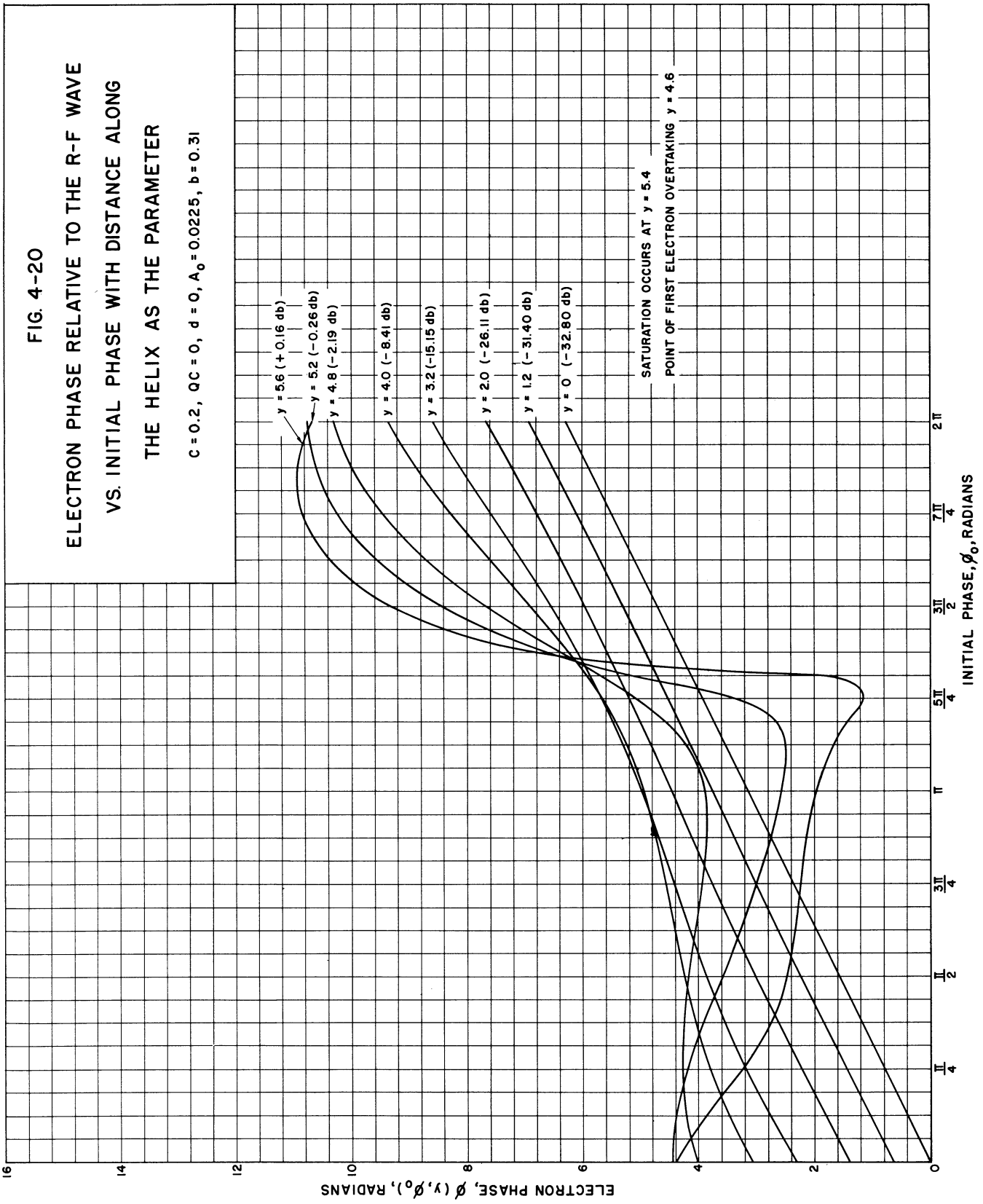

FIG. 4-20

ELECTRON PHASE RELATIVE TO THE R-F WAVE VS. INITIAL PHASE WITH DISTANCE ALONG THE HELIX AS THE PARAMETER

C = 0.2, QC = 0, d = 0, A_0 = 0.0225, b = 0.31

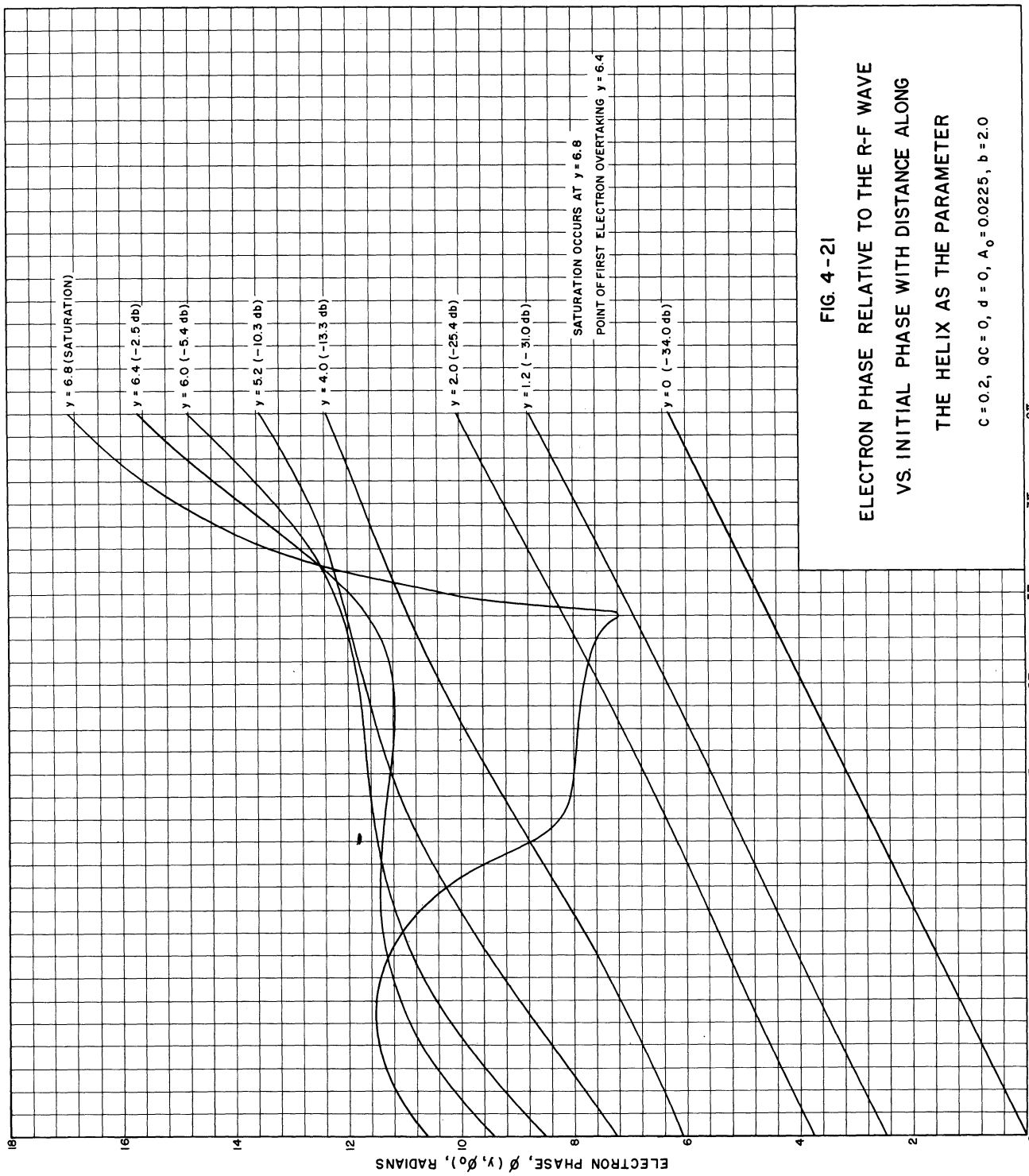

FIG. 4-21

ELECTRON PHASE RELATIVE TO THE R-F WAVE VS. INITIAL PHASE WITH DISTANCE ALONG THE HELIX AS THE PARAMETER

C = 0.2, QC = 0, d = 0, A_o = 0.0225, b = 2.0

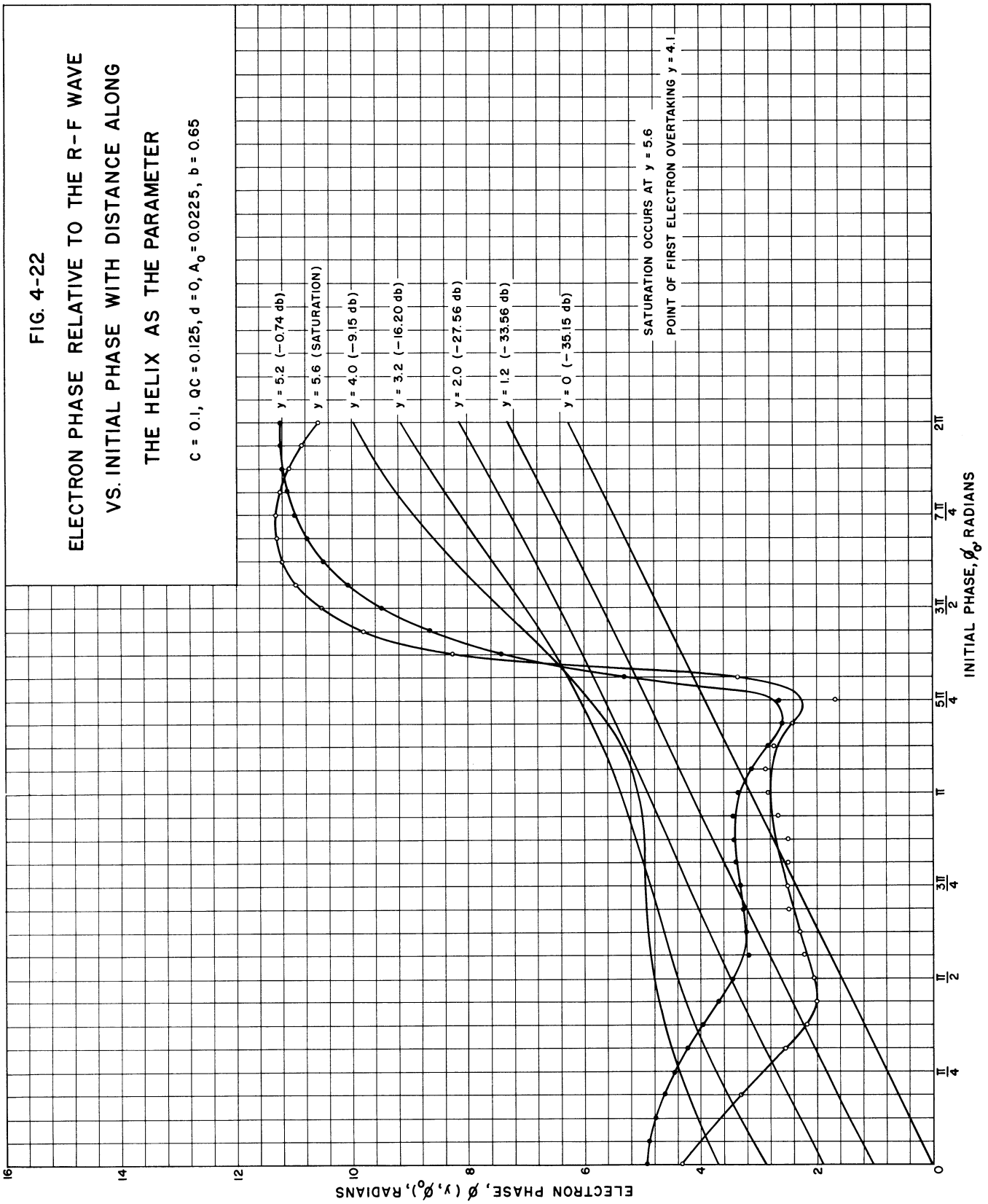
FIG. 4-22
ELECTRON PHASE RELATIVE TO THE R-F WAVE VS. INITIAL PHASE WITH DISTANCE ALONG THE HELIX AS THE PARAMETER
C = 0.1, QC = 0.125, d = 0, A_0 = 0.0225, b = 0.65
y = 5.2 (−0.74 db)
y = 5.6 (SATURATION)
y = 4.0 (−9.15 db)
y = 3.2 (−16.20 db)
y = 2.0 (−27.56 db)
y = 1.2 (−33.56 db)
y = 0 (−35.15 db)
SATURATION OCCURS AT y = 5.6
POINT OF FIRST ELECTRON OVERTAKING y = 4.1
ELECTRON PHASE, ∅ (y, $∅_0$), RADIANS
INITIAL PHASE, $∅_0$, RADIANS
0
2
4
6
8
10
12
14
16
π/4
π/2
3π/4
π
5π/4
3π/2
7π/4
2π

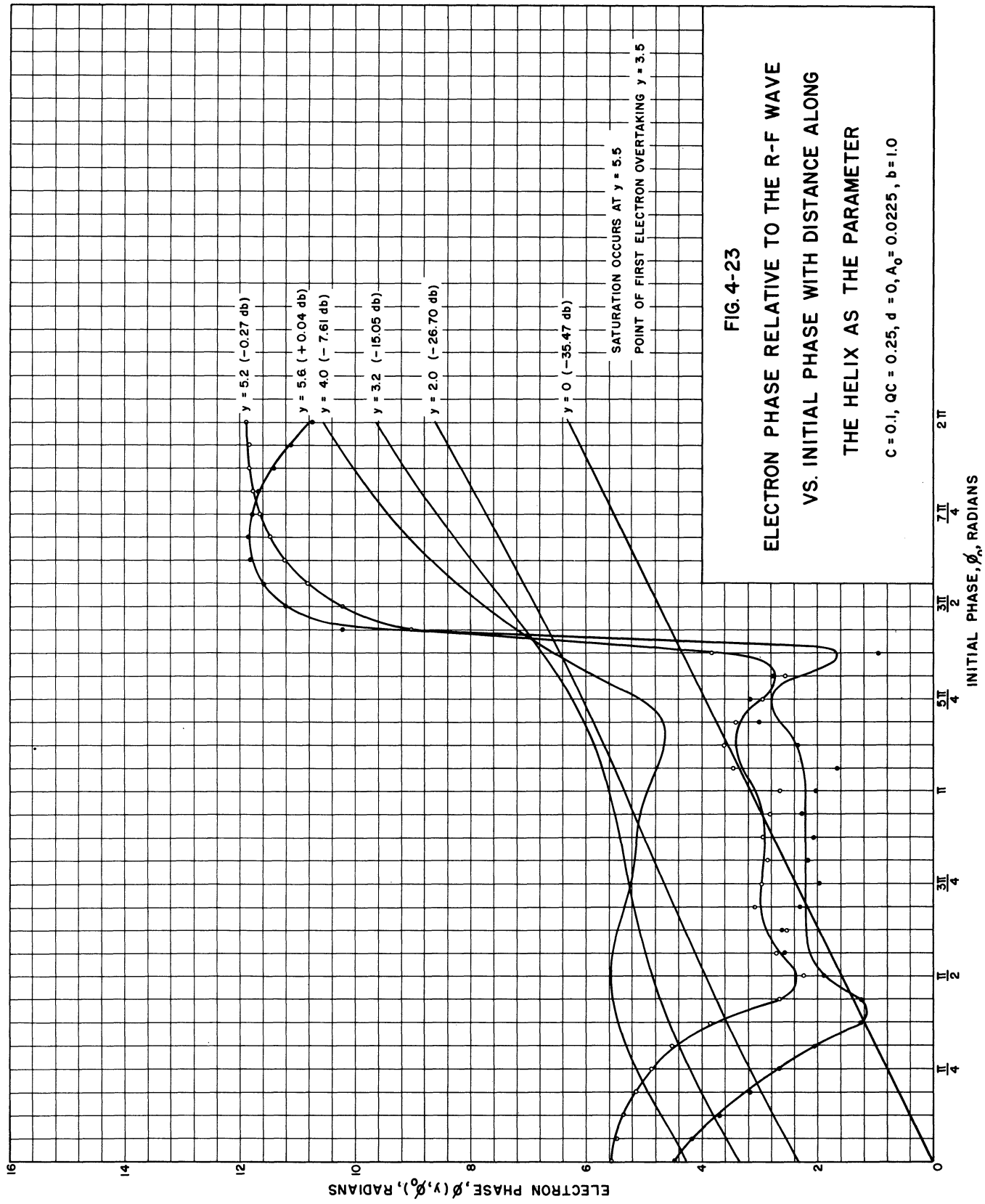
FIG. 4-23
ELECTRON PHASE RELATIVE TO THE R-F WAVE
VS. INITIAL PHASE WITH DISTANCE ALONG
THE HELIX AS THE PARAMETER
C = 0.1, QC = 0.25, d = 0, A_0 = 0.0225, b = 1.0
SATURATION OCCURS AT y = 5.5
POINT OF FIRST ELECTRON OVERTAKING y = 3.5
y = 5.2 (−0.27 db)
y = 5.6 (+0.04 db)
y = 4.0 (− 7.61 db)
y = 3.2 (−15.05 db)
y = 2.0 (−26.70 db)
y = 0 (−35.47 db)
ELECTRON PHASE, $\phi(y,\phi_0)$, RADIANS
INITIAL PHASE, ϕ_0, RADIANS
0
2
4
6
8
10
12
14
16
$\frac{\pi}{4}$
$\frac{\pi}{2}$
$\frac{3\pi}{4}$
π
$\frac{5\pi}{4}$
$\frac{3\pi}{2}$
$\frac{7\pi}{4}$
2π

4.4 Normalized Electron Velocity Deviation

4.4.1 Velocity Deviation vs. Initial Phase. The total velocity of an electron as a function of position is given by the expression

$$u_t(y,\phi_o) = u_o[1 + 2Cu(y,\phi_o)] \quad . \qquad (2\text{-}14)$$

In this equation it can be seen that the quantity $2Cu(y,\phi_o)$ is the normalized fractional velocity deviation from u_o for a particular electron. This velocity deviation term is plotted against the initial phase ϕ_o in Figs. 4-24 through 4-31 for the same values of b as those for which the electron-phase curves are presented in Section 4.3. The parameter is again distance measured from the input, and the signal level for each y is given in db relative to the saturation level.

In these curves the maximum percent velocity deviation increases as saturation is approached and has its largest value there. The maximum percent deviation at saturation increases with increasing C. With b adjusted for maximum saturation gain, C values of 0.05, 0.1, and 0.2 correspond to maximum saturation velocity deviations of 24, 50, and 86 percent respectively at QC = 0. At QC = 0.125 and 0.25 the maximum saturation velocity deviations are 55 and 40 percent respectively. For still larger QC values the maximum percent velocity deviation at saturation should continue to decrease.

For the cases in which $QC \neq 0$ the results were somewhat inaccurate, especially in regions where overtaking occurs, due to errors in evaluating the space-charge forces as discussed in Section 3.5.1. When this occurs the computed points are indicated on the graphs and a curve faired through them. As pointed out earlier, the dependent variables A(y) and $\Theta(y)$ are relatively insensitive to errors in the variables $\phi(y,\phi_o)$ and $u(y,\phi_o)$.

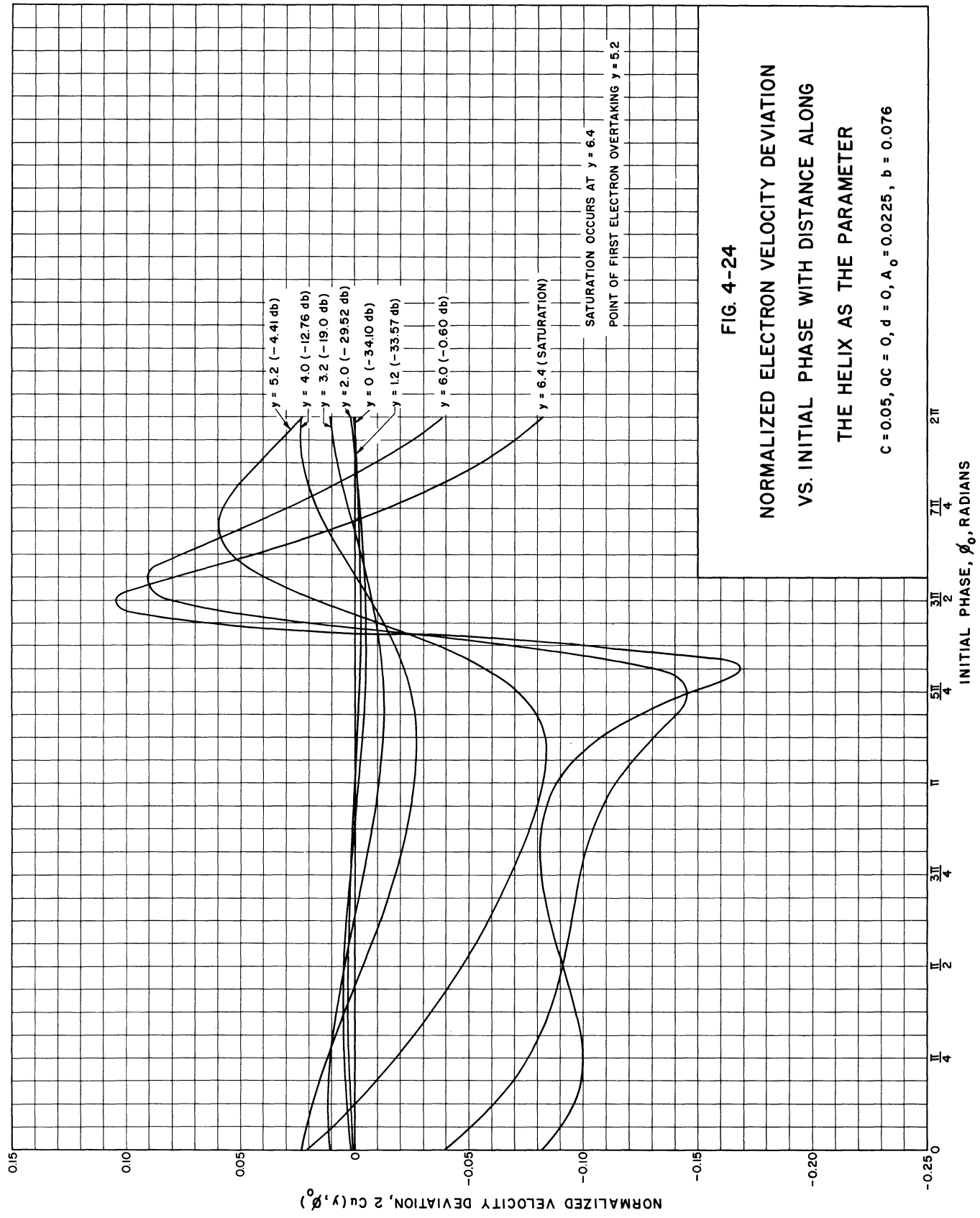
FIG. 4-24
NORMALIZED ELECTRON VELOCITY DEVIATION
VS. INITIAL PHASE WITH DISTANCE ALONG
THE HELIX AS THE PARAMETER
C = 0.05, QC = 0, d = 0, A_0 = 0.0225, b = 0.076
y = 5.2 (−4.41 db)
y = 4.0 (−12.76 db)
y = 3.2 (−19.0 db)
y = 2.0 (−29.52 db)
y = 0 (−34.10 db)
y = 1.2 (−33.57 db)
y = 6.0 (−0.60 db)
y = 6.4 (SATURATION)
SATURATION OCCURS AT y = 6.4
POINT OF FIRST ELECTRON OVERTAKING y = 5.2
NORMALIZED VELOCITY DEVIATION, 2 Cu(y, ϕ_0)
INITIAL PHASE, ϕ_0, RADIANS
0.15
0.10
0.05
0
−0.05
−0.10
−0.15
−0.20
−0.25
0
π/4
π/2
3π/4
π
5π/4
3π/2
7π/4
2π

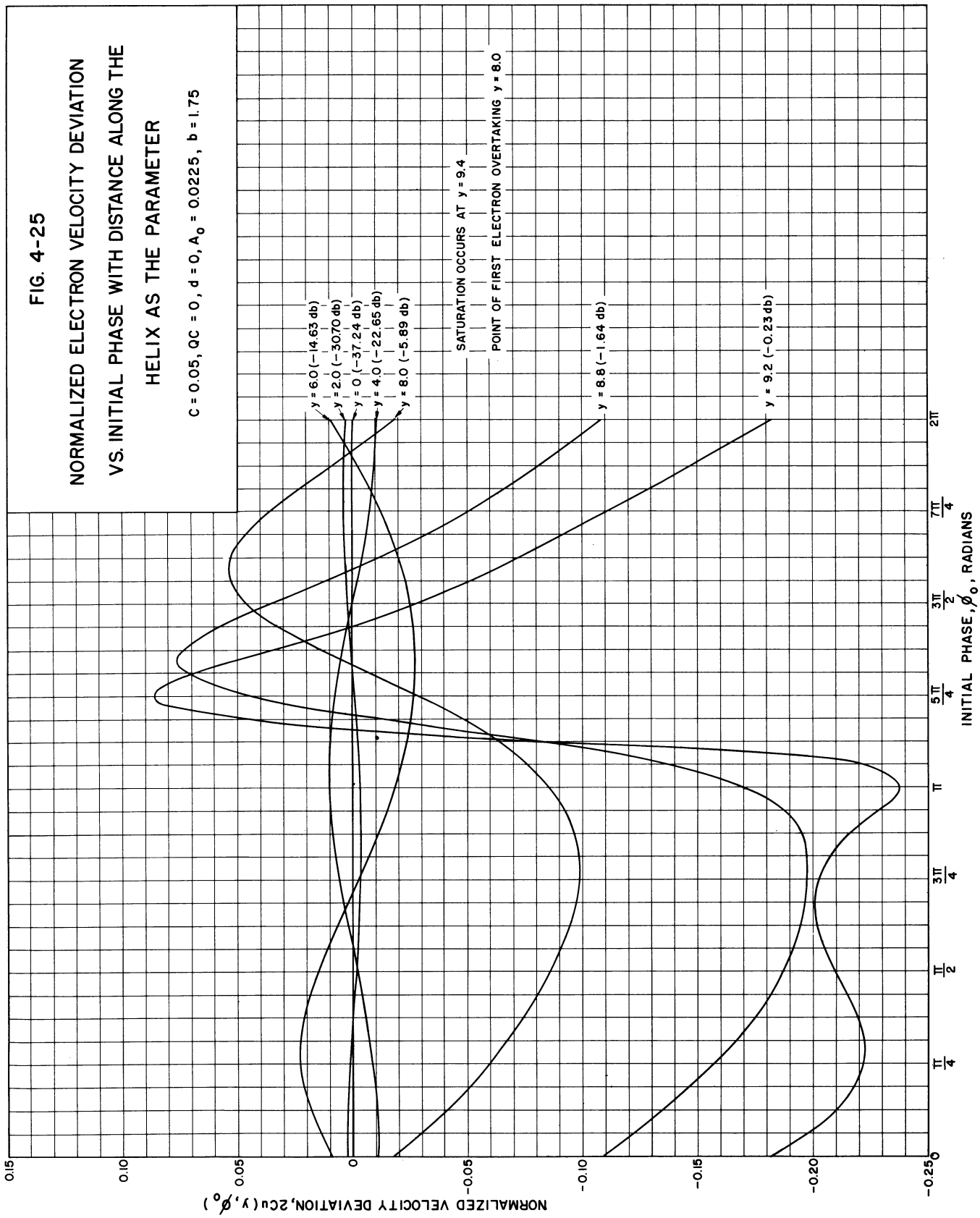
FIG. 4-25
NORMALIZED ELECTRON VELOCITY DEVIATION
VS. INITIAL PHASE WITH DISTANCE ALONG THE
HELIX AS THE PARAMETER
C = 0.05, QC = 0, d = 0, A_0 = 0.0225, b = 1.75
y = 6.0 (−14.63 db)
y = 2.0 (−30.70 db)
y = 0 (−37.24 db)
y = 4.0 (−22.65 db)
y = 8.0 (−5.89 db)
SATURATION OCCURS AT y = 9.4
POINT OF FIRST ELECTRON OVERTAKING y = 8.0
y = 8.8 (−1.64 db)
y = 9.2 (−0.23 db)
NORMALIZED VELOCITY DEVIATION, $2C u(y, \phi_0)$
0.15
0.10
0.05
0
-0.05
-0.10
-0.15
-0.20
-0.25
0
$\frac{\pi}{4}$
$\frac{\pi}{2}$
$\frac{3\pi}{4}$
π
$\frac{5\pi}{4}$
$\frac{3\pi}{2}$
$\frac{7\pi}{4}$
2π
INITIAL PHASE, ϕ_0, RADIANS

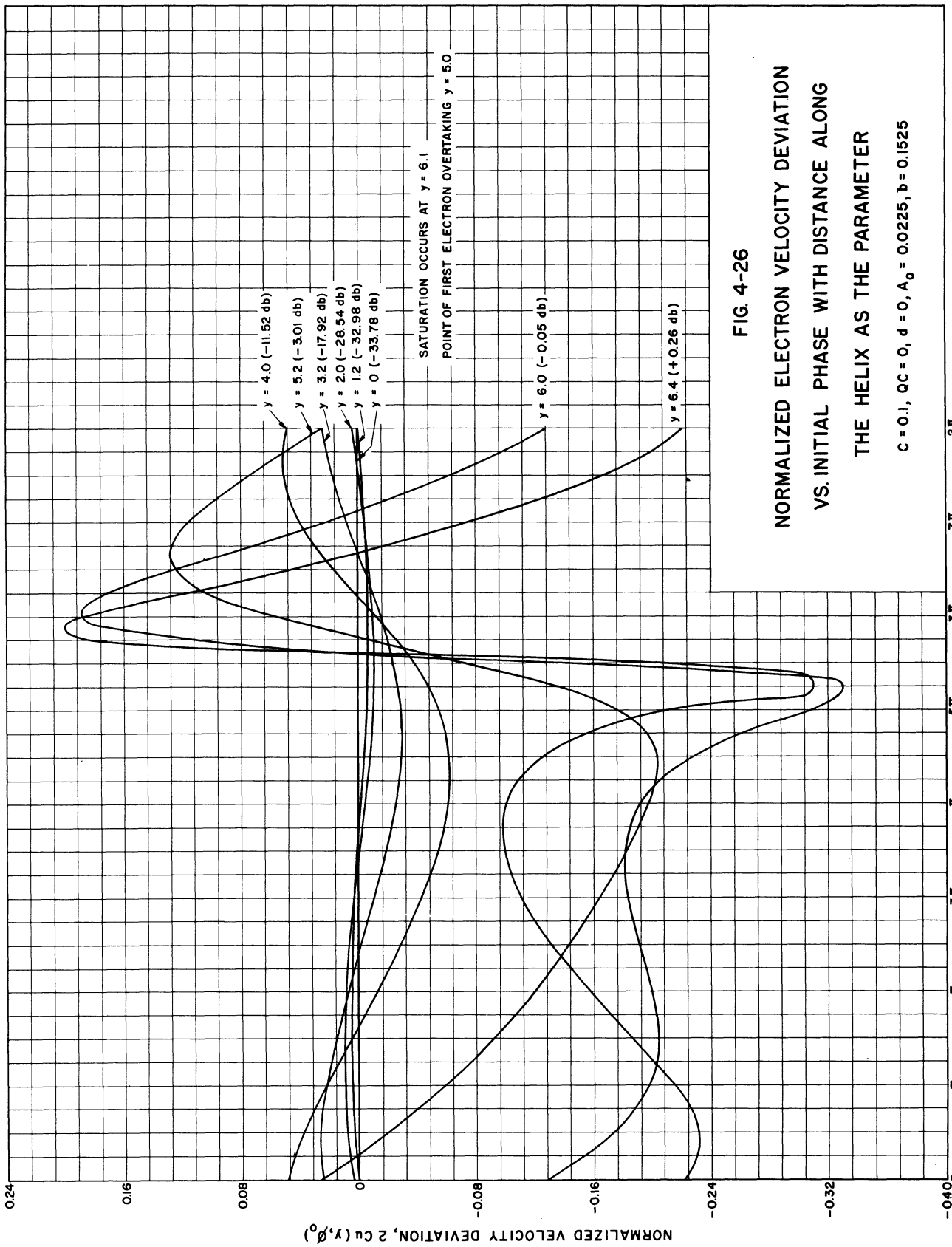
FIG. 4-26
NORMALIZED ELECTRON VELOCITY DEVIATION
VS. INITIAL PHASE WITH DISTANCE ALONG
THE HELIX AS THE PARAMETER
C = 0.1, QC = 0, d = 0, A0 = 0.0225, b = 0.1525
SATURATION OCCURS AT y = 6.1
POINT OF FIRST ELECTRON OVERTAKING y = 5.0
y = 4.0 (−11.52 db)
y = 5.2 (−3.01 db)
y = 3.2 (−17.92 db)
y = 2.0 (−28.54 db)
y = 1.2 (−32.98 db)
y = 0 (−33.78 db)
y = 6.0 (−0.05 db)
y = 6.4 (+0.26 db)
NORMALIZED VELOCITY DEVIATION, 2 Cu (y,ø0)
0.24
0.16
0.08
0
-0.08
-0.16
-0.24
-0.32
-0.40
0
π/4
π/2
3π/4
π
5π/4
3π/2
7π/4
2π
INITIAL PHASE, ø0, RADIANS

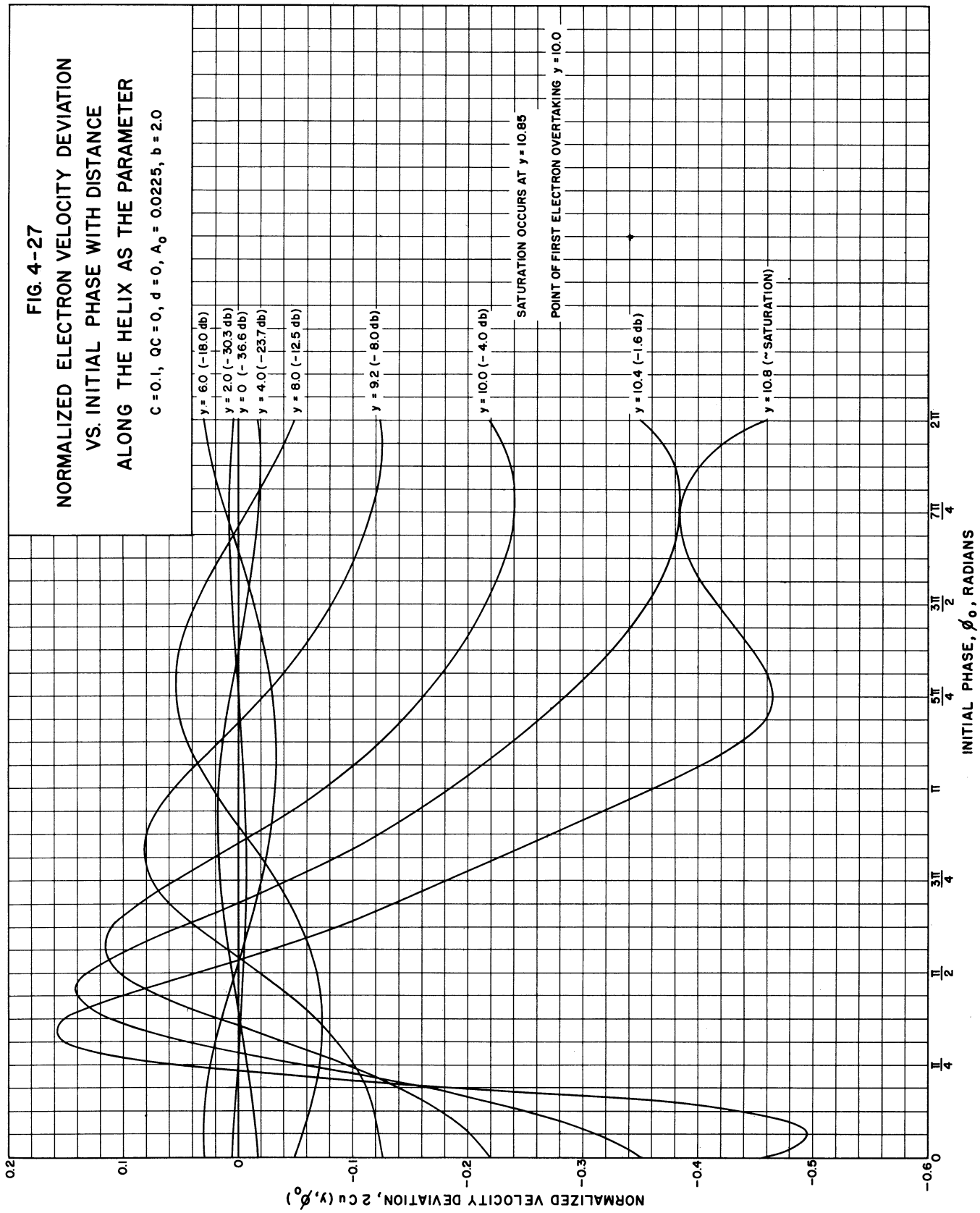
FIG. 4-27
NORMALIZED ELECTRON VELOCITY DEVIATION
VS. INITIAL PHASE WITH DISTANCE
ALONG THE HELIX AS THE PARAMETER
C = 0.1, QC = 0, d = 0, A_0 = 0.0225, b = 2.0
y = 6.0 (-18.0 db)
y = 2.0 (- 30.3 db)
y = 0 (- 36.6 db)
y = 4.0 (-23.7 db)
y = 8.0 (-12.5 db)
y = 9.2 (- 8.0 db)
y = 10.0 (- 4.0 db)
SATURATION OCCURS AT y = 10.85
POINT OF FIRST ELECTRON OVERTAKING y = 10.0
y = 10.4 (-1.6 db)
y = 10.8 (~SATURATION)
NORMALIZED VELOCITY DEVIATION, 2 C u (y, ϕ_0)
INITIAL PHASE, ϕ_0, RADIANS
0.2
0.1
0
-0.1
-0.2
-0.3
-0.4
-0.5
-0.6
0
$\frac{\pi}{4}$
$\frac{\pi}{2}$
$\frac{3\pi}{4}$
π
$\frac{5\pi}{4}$
$\frac{3\pi}{2}$
$\frac{7\pi}{4}$
2π

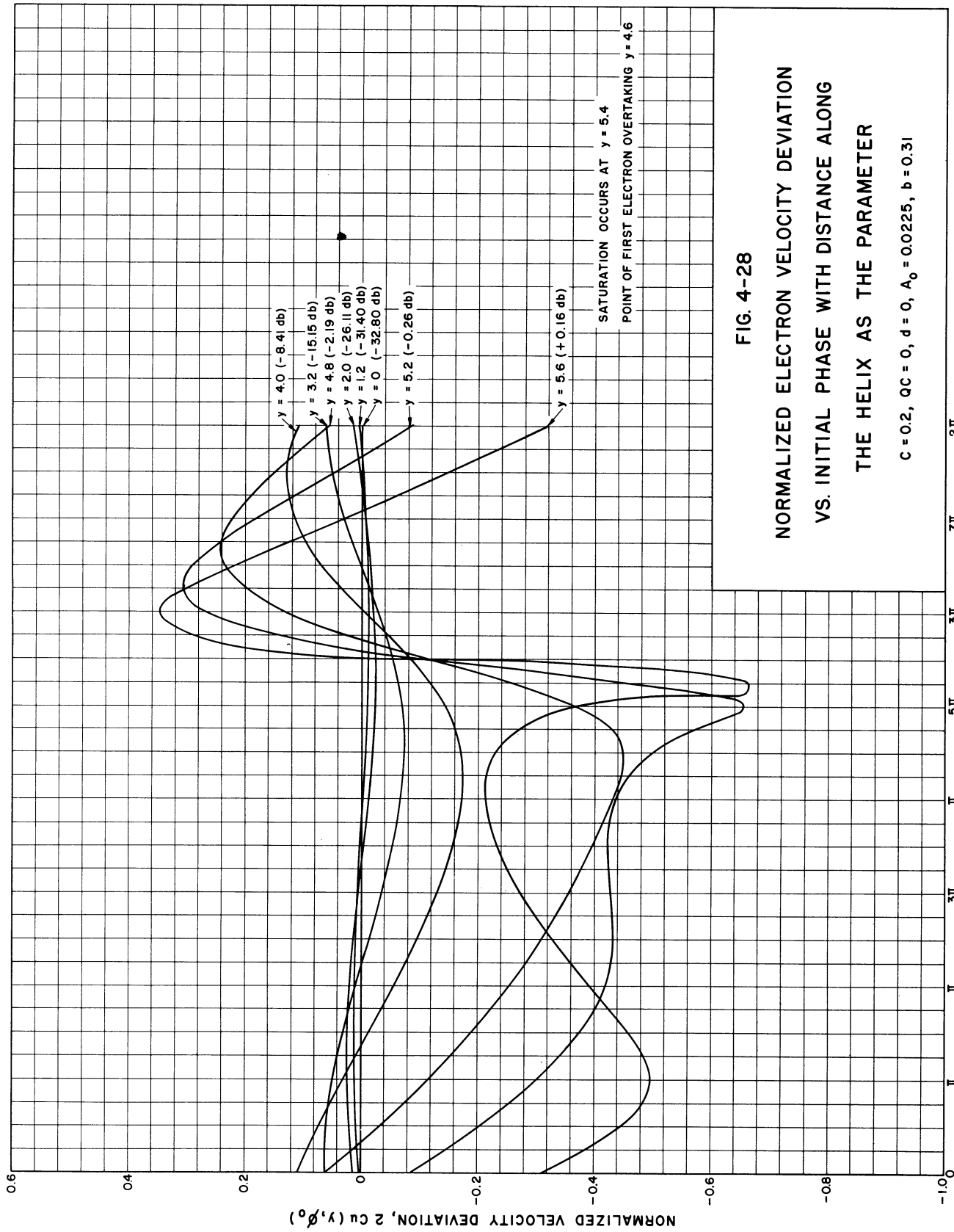
FIG. 4-28
NORMALIZED ELECTRON VELOCITY DEVIATION
VS. INITIAL PHASE WITH DISTANCE ALONG
THE HELIX AS THE PARAMETER
C = 0.2, QC = 0, d = 0, A_0 = 0.0225, b = 0.31
SATURATION OCCURS AT y = 5.4
POINT OF FIRST ELECTRON OVERTAKING y = 4.6
y = 4.0 (-8.41 db)
y = 3.2 (-15.15 db)
y = 4.8 (-2.19 db)
y = 2.0 (-26.11 db)
y = 1.2 (-31.40 db)
y = 0 (-32.80 db)
y = 5.2 (-0.26 db)
y = 5.6 (+0.16 db)
NORMALIZED VELOCITY DEVIATION, 2 Cu (y, ϕ_0)
0.6
0.4
0.2
0
-0.2
-0.4
-0.6
-0.8
-1.0
$\frac{\pi}{4}$
$\frac{\pi}{2}$
$\frac{3\pi}{4}$
π
$\frac{5\pi}{4}$
$\frac{3\pi}{2}$
$\frac{7\pi}{4}$
2π
INITIAL PHASE, ϕ_0, RADIANS

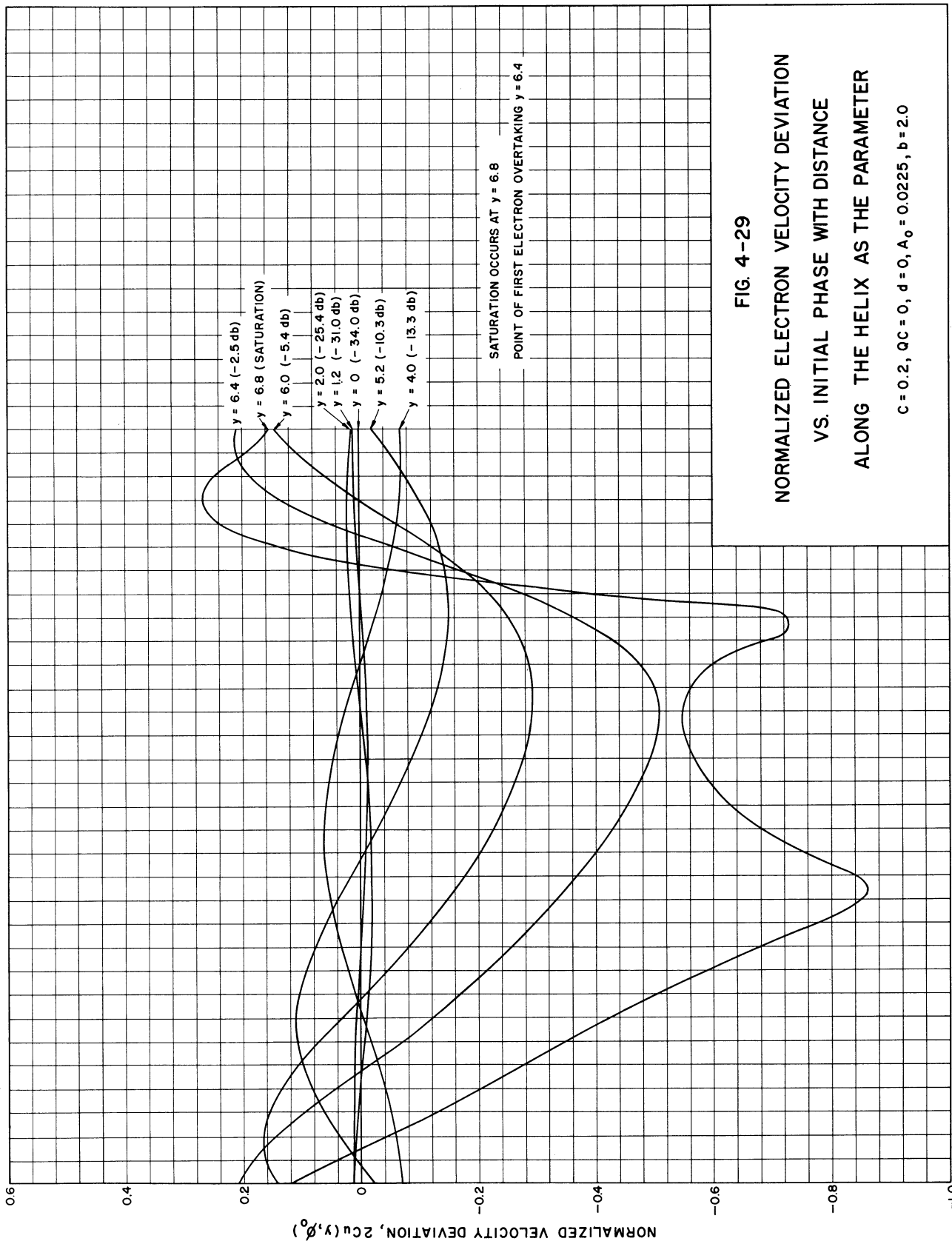
FIG. 4-29
NORMALIZED ELECTRON VELOCITY DEVIATION
VS. INITIAL PHASE WITH DISTANCE
ALONG THE HELIX AS THE PARAMETER
C = 0.2, QC = 0, d = 0, A_o = 0.0225, b = 2.0
SATURATION OCCURS AT y = 6.8
POINT OF FIRST ELECTRON OVERTAKING y = 6.4
y = 6.4 (−2.5 db)
y = 6.8 (SATURATION)
y = 6.0 (−5.4 db)
y = 2.0 (−25.4 db)
y = 1.2 (−31.0 db)
y = 0 (−34.0 db)
y = 5.2 (−10.3 db)
y = 4.0 (−13.3 db)
NORMALIZED VELOCITY DEVIATION, 2Cu(y,ϕ_o)
0.6
0.4
0.2
0
−0.2
−0.4
−0.6
−0.8
−1.0
0
$\frac{\pi}{4}$
$\frac{\pi}{2}$
$\frac{3\pi}{4}$
π
$\frac{5\pi}{4}$
$\frac{3\pi}{2}$
$\frac{7\pi}{4}$
2π
INITIAL PHASE, ϕ_o, RADIANS

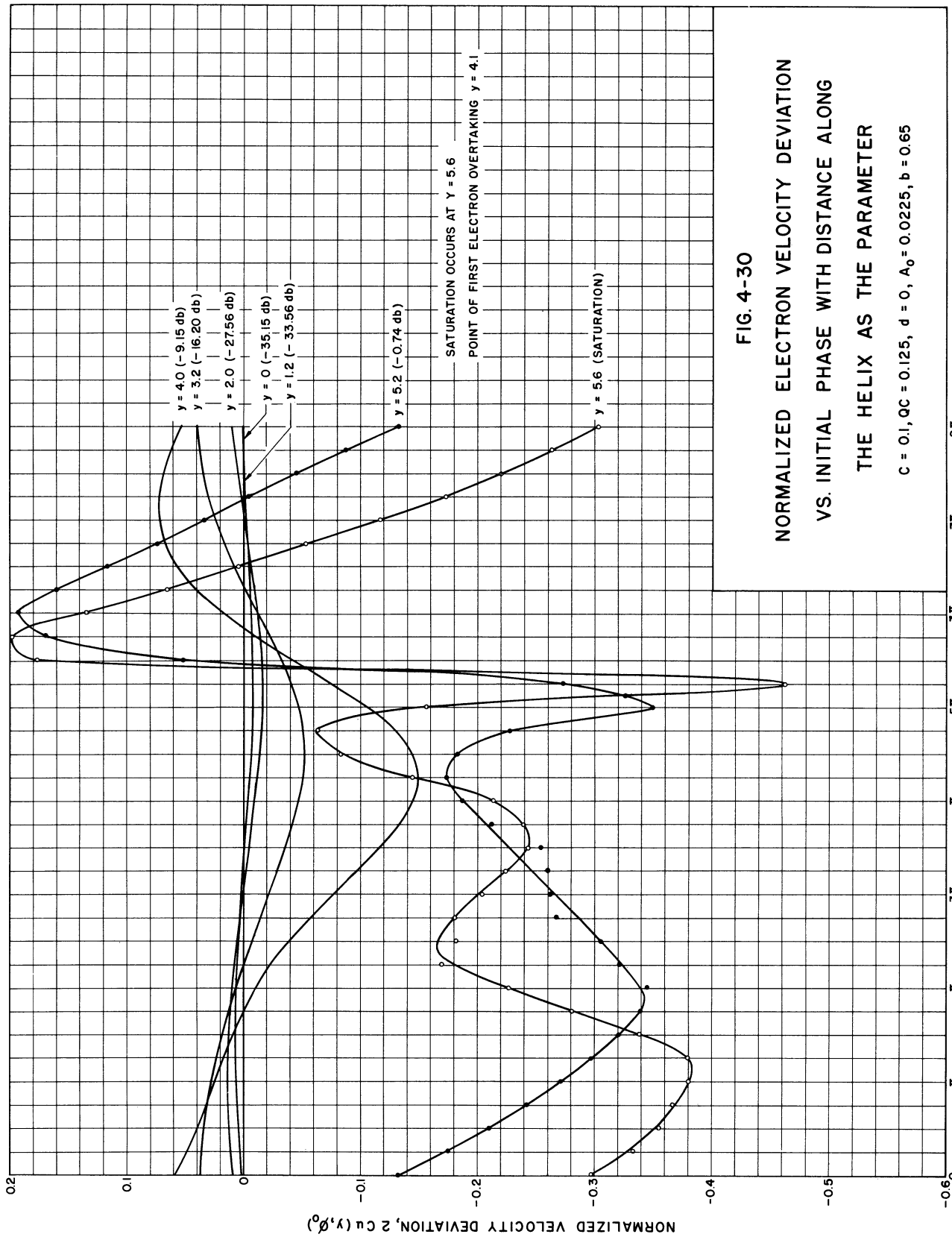
FIG. 4-30
NORMALIZED ELECTRON VELOCITY DEVIATION
VS. INITIAL PHASE WITH DISTANCE ALONG
THE HELIX AS THE PARAMETER
C = 0.1, QC = 0.125, d = 0, A0 = 0.0225, b = 0.65
y = 4.0 (−9.15 db)
y = 3.2 (−16.20 db)
y = 2.0 (−27.56 db)
y = 0 (−35.15 db)
y = 1.2 (−33.56 db)
y = 5.2 (−0.74 db)
y = 5.6 (SATURATION)
SATURATION OCCURS AT Y = 5.6
POINT OF FIRST ELECTRON OVERTAKING y = 4.1
NORMALIZED VELOCITY DEVIATION, 2 Cu (y,ϕo)
INITIAL PHASE, ϕo, RADIANS
0.2
0.1
0
-0.1
-0.2
-0.3
-0.4
-0.5
-0.6
0
π/4
π/2
3π/4
π
5π/4
3π/2
7π/4
2π

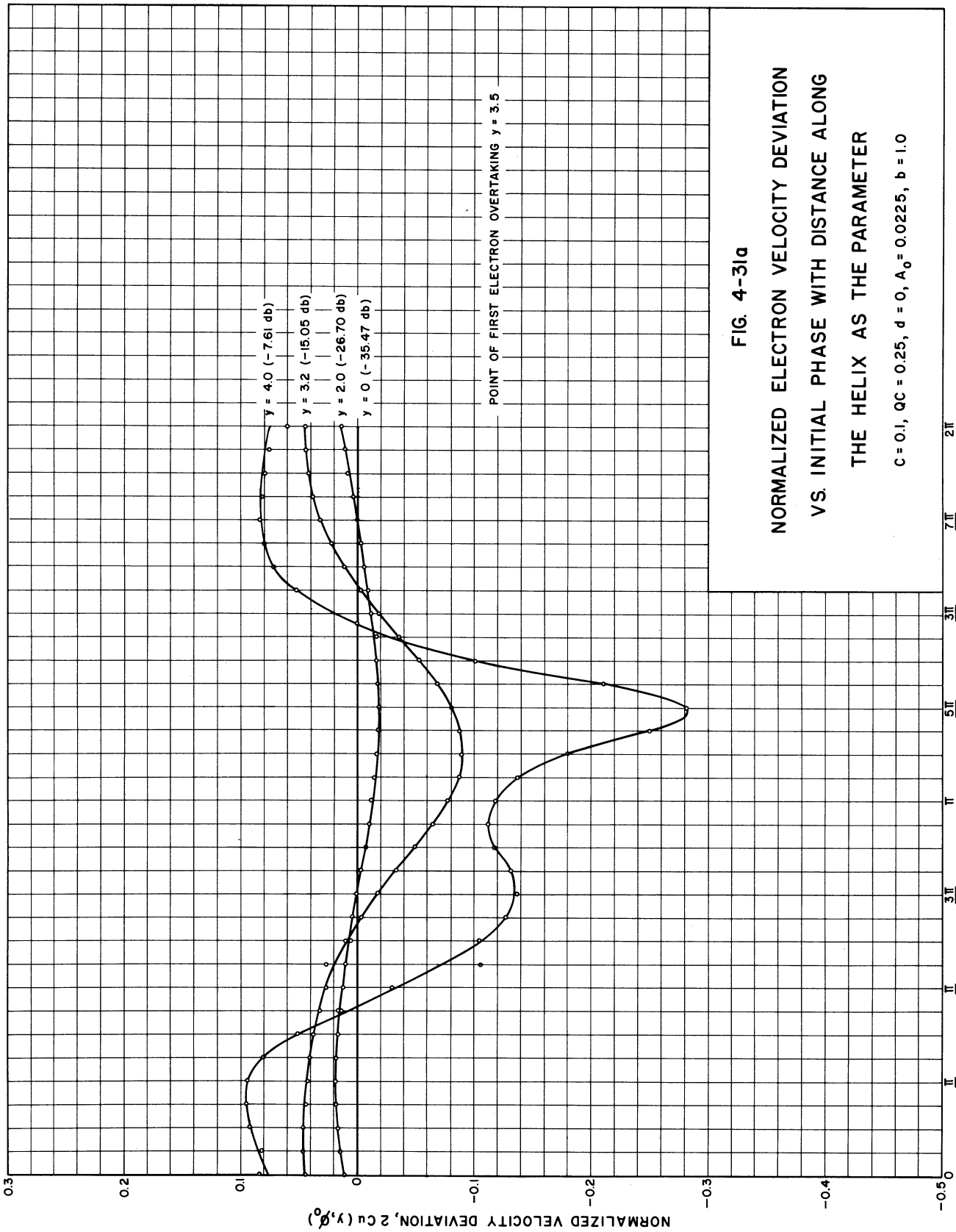
FIG. 4-31a
NORMALIZED ELECTRON VELOCITY DEVIATION
VS. INITIAL PHASE WITH DISTANCE ALONG
THE HELIX AS THE PARAMETER
C = 0.1, QC = 0.25, d = 0, A_o = 0.0225, b = 1.0
POINT OF FIRST ELECTRON OVERTAKING y = 3.5
y = 4.0 (-7.61 db)
y = 3.2 (-15.05 db)
y = 2.0 (-26.70 db)
y = 0 (-35.47 db)
NORMALIZED VELOCITY DEVIATION, 2 Cu (y, ϕ_o)
INITIAL PHASE, ϕ_o, RADIANS
0.3
0.2
0.1
0
-0.1
-0.2
-0.3
-0.4
-0.5
0
$\frac{\pi}{4}$
$\frac{\pi}{2}$
$\frac{3\pi}{4}$
π
$\frac{5\pi}{4}$
$\frac{3\pi}{2}$
$\frac{7\pi}{4}$
2π

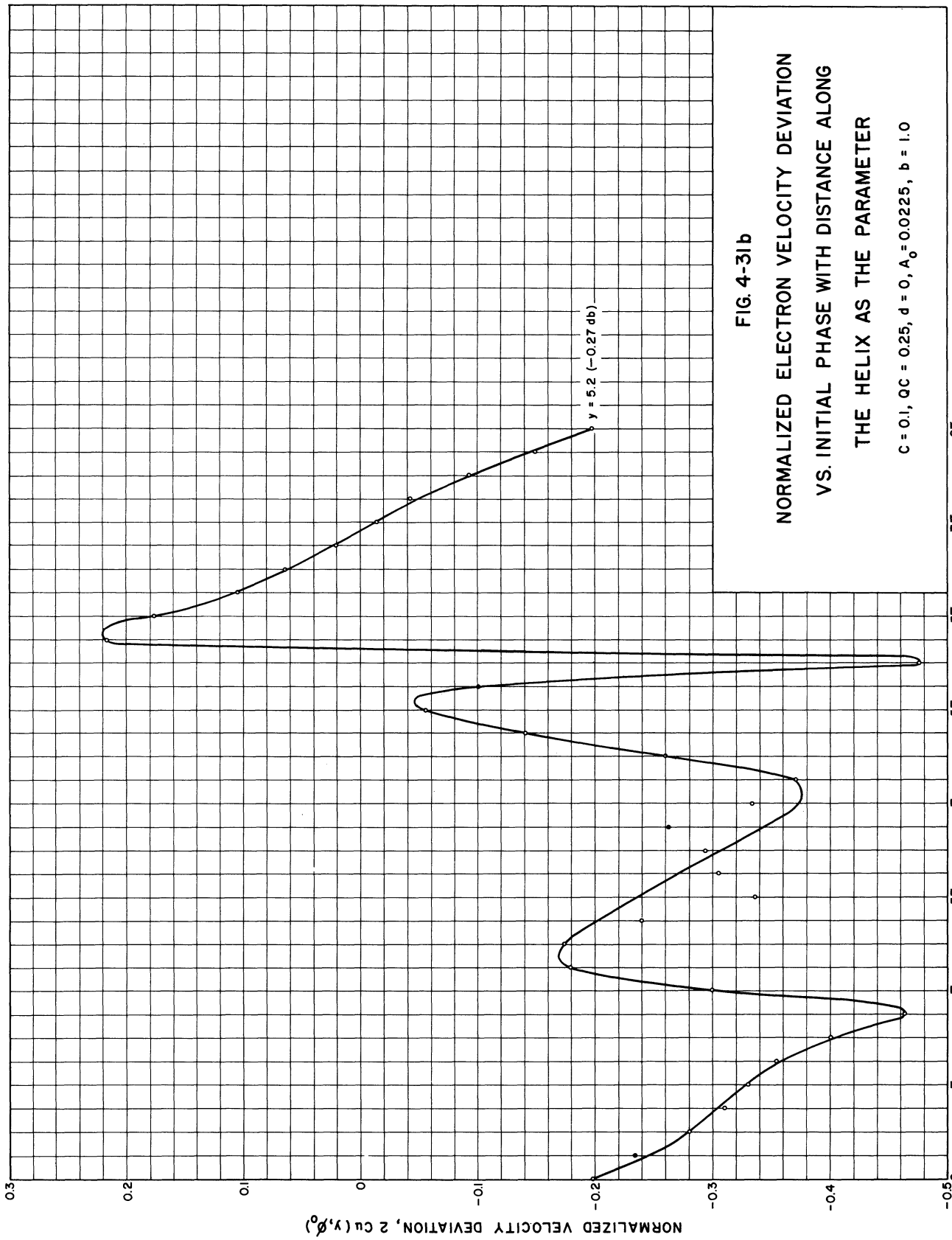
FIG. 4-31b
NORMALIZED ELECTRON VELOCITY DEVIATION
VS. INITIAL PHASE WITH DISTANCE ALONG
THE HELIX AS THE PARAMETER
C = 0.1, QC = 0.25, d = 0, A_o = 0.0225, b = 1.0
y = 5.2 (−0.27 db)
NORMALIZED VELOCITY DEVIATION, 2 Cu (y, ϕ_o)
INITIAL PHASE, ϕ_o, RADIANS
0.3
0.2
0.1
0
-0.1
-0.2
-0.3
-0.4
-0.5
0
$\frac{\pi}{4}$
$\frac{\pi}{2}$
$\frac{3\pi}{4}$
π
$\frac{5\pi}{4}$
$\frac{3\pi}{2}$
$\frac{7\pi}{4}$
2π

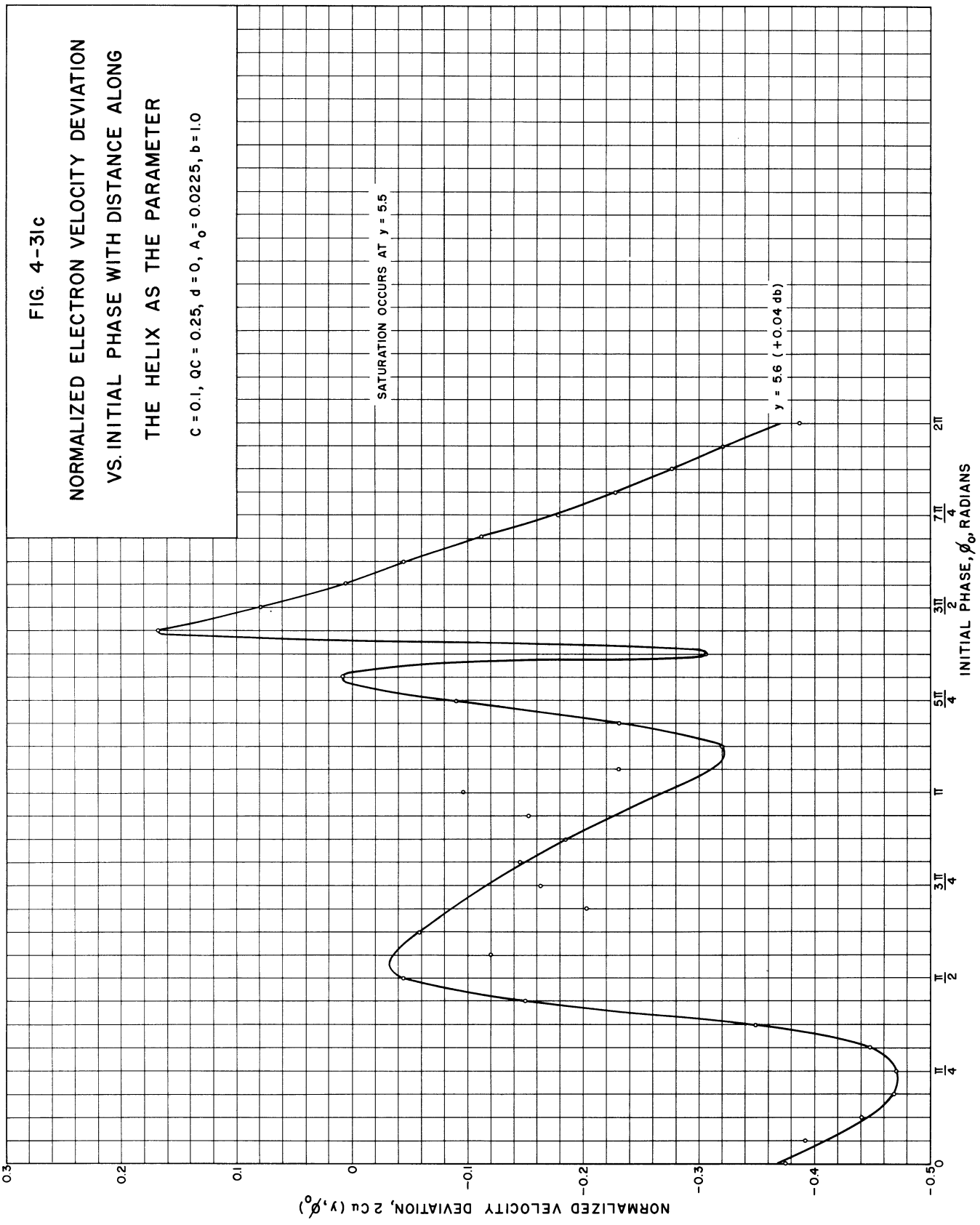
FIG. 4-31c
NORMALIZED ELECTRON VELOCITY DEVIATION VS. INITIAL PHASE WITH DISTANCE ALONG THE HELIX AS THE PARAMETER
C = 0.1, QC = 0.25, d = 0, A_0 = 0.0225, b = 1.0
SATURATION OCCURS AT y = 5.5
y = 5.6 (+0.04 db)
NORMALIZED VELOCITY DEVIATION, 2 Cu (y, ϕ_0)
INITIAL PHASE, ϕ_0, RADIANS
0.3
0.2
0.1
0
-0.1
-0.2
-0.3
-0.4
-0.5
0
$\frac{\pi}{4}$
$\frac{\pi}{2}$
$\frac{3\pi}{4}$
π
$\frac{5\pi}{4}$
$\frac{3\pi}{2}$
$\frac{7\pi}{4}$
2π

4.4.2 Velocity Deviation vs. Electron Phase. The normalized electron velocity deviation may also be plotted against $\phi(y,\phi_o)$, the electron phase, to give the electron velocity distribution vs. arrival phase at a particular position y along the tube. These curves are presented as Figs. 4-32 through 4-39. Regions of electron overtaking are characterized by vertical tangents to the velocity curves, since a vertical tangent can first be drawn just as overtaking occurs, and beyond that point the velocity is a multi-valued function of the electron phase $\phi(y,\phi_o)$.

In all cases, the electron velocity distribution is essentially sinusoidal with ϕ near the input, but as y increases more and more electrons are decelerated and the velocity curve twists around the point $\phi = \pi$ further and further as saturation is neared. The electrons followed through the interaction region are indicated by circles on the curves so as to give an idea of the percentage of the total number of electrons that are decelerated or accelerated at any point along the tube. The corresponding drop in the average velocity of the stream may be obtained by performing a Fourier analysis on the velocity-distribution curve to determine its average value and subtracting this quantity from u_o to get the final d-c velocity value. Clear u_o decreases with distance, since when the electrons are in a retarding field they give up energy to the r-f wave on the helix.

As with the space-charge solutions of Sections 4.3 and 4.4.1, the space-charge curves of this group do not vary as smoothly as those for QC = 0 due to the inaccuracies introduced in evaluating the space-charge weighting function $F(\phi-\phi')$ as pointed out in Section 3.5.1.

4.5 Electron Flight-Line Diagrams

One of the most interesting and useful graphs that can be plotted from the data obtained for a particular set of conditions is an electron

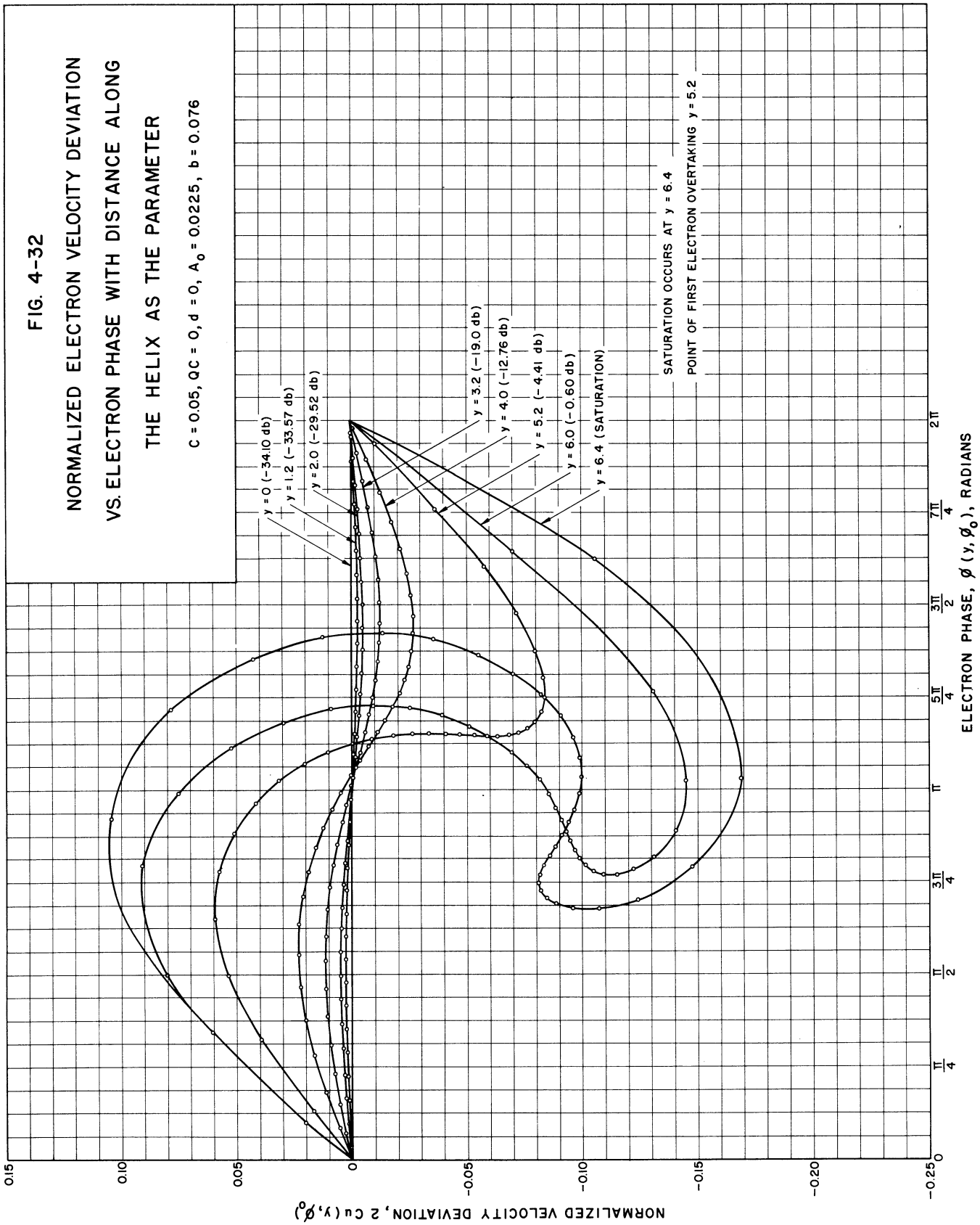
FIG. 4-32
NORMALIZED ELECTRON VELOCITY DEVIATION
VS. ELECTRON PHASE WITH DISTANCE ALONG
THE HELIX AS THE PARAMETER
C = 0.05, QC = 0, d = 0, A_o = 0.0225, b = 0.076
y = 0 (-34.10 db)
y = 1.2 (-33.57 db)
y = 2.0 (-29.52 db)
y = 3.2 (-19.0 db)
y = 4.0 (-12.76 db)
y = 5.2 (-4.41 db)
y = 6.0 (-0.60 db)
y = 6.4 (SATURATION)
SATURATION OCCURS AT y = 6.4
POINT OF FIRST ELECTRON OVERTAKING y = 5.2
NORMALIZED VELOCITY DEVIATION, 2 Cu (y, ϕ_o)
ELECTRON PHASE, ϕ (y, ϕ_o), RADIANS

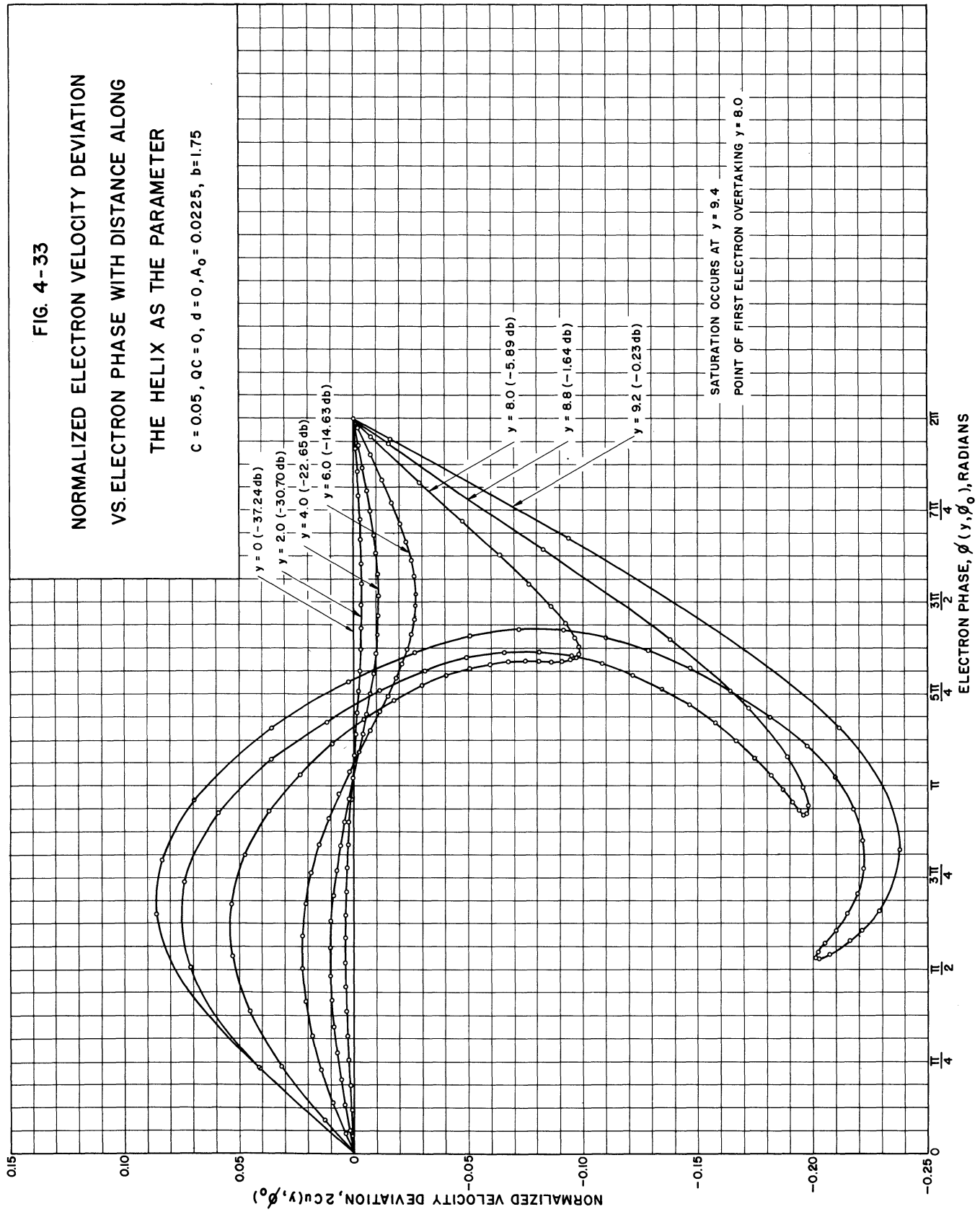
FIG. 4-33
NORMALIZED ELECTRON VELOCITY DEVIATION
VS. ELECTRON PHASE WITH DISTANCE ALONG
THE HELIX AS THE PARAMETER
C = 0.05, QC = 0, d = 0, A_0 = 0.0225, b=1.75
y = 0 (-37.24 db)
y = 2.0 (-30.70 db)
y = 4.0 (-22.65 db)
y = 6.0 (-14.63 db)
y = 8.0 (-5.89 db)
y = 8.8 (-1.64 db)
y = 9.2 (-0.23 db)
SATURATION OCCURS AT y = 9.4
POINT OF FIRST ELECTRON OVERTAKING y = 8.0
NORMALIZED VELOCITY DEVIATION, 2Cu(y, ϕ_0)
0.15
0.10
0.05
0
-0.05
-0.10
-0.15
-0.20
-0.25
$\frac{\pi}{4}$
$\frac{\pi}{2}$
$\frac{3\pi}{4}$
π
$\frac{5\pi}{4}$
$\frac{3\pi}{2}$
$\frac{7\pi}{4}$
2π
ELECTRON PHASE, $\phi(y, \phi_0)$, RADIANS

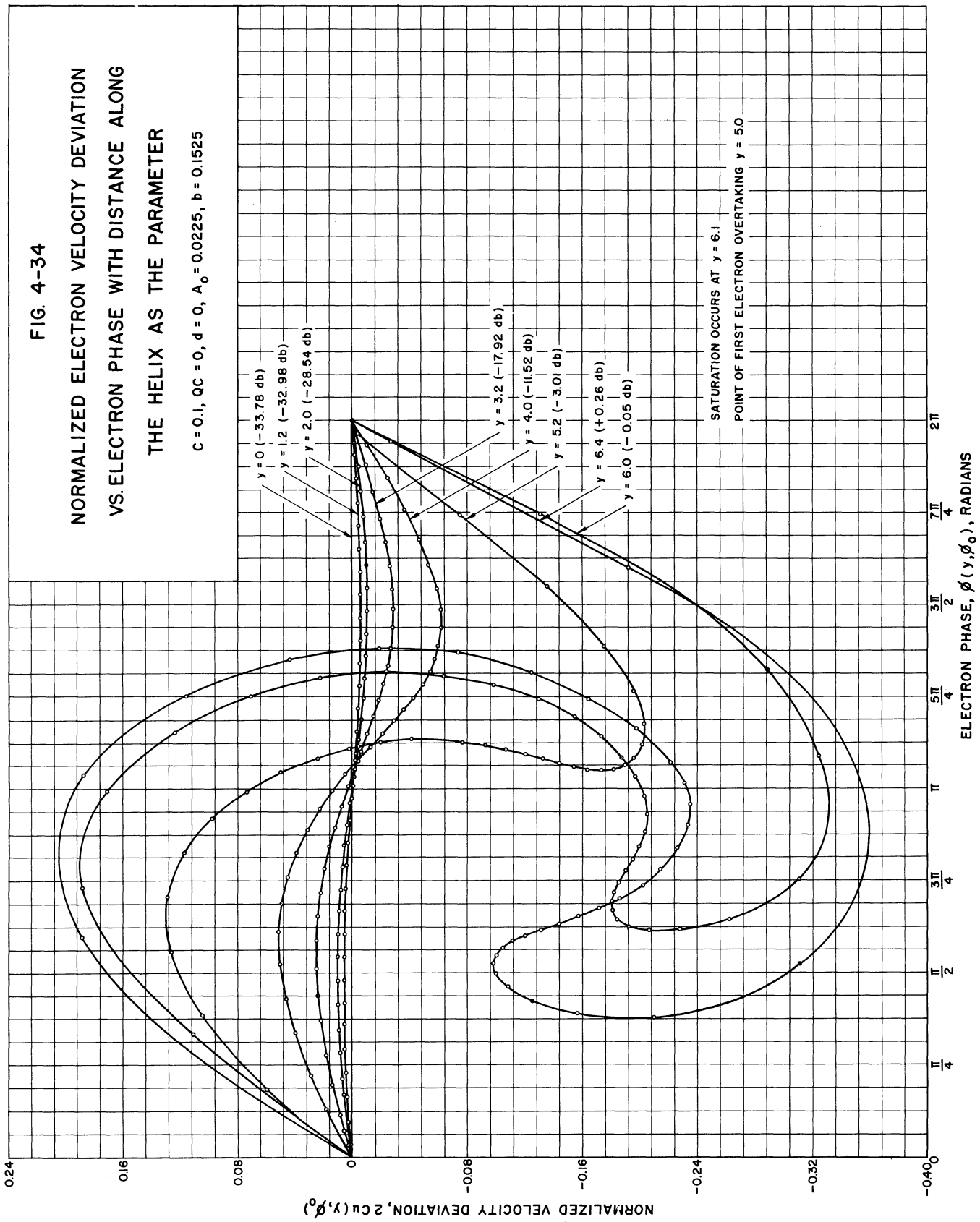
FIG. 4-34
NORMALIZED ELECTRON VELOCITY DEVIATION
VS. ELECTRON PHASE WITH DISTANCE ALONG
THE HELIX AS THE PARAMETER
C = 0.1, QC = 0, d = 0, A_0 = 0.0225, b = 0.1525
y = 0 (−33.78 db)
y = 1.2 (−32.98 db)
y = 2.0 (−28.54 db)
y = 3.2 (−17.92 db)
y = 4.0 (−11.52 db)
y = 5.2 (−3.01 db)
y = 6.4 (+0.26 db)
y = 6.0 (− 0.05 db)
SATURATION OCCURS AT y = 6.1
POINT OF FIRST ELECTRON OVERTAKING y = 5.0
NORMALIZED VELOCITY DEVIATION, 2 Cu (y, ϕ_0)
0.24
0.16
0.08
0
−0.08
−0.16
−0.24
−0.32
−0.40
0
$\frac{\pi}{4}$
$\frac{\pi}{2}$
$\frac{3\pi}{4}$
π
$\frac{5\pi}{4}$
$\frac{3\pi}{2}$
$\frac{7\pi}{4}$
2π
ELECTRON PHASE, $\phi(y, \phi_0)$, RADIANS

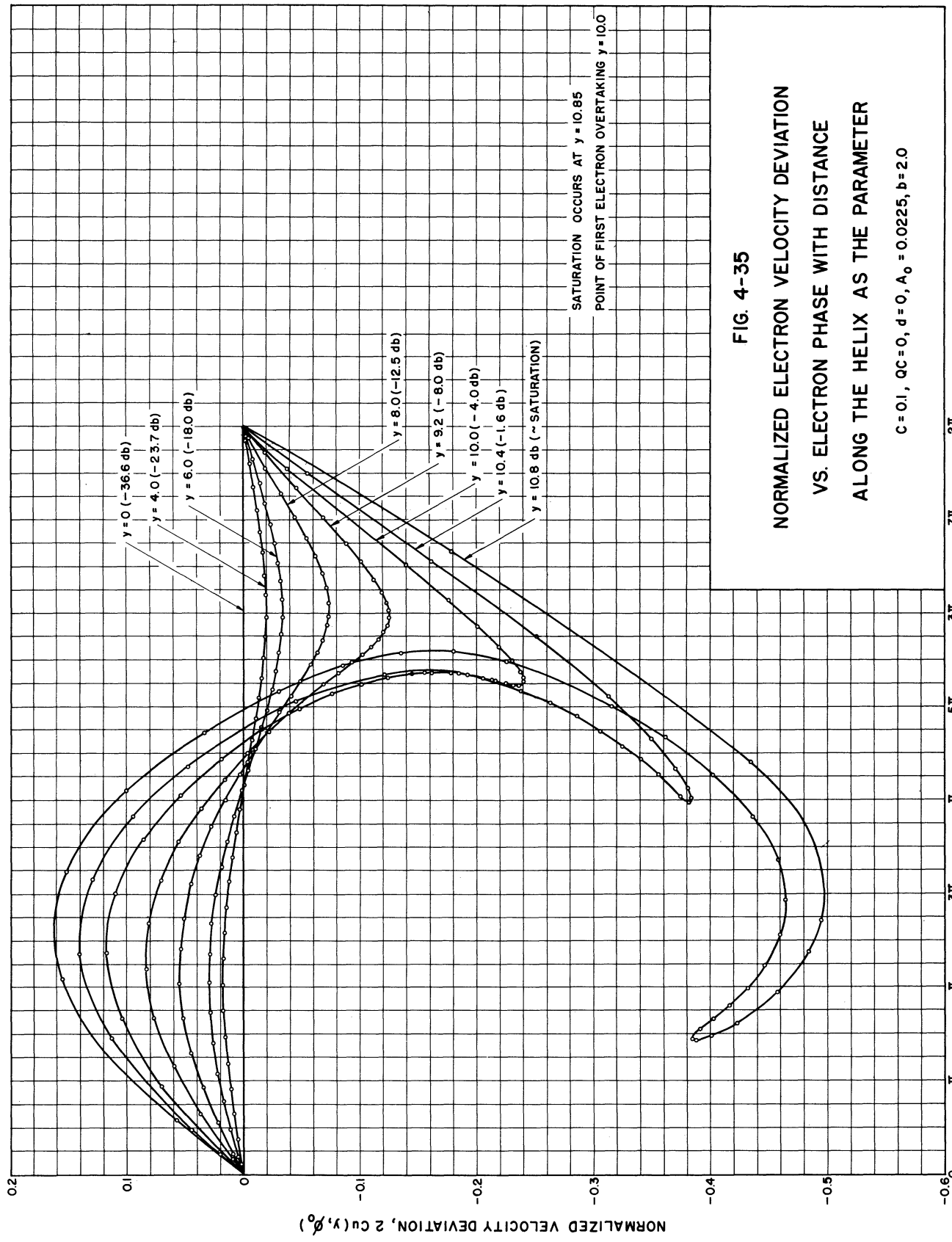
FIG. 4-35
NORMALIZED ELECTRON VELOCITY DEVIATION
VS. ELECTRON PHASE WITH DISTANCE
ALONG THE HELIX AS THE PARAMETER
C = 0.1, QC = 0, d = 0, A_0 = 0.0225, b = 2.0
SATURATION OCCURS AT y = 10.85
POINT OF FIRST ELECTRON OVERTAKING y = 10.0
y = 0 (−36.6 db)
y = 4.0 (−23.7 db)
y = 6.0 (−18.0 db)
y = 8.0 (−12.5 db)
y = 9.2 (−8.0 db)
y = 10.0 (−4.0 db)
y = 10.4 (−1.6 db)
y = 10.8 db (~SATURATION)
NORMALIZED VELOCITY DEVIATION, 2 Cu(y, ϕ_0)
ELECTRON PHASE, $\phi(y, \phi_0)$, RADIANS

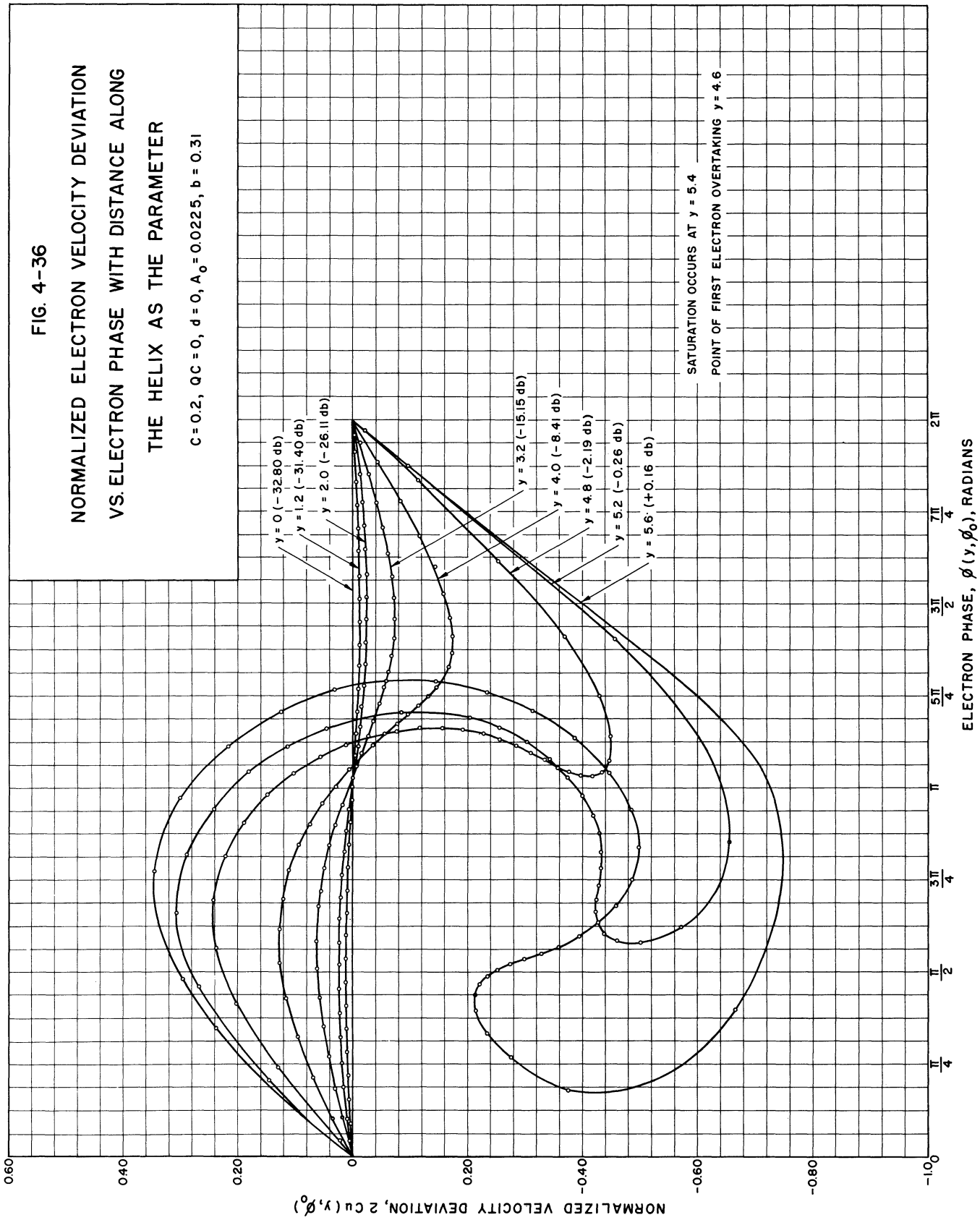
FIG. 4-36
NORMALIZED ELECTRON VELOCITY DEVIATION VS. ELECTRON PHASE WITH DISTANCE ALONG THE HELIX AS THE PARAMETER
C = 0.2, QC = 0, d = 0, A_0 = 0.0225, b = 0.31
y = 0 (−32.80 db)
y = 1.2 (−31.40 db)
y = 2.0 (−26.11 db)
y = 3.2 (−15.15 db)
y = 4.0 (−8.41 db)
y = 4.8 (−2.19 db)
y = 5.2 (−0.26 db)
y = 5.6 (+0.16 db)
SATURATION OCCURS AT y = 5.4
POINT OF FIRST ELECTRON OVERTAKING y = 4.6
NORMALIZED VELOCITY DEVIATION, 2 Cu (y, ϕ₀)
0.60
0.40
0.20
0
0.20
-0.40
-0.60
-0.80
-1.0
π/4
π/2
3π/4
π
5π/4
3π/2
7π/4
2π
ELECTRON PHASE, ϕ (y, ϕ₀), RADIANS

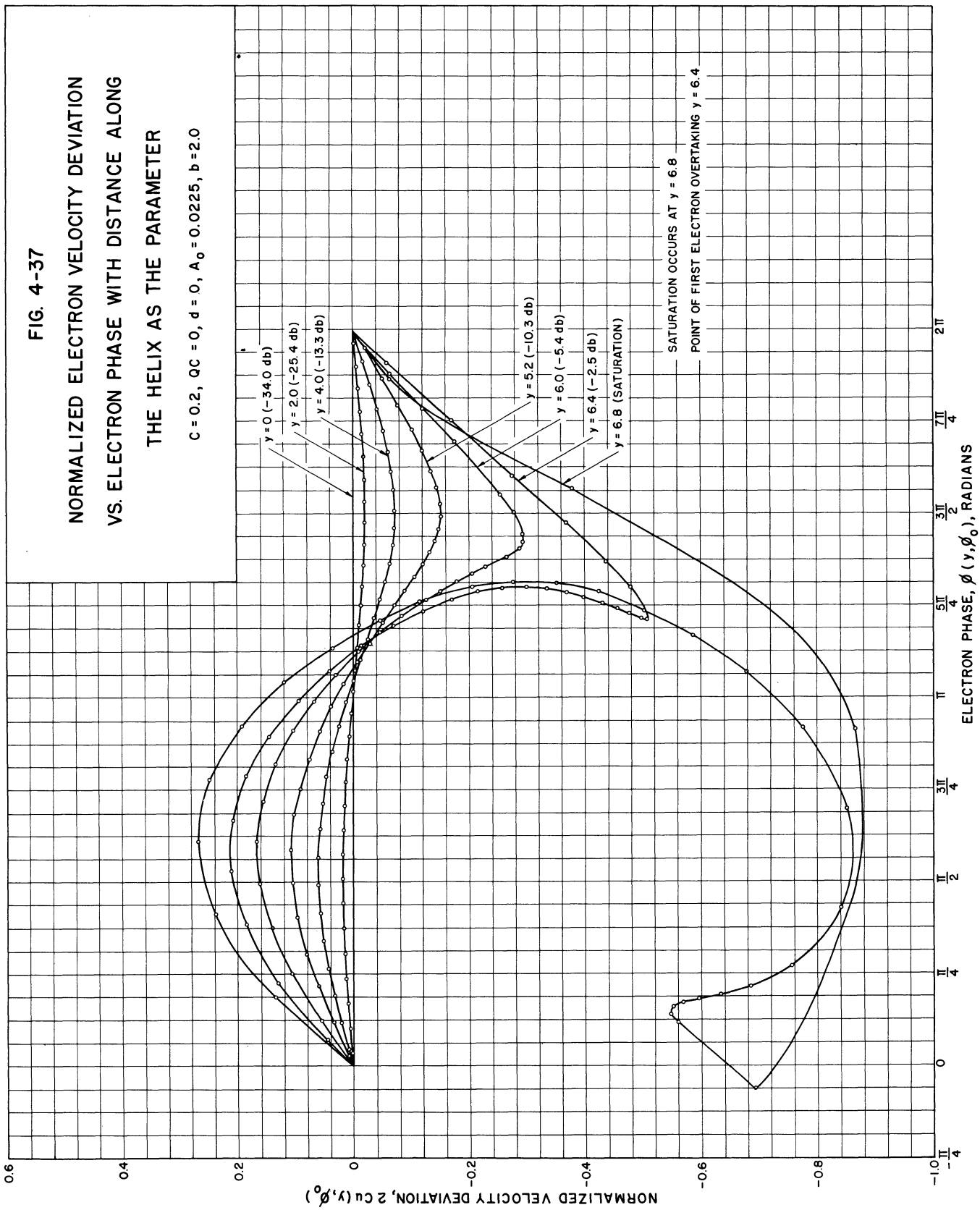
FIG. 4-37
NORMALIZED ELECTRON VELOCITY DEVIATION
VS. ELECTRON PHASE WITH DISTANCE ALONG
THE HELIX AS THE PARAMETER
C = 0.2, QC = 0, d = 0, A_0 = 0.0225, b = 2.0
y = 0 (−34.0 db)
y = 2.0 (−25.4 db)
y = 4.0 (−13.3 db)
y = 5.2 (−10.3 db)
y = 6.0 (−5.4 db)
y = 6.4 (−2.5 db)
y = 6.8 (SATURATION)
SATURATION OCCURS AT y = 6.8
POINT OF FIRST ELECTRON OVERTAKING y = 6.4
NORMALIZED VELOCITY DEVIATION, 2 Cu (y, ϕ_0)
ELECTRON PHASE, ϕ (y, ϕ_0), RADIANS

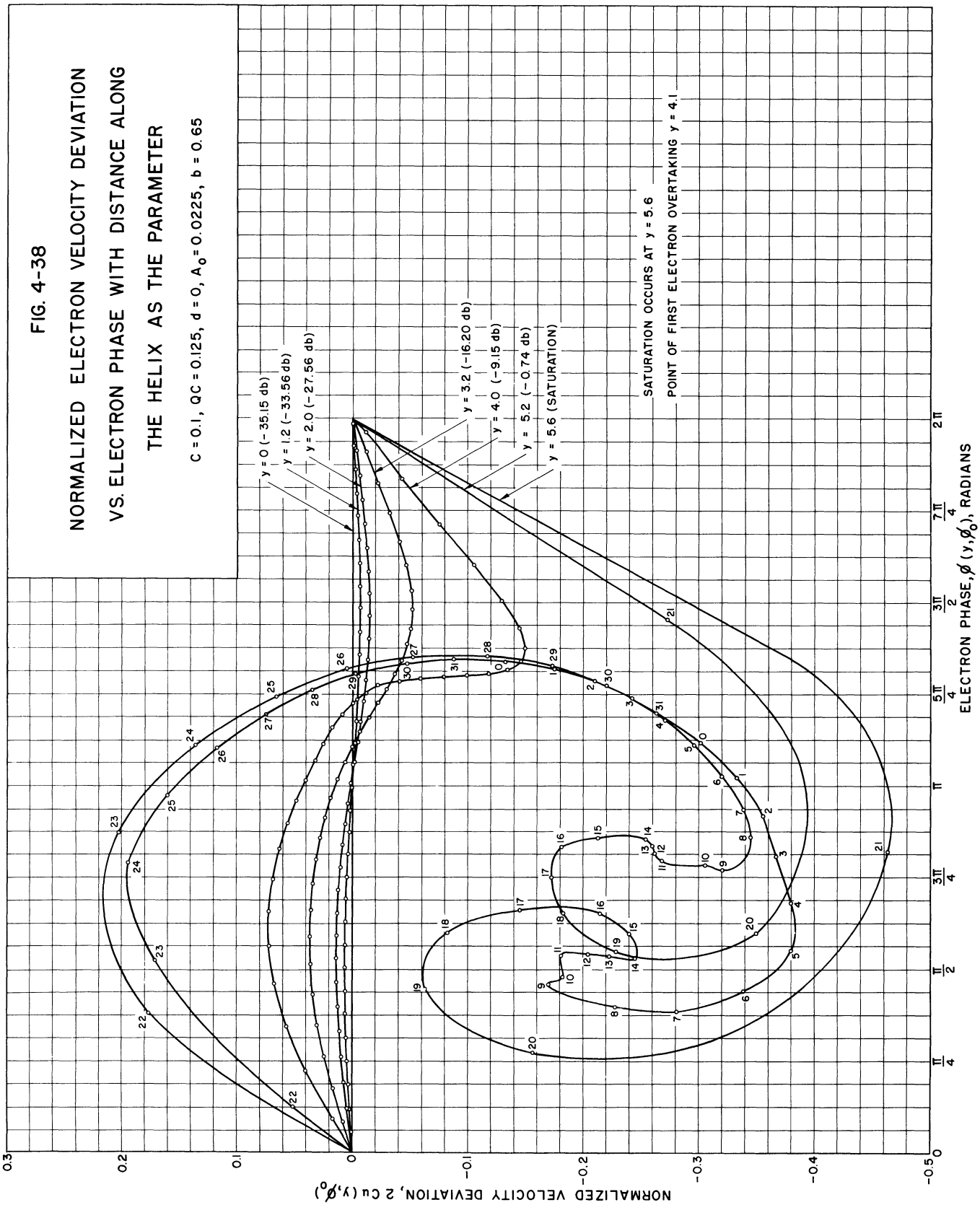
FIG. 4-38
NORMALIZED ELECTRON VELOCITY DEVIATION
VS. ELECTRON PHASE WITH DISTANCE ALONG
THE HELIX AS THE PARAMETER
C = 0.1, QC = 0.125, d = 0, A_0 = 0.0225, b = 0.65
y = 0 (−35.15 db)
y = 1.2 (−33.56 db)
y = 2.0 (−27.56 db)
y = 3.2 (−16.20 db)
y = 4.0 (−9.15 db)
y = 5.2 (−0.74 db)
y = 5.6 (SATURATION)
SATURATION OCCURS AT y = 5.6
POINT OF FIRST ELECTRON OVERTAKING y = 4.1
NORMALIZED VELOCITY DEVIATION, 2 Cu (y,ϕ_0)
ELECTRON PHASE, ϕ (y,ϕ_0), RADIANS

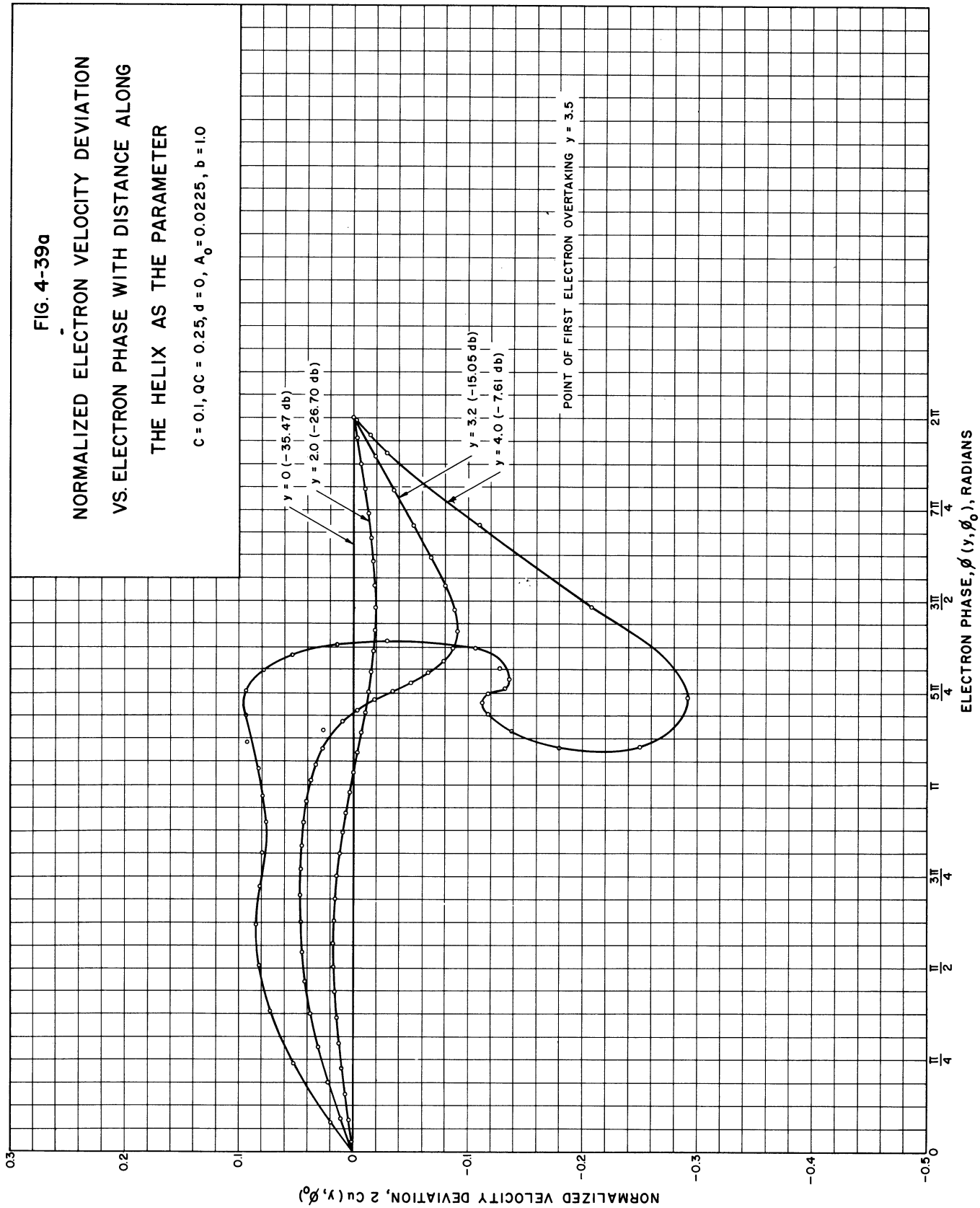
FIG. 4-39a
NORMALIZED ELECTRON VELOCITY DEVIATION
VS. ELECTRON PHASE WITH DISTANCE ALONG
THE HELIX AS THE PARAMETER
C = 0.1, QC = 0.25, d = 0, A_o=0.0225, b = 1.0
y = 0 (−35.47 db)
y = 2.0 (−26.70 db)
y = 3.2 (−15.05 db)
y = 4.0 (− 7.61 db)
POINT OF FIRST ELECTRON OVERTAKING y = 3.5
NORMALIZED VELOCITY DEVIATION, 2 Cu (y, ϕ_o)
ELECTRON PHASE, ϕ (y, ϕ_o), RADIANS
0.3
0.2
0.1
0
-0.1
-0.2
-0.3
-0.4
-0.5
0
$\frac{\pi}{4}$
$\frac{\pi}{2}$
$\frac{3\pi}{4}$
π
$\frac{5\pi}{4}$
$\frac{3\pi}{2}$
$\frac{7\pi}{4}$
2π

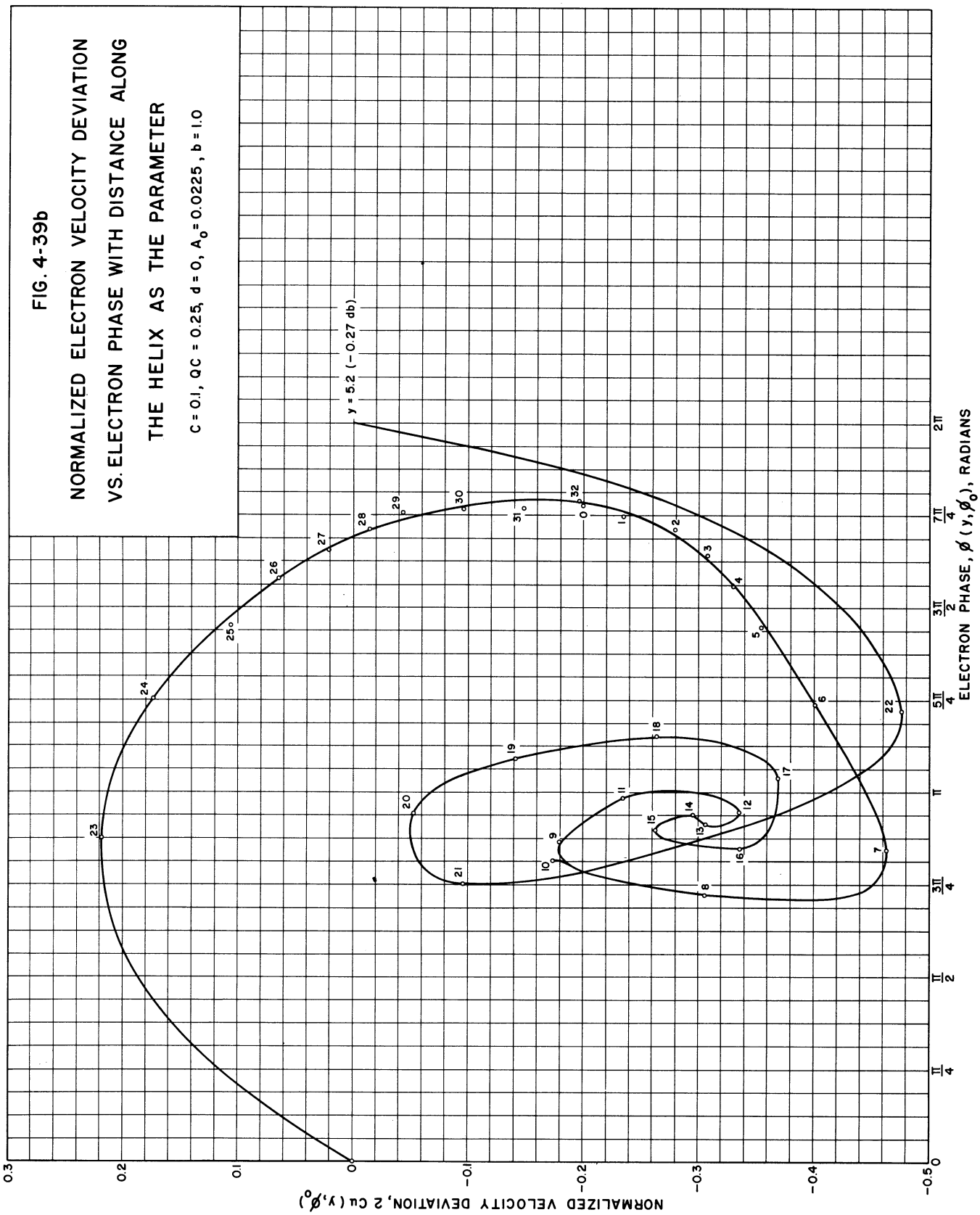
FIG. 4-39b
NORMALIZED ELECTRON VELOCITY DEVIATION
VS. ELECTRON PHASE WITH DISTANCE ALONG
THE HELIX AS THE PARAMETER
C = 0.1, QC = 0.25, d = 0, A_0 = 0.0225, b = 1.0
y = 5.2 (−0.27 db)
NORMALIZED VELOCITY DEVIATION, 2 Cu (y,ϕ_0)
ELECTRON PHASE, ϕ (y,ϕ_0), RADIANS
0.3
0.2
0.1
0
−0.1
−0.2
−0.3
−0.4
−0.5
$\frac{\pi}{4}$
$\frac{\pi}{2}$
$\frac{3\pi}{4}$
π
$\frac{5\pi}{4}$
$\frac{3\pi}{2}$
$\frac{7\pi}{4}$
2π

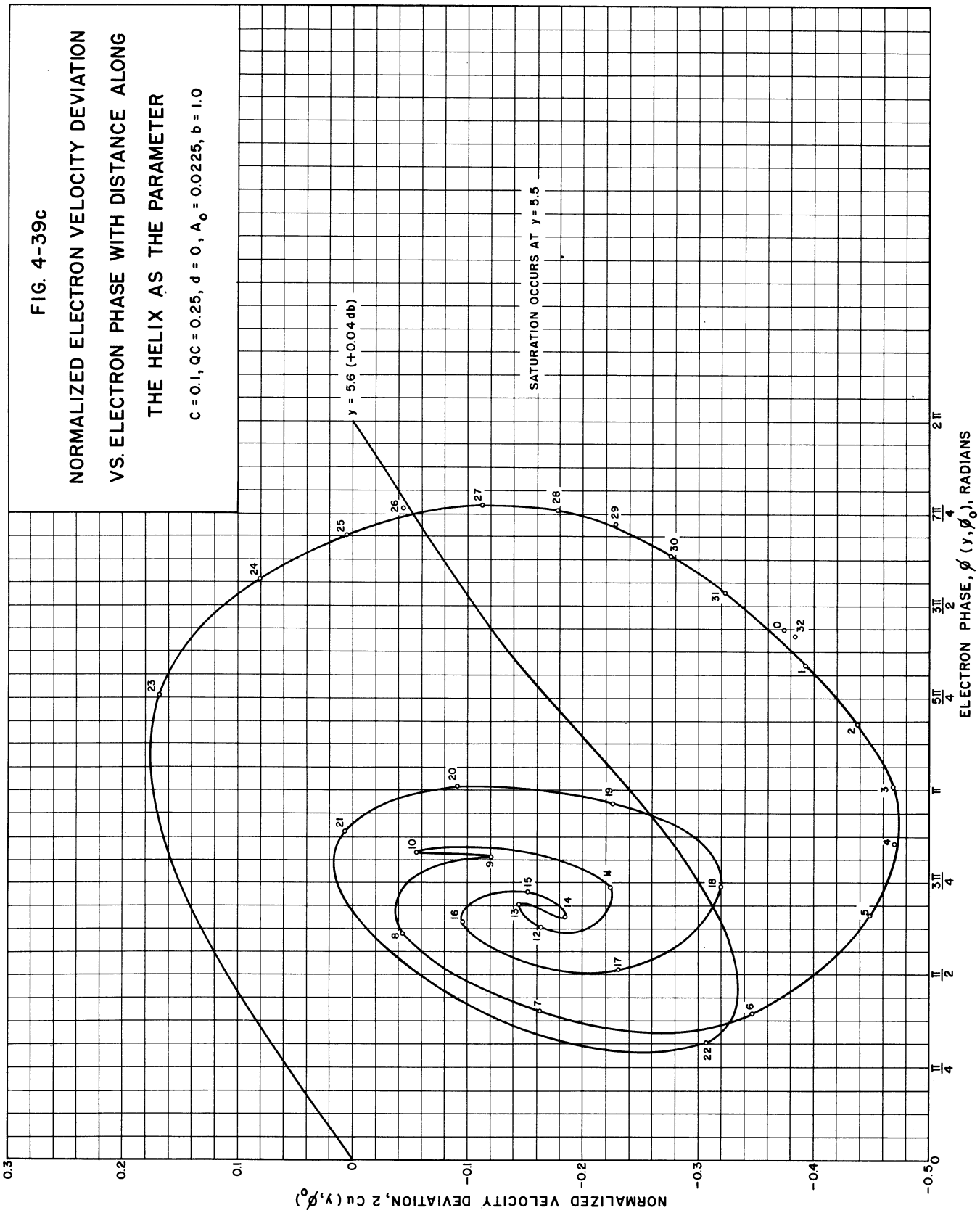
FIG. 4-39c
NORMALIZED ELECTRON VELOCITY DEVIATION
VS. ELECTRON PHASE WITH DISTANCE ALONG
THE HELIX AS THE PARAMETER
C = 0.1, QC = 0.25, d = 0, A_0 = 0.0225, b = 1.0
y = 5.6 (+0.04 db)
SATURATION OCCURS AT y = 5.5
NORMALIZED VELOCITY DEVIATION, 2 Cu (y, ϕ_0)
ELECTRON PHASE, ϕ (y, ϕ_0), RADIANS
0.3
0.2
0.1
0
-0.1
-0.2
-0.3
-0.4
-0.5
$\frac{\pi}{4}$
$\frac{\pi}{2}$
$\frac{3\pi}{4}$
π
$\frac{5\pi}{4}$
$\frac{3\pi}{2}$
$\frac{7\pi}{4}$
2π

flight-line diagram, which is similar to the well-known "Applegate diagram" associated with klystrons. The corresponding flight-line diagrams for the traveling-wave amplifier are plots of distance along the tube vs. electron phase (i.e., arrival phase) with entrance phase as the parameter. This "space-phase" diagram affords an opportunity to follow the electron trajectories through the interaction region and see just how their motions are affected by conditions in the stream.

Figures 4-40 through 4-49 are the electron flight-line diagrams for the cases studied. Each flight line represents 1 electron; 32 electrons were followed through the integrations, but only those which are particularly interesting have been plotted. On each figure the saturation level and point of first electron overtaking are noted. The point of first overtaking is clearly the point y at which the flight lines begin to cross. Hence the closeness of the curves indicates the degree of bunching in the stream.

The entrance phase of an electron is given by

$$\phi_{oj} = \frac{2\pi j}{32} \qquad j = 0,1,2 \ldots 32 \tag{4-5}$$

and hence the numbers identifying individual curves represent the initial phases in units of $\pi/16$ radians.

Over the interval in which $\phi(y,\phi_o)$ varies from 0 to π, the circuit electric potential gradient is positive; hence the electrons are accelerated in the direction of increasing y and they accept energy from the circuit. On the other hand, between π and 2π the circuit electric potential gradient is negative; accordingly the electrons are decelerated in the direction of increasing y and they are delivering energy to the circuit. Initially and for some distance the average velocity of the electrons is equal to or greater than the phase velocity of the wave and hence the electrons are seen

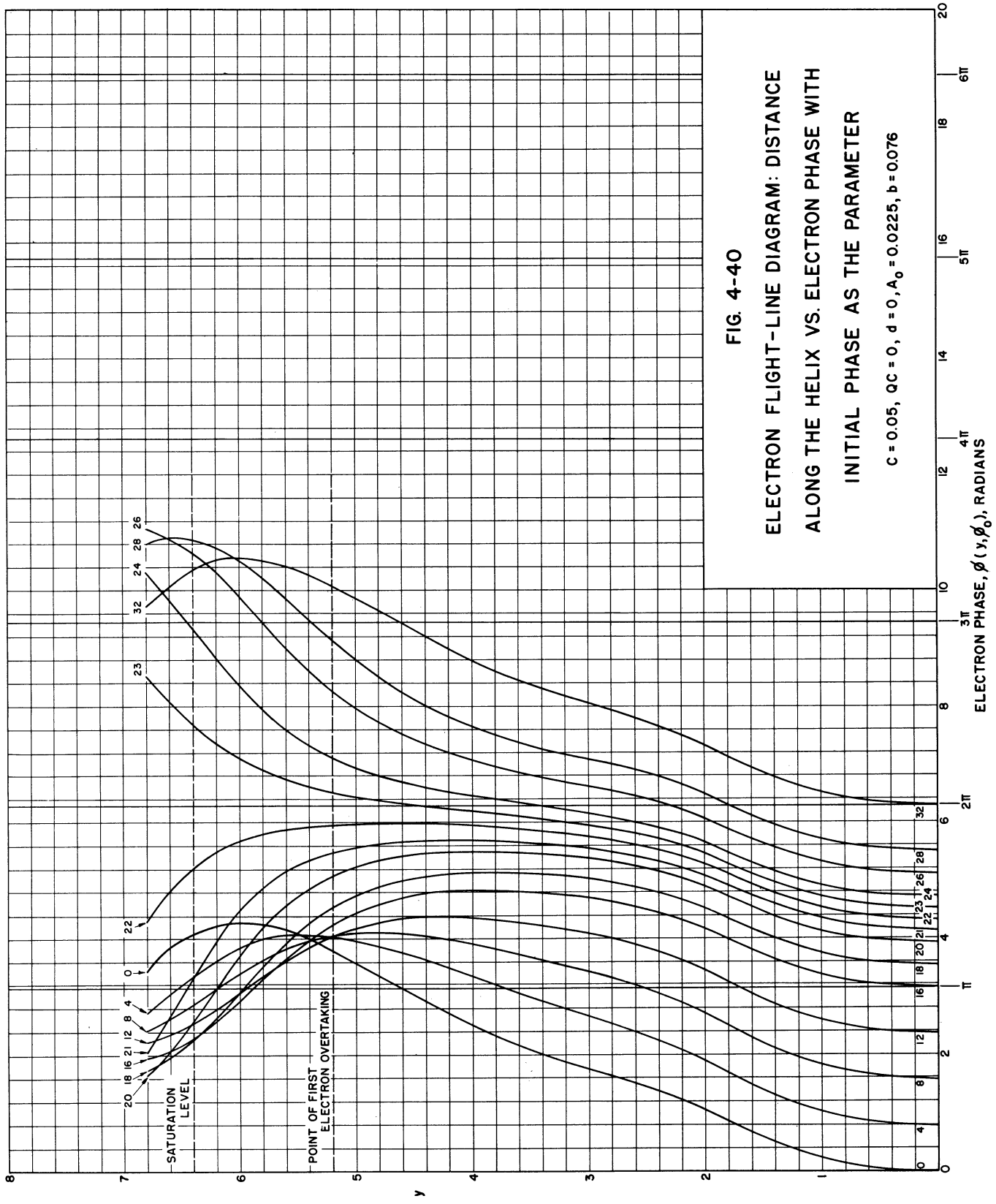
FIG. 4-40
ELECTRON FLIGHT-LINE DIAGRAM: DISTANCE ALONG THE HELIX VS. ELECTRON PHASE WITH INITIAL PHASE AS THE PARAMETER
C = 0.05, QC = 0, d = 0, A_0 = 0.0225, b = 0.076
SATURATION LEVEL
POINT OF FIRST ELECTRON OVERTAKING
y
ELECTRON PHASE, $\phi(y,\phi_0)$, RADIANS

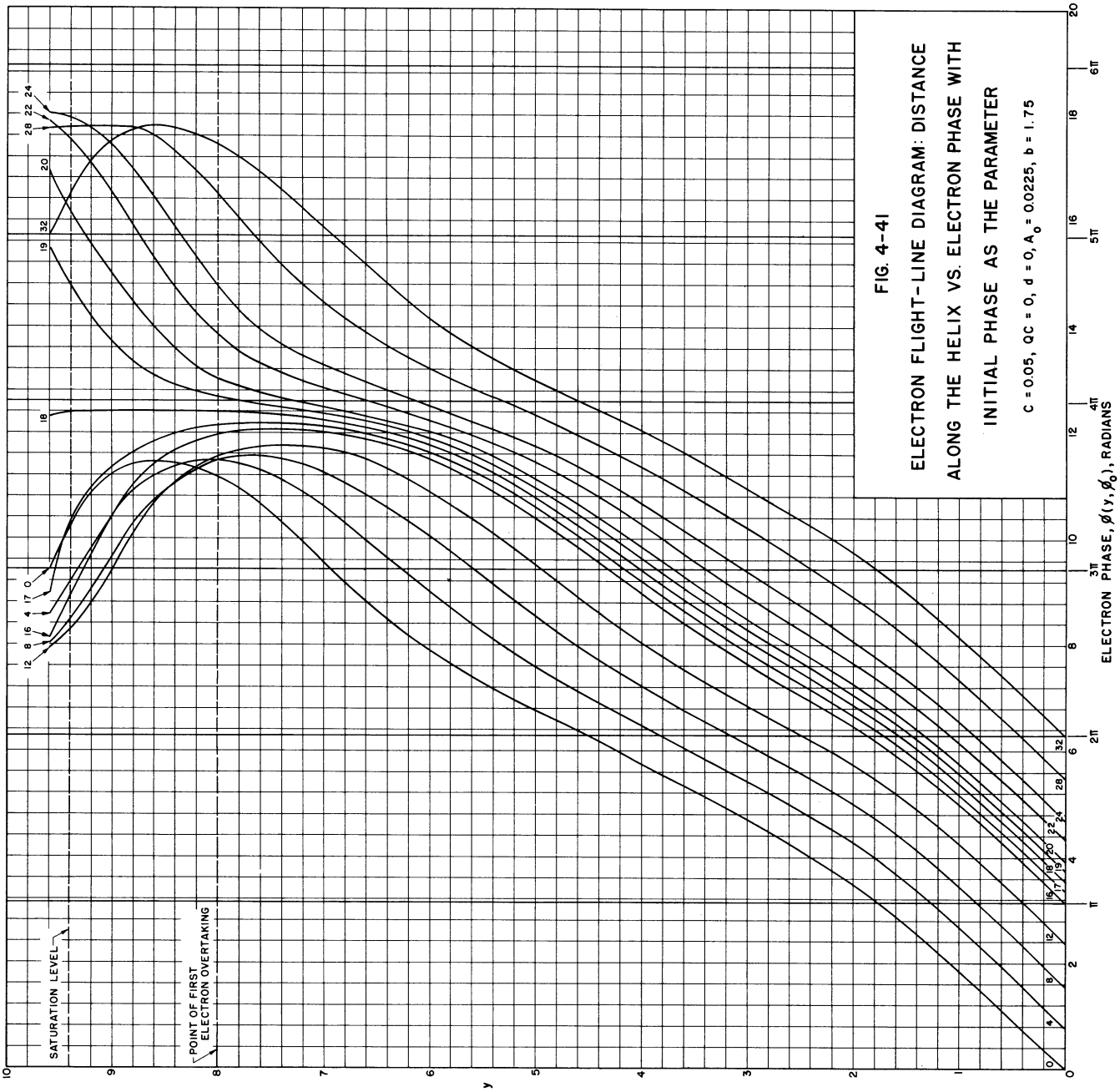

FIG. 4-41

ELECTRON FLIGHT-LINE DIAGRAM: DISTANCE ALONG THE HELIX VS. ELECTRON PHASE WITH INITIAL PHASE AS THE PARAMETER

C = 0.05, QC = 0, d = 0, A_0 = 0.0225, b = 1.75

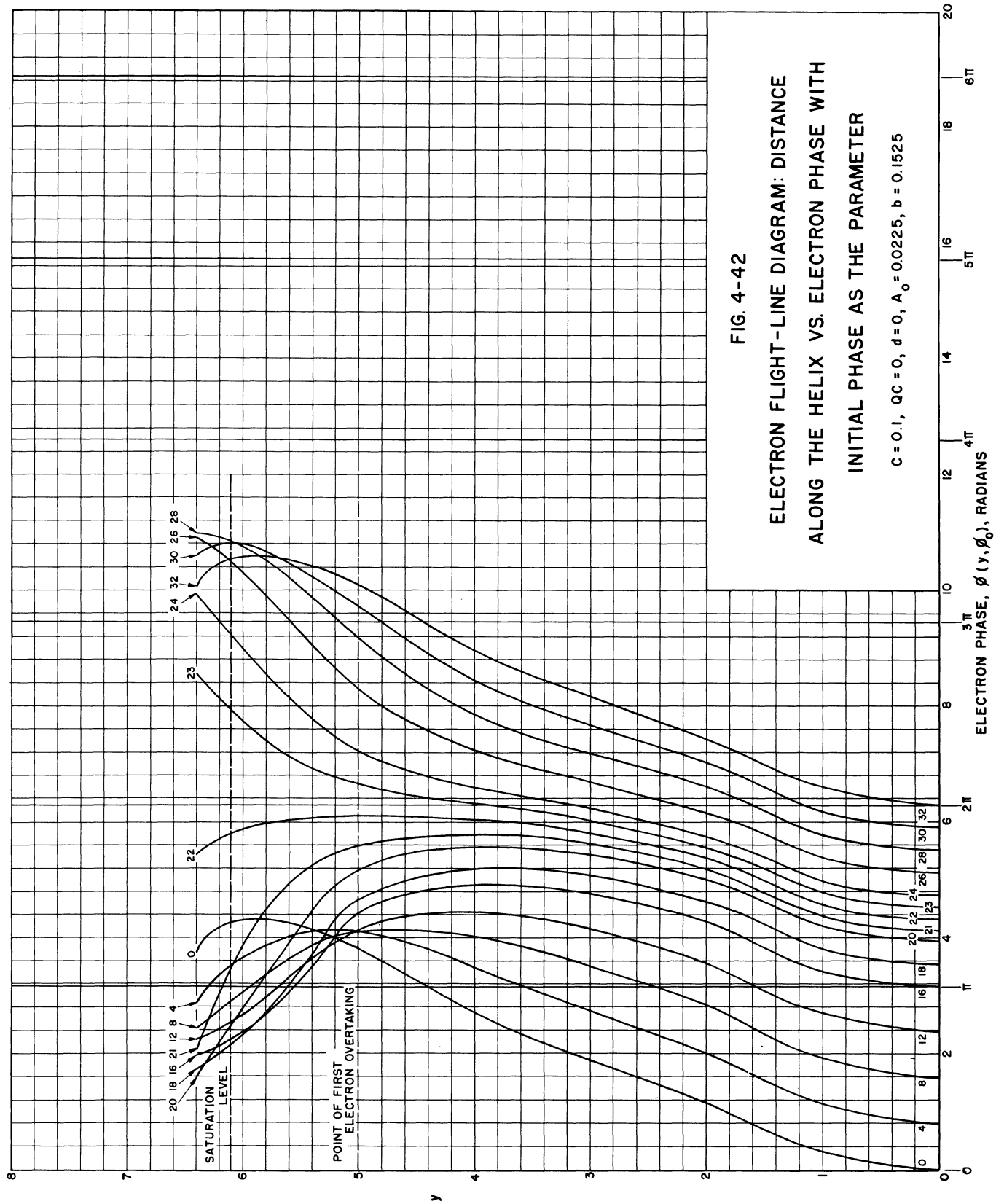
FIG. 4-42
ELECTRON FLIGHT-LINE DIAGRAM: DISTANCE ALONG THE HELIX VS. ELECTRON PHASE WITH INITIAL PHASE AS THE PARAMETER
C = 0.1, QC = 0, d = 0, A_0 = 0.0225, b = 0.1525
y
ELECTRON PHASE, $\phi(y,\phi_0)$, RADIANS
SATURATION LEVEL
POINT OF FIRST ELECTRON OVERTAKING
0
4
8
12
16
20
21
18
22
23
24
32
30
26
28

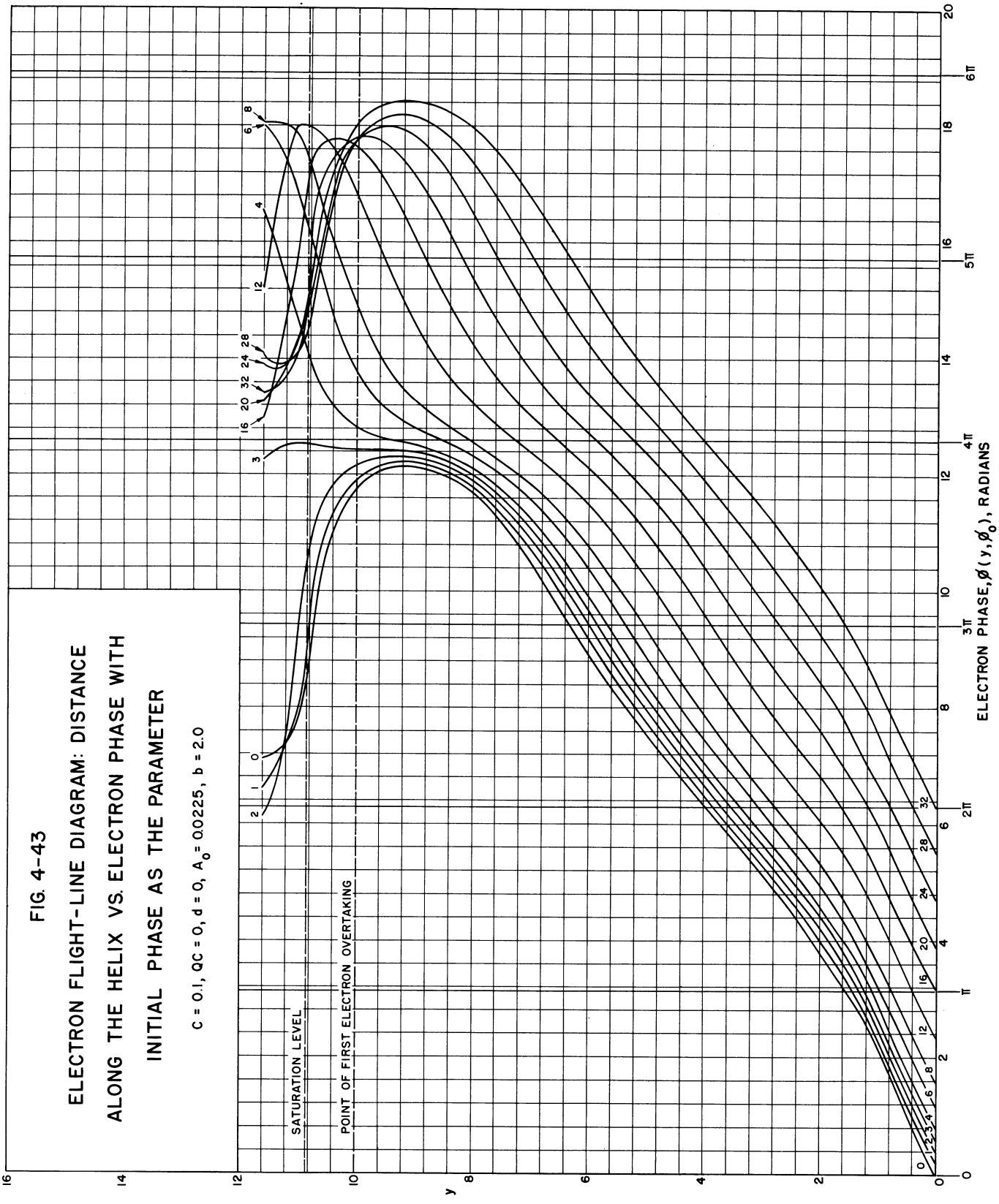

FIG. 4-43

ELECTRON FLIGHT-LINE DIAGRAM: DISTANCE ALONG THE HELIX VS. ELECTRON PHASE WITH INITIAL PHASE AS THE PARAMETER

C = 0.1, QC = 0, d = 0, A_0 = 0.0225, b = 2.0

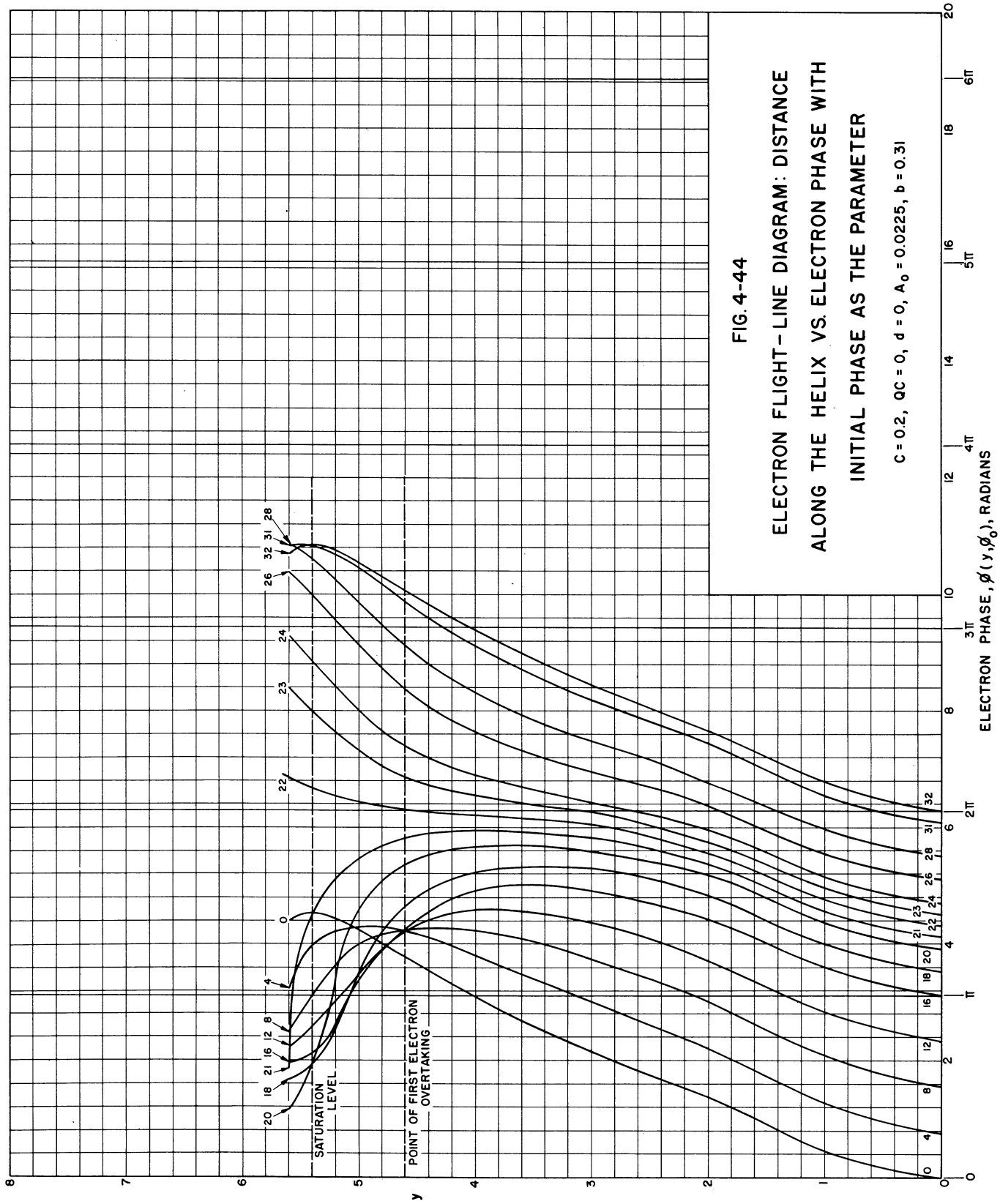
FIG. 4-44
ELECTRON FLIGHT-LINE DIAGRAM: DISTANCE ALONG THE HELIX VS. ELECTRON PHASE WITH INITIAL PHASE AS THE PARAMETER
C = 0.2, QC = 0, d = 0, A_0 = 0.0225, b = 0.31
y
ELECTRON PHASE, $\phi(y,\phi_0)$, RADIANS
SATURATION LEVEL
POINT OF FIRST ELECTRON OVERTAKING
0 4 8 12 16 18 21 20
22 23 24 26 28 31 32
0 π 2π 3π 4π 5π 6π

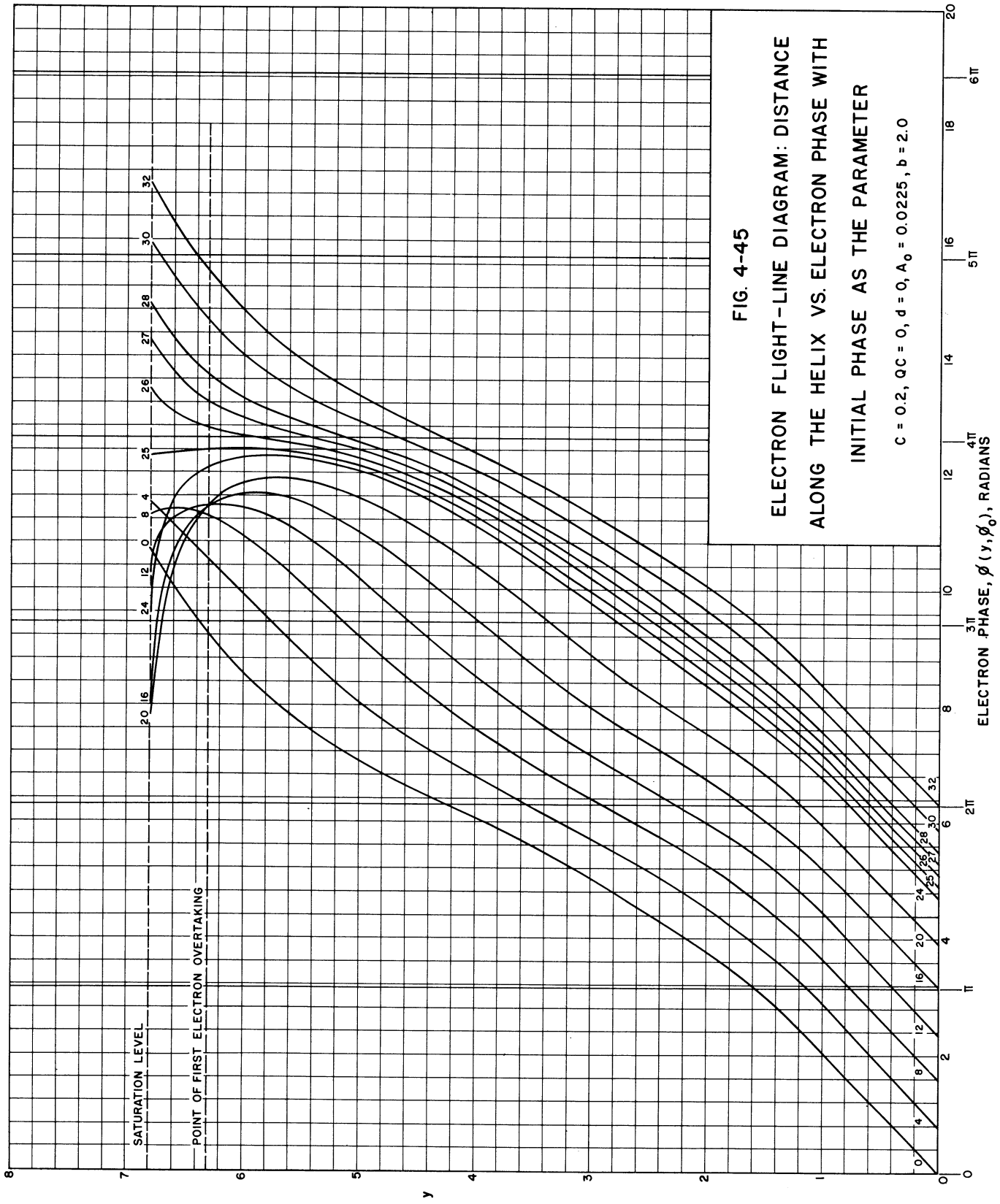
SATURATION LEVEL
POINT OF FIRST ELECTRON OVERTAKING
y
ELECTRON PHASE, ϕ (y, ϕ0), RADIANS
0
π
2π
3π
4π
5π
6π
FIG. 4-45
ELECTRON FLIGHT-LINE DIAGRAM: DISTANCE ALONG THE HELIX VS. ELECTRON PHASE WITH INITIAL PHASE AS THE PARAMETER
C = 0.2, QC = 0, d = 0, A0 = 0.0225, b = 2.0

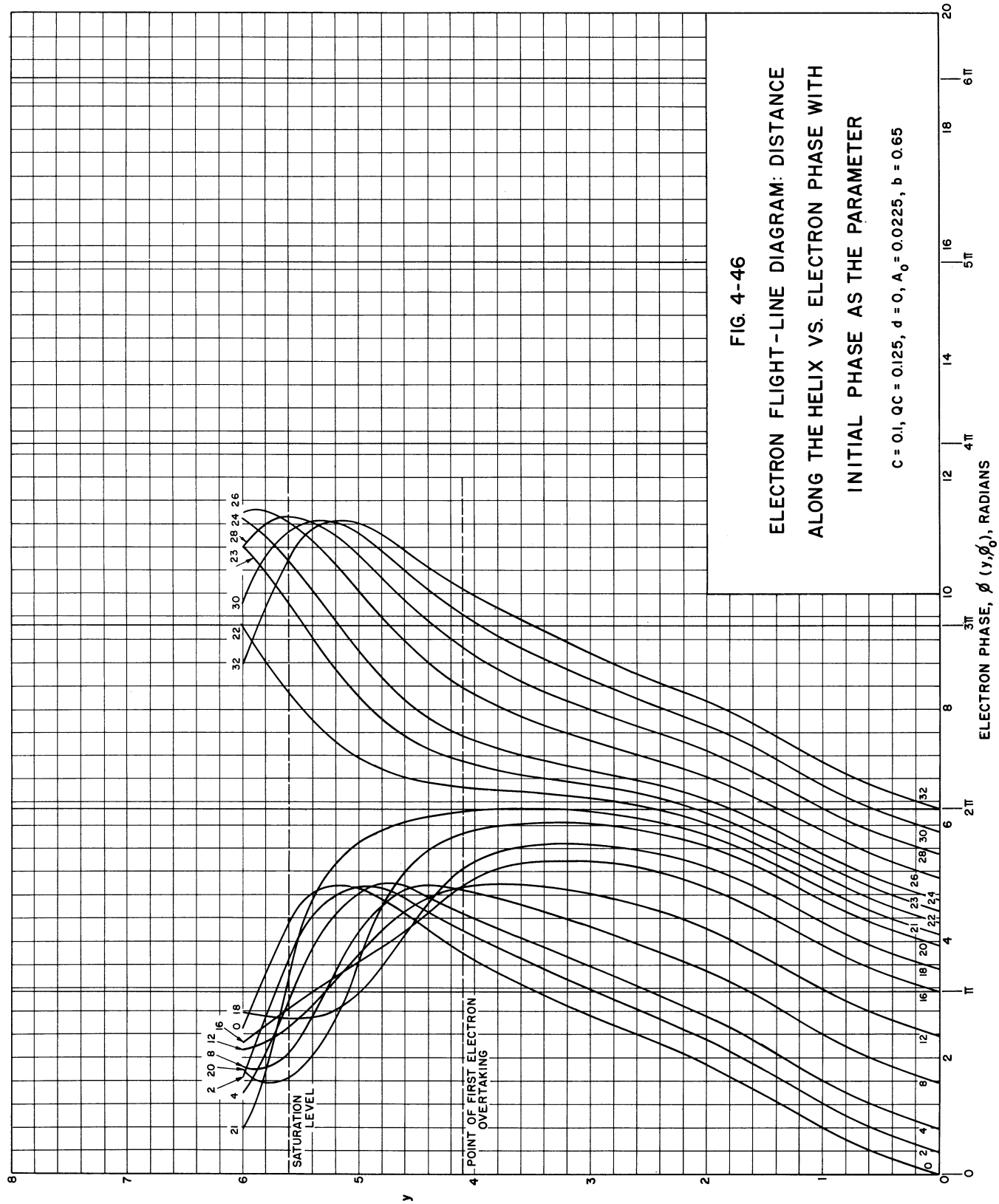
FIG. 4-46
ELECTRON FLIGHT-LINE DIAGRAM: DISTANCE ALONG THE HELIX VS. ELECTRON PHASE WITH INITIAL PHASE AS THE PARAMETER
C = 0.1, QC = 0.125, d = 0, A_0 = 0.0225, b = 0.65
SATURATION LEVEL
POINT OF FIRST ELECTRON OVERTAKING
y
ELECTRON PHASE, ϕ (y,ϕ_0), RADIANS
0
π
2π
3π
4π
5π
6π

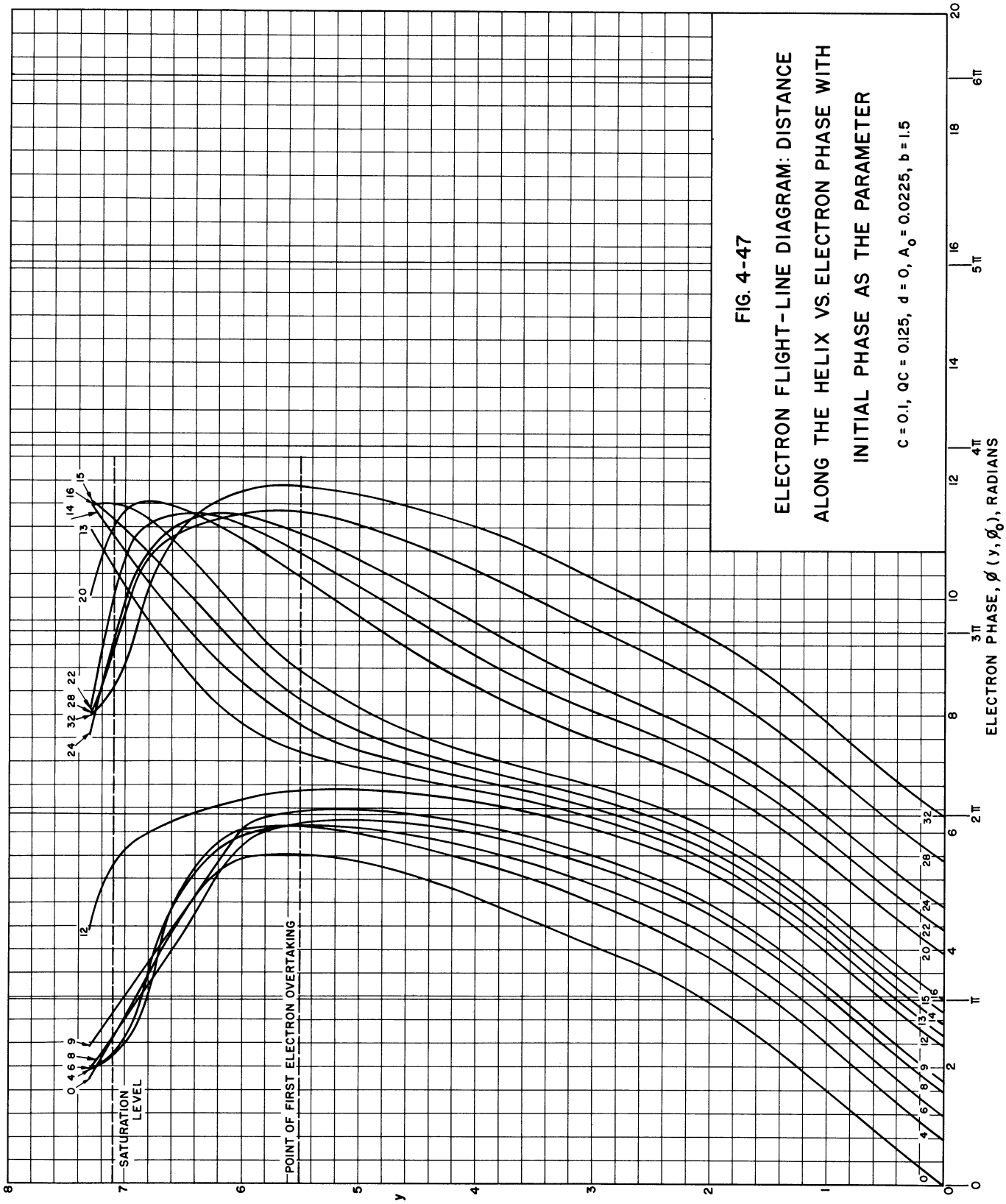
FIG. 4-47
ELECTRON FLIGHT-LINE DIAGRAM: DISTANCE ALONG THE HELIX VS. ELECTRON PHASE WITH INITIAL PHASE AS THE PARAMETER
C = 0.1, QC = 0.125, d = 0, A_0 = 0.0225, b = 1.5
SATURATION LEVEL
POINT OF FIRST ELECTRON OVERTAKING
y
ELECTRON PHASE, $\phi(y, \phi_0)$, RADIANS
0 4 6 8 9 12 13 14 16 15 20 24 32 28 22

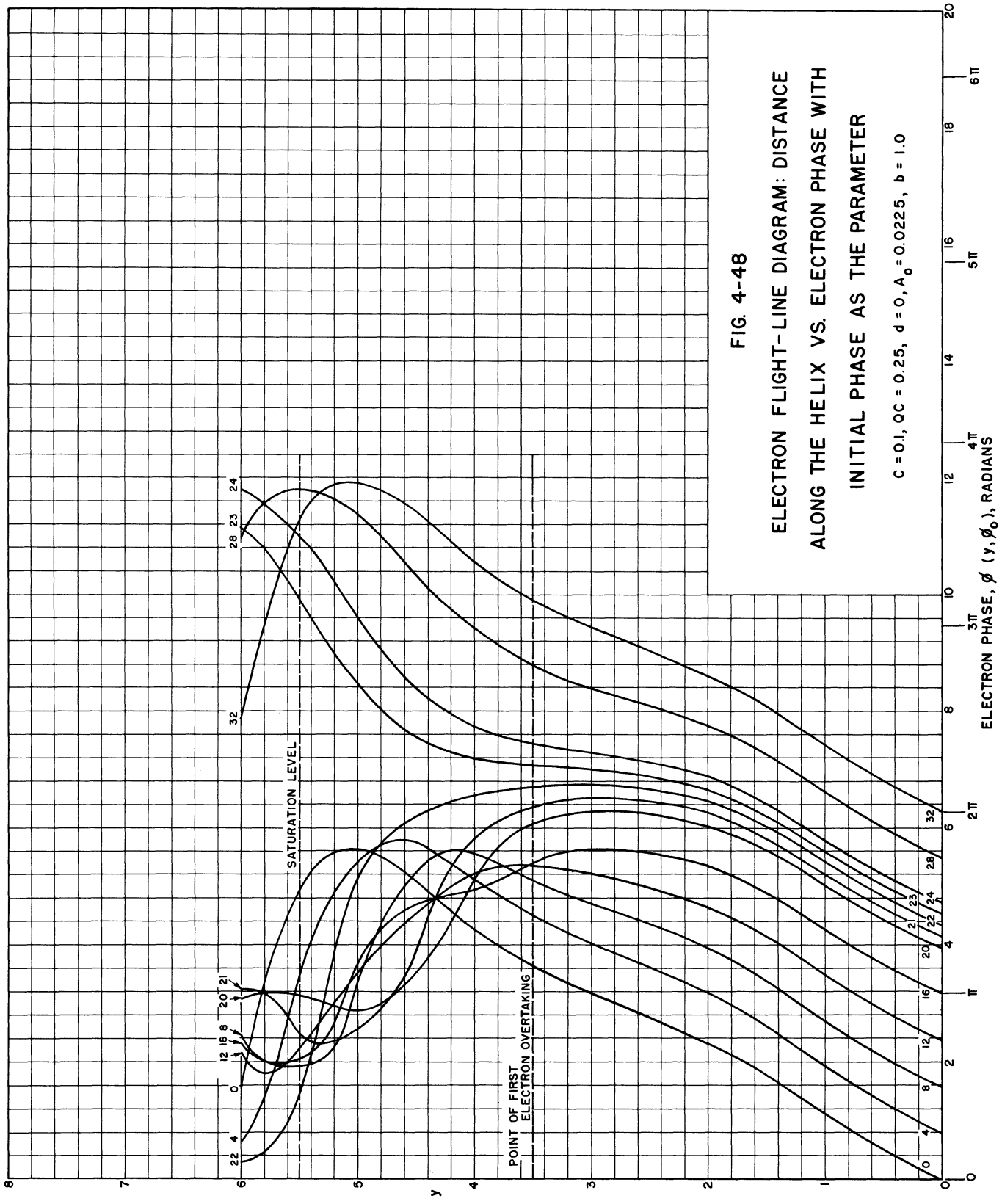
FIG. 4-48
ELECTRON FLIGHT-LINE DIAGRAM: DISTANCE ALONG THE HELIX VS. ELECTRON PHASE WITH INITIAL PHASE AS THE PARAMETER
C = 0.1, QC = 0.25, d = 0, A0 = 0.0225, b = 1.0
SATURATION LEVEL
POINT OF FIRST ELECTRON OVERTAKING
y
ELECTRON PHASE, ∅ (y, ∅0), RADIANS
0
π
2π
3π
4π
5π
6π

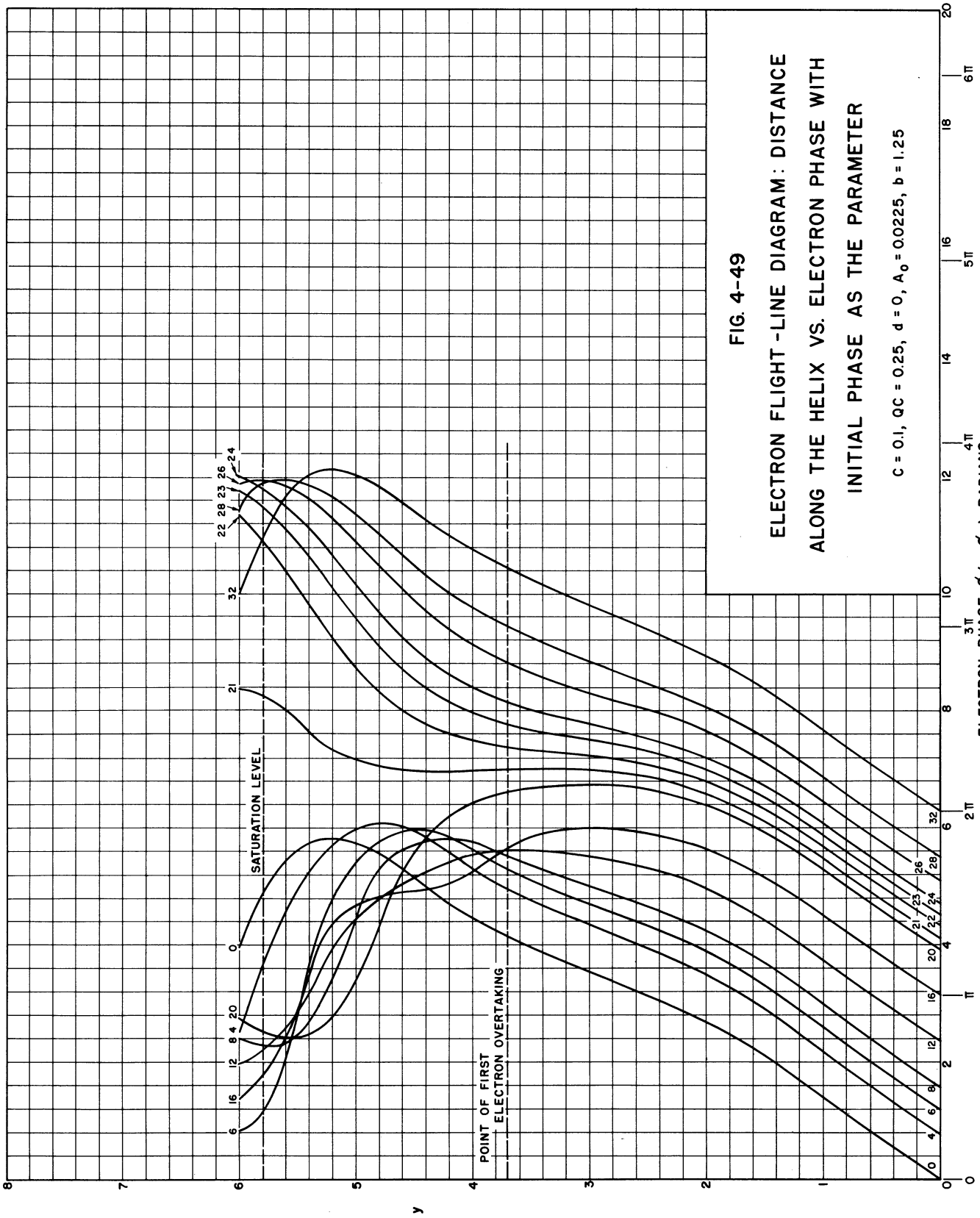
FIG. 4-49
ELECTRON FLIGHT-LINE DIAGRAM: DISTANCE ALONG THE HELIX VS. ELECTRON PHASE WITH INITIAL PHASE AS THE PARAMETER
C = 0.1, QC = 0.25, d = 0, A_0 = 0.0225, b = 1.25
SATURATION LEVEL
POINT OF FIRST ELECTRON OVERTAKING
y
ELECTRON PHASE, $\phi(y,\phi_0)$, RADIANS

to advance continually in phase until some of them are slowed down and become trapped in the negative-potential wells of the field. At saturation some of the electrons have not yet been trapped, but if the solution were carried beyond the first saturation point all the electrons would eventually become trapped in the negative-potential wells.

As would be expected, the larger the value of b the faster the electrons advance in phase with respect to the circuit wave; this effect is indicated by the decreased initial slope of the curves, i.e., $dy/d\phi$ is less.

Flight-line diagrams are presented for various values of C and QC so that the electron motions may be compared for the different cases. As a typical set of curves consider Fig. 4-42, where C = 0.1, QC = 0, and b = 0.1525. At y = 4 electrons 4 through 22 are in a retarding-field region and hence are decelerated and must have velocities less than the wave velocity. These electrons are giving up energy to the circuit wave. Electron 23, on the other hand, has sufficient velocity with respect to the wave not to be trapped, so it continues to advance in phase. Electrons of this latter class become trapped after they cross the $\phi = 3\pi$ boundary. Electrons in the category of No. 22 have velocities comparable to the wave velocity and hence continue to advance with the wave, forming the core of the bunch contributing energy to the circuit. Electrons 4 through 21 become trapped and near y = 5.5 they cross back over the $\phi = \pi$ boundary from a decelerating to an accelerating region. Between $\phi = 0$ and $\phi = \pi$ the electrons are accelerated, gaining in kinetic energy due to transfer of energy from the circuit to the stream.

4.6 Normalized Linear Current Density vs. Electron Phase

Information on the current distribution in the electron stream at any position y may be obtained by evaluating the expression

$$\frac{|I|}{I_o} = \frac{\rho(y,\phi_o)u_o}{I_o} = \sum \left|\frac{\partial\phi_o}{\partial\phi}\right| \frac{1}{1 + 2Cu(y,\phi_o)} \qquad (4\text{-}6)$$

for a particular value of y. The summation sign in Eq. 4-6 is necessary because when overtaking occurs then there are in general three terms contributing to the total current density, as can be seen clearly from the electron-phase curves of Section 4.4.

The current-density curves for the same parameters and the same values of b as were used previously are presented in Figs. 4-50 through 4-57. The data for these curves are easily obtained from the curves of electron phase and velocity deviation of Sections 4.3 and 4.4 respectively. In this group the current density is plotted against one period of the electron phase. The signal level on the helix is given in db referenced to the saturation level for convenience.

The infinite peaks in the current-density curves arise from the regions of zero slope in the ϕ vs. ϕ_o curves of Section 4.3. These infinite peaks do not indicate infinite current density, since the charge is conserved. An estimate of the actual current density at these points may be obtained from the flight-line diagrams of Section 4.5.

In each case it is noticed that the initial electron bunch forms between $\phi = 5\pi/4$ and $\phi = 3\pi/2$ and remains invariant with distance. As saturation is approached a second bunch is formed which at saturation is displaced approximately π radians from the first bunch. At saturation one bunch is in a decelerating region and the other is in an accelerating region of the field, so that one bunch contributes energy to the helix and the other receives energy from the circuit wave. Clearly at saturation these energy transfers balance one another, since by definition there is no net transfer of energy between the wave and the stream.

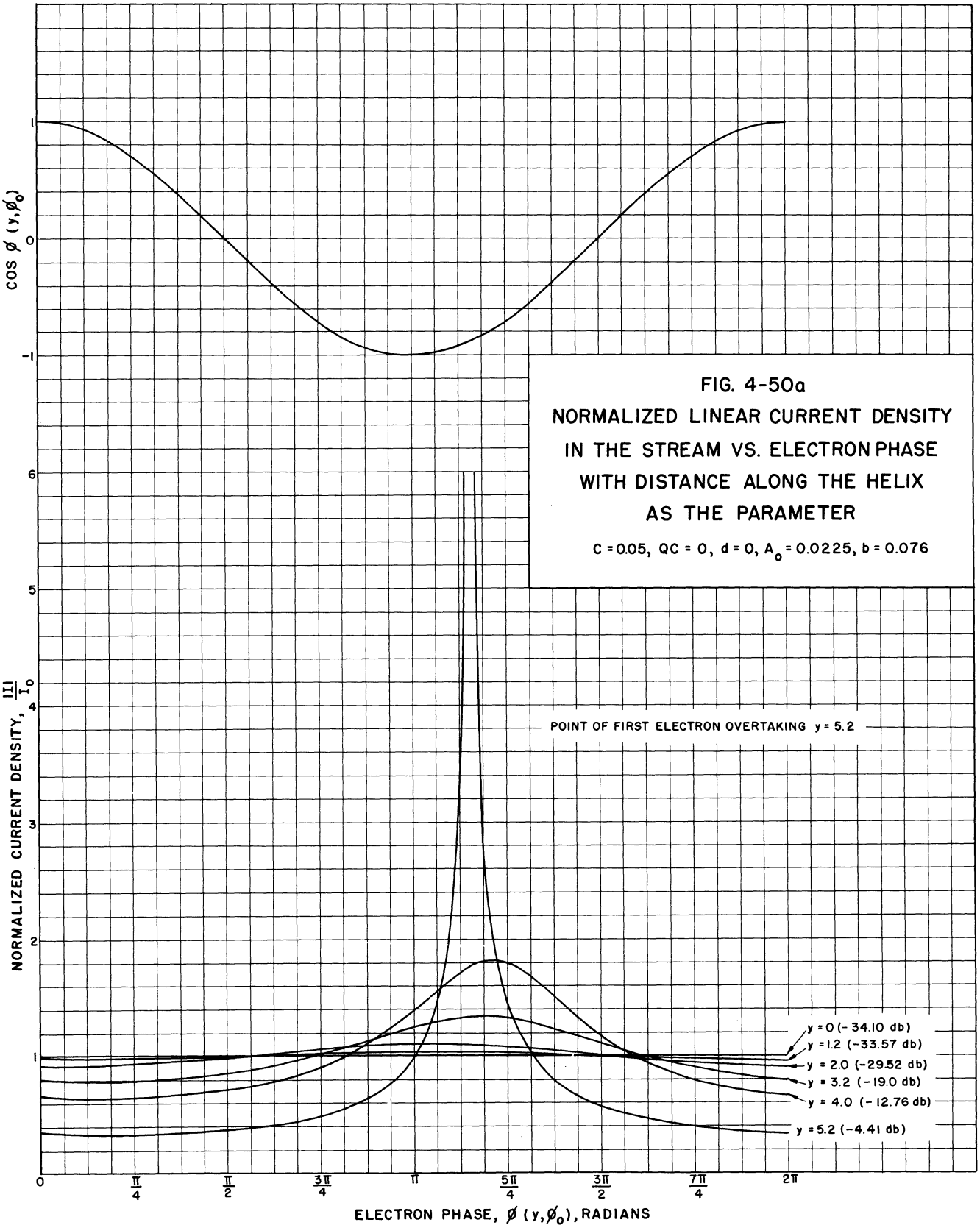

FIG. 4-50a
NORMALIZED LINEAR CURRENT DENSITY IN THE STREAM VS. ELECTRON PHASE WITH DISTANCE ALONG THE HELIX AS THE PARAMETER

C = 0.05, QC = 0, d = 0, A_o = 0.0225, b = 0.076

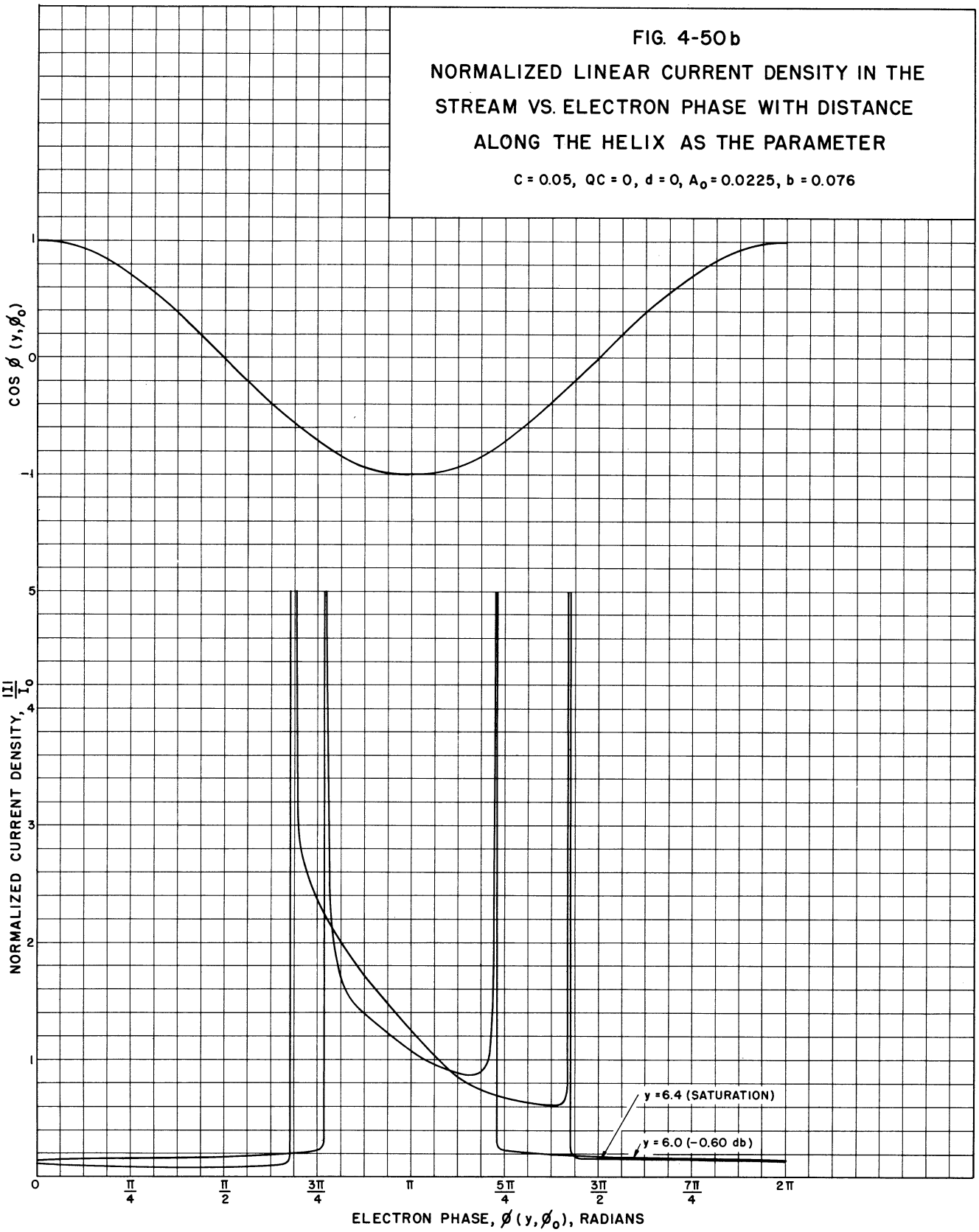
FIG. 4-50b
NORMALIZED LINEAR CURRENT DENSITY IN THE STREAM VS. ELECTRON PHASE WITH DISTANCE ALONG THE HELIX AS THE PARAMETER
C = 0.05, QC = 0, d = 0, A0 = 0.0225, b = 0.076
COS ∅ (y,∅0)
NORMALIZED CURRENT DENSITY, |I|/I0
y = 6.4 (SATURATION)
y = 6.0 (−0.60 db)
ELECTRON PHASE, ∅ (y,∅0), RADIANS

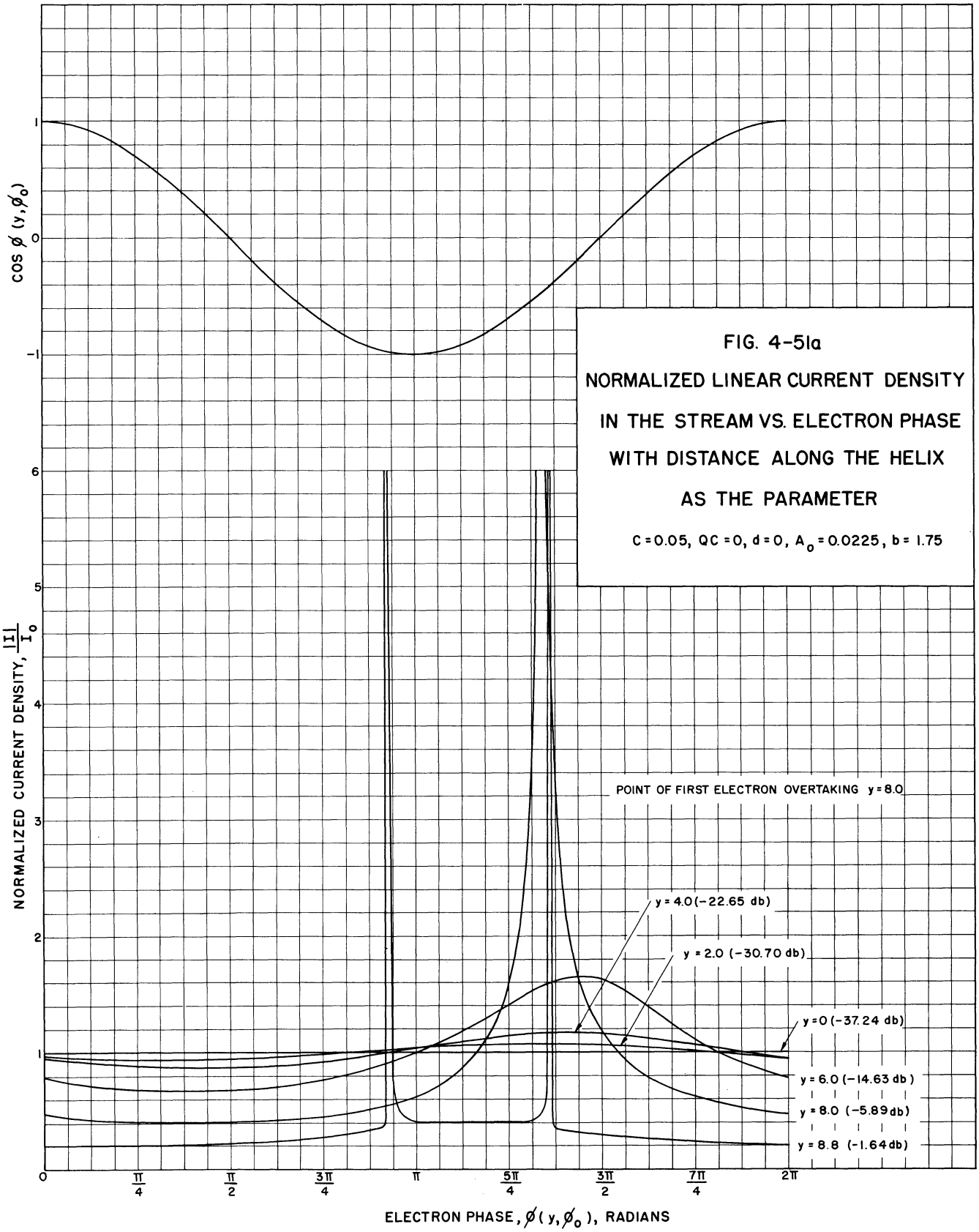

FIG. 4-51a

NORMALIZED LINEAR CURRENT DENSITY IN THE STREAM VS. ELECTRON PHASE WITH DISTANCE ALONG THE HELIX AS THE PARAMETER

C = 0.05, QC = 0, d = 0, A_0 = 0.0225, b = 1.75

FIG. 4-51b

NORMALIZED LINEAR CURRENT DENSITY

IN THE STREAM VS. ELECTRON PHASE WITH DISTANCE

ALONG THE HELIX AS THE PARAMETER

C = 0.05, QC = 0, d = 0, A_0 = 0.0225, b = 1.75

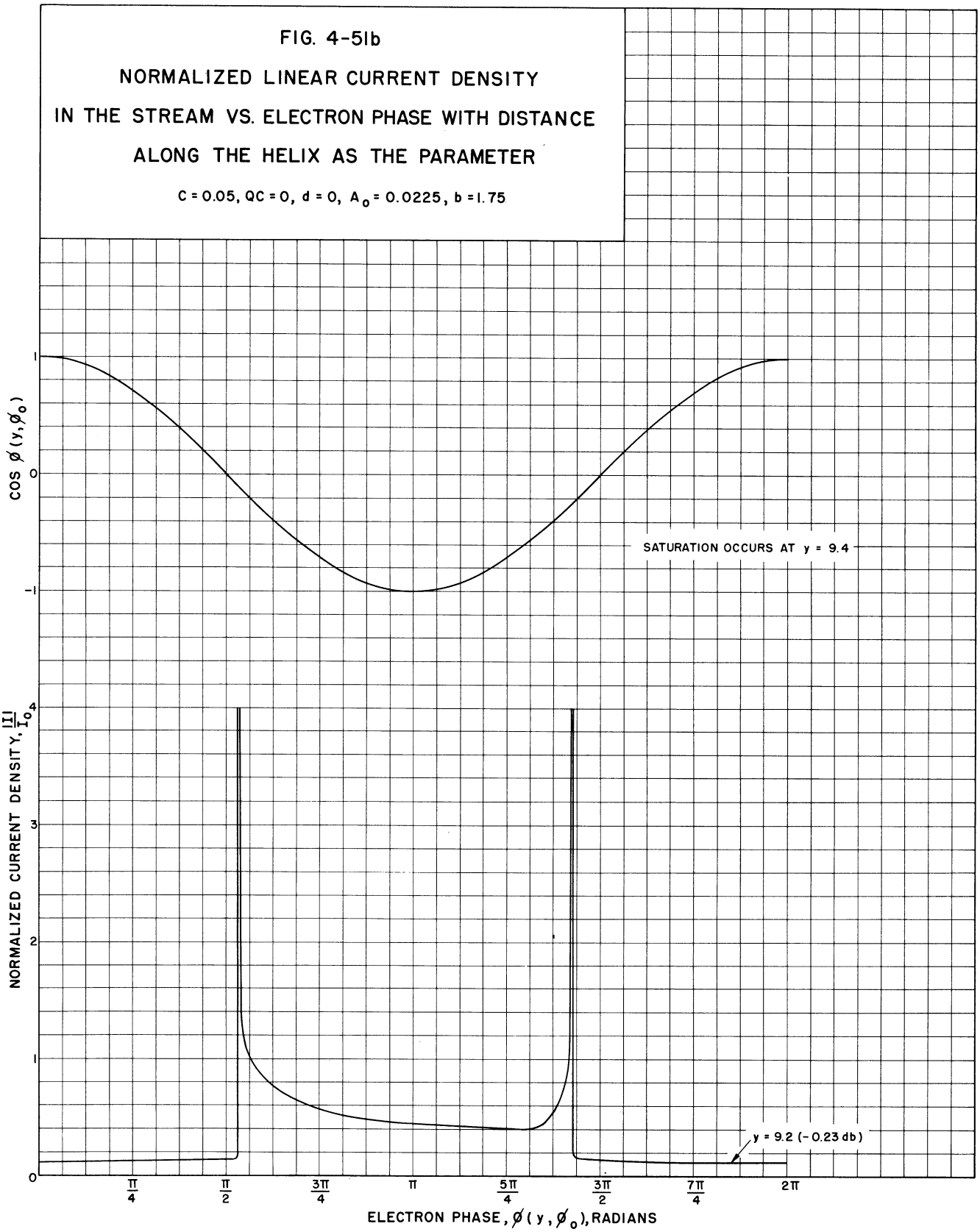

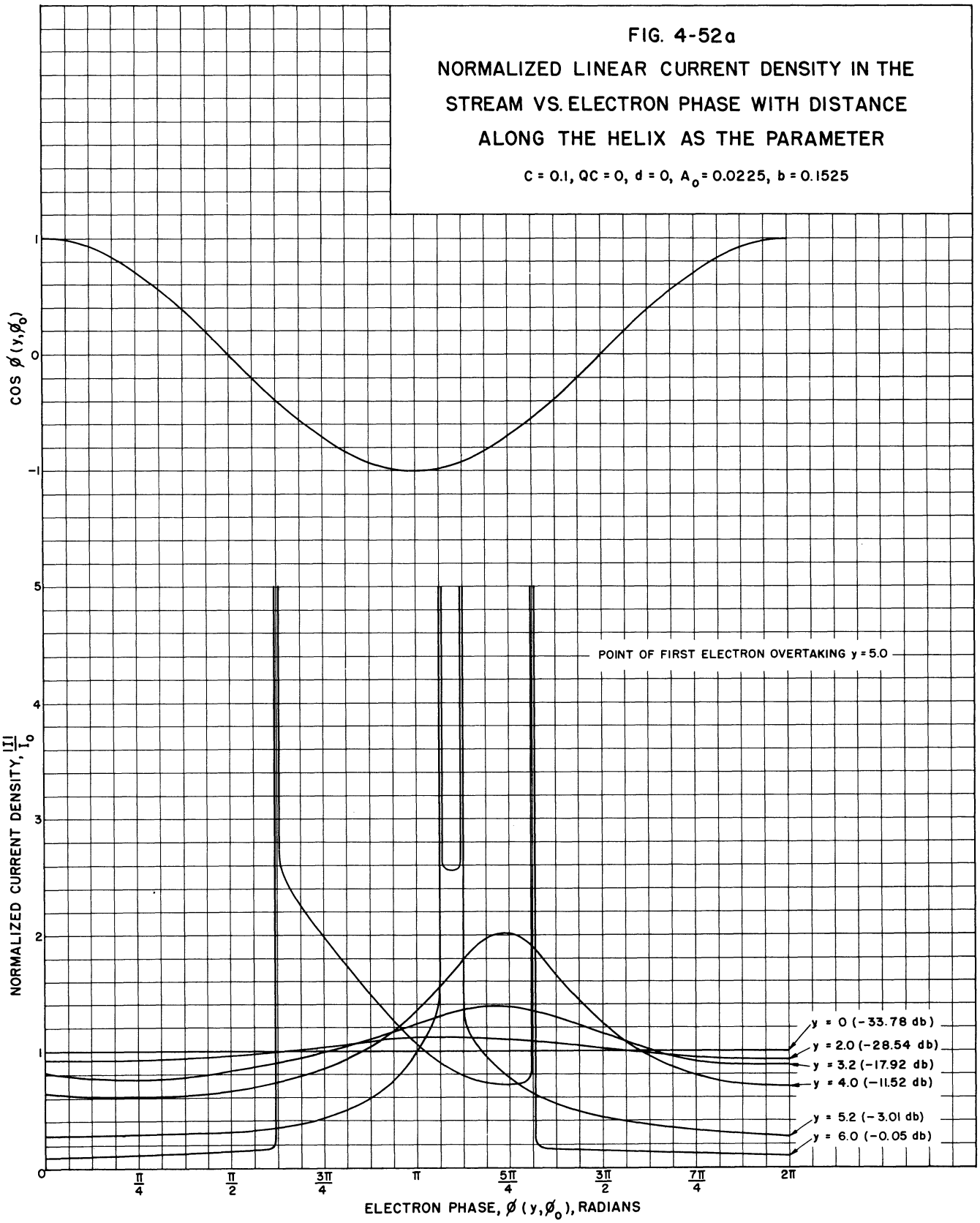
FIG. 4-52a
NORMALIZED LINEAR CURRENT DENSITY IN THE STREAM VS. ELECTRON PHASE WITH DISTANCE ALONG THE HELIX AS THE PARAMETER
C = 0.1, QC = 0, d = 0, A0 = 0.0225, b = 0.1525
COS ∅ (y,∅0)
NORMALIZED CURRENT DENSITY, |I1|/I0
POINT OF FIRST ELECTRON OVERTAKING y = 5.0
y = 0 (-33.78 db)
y = 2.0 (-28.54 db)
y = 3.2 (-17.92 db)
y = 4.0 (-11.52 db)
y = 5.2 (-3.01 db)
y = 6.0 (-0.05 db)
ELECTRON PHASE, ∅ (y,∅0), RADIANS

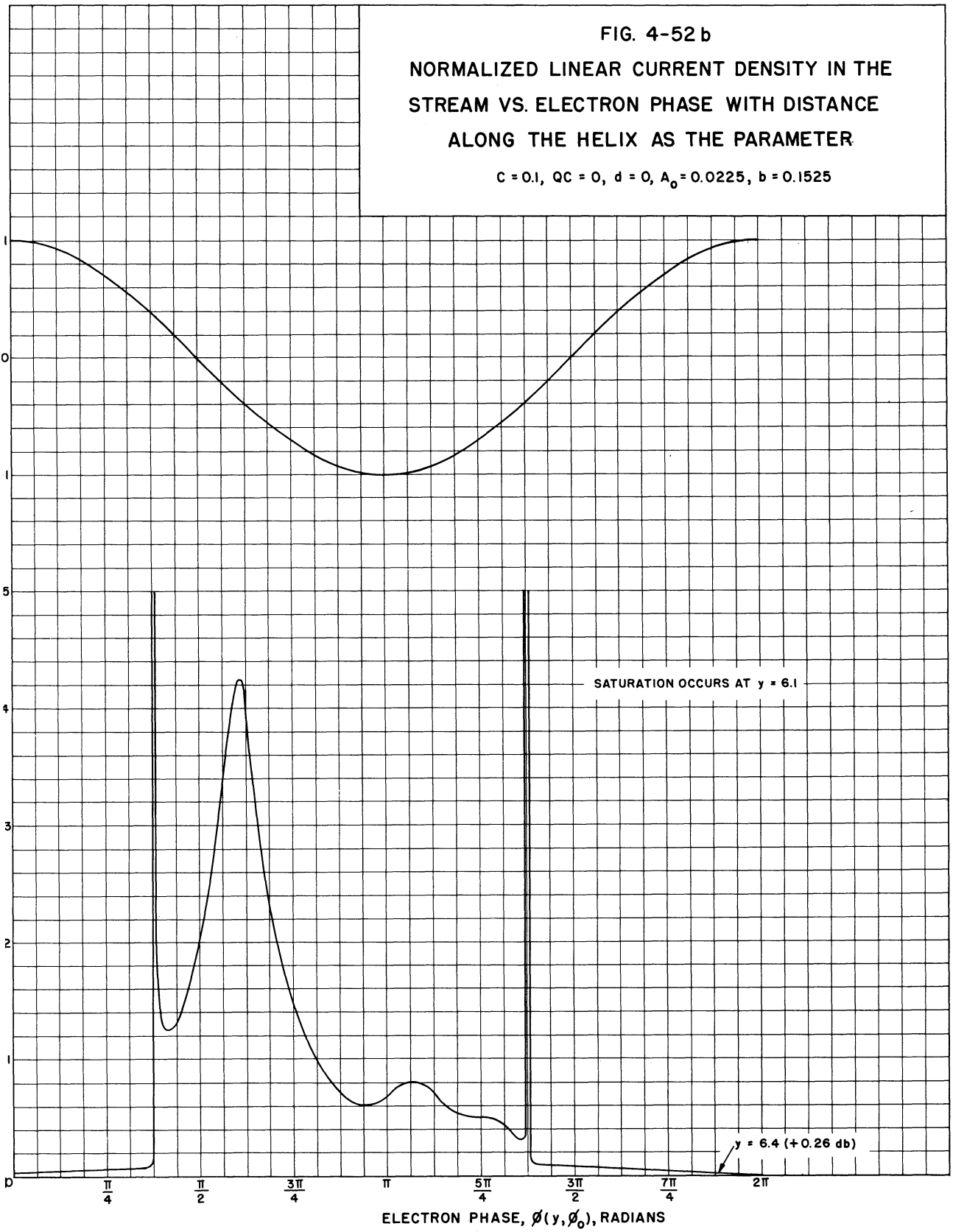
FIG. 4-52 b
NORMALIZED LINEAR CURRENT DENSITY IN THE STREAM VS. ELECTRON PHASE WITH DISTANCE ALONG THE HELIX AS THE PARAMETER
C = 0.1, QC = 0, d = 0, A0 = 0.0225, b = 0.1525
SATURATION OCCURS AT y = 6.1
y = 6.4 (+0.26 db)
1
0
1
5
4
3
2
1
0
π/4
π/2
3π/4
π
5π/4
3π/2
7π/4
2π
ELECTRON PHASE, ø(y,ø0), RADIANS

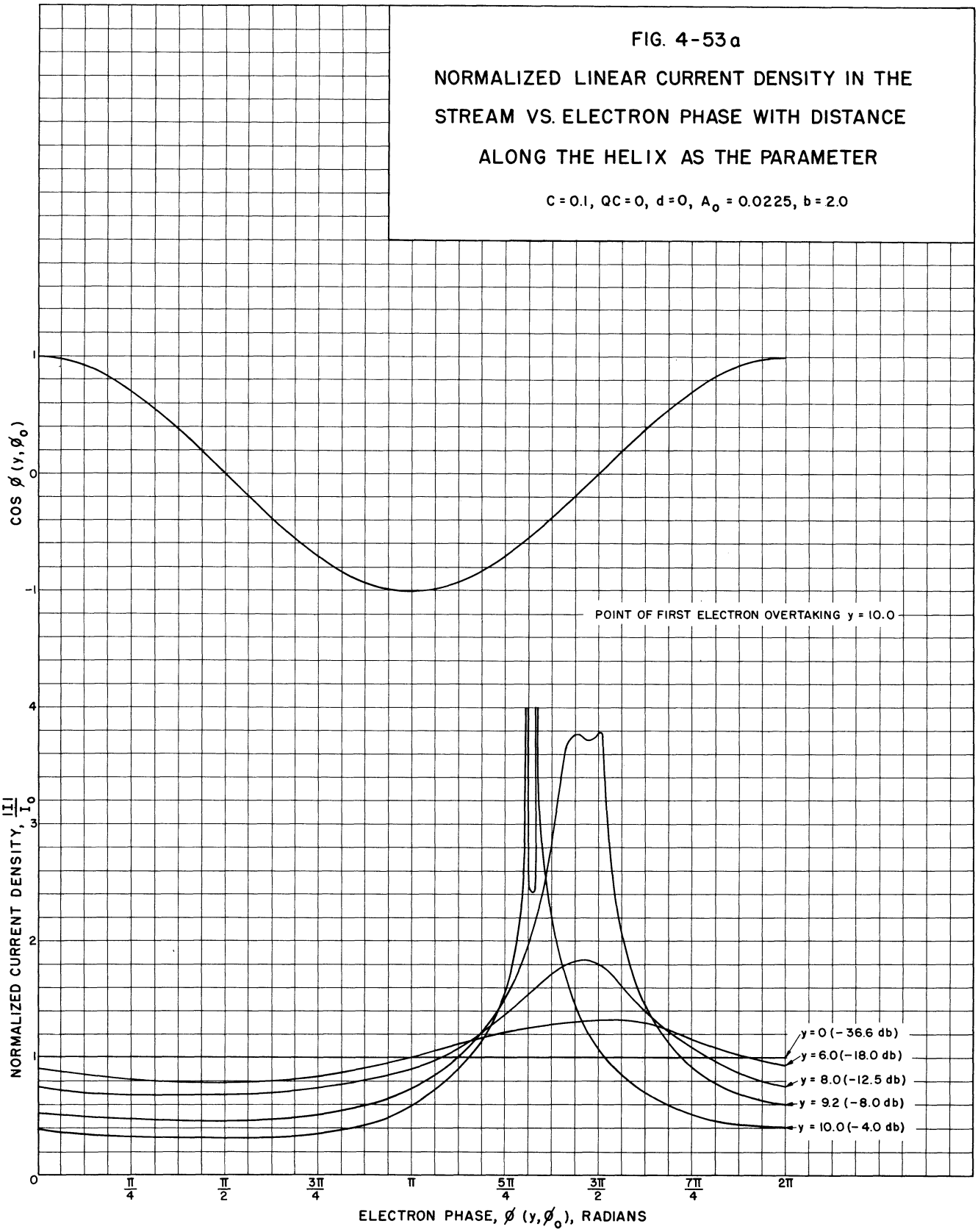
FIG. 4-53a
NORMALIZED LINEAR CURRENT DENSITY IN THE STREAM VS. ELECTRON PHASE WITH DISTANCE ALONG THE HELIX AS THE PARAMETER
C = 0.1, QC = 0, d = 0, A_0 = 0.0225, b = 2.0
COS ∅ (y, ∅o)
POINT OF FIRST ELECTRON OVERTAKING y = 10.0
NORMALIZED CURRENT DENSITY, |I1|/Io
y = 0 (- 36.6 db)
y = 6.0 (-18.0 db)
y = 8.0 (-12.5 db)
y = 9.2 (-8.0 db)
y = 10.0 (- 4.0 db)
ELECTRON PHASE, ∅ (y, ∅o), RADIANS

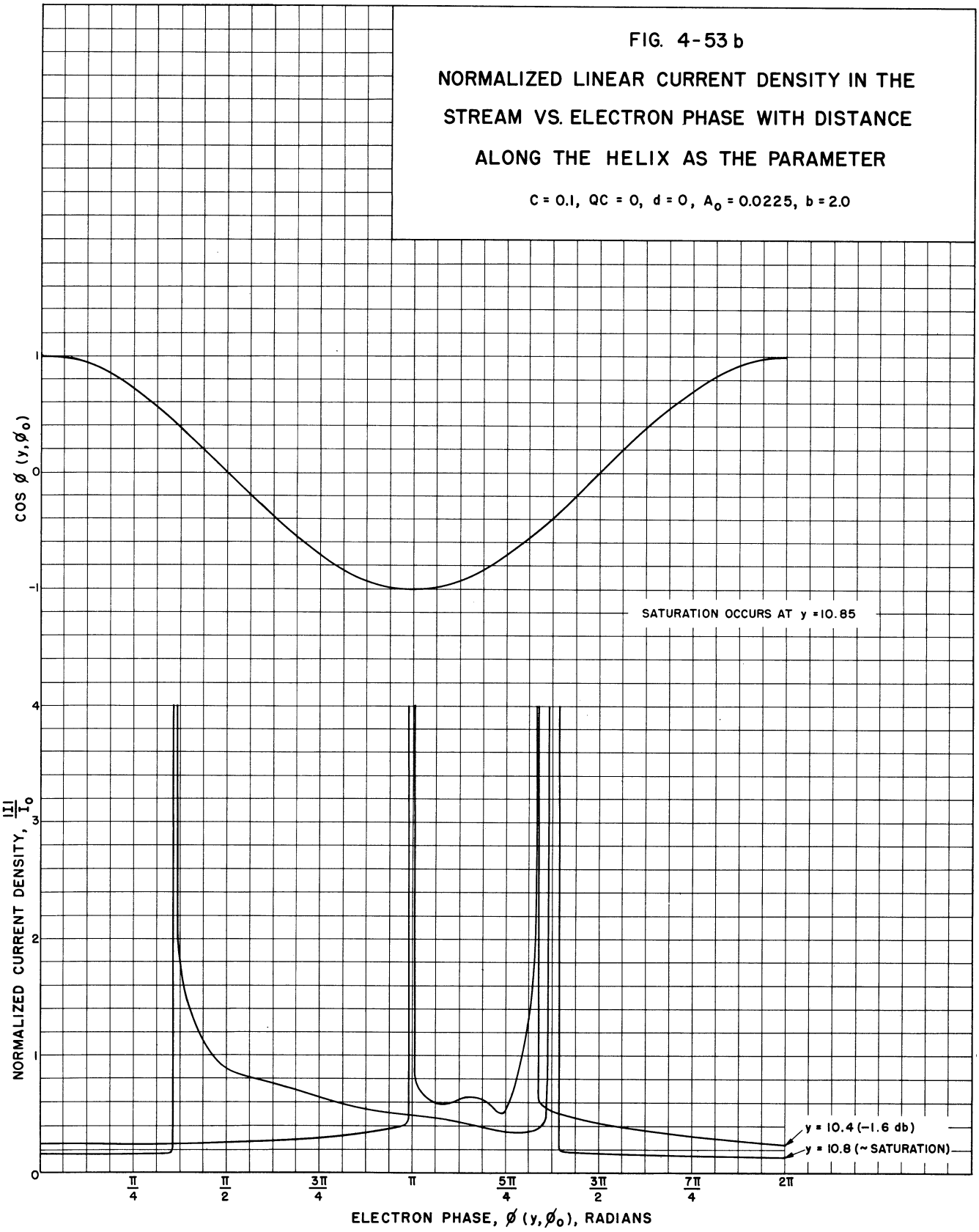
FIG. 4-53 b
NORMALIZED LINEAR CURRENT DENSITY IN THE STREAM VS. ELECTRON PHASE WITH DISTANCE ALONG THE HELIX AS THE PARAMETER
C = 0.1, QC = 0, d = 0, A_0 = 0.0225, b = 2.0
COS ∅ (y, $∅_0$)
SATURATION OCCURS AT y = 10.85
NORMALIZED CURRENT DENSITY, $\frac{|I|}{I_0}$
y = 10.4 (-1.6 db)
y = 10.8 (~ SATURATION)
ELECTRON PHASE, ∅ (y, $∅_0$), RADIANS

FIG. 4-54a

NORMALIZED LINEAR CURRENT DENSITY IN THE STREAM VS. ELECTRON PHASE WITH DISTANCE ALONG THE HELIX AS THE PARAMETER

C = 0.2, QC = 0, d = 0, A_0 = 0.0225, b = 0.31

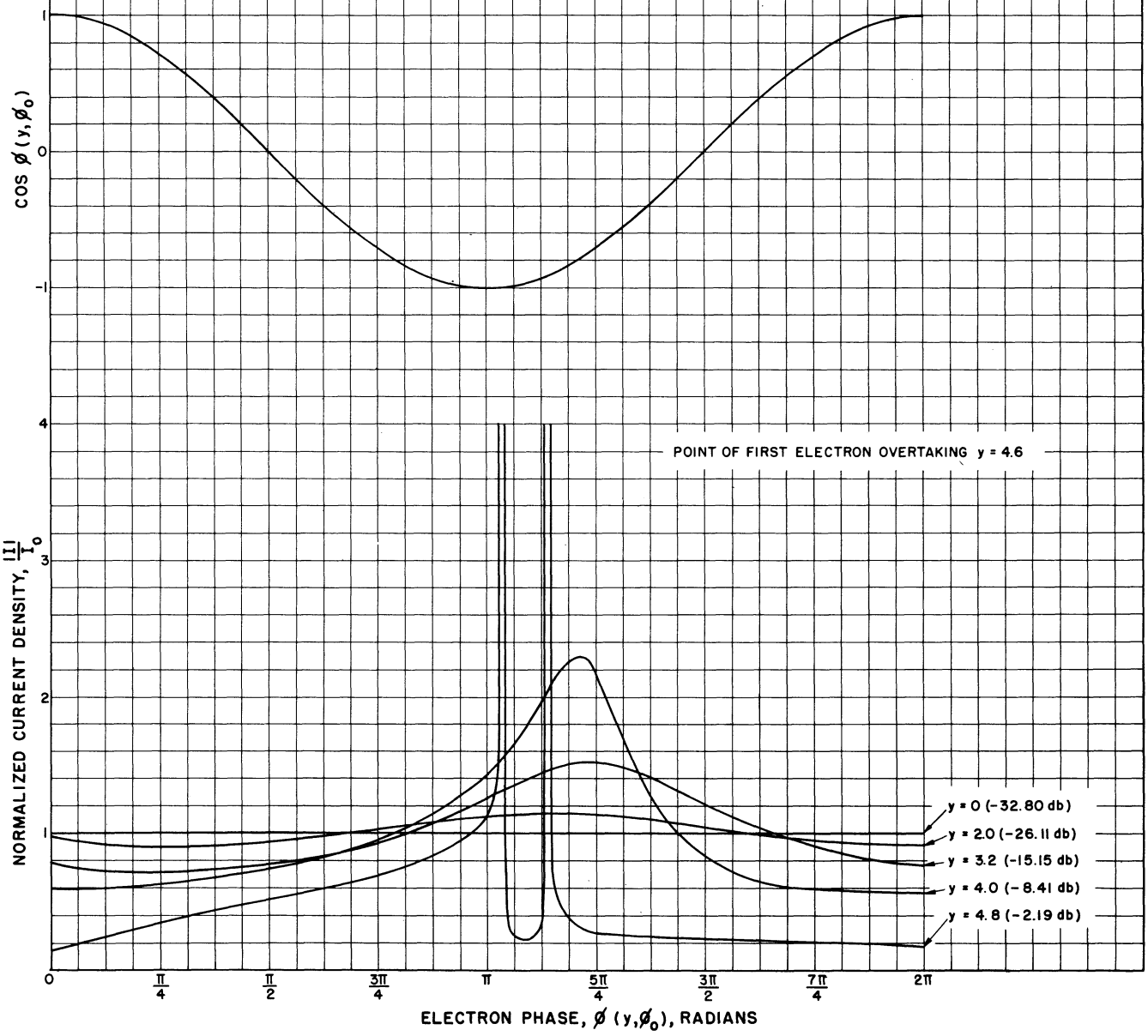

FIG. 4-54b

NORMALIZED LINEAR CURRENT DENSITY IN THE STREAM VS. ELECTRON PHASE WITH DISTANCE ALONG THE HELIX AS THE PARAMETER

C = 0.2, QC = 0, d = 0, A_0 = 0.0225, b = 0.31

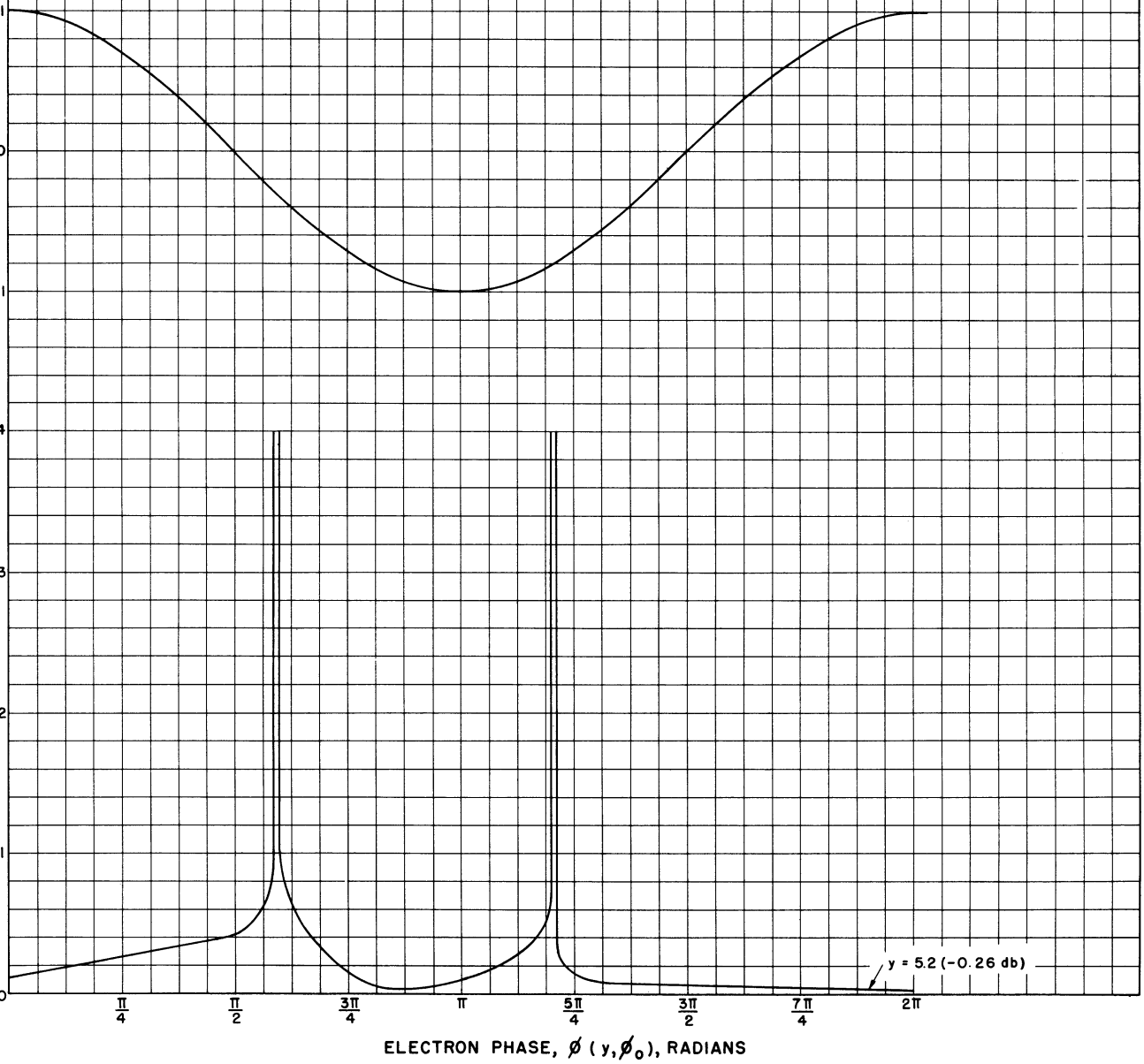

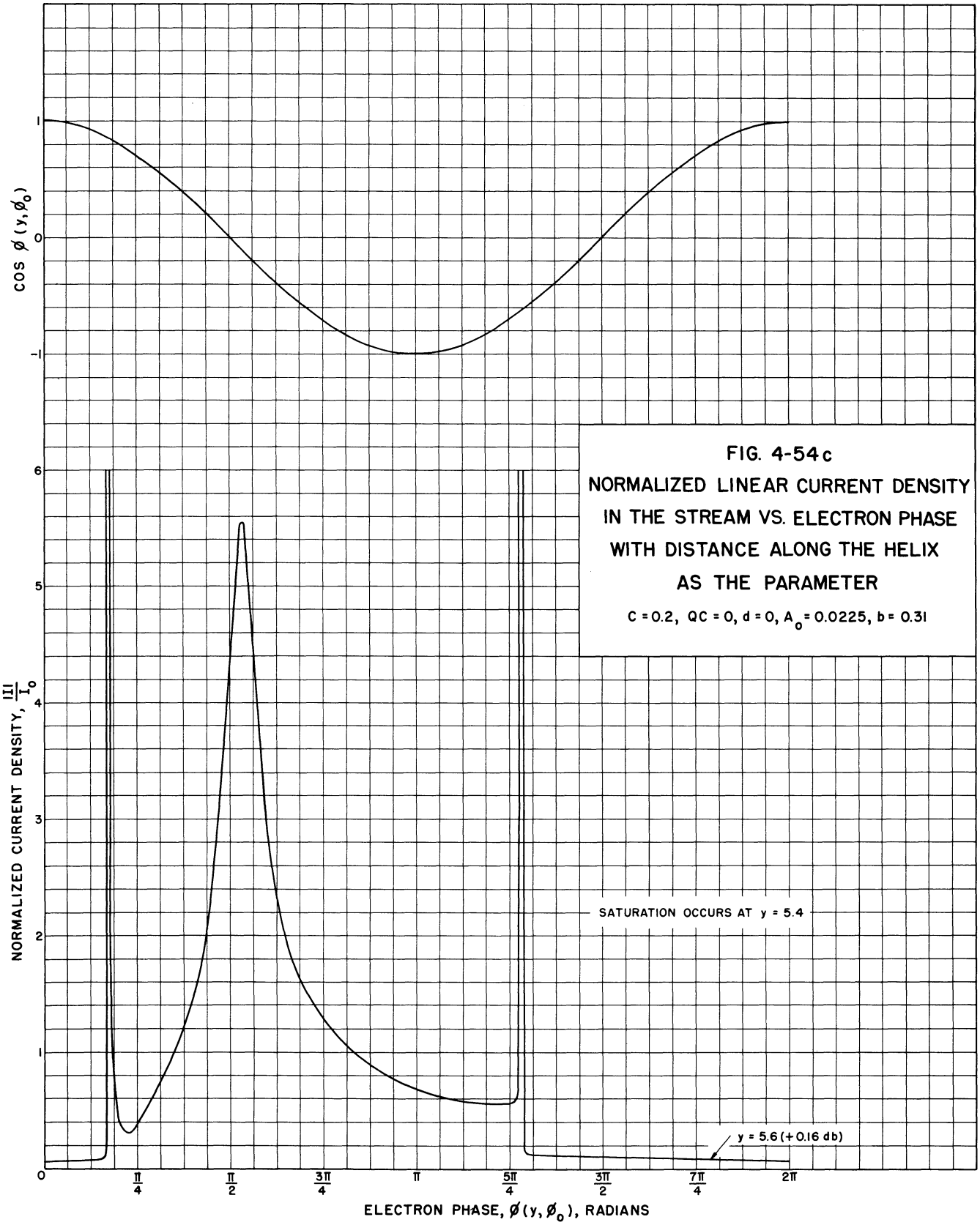

FIG. 4-54c
NORMALIZED LINEAR CURRENT DENSITY IN THE STREAM VS. ELECTRON PHASE WITH DISTANCE ALONG THE HELIX AS THE PARAMETER

C = 0.2, QC = 0, d = 0, A_0 = 0.0225, b = 0.31

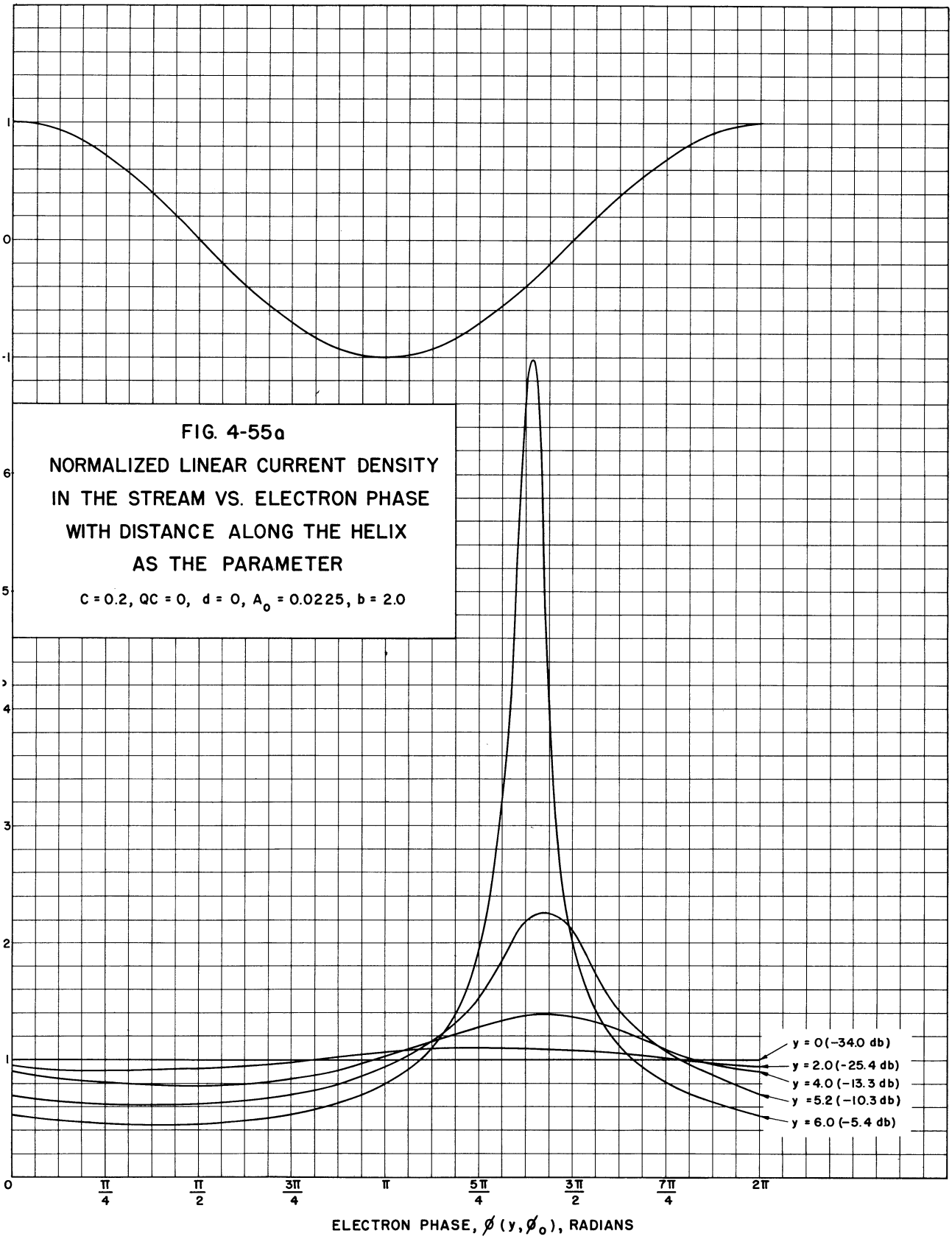

FIG. 4-55a
NORMALIZED LINEAR CURRENT DENSITY IN THE STREAM VS. ELECTRON PHASE WITH DISTANCE ALONG THE HELIX AS THE PARAMETER

C = 0.2, QC = 0, d = 0, A_0 = 0.0225, b = 2.0

FIG. 4-55b

NORMALIZED LINEAR CURRENT DENSITY IN THE STREAM VS. ELECTRON PHASE WITH DISTANCE ALONG THE HELIX AS THE PARAMETER

C = 0.2, QC = 0, d = 0, A_0 = 0.0225, b = 2.0

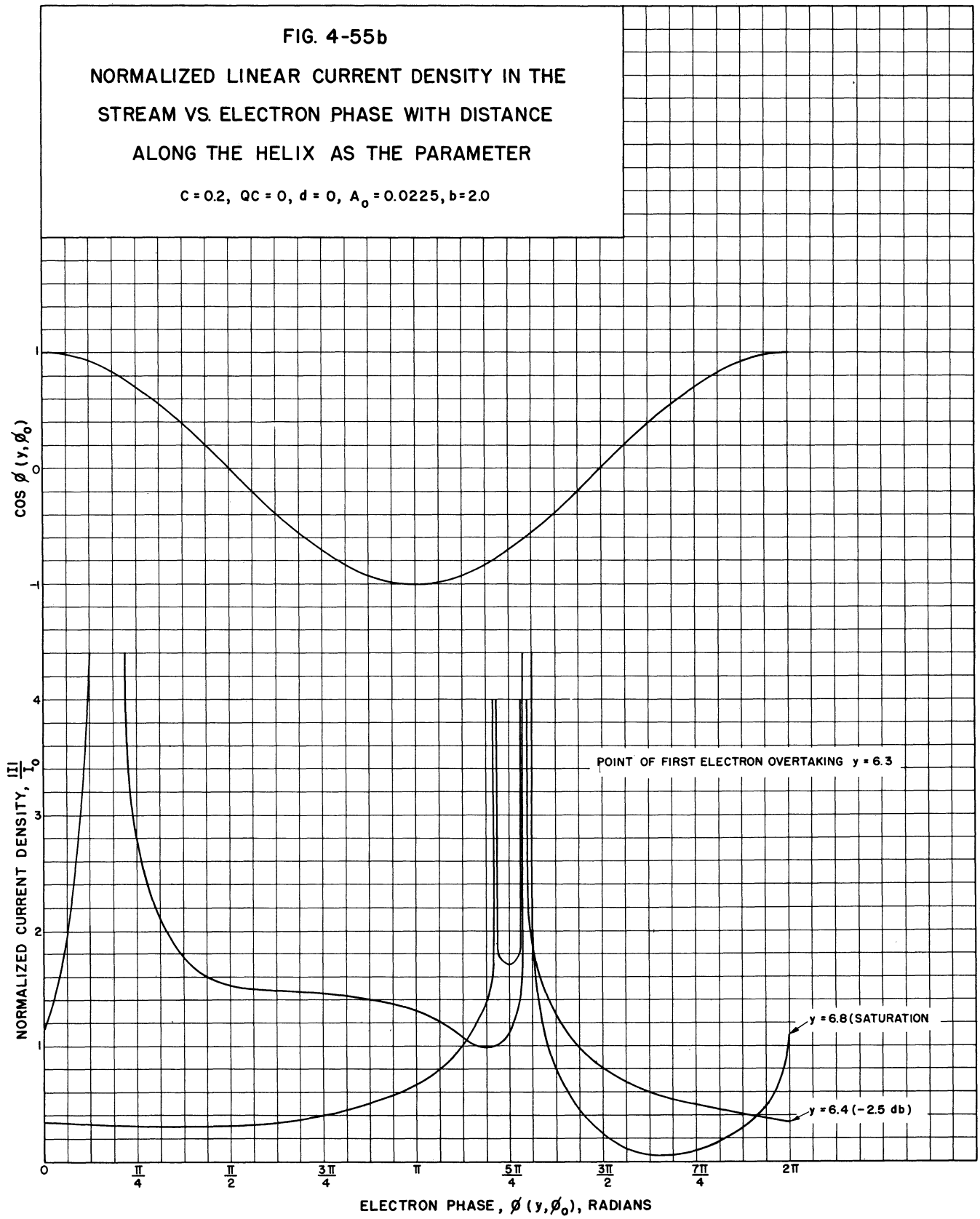

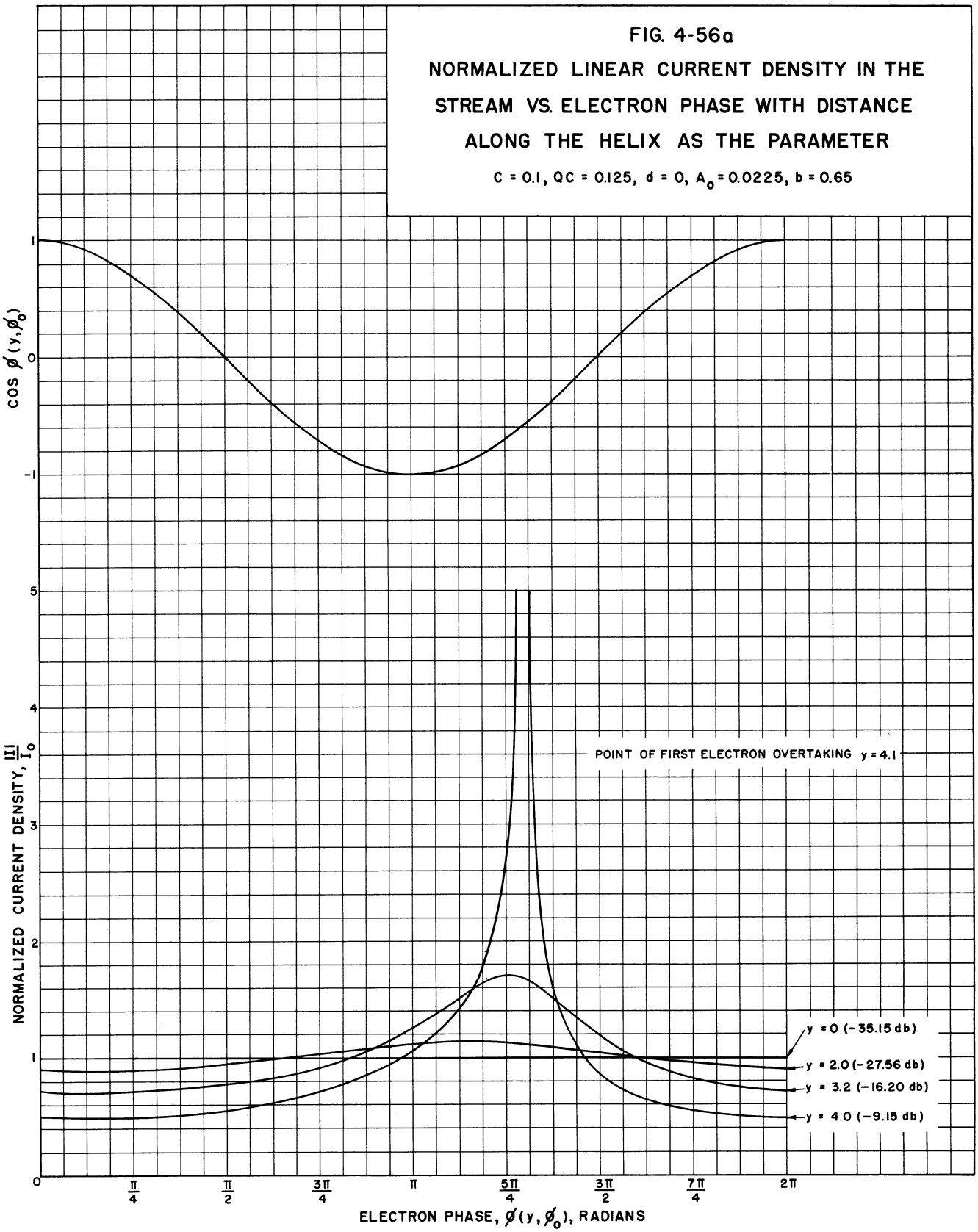
FIG. 4-56a
NORMALIZED LINEAR CURRENT DENSITY IN THE STREAM VS. ELECTRON PHASE WITH DISTANCE ALONG THE HELIX AS THE PARAMETER
C = 0.1, QC = 0.125, d = 0, A_0 = 0.0225, b = 0.65
COS $\phi(y,\phi_0)$
NORMALIZED CURRENT DENSITY, $\frac{|I|}{I_0}$
POINT OF FIRST ELECTRON OVERTAKING y = 4.1
y = 0 (-35.15 db)
y = 2.0 (-27.56 db)
y = 3.2 (-16.20 db)
y = 4.0 (-9.15 db)
ELECTRON PHASE, $\phi(y,\phi_0)$, RADIANS

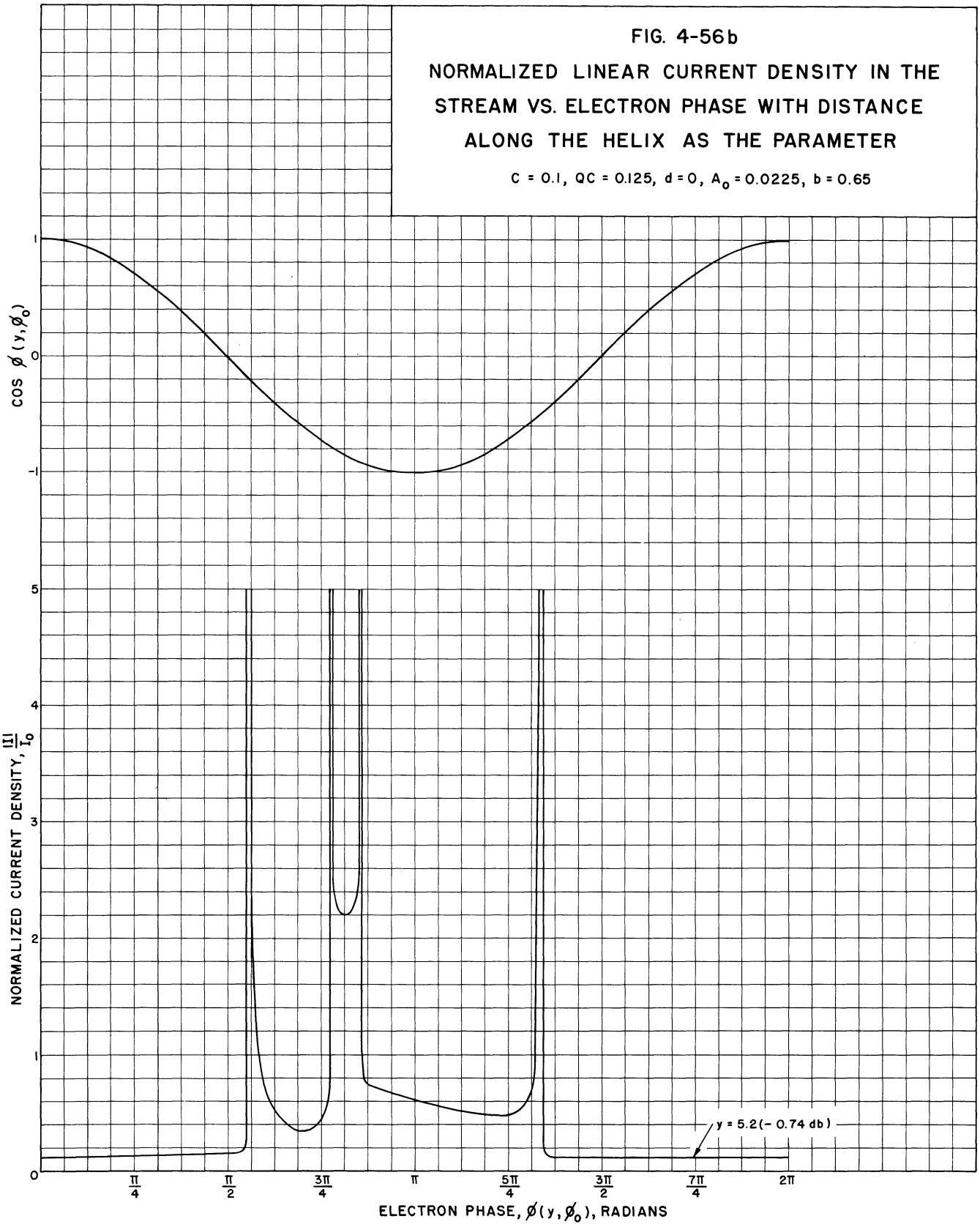
FIG. 4-56b
NORMALIZED LINEAR CURRENT DENSITY IN THE STREAM VS. ELECTRON PHASE WITH DISTANCE ALONG THE HELIX AS THE PARAMETER
C = 0.1, QC = 0.125, d = 0, A_0 = 0.0225, b = 0.65
COS $\phi(y,\phi_0)$
NORMALIZED CURRENT DENSITY, $\frac{|I|}{I_0}$
y = 5.2(- 0.74 db)
$\frac{\pi}{4}$ $\frac{\pi}{2}$ $\frac{3\pi}{4}$ π $\frac{5\pi}{4}$ $\frac{3\pi}{2}$ $\frac{7\pi}{4}$ 2π
ELECTRON PHASE, $\phi(y,\phi_0)$, RADIANS

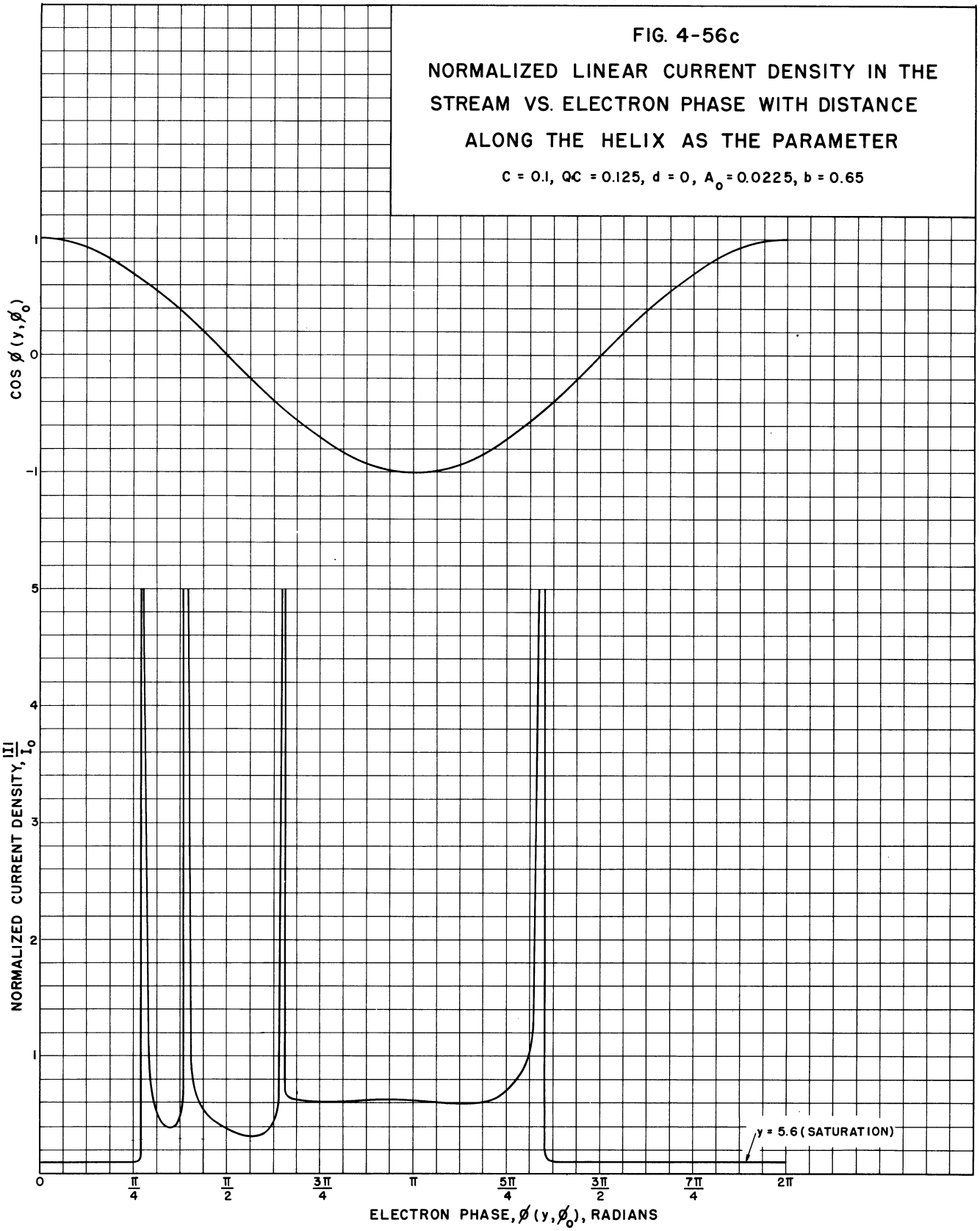
FIG. 4-56c
NORMALIZED LINEAR CURRENT DENSITY IN THE STREAM VS. ELECTRON PHASE WITH DISTANCE ALONG THE HELIX AS THE PARAMETER
C = 0.1, QC = 0.125, d = 0, A0 = 0.0225, b = 0.65
COS ∅ (y, ∅0)
1
0
-1
NORMALIZED CURRENT DENSITY, |I|/I0
5
4
3
2
1
y = 5.6 (SATURATION)
0
π/4
π/2
3π/4
π
5π/4
3π/2
7π/4
2π
ELECTRON PHASE, ∅ (y, ∅0), RADIANS

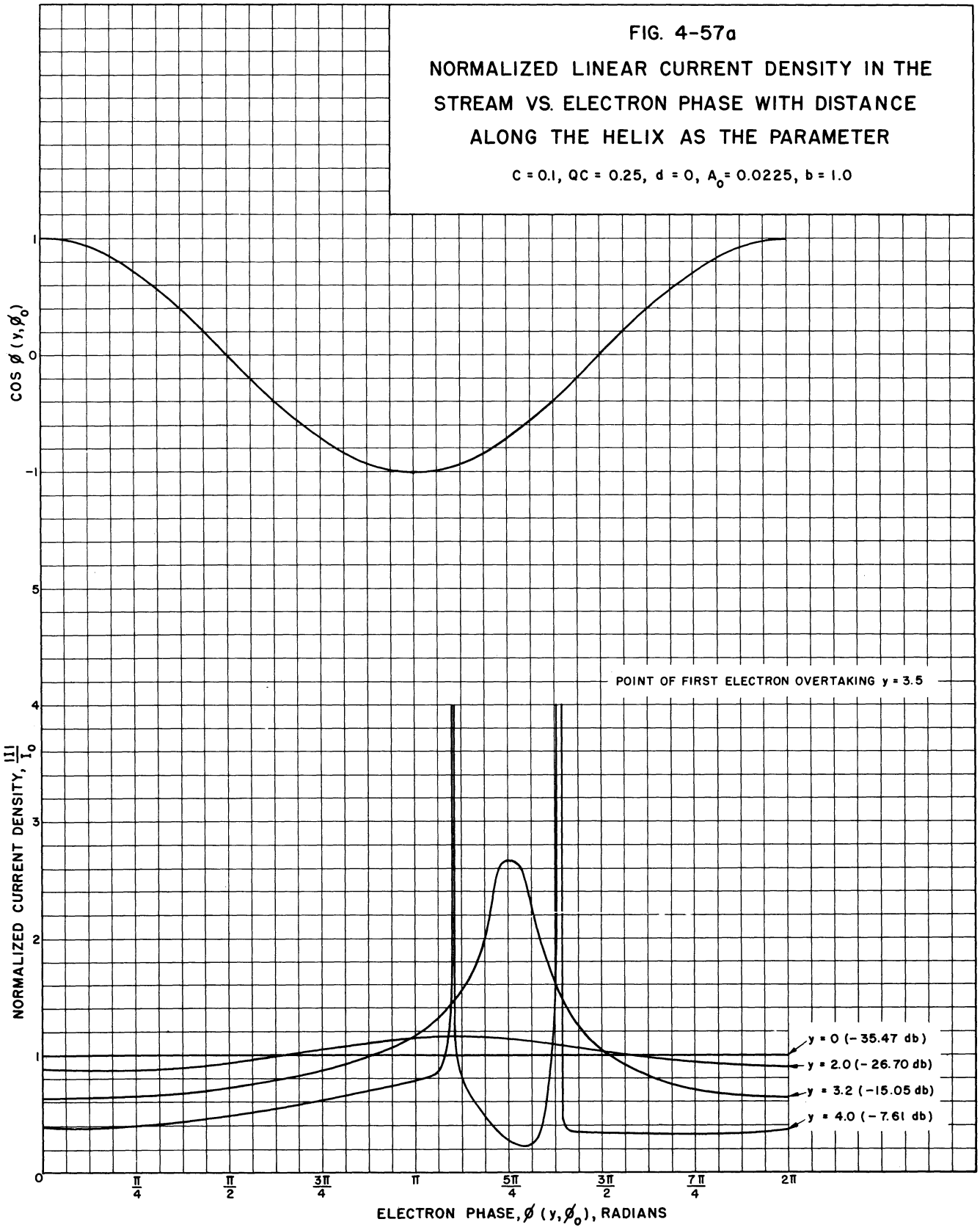
FIG. 4-57a
NORMALIZED LINEAR CURRENT DENSITY IN THE STREAM VS. ELECTRON PHASE WITH DISTANCE ALONG THE HELIX AS THE PARAMETER
C = 0.1, QC = 0.25, d = 0, A_0 = 0.0225, b = 1.0
COS ∅ (y, ∅₀)
1
0
-1
5
4
3
2
1
0
NORMALIZED CURRENT DENSITY, $\frac{|I|}{I_0}$
POINT OF FIRST ELECTRON OVERTAKING y = 3.5
y = 0 (- 35.47 db)
y = 2.0 (- 26.70 db)
y = 3.2 (-15.05 db)
y = 4.0 (- 7.61 db)
$\frac{\pi}{4}$
$\frac{\pi}{2}$
$\frac{3\pi}{4}$
π
$\frac{5\pi}{4}$
$\frac{3\pi}{2}$
$\frac{7\pi}{4}$
2π
ELECTRON PHASE, ∅ (y, ∅₀), RADIANS

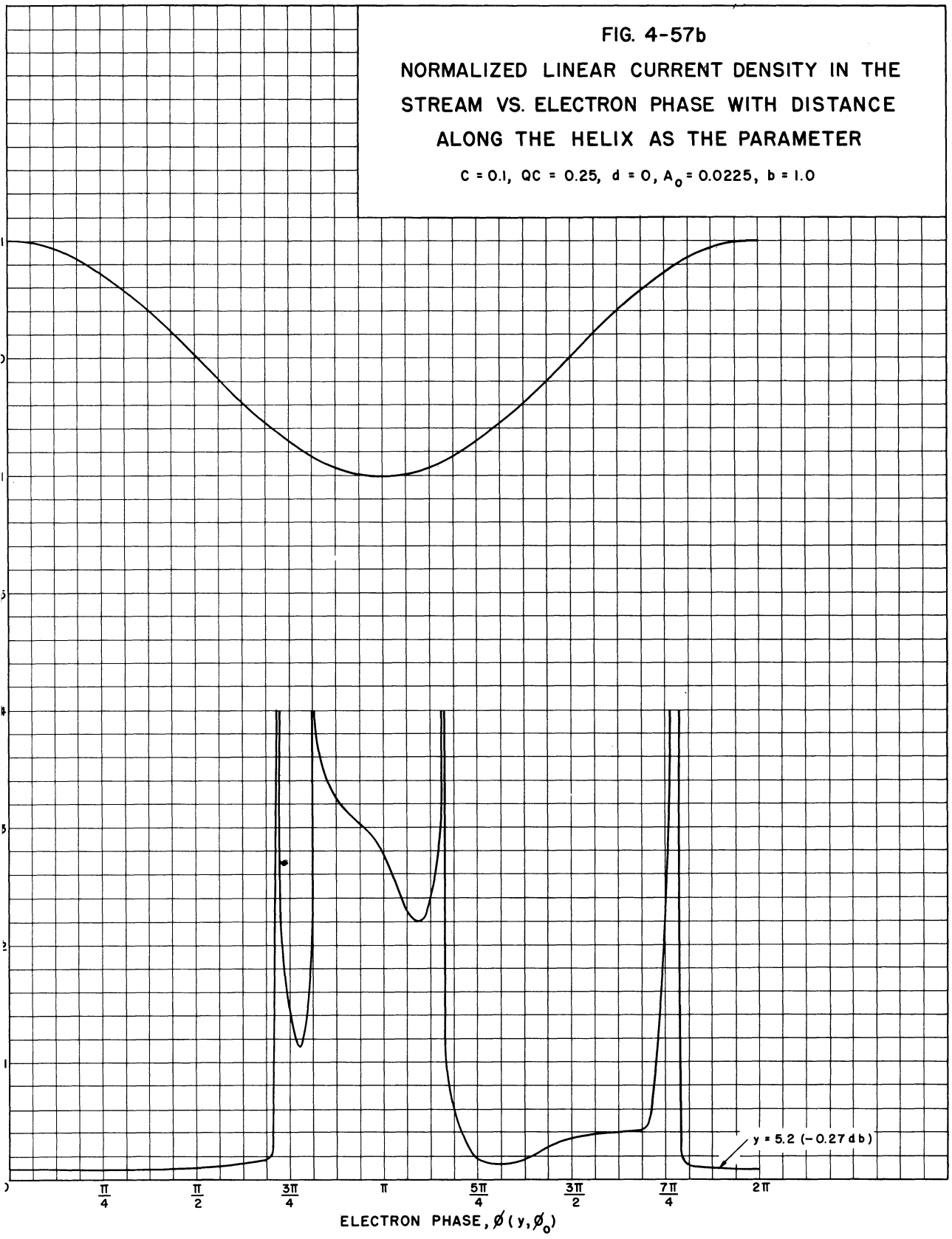

FIG. 4-57b

NORMALIZED LINEAR CURRENT DENSITY IN THE STREAM VS. ELECTRON PHASE WITH DISTANCE ALONG THE HELIX AS THE PARAMETER

C = 0.1, QC = 0.25, d = 0, A_0 = 0.0225, b = 1.0

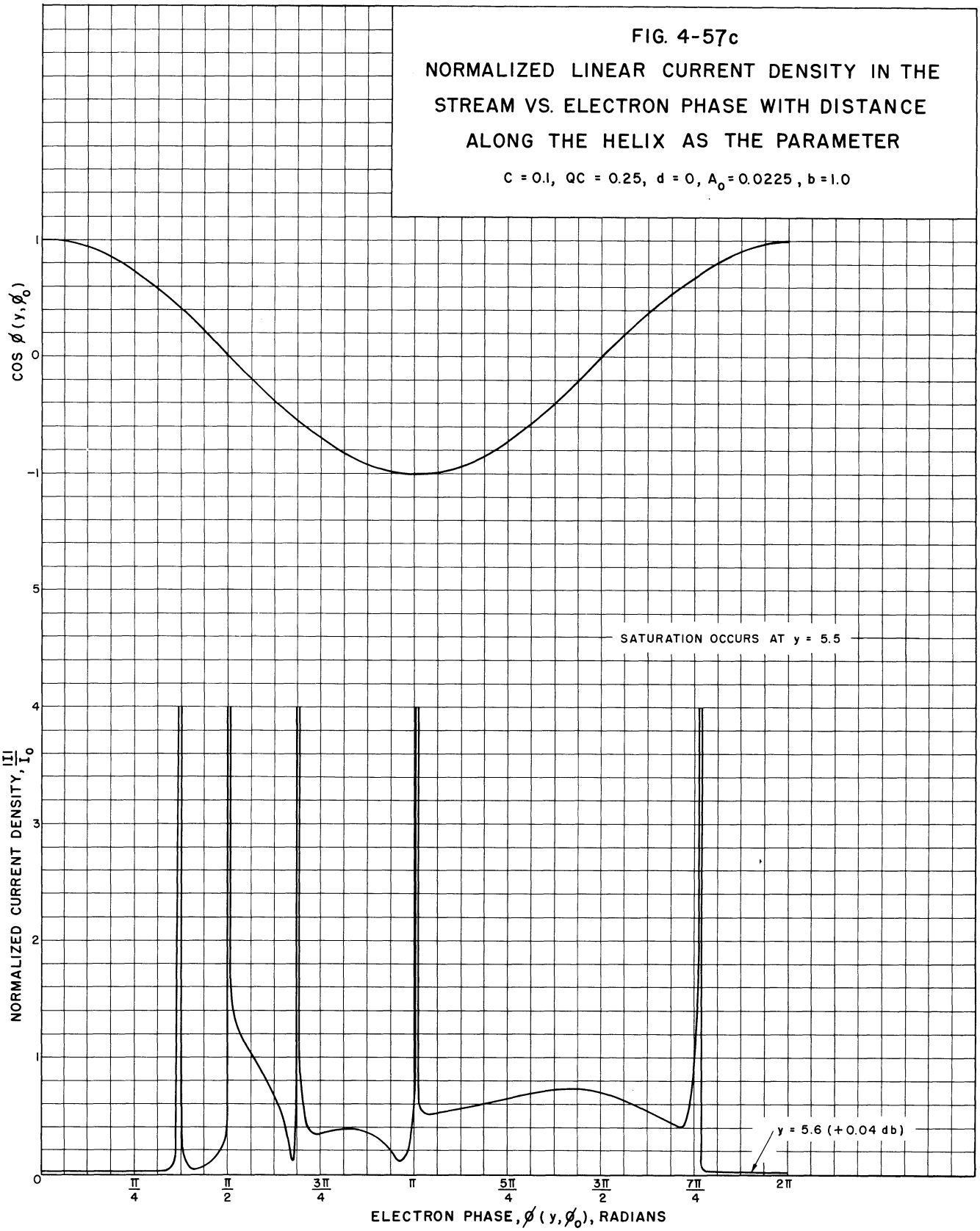
FIG. 4-57c
NORMALIZED LINEAR CURRENT DENSITY IN THE STREAM VS. ELECTRON PHASE WITH DISTANCE ALONG THE HELIX AS THE PARAMETER
C = 0.1, QC = 0.25, d = 0, A0 = 0.0225, b = 1.0
COS ∅(y, ∅0)
1
0
-1
5
4
3
2
1
0
SATURATION OCCURS AT y = 5.5
y = 5.6 (+0.04 db)
NORMALIZED CURRENT DENSITY, |I|/I0
π/4
π/2
3π/4
π
5π/4
3π/2
7π/4
2π
ELECTRON PHASE, ∅(y, ∅0), RADIANS

4.7 Variable Input-Signal Level

The input-signal level for all calculations heretofore presented has been the same, i.e., 30 db below CI_oV_o. This value of A_o was selected so that the input boundary conditions could be calculated from the linear theory.

The purpose of these calculations, however, is to analyze the operation of high-power amplifiers. For the value of A_o used here the saturation gain is between 30 and 40 db, but it has been found experimentally that the maximum gain in a loss-free region must be limited to approximately 20 db if the standing-wave ratio at the output transducer is of the order of 1.5:1. Hence where higher gains are necessary added external attenuation must be placed on the helix and consequently the saturation gain and power output are reduced. Thus it is not practical to build high gain and high power output in the same tube; instead, a short low-gain loss-free tube should be used when high power output is desired.

To shed some light on the tube characteristics under such conditions, solutions are presented for larger values of the input-signal level A_o. These solutions are shown in Figs. 4-58, 4-59, and 4-60 with ψ, the input-power level below CI_oV_o, having values of 5, 7, 10, 15, 20, 25, 30, and 40 db. The case selected for this investigation is C = 0.1, QC = 0.125, and b = 1.5.

The input boundary conditions on the initial phase $\phi(0,\phi_o)$ and the a-c velocity parameter $u(0,\phi_o)$ are taken to be the same as in the previous calculations. The value of $A'(y)$ at the input of a lossless helix is still zero since, as was pointed out in Section 2.4, the stream cannot influence the wave amplitude until it has become bunched. However, the value of $\theta'(y)$ at the input for large input-signal levels is open to question. The value of $\theta'(0)$ gives an apparent phase velocity of the total wave at the

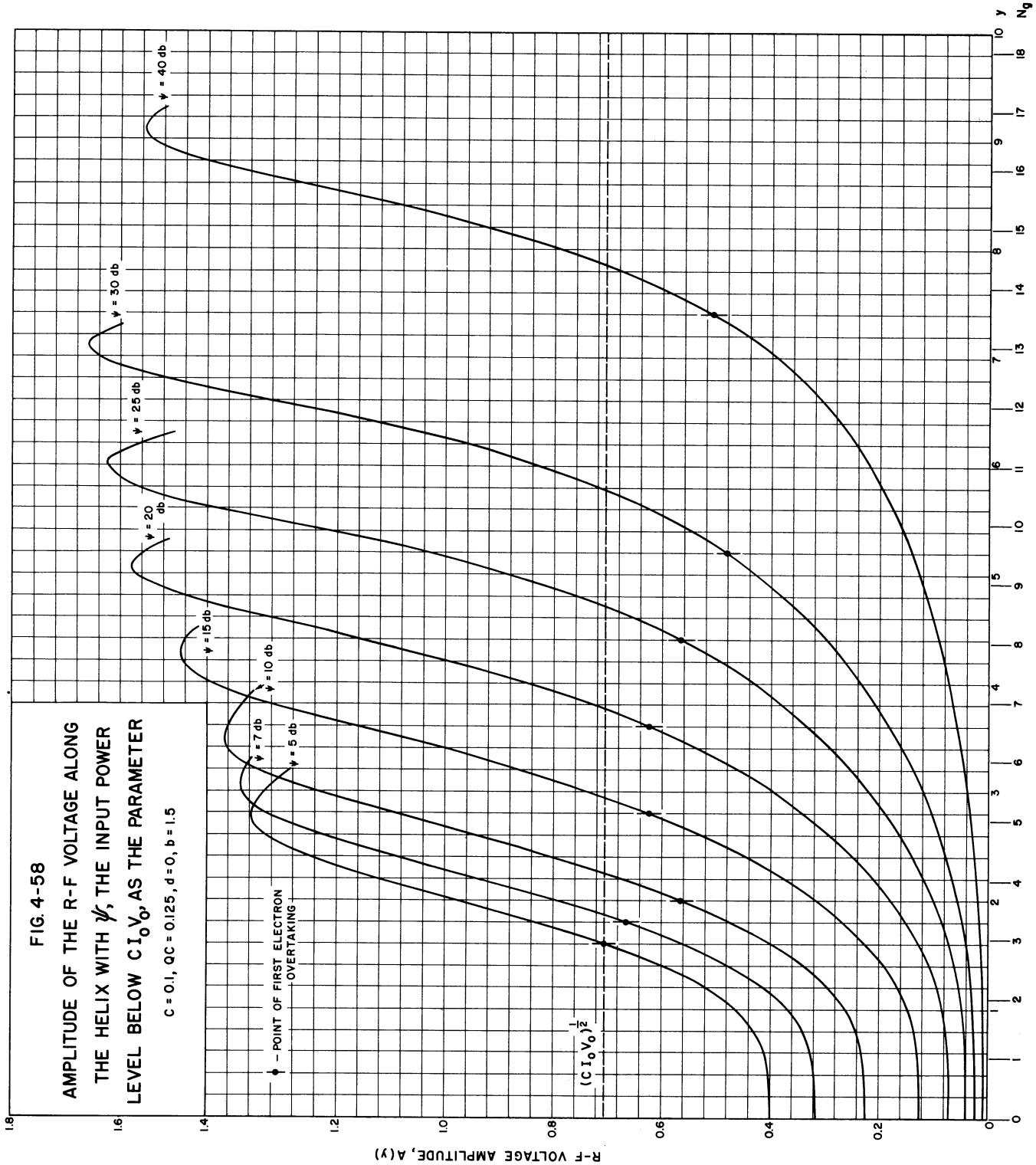
FIG. 4-58
AMPLITUDE OF THE R-F VOLTAGE ALONG THE HELIX WITH ψ, THE INPUT POWER LEVEL BELOW CI_0V_0, AS THE PARAMETER
C = 0.1, QC = 0.125, d = 0, b = 1.5
ψ = 40 db
ψ = 30 db
ψ = 25 db
ψ = 20 db
ψ = 15 db
ψ = 10 db
ψ = 7 db
ψ = 5 db
POINT OF FIRST ELECTRON OVERTAKING
$(CI_0V_0)^{\frac{1}{2}}$
R-F VOLTAGE AMPLITUDE, A(y)
y
N_g

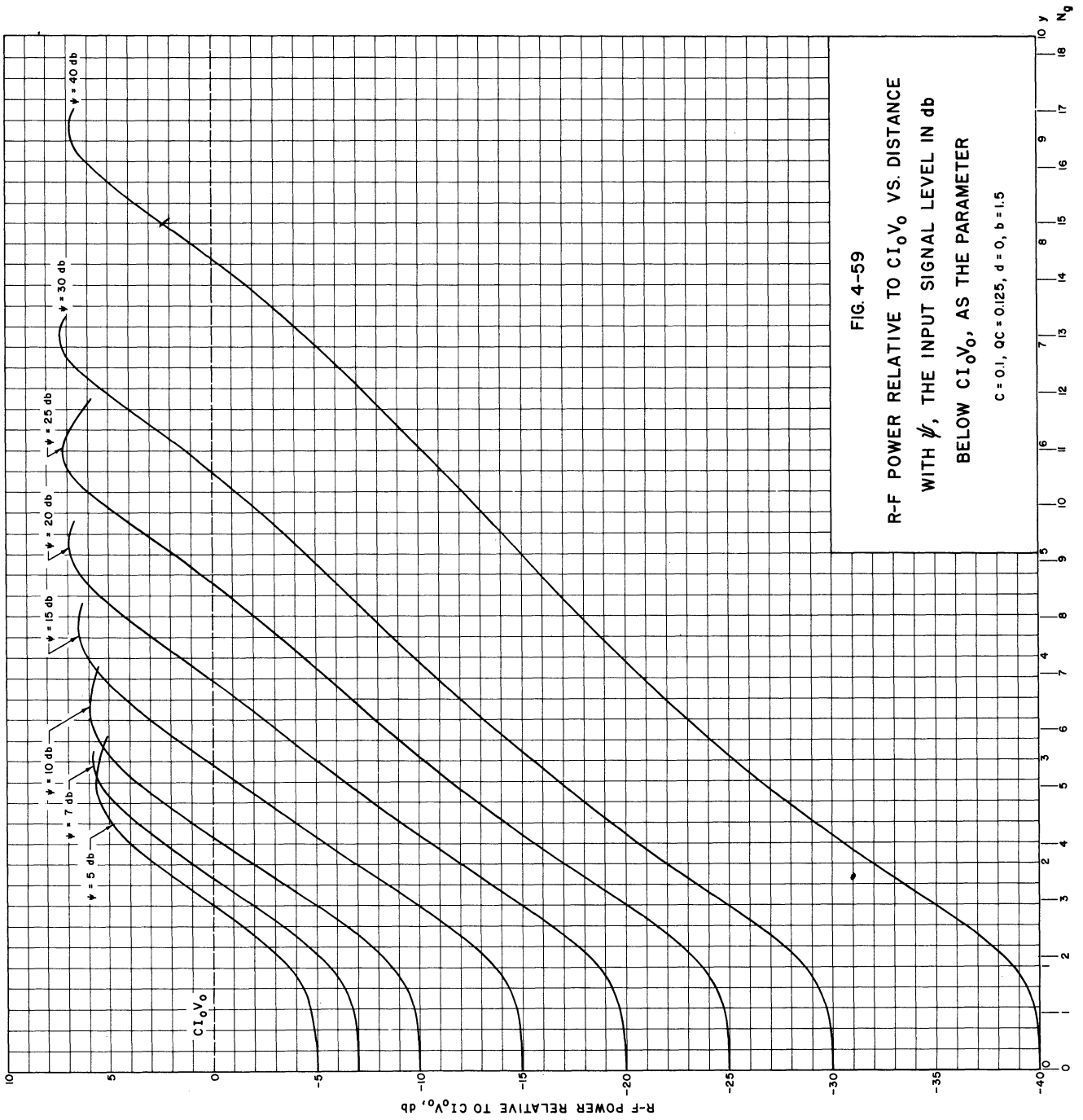

FIG. 4-59

R-F POWER RELATIVE TO CI_oV_o VS. DISTANCE WITH ψ, THE INPUT SIGNAL LEVEL IN db BELOW CI_oV_o, AS THE PARAMETER

C = 0.1, QC = 0.125, d = 0, b = 1.5

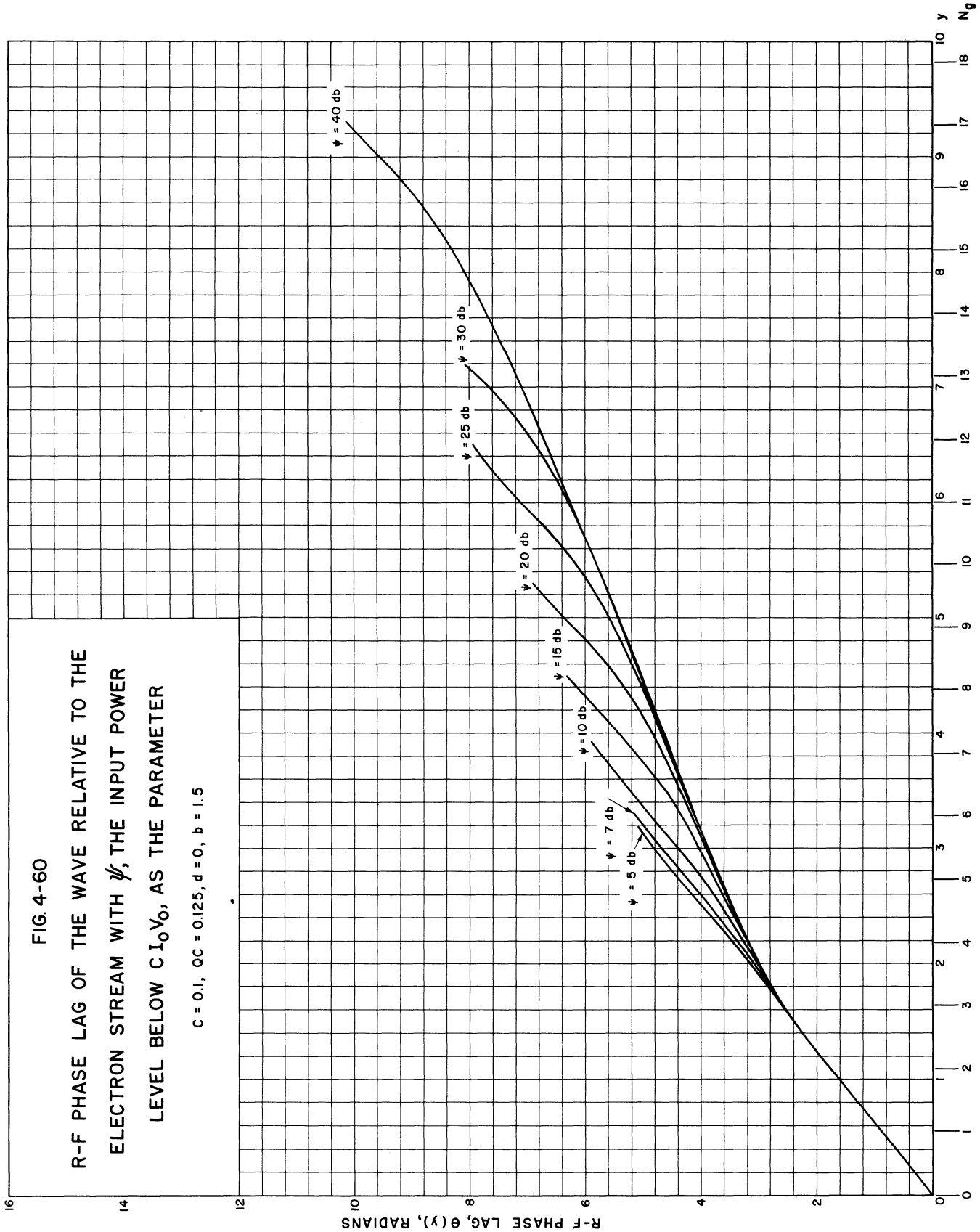
FIG. 4-60
R-F PHASE LAG OF THE WAVE RELATIVE TO THE ELECTRON STREAM WITH ψ, THE INPUT POWER LEVEL BELOW C I0V0, AS THE PARAMETER
C = 0.1, QC = 0.125, d = 0, b = 1.5
ψ = 40 db
ψ = 30 db
ψ = 25 db
ψ = 20 db
ψ = 15 db
ψ = 10 db
ψ = 7 db
ψ = 5 db
R-F PHASE LAG, θ(y), RADIANS
y
Ng

input which results when the three small-signal-theory waves are combined. Since no theory is available to calculate a more accurate value of $\theta'(0)$, the value given by the linear theory is used. This is tantamount to assuming that $\theta'(0)$ is independent of signal level, which is not considered to be a serious deviation from the truth. The insensitivity of the solutions to small errors in $\theta(y)$ and $A(y)$ further justifies this assumption.

Additional analysis of these solutions is presented in Chapter V.

4.8 Effect of Series Loss along the Helix

As was pointed out in Section 4.7, it is necessary to add series loss along the helix in high-gain amplifiers in order to insure stable operation. To assist in determining the effect of the amount and placement of this loss on the saturation gain and efficiency, solutions are presented for several values of the loss factor d at C = 0.1 and QC = 0.125. The values of d selected are 0.1, 0.25, 1.0, and 2.0, which, for C = 0.1, correspond to losses of approximately 0.56, 1.36, 5.45, and 10.9 db per undisturbed wavelength λ_g respectively. In addition, the effect of the placement of loss and the reduction in the optimum value of b in the presence of loss are discussed for d = 2.0.

The power flow along a lossy helix is given by

$$P_{oL}(y) = \text{Re}\,\frac{1}{2}\,VI^*$$

$$= \text{Re}\,\frac{VV^*}{2Z_{oL}^*} \quad , \tag{4-7}$$

where $Z_{oL} = Z_o(1 - jCd)$, the characteristic impedance of the lossy helix. Substitution of the defining expression for Z_{oL} and Eq. 2-12 for the voltage give, for the power flow along the lossy helix,

$$P_{oL}(y) = \frac{2CI_oV_o}{1 + jCd} A^2(y) \quad . \tag{4-8}$$

4.8.1 Variable Loss Factor d for Fixed Injection Velocity b. The solution selected for investigation is C = 0.1, QC = 0.125, and that value of b which gives maximum saturation gain when d = 0, i.e., b = 1.5. The method is to integrate for a distance of approximately three undisturbed wavelengths from the input with d = 0 and then to carry out solutions from this point to saturation for the values of d listed above. The results are presented as Figs. 4-61, 4-62, and 4-63.

Since the region in the vicinity of the point where the loss is first applied is of particular interest, this region has been expanded in Figs. 4-64 and 4-65 for the variables A(y) and $\theta(y)$. It can be seen that in the cases where d = 1.0 and 2.0 the signal level on the helix diminishes in amplitude for approximately one undisturbed wavelength after the loss is applied and then as the stream is continually being bunched resumes increasing in amplitude. This temporary decrease in r-f signal amplitude indicates that energy is being put back into the stream and appears as an increase in the kinetic energy of the stream. Hence the electrons are accelerated, which lessens the interaction between the wave and the stream so that the signal level on the helix drops until the stream becomes rebunched sufficiently to give energy back to the helix wave.

The slowing of the r-f wave due to the presence of series loss also contributes to a decreased interaction between the wave and the stream. The axial phase velocity of the wave in the presence of small amounts of loss is

$$v_{oL} = \frac{\omega}{\beta} = \frac{v_o}{\left(1 + \frac{C^2d^2}{2}\right)} \quad . \tag{4-9}$$

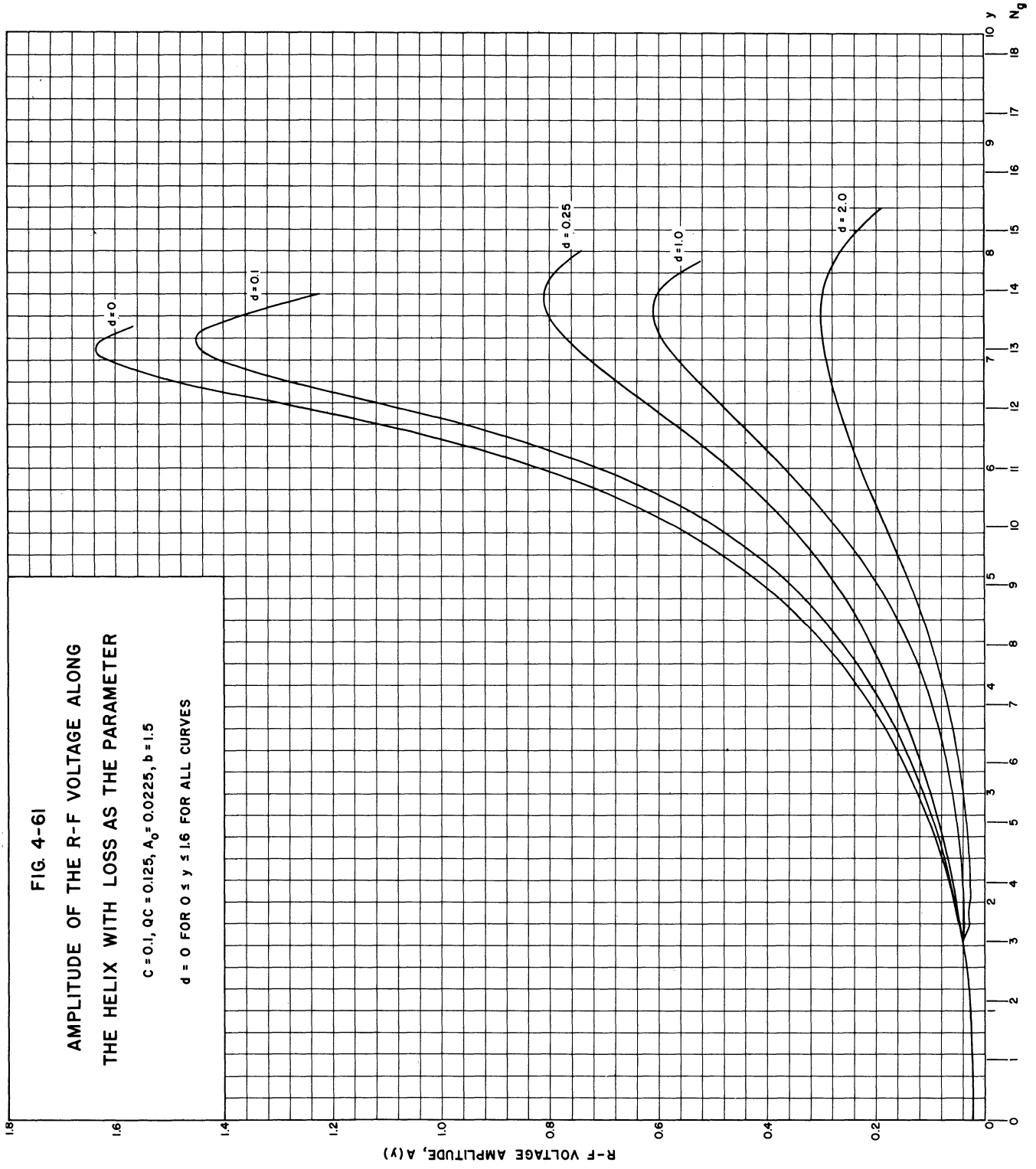

FIG. 4-61

AMPLITUDE OF THE R-F VOLTAGE ALONG THE HELIX WITH LOSS AS THE PARAMETER

C = 0.1, QC = 0.125, A_0 = 0.0225, b = 1.5

d = 0 FOR $0 \leq y \leq 1.6$ FOR ALL CURVES

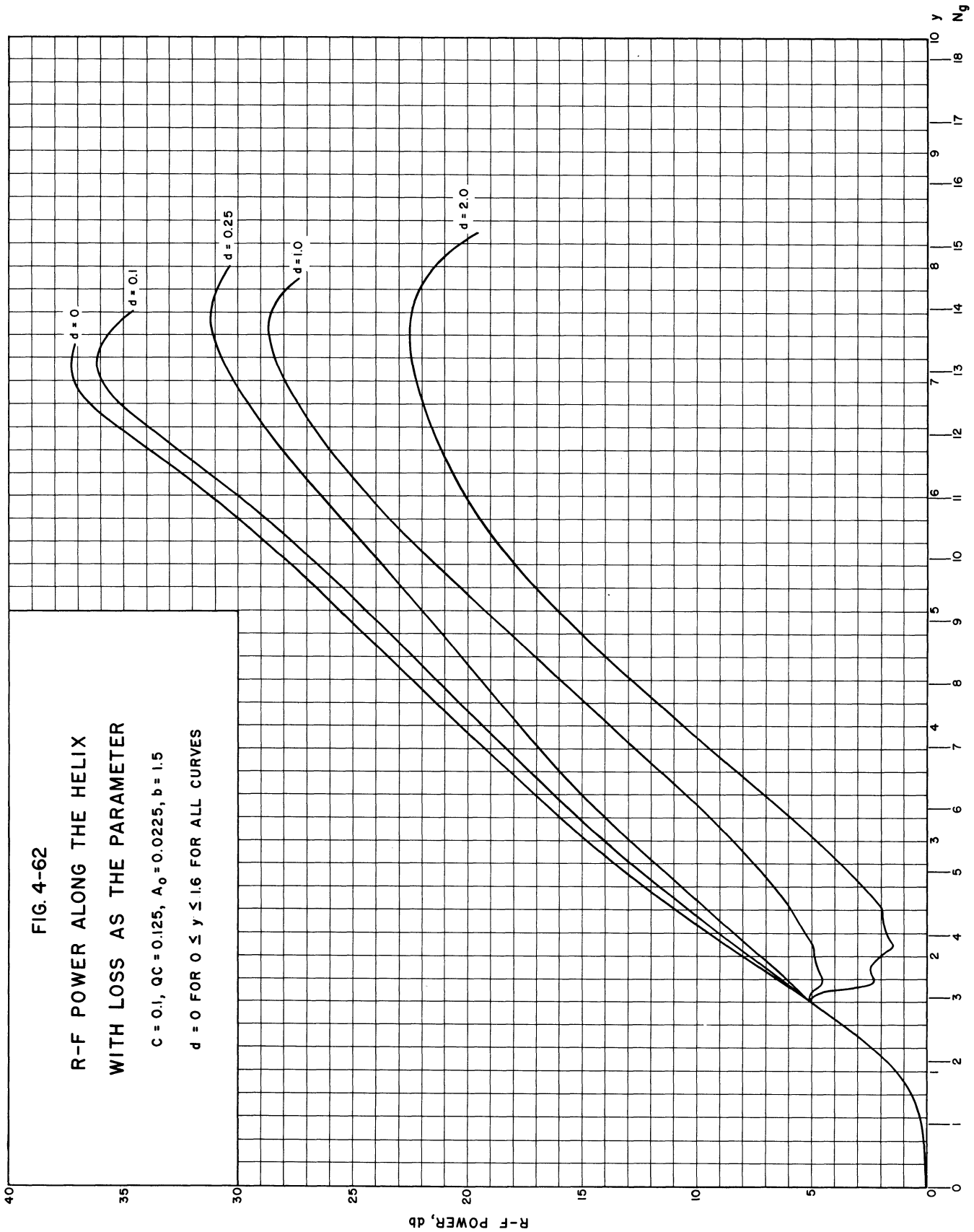
FIG. 4-62
R-F POWER ALONG THE HELIX
WITH LOSS AS THE PARAMETER
C = 0.1, QC = 0.125, A_0 = 0.0225, b = 1.5
d = 0 FOR 0 ≤ y ≤ 1.6 FOR ALL CURVES
d = 0
d = 0.1
d = 0.25
d = 1.0
d = 2.0
R-F POWER, db
y
N_g

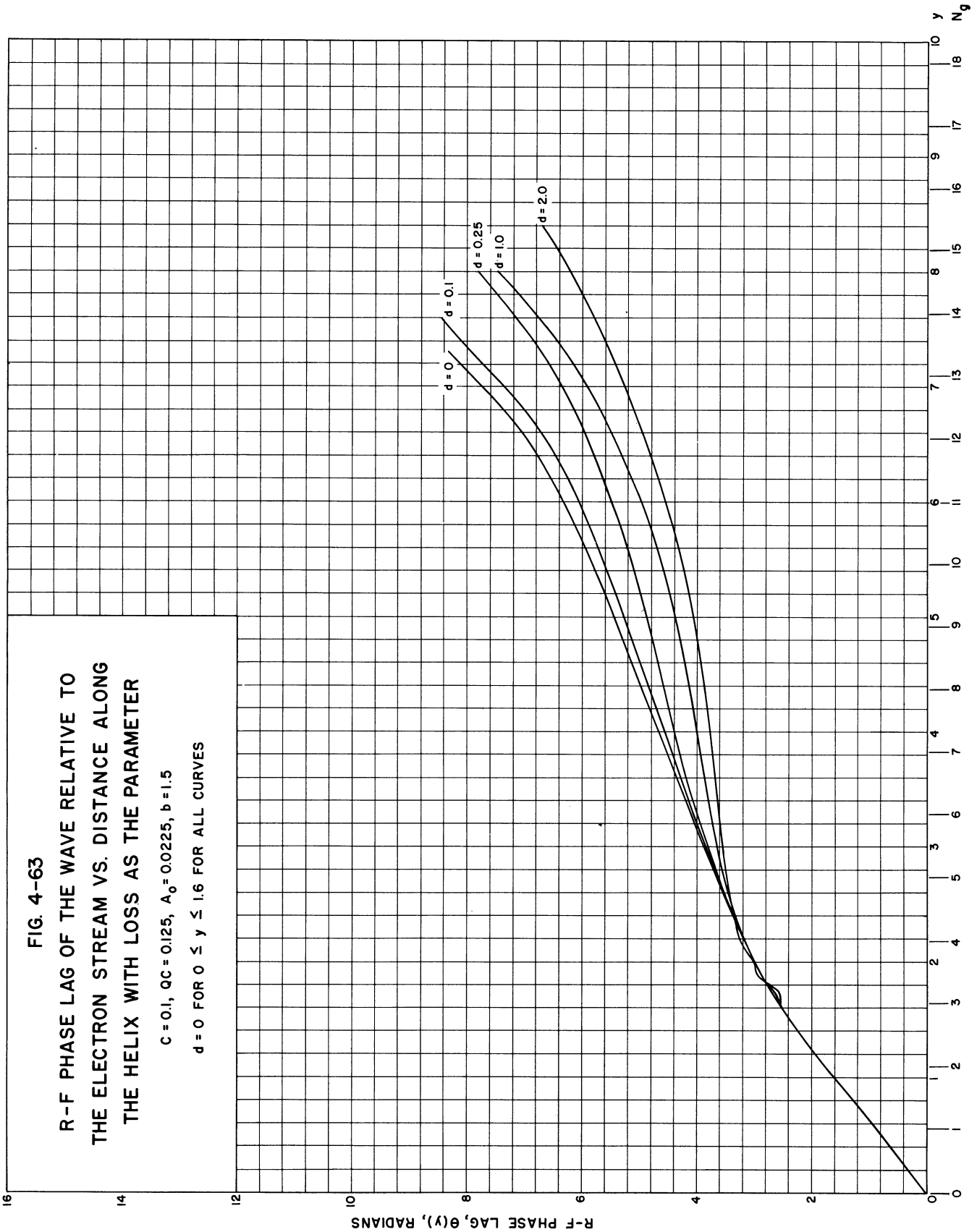

FIG. 4-63

R-F PHASE LAG OF THE WAVE RELATIVE TO THE ELECTRON STREAM VS. DISTANCE ALONG THE HELIX WITH LOSS AS THE PARAMETER

C = 0.1, QC = 0.125, A_o = 0.0225, b = 1.5

d = 0 FOR $0 \leq y \leq 1.6$ FOR ALL CURVES

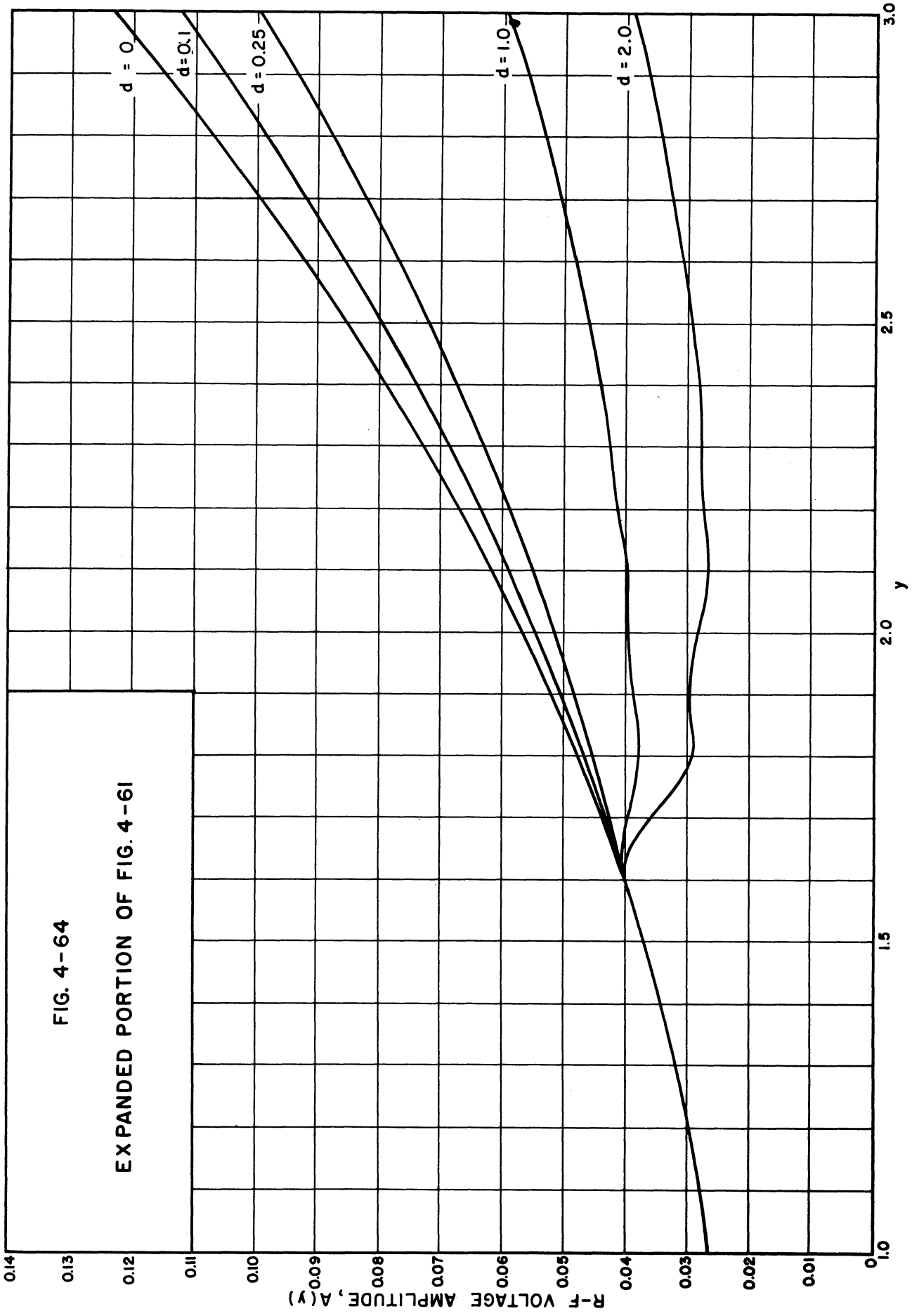
d = 0
d=0.1
d = 0.25
d = 1.0
d = 2.0
R-F VOLTAGE AMPLITUDE, A(y)
y
0.14
0.13
0.12
0.11
0.10
0.09
0.08
0.07
0.06
0.05
0.04
0.03
0.02
0.01
0
1.0
1.5
2.0
2.5
3.0
EXPANDED PORTION OF FIG. 4-61
FIG. 4-64

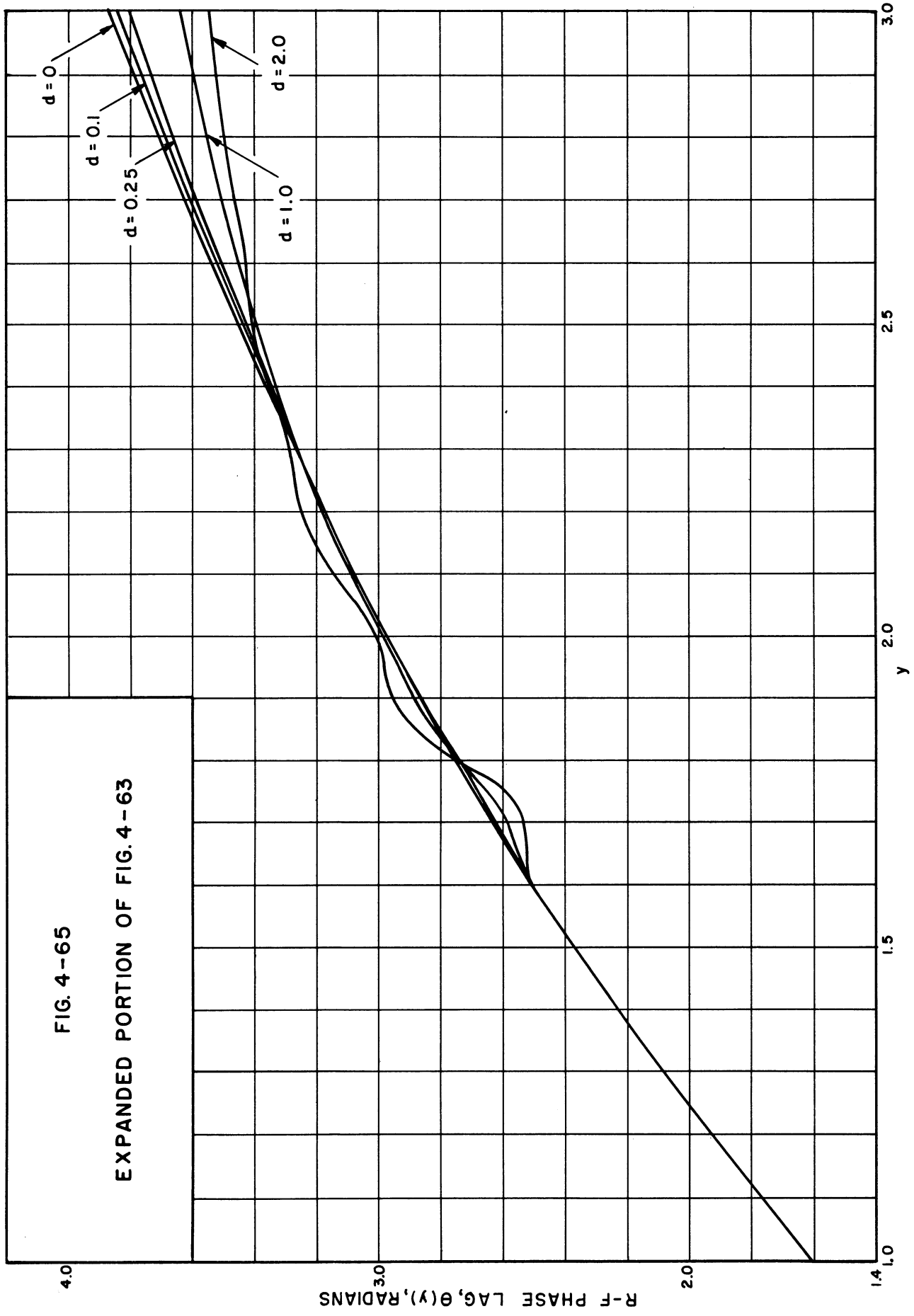

FIG. 4-65

EXPANDED PORTION OF FIG. 4-63

4.8.2 Variable Injection Velocity b for Fixed Loss Factor d. As discussed in Section 4.8.1, the effect of series loss along the helix is to decrease the wave velocity and thus reduce the interaction between the wave and the stream. The larger the value of d, the greater of course the decrease in wave velocity. In order to determine the amount by which the velocity is decreased and also the b associated with maximum saturation gain in the presence of loss, solutions have been carried out for several values of b with fixed loss. The value of d selected is 2.0 (10.9 db/λ_g). The results of these computations are presented in Figs. 4-66, 4-67, and 4-68. These curves are discussed in more detail in Chapter V.

4.8.3 Effect of Position of Loss for Fixed Loss Factor d and Fixed Injection Velocity b. In his development of the linear theory Pierce* found that the loss should be applied at least a distance corresponding to $CN_g = 0.2$ from the input, since at that value of CN_g the signal on the helix is just beginning to increase. It should be noted that Pierce's curve is plotted for the special case $QC = b = 0$.

In order to determine the effect of the placement of loss on a large-signal amplifier, the loss was introduced at $CN \simeq 0.2$ and $CN \simeq 0.4$ for the case $C = 0.1$, $QC = 0.125$, $b = 1.5$, and $d = 2.0$ (10.9 db/λ_g). A solution has already been obtained for the curves of Section 4.8.2 using these same conditions with the loss applied at $CN \simeq 0.3$. The three solutions are presented for comparison in Figs. 4-69, 4-70, and 4-71.

*Reference 8, p. 135, Fig. 9.1.

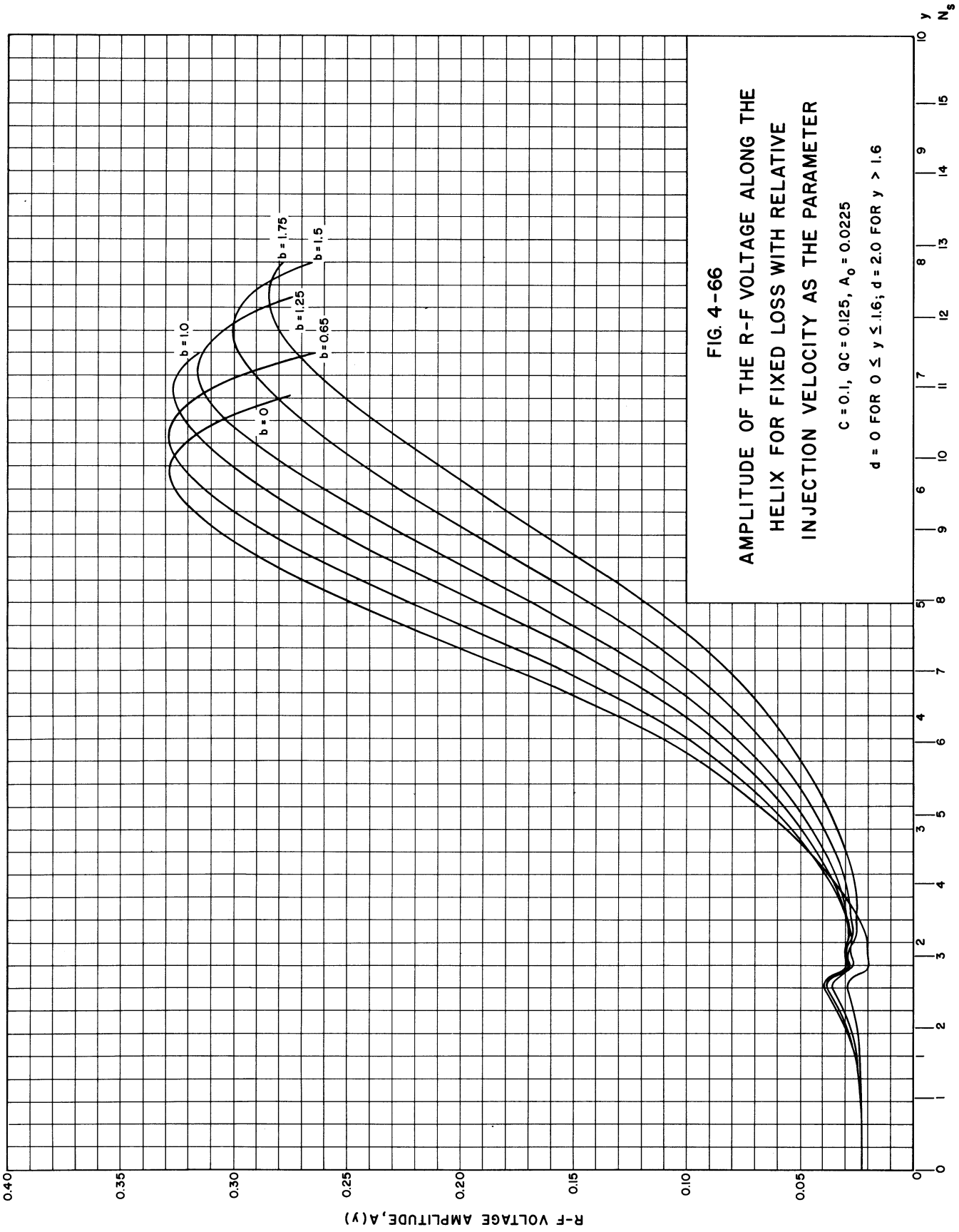
FIG. 4-66
AMPLITUDE OF THE R-F VOLTAGE ALONG THE HELIX FOR FIXED LOSS WITH RELATIVE INJECTION VELOCITY AS THE PARAMETER
C = 0.1, QC = 0.125, A_o = 0.0225
d = 0 FOR 0 ≤ y ≤ 1.6; d = 2.0 FOR y > 1.6
b = 1.75
b = 1.5
b = 1.25
b = 1.0
b = 0.65
b = 0
R-F VOLTAGE AMPLITUDE, A(y)
0.40
0.35
0.30
0.25
0.20
0.15
0.10
0.05
0
y
N_s

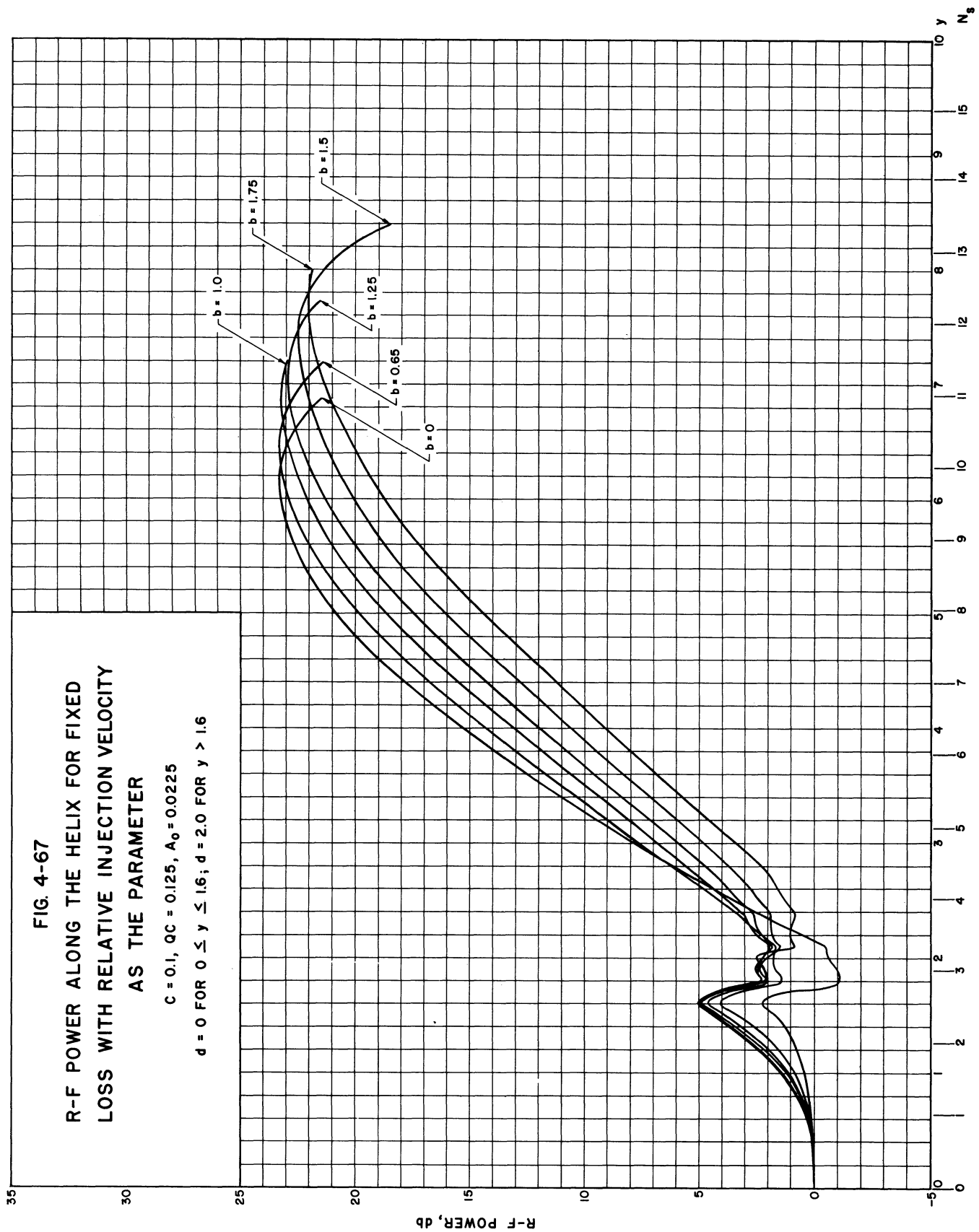

FIG. 4-67
R-F POWER ALONG THE HELIX FOR FIXED LOSS WITH RELATIVE INJECTION VELOCITY AS THE PARAMETER
C = 0.1, QC = 0.125, A_0 = 0.0225
d = 0 FOR $0 \leq y \leq 1.6$; d = 2.0 FOR $y > 1.6$

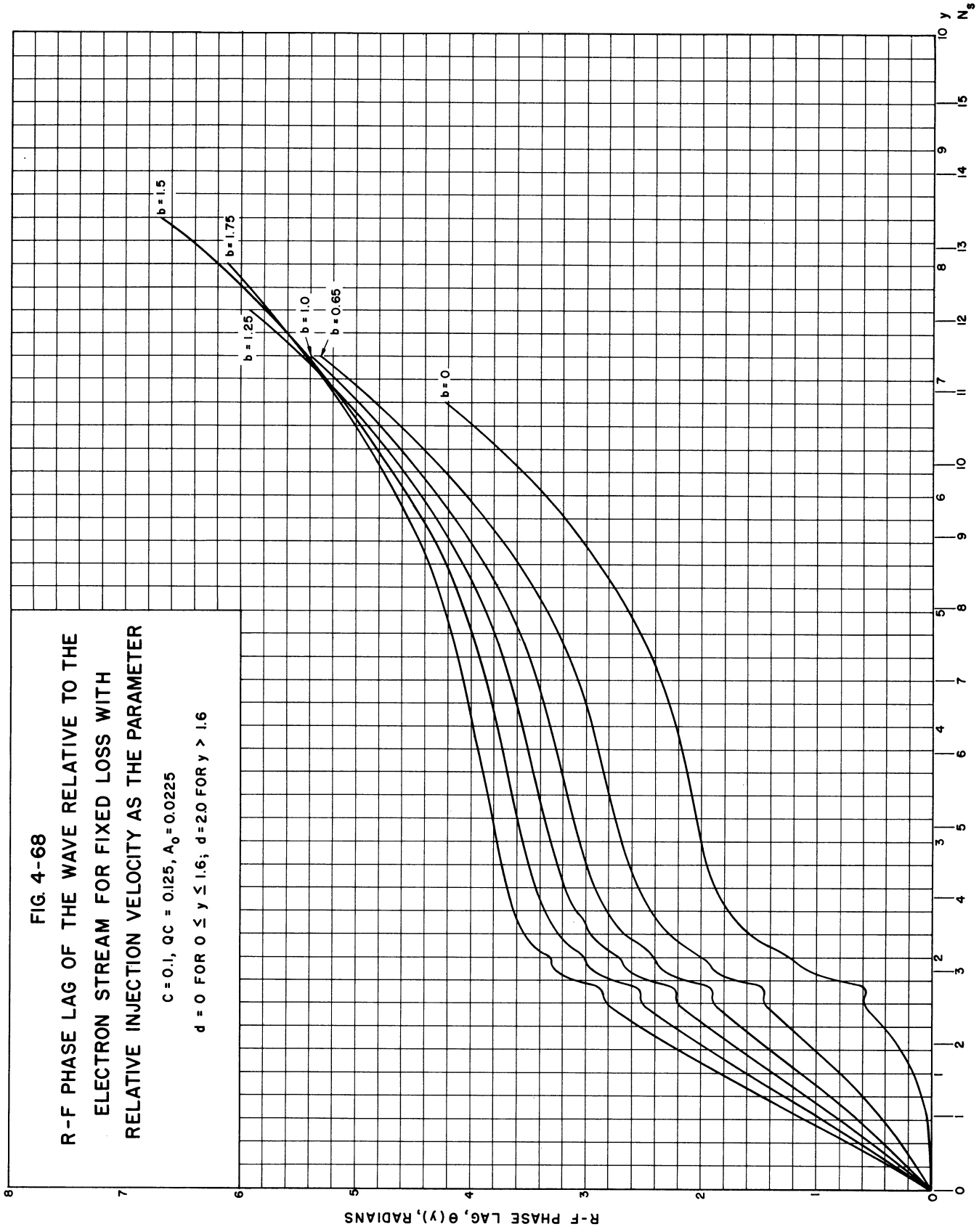

FIG. 4-68
R-F PHASE LAG OF THE WAVE RELATIVE TO THE ELECTRON STREAM FOR FIXED LOSS WITH RELATIVE INJECTION VELOCITY AS THE PARAMETER

C = 0.1, QC = 0.125, A_0 = 0.0225

d = 0 FOR $0 \leq y \leq 1.6$; d = 2.0 FOR $y > 1.6$

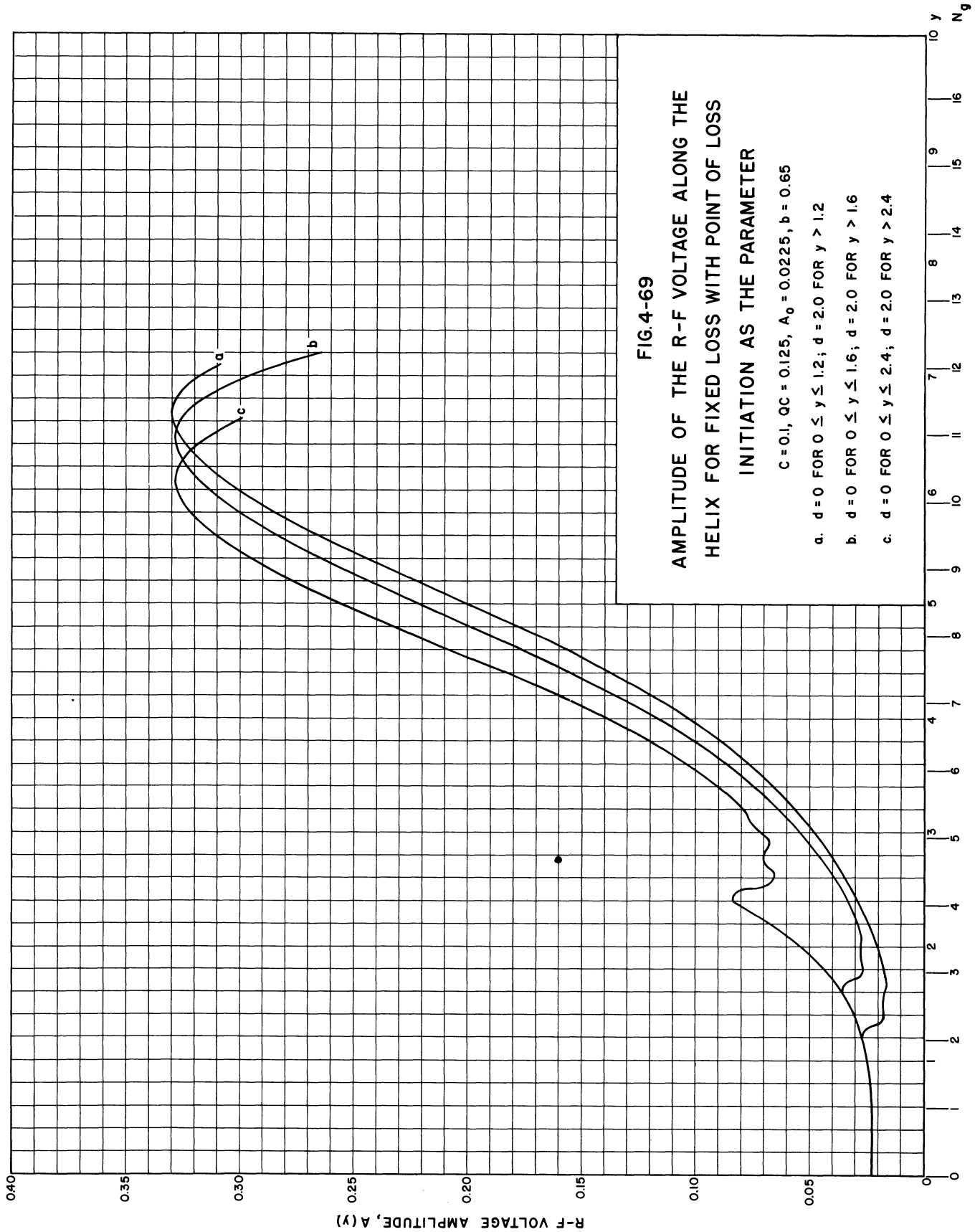

FIG. 4-69

AMPLITUDE OF THE R-F VOLTAGE ALONG THE HELIX FOR FIXED LOSS WITH POINT OF LOSS INITIATION AS THE PARAMETER

C = 0.1, QC = 0.125, A_o = 0.0225, b = 0.65

a. d = 0 FOR $0 \leq y \leq 1.2$; d = 2.0 FOR $y > 1.2$

b. d = 0 FOR $0 \leq y \leq 1.6$; d = 2.0 FOR $y > 1.6$

c. d = 0 FOR $0 \leq y \leq 2.4$; d = 2.0 FOR $y > 2.4$

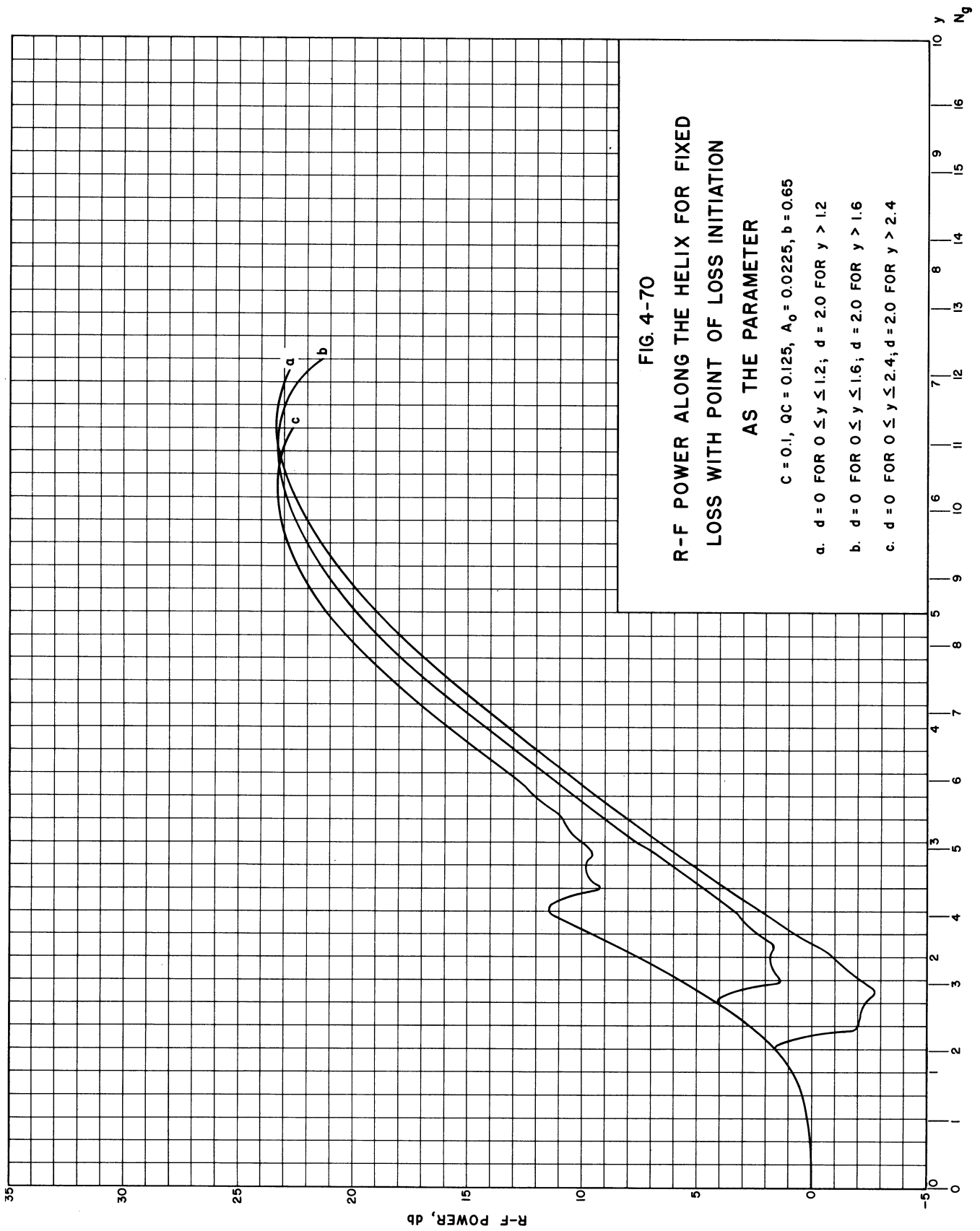

FIG. 4-70

R-F POWER ALONG THE HELIX FOR FIXED LOSS WITH POINT OF LOSS INITIATION AS THE PARAMETER

C = 0.1, QC = 0.125, A_0 = 0.0225, b = 0.65

a. d = 0 FOR $0 \leq y \leq 1.2$; d = 2.0 FOR $y > 1.2$

b. d = 0 FOR $0 \leq y \leq 1.6$; d = 2.0 FOR $y > 1.6$

c. d = 0 FOR $0 \leq y \leq 2.4$; d = 2.0 FOR $y > 2.4$

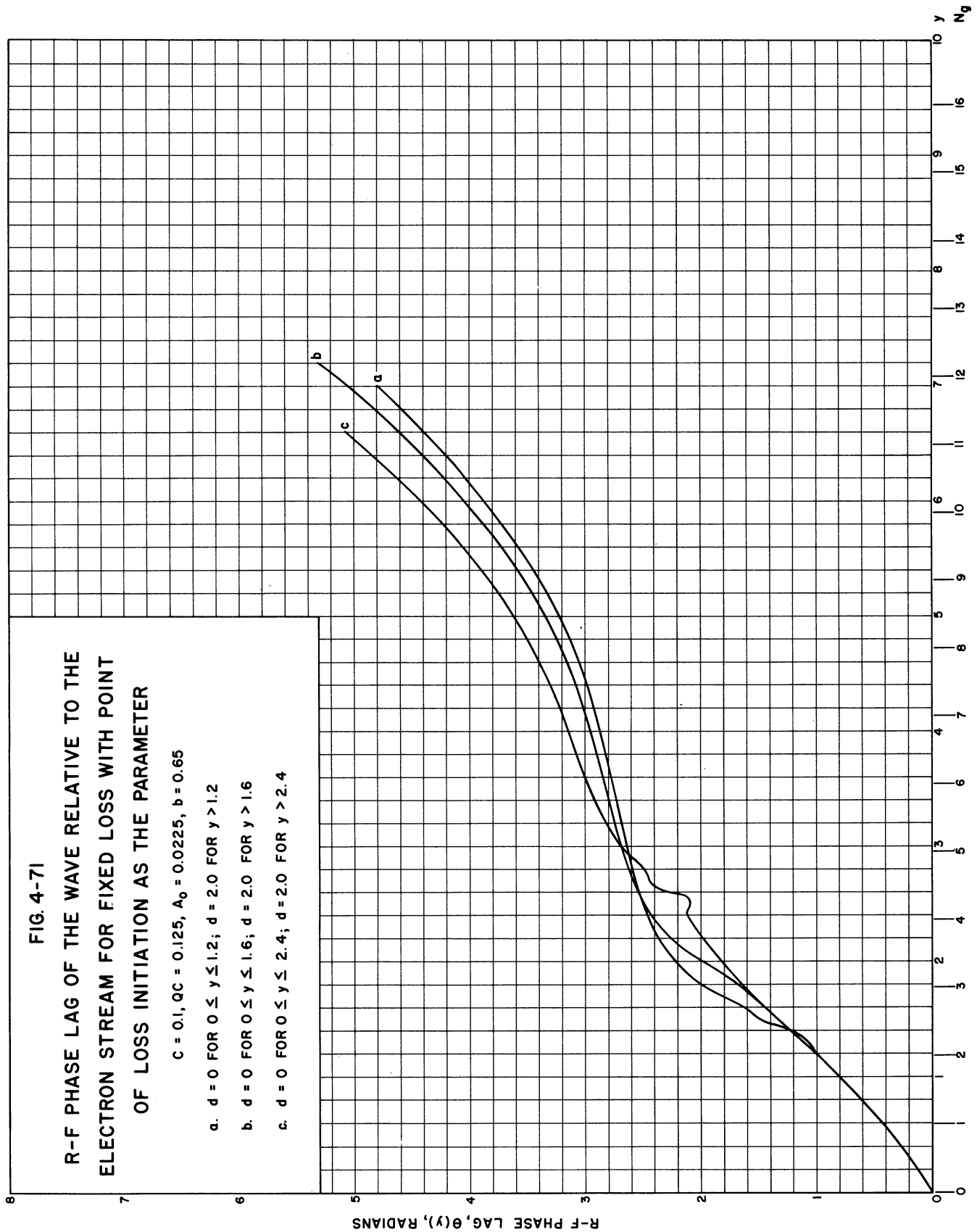

FIG. 4-71

R-F PHASE LAG OF THE WAVE RELATIVE TO THE ELECTRON STREAM FOR FIXED LOSS WITH POINT OF LOSS INITIATION AS THE PARAMETER

C = 0.1, QC = 0.125, A_o = 0.0225, b = 0.65

a. d = 0 FOR $0 \leq y \leq 1.2$; d = 2.0 FOR $y > 1.2$

b. d = 0 FOR $0 \leq y \leq 1.6$; d = 2.0 FOR $y > 1.6$

c. d = 0 FOR $0 \leq y \leq 2.4$; d = 2.0 FOR $y > 2.4$

CHAPTER V. ANALYSIS OF THE RESULTS

In addition to the basic curves drawn from the computed data on r-f voltage and phase lag and presented in Chapter IV, a number of curves may be drawn from the same data to emphasize certain especially interesting relationships and examine phenomena of particular importance in design applications.

5.1 Voltage Gain and Tube Length at Saturation

In order to determine the optimum injection velocity for particular C and QC values, the voltage gain and tube length in undisturbed wavelengths at saturation are plotted vs. b. The resulting curves are shown in Figs. 5-1 and 5-2.

The drop-out point of the voltage-gain curve is quite sharp, as it is in the linear case, and the value of b at which this drop of the gain to a very small value occurs is approximately that value of b for which the small-signal gain goes to zero. As can be seen from the figures of Section 4.1, for these large values of b the saturation tube length is very short, which is to be expected since the electron velocity is much greater than the wave speed and hence the interaction between the wave and the stream is negligible. In comparing the curves of this section with those of Section 4.1 it should be remembered that $\lambda_s/\lambda_g = 1 + Cb$.

In Fig. 5-1 the gain curve for C = 0.2 is shown dotted in the vicinity of b = 2.0 because the total velocity $u_t(y,\phi_o)$ approaches zero near saturation for this case. As pointed out in Chapter II, for values of C as large as 0.2 the neglect of space charge leads to appreciable errors and hence these particular results are questionable.

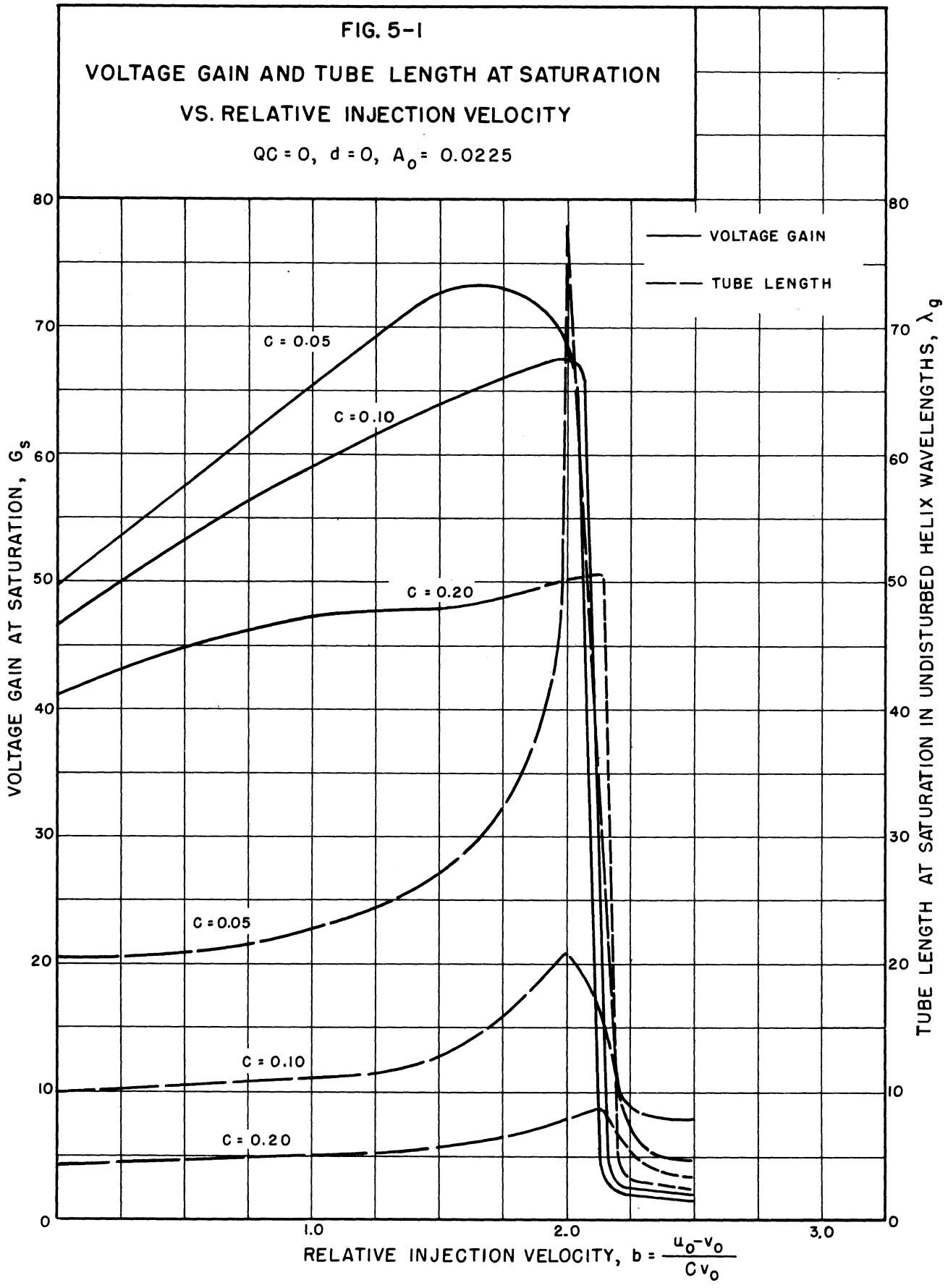
FIG. 5-1
VOLTAGE GAIN AND TUBE LENGTH AT SATURATION
VS. RELATIVE INJECTION VELOCITY
QC = 0, d = 0, A_0 = 0.0225
VOLTAGE GAIN
TUBE LENGTH
C = 0.05
C = 0.10
C = 0.20
C = 0.05
C = 0.10
C = 0.20
VOLTAGE GAIN AT SATURATION, G_s
TUBE LENGTH AT SATURATION IN UNDISTURBED HELIX WAVELENGTHS, λ_g
RELATIVE INJECTION VELOCITY, $b = \frac{u_0 - v_0}{C v_0}$
0
10
20
30
40
50
60
70
80
1.0
2.0
3.0

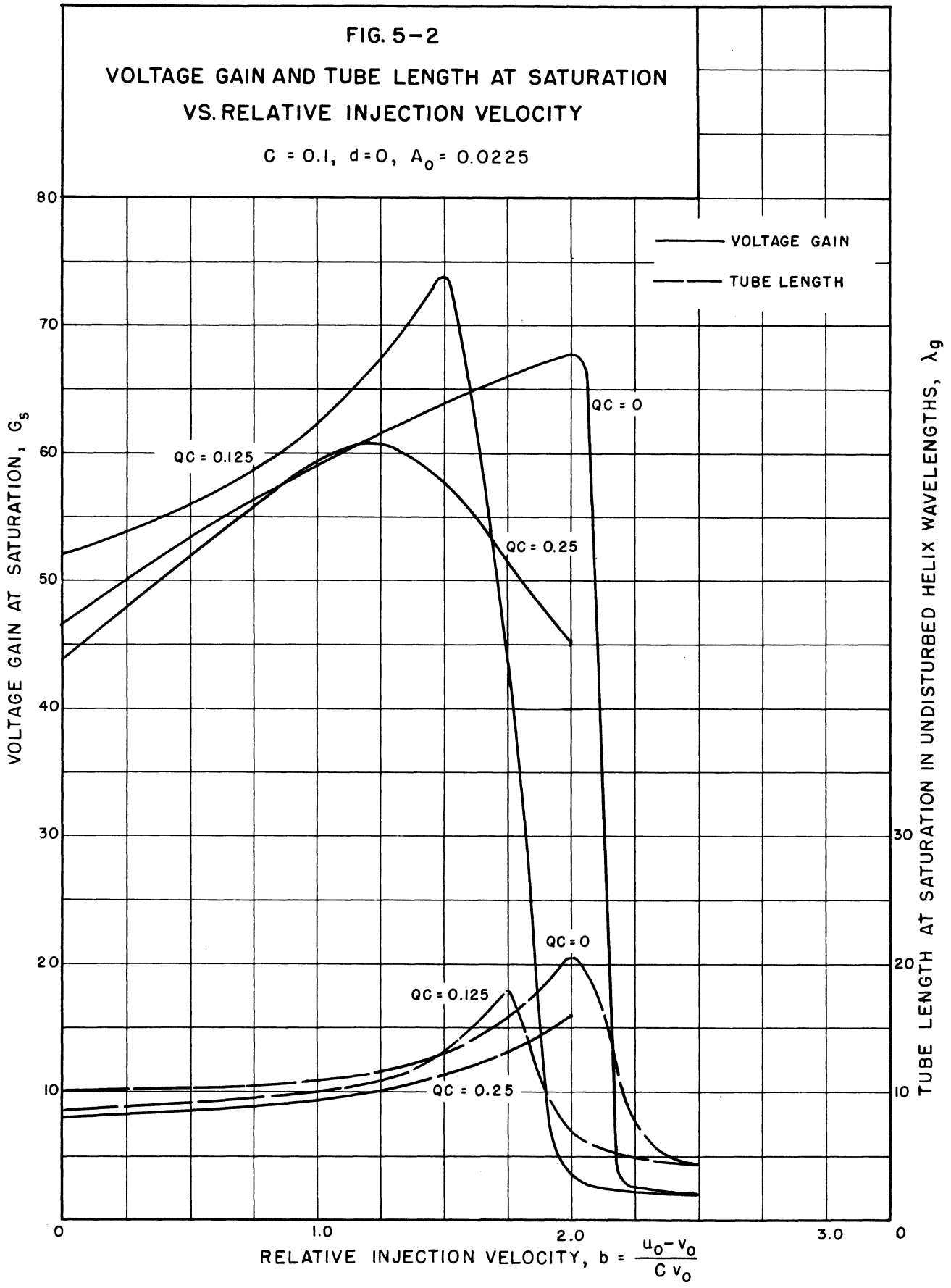
FIG. 5-2
VOLTAGE GAIN AND TUBE LENGTH AT SATURATION
VS. RELATIVE INJECTION VELOCITY
C = 0.1, d = 0, A_0 = 0.0225
VOLTAGE GAIN
TUBE LENGTH
QC = 0
QC = 0.125
QC = 0.25
QC = 0
QC = 0.125
QC = 0.25
VOLTAGE GAIN AT SATURATION, G_s
TUBE LENGTH AT SATURATION IN UNDISTURBED HELIX WAVELENGTHS, λ_g
RELATIVE INJECTION VELOCITY, $b = \frac{u_0 - v_0}{C v_0}$
0
10
20
30
40
50
60
70
80
1.0
2.0
3.0

The curves of Fig. 5-1 indicate that saturation gain decreases with increasing C. The nonlinearities which largely determine the gain in the large-signal region and which increase with increased coupling (i.e., larger C), are responsible for this decreased gain.

Maximum saturation gain for C = 0.1 and QC = 0 occurs at b = 2.0, which amounts to an 18.2-percent increase in velocity or 40-percent increase in the stream voltage V_o over that for maximum small-signal gain. As b is increased the tube length at saturation would be expected to be greater, since the electrons advance in phase with respect to the wave faster and hence it takes a greater distance for them to build up comparable a-c velocities. Also, the expected saturation gain should be greater for larger b, since the kinetic energy in the stream is greater by an amount proportional to b^2.

In Fig. 5-2 gain curves are shown for C = 0.1 and three values of the space-charge parameter QC. For QC = 0.125 and 0.25 it is noticed that the b for maximum saturation gain is less than that for QC = 0. However, for larger values of QC it is expected that the b for maximum saturation gain will increase as in the linear theory. Also, the saturation gain with small values of QC has increased over that for QC = 0, but as QC is increased further the gain decreases as is expected for large values of space charge. A qualitative explanation of this phenomenon is given in the following section.

5.2 Efficiency and Tube Length at Saturation

For the same data as discussed in Section 5.1, saturation efficiency and tube length may be plotted vs. the velocity parameter b. The saturation efficiency η_s is, from Eq. 4-1,

$$\eta_s = 2C\, A^2_{max.}(y) \quad . \qquad (5\text{-}1)$$

These curves are plotted with C and QC as the respective parameters in Figs. 5-3 and 5-4. For the QC = 0 case the efficiency is plotted both in percent and as η_s/C. The efficiency curves are seen to be quite similar to the voltage-gain curves, except that for increasing C the maximum efficiency increases whereas the saturation gain decreased. Obviously this increase is to be expected, since larger C values correspond to greater coupling between the circuit and the stream.

In Fig. 5-5 the maximum saturation efficiency is plotted vs. C for QC = 0. For each value of C the efficiency is maximized by optimizing the velocity parameter b. Figure 5-5 indicates that not much is gained in efficiency by increasing the gain parameter C beyond 0.10 or 0.12 for small values of space charge.

The maximum saturation efficiency divided by C is plotted against the small-signal space-charge parameter QC in Fig. 5-6 and against the large-signal space-charge amplitude parameter K in Fig. 5-7. Figures 5-6 and 5-7 might be interpreted qualitatively as follows. For small values of QC, up to approximately 0.125, the maximum saturation efficiency increases with QC, as might be expected since the charge density and the space-charge forces in the stream are very small and the increase in charge density associated with increasing QC appears as increased power output. However, for larger values of QC it is probable that the strong short-range space-charge forces inhibit the bunching severely enough to overcome the effect of the increased charge density.

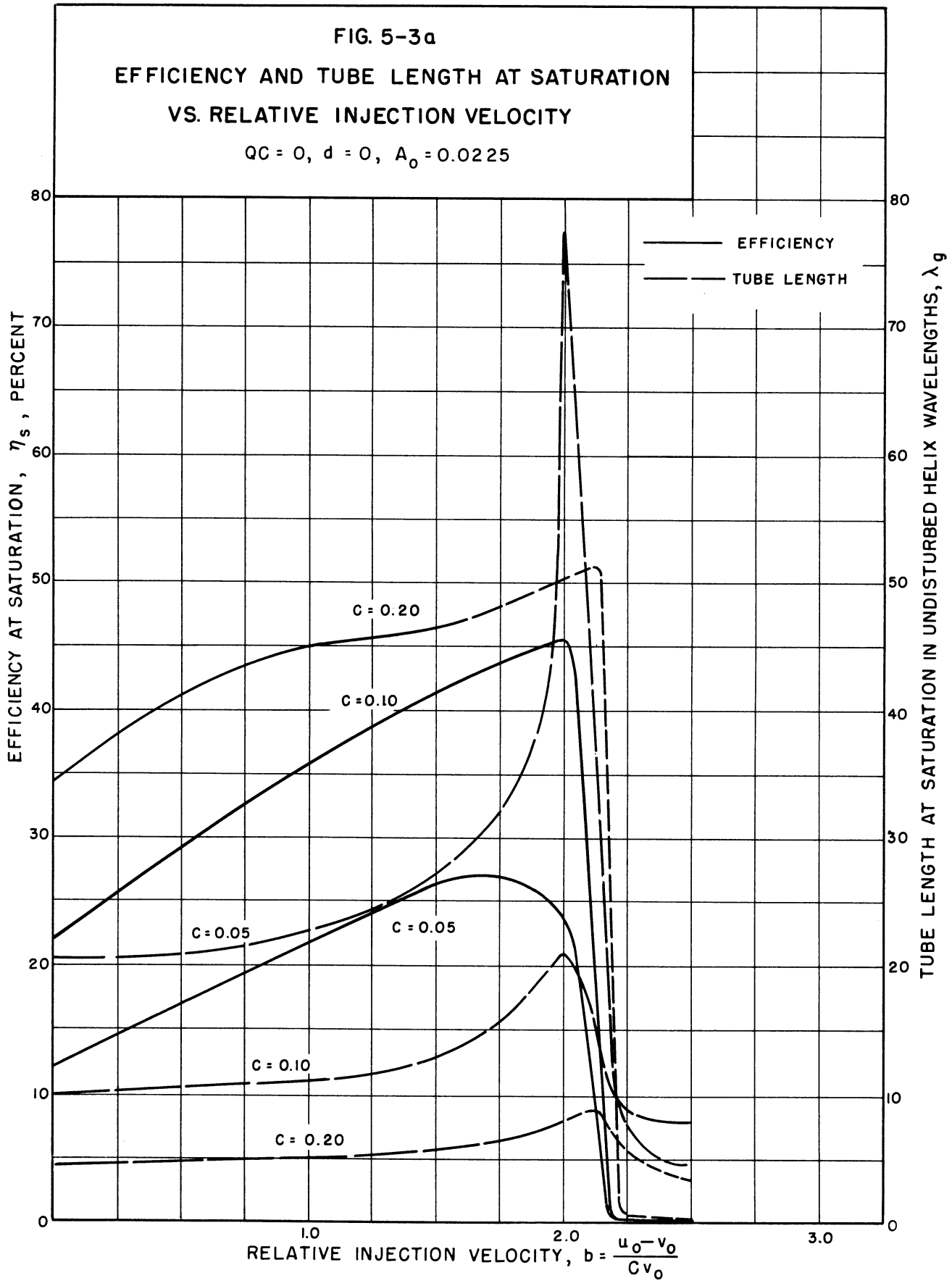
FIG. 5-3a
EFFICIENCY AND TUBE LENGTH AT SATURATION
VS. RELATIVE INJECTION VELOCITY
QC = 0, d = 0, A_0 = 0.0225
EFFICIENCY
TUBE LENGTH
C = 0.20
C = 0.10
C = 0.05
C = 0.05
C = 0.10
C = 0.20
EFFICIENCY AT SATURATION, η_s, PERCENT
TUBE LENGTH AT SATURATION IN UNDISTURBED HELIX WAVELENGTHS, λ_g
RELATIVE INJECTION VELOCITY, $b = \frac{u_0 - v_0}{Cv_0}$
0
10
20
30
40
50
60
70
80
1.0
2.0
3.0

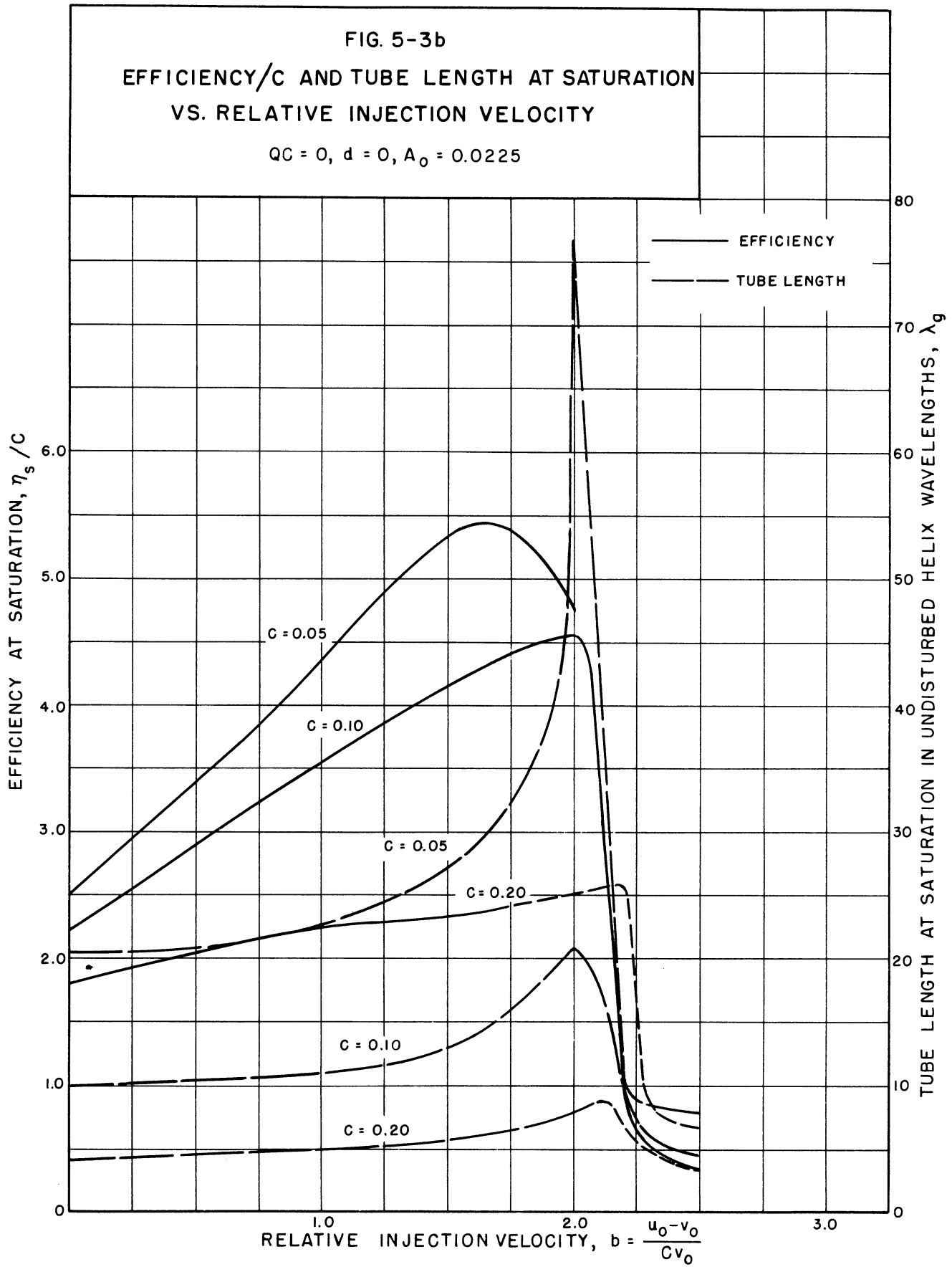
FIG. 5-3b
EFFICIENCY/C AND TUBE LENGTH AT SATURATION
VS. RELATIVE INJECTION VELOCITY
QC = 0, d = 0, A_0 = 0.0225
EFFICIENCY
TUBE LENGTH
C = 0.05
C = 0.10
C = 0.05
C = 0.20
C = 0.10
C = 0.20
EFFICIENCY AT SATURATION, η_s /C
TUBE LENGTH AT SATURATION IN UNDISTURBED HELIX WAVELENGTHS, λ_g
RELATIVE INJECTION VELOCITY, $b = \frac{u_0 - v_0}{Cv_0}$
0
1.0
2.0
3.0
4.0
5.0
6.0
10
20
30
40
50
60
70
80

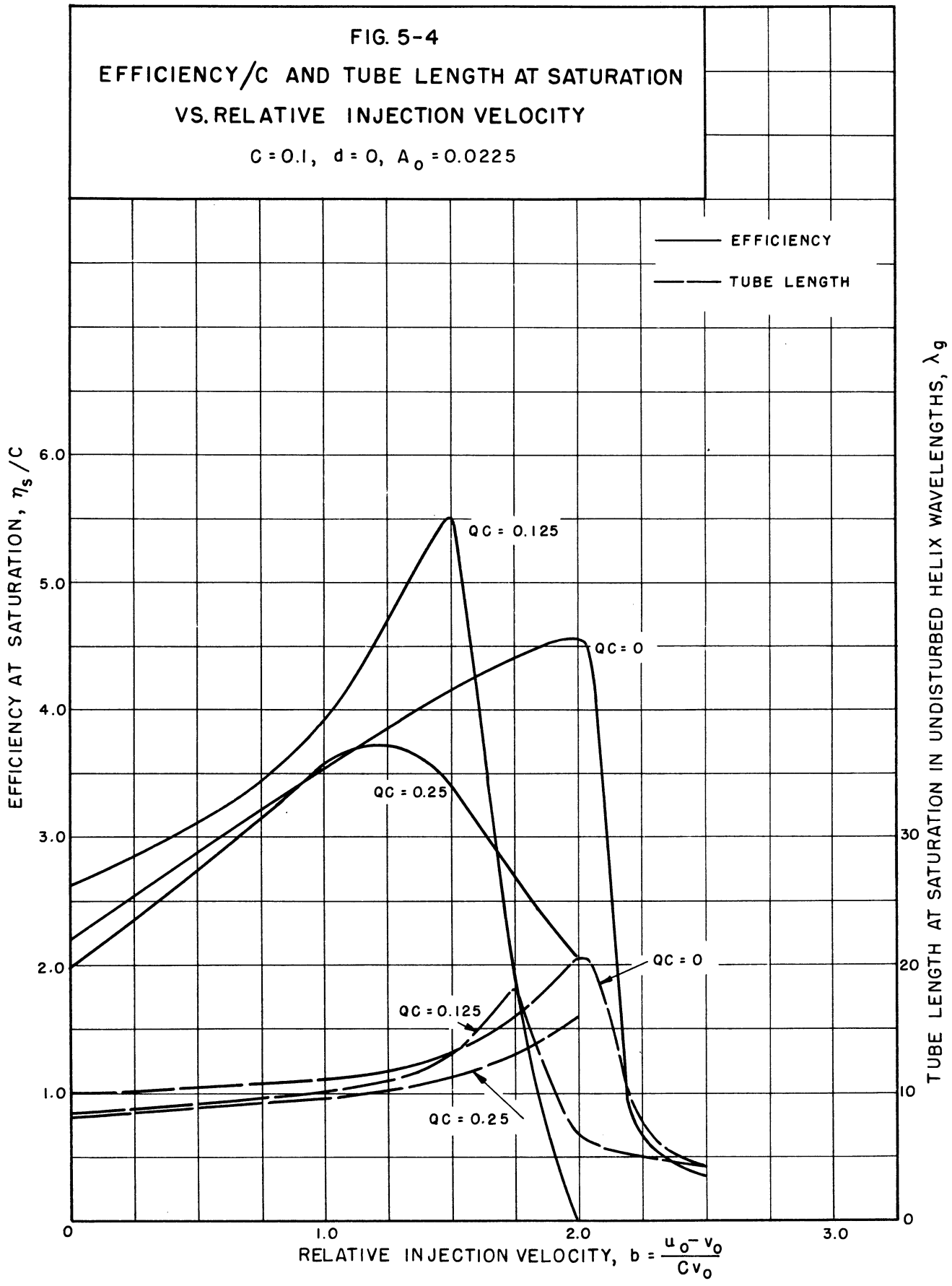
FIG. 5-4
EFFICIENCY/C AND TUBE LENGTH AT SATURATION
VS. RELATIVE INJECTION VELOCITY
C = 0.1, d = 0, A0 = 0.0225
EFFICIENCY
TUBE LENGTH
QC = 0.125
QC = 0
QC = 0.25
QC = 0
QC = 0.125
QC = 0.25
EFFICIENCY AT SATURATION, ηs/C
TUBE LENGTH AT SATURATION IN UNDISTURBED HELIX WAVELENGTHS, λg
RELATIVE INJECTION VELOCITY, b = (u0 − v0)/Cv0
0
1.0
2.0
3.0
1.0
2.0
3.0
4.0
5.0
6.0
10
20
30

FIG. 5-5

MAXIMUM SATURATION EFFICIENCY

VS. SMALL-SIGNAL GAIN PARAMETER

QC = 0, d = 0

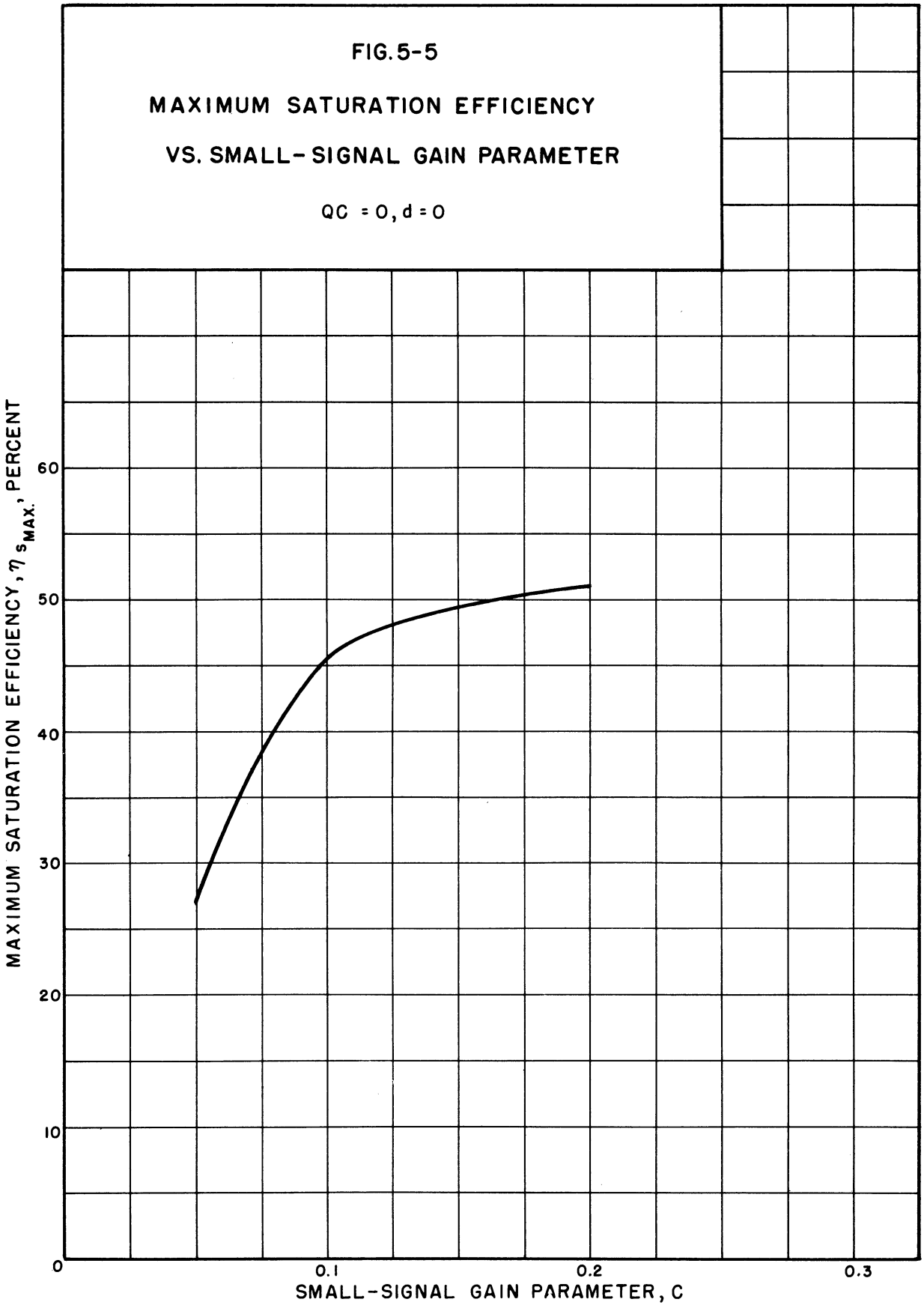

FIG. 5-6

MAXIMUM SATURATION EFFICIENCY/C VS. SMALL-SIGNAL SPACE-CHARGE PARAMETER

C = 0.1, d = 0

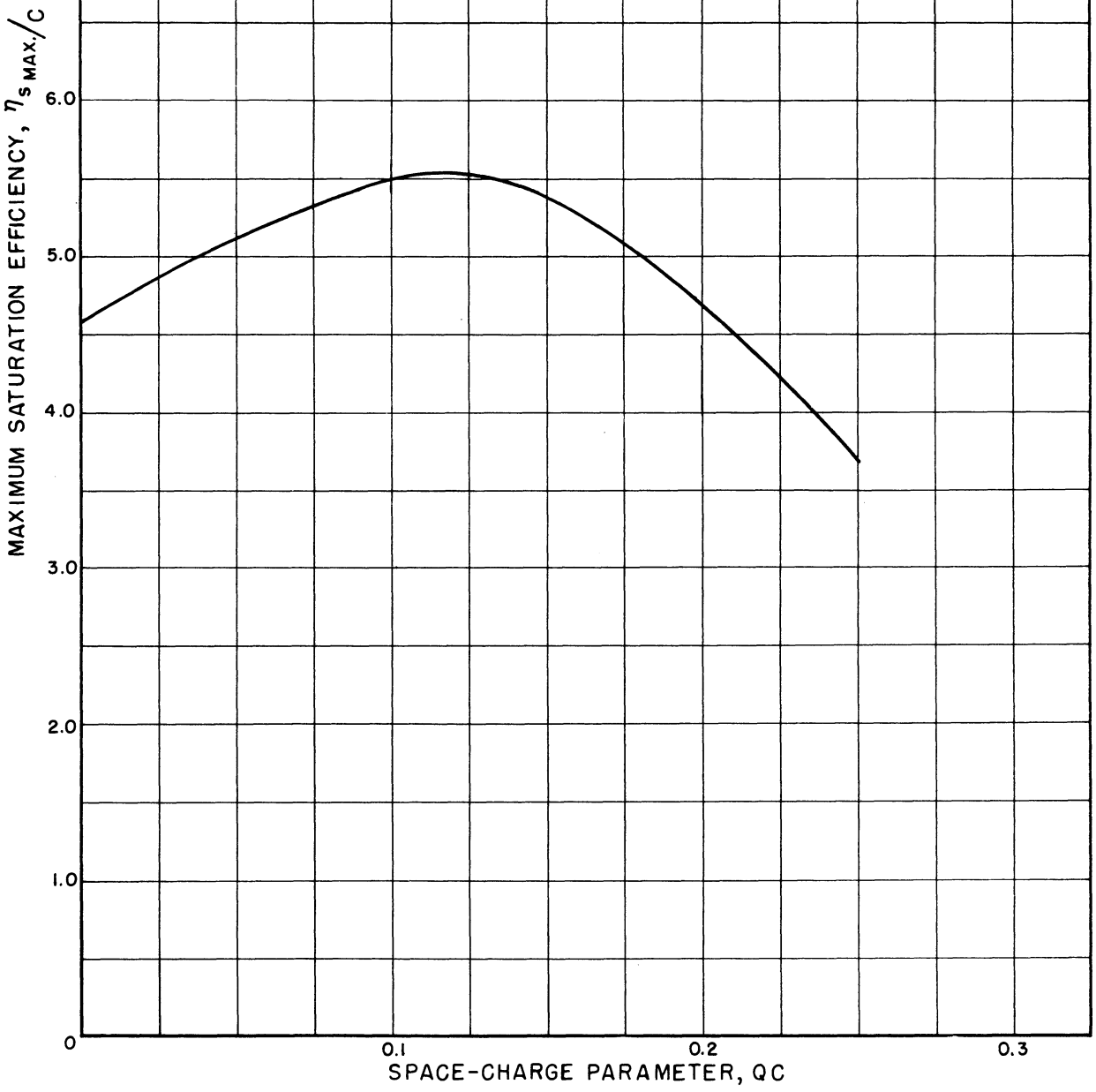

FIG. 5-7
MAXIMUM SATURATION EFFICIENCY/C
VS. LARGE-SIGNAL SPACE-CHARGE
AMPLITUDE PARAMETER, K
C = 0.1, d = 0

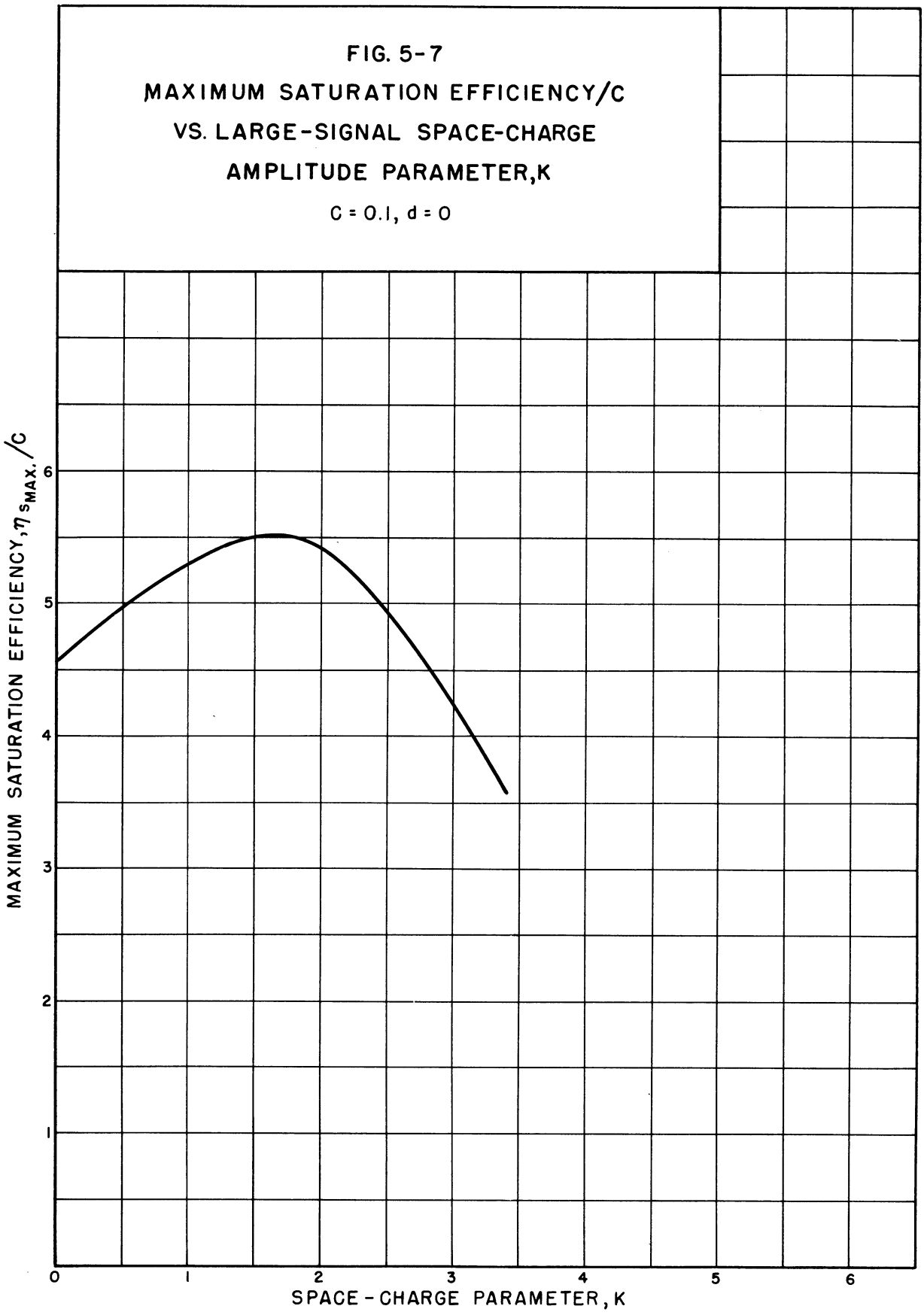

5.3 Variable Input-Signal Level

Some additional information on the operation of large-signal amplifiers when the input-signal level is varied may be obtained from the figures of Section 4.6. Since the saturation level is relatively independent of ψ, one such curve is a plot of the input-signal level vs. the saturation length, shown in Fig. 5-8. It can be seen that the optimum tube length is very nearly a linear function of the input-signal level for a wide range of ψ.

Figure 5-9 is a plot of the phase shift at saturation, relative to that for a very small input-signal level, vs. the input-signal level for a fixed tube length. The tube length chosen is $N_g = 5.5$ (i.e., $y = 3$); from the figure it can be seen that the tube would saturate at approximately $y = 3$ for $\psi = 7$ db. This curve indicates the amount of incidental phase modulation that would accompany a change in the input-signal level or amplitude modulation of the input signal. Clearly if the tube is to be amplitude-modulated it must be operated well below saturation and for small amplitudes of modulating voltage if linearity is desired.

For the same tube length, i.e., $N_g = 5.5$, a power-output vs. power-input curve prepared from the data of Fig. 4-66 is shown as Figs. 5-10a, 5-10b, and 5-10c. The power levels are plotted on a linear scale in Figs. 5-10a and 5-10b and on a logarithmic scale in Fig. 5-10c. In the small-signal region the power output is seen to be a linear function of the input power as expected; however, as the input power is increased still further the output power reaches a maximum and then decreases. Figure 5-10c indicates that for this case the saturation power output is approximately 3.75 db below that which would be obtained if the output were still linearly related to the input and it is seen from Fig. 5-10a that the power

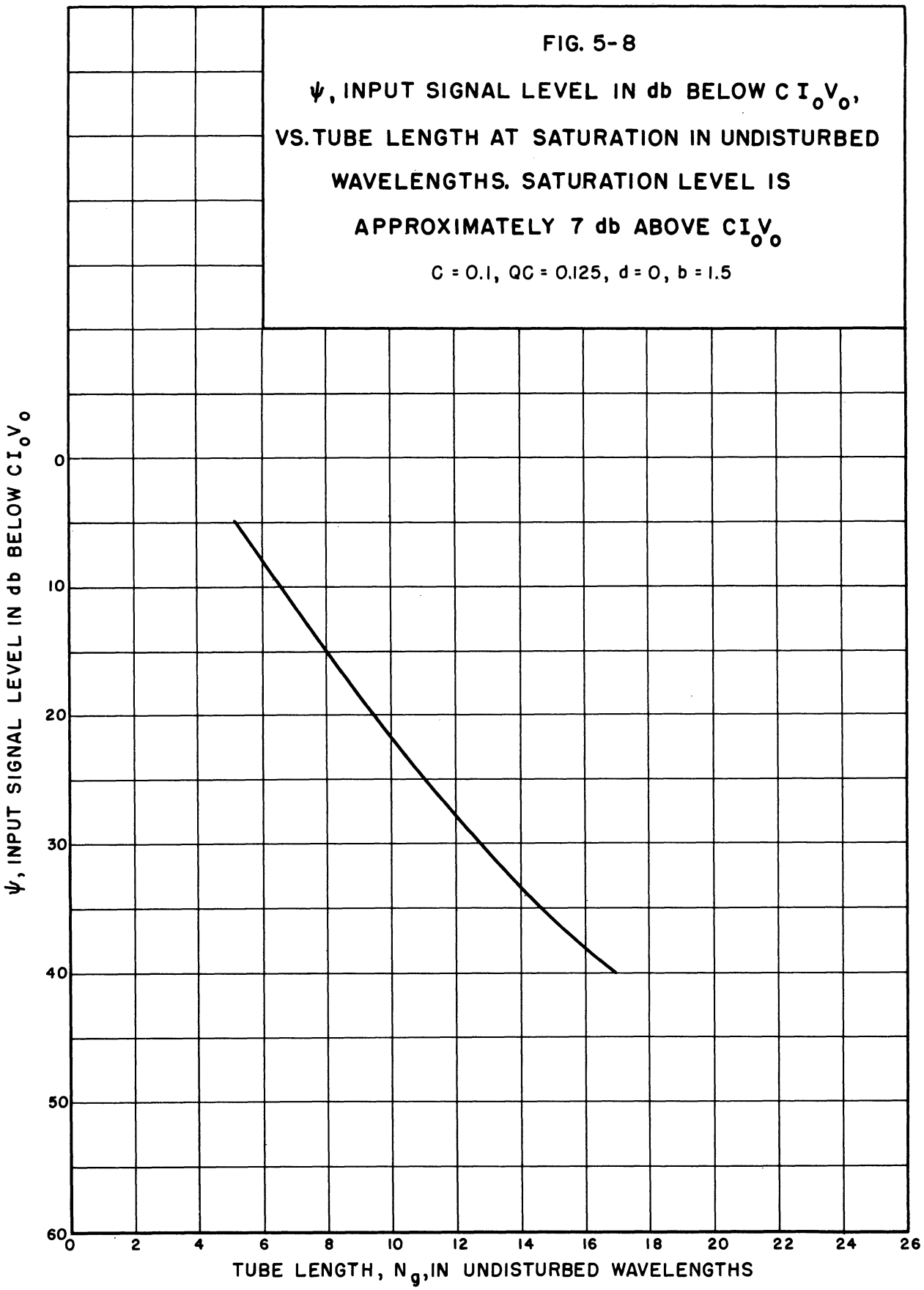
FIG. 5-8
ψ, INPUT SIGNAL LEVEL IN db BELOW C I0V0, VS. TUBE LENGTH AT SATURATION IN UNDISTURBED WAVELENGTHS. SATURATION LEVEL IS APPROXIMATELY 7 db ABOVE CI0V0
C = 0.1, QC = 0.125, d = 0, b = 1.5
ψ, INPUT SIGNAL LEVEL IN db BELOW CI0V0
0
10
20
30
40
50
60
0
2
4
6
8
10
12
14
16
18
20
22
24
26
TUBE LENGTH, Ng, IN UNDISTURBED WAVELENGTHS

FIG. 5-9

PHASE SHIFT VS. ψ FOR FIXED TUBE LENGTH

WITH VARIABLE INPUT-SIGNAL LEVEL

$C = 0.1$, $QC = 0.125$, $d = 0$, $b = 1.5$, $N_g = 5.5$

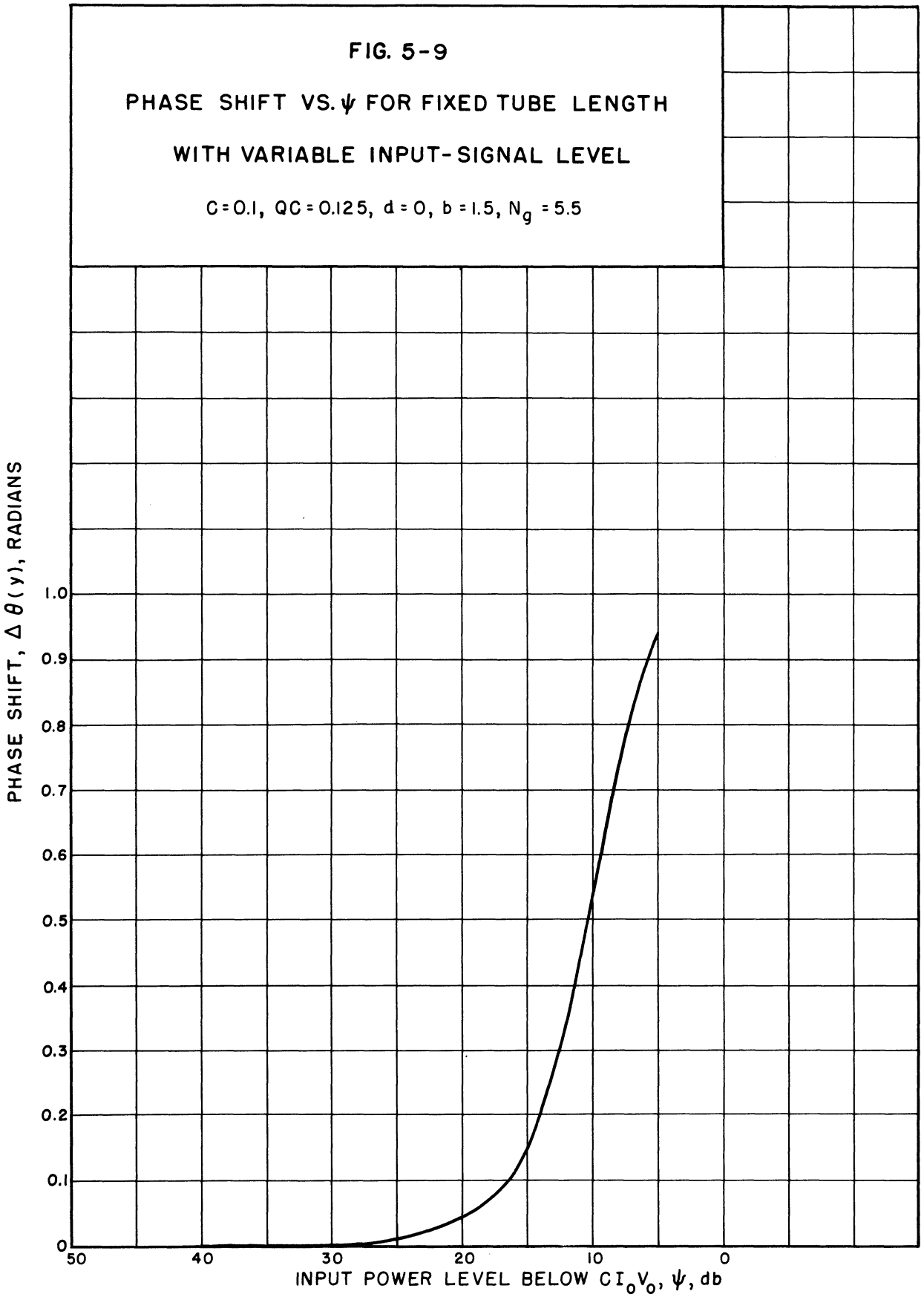

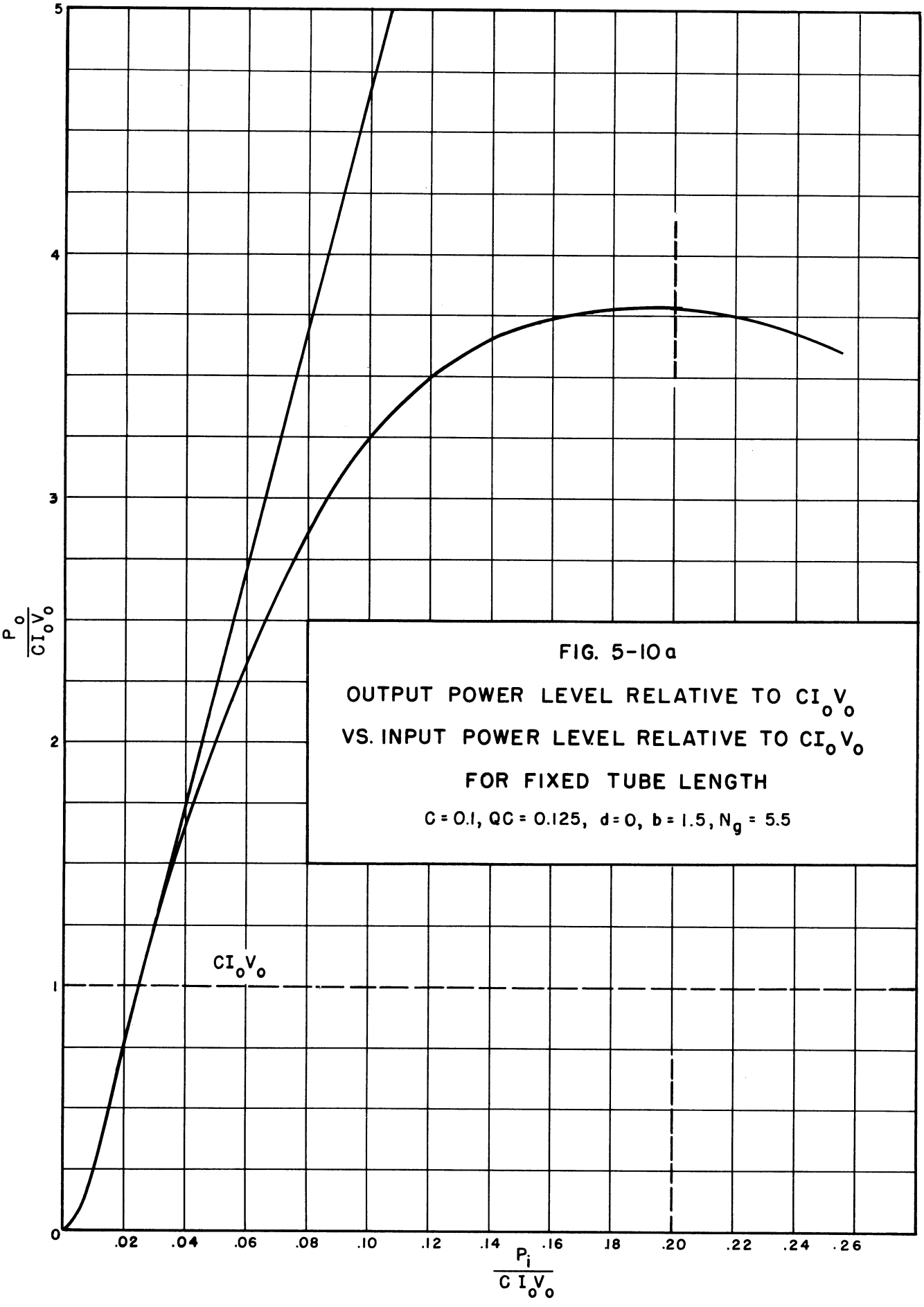

FIG. 5-10a

OUTPUT POWER LEVEL RELATIVE TO CI_oV_o

VS. INPUT POWER LEVEL RELATIVE TO CI_oV_o

FOR FIXED TUBE LENGTH

C = 0.1, QC = 0.125, d = 0, b = 1.5, N_g = 5.5

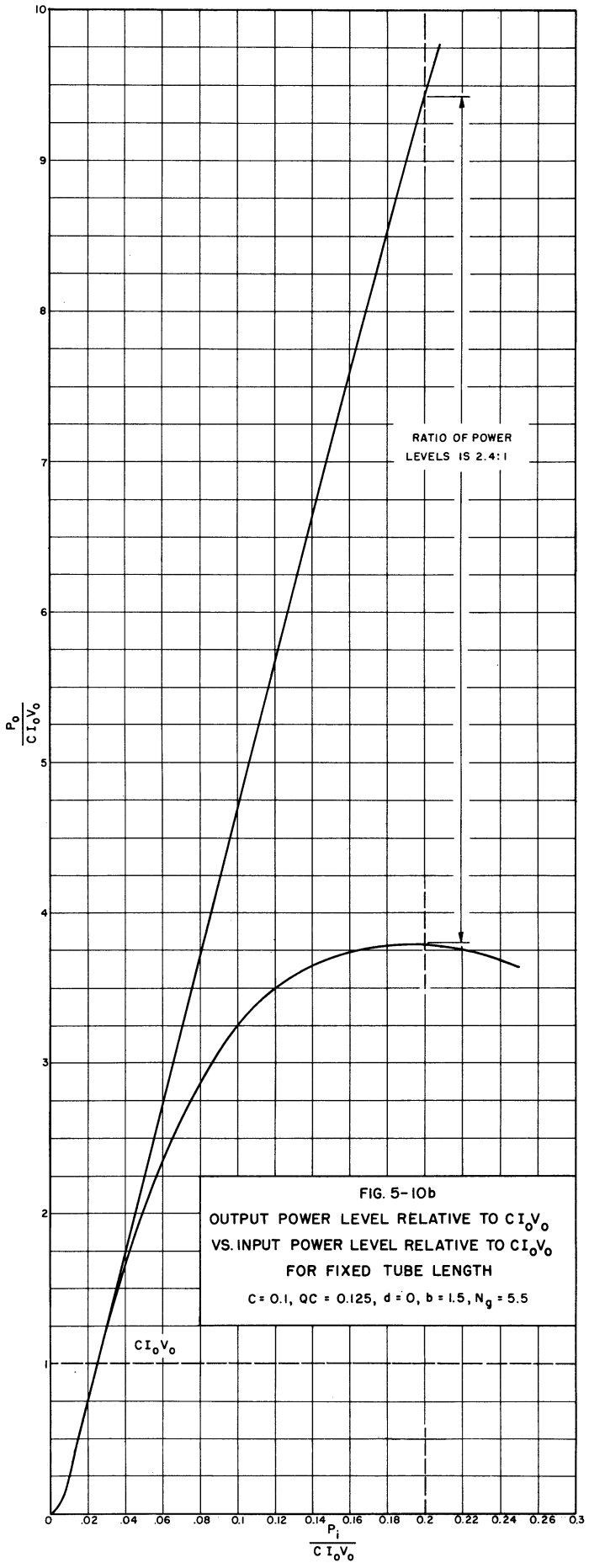

FIG. 5-10b

OUTPUT POWER LEVEL RELATIVE TO CI_0V_0 VS. INPUT POWER LEVEL RELATIVE TO CI_0V_0 FOR FIXED TUBE LENGTH

C = 0.1, QC = 0.125, d = 0, b = 1.5, N_g = 5.5

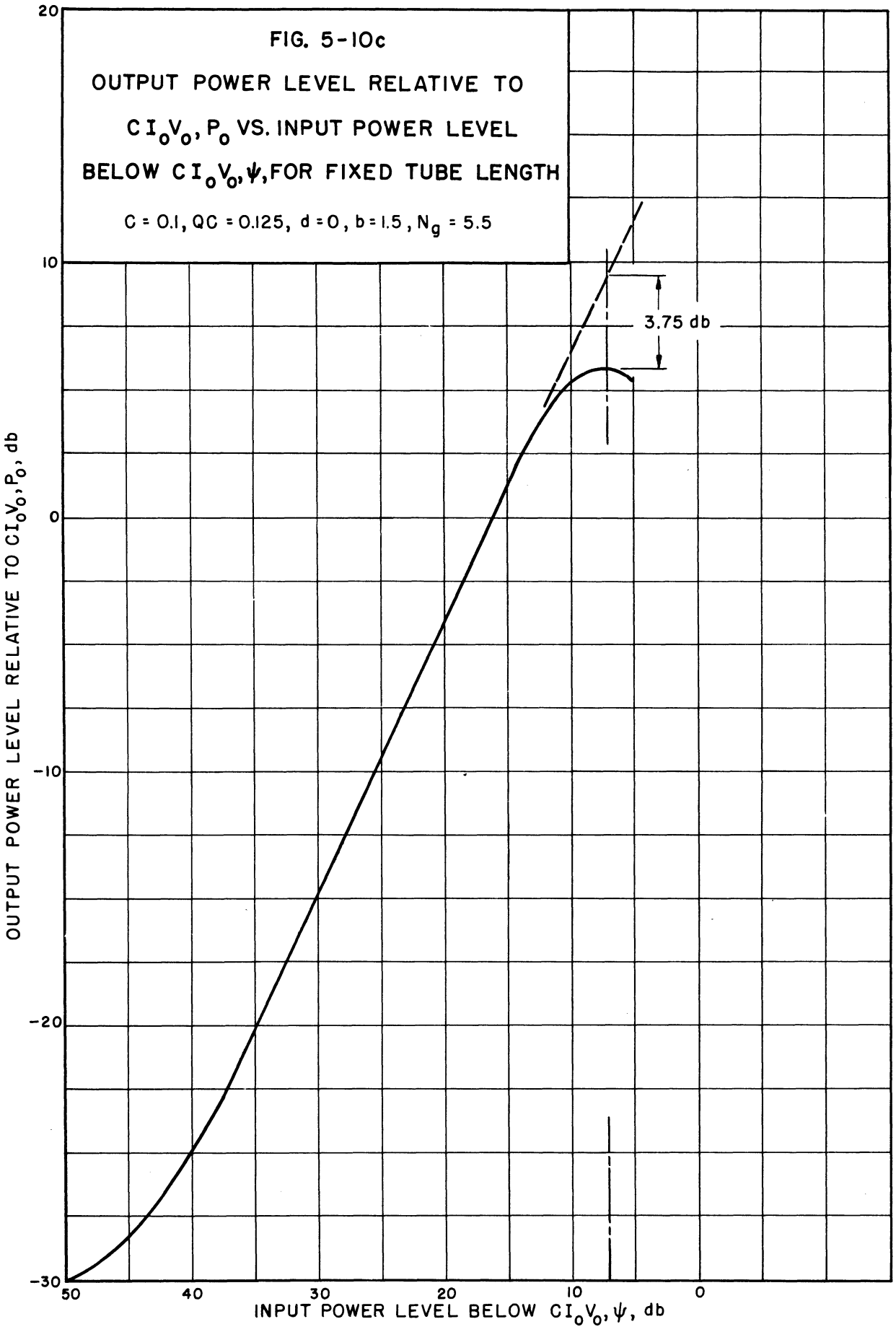
FIG. 5-10c
OUTPUT POWER LEVEL RELATIVE TO
CI_0V_0, P_0 VS. INPUT POWER LEVEL
BELOW CI_0V_0, ψ, FOR FIXED TUBE LENGTH
C = 0.1, QC = 0.125, d = 0, b = 1.5, N_g = 5.5
3.75 db
OUTPUT POWER LEVEL RELATIVE TO CI_0V_0, P_0, db
INPUT POWER LEVEL BELOW CI_0V_0, ψ, db
20
10
0
-10
-20
-30
50
40
30
20
10
0

output departs slowly from the straight-line value. When QC = 0.125 it was found that there is an increase in the output due to the presence of space charge, but for larger QC the output decreases. Hence for larger values of QC it is expected that the saturation power output should be more than 4 db below the extrapolated linear output value. Experimentally it has been found that when C = 0.1 and QC = 0.25 the best that can be achieved for saturation power is 5 to 6 db below the value predicted by the linear relationship.

5.4 Effect of Loss on Saturation Gain and Phase Shift

From the loss curves for constant injection velocity shown in Fig. 4-61, the percent reduction in saturation gain and phase shift are calculated and plotted in Figs. 5-11 and 5-12. For low values of loss the percent reduction in saturation gain increases rapidly, but for values of d greater than 0.2 (1.09 db/λ_g) the percent reduction increases more slowly.

The optimum injection velocity is reduced by the presence of loss as pointed out in Section 4.8.2. The saturation voltage gain is plotted vs. the velocity parameter for the case C = 0.1 and QC = 0.125 in Fig. 5-13, from which it is seen that the optimum b at d = 2 is 0.65 as compared to 1.5 for d = 0, a reduction of 8.5 percent in velocity above synchronism. The saturation gain is seen to vary only slightly for b between 0 and 0.65. Hence it would seem desirable to change the helix pitch under the attenuator of a traveling-wave amplifier in order to realize an increased gain. This is especially true if the loss per wavelength is large. In the above-mentioned case an improvement in the saturation gain in the lossy region of 1 db would be realized. The reduction in optimum b would obviously be less for smaller values of loss.

FIG. 5-11

PERCENT REDUCTION IN SATURATION GAIN VS. LOSS FACTOR FOR FIXED INJECTION VELOCITY

C = 0.1, QC = 0.125, A_0 = 0.0225, b = 1.5

d = 0 FOR $0 \leq y \leq 1.6$

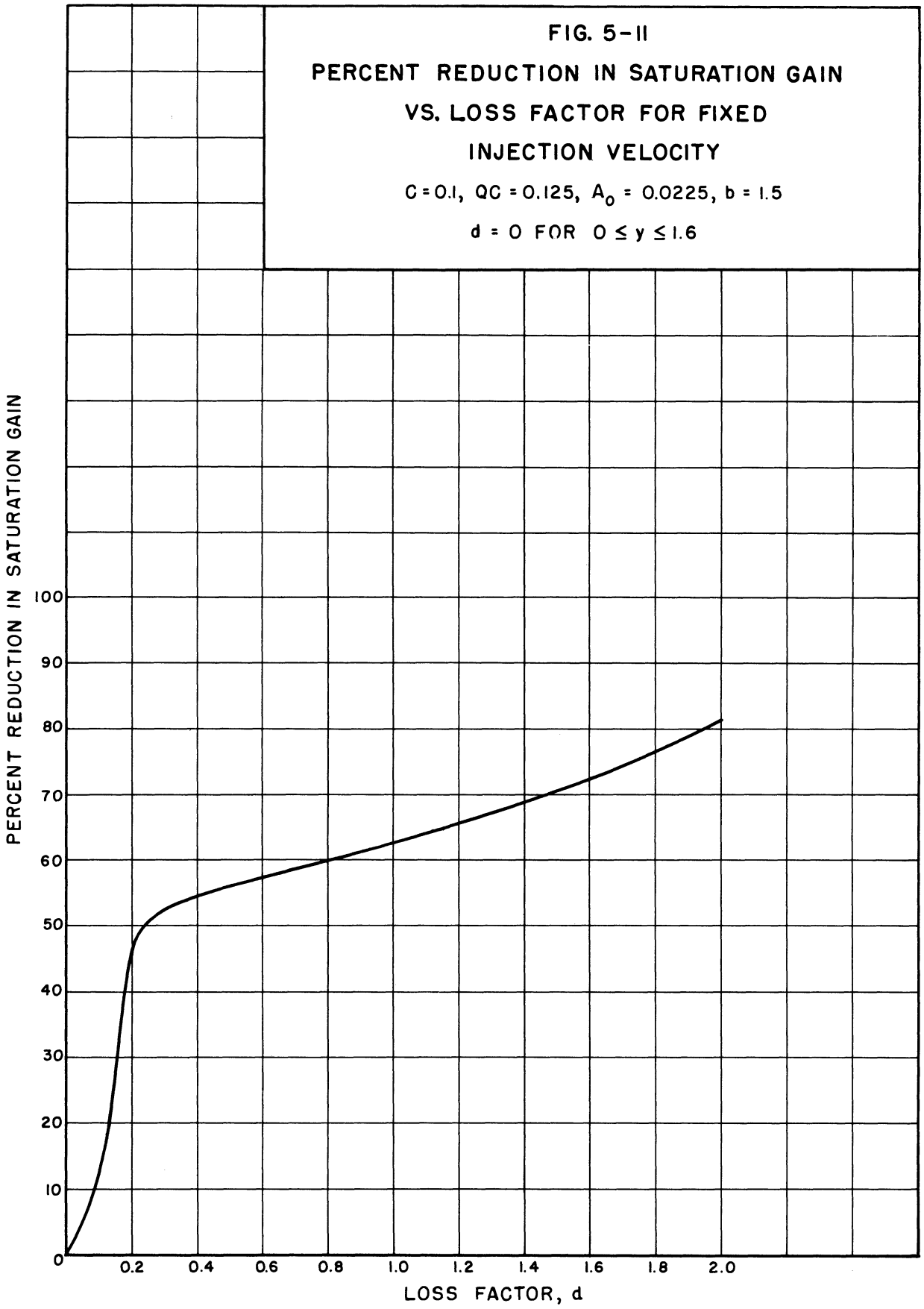

FIG. 5-12

PERCENT REDUCTION IN PHASE SHIFT AT SATURATION VS. LOSS FACTOR FOR FIXED INJECTION VELOCITY

$C = 0.1, QC = 0.125, A_0 = 0.0225, b = 1.5$

$d = 0$ FOR $0 \leq y \leq 1.6$

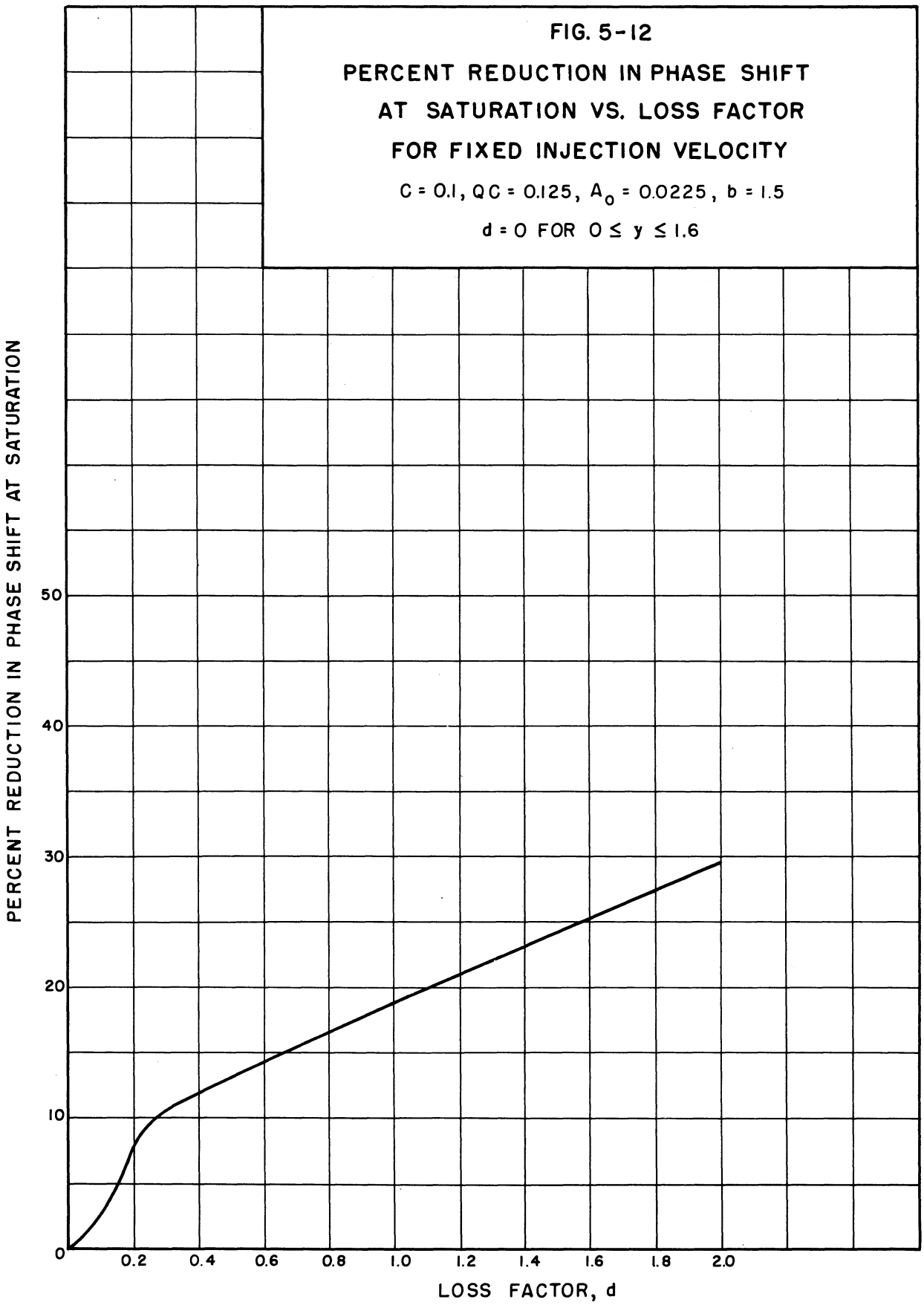

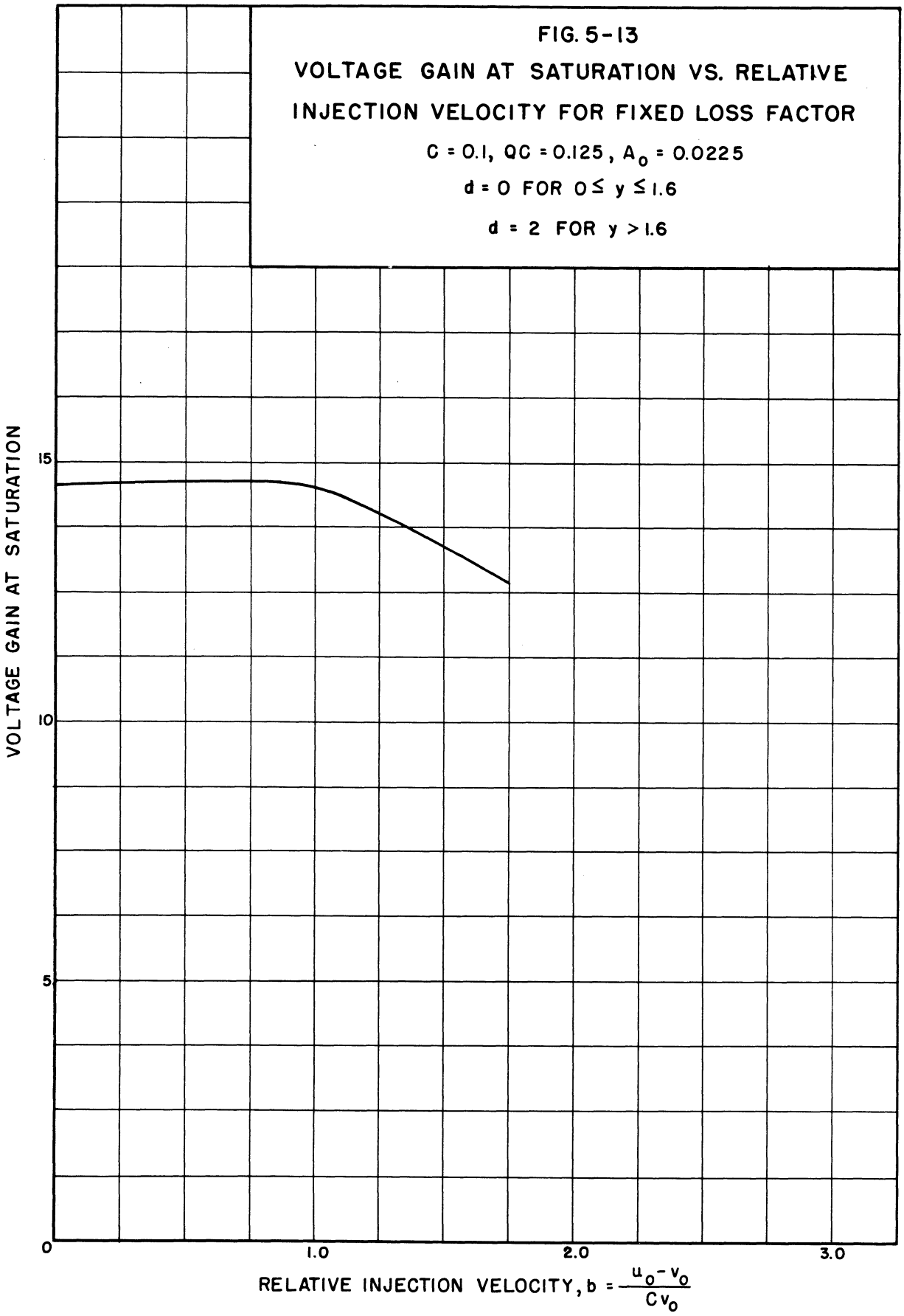
FIG. 5-13
VOLTAGE GAIN AT SATURATION VS. RELATIVE INJECTION VELOCITY FOR FIXED LOSS FACTOR
C = 0.1, QC = 0.125, A_0 = 0.0225
d = 0 FOR 0 ≤ y ≤ 1.6
d = 2 FOR y > 1.6
VOLTAGE GAIN AT SATURATION
15
10
5
0
1.0
2.0
3.0
RELATIVE INJECTION VELOCITY, $b = \frac{u_0 - v_0}{C v_0}$

5.5 Comparison with Experimental Results

C. C. Cutler of the Bell Telephone Laboratories has made some rather interesting measurements on the velocity distribution in the electron stream of a traveling-wave amplifier as a function of the signal level at the output end of the tube. Cutler's tube is a scale-model traveling-wave amplifier operating at 100 mc. Figures 5-14 and 5-15 are some typical results obtained by Cutler. These curves are similar to the plots of electron velocity deviation vs. electron phase of Section 4.4.2. Although the parameters (i.e., C, QC, $\beta b'$ and b) are not exactly those of any curves presented in Section 4.4.2 the similarity between Cutler's experimental results and the theoretical curves is striking.

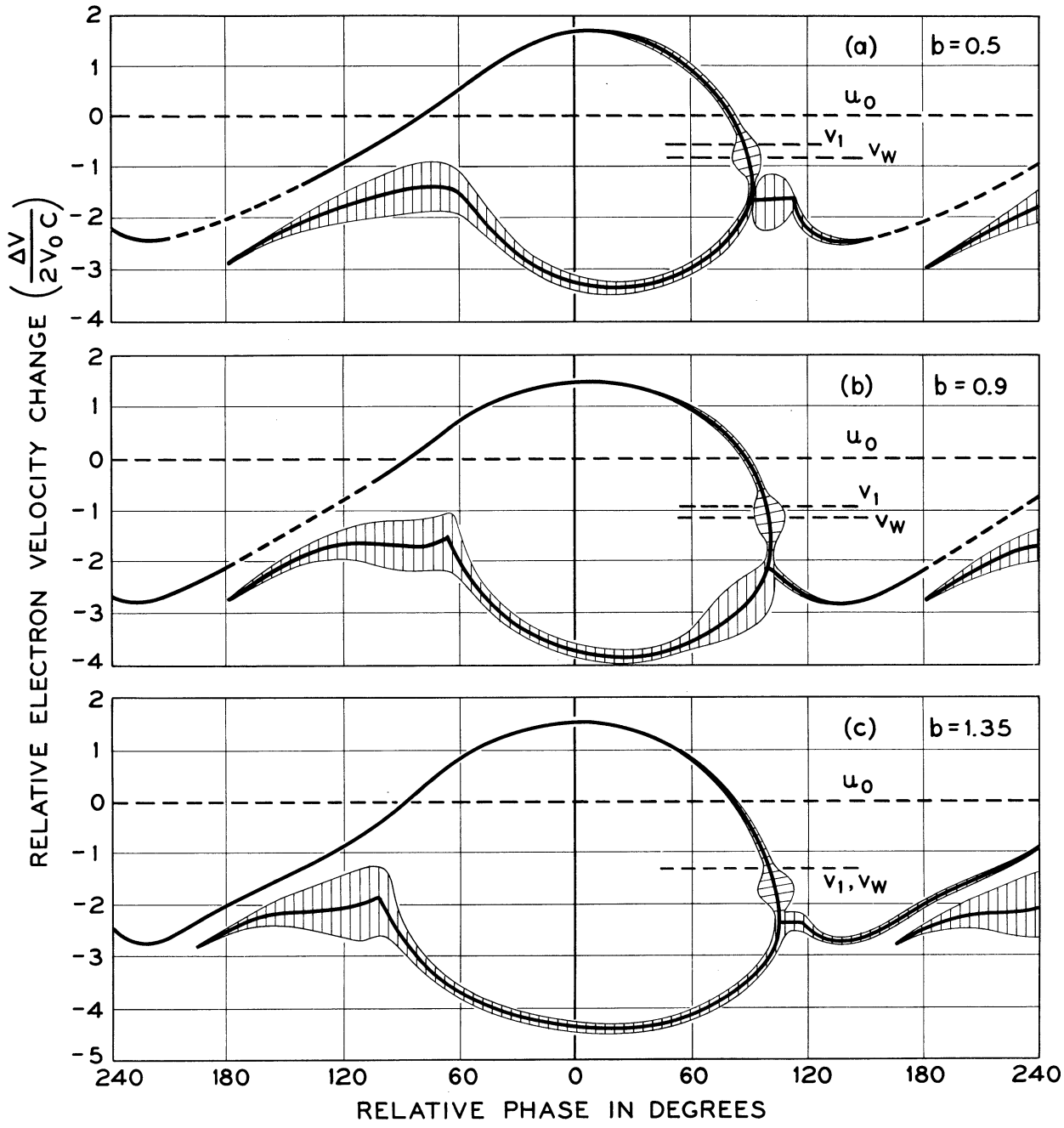

FIG. 5-14

VELOCITY AND CURRENT IN THE STREAM AT SATURATION VS. RELATIVE ELECTRON PHASE WITH RELATIVE INJECTION VELOCITY AS THE PARAMETER

$C = 0.075$, $QC = 0.22$, $\beta b' = 0.388$

a. $b = 0.5$ (ADJUSTED FOR $X_{1\,max.}$)

b. $b = 0.9$

c. $b = 1.35$ (ADJUSTED FOR MAXIMUM SATURATION GAIN)

(COURTESY OF C.C. CUTLER, BELL TELEPHONE LABORATORIES)

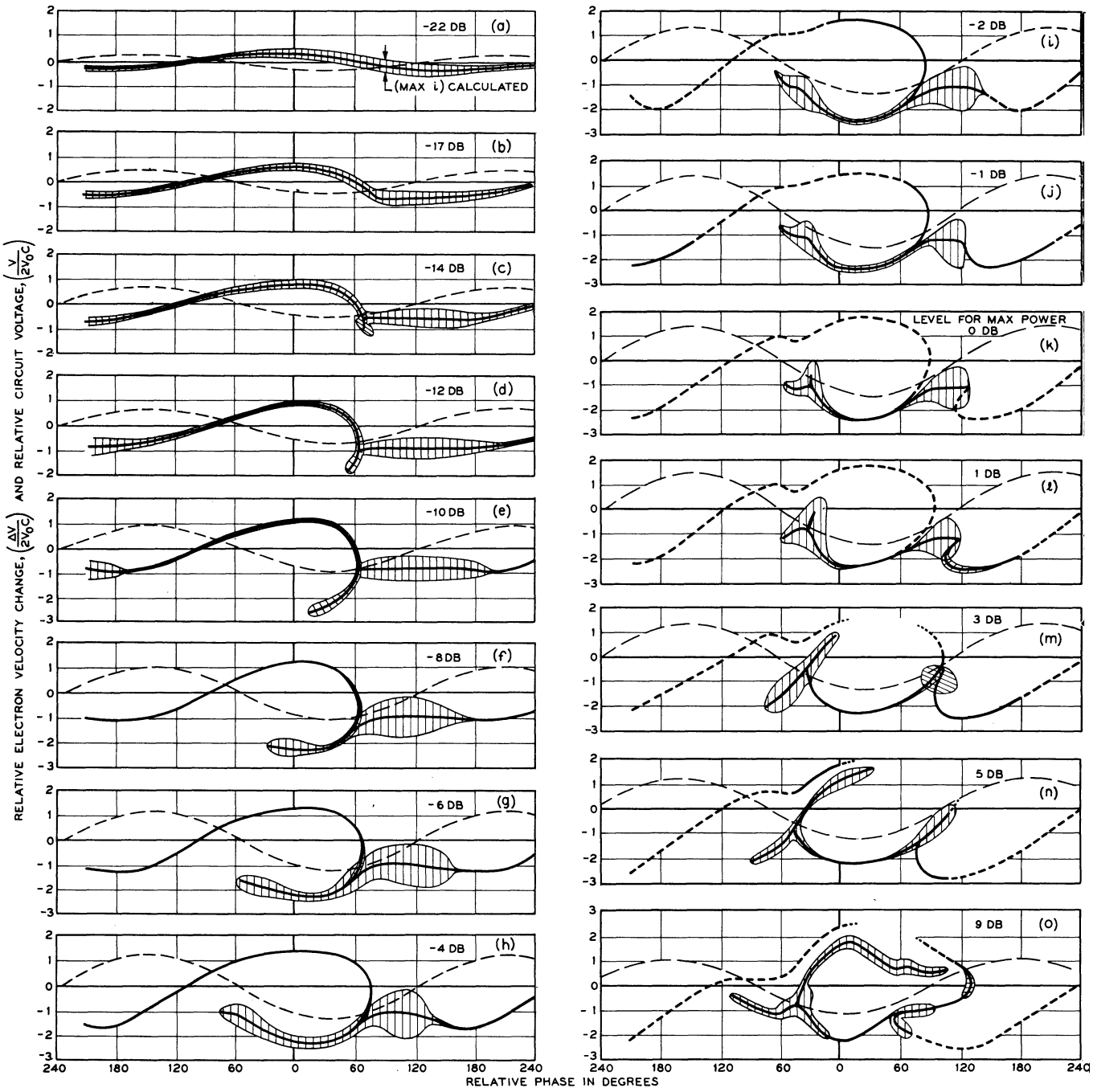

FIG. 5-15

VELOCITY AND CURRENT IN THE STREAM VS. RELATIVE ELECTRON PHASE WITH INPUT-SIGNAL LEVEL AS THE PARAMETER

C = 0.1, QC = 0.064, $\beta b' = 0.412$, b = 0.26

HEAVY LINE – ELECTRON VELOCITY

SHADED WIDTHS PROPORTIONAL TO CURRENT

LIGHT DASHED LINE – CIRCUIT VOLTAGE

(COURTESY OF C.C. CUTLER, BELL TELEPHONE LABORATORIES)

CHAPTER VI. CONCLUSIONS

6.1 Introduction

In the preceding chapters the large-signal traveling-wave amplifier equations have been derived and solved for several values of the gain parameter C, the space-charge parameter QC, the loss factor d, and the velocity parameter b. Solutions were also obtained for variable input-signal level. The assumptions made in deriving the large-signal equations are listed in Section 2.1. It is believed the chief limiting assumptions are that the electric field is constant across the electron stream and that the space-charge density has a sinusoidal variation with z but does not vary with radius.

6.2 Accuracy of the Results

As discussed in Chapter III, the various errors which arise in the course of computation have been analyzed and found to affect the results as follows:

1. Truncation error was found to be insignificant for a Δy of 0.025 or less.
2. Round-off error, on the other hand, is insignificant for a Δy of 0.025 or more.
3. The value $\Delta y = 0.025$ was therefore selected as the optimum value to give a minimum rms error and require the least computation time for minimum error.
4. The analysis of truncation and round-off error showed the results to be accurate solutions of the differential equations to approximately 5 decimal places.

5. The solutions were found to be stable with respect to the propagation of error.

6. The number of representative electrons that must be followed through the interaction region depends on the magnitude of the space-charge parameter QC. For QC less than 0.5, 32 electrons are sufficient; but for $0.5 < QC < 1.0$, 64 electrons are required. For $QC > 1.0$ it is necessary to follow an even larger number of electrons to obtain reasonably accurate results.

6.3 Summary of the Results

From the graphical analysis of the resulting data the following characteristics are notable:

1. The optimum relative injection velocity b increases with C for zero space charge ($QC = 0$). Typically, for $C = 0.1$ and $QC = 0$ the optimum b is 2.0.

2. When $QC \neq 0$ and $C = 0.1$ the optimum b decreases with increasing QC up to $QC = 0.25$, for which the optimum b is 1.25. However, it is expected that the optimum b will increase with QC beyond that point. If the experimentally determined optimum value of b is larger than that predicted by the curves of Chapter V, a possible explanation is that the potential depression in the electron stream due to the average space charge lowers the stream voltage significantly below the helix voltage.

3. In the absence of space-charge forces, the saturation gain was found to decrease with increasing C, but the saturation efficiency increases with C.

4. For zero space charge the maximum saturation efficiency increases rapidly with C up to approximately C = 0.1; beyond this value the increase in efficiency is slower. Hence there is a value of C around 0.1 to 0.12 beyond which the increase in maximum efficiency probably does not justify the corresponding loss in gain noted in (3) above.
5. The drop-out of each voltage gain vs. relative injection velocity curve is quite sharp, as in the small-signal case, and the value of b at which this drop of the gain to a very small value occurs is approximately that value of b for which the small-signal gain goes to zero.
6. At C = 0.1 the optimum tube length for QC between 0 and 0.25 is between 10 and 20 undisturbed wavelengths.
7. For small values of space charge and C = 0.1, the saturation gain and efficiency both increase with increasing QC up to about QC = 0.125 and then both decrease as QC increases further.
8. For a typical case, C = 0.1 and QC = 0.125, the saturation power output is approximately 3.75 db below the value predicted by the linear theory. The difference would be still greater for larger QC (see Figs. 5-10a and 5-10b).
9. The presence of series loss along the helix has two important effects. First, the loss reduces the value of b for optimum gain, for example from 1.5 to 0.65 in the case of d = 2.0 (10.9 db/λ_g) for C = 0.1 and QC = 0.125.

Second, a series loss as high as d = 2.0 reduces the saturation gain to 18.3 percent of its value for d = 0 where C = 0.1, QC = 0.125, and b = 1.5.

10. The point at which loss is introduced at a distance of CN $\simeq$ 0.2, 0.3, or 0.4 from the input has little effect on the saturation gain for C = 0.1, QC = 0.125, and b = 0.65.

11. The curves of Chapters IV and V are very useful for designing and predicting the performance of large-signal traveling-wave amplifiers.

6.4 Suggestions for Further Research

During the course of this investigation a number of points were touched upon which were aside from the main direction of this research but which seemed to hold promise for fruitful work. Several of the most interesting of these ideas are listed below.

1. In tubes with especially large stream diameters the effect on the saturation power output of variation of the field across the stream diameter is of particular interest. Equations can be derived to express this effect by dividing the electron stream up into several sections, but the resulting expressions are even more complex than the set solved for this dissertation and the computation time would be correspondingly great. Perhaps improved computer techniques will make this problem feasible in the near future, however.

2. Investigations of the effect on A(y) and Θ(y) of varying the stream diameter $\beta b'$ and the ratio of the helix diameter to the stream diameter should produce worthwhile results.

3. Solutions for additional values of the gain parameter C and the space-charge parameter QC beyond the range investigated here would be of interest and usefulness as higher-power traveling-wave amplifiers are developed.

4. Loss calculations for many other values of the loss parameter d and various configurations of loss along the helix constitute an interesting area for further investigation.

5. Plots of power output P_o vs. power input P_i for additional values of QC, C, and d would also provide useful information.

APPENDIX A. DERIVATION OF THE GENERAL TRANSMISSION-LINE EQUATION

A.1 Equivalent Circuit

The interaction of an electron stream and a radio-frequency wave propagating along a helical slow-wave structure can be studied in terms of the simplified model shown in Fig. A-1. The electron velocity and the phase velocity of the radio-frequency wave are approximately equal and about one-tenth the velocity of light; hence, relativistic effects may be neglected.

The helical slow-wave structure is represented by a distributed-constant transmission line made up of series inductance and resistance and shunt capacitance. The inductance and capacitance of the equivalent line are chosen to match the phase velocity of the radio-frequency wave and the field strength of the longitudinal electric field acting on the electron stream. The transmission line is then divided into a number of lumped-constant sections which are short compared to the helix wavelength λ_g.

Probably the best justification for using this simplified equivalent circuit for the helical slow-wave structure is that results obtained with such a circuit agree well with experimental evidence.

A.2 Definition of Variables

The following variables are used in the derivation of the general transmission-line equation:

L_o = Ld_o, the self induction per section $\Delta z = d_o$, henries/m;

R_o = Rd_o, the resistance per section, ohms/m;

C_o = Cd_o, the capacitance per section, farads/m;

I_n = the current in L_o and R_o in section n, amp;

q'_n = $\rho_n d_o$, the electric charge of the stream in section n, coulombs;

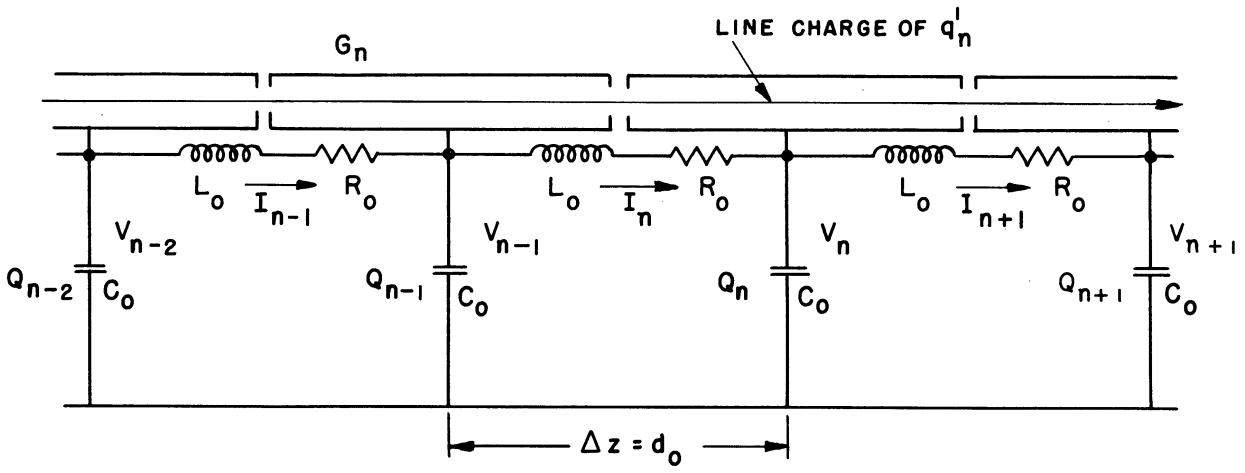

FIG. A-1

GENERAL EQUIVALENT CIRCUIT
OF A TRAVELING-WAVE TUBE

u_o = the electron velocity in the stream, m/sec;

Q_n = the charge on the capacitance of section n, coulombs;

V_n = the potential on the capacitance of section n, volts;

q_n = the charge brought on the capacitance of section n by the currents occurring in the line, coulombs; and

G_n = a guiding section of the electron stream.

A.3 Derivation of the Equation

From the equivalent circuit described in section A.1, the following equations are obtained along the transmission line:

$$I_n - I_{n+1} = \frac{\partial q_n}{\partial t} , \tag{A-1}$$

$$V_{n-1} - V_n = L_o \frac{\partial I_n}{\partial t} + R_o I_n , \tag{A-2}$$

$$Q_n = q_n + q_n' = q_n + \rho_n d_o , \tag{A-3}$$

and

$$V_n = \frac{Q_n}{C_o} , \tag{A-4}$$

where $R_o I_n^2$ represents the dissipation in the transmission line.

The electron stream has a charge of q_n' in the section G_n, and thus induces a charge $-q_n'$ on the helix wall of that section, which produces an additional charge q_n' on the capacitance of G_n. The time derivative of Eq. A-1 is

$$\frac{\partial I_n}{\partial t} - \frac{\partial I_{n+1}}{\partial t} = \frac{\partial^2 q_n}{\partial t^2} . \tag{A-5}$$

Solving Eq. A-2 for $\partial I_n/\partial t$ gives

$$\frac{\partial I_n}{\partial t} = \frac{V_{n-1} - V_n}{L_o} - \frac{R_o}{L_o} I_n \quad . \tag{A-6}$$

By analogy,

$$\frac{\partial I_{n+1}}{\partial t} = \frac{V_n - V_{n+1}}{L_o} - \frac{R_o}{L_o} I_{n+1} \quad . \tag{A-7}$$

Substituting Eqs. A-6 and A-7 into Eq. A-5 and collecting terms gives

$$\frac{V_{n-1} + V_{n+1} - 2V_n}{L_o} + \frac{R_o}{L_o} (I_{n+1} - I_n) = \frac{\partial^2 q_n}{\partial t^2} \quad . \tag{A-8}$$

Substituting Eq. A-4 into Eq. A-3 and taking the second time derivative yields

$$\frac{\partial^2 q_n}{\partial t^2} = C_o \frac{\partial^2 V_n}{\partial t^2} - \frac{\partial^2 \rho_n}{\partial t^2} d_o \quad . \tag{A-9}$$

Equating Eq. A-9 to Eq. A-8 and rearranging terms results in the following:

$$\frac{V_{n-1} + V_{n+1} - 2V_n}{d_o^2} - LC \frac{\partial^2 V_n}{\partial t^2} = -L \frac{\partial^2 \rho_n}{\partial t^2} + \frac{R}{d_o} (I_n - I_{n+1}) \quad . \tag{A-10}$$

Equations A-1 and A-3 may be utilized to rewrite the last term of Eq. A-10 as

$$I_n - I_{n+1} = \frac{\partial q_n}{\partial t} = Cd_o \frac{\partial V_n}{\partial t} - d_o \frac{\partial \rho_n}{\partial t} \quad . \tag{A-11}$$

Hence Eq. A-10 may be rewritten as

$$\frac{V_{n-1} + V_{n+1} - 2V_n}{d_o^2} - LC \frac{\partial^2 V_n}{\partial t^2} = -L \frac{\partial^2 \rho_n}{\partial t^2} + RC \frac{\partial V_n}{\partial t} - R \frac{\partial \rho_n}{\partial t} \quad . \tag{A-12}$$

The sections of the equivalent transmission line shown in Fig. A-1 are considered to be very short compared to the helix wavelength λ_g. Thus in Eq. A-12 d_o is allowed to approach zero and the limit taken

$$\frac{\partial^2 \overline{V}(z,t)}{\partial z^2} - LC \frac{\partial^2 \overline{V}(z,t)}{\partial t^2} = -L \frac{\partial^2 \overline{\rho}(z,t)}{\partial t^2} + RC \frac{\partial \overline{V}(z,t)}{\partial t} - R \frac{\partial \overline{\rho}(z,t)}{\partial t} . \quad \text{(A-13)}$$

Substituting

$$v_o = \frac{1}{\sqrt{LC}} = \text{the undisturbed phase velocity of the line, m/sec,}$$

and

$$Z_o = \sqrt{L/C} \cong \frac{E_z^2(0)}{2\beta^2 P} = \text{the characteristic impedance of the lossless line, ohms,}$$

where $E_z^2(0)$ = the maximum value of the longitudinal electric field intensity on the axis of the helix carrying power P with a phase constant β, volts/m, reduces A-13 to

$$\frac{\partial^2 \overline{V}(z,t)}{\partial t^2} - v_o^2 \frac{\partial^2 \overline{V}(z,t)}{\partial z^2} + \frac{R}{L} \frac{\partial \overline{V}(z,t)}{\partial t}$$

$$= v_o Z_o \frac{\partial^2 \overline{\rho}(z,t)}{\partial t^2} + \frac{R}{L} v_o Z_o \frac{\partial \overline{\rho}(z,t)}{\partial t} . \quad \text{(A-14)}$$

In terms of the notation introduced by J. R. Pierce in Traveling-Wave Tubes[8], the quantity R/L in the above equation may be replaced by $2\omega Cd$, where

ω = angular frequency of the wave impressed on the helix, radians;

C = the gain parameter defined by $C^3 = |\eta| Z_o I_o / 2u_o^2$;

I_o = the d-c stream current, amp;

η = q/m, the charge-to-mass ratio for the electron, coulombs/kg;

d = 0.01836 ℓ/C, the loss factor; and

ℓ = the series loss expressed in db per undisturbed wavelength along the helix.

Thus Eq. A-14 may be written

$$\frac{\partial^2 \overline{V}(z,t)}{\partial t^2} - v_o^2 \frac{\partial^2 \overline{V}(z,t)}{\partial z^2} + 2\omega C d \frac{\partial \overline{V}(z,t)}{\partial t}$$

$$= v_o Z_o \frac{\partial^2 \overline{\rho}(z,t)}{\partial t^2} + 2\omega C d v_o Z_o \frac{\partial \overline{\rho}(z,t)}{\partial t} . \qquad \text{(A-15)}$$

For the case of a lossless line, Eq. A-15 reduces to

$$\frac{\partial^2 \overline{V}(z,t)}{\partial t^2} - v_o^2 \frac{\partial^2 \overline{V}(z,t)}{\partial z^2} = v_o Z_o \frac{\partial^2 \overline{\rho}(z,t)}{\partial t^2} . \qquad \text{(A-16)}$$

A similar expression for this special case has been derived by Brillouin.[11]

APPENDIX B. DERIVATION OF THE SPACE-CHARGE FIELD EXPRESSION

B.1 Underlying Assumptions

A number of basic assumptions are essential to the derivation of a usable expression for the space-charge field in a traveling-wave amplifier. The assumptions underlying the derivation in section B.2 are as follows:

1. The radio-frequency wave impressed on the helix bunches the stream in such a manner that the space-charge density is constant in amplitude (i.e., has no radial variation) and varies sinusoidally with axial distance. (In calculating the space-charge forces it is assumed that the growth constant of the growing space-charge wave is small compared to unity.)
2. The relationships may be described using nonrelativistic mechanics; i.e., the squares of the ratios of the stream velocity u_o and the wave velocity v to the velocity of light are small compared to unity, and hence the motion of the electrons is sufficiently slow that the formulas of electrostatics are valid. Thus, the solution will be found for the static stream of electrons with the same a-c charge distribution as the moving stream of electrons.
3. The electron stream is in a strong axial d-c magnetic field (rectilinear flow), so that the electrons are constrained to follow linear paths. Consequently there is considered to be no transverse motion and the stream boundary is smooth.

4. A sufficient quantity of positive ions is present to neutralize the average space charge.

Assumption 1 is considered to be a reasonable supposition, the sine variation having been selected for its mathematical convenience. Assumption 2 is valid even for accelerating voltages of the order of 20 kv, while Assumption 4 does not appreciably limit the generality of the derivation.

Assumption 3 is exact only for an infinite focusing field. However, this is one of the usual assumptions made in dealing with space-charge waves in electron streams and is probably valid in practice where the magnetic field is such that the cyclotron frequency is several times the electron plasma frequency. The effect of considering transverse motion of the electrons in wave propagation along an electron stream has been investigated by Rigrod and Lewis[29], who found that the growth constant is somewhat larger for Brillouin flow (finite magnetic field) than for rectilinear flow (infinite magnetic field).

B.2 Derivation of the Equation

For purposes of calculating the space-charge field, the helical slow-wave structure is replaced by a drift tube related to the helix as shown in Fig. B-1.

The equations satisfied by a stationary charge distribution may be obtained directly from Maxwell's equations by setting all the derivatives with respect to time equal to zero. Hence, we may write at all regular points of the electrostatic field:

$$\nabla \times E = 0 \qquad \text{(B-1)}$$

and

$$\nabla \cdot D = \rho \quad . \qquad \text{(B-2)}$$

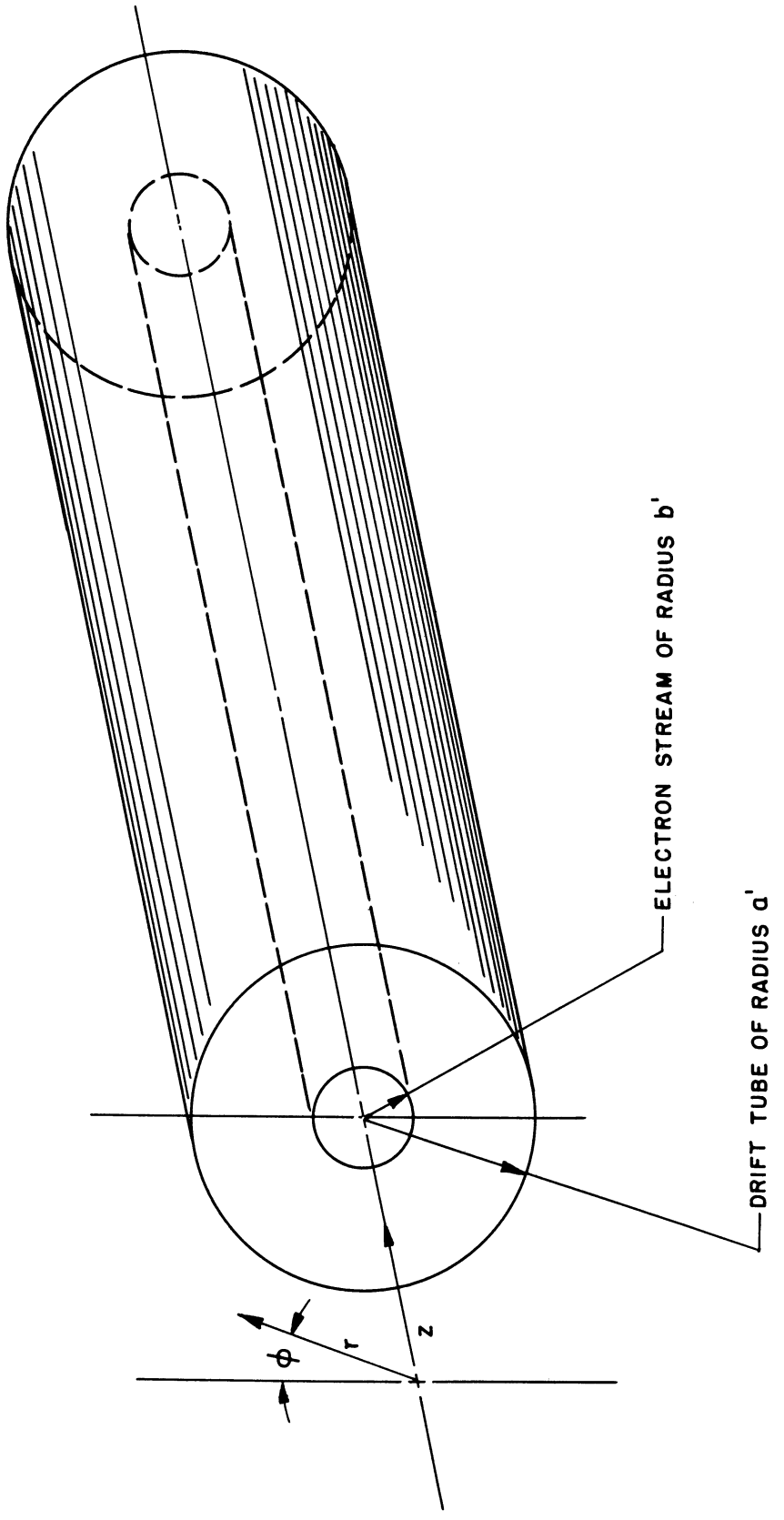

FIG. B-1 SKETCH OF THE ELECTRON STREAM AND DRIFT TUBE USED TO DERIVE THE SPACE-CHARGE FIELD EXPRESSION

The conservative nature of the electrostatic field as indicated in Eq. B-1 is a necessary and sufficient condition for the existence of a scalar electric potential whose gradient is E. Hence,

$$E = -\nabla V \quad . \tag{B-3}$$

Since the electron stream is homogeneous, V must be a solution of Poisson's equation within the stream; and between the stream boundary and the drift tube Laplace's equation must be satisfied.

Within the electron stream Poisson's equation may be written as follows for the case of cylindrical geometry:

$$\nabla^2 V = \frac{1}{r}\frac{\partial}{\partial r}\left(r\frac{\partial V}{\partial r}\right) + \frac{1}{r^2}\frac{\partial^2 V}{\partial \phi^2} + \frac{\partial^2 V}{\partial z^2} = \frac{-\rho(z)}{\epsilon\pi b'^2} \quad , \tag{B-4}$$

where $V(r,z)$ = scalar electric potential within the electron stream, volts;

$\rho(z)$ = instantaneous linear space-charge density, coulombs/m; and

b' = radius of the electron stream, m.

If it is assumed that there is no variation with ϕ, the polar angle about the axis, and the first term is expanded, Eq. B-4 becomes

$$\nabla^2 V(r,z) = \frac{\partial^2 V(r,z)}{\partial r^2} + \frac{1}{r}\frac{\partial V(r,z)}{\partial r} + \frac{\partial^2 V(r,z)}{\partial z^2} = -\frac{\rho(z)}{\epsilon\pi b'^2}$$

$$= A\rho(z)e^{-j\beta z} \quad . \tag{B-5}$$

As discussed above, in the region between the electron stream and the drift tube Eq. B-5 reduces to Laplace's equation,

$$\nabla^2 V'(r,z) = 0 \quad . \tag{B-6}$$

The solution of Poisson's equation (Eq. B-5) may be written directly as follows:

$$V(r)\, e^{-j\beta z} = \left[\frac{A\rho(z)}{\beta^2} + BI_o(\beta r)\right] e^{-j\beta z} , \qquad (B\text{-}7)$$

where $I_o(\beta r)$ = the zero-order modified Bessel function, first kind, of argument βr, and

$\beta = \frac{\omega}{v}$ = phase constant determined by the impressed r-f wave on the helix, radians/m.

The electric field intensity within the electron stream is given by

$$E_z(r,z) = -\frac{\partial V}{\partial z} = -\frac{\partial}{\partial z}\left[V(r)\, e^{-j\beta z}\right]$$

$$= j\beta\, V(r)\, e^{-j\beta z} . \qquad (B\text{-}8)$$

Substituting for V(r) from Eq. B-7 gives

$$E_z(r,z) = j\beta\left[\frac{A\rho(z)}{\beta^2} + BI_o(\beta r)\right] e^{-j\beta z} . \qquad (B\text{-}9)$$

Equation B-9 represents the electric field intensity within the stream in terms of the space-charge density and the constants A and B, which are to be determined from the boundary conditions. The boundary conditions to be satisfied are that the radial and longitudinal components of the electric field intensity are continuous across the stream boundary and that the longitudinal component of electric field intensity is zero at the drift tube. B in Eq. B-9 can be evaluated from these boundary conditions, and Eq. B-9 written as

$$E_z(r,z) = \frac{j\rho(z)A}{\beta}\left[1 - \beta b' \frac{I_o(\beta r)}{I_o(\beta a')}\left(I_1(\beta b')\, K_o(\beta a') + I_o(\beta a')\, K_1(\beta b')\right)\right] e^{-j\beta z} \quad . \qquad \text{(B-10)}$$

The space-charge field is obtained from Eq. B-10 by evaluating the field on the axis as follows:

$$E_z(r=0) = \frac{j\rho(z)A}{\beta} R^2\, e^{-j\beta z} \quad , \qquad \text{(B-11)}$$

where

$$R^2 \triangleq 1 - \frac{\beta b'}{I_{oa}}\left(I_{1b'}K_{oa'} + I_{oa'}K_{1b'}\right) \qquad \text{(B-12)}$$

$$I_{1b'} \equiv I_1(\beta b')$$

and

$$K_{oa'} \equiv K_o(\beta a') \quad .$$

For convenience in computation, the radian electron-plasma frequency ω_p is introduced. Physically ω_p is the natural oscillation frequency of an infinite plasma of uniform electron distribution[30]. The plasma radian frequency for an electron is defined as

$$\omega_p^2 \triangleq \frac{|I_o|\,|\eta|}{\pi\epsilon b'^2 u_o} \quad . \qquad \text{(B-13)}$$

For typical electron streams in traveling-wave amplifiers, the plasma frequency is of the order of several hundred megacycles per second. Figure B-2 is a nomograph for computing ω_p from the stream parameters.

FIG. B-2 NOMOGRAPH FOR OBTAINING RADIAN ELECTRON-PLASMA FREQUENCY FROM THE VOLTAGE, CURRENT, AND DIAMETER OF AN ELECTRON STREAM.

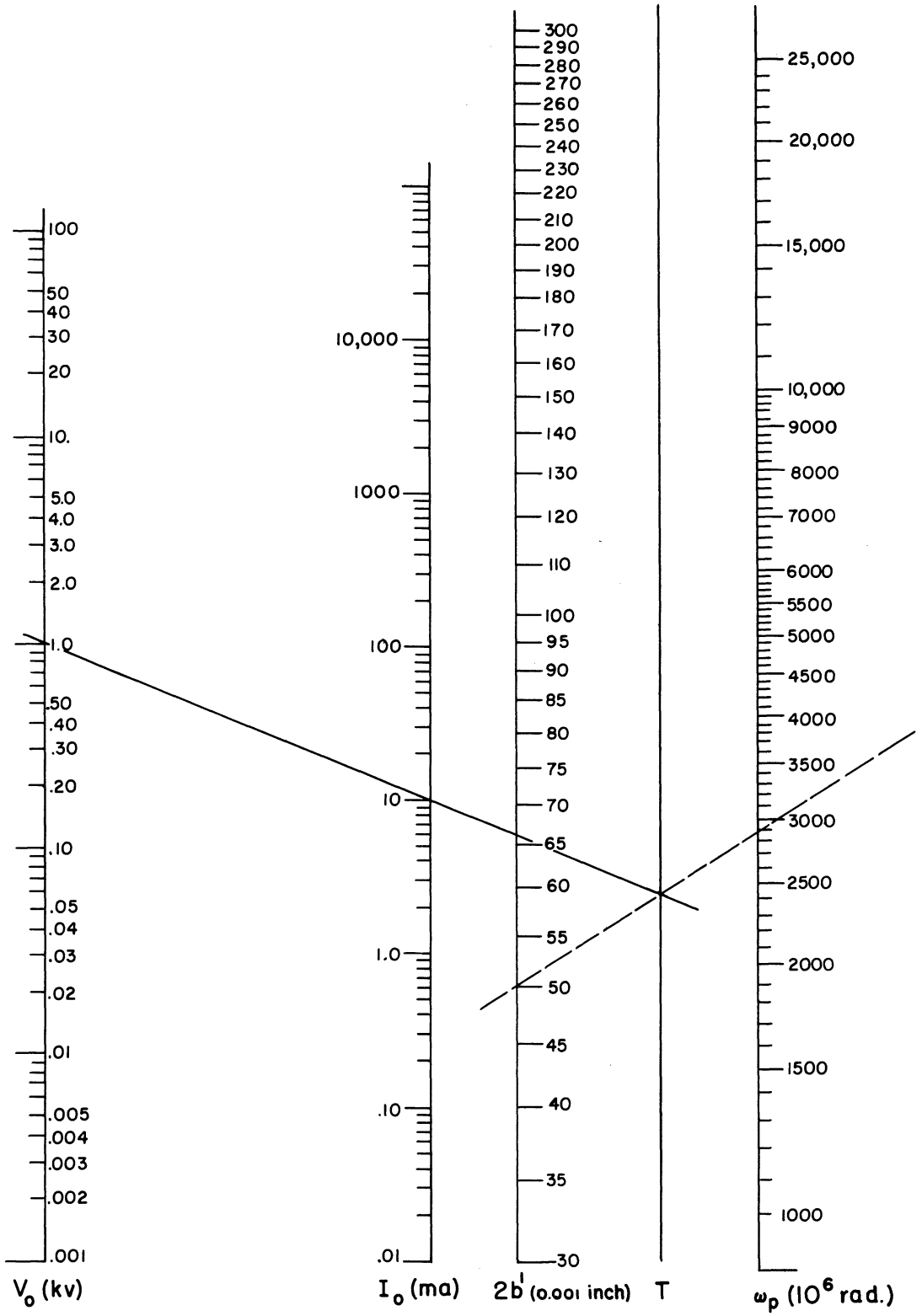

Also defined is an effective plasma frequency,

$$\omega_{qn}^2 \triangleq \omega_p^2 R_n^2 \quad , \tag{B-14}$$

where

$$R_n^2 \triangleq 1 - \frac{n\beta b'}{I_{ona'}} \left(I_{inb'}K_{ona'} + I_{ona'}K_{inb'}\right) \tag{B-15}$$

The quantity R_n is defined as the electron-plasma-frequency reduction factor for axial symmetry, and a plot of Eq. B-15 is shown in Fig. B-3. The reduction factor as calculated here for a stream within a helix is in good agreement with the calculations of Fletcher[7].

With the value of ω_q/ω thus calculated, the small-signal space-charge parameter QC may be found for a particular value of C from Fig. B-4 or it may be calculated from the following relationship:

$$\sqrt{4QC^3} = \frac{\omega_q/\omega}{1 + \omega_q/\omega} \quad , \tag{B-16}$$

which when solved for QC gives

$$QC = \frac{1}{4C^2}\left(\frac{\omega_q/\omega}{1 + \omega_q/\omega}\right)^2 \quad . \tag{B-17}$$

Suggested new space-charge parameters are discussed in Section 2.1.

Substituting Eqs. B-13 and B-14 into Eq. B-11 gives the space-charge field as

$$E_s = \sum_{n=1}^{\infty} \rho_n \, e^{-j(\phi + \pi/2)} \left(\frac{\omega_{qn}}{\omega}\right)^2 \frac{\omega}{\frac{I_o}{u_o^2}\,|\eta|n(1+Cb)} \quad . \tag{B-18}$$

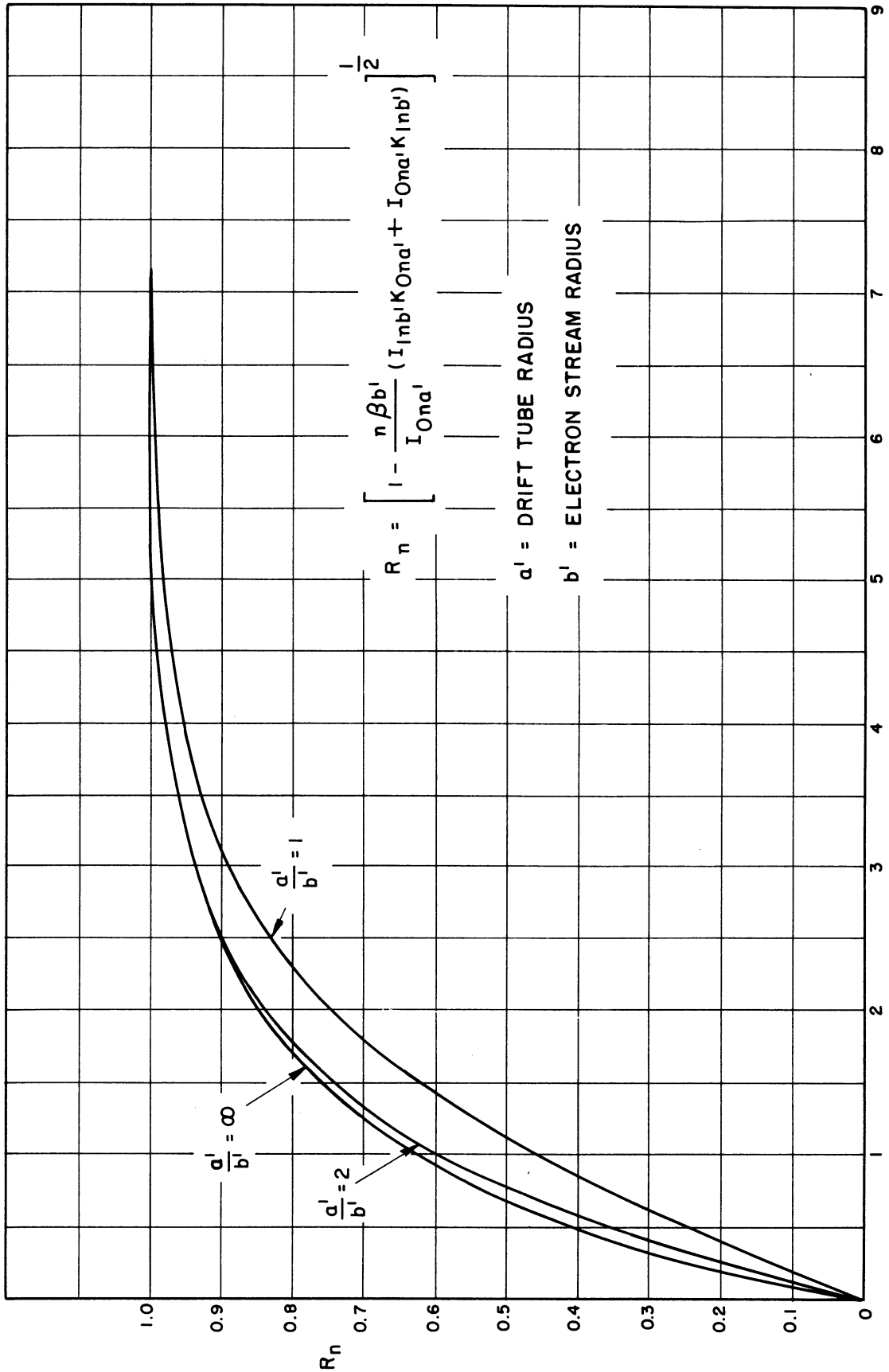

FIG. B-3 ELECTRON PLASMA FREQUENCY REDUCTION FACTOR FOR AXIAL SYMMETRY

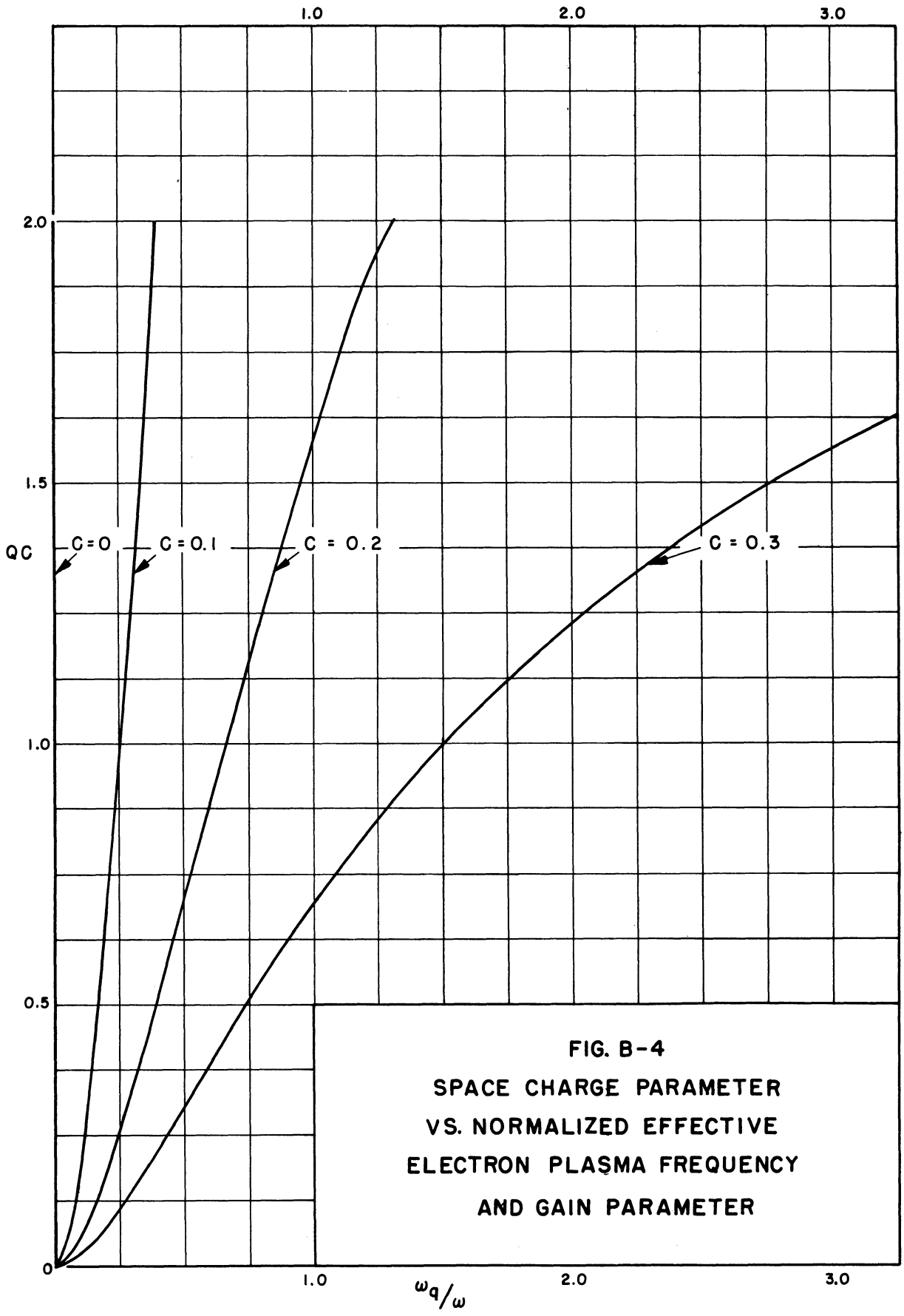

FIG. B-4
SPACE CHARGE PARAMETER
VS. NORMALIZED EFFECTIVE
ELECTRON PLASMA FREQUENCY
AND GAIN PARAMETER

In Eq. B-18, β, the phase constant of the space-charge waves in the stream, is written as

$$\beta = \frac{\omega}{v} = \left(\frac{\omega}{u_o}\right)\left(\frac{u_o}{v}\right) . \qquad \text{(B-19)}$$

From the small-signal calculations shown in Appendix C and Fig. B-5 it is seen that $v \cong v_o$, particularly for large values of the space-charge parameter QC; therefore an approximate expression for β is

$$\beta \cong \left(\frac{\omega}{u_o}\right)\left(\frac{u_o}{v_o}\right) = \frac{\omega}{u_o}\,(1 + Cb) . \qquad \text{(B-20)}$$

The Fourier expansion of space-charge density given in Eq. 2-24 may be used to rewrite one factor of Eq. B-18 as

$$\sum_{n=1}^{\infty} \rho_n e^{-j(n\phi + \pi/2)} \left(\frac{\omega_{qn}}{\omega}\right)^2 \frac{1}{n}$$

$$= \frac{I_o}{u_o} \sum_{n=1}^{\infty} \left(\frac{\omega_p}{\omega}\right)^2 R_n^2 \frac{1}{n} e^{-j(n\phi + \pi/2)} \left\{\frac{1}{2\pi} \int_0^{2\pi} \frac{e^{jn\phi(y,\phi_o')} d\phi_o'}{1 + 2Cu(y,\phi_o')}\right\} . \qquad \text{(B-21)}$$

Thus the space-charge field has been expanded into a Fourier series in the time variable $\phi(y,\phi_o)$ at a particular point in space and will be evaluated for electrons within one cycle of ϕ. Actually the space-charge field pattern for the nearest neighboring cycle will be very like its own, but the ones further away may be very different. However it is believed that this assumption is sufficiently accurate for practical purposes, as the influence of space charge does not extend further than two or three cycles in either direction.

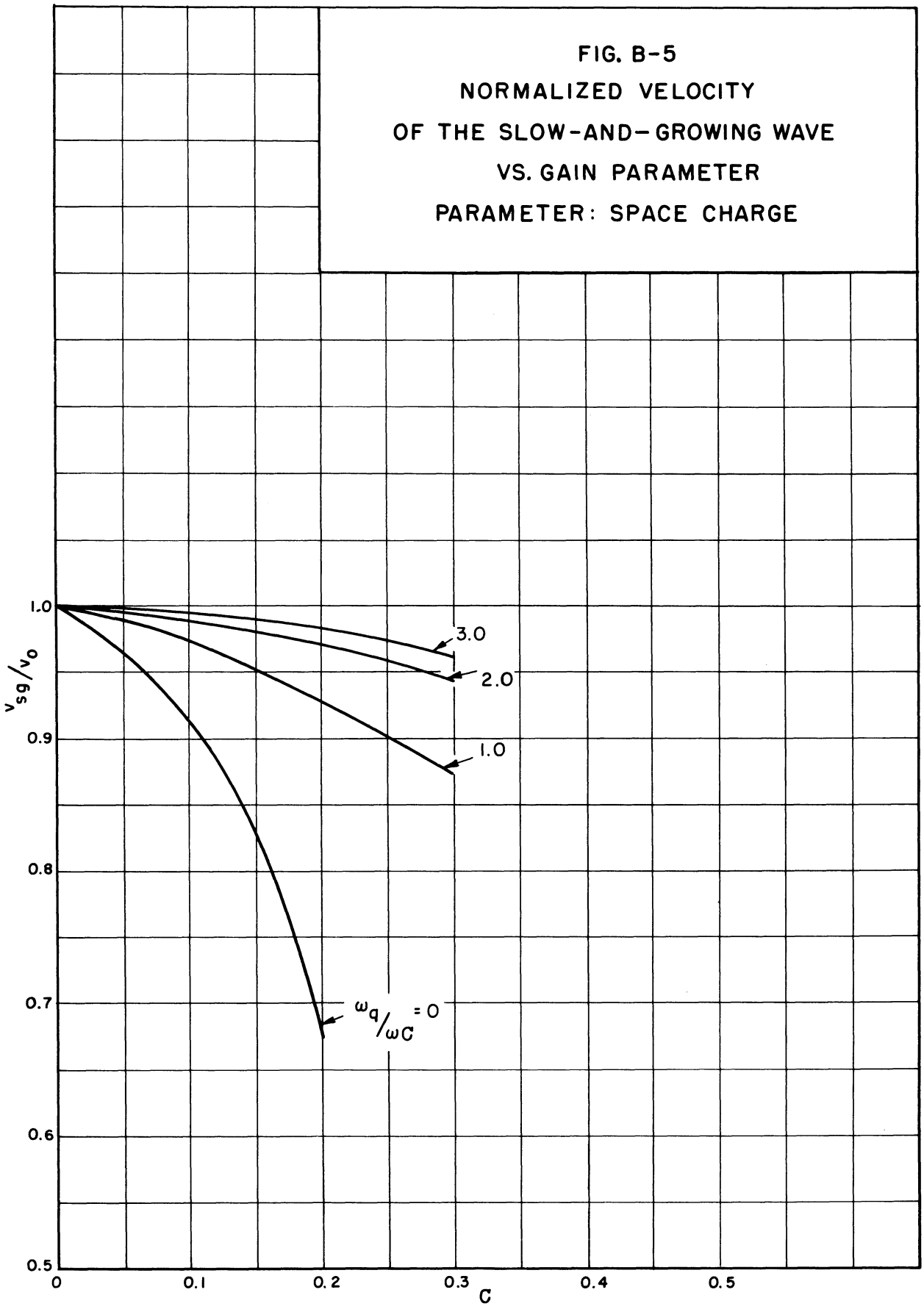
FIG. B-5
NORMALIZED VELOCITY
OF THE SLOW-AND-GROWING WAVE
VS. GAIN PARAMETER
PARAMETER: SPACE CHARGE
v_{sg}/v_o
1.0
0.9
0.8
0.7
0.6
0.5
0
0.1
0.2
0.3
0.4
0.5
C
3.0
2.0
1.0
$\omega_q/\omega_C = 0$

The distribution of electrons in space for constant time is very nearly the same as their distribution in time for a small interval of y even for relatively large a-c velocities, since it is the closely spaced electrons about ϕ which are important in evaluating the space-charge force at ϕ as indicated in Fig. B-6.

In Eq. B-21, since the function under the integral sign converges uniformly to the sum, the order of summation and integration may be interchanged, as follows:

$$\sum_{n=1}^{\infty} \rho_n e^{-j(n\phi + \pi/2)} \left(\frac{\omega_{qn}}{\omega}\right)^2 \left(\frac{1}{n}\right)$$

$$= \frac{I_o}{u_o}\left(\frac{\omega_p}{\omega}\right)^2 \int_0^{2\pi} \left[\sum_{n=1}^{\infty} e^{-jn(\phi-\phi') - j\pi/2} R_n^2 \frac{1}{2\pi n}\right] \frac{d\phi_o'}{1 + 2Cu(y,\phi_o')} . \quad \text{(B-22)}$$

Since a sinusoidal variation of space-charge density was postulated, this may be obtained by taking the real part of Eq. B-22, which gives

$$\mathrm{Re}\left\{\sum_{n=1}^{\infty} \rho_n e^{-j(n\phi + \pi/2)} \left(\frac{\omega_{qn}}{\omega}\right)^2 \left(\frac{1}{n}\right)\right\}$$

$$= -\frac{2I_o}{u_o}\left(\frac{\omega_p}{\omega}\right)^2 \int_0^{2\pi} \left[\sum_{n=1}^{\infty} \frac{\sin n(\phi-\phi') R_n^2}{2\pi n}\right] \frac{d\phi_o'}{1 + 2Cu(y,\phi_o')} . \quad \text{(B-23)}$$

The space-charge-field weighting function $F(\phi-\phi')$, which weights the influence of an electron at ϕ' on the electron at ϕ in determining the space-charge-field force, is shown in Fig. B-6 and defined as

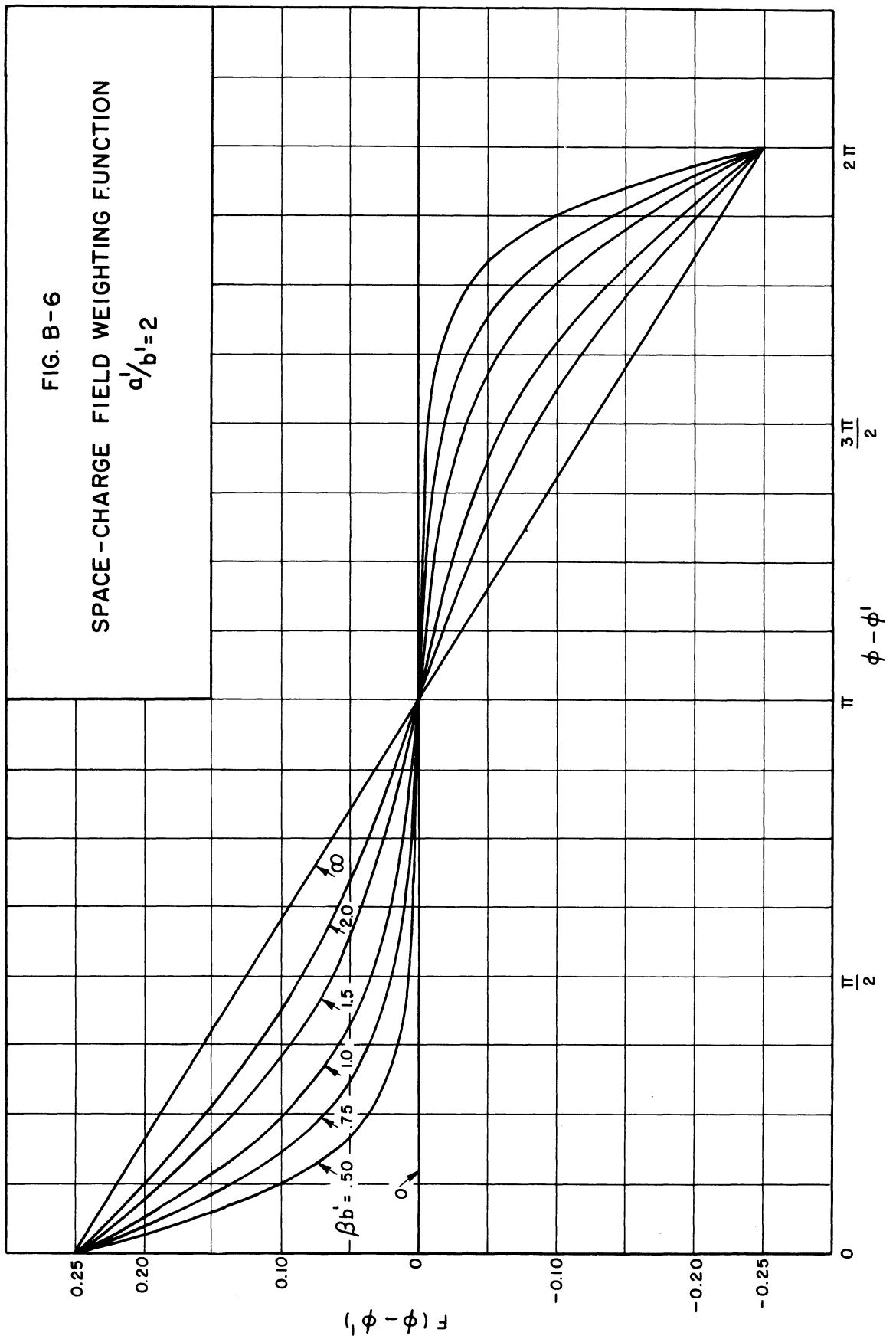
FIG. B-6
SPACE-CHARGE FIELD WEIGHTING FUNCTION
a'/b'=2
F(φ − φ')
φ − φ'
0
π/2
π
3π/2
2π
0.25
0.20
0.10
0
-0.10
-0.20
-0.25
βb' = .50
.75
1.0
1.5
2.0
∞

$$F(\phi-\phi') \triangleq \sum_{n=1}^{\infty} \frac{\sin n(\phi-\phi')\, R_n^2}{2\pi n} \quad . \tag{B-24}$$

The form of the space-charge weighting function indicates that for $(\phi-\phi')$ very much different from 0 or 2π the influence of space charge decreases rapidly. The closed form of Eq. B-24 is derived in Section 3.4.3.

Equation B-23 may then be rewritten as follows:

$$\mathrm{Re}\left\{\sum_{n=1}^{\infty} \rho_n e^{-j(n\phi + \pi/2)} \left(\frac{\omega_{qn}}{\omega}\right)^2 \left(\frac{1}{n}\right)\right\} = -\frac{2I_o}{u_o}\left(\frac{\omega_p}{\omega}\right)^2 \int_0^{2\pi} \frac{F(\phi-\phi')\, d\phi_o'}{1 + 2Cu(y,\phi_o')} \quad . \tag{B-25}$$

Substitution of the right-hand side of Eq. B-25 into Eq. B-18 yields the desired expression for the space-charge field within the electron stream:

$$E_s = -\frac{2\omega u_o}{|\eta|\,(1+Cb)}\left(\frac{\omega_p}{\omega}\right)^2 \int_0^{2\pi} \frac{F(\phi-\phi')\, d\phi_o'}{1 + 2Cu(y,\phi_o')} \quad . \tag{B-26}$$

An expression for the space-charge field has been derived in a similar manner by Poulter[13].

APPENDIX C. CALCULATION OF THE SMALL-SIGNAL PROPAGATION CONSTANTS

The initial conditions for the large-signal traveling-wave-amplifier problem are given by the solutions to the small-signal equations. The small-signal equations are therefore presented here and the method of solution is indicated. The notation used is that of Pierce[8], and it will be assumed that the reader is sufficiently familiar with the notation and the basic assumptions underlying the fundamental equations that a detailed derivation is unnecessary.

The method of solving the small-signal determinantal equation will be outlined; in addition solutions will be given in terms of some newly defined parameters in order to convert the small-signal solutions to a more convenient form.

In the small-signal analysis the following determinantal equation in the propagation constant Γ is obtained when the circuit and stream equations, which describe the action of the circuit on the stream and in turn the stream on the circuit, are combined:

$$1 = \frac{jI_o\beta_e}{2V_o(j\beta_e - \Gamma)^2}\left[\frac{\Gamma\Gamma_1(E^2/\beta^2P)}{2(\Gamma_1^2 - \Gamma^2)} - \frac{j\Gamma}{\omega C_1}\right] . \qquad (C\text{-}1)$$

The propagation constants $-\Gamma$ and $-\Gamma_1$ describing propagation respectively in the presence and absence of the electron stream are

$$-\Gamma = -j\beta_e(1 + jC\delta) \qquad (C\text{-}2)$$

and

$$-\Gamma_1 = -j\beta_e(1 + Cb - jCd) . \qquad (C\text{-}3)$$

Substitution of Eqs. C-2 and C-3 into Eq. C-1 results in the expression

$$\delta^2 = \frac{[1 + C(2j\delta - C\delta^2)][1 + C(b - jd)]}{-b + jd + j\delta + C\left(jbd - \frac{b^2}{2} + \frac{d^2}{2} - \frac{\delta^2}{2}\right)} - 4QC[1 + C(2j\delta - C\delta^2)] \quad , \qquad (C\text{-}4)$$

where

δ = $x + jy$;

x = growth constant of the wave;

y = propagation constant of the wave;

C = gain parameter;

b = $\frac{u_o - v_o}{Cv_o}$ = relative injection velocity;

u_o = d-c beam velocity, m/sec;

v_o = undisturbed phase velocity of the wave, m/sec;

d = loss factor; and

QC = space-charge parameter defined by $Q = \frac{\beta_e}{\omega C_1 (E^2/\beta^2 P)}$.

The four roots of the quartic equation, C-4, are the propagation constants of the four waves which are identifiable in a traveling-wave tube where the interaction is negligible.

In order to show how the four wave solutions arise, Eq. C-4 has been rewritten by Brewer and Birdsall[1] as follows:

$$\left(\delta + \frac{j\sqrt{4QC}}{1 - \sqrt{4QC^3}}\right)\left(\delta - \frac{j\sqrt{4QC}}{1 + \sqrt{4QC^3}}\right)(\delta + jb + d)\left(\delta - jb - d - \frac{2j}{C}\right)$$

$$= \left(\delta - \frac{j}{C}\right)^2 \frac{2C(1+Cb-jCd)}{1 - 4QC^3} \quad . \qquad (C\text{-}5)$$

Solutions of Eq. C-5 for the growing wave, the unchanging wave, and the fast wave are given by Brewer and Birdsall[1] for a wide range of the parameters QC, C, b, and d.

Sensiper[9] has derived explicit expressions for the small-signal propagation constants by expanding about the electron-beam propagation constant. From these expressions, values of the propagation constants may be computed readily, but the expressions given are valid only over a somewhat limited range of the parameters QC, C, b, and d.

The initial conditions for the large-signal traveling-wave-tube analysis of this investigation were obtained, for the most part, from the solutions presented in References 1 and 4, quoted previously. In all cases where data were not available the solutions were found directly from the quartic determinantal equation C-4.

In order to present the data obtained from the small-signal solutions in a more convenient form, gain curves have been constructed for several values of the parameters QC, C, and d with newly defined variables as follows:

$$v_d = u_o - v_o \tag{C-6}$$

and

$$v_\phi = v_{sg} - v_o \quad , \tag{C-7}$$

where v_{sg} = phase velocity of the slow-and-growing wave.

In terms of Pierce's notation these variables are

$$u_o/v_{sg} = 1-Cy \tag{C-8}$$

$$u_o/v_o = 1+Cb \tag{C-9}$$

$$v_\phi/v_o = \frac{1+Cb}{1-Cy} - 1 \tag{C-10}$$

$$v_d/v_o = Cb \quad . \tag{C-11}$$

The small-signal gain of the traveling-wave tube is given by

$$G_{db} = A + BCN \quad , \tag{C-12}$$

where A = total transition loss suffered by the signal at the input and output, db;

N = length of tube in electron wavelengths; and

B = 54.6x.

Hence Eq. C-12 may be written as

$$G_{db} = A + 54.6x\ CN \quad . \tag{C-13}$$

Dividing both sides of Eq. C-13 by 54.6N(1+Cb) gives

$$\frac{G_{db}}{54.6N(1+Cb)} = \frac{A}{54.6N(1+Cb)} + \frac{Cx}{1+Cb} \quad ; \tag{C-14}$$

but

$$N_g = N(1+Cb) = \frac{\beta_o}{2\pi} \quad , \tag{C-15}$$

where N_g = number of circuit wavelengths. Hence Eq. C-14 may now be re-written as

$$\frac{G_{db}}{8.68\ \beta_o} = \frac{A}{8.68\ \beta_o} + \frac{\alpha\phi}{\beta_o} \quad , \tag{C-16}$$

where

$$\frac{\alpha\phi}{\beta_o} = \frac{Cx}{1+Cb} \tag{C-17}$$

and $\alpha\phi = \alpha$ = gain constant of the growing wave. When new variables

$$g = \frac{G_{db}}{8.68} \qquad \text{(C-18)}$$

and

$$a = \frac{A}{8.68} \qquad \text{(C-18)}$$

are defined and substituted in Eq. C-16, it becomes

$$\frac{g}{\beta_o} = \frac{a}{\beta_o} + \frac{\alpha_\phi}{\beta_o} \quad . \qquad \text{(C-19)}$$

Figures C-1 through C-6 show the variation of α_ϕ/β_o with v_d/v_o, using QC and C as parameters.

Figures C-7 and C-8 similarly indicate the variation of g/β_o with v_d/v_o for three values of N_g, using QC and C as parameters.

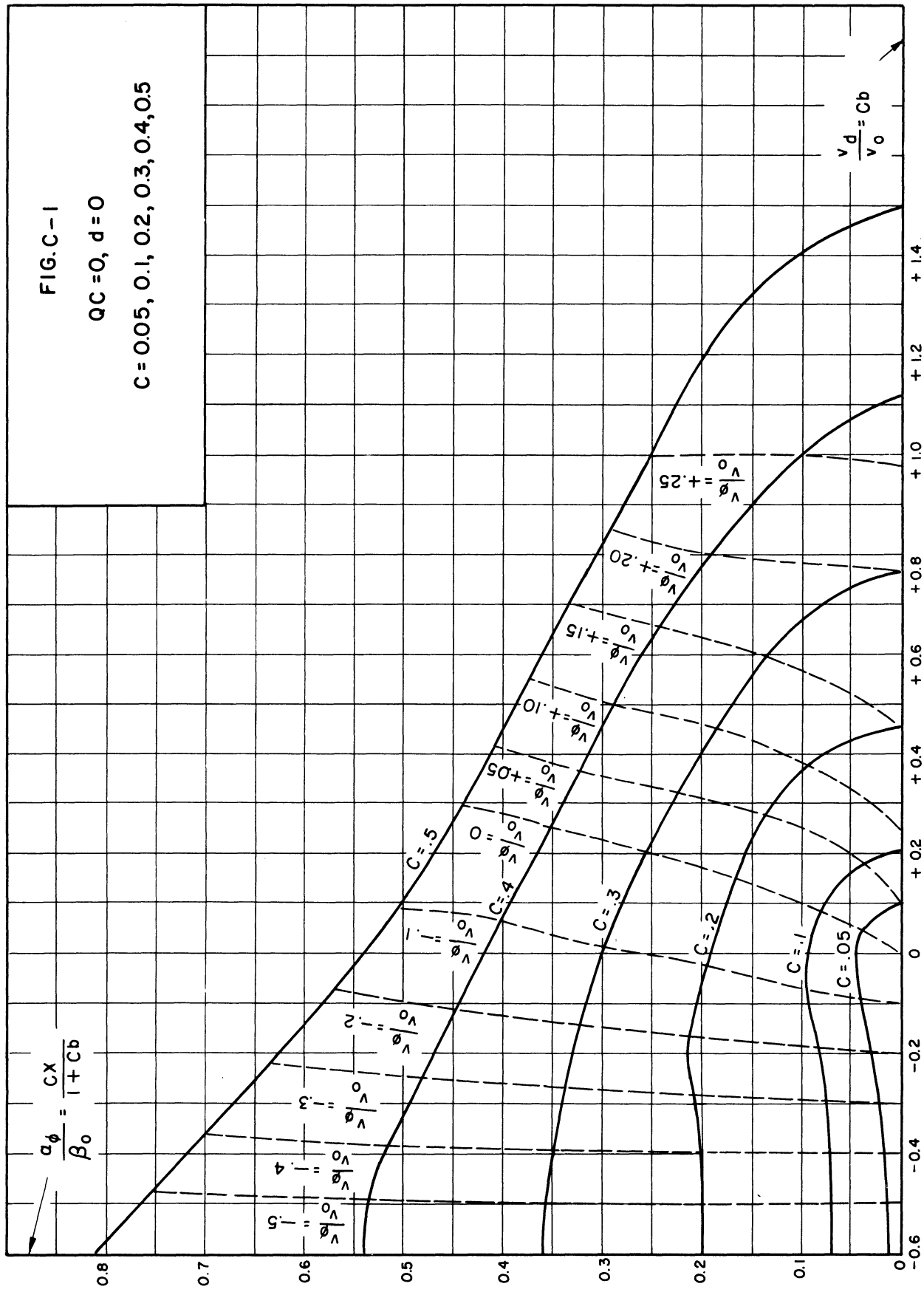
FIG. C-1
QC = 0, d = 0
C = 0.05, 0.1, 0.2, 0.3, 0.4, 0.5
$\frac{v_d}{v_o} = Cb$
$\frac{a_\phi}{\beta_o} = \frac{CX}{1+Cb}$
$\frac{v_\phi}{v_o} = +.25$
$\frac{v_\phi}{v_o} = +.20$
$\frac{v_\phi}{v_o} = +.15$
$\frac{v_\phi}{v_o} = +.10$
$\frac{v_\phi}{v_o} = +.05$
$\frac{v_\phi}{v_o} = 0$
$\frac{v_\phi}{v_o} = -.1$
$\frac{v_\phi}{v_o} = -.2$
$\frac{v_\phi}{v_o} = -.3$
$\frac{v_\phi}{v_o} = -.4$
$\frac{v_\phi}{v_o} = -.5$
C = .5
C = .4
C = .3
C = .2
C = .1
C = .05
0.8
0.7
0.6
0.5
0.4
0.3
0.2
0.1
0
-0.6
-0.4
-0.2
0
+0.2
+0.4
+0.6
+0.8
+1.0
+1.2
+1.4

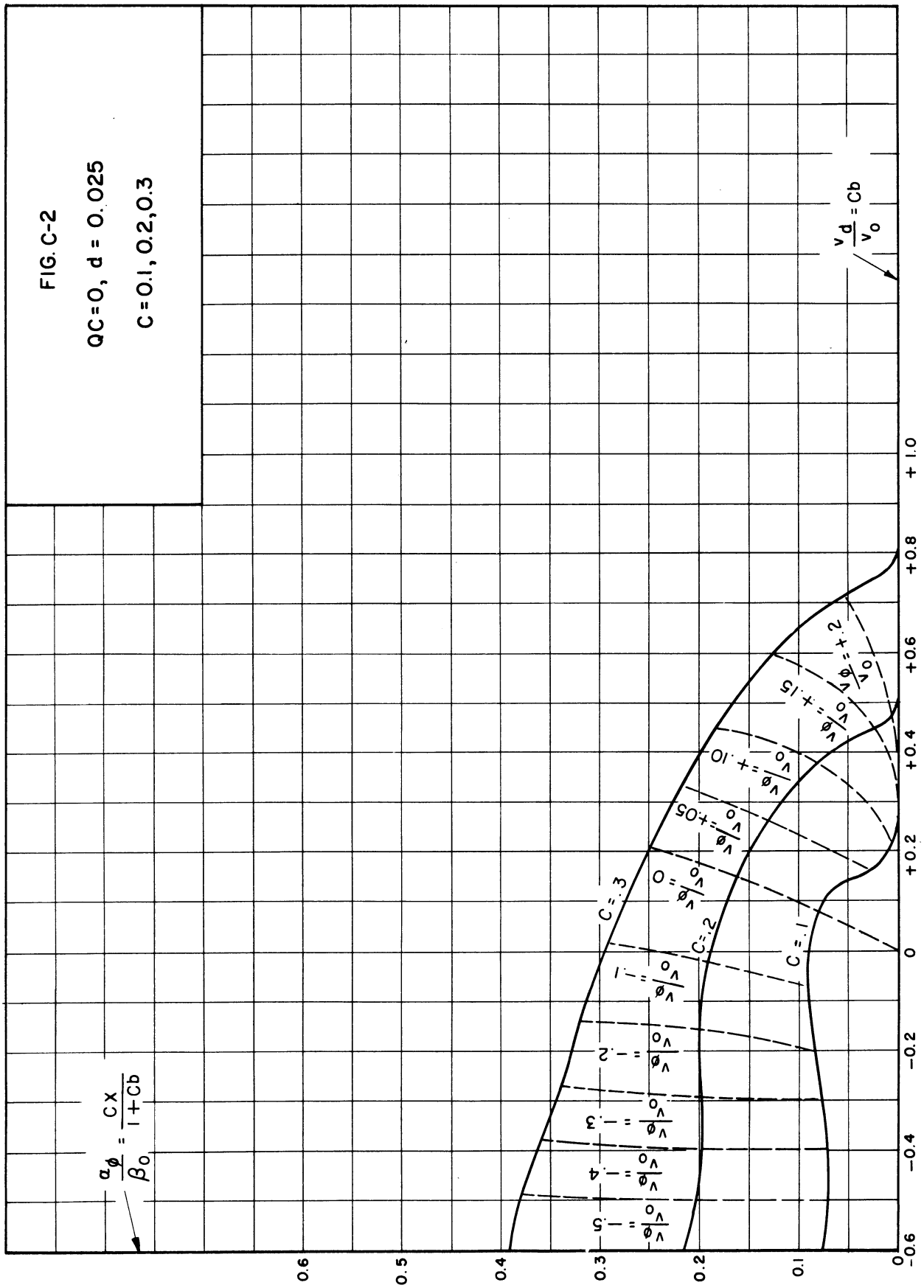
FIG. C-2
QC=0, d = 0.025
C=0.1, 0.2, 0.3
$\frac{v_d}{v_o} = Cb$
$\frac{a_\phi}{\beta_o} = \frac{Cx}{1+Cb}$
C=.3
C=.2
C=.1
$\frac{v_\phi}{v_o} = -.5$
$\frac{v_\phi}{v_o} = -.4$
$\frac{v_\phi}{v_o} = -.3$
$\frac{v_\phi}{v_o} = -.2$
$\frac{v_\phi}{v_o} = -.1$
$\frac{v_\phi}{v_o} = 0$
$\frac{v_\phi}{v_o} = +.05$
$\frac{v_\phi}{v_o} = +.10$
$\frac{v_\phi}{v_o} = +.15$
$\frac{v_\phi}{v_o} = +.2$
0.6
0.5
0.4
0.3
0.2
0.1
0
-0.6
-0.4
-0.2
0
+0.2
+0.4
+0.6
+0.8
+1.0

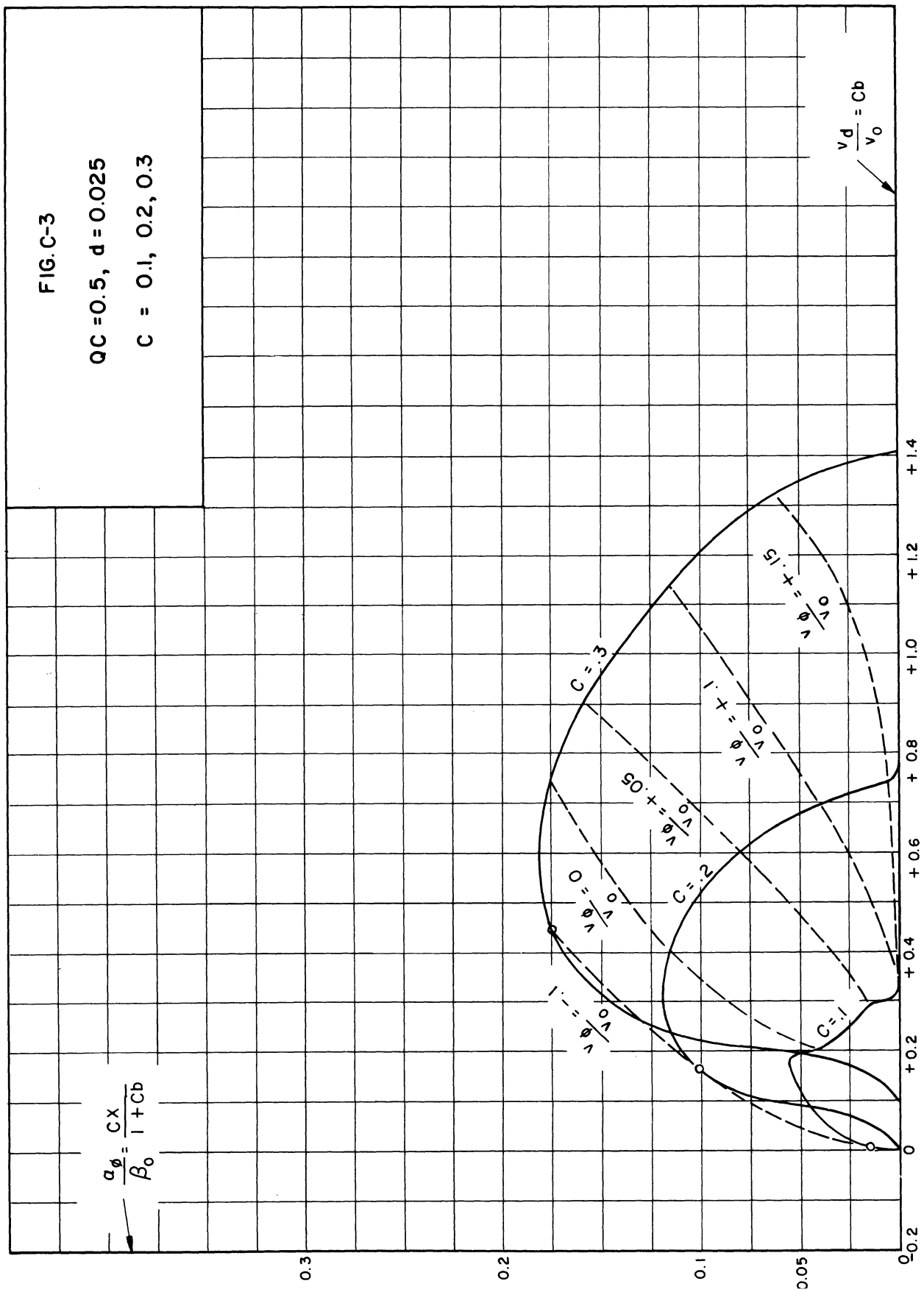
FIG. C-3
QC = 0.5, d = 0.025
C = 0.1, 0.2, 0.3
$\frac{v_d}{v_o} = Cb$
$\frac{a_\phi}{\beta_o} = \frac{Cx}{1+Cb}$
C = .3
C = .2
C = .1
$\frac{v_\phi}{v_o} = +.15$
$\frac{v_\phi}{v_o} = +.1$
$\frac{v_\phi}{v_o} = +.05$
$\frac{v_\phi}{v_o} = 0$
$\frac{v_\phi}{v_o} = -.1$
0.3
0.2
0.1
0.05
0
-0.2
+0.2
+0.4
+0.6
+0.8
+1.0
+1.2
+1.4

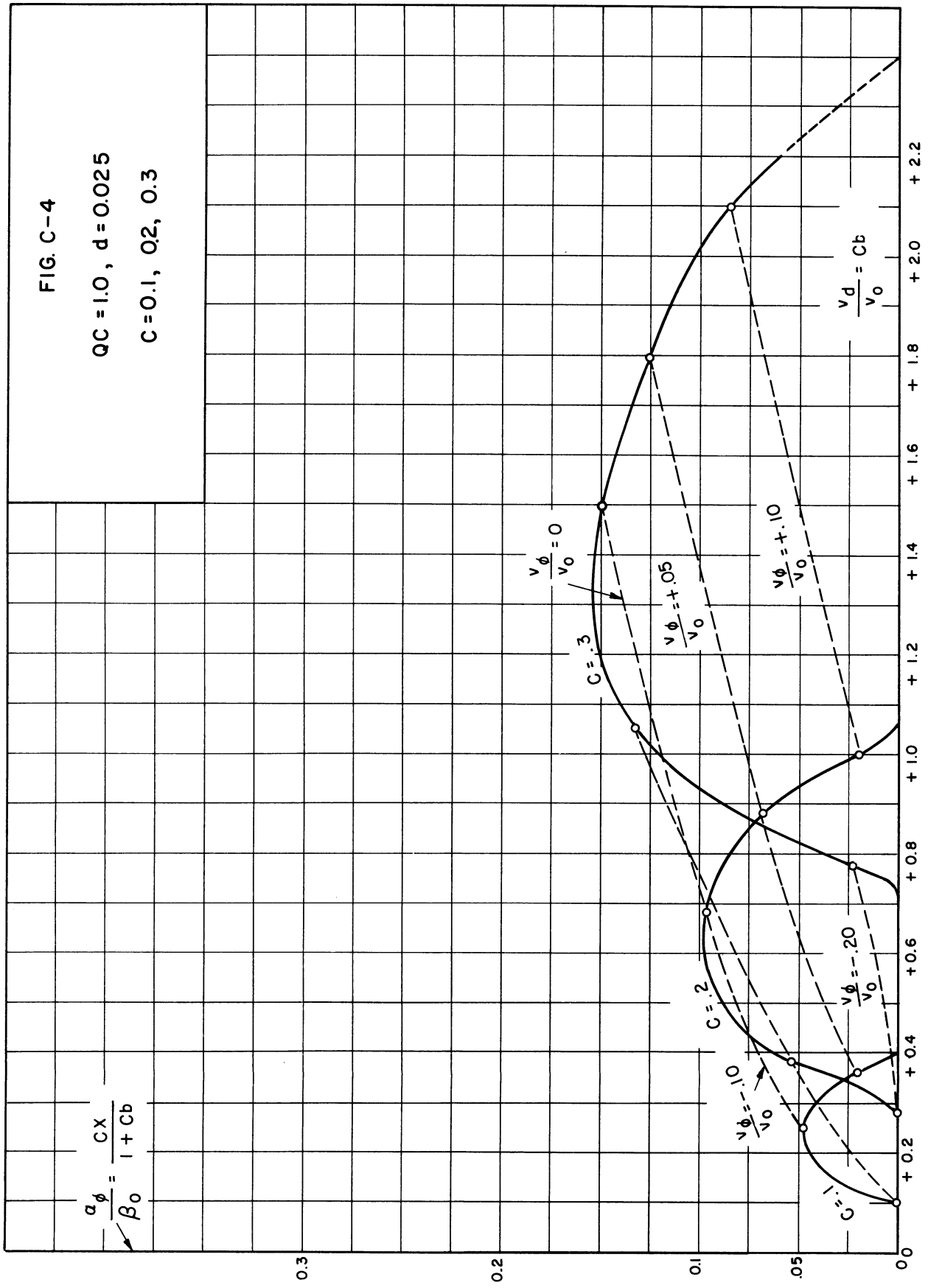
FIG. C-4
QC = 1.0, d = 0.025
C = 0.1, 0.2, 0.3
$\frac{\alpha_\phi}{\beta_o} = \frac{CX}{1 + Cb}$
$\frac{v_d}{v_o} = Cb$
$\frac{v_\phi}{v_o} = 0$
$\frac{v_\phi}{v_o} = +.05$
$\frac{v_\phi}{v_o} = +.10$
$\frac{v_\phi}{v_o} = -.10$
$\frac{v_\phi}{v_o} = -.20$
C = .3
C = .2
C = .1
0.3
0.2
0.1
.05
0.0
+ 0.2
+ 0.4
+0.6
+ 0.8
+ 1.0
+ 1.2
+ 1.4
+ 1.6
+ 1.8
+ 2.0
+ 2.2

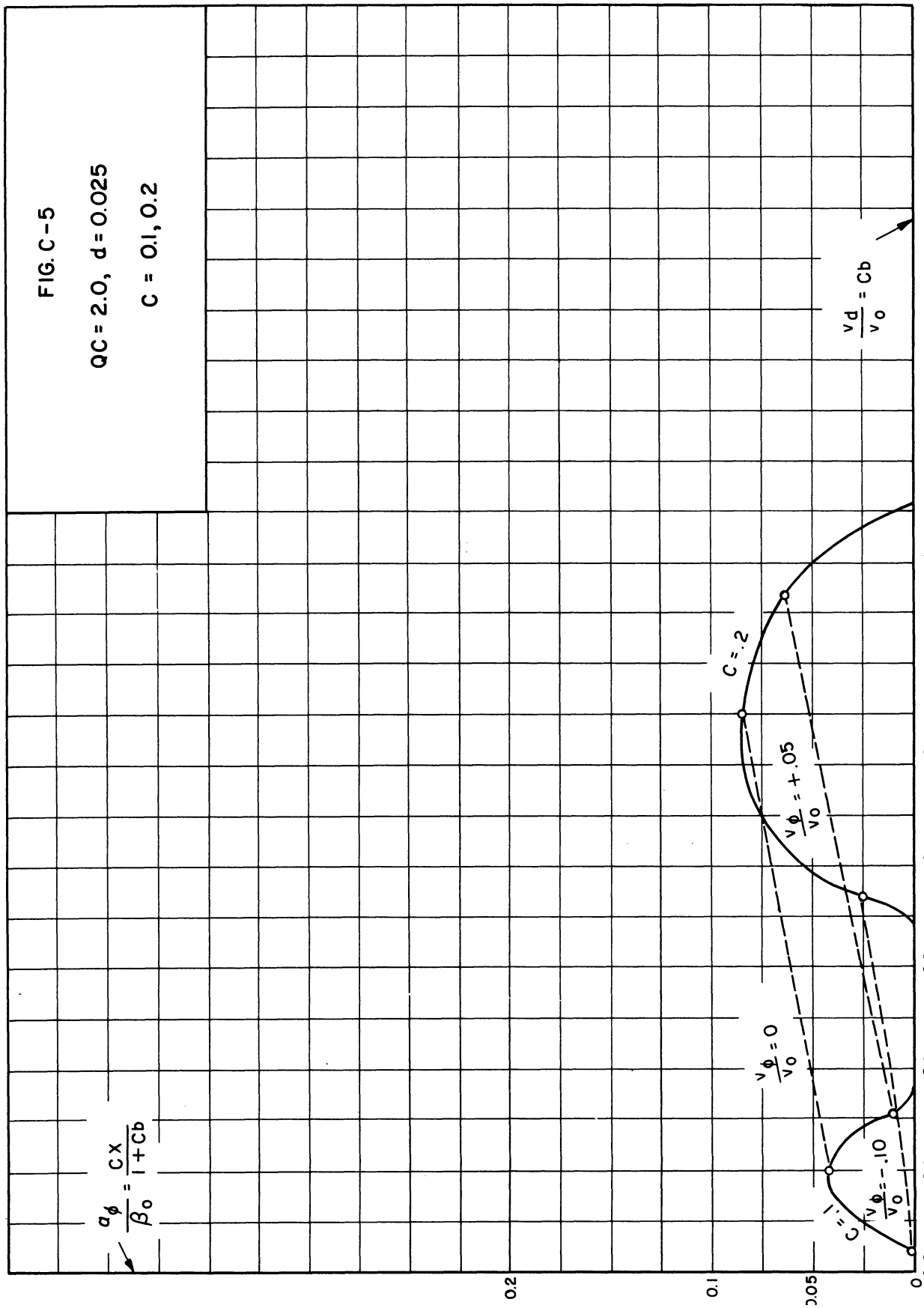
FIG. C-5
QC = 2.0, d = 0.025
C = 0.1, 0.2
$\frac{a_\phi}{\beta_0} = \frac{Cx}{1+Cb}$
$\frac{vd}{v_0} = Cb$
C = .2
C = .1
$\frac{v_\phi}{v_0} = +.05$
$\frac{v_\phi}{v_0} = 0$
$\frac{v_\phi}{v_0} = -.10$
0.2
0.1
0.05
0
+0.2
+0.4
+0.6
+0.8
+1.0
+1.2
+1.4
+1.6

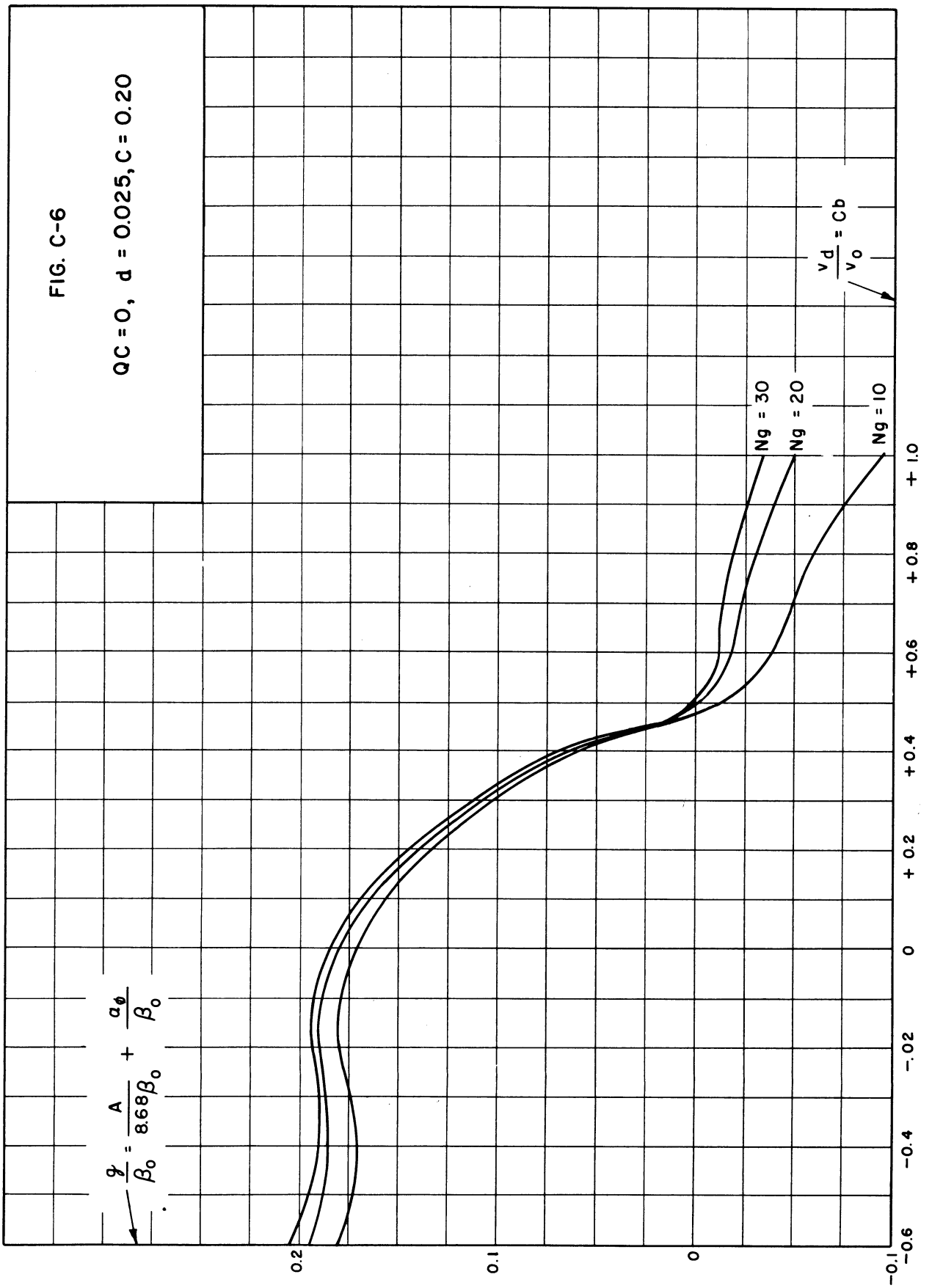
FIG. C-6
QC = 0, d = 0.025, C = 0.20
$\frac{g}{\beta_o} = \frac{A}{8.68\beta_o} + \frac{a_\phi}{\beta_o}$
$\frac{v_d}{v_o} = Cb$
Ng = 30
Ng = 20
Ng = 10
0.2
0.1
0
-0.1
-0.6
-0.4
-.02
0
+0.2
+0.4
+0.6
+0.8
+1.0

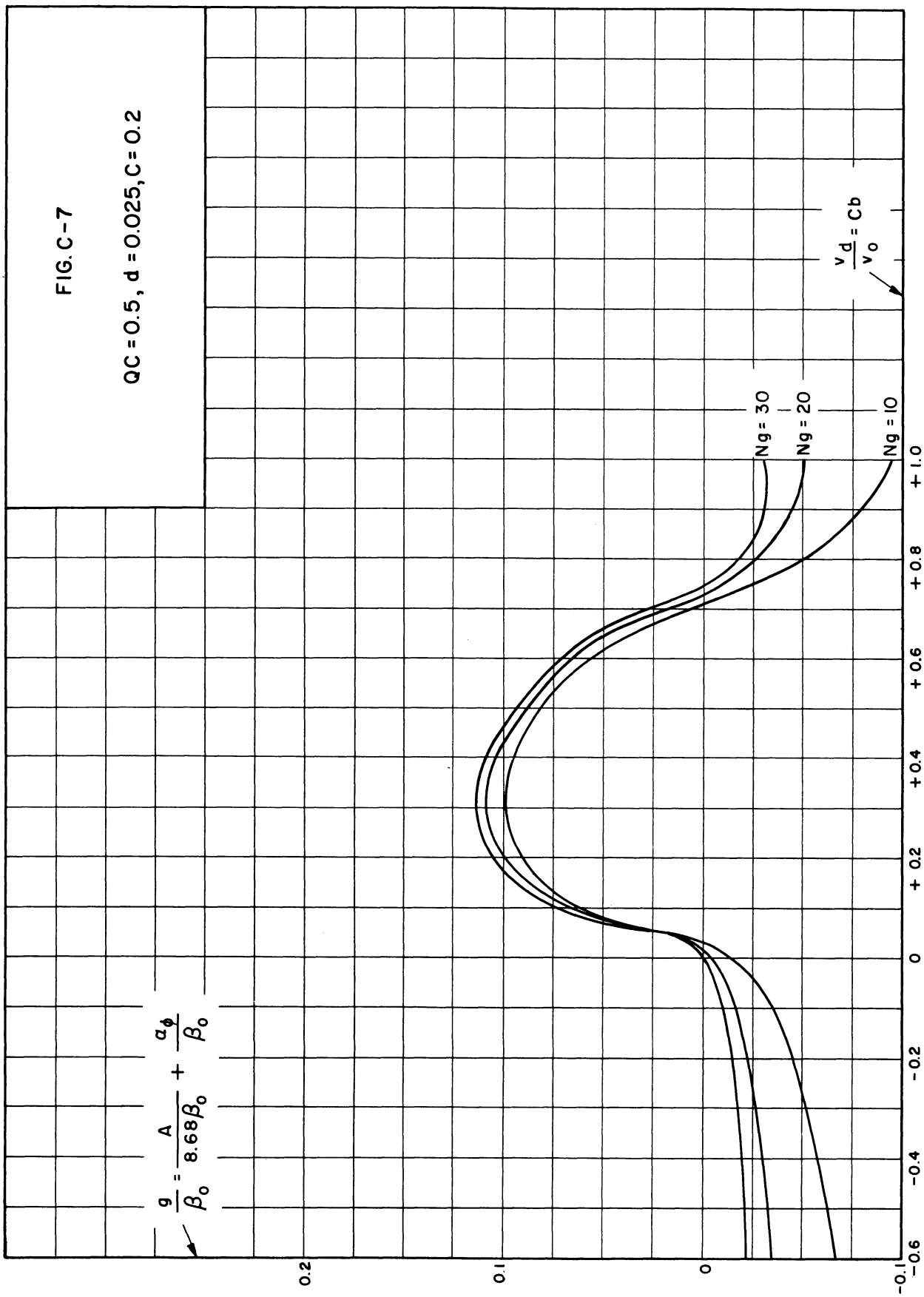
FIG. C-7
QC = 0.5, d = 0.025, C = 0.2
$\frac{g}{\beta_0} = \frac{A}{8.68\beta_0} + \frac{\alpha_\phi}{\beta_0}$
$\frac{v_d}{v_0} = Cb$
Ng = 30
Ng = 20
Ng = 10
0.2
0.1
0
-0.1
-0.6
-0.4
-0.2
0
+0.2
+0.4
+0.6
+0.8
+1.0

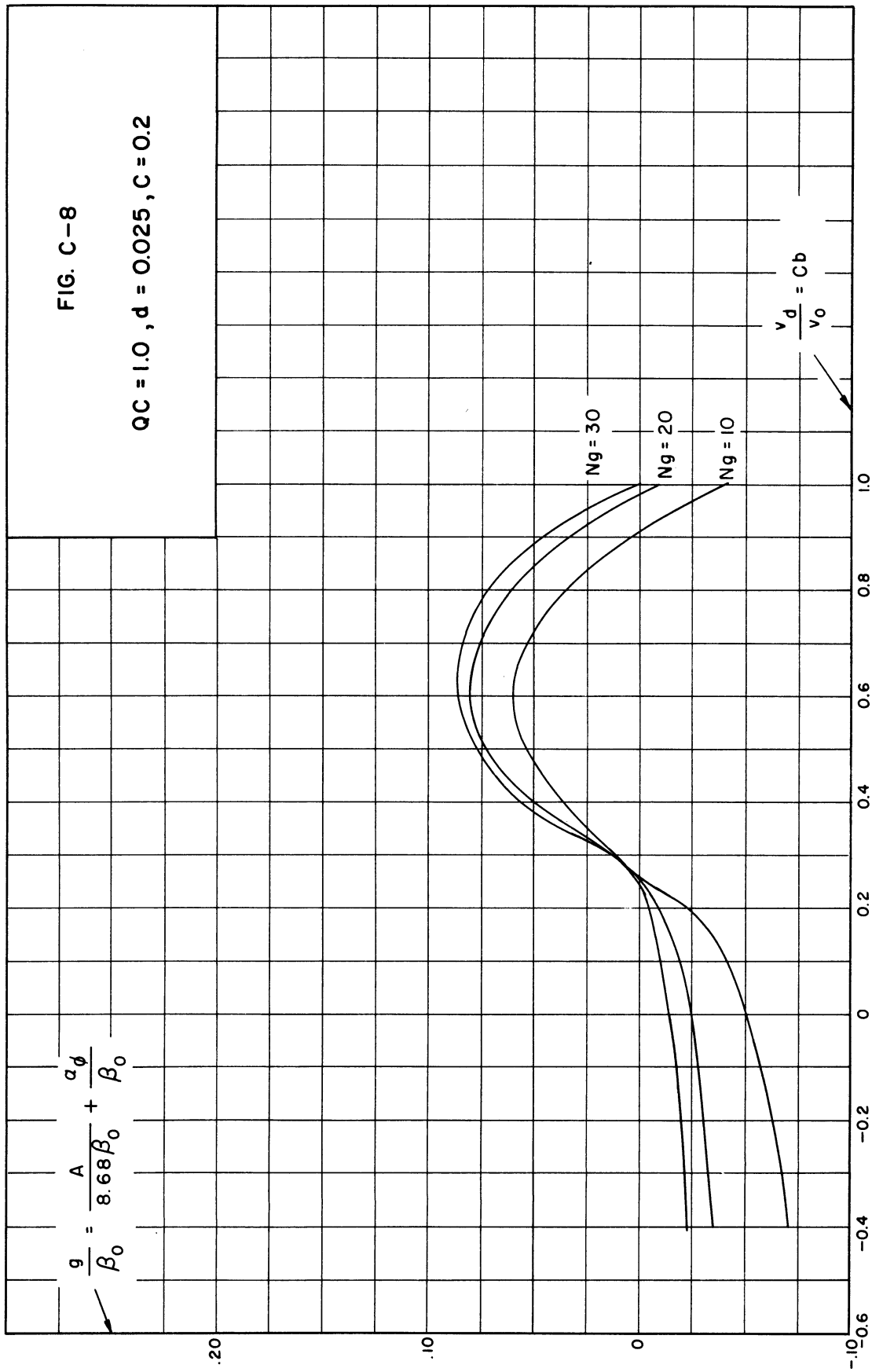
FIG. C-8
QC = 1.0 , d = 0.025 , C = 0.2
$\frac{g}{\beta_0} = \frac{A}{8.68\beta_0} + \frac{a\phi}{\beta_0}$
$\frac{v_d}{v_0} = Cb$
Ng = 30
Ng = 20
Ng = 10
.20
.10
0
-.10
-0.6
-0.4
-0.2
0
0.2
0.4
0.6
0.8
1.0

APPENDIX D. MIDAC PROGRAM AND OPERATING INSTRUCTIONS

For the sake of completeness the various programs that were used in obtaining the solution to the problem on MIDAC are presented in this appendix. The following programs are included:

1. For 32 electrons (13MOm23,24):
   a) The operating instructions.
   b) The program used in the beginning of the problem with the following scaling:
      $A \cdot 2^{-1}$, $\theta \cdot 2^{-2}$, $\phi \cdot 2^{-4}$, and $u \cdot 2^{-3}$.
   c) The program used from the point where θ reached an absolute value greater than 3.75. This program has the following scaling:
      $A \cdot 2^{-4}$, $\theta \cdot 2^{-6}$, $\phi \cdot 2^{-6}$, and $u \cdot 2^{-3}$.
   d) The program for the parameter tape.
2. For 64 electrons (13M13m7):
   a) The operating instructions.
   b) The program used, with the following scaling:
      $A \cdot 2^{-4}$, $\theta \cdot 2^{-6}$, $\phi \cdot 2^{-6}$, and $u \cdot 2^{-3}$.
   c) The program for the parameter tape.
3. The program and operating instructions for converting voltage gain into power gain in db (13M12m2).

TRAVELING-WAVE TUBE: PROGRAM NO. 13M0m23,24

Operating Instructions for Run No. ___

A. General Information

The output of this program is a sequence of 4 groups of 3 words and 2 groups of 33 words. It can be determined if the program is proceeding correctly by examining the last 2 words in the groups of 3: the second word in each group of 3 should be a positive number and these numbers should increase continuously until a maximum is reached and the problem is terminated (see below), while the third word in each group of 3 should be a negative number and these numbers should increase negatively throughout the entire problem. If at any stage of the problem these numbers do not follow the right pattern, then the computer should be halted and computation resumed at a point where the numbers are of the correct form.

B. Initial Computations

1. Insert 13M0m14. The memory sums should agree. The entire tape does not read in. Read in the last word on run. Halt the computer while the last words on this tape read in.
2. Place 13M0m23 on the Ferranti and press the start. The tape reads in and the memory sums should agree. Do not read in the last word.
3. Place the parameter tape 13M0p___ on the Ferranti and press the start button. Read in the last word on halt.
4. Patch Panel Settings: Decimal point at 1
   Tab at 7
   Carriage return at 11
5. Put the output switch on patch.

6. Put overflow on automatic. Put on run and press start. If everything works all right, run this problem until the second word in a group of 3 in the print-out reaches a maximum and starts to decrease. Let a final set of 2 groups of 33 words print out.
7. Place tape 13MOm10 (in the form of a loop) on the Ferranti and, starting after the first 2 groups of 33 in the print-out, do the following:

   While the last word in the second group of 33 words in the print-out is being typed out, halt the computer. Clear the counters and insert one word from 001. Then put the computer on run and press the start button. This reads in tape no. 13MOm10. This tape dumps the internal memory on the drum and then automatically resumes computation. Repeat this process every 10 or 15 minutes throughout the program.
8. When the last word in a group of 3 gets close to 3.75, the computer will halt after printing out the word f.fffff. When this happens, take the output off of patch and put on 1 column. Then clear the counters and place 13MOm24 on the Ferranti. Take overflow off automatic. Insert this tape in the standard manner. The memory sums should agree. Put overflow back on automatic and the output to patch. Read in the last word on run. This resumes computation again. After the next 2 groups of 33 print out, repeat 7.
9. Print-out should occur at least every 5 minutes. If the computer gets stuck in a loop (i.e., print-out does not occur as often as it should), halt the computer and read out the counter. If the counter is in the range of 08d to 0a5 then step through until

the counter reads 0a2 or 0a3. Then read out one word from 009. Insert into 0f3 a positive word which is just larger (in the first significant hex digit) than the word just read out of 009. Put on run and press the start button. If the counter is not in this range, then run a changed-word post mortem on 13M0m20 or 13M0m24, depending on which program is currently in the memory.

10. If overflow occurs the computer will halt. Take the output off patch and read out the counter. Put back on patch and place 13M0m11 on the Ferranti. Clear the counters and insert one word from 001. Put the computer on run and press the start button. Computation should resume. However, if the computer immediately prints out 0.0bad0 and halts, then reset the carriage, press the format reset button and press the start button again. If the same thing happens, try once more. If the same thing happens again, put the punch on and tape feed, insert, and process with 1-column output

+ 1f1 00e 000 0f ,

which dumps the memory on tape. Then use a changed-word post mortem on either 13M0m23 or 13M0m24, depending on which is in the memory. IF OVERFLOW OCCURS MORE THAN 3 TIMES AT ANY ONE POINT IN THE PROGRAM, THEN DO STEP 11 BELOW AND QUIT.

11. If at any time during the program a short word prints out (except the f.fffff word mentioned in step 8) and the computer halts, then clear the counters, put 13M0m11 on the Ferranti and insert the first word. Leave the computer on halt and step through until the counter reads 004. Then put on 1-column-output format, put the punch on and some tape feed, and insert and process the

word

+ 1f1 00e 000 0f ,

which punches out the mercury memory. Then take the punch off and use a changed-word post mortem on either 13M0m23 or 13M0m24, depending on which is the last program in the memory.

12. Halting the Computer for Purposes of Time: To store the program on the drum overnight, insert and process

1f1 00e 6c0 0f .

C. Resuming Computations

1. Read in tape 13M0m14 with the last word on run.
2. Insert and process 1f1 6c0 00e 00.
3. Put the overflow switch on automatic and set the patch panel as in section B4.
4. Jump to 068 and begin computing.

CONTROL COMBINATION	TRAVELING-WAVE AMPLIFIER PROGRAM NO. 1 32 ELECTRONS				EXPLANATION
Scaling:	$A \cdot 2^{-1}$,	$\theta \cdot 2^{-2}$,	$\phi \cdot 2^{-4}$ and	$u \cdot 2^{-3}$	Program Tape No. 13M0m23
AC 006					
cd 238					
FA B11	000	000	000	su	set up 000
	-6c01	-6c01	-6c01	-su	clear tallys
	-001	003	B11	ba	"
	B10	001	B09	fi	Find constants
FA B12	1e	-0e03	2c05	-mr	$2c05 = 2Cu\ 2^{-4}$
	13d	2c05	1c05	ad	$1c05 = (1+2Cu)2^{-4}$
	1c05	27d	-0e07	-sn	$0e07 = (1+2Cu)2^{-2}$
	-001	033	B12	ba	
FA B17	7e	8c01	8c01	ad	$\Delta y + y \rightarrow y$
	1e06	3e06	5c	su	$5c = (\theta_{i+1} - \theta_i) \cdot 2^{-2}$
	5c	25d	8c	sn	$8c =$ " 2^{-1}
	1e	8c	4c	mr	$4c = C($ " $) 2^{-1}$
	0e06	2e06	6c	su	$6c = (A_{i+1} - A_i)2^{-1}$
	6c	1e	6c	mr	$6c = C($ " $)2^{-1}$
	10e	4c	7c	su	$7c = [\Delta y - C(\theta_{i+1} - \theta_i)]\ 2^{-1}$
FA A00	5e	-0e03	2c	-mr	$2c = 2\Delta yu2^{-4}$
	-0e07	2c	1c	-dv	$1c = \frac{2\Delta yu}{1+2Cu}\ 2^{-2}$
	1c	5c	1c	su	$1c = \left(\theta_i - \theta_{i+1} + \frac{2\Delta yu}{1+2Cu}\right) \cdot 2^{-2}$
	1c	5d	1c	sn	$1c =$ " 2^{-4}
	1c	-0e02	-0e01	-ad	Store new $\phi\ 2^{-4}$
	-001	033	A00	ba	"
FA B19	-0e02	4d	1c	-ad	$1c = \phi_{i,j} = T \cdot 2^{-4}$
	B22	-001	B25	-fi	File base counter

CONTROL COMBINATION					EXPLANATION
FA B25	11c	11c	11c	su	clear 11c
FA B20	1c	-0e02	2c	-su -	$2c=x=T-\phi_{i,0}\ 2^{-4}$
	A37	001	A30	fi	$2c=F(x)\ 2^{-6}$
	-0e07	2c	2c	-dv -	$2c=\frac{F(x)}{1+2Cu}=I_o\ 2^{-4}$
	2c	11c	11c	ad	$11c=\frac{2}{h}\int 2^{-4}$
	-032	064	B20	ba	$11c=\frac{2}{h}\int 2^{-4}$
	11c	8d	11c	sn	$11c=\frac{1}{h}\int 2^{-4}$
FA B21	1c	-1e02	2c	-su	$2c=x\ 2^{-4}$
	A37	001	A30	fi	$2c=F(x)\ 2^{-6}$
	-1e07	2c	2c	-dv -	$2c=\frac{F(x)}{1+2Cu}\ 2^{-4}$
	2c	11c	11c	ad	$11c=\frac{1}{h}\int 2^{-4}$
	-001	031	B21	ba	11c= "
	11c	30d	11c	mr -	$11c=\int 2^{-4}$
FA B22	[000]	511	B23	ba	Reset C_B
FA B23	9c01	11c	11c	mr -	$11c=K_1\ .2^{-8}$
	6c	-0e05	1c	-mr	$1c=c(A_{i+1}-A_i)\cos\phi\ 2^{-2}$
	2e06	7c	2c	mr	$2c=A_i\left[\Delta y-C(\theta_{i+1}-\theta_i)\right]2^{-2}$
	2c	-0e04	2c	-mr	$2c=A_i$ ["] $\sin\phi 2^{-3}$
	2c	10d	2c	sn	2c= " 2^{-8}
	1c	11d	1c	sn	$1c=C(A_{i+1}-A_i)\cos\phi\ 2^{-8}$
	2c	1c	1c	su -	$1c=K_2\ .\ 2^{-8}$
	-0e07	-0e03	2c	-mr	$2c=u(1+2Cu)\ 2^{-5}$
	2c	21d	2c	sn -	$2c=K_3\ .\ 2^{-8}$
	1c	2c	1c	ad	$1c=(K_2+K_3)\ 2^{-8}$

CONTROL COMBINATION					EXPLANATION
	1c	11c	1c	su	1c= ($-K_1 + K_2 + K_3$) 2^{-8}
	1c	26d	1c	sn	1c= " 2^{-5}
	-0e07	1c	-0e03	-dv	store u . 2^{-3}
	-001	033	B19	ba	
FA B24	-0e01	4d	-0e02	-ad	Store new ϕ "s
	1e	-0e03	2c	-mr	2c= 2Cu 2^{-4}
	13d	2c	1c	ad	1c= (1+2Cu) 2^{-4}
	1c	27d	-0e07	-sn	0e07=(1+2Cu) 2^{-2}
	-001	033	B24	ba	Store new (1+2Cu)2^{-2}
	6c01	25d	6c01	ad	T_{A+1} ---> T_A
	7c01	25d	7c01	ad	$T_{\phi+1}$ ----> T_ϕ
	6c01	9e	A04	cn	jump if no print out
	6c01	6c01	6c01	su	Clear tally
	4d	30d	000	ad	set up 000
FA B27	064	1024m	A05	ri	Call in P. O. routine
	002	002	002	su	Clear 002
	003	003	003	su	Clear 003
FA B26	-A05	002	002	-ad	Form memory sum in 002
	-001	064	B26	ba	
	002	33d	002	su	002 = Δ(m.s.)
	4d	002	B28	cm	Is 0 < $\lvert \Delta \rvert$
	000	000	000	su	resct 000
	0d	4d	511	ad	511= 4 2^{-44}
	8c01	4d	510	ad	510= y 2^{-4}
	A05	001	1A05	fi	
	002	510	000	ro	read out y

CONTROL COMBINATION					EXPLANATION
	0E06	4d	510	ad	A → 510
	25d	4d	511	ad	1 → 511
	A05	001	1A05	fi	
	002	510	000	ro	read out A
	1e06	4d	510	ad	510 = θ
	4d	5d	511	su	511 = 2
	A05	001	1A05	fi	
	002	510	000	ro	read out θ
	-001	22d	000	ro	1 carriage return
	7c01	8e	A04	cn	Is $T\phi$ < $C\phi$
	7c01	7c01	7c01	su	clear tally
FA B31	-0e02	4d	510	-ad	510 = $\phi\ 2^{-4}$
	0d	4d	511	ad	511 = 4
	A05	001	1A05	fi	
	002	510	000	ro	print out ϕ
	-001	033	B31	ba	
	-001	22d	000	ro	1 carriage return
FA B32	-0e03	4d	510	-ad	510 = u
	26d	4d	511	ad	511 = 3
	A05	001	1A05	fi	
	002	510	000	ro	print out u
	-001	033	B32	ba	
	-003	22d	000	ro	3 carriage returns
FA A04	1e06	6e31	2A04	cm	Is $\lvert\theta\rvert$ < 3.75
	001	28d	000	ro-	Halt

CONTROL COMBINATION					EXPLANATION
FA A04	d31	4d	000	ad	set up 000
	061	1032m	A05	ri-	Call in sin-cos routine
FA B39	-003	-003	-003	-su	Clear 003.....010
	-001	008	B39	ba	
FA B33	-A05	003	003	-ad	Form memory sum
	-001	061	B33	ba	in 003
	003	34d	003	su	003 = Δ(ms)
	4d	003	B34	cm	Is 0 < $\lvert\Delta\rvert$
	000	000	000	su	reset 000
FA A21	-0E02	4d	lc	-ad	lc = $\phi\ 2^{-4}$
	lc	4d	2c	ex	2c = sign of ϕ
	0d	4d	lc	ex	lc = $\lvert\phi\rvert\ 2^{-4}$
FA A02	lc	19d	A03	cm	Is $\lvert\phi\rvert < 2\pi$
	lc	19d	lc	su	lc = $(\phi - 2\pi)\ 2^{-4}$
	4d	0d	A02	cn	jump
FA A03	2c	4d	lc	ex	lc = $\pm\ \phi\ 2^{-4}$
	lc	25d	511	sn	511 = $\phi\ 2^{-3}$
	A05	001	lA05	fi	510=sin$\phi 2^{-1}$ 511=cos$\phi 2^{-1}$
	510	4d	-0e04	-ad	Store sin$\phi\ 2^{-1}$
	511	4d	-0E05	-ad	Store cos$\phi\ 2^{-1}$
	-001	033	A21	ba	
	d32	4d	000	ad	setup 000
FA B35	064	1054m	A05	ri-	read in 64 inst. from drum

CONTROL COMBINATION					EXPLANATION
	003	003	003	su	clear 003
	004	004	004	su	clear 004
FA B36	-A05	003	003	-ad	form memory sum
	-001	064	B36	ba	in 002, 003
	003	35d	003	su	003 = Δ(m.s.)
	4d	003	B37	cm	Is 0 < $\lvert\Delta\rvert$
	000	000	000	su	reset 000
FA A05	-1e04	11d	2c	-sn	2c=sinϕ 2^{-7}
	-1e05	11d	3c	-sn	3c=cosϕ 2^{-7}
	-1e07	2c	2c	-dv	2c = $\frac{\sin\phi}{1+2Cu}$ 2^{-5}
	-1e07	3c	3c	-dv	3c= $\frac{\cos\phi}{1+2Cu}$ 2^{-5}
	2c	5d	2c	sn	2c=$\frac{\sin\phi}{1+2Cu}$ 2^{-7}
	3c	5d	3c	sn	3c = $\frac{\cos\phi}{1+2Cu}$ 2^{-7}
	2c	5c	5c	ad	5c= 4($\sum y_1 \sin$) 2^{-9}
	3c	6c	6c	ad	6c= 4($\sum y_1 \cos$) 2^{-9}
	-002	032	A05	ba	
FA A06	-2e04	11d	2c	-sn	2c=sinϕ 2^{-7}
	-2e05	11d	3c	-sn	3c=cosϕ 2^{-7}
	-2e07	2c	2c	-dv	2c= $\frac{\sin\phi}{1+2Cu}$ 2^{-5}
	2c	21d	2c	sn	2c= " 2^{-8}
	-2e07	3c	3c	-dv	3c= $\frac{\cos\phi}{1+2Cu}$ 2^{-5}
	3c	21d	3c	sn	3c= " 2^{-8}
	2c	7c	7c	ad	7c= 2($\sum y_1 \sin$) 2^{-9}
	3c	8c	8c	ad	8c= 2($\sum y_1 \cos$) 2^{-9}
	-002	030	A06	ba	

CONTROL COMBINATION					EXPLANATION
FA A07	-0e04	11d	2c	-sn	2c= $\sin\phi\ 2^{-7}$
	-0e05	11d	3c	-sn	3c= $\cos\phi\ 2^{-7}$
	-0e07	2c	2c	-dv	2c= $\frac{\sin\phi}{1+2Cu}\ 2^{-5}$
	2c	3d	2c	sn	2c= " 2^{-9}
	-0e07	3c	3c	-dv	3c= $\frac{\cos\phi}{1+2Cu}\ 2^{-5}$
	3c	3d	3c	sn	3c= " 2^{-9}
	2c	9c	9c	ad	9c= $\sum y_i \sin\ 2^{-9}$
	3c	10c	10c	ad	10c= $\sum y_i \cos\ 2^{-9}$
	-032	064	A07	ba	
FA A08	-5c	12d	-5c	-mr	5c= $\frac{h}{3}\ 4\sum\ 2^{-7}$
	-6c	12d	-6c	-mr	6c= "
	-002	006	A08	ba	
	5c	7c	5c	ad	5c= $(4\sum \sin +2\sum)\ 2^{-7}$
	5c	9c	9c	ad	9c= $(4\sum +2\sum +\sum)\ 2^{-7}$
	6c	8c	6c	ad	6c= $(4\sum \cos +2\sum)\ 2^{-7}$
	6c	10c	10c	ad	10c= $(4\sum +2\sum +\sum)\ 2^{-7}$
FA A09	1c01	-9c	-1c	-mr	1c= 2Cd $\int \sin\ 2^{-9}$
	-9c	5d	-9c	-sn-	9c= $\int \sin\ 2^{-9}$
	-001	002	A09	ba	2c=2Cd $\int \cos 2^{-9}$, 10c= $\int \cos 2^{-9}$
	1c	10c	3c	ad	3c= $(\int \cos +2Cd \int \sin)\ 2^{-9}$
	9c	2c	2c	su	2c= $(\int \sin -2Cd \int \cos) 2^{-9}$
	2c01	3c	1c	mr-	1c= $\Lambda\ 2^{-5}$
	2c01	2c	2c	mr-	2c= $\Upsilon\ 2^{-5}$
	3e06	3d	3c	sn	3c= $\theta_{i-1} \cdot 2^{-6}$
	3e06	3c01	3c	ad	3c= $\left(\theta_{i-1} + \frac{2\Delta y}{C}[\ ]\right) 2^{-6}$
	0e06	3c	3c	mr-	3c= $\Psi\ 2^{-7}$

CONTROL COMBINATION					EXPLANATION
	1e06	1e06	4c	mr	$4c = \theta_i^2 \; 2^{-4}$
	5c01	1e06	5c	mr	$5c = \frac{\Delta y}{C} \theta_i \; 2^{-2}$
	5c	8d	5c	sn	$5c = 2 \; " \; 2^{-4}$
	4c01	17d	9c	sn	$9c = (4c01) \; 2^{-4}$
	4c	9c	4c	su	$4c = [\theta_i^2 - \Delta y^2 (\frac{b}{C}) ..] \; 2^{-4}$
	4c	5c	4c	ad	$4c = [" \; \frac{2\Delta y}{C} \theta_i \;] \; 2^{-4}$
	0e06	4c	4c	mr	$4c = A_i [\quad] 2^{-5}$
	2e06	3d	6c	sn	$6c = A_{i-1} \; 2^{-5}$
	1c	6c	1c	su	$1c = (\Lambda - A_{i-1}) \; 2^{-5}$
	1c	4c	1c	ad	$1c = \Pi \; 2^{-5}$
	5c01	5d	4c	sn	$4c = \frac{\Delta y}{C} \; 2^{-2}$
	1e06	4c	4c	ad	$4c = [\theta_i + \frac{\Delta y}{C}] \; 2^{-2}$
	1c	4c	5c	mr	$5c = \Pi [\theta_i + \frac{\Delta y}{C}] \; 2^{-7}$
	5c	8d	5c	sn	$5c = 2 \; " \quad 2^{-9}$
	3c	5d	3c	sn	$3c = \Psi \; .2^{-9}$
	2c	3d	2c	sn	$2c = \Upsilon \; .2^{-9}$
	3c	2c	2c	su	$2c = (\Psi - \Upsilon) \; 2^{-9}$
FA A10	2c	5c	2c	su-	$2c = U \; 2^{-9}$

CONTROL COMBINATION					EXPLANATION
	D33	4d	000	ad	set up 000
FA E35	042	1062m	A05	ri	call in instructions
	10c	10c	10c	su	clear 10c
	11c	11c	11c	su	clear 11c
FA E31	-A05	10c	10c	-ad	form memory sum
	-001	042	E31	ba	in 10c
	10c	38d	10c	su	10c= Δ m.s.
	4d	10c	E30	cm	Is 0 < | Δ |
	000	000	000	su	reset 000
	4d	0d	A05	cm	jump to A05
	3840m	000	000	ri	Dummy inst.
FA D30	4d	0d	1b26	cn	constant instr.
FA D31	4d	0d	1b33	cn	const. instr.
FA D32	4d	0d	1b36	cn	const. instr.
FA D33	4d	0d	1e31	cn	const. instr.

CONTROL COMBINATION	BEGINNING OF INSTRUCTIONS FOR DRUM				EXPLANATION
FA A05	4c	4c	5c	mr	$5c = 4(\theta_i + \frac{\Delta y}{C})^2 \; 2^{-6}$
	5c	16d	5c	su	$5c = [\;" \qquad -1]\; 2^{-6}$
	0e06	5c	5c	mr	$5c = A_i [\qquad]\, 2^{-7}$
	1c	8d	3c	sn	$3c = 2\,\Pi\; 2^{-7}$
	3c	5c	3c	ad-	$3c = \Sigma\; 2^{-7}$
	0e06	9d	6c	mr	$6c = {}^{6}A_i\; 2^{-4}$
	6c	4c	6c	mr-	$6c = Y\; 2^{-6}$

CONTROL COMBINATION	NEWTON RAPHSON METHOD				EXPLANATION
	1e06	4d	5c	ad	$5c = \theta\ 2^{-2}$
	5c	0e06	7c	mr	$7c = X\theta\ 2^{-4}$
	5c	5c	8c	mr	$8c = \theta^2\ 2^{-4}$
	7c	8c	7c	mr	$7c = X\theta^3 \cdot 2^{-8}$
	7c	5d	7c	sn	$7c =$ " 2^{-10}
	6c	8c	9c	mr	$9c = Y\theta^2\ 2^{-10}$
	7c	9c	7c	su	$7c = (X\theta^3 - Y\theta^2)\ 2^{-10}$
	7c	25d	7c	sn	$7c = (\quad$ " $) .2^{-9}$
	3c	5c	10c	mr	$10c = Z\theta\ 2^{-9}$
	7c	10c	7c	ad	$7c = (X\theta^3 - Y\theta^2 + Z\theta)\ 2^{-9}$
	7c	2c	7c	ad	$7c = f(\theta)\ 2^{-9}$
	5c	6c	10c	mr	$10c = 2Y\theta\ 2^{-9}$
	0e06	9d	9c	mr	$9c = 3X\ 2^{-4}$
	9c	8c	9c	mr	$9c = 3X\theta^2\ 2^{-8}$
	9c	8d	9c	sn	$9c =$ " 2^{-9}
	9c	10c	9c	su	$9c = (3X\theta^2 - 2Y\theta)\ 2^{-9}$
	9c	27d	9c	sn	$9c =$ " 2^{-7}
	9c	3c	9c	ad	$9c = f'(\theta)\ 2^{-7}$
	9c	7c	7c	dv	$7c = f/f'\ 2^{-2}$
	5c	7c	7c	su	$7c =$ new $\theta^{(i+1)}\ 2^{-2}$
	7c	5c	9c	su	$9c = (\theta^{(i+1)} - \theta^{(i)})\ 2^{-2}$
	9c	A19	31A05	cm	Is $\lvert\Delta\theta\rvert < 2^{-17}$
	7c	4d	5c	ad	$5c = \theta^{i+1}$
	4d	0d	8A05	cn	jump

CONTROL COMBINATION					EXPLANATION
	0e06	7c	9c	mr	$9c = A_i \theta_{i+1}\ 2^{-3}$
	9c	7c	10c	mr	$10c = A_i \theta^2_{i+1}\ 2^{-5}$
	4c	9c	9c	mr	$9c = A_i(\theta_i + \frac{\Delta y}{c})\theta_{i+1} 2^{-5}$
	10c	9c	10c	su	$10c = [\ A_i \theta^2_{i+1}$ -" $]\ 2^{-5}$
	10c	9c	10c	su	$10c = [\ A_i \theta^2_{i+1}$ -2" $]\ 2^{-5}$
	10c	1c	10c	ad	$10c = A_{i+1}\ 2^{-5}$
	10c	0d	6c	sn	$6c = A_{i+1}\ 2^{-1}$
	-0e06	4d	-2e06	-ad	$A_{i+1} \longrightarrow A_i$
	-6c	4d	-0e06	-ad	$A_{i+2} \longrightarrow A_{i+1}$
	-001	002	38A05	ba	$\theta_{i+1} \longrightarrow \theta_i$, $\theta_{i+2} \longrightarrow \theta_{i+1}$
	4d	0d	B17	cn	Jump

CONTROL COMBINATION					EXPLANATION
FA A30	3c	3c	3c	su-	clear 3c
	2c	4d	28d	ex	sign of x onto fffff
FA A31	1d	4d	2c	ex-	$\|x\|\ 2^{-4}$
FA A32	2c	19d	A33	cn	Is $x < 2\pi$
	2c	19d	2c	su	$x - 2\pi \longrightarrow x$
FA A33	2c	30d	A34	cn	is $x < \pi\ \ 2^{-4}$
	19d	2c	2c	su-	$2\pi - x \longrightarrow x$
	28d	29d	28d	mr-	28d= $\pm$ 1
FA A34	2c	37d	A37	cm	Is $\|x\|\ 2^{-4} < \epsilon$
	2c	27d	2c	sn	2c= X 2^{-2}
	A36	-001	A35	-fi	File C_B
FA A35	-11e	3c	3c	-ad-	3c= $a_5\ 2^6$
	3c	2c	3c	mr-	3c= $Xa_5 2^4$
	-001	005	A35	ba	3c=$(a_5X^5+a_4X^4+\ldots a_1X)\ 2^{-4}$
	3c	16e	3c	ad-	3c= F(X) 2^{-4}
	3c	28d	3c	mr	3c= $\pm$ F(X)
	3c	5d	2c	sn	2c= F(X) 2^{-6}
	4d	29d	28d	su	Reset fff
FA A36	[-000]	511	A37	ba	Reset C_B
FA A37	4d	0d	[000]	cn	jump

CONTROL COMBINATION					EXPLANATION
FA B28	25d	003	003	ad	$1 \rightarrow T_{po}$
	003	26d	B27	cn	Is $T_{po} < 3$
FA B29	001	B27	000	ro-	error halt
FA B34	25d	004	004	ad	$1 \rightarrow T_{sc}$
	004	26d	A04	cn	Is $T_{sc} < 3$
	001	A04	000	ro-	error halt
FA B37	25d	004	004	ad	$1 \rightarrow T_i$
	004	26d	B35	cn	Is $T_i < 3$
	001	B35	000	ro-	error halt
FA E30	25d	11c	11c	ad	$1 \rightarrow T_i$
	11c	26d	E35	cn	Is $T_i < 3$
	001	E30	000	ro-	Error halt
FA A19	000	000	100	ri	N.R. comp. const.

CONTROL COMBINATION	CONSTANTS			EXPLANATION
FA D00				
DA 036	000 000 000 04			0d
	02			1d
	-000 000 000 08			2d
	-000 000 000 04			3d
	-0			4d
	-000 000 000 02			5d
	000 000 000 06			6d
	000 000 000 05			7d
	-000 000 000 01			8d
	c0			9d= $3 \cdot 2^{-2}$
	-000 000 000 05			10d
	-000 000 000 06			11d
	430 547 9e9 58			12d= $\pi/48 \quad 2^2$
	10			13d
	c90 fda a22 16			14d= $\pi \; 2^{-2}$
	20			15d
	04			16d
	000 000 000 8			17d
	000 000 000 0c			18d
	6487ed511ob			19d = $2\pi \; 2^{-4}$
	0004			20d
	-000 000 000 03			21d
	d4			22d
	d4			23d
	d4			24d
	000 000 000 01			25d
	000 000 000 03			26d

CONTROL COMBINATION				EXPLANATION
	000 000 000 02			27d
	fff fff fff ff			28d
	-fff fff fff ff			29d
	324 3f6 a88 86			30d= $\pi\ 2^{-4}$ = h
	-000 000 000 09			31d
	0C9 0Fd aa 221			32d = $\pi\ 2^{-6}$
	-3ad 330619 62			33d = M.S. for P.O.
	644 ed9 abf a9			34d= M.S. for s-c
	d060b2449ed			35d= M.S. for 64 instr.
	-000 000 000 0a			36d
	-000 000 000 0c			37d
	e092246adfc			38d = M.S. for 42 instr.

CONTROL COMBINATION					EXPLANATION
FA B09 (E07)	1e	3e	1c	mr	$1c = Cd\ 2^{-2}$
	1c	1c	1c01	ad	$1c01 = 2Cd\ 2^{-2}$
	6e	6e	1c	mr	$1c = (\Delta y)^2 2^8$
	1e	2e	2c	mr	$2c = Cb\ 2^{-4}$
	13d	2c	2c	ad	$2c = (1+Cb)\ 2^{-4}$
	14d	1e	3c	mr	$3c = \pi C\ 2^{-2}$
	2c	5d	4c	sn	$4c = (1+Cb)\ 2^{-6}$
	3c	4c	3c	dv	$3c = \frac{(1+Cb)}{\pi C}\ 2^{-4}$
	1c	3c	2c01	mr-	$2c01 = (\Delta y)^2$ " 2^4
	2e	3d	3c	sn	$3c = b\ 2^{-8}$
	1e	3c	3c	dv	$3c = [b/C]\ 2^{-8}$
	13d	2c	5c	ad	$5c = (2+Cb)\ 2^{-4}$
	3c	1c	3c	mr	$3c = (\Delta y)^2\ b/C\ 2^0$
	3c	5c	3c	mr	$3c =$ " $(2+Cb)\ 2^{-4}$
	3c	15d	4c01	su	$4c01 = [$ " $-2]2^{-4}$
	4c01	2d	4c01	sn	$4c01 = [$ " $]2^{-12}$
	2c	5e	7c	dv	$7c = \frac{\Delta y}{1+Cb}\ 2^4$

CONTROL COMBINATION					EXPLANATION
	1e	1e	8c	mr	$8c = C^2\ 2^0$
	4e	4e	9c	mr	$9c = [\omega_p/\omega]^2\ 2^{-8}$
	8c	9c	9c	dv	$9c = [\omega_p/C\omega]^2\ 2^{-8}$
	7c	9c	9c01	mr	$9c01 = \frac{\Delta y}{1+Cb}\ [\omega_p/\omega]^2\ 2^{-4}$
	1e	5e	5c01	dv	$5c01 = \Delta y/C\ 2^0$
	2c	2c	2c	mr	$2c = (1+Cb)^2\ 2^{-8}$
	3c	6e	3c	mr	$3c = d\Delta y\ 2^2$
	2c	3c	2c	mr	$2c = d\Delta y(1+Cb)^2\ 2^{-6}$
	16d	2c	2c	su	$2c = [1 - "]\ 2^{-6}$
	5c01	2c	2c	mr	$2c = \Delta y/C\ [\ "\ ]\ 2^{-6}$
	2c	2c	3c01	ad	$3c01 = 2\Delta y/C\ [\quad]\ 2^{-6}$
FA B10	4d	0d	[000]	cn	Jump
	000	000	000	ri	Dummy order
	000	000	000	ri	"
	000	000	000	ri	"
	000	000	000	ri	"

CONTROL COMBINATION					EXPLANATION
FA e01					$\phi_{i+1}\ 2^{-4}$
DA 033					
FA e02					$\phi_i\ 2^{-4}$
DA 033					
FA e04					$\sin\phi\ 2^{-1}$
DA 033					
FA e05					$\cos\phi\ 2^{-1}$
DA 033					
FA e03					$u\ 2^{-3}$
AC B09					
FA e07					$(1+2cu)\ 2^{-2}$
AC 33e03					
FA e06					$A_1 \cdot 2^{-1}, \theta_1 2^{-2}, A_o \cdot 2^{-1}, \theta_o \cdot 2^{-2}$
AC 3e06					
FA e00					Parameters
AC 16e00					
FA c01					temporaries
AC 9c01					
FA c05					temporaries
AC 000					
FA c00					
BC B11					

CONTROL COMBINATION	PARAMETERS				EXPLANATION
1e00	C 2^{0}				
2e00	b 2^{-4}				
3e00	d 2^{-2}				
4e00	ω_p/ω 2^{-4}				
5e00	Δy 2^{0}				
6e00	Δy 2^{4}				
7e00	$\Delta y 2^{-4}$				
8e00	ϕ, u comparison constant 2^{-44}				
9e000	A, θ comparison constant 2^{-44}				
10e00	Δy 2^{-1}				
11e00	a_5 2^{6}				
12e00	a_4 2^{4}				
13e00	a_3 2^{2}				
14e00	a_2 2^{0}				
15e00	$a_1 2^{-2}$				
16e00	a_o 2^{-4}				
	$A_1 \cdot 2^{-1}$				
	$\theta_1 \cdot 2^{-2}$				
	$A_o \cdot 2^{-1}$				
	$\theta_o \cdot 2^{-2}$				
	$\phi \cdot 2^{-4}$				

CONTROL COMBINATION	TEMPORARIES			EXPLANATION
1c01	$2Cd\ 2^{-2}$			
2c01	$(\Delta y)^2\ \frac{(1 + Cb)}{\pi C}\ 2^4$			
3c01	$2\Delta y/C\ \ [1 - d\Delta y(1+Cb)^2]\ 2^{-6}$			
4c01	$(\Delta y)^2 (^b/_{C_1'})\ (2+Cb)\ -2$	2^{-2}		
5c01	$\Delta y/C\ 2^0$			
6c01	Tally for A, Θ print out			
7c01	Tally for ϕ_1', u print out			
8c01	$y\ 2^{-4}$			
9c01	$\frac{\Delta y}{(1+Cb)}\ [\omega_p/C\omega]^2\ 2^{-4}$			
1co5				
2co5				
1c00				
2c00				
3c00				
4c00				
5c00				
6c00				
7c00				
8c00				
9c00				
10c00				
11c00				

CONTROL COMBINATION	TRAVELING-WAVE AMPLIFIER PROGRAM NO. 2 32 ELECTRONS				EXPLANATION
Scaling:	$A \cdot 2^{-4}$,	$\theta \cdot 2^{-6}$, $\phi \cdot 2^{-6}$ and		$u \cdot 2^{-3}$	Program Tape No. 13M0m24
AC 006					
CD 238					
FA B11	000	000	000	su	set up 000
	-6col	-6col	-6col	-su	clear tallys
	-001	003	B11	ba	"
	B10	001	B09	fi	Find constants
FA B12	1e	-0e03	2c05	-mr	$2c05 = 2Cu\ 2^{-4}$
	13d	2c05	1c05	ad	$1c05 = (1+2Cu)2^{-4}$
	1c05	27d	-0e07	-sn	$0e07 = (1+2Cu)2^{-2}$
	-001	033	B12	ba	
FA B17	7e	8c01	8c01	ad	$\Delta y + y \rightarrow y$
	1e06	3e06	5c	su	$5c = (\theta_{i+1} - \theta_i)\ 2^{-6}$
	5c	7d	8c	sn	$8c =$ " 2^{-1}
	1e	8c	4c	mr	$4c = C($ " $)2^{-1}$
	0e06	2e06	6c	su	$6c = (A_{i+1} - A_i)2^{-4}$
	6c	26d	6c	sn	$6c = ($ " $)2^{-1}$
	6c	1e	6c	mr	$6c = C($ " $)2^{-1}$
	10e	4c	7c	su	$7c = [\Delta y - C(\theta_{i+1} - \theta_i)]\ 2^{-1}$
FA A00	5e	-0e03	2c	-mr	$2c = 2\Delta yu 2^{-4}$
	-0e07	2c	1c	-dv	$1c = \frac{2\Delta yu}{1+2Cu}\ 2^{-2}$
	1c	3d	1c	sn	$1c =$ " 2^{-6}
	1c	5c	1c	su	$1c = (\theta_i - \theta_{i+1} + \frac{2\Delta yu}{1+2Cu})\ 2^{-6}$
	000	000	000	su	Dummy order
	1c	-0e02	-0e01	-ad	Store new $\phi\ 2^{-6}$
	-001	033	A00	ba	"

CONTROL COMBINATION					EXPLANATION
FA B19	-0e02	4d	1c	-ad	1c= $\phi_{i,j}$ = T
	B22	-001	B25	-fi	File base counter
FA B25	11c	11c	11c	su	clear 11c
FA B20	1c	-0e02	2c	-su -	2c= x= $T-\phi_{i,0}$ 2^{-6}
	A37	001	A30	fi	2c= F(x) 2^{-6}
	-0e07	2c	2c	-dv -	2c= $\frac{F(x)}{1+2Cu}$ = I_o 2^{-4}
	2c	11c	11c	ad	11c= $\frac{2}{h}\int$ 2^{-4}
	-032	064	B20	ba	11c= $\frac{2}{h}\int$ 2^{-4}
	11c	8d	11c	sn	11c= $\frac{1}{h}\int$ 2^{-4}
FA B21	1c	-1e02	2c	-su	2c= x 2^{-6}
	A37	001	A30	fi	2c= F (x) 2^{-6}
	-1e07	2c	2c	-dv -	2c=$\frac{F(x)}{1+2Cu}$ 2^{-4}
	2c	11c	11c	ad	11c= $\frac{1}{h}\int$ 2^{-4}
	-001	031	B21	ba	11c= "
	11c	30d	11c	mr -	11c = $\int$ 2-4
FA B22	[000]	511	B23	ba	Reset C_B
FA B23	9c01	11c	11c	mr -	11c= K_1 2^{-8}
	6c	-0e05	1c	-mr	1c=C(A_{i+1}- A_i) cosϕ 2^{-2}
	2e06	7c	2c	mr	2c= A_i [Δy-C(θ_{i+1}-θ_i)]2^{-5}
	2c	-0e04	2c	-mr	2c= A_i ["] sin$\phi 2^{-6}$
	2c	5d	2c	sn	2c= " 2^{-8}
	1c	11d	1c	sn	1c= C(A_{i+1}- A_i)cosϕ 2^{-8}
	2c	1c	1c	su -	1c= K_2 2^{-8}
	-0e07	-0e03	2c	-mr	2c= u(1+2Cu) 2^{-5}
	2c	21d	2c	sn -	2c= K_3 2^{-8}
	1c	2c	1c	ad	1c= (K_2 + K_3) 2^{-8}

CONTROL COMBINATION					EXPLANATION
	lc	11c	lc	su	lc= $(-K_1+K_2+K_3)\ 2^{-8}$
	lc	26d	lc	sn	lc= " 2^{-5}
	-0e07	lc	-0e03	-dv	store u 2^{-3}
	-001	033	B19	ba	
FA B24	-0E01	4d	-0e02	-ad	Store new ϕ 's
	le	-0e03	2c	-mr	2c= 2Cu 2^{-4}
	13d	2c	lc	ad	lc= (1+2Cu) 2^{-4}
	lc	27d	-0e07	-sn	0e07=(1+2Cu) 2^{-2}
	-001	033	B24	ba	Store new (1+2Cu) 2^{-2}
	6c01	25d	6c01	ad	$T_{A+1} \longrightarrow T_A$
	7c01	25d	7c01	ad	$T_{\phi+1} \longrightarrow T_\phi$
	6c01	9e	A04	cn	jump if no print out
	6c01	6c01	6c01	su	Clear tally
	4d	30d	000	ad	Set up 000
FA B27	064	1024m	A05	ri	Call in P. O. routine
	002	002	002	su	Clear 002
	003	003	003	su	Clear 003
FA B26	-A05	002	002	-ad	Form memory sum in
	-001	064	B26	ba	002
	002	33d	002	su	002 = Δ(m.s.)
	4d	002	B28	cm	Is 0 < $\lvert\Delta\rvert$
	000	000	000	su	reset 000
	0d	4d	511	ad	511 = 4 2^{-44}
	8c01	4d	510	ad	510 = y 2^{-4}
	A05	001	1A05	fi	

CONTROL COMBINATION					EXPLANATION
	002	510	000	ro	read out y
	0E06	4d	510	ad	A → 510
	0d	4d	511	ad	4 → 511
	A05	001	1A05	fi	
	002	510	000	ro	read out A
	1e06	4d	510	ad	510 = θ
	4d	11d	511	su	511 = 6
	A05	001	1A05	fi	
	002	510	000	ro	read out θ
	-001	22d	000	ro	1 carriage return
	7c01	8e	A04	cn	Is $T_{\phi} < C_{\phi}$
	7c01	7c01	7c01	su	clear tally
FA B31	-0e02	4d	510	-ad	510 = ϕ 2^{-6}
	6d	4d	511	ad	511 = 6
	A05	001	1A05	fi	
	002	510	000	ro	print out ϕ
	-001	033	B31	ba	
	-001	22d	000	ro	1 carriage return
FA B32	-0e03	4d	510	-ad	510 = u
	26d	4d	511	ad	511 = 3
	A05	001	1A05	fi	
	002	510	000	ro	print out u
	-001	033	B32	ba	
	-003	22d	000	ro	3 carriage returns

CONTROL COMBINATION					EXPLANATION
FA A04	31d	4d	000	ad	set up 000
	061	1032m	A05	ri-	Call in sin-cos routine
FA B39	-003	-003	-003	-su	clear 003 010
	-001	008	B39	ba	
FA B33	-A05	003	003	-ad	Form memory sum
	-001	061	B33	ba	in 003
	003	34d	003	su	003 = Δ(ms)
	4d	003	B34	cm	Is 0 < $\lvert\Delta\rvert$
	000	000	000	su	reset 000
FA A21	-0E02	4d	lc	-ad	lc = $\phi\ 2^{-6}$
	lc	4d	2c	ex	2c = sign of ϕ
	0d	4d	lc	ex	lc = $\lvert\phi\rvert\ 2^{-6}$
FA A02	lc	19d	A03	cm	Is $\lvert\phi\rvert < 2\pi$
	lc	19d	lc	su	lc = (ϕ - 2π) 2^{-6}
	4d	0d	A02	cn	jump
FA A03	2c	4d	lc	ex	lc = $\pm\ \phi\ 2^{-6}$
	lc	26d	511	sn	511 = ϕ 2-3
	A05	001	1A05	fi	510 = sinϕ2-1 511=cosϕ2-1
	510	4d	-0e04	-ad	Store sinϕ 2^{-1}
	511	4d	-0E05	-ad	Store cosϕ 2^{-1}
	-001	033	A21	ba	
	d32	4d	000	ad	setup 000
FA B35	064	1040m	A05	ri-	read in 64 inst. from drum

CONTROL COMBINATION					EXPLANATION
	003	003	003	su	clear 003
	004	004	004	su	clear 004
FA B36	-A05	003	003	-ad	form memory sum
	-001	064	B36	ba	in 002, 003
	003	35d	003	su	003 = Δ(m.s.)
	4d	003	B37	cm	Is 0 < $\lvert\Delta\rvert$
	000	000	000	su	reset 000
FA A05	-1e04	31d	2c	-sn	2c= sinϕ 2^{-10}
	-1e05	31d	3c	-sn	3c= cosϕ 2^{-10}
	-1e07	2c	2c	-dv	2c = $\frac{\sin\phi}{1+2Cu}$ 2^{-8}
	-1e07	3c	3c	-dv	3c = $\frac{\cos\phi}{1+2Cu}$ 2^{-8}
	2c	5d	2c	sn	2c = $\frac{\sin\phi}{1+2Cu}$ 2^{-10}
	3c	5d	3c	sn	3c = $\frac{\cos\phi}{1+2Cu}$ 2^{-10}
	2c	5c	5c	ad	5c = 4($\sum y_i \sin$) 2^{-12}
	3c	6c	6c	ad	6c = 4($\sum y_i \cos$) 2^{-12}
	-002	032	A05	ba	
FA A06	-2e04	31d	2c	-sn	2c=sinϕ 2^{-10}
	-2e05	31d	3c	-sn	3c= cosϕ 2^{-10}
	-2e07	2c	2c	-dv	2c= $\frac{\sin\phi}{1+2Cu}$ 2^{-8}
	2c	21d	2c	sn	2c= " 2^{-11}
	-2e07	3c	3c	-dv	3c = $\frac{\cos\phi}{1+2Cu}$ 2^{-8}
	3c	21d	3c	sn	3c = " 2^{-11}
	2c	7c	7c	ad	7c = 2($\sum y_i \sin$) 2^{-12}
	3c	8c	8c	ad	8c = 2($\sum y_i \cos$) 2^{-12}
	-002	030	A06	ba	

CONTROL COMBINATION					EXPLANATION
FA A07	-0e04	31d	2c	-sn	2c= sinϕ 2^{-10}
	-0e05	31d	3c	-sn	3c= cosϕ 2^{-10}
	-0e07	2c	2c	-dv	2c=$\frac{\sin\phi}{1+2Cu}$ 2^{-8}
	2c	3d	2c	sn	2c= " 2^{-12}
	-0e07	3c	3c	-dv	3c=$\frac{\cos\phi}{1+2Cu}$ 2^{-8}
	3c	3d	3c	sn	3c= " 2^{-12}
	2c	9c	9c	ad	9c= Σ $y_i$sin 2^{-12}
	3c	10c	10c	ad	10c= Σ $y_i$cos 2^{-12}
	-032	064	A07	ba	
FA A08	-5c	12d	-5c	-mr	5c= $\frac{h}{3}$ 4 Σ 2-10
	-6c	12d	-6c	-mr	6c "
	-002	006	A08	ba	
	5c	7c	5c	ad	5c= (4Σ sin +2Σ) 2^{-10}
	5c	9c	9c	ad	9c= (4Σ +2Σ + Σ) 2^{-10}
	6c	8c	6c	ad	6c= (4Σ cos +2Σ) 2^{-10}
	6c	10c	10c	ad	10c= (4Σ +2Σ + Σ) 2^{-10}
FA A09	1c01	-9c	-1c	-mr	1c = 2cd $\int$ sin 2^{-12}
	-9c	5d	-9c	-sn-	9c= $\int$ sin 2^{-12}
	-001	002	A09	ba	2c=2cd $\int$sin2^{-12},10c=
					$\int$cos2-12
	1c	10c	3c	ad	3c= ($\int$cos+2cd $\int$sin) 2^{-12}
	9c	2c	2c	su	2c= ($\int$sin-2cd $\int$cos) 2^{-12}
	2c01	3c	1c	mr-	1c= Λ 2^{-8}
	2c01	2c	2c	mr-	2c= Υ 2^{-8}
	3e06	3c01	3c	ad	3c= (θ_{i-1} +$\frac{2\Delta y}{C}$ [ ])2^{-6}
	0e06	3c	3c	mr-	3c= Ψ 2^{-10}

CONTROL COMBINATION					EXPLANATION
	1e06	1e06	4c	mr	4c= θ_i^2 2^{-12}
	5c01	1e06	5c	mr	5c= $\frac{\Delta y}{c}$ θ_i 2^{-6}
	5c	10d	5c	sn	5c= 2 " " 2^{-12}
	4c	4c01	4c	su	4c= $[\theta_i^2 - \Delta y^2 (\frac{b}{c})..]$ 2^{-12}
	4c	5c	4c	ad	4c= [" + $\frac{2\Delta y}{c}$ θ_i] 2^{-12}
	0e06	4c	4c	mr	4c= A_i ["] 2^{-16}
	1c	3d	1c	sn	1c= Λ 2^{-12}
	2e06	2d	6c	sn	6c= A_{i-1} 2^{-12}
	1c	6c	1c	su	1c= (Λ - A_{i-1}) 2^{-12}
	1c	3d	1c	sn	1c= (Λ -A_{i-1}) 2^{-16}
	1c	4c	1c	ad	1c= Π 2^{-16}
	1c	27d	1c05	sn	1c05= Π 2^{-14}
	5c01	11d	4c	sn	4c= $\frac{\Delta y}{c}$ 2^{-6}
	1e06	4c	4c	ad	4c= [θ_i + $\frac{\Delta y}{c}$] 2^{-6}
	1c05	4c	5c	mr	5c= Π [θ_i + $\frac{\Delta y}{c}$] 2^{-20}
	5c	5c	5c	ad	5c= 2 " 2^{-20}
	3c	36d	3c	sn	3c= Ψ 2^{-20}
	2c	37d	2c	sn	2c= Υ 2^{-20}
	3c	2c	2c	su	2c= (Ψ - Υ) 2^{-20}
FA A10	2c	5c	2c	su -	2c= U 2^{-20}
	D33	4d	000	ad	set up 000
FA E35	043	1048m	A05	ri	call in instructions
	10c	10c	10c	su	clear 10c
	11c	11c	11c	su	clear 11c

CONTROL COMBINATION					EXPLANATION
FA E31	-A05	10c	10c	-ad	form memory sum
	-001	043	E31	ba	in 10c
	10c	38d	10c	su	10c= Δ m.s.
	4d	10c	E30	cm	Is 0 < $\lvert\Delta\rvert$
	000	000	000	su	reset 000
	4d	0d	A05	cm	jump to A05
FA D30	4d	0d	1b26	cn	constant instr.
FA D31	4d	00d	1b33	cn	const. instr.
FA D32	4d	0d	1B36	cn	const. instr.
FA D33	4d	0d	1E31	cn	const. instr.

CONTROL COMBINATION	BEGINNING OF INSTRUCTIONS FOR DRUM				EXPLANATION
FA A05	4c	4c	5c	mr	$5c = 4(\theta_1 + \frac{\Delta y}{c})^2 \; 2^{-14}$
	5c	20d	5c	su	5c= [" -1] 2^{-14}
	0e06	5c	5c	mr	5c= A_1["] 2^{-18}
	5c	0d	5c	sn	5c= " 2^{-14}
	1c05	1c05	3c	ad	3c= $2\Pi \; 2^{-14}$
	3c	5c	3c	ad -	3c= Z 2^{-14}
	0e06	9d	6c	mr	6c= $6A_1 \; 2^{-7}$
	6c	4c	6c	mr -	6c= Y 2^{-13}

CONTROL COMBINATION	NEWTON RAPHSON METHOD				EXPLANATION
	1e06	4d	5c	ad	5c= $\theta\ 2^{-6}$
	5c	0e06	7c	mr	7c= $X\theta\ 2^{-11}$
	5c	5c	8c	mr	8c= $\theta^2\ 2^{-12}$
	7c	8c	7c	mr	7c= $X\theta^3 . 2^{-23}$
	7c	26d	7c	sn	7c= " 2^{-20}
	6c	8c	9c	mr	9c= $Y\theta^2\ 2^{-25}$
	9c	7d	9c	sn	9c= " 2^{-20}
	7c	9c	7c	su	7c= $(X\theta^3 - Y\theta^2)\ 2^{-20}$
	3c	5c	10c	mr	10c= $Z\theta\ 2^{-20}$
	7c	10c	7c	ad	7c= $(X\theta^3 - Y\theta^2 + Z\theta\ )\ 2^{-20}$
	7c	2c	7c	ad	7c= $f(\theta)\ 2^{-20}$
	5c	6c	10c	mr	10c= $2Y\theta\ 2^{-20}$
	0e06	9d	9c	mr	9c= $3X\ 2^{-7}$
	9c	8c	9c	mr	9c= $3X\theta^2\ 2^{-19}$
	9c	8d	9c	sn	9c= " 2^{-20}
	9c	10c	9c	su	9c= $(3X\theta^2 - 2Y\theta)\ 2^{-20}$
	9c	6d	9c	sn	9c= " 2^{-14}
	9c	3c	9c	ad	9c= $f'(\theta)\ 2^{-14}$
	9c	7c	7c	dv	7c= $f/f'\ 2^{-6}$
	5c	7c	7c	su	7c= new $\theta^{(i+1)}\ 2^{-6}$
	7c	5c	9c	su	9c= $(\theta(i+1)_{-}\theta\ (i))\ 2^{-6}$
	9c	A19	32A05	cm	Is $\lvert\Delta\theta\rvert < 2^{-17}$
	7c	4d	5c	ad	5c= θ^{i+1}
	4d	0d	9A05	cn	jump

CONTROL COMBINATION					EXPLANATION
	0e06	7c	9c	mr	$9c = A_i\theta_{i+1}\ 2^{-10}$
	9c	7c	10c	mr	$10c = A_i\theta_{i+1}^2\ 2^{-16}$
	4c	9c	9c	mr	$9c = A_i(\theta_i + \frac{\Delta y}{c})\theta_{i+1}\ 2^{-16}$
	10c	9c	10c	su	$10c = A_i\theta_{i+1}^2$ - " 2^{-16}
	10c	9c	10c	su	$10c = A_i\theta_{i+1}^2$ -2 " 2^{-16}
	10c	1c	10c	ad	$10c = A_{i+1}\ 2^{-16}$
	10c	18d	6c	sn	$6c = A_{i+1}\ 2^{-4}$
	-0e06	4d	-2e06	-ad	$A_{i+1} \longrightarrow A_i$
	-6c	4d	-0e06	-ad	$A_{i+2} \longrightarrow A_{i+1}$
	-001	002	39A05	ba	$\theta_{i+1} \longrightarrow \theta_i$, $\theta_{i+2} \longrightarrow \theta_{i+1}$
	4d	0d	B17	cn	Jump
FA A30	3c	3c	3c	su -	clear 3c
	2c	4d	28d	ex	sign of x onto fffff
FA A31	1d	4d	2c	ex -	$\lvert x \rvert\ 2^{-6}$
FA A32	2c	19d	A33	cn	Is $x < 2\pi$
	2c	19d	2c	su	$x - 2\pi \longrightarrow x$
FA A33	2c	32d	A34	cn	is $x < \pi\ 2^{-6}$
	19d	2c	2c	su -	$2\pi - x \dashrightarrow x$
	28d	29d	28d	mr -	$28d = \pm 1$
FA A34	2c	37d	A37	cm	Is $\lvert x \rvert\ 2^{-6} < \epsilon$
	2c	0d	2c	sn	$2c = X\ 2^{-2}$
	A36	-001	A35	-fi	File C_B
FA A35	-11e	3c	3c	-ad -	$3c = a_5\ 2^6$
	3c	2c	3c	mr -	$3c = Xa_5 2^4$

CONTROL COMBINATION					EXPLANATION
	-001	005	A35	ba	$3c=(a_5X^5+a_4X^4 + \ldots a_1X)2^{-4}$
	3c	16e	3c	ad -	$3c= F(X)\ 2^{-4}$
	3c	28d	3c	mr	$3c= \pm F(X)$
	3c	5d	2c	sn	$2c= F(X)\ 2^{-6}$
	4d	29d	28d	su	Reset ffff
FA A36	[-000]	511	A37	ba	Reset C_B
FA A37	4d	0d	[000]	cn	jump
FA B28	25d	003	003	ad	$1 \rightarrow T_{po}$
	003	26d	B27	cn	Is $T_{po} < 3$
FA B29	001	B27	000	ro-	error halt
FA B34	25d	004	004	ad	$1 \rightarrow T_{sc}$
	004	26d	A04	cn	Is $T_{sc} < 3$
	001	A04	000	ro-	error halt
FA B37	25d	004	004	ad	$1 \rightarrow T_1$
	004	26d	B35	cn	Is $T_1 < 3$
	001	B35	000	ro-	error halt
FA E30	25d	11c	11c	ad	$1 \rightarrow T_1$
	11c	26d	E35	cn	Is $T_1 < 3$
	001	E30	000	ro-	Error halt
FA A19	000	001	000	ri	N. R. comp. const.

CONTROL COMBINATION	CONSTANTS			EXPLANATION
FA D00				
DA 036	000 000 000 04			0d
	02			1d
	-000 000 000 08			2d
	-000 000 000 04			3d
	-0			4d
	-000 000 000 02			5d
	000 000 000 06			6d
	000 000 000 05			7d
	-000 000 000 01			8d
	c0			9d
	-000 000 000 05			10d
	-000 000 000 06			11d
	430 547 9e9 58			12d= $\pi/48\ \ 2^2$
	10			13d
	c90 fda a22 16			14d= $\pi\ 2^{-2}$
	20			15d
	04			16d
	000 000 000 8			17d
	000 000 000 0c			18d
	192 1fb 544 44			19d = $2\pi\ 2^{-6}$
	0004			20d
	-000 000 000 03			21d
	d4			22d
	d4			23d
	d4			24d
	000 000 000 01			25d
	000 000 000 03			26d

CONTROL COMBINATION				EXPLANATION
	000 000 000 02			27d
	fff fff fff ff			28d
	-fff fff fff ff			29d
	324 3f6 a88 86			30d= $\pi\ 2^{-4}$ = h
	-000 000 000 09			31d
	0c9 0fd aa2 21			32d = $\pi\ 2^{-6}$
	-3ad 33061962			33d= M. S. for P. O.
	644 ed9 abf a9			34d= M. S. for s-c
	ceof455b7f2			35d= M. S. for 64 instr.
	-000 000 000 0a			36d
	-000 000 000 0c			37d
	00d 41e 6ba 01			38d = M. S. for 43 instr.

CONTROL COMBINATION					EXPLANATION
FA B09	1e	3e	1c	mr	$1c = Cd\ 2^{-2}$
	1c	1c	1c01	ad	$1c01 = 2Cd\ 2^{-2}$
	6e	6e	1c	mr	$1c = (\Delta y)^2 2^8$
	1e	2e	2c	mr	$2c = Cb\ 2^{-4}$
	13d	2c	2c	ad	$2c = (1+Cb)\ 2^{-4}$
	14d	1e	3c	mr	$3c = \pi C\ 2^{-2}$
	2c	5d	4c	sn	$4c = (1+Cb)\ 2^{-6}$
	3c	4c	3c	dv	$3c = \frac{(1+Cb)}{\pi C}\ 2^{-4}$
	1c	3c	2c01	mr-	$2c01 = (\Delta y)^2\ "\ \cdot 2^4$
	2e	3d	3c	sn	$3c = b\ 2^{-8}$
	1e	3c	3c	dv	$3c = [b/C]\ 2^{-8}$
	13d	2c	5c	ad	$5c = (2+Cb)\ 2^{-4}$
	3c	1c	3c	mr	$3c = (\Delta y)^2\ [b/C]\ 2^0$
	3c	5c	3c	mr	$3c = "\ (2+Cb)\ 2^{-4}$
	3c	15d	4c01	su	$4c01 = [\ "\ -2\ ]\ 2^{-4}$
	4c01	2d	4c01	sn	$4c01 = [\ "\ ]\ 2^{-12}$
	2c	5e	7c	dv	$7c = \frac{\Delta y}{1+Cb}\ 2^4$
	1e	1e	8c	mr	$8c = C^2\ 2^0$
	4e	4e	9c	mr	$9c = [\omega_p/\omega]^2\ 2^{-8}$
	8c	9c	9c	dv	$9c = [\omega_p/C\omega]^2\ 2^{-8}$
	7c	9c	9c01	mr	$9c01 = \frac{\Delta y}{1+Cb}[\omega_p/C\omega]^2\ 2^{-4}$
	1e	5e	5c01	dv	$5c01 = \Delta y/C\ 2^0$
	2c	2c	2c	mr	$2c = (1+Cb)^2\ 2^{-8}$
	3e	6e	3c	mr	$3c = d\Delta y\ 2^2$
	2c	3c	2c	mr	$2c = d\Delta y(1+Cb)^2\ 2^{-6}$
	16d	2c	2c	su	$2c = [1 - "]\ 2^{-6}$
	5c01	2c	2c	mr	$2c = \Delta y/C\ [\ "\ ]\ 2^{-6}$

CONTROL COMBINATION					EXPLANATION
	2c	2c	3c01	ad	3c01= 2^{Δ}v/c ["] 2^{-6}
FA B10	4d	0d	[000]	cn	jump
	000	000	000	ri	Dummy order
	000	000	000	ri	"
	000	000	000	ri	"
	000	000	000	ri	"

CONTROL COMBINATION				EXPLANATION
FA e01				$\phi_{i+1}\ 2^{-6}$
DA 033				
FA e02				$\phi_i\ 2^{-6}$
DA 033				
FA e04				$\sin\phi\ 2^{-1}$
DA 033				
FA e05				$\cos\phi\ 2^{-1}$
DA 033				
FA e03				$u\ 2^{-3}$
AC B09				
FA e07				$(1+2Cu)\ 2^{-2}$
AC 33e03				
FA e06				$A_1 .2^{-4}, \theta_1 2^{-6}, A_o .2^{-4}, \theta_o 2^{-6}$
AC 3e06				
FA e00				Parameters
AC 16e00				
FA c01				temporaries
AC 9c01				
FA c05				temporaries
AC 000				
FA c00				
BC B11				

CONTROL COMBINATION	PARAMETERS	EXPLANATION
1e00	C 2^0	
2e00	b 2^{-4}	
3e00	d 2^{-2}	
4e00	ω_p/ω 2^{-4}	
5e00	Δy 2^0	
6e00	Δy 2^4	
7e00	$\Delta y 2^{-4}$	
8e00	ϕ, u comparison constant 2^{-44}	
9e000	A,θ comparison constant 2^{-44}	
10e00	Δy 2^{-1}	
11e00	a_5 2^6	
12e00	a_4 2^4	
13e00	a_3 2^2	
14e00	a_2 2^0	
15e00	$a_1 2^{-2}$	
16e00	a_0 2^{-4}	
	$A_1 \cdot 2^{-4}$	
	$\theta_1 \cdot 2^{-6}$	
	$A_0 \cdot 2^{-4}$	
	$\theta_0 \cdot 2^{-6}$	
	$\phi \cdot 2^{-6}$	

CONTROL COMBINATION	TEMPORARIES			EXPLANATION
1c01	$2Cd\ 2^{-2}$			
2c01	$(\Delta y)^2 \frac{(1+Cb)}{\pi C}\ 2^4$			
3c01	$2\Delta y/C\ [1 + d\Delta y(1+Cb)^2]\ 2^{-6}$			
4c01	$[(\Delta y)^2(b/C)\ (2+Cb)\ -2]\ 2^{-12}$			
5c01	$\Delta y/C\ 2^0$			
6c01	Tally for A, θ print	out		
7c01	Tally for ϕ, u print	out		
8c01	$y\ 2^{-4}$			
9c01	$\frac{\Delta y}{(1+Cb)}[\omega_p/C\omega]^2\ 2^{-4}$			
1co5				
2co5				
1c00				
2c00				
3c00				
4c00				
5c00				
6c00				
7c00				
8c00				
9c00				
10c00				
11c00				

CONTROL COMBINATION	PARAMETER TAPE FOR TRAVELING-WAVE TUBE PROBLEM TRANSLATE by INTERIM HEX ITP				EXPLANATION
AC 481					Program Tape No. 13 MO
de 020 df					
				-1b	A_1 2^{-1}
				-2b	θ_1 2^{-2}
				-1b	A_o 2^{-1}
				-2b	θ_o 2^{-2}
				0b	C 2^0
				-4b	b 2^{-4}
				-2b	d 2^{-2}
				-4b	(ω_p/ω) 2^{-4}
	.25		-1d	0b	Δy 2^0
	.25		-1d	4b	Δy 2^4
	.25		-1d	-4b	Δy 2^{-4}
	.16		2d	-44b	ϕ, u comp. const. 2^{-44}
	.4		1d	-44b	A, θ comp. const. 2^{-44}
	.25		-1d	-1b	Δy 2^{-1}
				6b	a_5 2^6
				4b	a_4 2^4
				2b	a_3 2^2
				0b	a_2 2^0
				-2b	a_1 2^{-2}
				-4b	a_o 2^{-4}
BC 006					

TRAVELING-WAVE TUBE: PROGRAM NO. 13M13m7

Operating Instructions for Run No. ____

A. General Information

The output of this program is a sequence of 4 groups of 3 words and 2 groups of 65 words. It can be determined if the program is proceeding correctly by examining the last 2 words in the groups of 3: the second word in each group of 3 should be a positive number and these numbers should increase continuously until a maximum is reached and the problem is terminated (see below), while the third word in each group of 3 should be a negative number and these numbers should increase negatively throughout the entire problem. If at any stage of the problem these numbers do not follow the right pattern, then the computer should be halted and computation resumed at a point where the numbers are of the correct form (see B.7).

B. Initial Computations

1. Tape 13M13m7: Insert and process the first word on tape no. 13M13m7. With all the switches set on normal, begin computing. As the tape is read in, 4 groups of 3 identical memory sums are read out for drum transfers and 1 group of 2 for transfers to the acoustic memory only.
2. After 13M13m7 is in the machine, place 13m13p ___ in the Ferranti and begin computing. This will read in the tape and read out 2 memory sums, halting the process. Read in the last word on halt.
3. Patch Panel Settings: Decimal point at 2
   Carriage return at 8
4. With overflow switch on halt and format on patch, begin computing.

5. Intermittent Read-out without Machine Halting: Occasionally several intermittent read-outs will occur during computations. Usually this read-out is less than 5 words; however, if it should be much greater halt the machine and proceed to the section on program malfunction (B.7).
6. If everything is working correctly, run the program until the second number in the groups of 3 begins to decrease. After this point let the computations continue until a print-out of 2 sets of 65 words occurs. After each set of 3 words the computer halts to permit the operator to check the output with previous outputs. Computations are resumed by pushing the start button.
7. Program Malfunction: A program malfunction is here understood to be any difficulty arising from rapid, unexpected changes in the second and third words in the groups of 3 words, overflow, or cessation of computation other than those described earlier. In the event of a program malfunction:
    a. Read out the counter, gamma, and instruction. Also read out register 00c.
    b. Clear the acoustic memory.
    c. Insert and process the first word of 13M13p10.
    d. With the overflow switch on halt, begin computing.
    e. Repeat a-d several times if necessary. If the malfunction repeats successively at the same point, read out 088 (hex) words from 00c. That is all.
8. Halting the Computer for Purposes of Time: The operator should halt the computer approximately 15 seconds after the computer halts on a 3-word output and the start button is pushed.

C. Resuming Computations

1. Tape 13M13m7: Insert and process the first word of 13M13m7. With all the switches on normal, begin computing. As the tape is read in, 4 groups of 3 identical memory sums are read out for drum transfers and 1 group of 2 for transfers to the acoustic memory only.
2. After 13M13m7 is in the machine, clear the acoustic memory.
3. Insert and process the first word of 13M13p10.
4. Patch Panel Settings: Decimal point 2
   Carriage return at 8
5. With overflow switch on halt and format on patch, begin computing. Proceed with instructions B.6-B.8.

CONTROL COMBINATION	TRAVELING-WAVE TUBE PROBLEM 64 ELECTRONS				EXPLANATION
	READ IN INSTRUCTIONS				
	(READS IN SIN-COS BLOCK)				
AC 001					PROGRAM TAPE NO. 13M13
CD 014					
	014	001	001	ri	Read in 14 words
	[000]	001	015	ri	Read in X words to 015
	000	000	000	su	Clear 000
	-016	000	000	-ad	Obtain Memory
	-001	[000]	003	ba	Sum
	001	000	001	ro	Read out computed M. S.
	001	015	001	ro	Read out correct M. S.
	[000]	[016]	[000]	ro	Transfer to Drum
	[000]	[000]	160	ri	Read in from Drum
	000	000	000	su	Clear 000
	000	-160	000	-ad	Obtain drum
	-001	[000]	010	ba	Memory sum
	001	000	001	ro	Read out M. S.
	001	001	001	ri	Read in 1-word to 001
	1024m	001	001	fi	Transfer Control to 001
	Sin-Cos Block				
	013	001	002	ri	Read in 13 words to 002

CONTROL COMBINATION	Cont. -- (READS IN BLOCKS 2, 3, and 4)				EXPLANATION
AC 002					
CD 013	[000]	001	015	ri	Read in X words to 015
	000	000	000	su	Clear 000
	000	-016	000	-ad	Obtain
	-001	[000]	004	ba	Memory sum
	001	000	001	ro	Read out computed M. S.
	001	015	001	ro	Read out correct M. S.
	[000]	016	[000]	ro	Transfer to Drum
	[000]	[000]	160	ri	Read in from drum
	000	000	000	su	Clear 000
	000	160	000	-ad	Obtain
	-001	[000]	011	ba	Memory sum
	001	000	000	ro	Read out M. S.
	1024m	001	001	fi	Transfer control to 001

CONTROL COMBINATION	Cont. -- (Reads in Block 1)				EXPLANATION
AC 002					
CD 013					
	[000]	001	011	ri	Read in X words
	000	000	000	su	Clear 000
	000	-012	000	-ad	Obtain
	-001	[000]	004	ba	Memory sum
	001	000	001	ro	Read out computed M. S.
	001	011	001	ro-	Read out correct M. S.
	001	001	000	ri	Read in 1 word to 000
	1024m	001	000	fi	Transfer control to 000
	000	000	000	ri	0
	000	000	000	ri	0
	000	000	000	ri	0
	000	000	000	ri	0
	000	000	000	ri	0

CONTROL COMBINATION	DIRECTORY				EXPLANATION
	Register Number	Hex. No. of Register	Location		Hex Location on Drum
ϕ_{i+1}	65	41	1024m	1032m	400
Sin $\phi \cdot 2^{-1}$	65	41	1042m	1050m	412
Sin-cos sub-	61	3D	1051m	1058m	41B
routine					
Block No. 1	58	3A	12	70	Not stored on drum
Block No. 2	84	53	1059m	1069m	423
Block No. 3	98	62	1070m	1082m	42E
Block No. 4	136	88	1083m	1099m	43B
Dead Storage					
ϕ_i	65	41	1728m	1736m	6C0
u_i	65	41	1737m	1745m	6C9
Sections A, B,	31	1F	1746m	1749m	6D2
and C					

CONTROL COMBINATION	SCALING: $A\cdot2^{-4}$, $\theta\cdot2^{-6}$, $\phi\cdot2^{-6}$ and $u\cdot2^{-3}$				EXPLANATION
AC 012					Block No. 1
CD 048					
FA B00	083	1059m	B00	ri	Read in next block
	061	1051m	E07	ri	Read in Sin-cos Routine
	512	D17	000	su	$-\pi\cdot2^{-8} \rightarrow \Delta$
FA B01	D17	000	000	ad	$\pi\cdot2^{-8} + \Delta \rightarrow \Delta$
	512	000	511	ad	$\Delta \rightarrow$ 511
	E07	001	1E07	fi	Sin $\phi\cdot2^{-1}$, Cos $\phi\cdot2^{-1}$
	000	D18	-E02	-sn	$\Delta \rightarrow \phi_i\cdot2^{-6}$
	512	510	-E04	-ad	Store Sin $\phi\cdot2^{-1}$
	512	511	-E05	-ad	Store Cos $\phi\cdot2^{-1}$
	-001	065	B01	ba	
	065	E04	1042m	ro	Store Sin ϕ on drum
	065	E02	1728m	ro	Store $\phi\cdot2^{-6}$ on drum
FA B12	512	D19	-E07	-ad	$(1+2Cu)\cdot2^{-2}$
	-E03	-E03	-E03	-su	Clear u_i
	-001	065	B12	ba	
	065	E03	1737m	ro	Store $u_i\cdot2^{-3}$
FA B09	-6C01	-6C01	-6C01	-su	Clear tallys
	-001	000	B09	ba	
	1e	3e	1c	mr	$1c = 2Cd\cdot2^{-2}$
	1c	1c	1c01	ad	$1c01 = 2Cd\cdot2^{-2}$
	6e	6e	1c	mr	$1c = (\Delta y)^2\cdot2^{8}$
	1e	2e	2c	mr	$2c = Cb\cdot2^{-4}$
	D13	2c	2c	ad	$2c = (1+Cb)\cdot2^{-4}$
	D14	1e	3c	mr	$3c = (\pi C)2^{-2}$
	2c	D05	4c	sn	$4c = (1+Cb)\ 2^{-6}$
	3c	4c	3c	dv	$3c = \left[\frac{1+Cb}{\pi C}\right]\cdot2^{-4}$

CONTROL COMBINATION					EXPLANATION
	1c	3c	2c01	mr-	$2c01 = (\Delta y)^2 \left[\frac{1+Cb}{\pi C}\right] \cdot 2^4$
	2e	D03	3c	sn	$3c = b \cdot 2^{-8}$
	1e	3c	3c	dv	$3c = (b/C) \cdot 2^{-8}$
	D13	2c	5c	ad	$5c = (2+Cb)\ 2^{-4}$
	3c	1c	3c	mr	$3c = (\Delta y)^2\ (b/C) \cdot 2^0$
	3c	5c	3c	mr	$3c = (\Delta y)^2\ (2+Cb)\ 2^{-4}$
	3c	D15	4c01	su	$4c01 = [\ "\ -2] \cdot 2^{-4}$
	4c01	D02	4C01	sn	$4c01 = [\ "\ ]\ 2^{-12}$
	2c	5e	7c	dv	$7c = \left[\frac{\Delta y}{1+Cb}\right] \cdot 2^4$
	1e	1e	8c	mr	$8c = C^2 \cdot 2^0$
	4e	4e	9c	mr	$9c = [\omega_p/\omega]^2 \cdot 2^{-8}$
	8c	9c	9c	dv	$9c = [\omega_p/C\omega]^2 \cdot 2^{-8}$
	7c	9c	9c01	mr	$9c01 = \frac{\Delta y}{1+Cb} [\omega_p/C\omega]^2 \cdot 2^{-4}$
	1e	5e	5c01	dv	$5c01 = [\Delta y/C]\ 2^0$
	2c	2c	2c	mr	$2c = (1+Cb)^2 \cdot 2^{-8}$
	3e	6e	3c	mr	$3c = (d\Delta y)\ 2^2$
	2c	3c	2c	mr	$2c = d\Delta y\ (1+Cb)^2 \cdot 2^{-6}$
	D16	2c	2c	su	$2c = [1 - "\ ]\ 2^{-6}$
	5c01	2c	2c	mr	$2c = \Delta y/C\ [\ "\ ]\ 2^{-6}$
	2c	2c	3c01	ad	$3c01 = 2\Delta y/C\ [\ "\ ]\ 2^{-6}$
	031	E06	1746m	ro	Read A, B, and C onto drum
FA B10	512	001	B00	fi	Jump
Constants					
FA D13					
DA 001	10				D13
FA D14					
DA 001	C90 FDA	A22 16			$D14 = \pi \cdot 2^{-2}$

CONTROL COMBINATION				EXPLANATION
FA D05				
DA 001	-000 000 000 02			D05= $-2 \cdot 2^{-44}$
FA D03				
DA 001	-000 000 000 4			D03= $-4 \cdot 2^{-44}$
FA D15				
DA 001	20			D15= $2 \cdot 2^{-4}$
FA D02				
DA 001	-000 000 000 08			D02= $-8 \cdot 2^{-44}$
FA D16				
DA 001	04			D16
FA D17				
DA 001	032 43F 6A8 88			D17= $\pi \cdot 2^{-8}$
FA D18				
DA 001	-000 000 000 03			D18= $-3 \cdot 2^{-44}$
FA D19				
DA 001	400 000 000 00			D19= 2^{-2}

CONTROL COMBINATION				EXPLANATION
AC 136 B00				
FA E02				$\phi_1 \cdot 2^{-6}$
AC 65 E02				
FA E04				Sin $\phi \cdot 2^{-1}$
AC 65 E04				
FA E05				Cos $\phi \cdot 2^{-1}$
AC 65E05				
FA E03				$u \cdot 2^{-3}$
AC 65 E03				
FA E07				$(1+2Cu)\ 2^{-2}$
AC 65 E07				
FA E06		SECTION	A	$A_1 2^{-4}, \Theta_1 \cdot 2^{-6}, A_0 \cdot 2^{-4}, \Theta_0 \cdot 2^{-6}$
AC 3E06				
FA E00		SECTION	B	Parameters
AC 16E00				
FA C01		SECTION	C	Temporaries
AC 9C01				
FA C05				Temporaries
AC 000				
FA C00				
BC 000				

CONTROL COMBINATION					EXPLANATION
AC 012					Block No. 2
CD 068					
FA B00	098	1070m	B00	ri	Read in next block
FA B17	7e	8c01	8c01	ad	$\Delta y + y \longrightarrow y$
	1e06	3e06	5c	su	$5c = (\theta_{i+1} - \theta_i)\ 2^{-6}$
	5c	D07	8c	sn	$8c =$ " $\cdot 2^{-1}$
	1e	8c	4c	mr	$4c = C$ (") 2^{-1}
	e06	2e06	6c	su	$6c = (A_{i+1} - A_i)\ 2^{-4}$
	6c	D26	6c	sn	$6c =$ (") 2^{-1}
	6c	1e	6c	mr	$6c = C$ (") 2^{-1}
	10e	4c	7c	su	$7c = [\Delta y - C(\theta_{i+1} - \theta_i)]\ 2^{-1}$
FA A00	5e	-e03	2c	-mr	$2c = 2\Delta y\ u \cdot 2^{-4}$
	-e07	2c	1c	-dv	$1c = \left[\frac{2\Delta yu}{1+2Cu}\right]\ 2^{-2}$
	1c	D03	1c	sn	$1c =$ " $\cdot 2^{-6}$
	1c	5c	1c	su	$1c = \left[\theta_i - \theta_{i+1} + \frac{2\Delta yu}{1+2Cu}\right]\ 2^{-6}$
	1c	-e02	-e04	-ad	Store new $\phi \cdot 2^{-6}$
	-001	065	A00	ba	"
	065	e04	1024m	ro	Read out ϕ_{i+1}'s to Drum
	065	1042m	e04	ri	Read in Sin ϕ's
FA B19	-e02	D04	1c	-ad	$1c = \phi_{ij} = T$
	B22	-001	B25	-fi	File Base Counter
FA B25	11c	11c	11c	su	Clear 11c
FA B20	1c	-e02	2c	-su-	$2c = x = T - \phi_{i,o} \cdot 2^{-6}$
	A37	001	A30	fi	$2c = F(x) \cdot 2^{-6}$
	-e07	2c	2c	-dv-	$2c = \frac{F(x)}{1+2Cu} = I_o \cdot 2^{-4}$
	2c	11c	11c	ad	$11c = 2/h \int \cdot 2^{-4}$
	-064	128	B20	ba	$11c = 2/h \int \cdot 2^{-4}$
	11c	D08	11c	sn	$11c = 1/h \int \cdot 2^{-4}$

CONTROL COMBINATION					EXPLANATION
FA B21	1c	-1e02	2c	-su	$2c = x \cdot 2^{-6}$
	A37	001	A30	fi	$2c = F(x) \cdot 2^{-6}$
	-1e07	2c	2c	-dv-	$2c = \frac{F(x)}{1+2Cu} \cdot 2^{-4}$
	2c	11c	11c	ad	$11c = 1/h \int \cdot 2^{-4}$
	-001	063	B21	ba	11c= "
	11c	D19	11c	mr-	$11c = \int \cdot 2^{-4}$
FA B22	-[000]	511	B23	ba	Reset C_b
FA B23	9c01	11c	11c	mr-	$11c = K_1 \cdot 2^{-8}$
	6c	-e05	1c	-mr	$1c = C\ (A_{i+1} - A_i)\ \text{Cos}\ \phi \cdot 2^{-2}$
	2e06	7c	2c	mr	$2c = A_i\ [\Delta y - C(\theta_{i+1} - \theta_i)]\ 2^{-5}$
	2c	-e04	2c	-mr	$2c = A_i\ [\text{"}]\ \text{Sin}\ \phi \cdot 2^{-6}$
	2c	D05	2c	sn	2c= " 2^{-8}
	1c	D11	1c	sn	$1c = C\ (A_{i+1} - A_i)\ \text{Cos}\ \phi \cdot 2^{-8}$
	2c	1c	1c	su-	$1c = K_2 \cdot 2^{-8}$
	-e07	-e03	2c	-mr	$2c = u(1+2Cu)\ 2^{-5}$
	2c	D21	2c	sn-	$2c = K_3 \cdot 2^{-8}$
	1c	2c	1c	ad	$1c = (K_2 + K_3)\ 2^{-8}$
	1c	11c	1c	su	$1c = (-K_1 + K_2 + K_3)\ 2^{-8}$
	1c	D26	1c	sn	1c= " $\cdot 2^{-5}$
	-e07	1c	-e03	-dv	$u_i \cdot 2^{-3}$
	-001	065	B19	ba	
	512	001	B00	fi	Jump
FA A30	3c	3c	3c	su-	Clear 3c
	2c	D04	D28	ex	Extract sign of x onto fff
FA A31	D01	D04	2c	ex-	$\lvert x \rvert \cdot 2^{-6}$
FA A32	2c	D19	A33	cn	Is $x < 2\pi$
	2c	D19	2c	su	$x - 2\pi \rightarrow x$
FA A33	2c	D32	A34	cn	Is $x < \pi \cdot 2^{-6}$

CONTROL COMBINATION					EXPLANATION
	D19	2c	2c	su-	$2\pi - x \rightarrow x$
	D28	D29	D28	mr-	D28 = $\pm$ 1
FA A34	2c	D37	A37	cm	Is $\lvert x \rvert \cdot 2^{-6} < \epsilon$
	2c	D00	2c	sn	$2c = x \cdot 2^{-2}$
	A36	-001	A35	-fi	File C_b
FA A35	-11e	3c	3c	-ad-	$3c = a_5 \cdot 2^6$
	3c	2c	3c	mr-	$3c = x\, a_5 \cdot 2^4$
	-001	005	A35	ba	$3c = \left(\sum_1^5 a_i x^i\right) 2^{-5}$
	3c	16e	3c	ad-	$3c = F(x) \cdot 2^{-4}$
	3c	D28	3c	mr-	$3c = \pm F(x)$
	3c	D05	2c	sn	$2c = F(x) \cdot 2^{-6}$
	D04	D29	D28	su	Reset fff
FA A36	[-000]	511	A37	ba	Reset C_b
FA A37	D04	D00	[000]	cn	Jump
Constants					
FA D07					
DA 001	000 000	000 05			D07
FA D26					
DA 001	000 000	000 03			D26
FA D03					
DA 001	-000 000	000 04			D03
FA D04					
DA 001	-0				D04
FA D08					
DA 001	-000 000	000 01			D08
FA D05					
DA 001	-000 000	000 02			D05

CONTROL COMBINATION				EXPLANATION
FA D11				
DA 001	-000 000 000 06			D11
FA D21				
DA 001	-000 000 000 03			D21
FA D28				
DA 001	fff fff fff ff			D28
FA D29				
DA 001	-fff fff fff ff			D29
FA D01				
DA 001	02			D01
FA D19				
DA 001	192 1FB 544 44			D19=h=$(2\pi)2^{-6}$
FA D32				
DA 001	0C9 0FD AA2 21			D32 = $(\pi)2^{-6}$
FA D37				
DA 001	-000 000 000 0C			D37
FA D00				
DA 001	000 000 000 04			D00

CONTROL COMBINATION				EXPLANATION
AC 136 B00				
FA E02				$\phi_i \cdot 2^{-6}$
AC 65 E02				
FA E04				Sin $\phi \cdot 2^{-1}$
AC 65 E04				
FA E05				Cos $\phi \cdot 2^{-1}$
AC 65 E05				
FA E03				$u \cdot 2^{-3}$
AC 65 E03				
FA E07				$(1+2Cu)\ 2^{-2}$
AC 65 E07				
FA E06		SECTION	A	$A_1 \cdot 2^{-4}, \theta_1 \cdot 2^{-6}, A_0 \cdot 2^{-4}, \theta_0 \cdot 2^{-6}$
AC 3E06				
FA E00		SECTION	B	Parameters
AC 16E00				
FA C01		SECTION	C	Temporaries
AC 9C01				
FA C05				Temporaries
AC 000				
FA C00				
BC 000				

CONTROL COMBINATION					EXPLANATION
AC 012					Block No. 3
CD 060					
FA B00	136	1083m	B00	ri	Read in next block
	065	1024m	e02	ri	Read in ϕ_{i+1}
	6c01	D25	6c01	ad	$T_{A+1} \rightarrow T_A$
	7c01	D25	7c01	ad	$T_{\phi+1} \rightarrow T_\phi$
	6c01	9e	A04	cn	
	6c01	6c01	6c01	su	Clear Tally
	D00	D04	510	ad	$510 = 4 \cdot 2^{-44}$
	8c01	D04	511	ad	$511 = y \cdot 2^{-44}$
	B09	001	1B09	fi	Read out y
	e06	D04	511	ad	A → 511
	B09	001	1B09	fi	Read out A
	D04	D11	510	su	510=6
	1e06	D04	511	ad	$510=\theta$
	B09	001	1B09	fi	Read out θ
	-001	D22	001	ro-	Read out 1-C. R.
	7c01	8e	A04	cn	is $T_\phi < C_\phi$
	7c01	7c01	7c01	su	Clear Tally
	D06	D04	510	ad	510 = 6
FA B31	-e02	D04	511	-ad	$511 = \phi \cdot 2^{-6}$
	B09	001	1B09	fi	
	-001	065	B31	ba	
	-001	D22	000	ro	Read out 1 - C. R.
	D26	D04	510	ad	510 = 3
FA B32	-e03	D04	511	-ad	511 = u
	B09	001	1B09	fi	Read out u
	-001	065	B32	ba	

CONTROL COMBINATION					EXPLANATION
FA A04	065	e02	1728m	ro	Read out $\phi_{i+1,j}$ to drum
	065	e03	1737m	ro	Read out $u_{i+1,j}$ to drum
	031	e06	1746m	ro	Read out Sec.A, B and C to Drum
	061	1051m	e07	ri	Call in Sin-cos routine
FA B39	-003	-003	-003	su	Clear 003 --- 010
	-001	008	B39	ba	
FA A21	-e02	D04	1c	-ad	$1c = \phi \cdot 2^{-6}$
	1c	D04	2c	ex	2c= Sign of ϕ
	D00	D04	1c	ex	$1c = \lvert\phi\rvert \cdot 2^{-6}$
FA A02	1c	D19	A03	cm	Is $\lvert\phi\rvert < 2\pi$
	1c	D19	1c	su	$1c = (\phi - 2\pi)\, 2^{-6}$
	D04	D00	A02	cn	Jump
FA A03	2c	D04	1c	ex	$1c = \pm \phi \cdot 2^{-6}$
	1c	D26	511	sn	$511 = \phi \cdot 2^{-3}$
	e07	001	1e07	fi	$510 = \sin\phi \cdot 2^{-1}$; $511 = \cos\phi \cdot 2^{-1}$
	510	D04	-e04	-ad	Store Sin $\phi \cdot 2^{-1}$
	511	D04	-e05	-ad	Store Cos $\phi \cdot 2^{-1}$
	-001	065	A21	ba	
FA B24	1e	-e03	2c	-mr	$2c = 2Cu \cdot 2^{-4}$
	D13	2c	1c	ad	$(1+2Cu) \cdot 2^{-4}$
	1c	D27	-e07	-sn	$e07 = (1+2Cu)\, 2^{-2}$
	-001	065	B24	ba	
	065	-e04	1042m	ro	Store Sin $\phi \cdot 2^{-1}$
	512	001	B00	fi	Jump
Printout Subroutine					
FA B09	512	001	000	fi	exit
	510	D01	18D06	su	K - 44 - K'
	511	511	D05	sn	N_f

CONTROL COMBINATION					EXPLANATION
	511	18D06	511	sn	$N_i \cdot 2^{-44}$
	D29	001	1D29	fi	
	511	D02	511	sn	$N_i \cdot 2^{-12}$
	D05	001	D05	bd	
	D05	D03	D05	sn	$N_f \cdot 2^{-12}$
	D05	511	511	ad	$(N_i+N_f)\ 2^{-12}$
	001	511	001	ro	
	512	001	B09	fi	Jump
Constants					
FA D01					
DA 001	000 000	000 2C			D01= $44 \cdot 2^{-44}$
FA D02					
DA 001	000 000	000 20			D02= $32 \cdot 2^{-44}$
FA D03					
DA 001	-000 000	000 0C			D03= $12 \cdot 2^{-44}$
FA D05					
DA 001	0				D05= $N \cdot 2^{k}$
FA D25					
DA 001	000 000	000 01			D25
FA D00					
DA 001	000 000	000 04			D00
FA D04					
DA 001	-0				D04
FA D11					
DA 001	-000 000	000 06			D11
FA D22					
DA 003	d4				D22
	d4				D22

CONTROL COMBINATION				EXPLANATION
	d4			D22
FA D06				
DA 001	000 000 000 06			D06
FA D26				
DA 001	000 000 000 03			D26
FA D19				
DA 001	192 1FB 544 44			D19 = $2\pi \cdot 2^{-8}$
FA D13				
DA 001	10			D13
FA D27				
DA 001	000 000 000 02			D27
FA D29				
DA 022	Tape 14 D2m4			Integer Subroutine

CONTROL COMBINATION				EXPLANATION
AC 136 B00				
FA E02				$\phi \cdot 2^{-6}$
AC 65 E02				
FA E04				Sin $\phi \cdot 2^{-1}$
AC 65 E04				
FA E05				Cos $\phi \cdot 2^{-1}$
AC 65 E05				
FA A03				$u \cdot 2^{-3}$
AC 65 E03				
FA E07				$(1+2Cu)\ 2^{-2}$
AC 65 E07				
FA E06		SECTION	A	$A_1 \cdot 2^{-4}, \theta_1 \cdot 2^{-6}, A_o \cdot 2^{-4}, \theta_o \cdot 2^{-6}$
AC 3E06				
FA E00		SECTION	B	Temporaries
AC 16 E00				
FA C01		SECTION	C	Temporaries
AC 9C01				
FA C05				Temporaries
AC 000				
FA C00				
BC 000				

CONTROL COMBINATION					EXPLANATION
AC 012					Block No. 4
CD 113					
FA B00	083	1059m	B00	ri	Read in next block
FA A05	-1e04	D31	2c	-sn	$2c=\text{Sin}\ \phi \cdot 2^{-10}$
FA A05	-1e04	D31	3c	-sn	$3c=\text{Cos}\ \phi \cdot 2^{-10}$
	-1e07	2c	2c	-dv	$2c=\frac{\text{Sin}\ \phi}{1+2Cu} \cdot 2^{-8}$
	-1e07	3c	3c	-dv	$3c=\frac{\text{Cos}\ \phi}{1+2Cu} \cdot 2^{-8}$
	2c	D04	2c	sn	$2c=\frac{\text{Sin}\ \phi}{1+2Cu} \cdot 2^{-10}$
	3c	D05	3c	sn	$3c=\frac{\text{Cos}\ \phi}{1+2Cu} \cdot 2^{-10}$
	2c	5c	5c	ad	$5c=4(\Sigma\ y_i \text{Sin}\ )\ 2^{-12}$
	3c	6c	6c	ad	$6c=4(\Sigma\ y_i \text{Cos}\ )\ 2^{-12}$
	-002	064	A05	ba	
FA A06	-2e04	D31	2c	-sn	$2c=\text{Sin}\ \phi \cdot 2^{-10}$
	-2e05	D31	3c	-sn	$3c=\text{Cos}\ \phi \cdot 2^{-10}$
	-2e07	2c	2c	-dv	$2c=\frac{\text{Sin}\ \phi}{1+2Cu} \cdot 2^{-8}$
	2c	D21	2c	sn	2c= " $\cdot 2^{-11}$
	-2e07	3c	3c	-dv	$3c=\frac{\text{Cos}\ \phi}{1+2Cu} \cdot 2^{-8}$
	3c	D21	3c	sn	3c= " $\cdot 2^{-11}$
	2c	7c	7c	ad	$7c=2(\Sigma\ y_i \text{Sin}\ )\ 2^{-12}$
	3c	8c	8c	ad	$8c=2(\Sigma\ y_i \text{Cos}\ )\ 2^{-12}$
	-002	062	A06	ba	
FA A07	-e04	D31	2c	-sn	$2c=\text{Sin}\ \phi \cdot 2^{-10}$
	-e05	D31	3c	-sn	$3c=\text{Cos}\ \phi \cdot 2^{-10}$
	-e07	2c	2c	-dv	$2c=\frac{\text{Sin}\ \phi}{1+2Cu} \cdot 2^{-8}$
	2c	D03	2c	sn	2c= " $\cdot 2^{-12}$
	-e07	3c	3c	-dv	$3c=\frac{\text{Cos}\ \phi}{1+2Cu} \cdot 2^{-8}$
	3c	D03	3c	sn	3c= " $\cdot 2^{-12}$
	2c	9c	9c	ad	$9c=\Sigma y_i \text{Sin} \cdot 2^{-12}$

CONTROL COMBINATION					EXPLANATION
	3c	10c	10c	ad	$10c = \Sigma\, y_i \mathrm{Cos} \cdot 2^{-12}$
	-064	128	A07	ba	
FA A08	-5c	D12	-5c	-mr	$5c = \frac{4h}{\lambda} \Sigma \cdot 2^{-10}$
	-6c	D12	-6c	-mr	6c= "
	-002	006	A08	ba	
	5c	7c	5c	ad	$5c = (4\,\Sigma\, \mathrm{Sin} + 2\,\Sigma)\, 2^{-10}$
	5c	9c	9c	ad	$9c = (4\Sigma + 2\,\Sigma + \Sigma)\, 2^{-10}$
	6c	8c	6c	ad	$6c = (4\,\Sigma\, \mathrm{Cos} + 2\,\Sigma)\, 2^{-10}$
	6c	10c	10c	ad	$10c = (4\,\Sigma + 2\,\Sigma + \Sigma)\, 2^{-10}$
FA A09	1c01	-9c	-1c	-mr	$1c = 2Cd \int \mathrm{Sin} \cdot 2^{-12}$
	-9c	D05	-9c	-sn-	$9c = \int \mathrm{Sin} \cdot 2^{-12}$
	-001	002	A09	ba	$2c = 2Cd \int \mathrm{Cos} \cdot 2^{-12}; 10c = \int \mathrm{Cos} \cdot 2^{-12}$
	1c	10c	3c	ad	$3c = (\int \mathrm{Cos} + 2Cd \int \mathrm{Sin}) \cdot 2^{-12}$
	9c	2c	2c	su	$2c = (\int \mathrm{Sin} - 2Cd \int \mathrm{Cos})\, 2^{-12}$
	2c01	3c	1c	mr-	$1c = \Lambda \cdot 2^{-8}$
	2c01	2c	2c	mr-	$2c = \Upsilon \cdot 2^{-8}$
	3e06	3c01	3c	ad	$3c = \theta_{i-1} + \frac{2\Delta y}{C} [\quad] 2^{-6}$
	0e06	3c	3c	mr-	$3c = \Psi \cdot 2^{-10}$
	1e06	1e06	4c	mr	$4c = \theta_i^2 \cdot 2^{-12}$
	5c01	1e06	5c	mr	$5c = \Delta y / C \cdot \theta_i \cdot 2^{-6}$
	5c	D10	5c	sn	5c= 2 " $\cdot 2^{-12}$
	4c	4c01	4c	su	$4c = [\theta_i^2 - (\Delta y)^2 b / C \cdots] \cdot 2^{-12}$
	4c	5c	4c	ad	$4c = [\ " + \frac{2\Delta y}{C} \theta_i\ ] \cdot 2^{-12}$
	e06	4c	4c	mr	$4c = A_i [\quad] \cdot 2^{-16}$
	1c	D03	1c	sn	$1c = \Lambda \cdot 2^{-12}$
	2e06	D02	6c	sn	$6c = A_{i-1} \cdot 2^{-12}$
	1c	6c	1c	su	$1c = (\Lambda - A_{i-1})\, 2^{-12}$
	1c	D03	1c	sn	1c= " $\cdot 2^{-16}$

CONTROL COMBINATION					EXPLANATION
	1c	4c	1c	ad	1c= $\Pi \cdot 2^{-16}$
	1c	D27	1c05	sn	1c05= $\Pi \cdot 2^{-14}$
	5c01	D11	4c	sn	4c= $\Delta y/c \cdot 2^{-6}$
	1e06	4c	4c	ad	4c= $[\theta_i + \Delta y/c] \cdot 2^{-6}$
	1c05	4c	5c	mr	5c= $\Pi [\theta_i + \Delta y/c] \cdot 2^{-6}$
	5c	5c	5c	ad	5c= 2 " $\cdot 2^{-20}$
	3c	D36	3c	sn	3c= $\Psi \cdot 2^{-20}$
	2c	D37	2c	sn	2c= $\Upsilon \cdot 2^{-20}$
	3c	2c	2c	su	2c= $(\Psi - \Upsilon) \cdot 2^{-20}$
FA A10	2c	5c	2c	su-	2c= $U \cdot 2^{-20}$
FA E35	4c	4c	5c	mr	5c= 4 $(\theta_i + \frac{\Delta y}{c})^2 \cdot 2^{-14}$
	5c	D20	5c	su	5c= [-1] 2^{-14}
	e06	5c	5c	mr	5c= A_i [ ] 2^{-18}
	5c	D00	5c	sn	5c= " 2^{-12}
	1c05	1c05	3c	ad	3c= 2 $\Pi \cdot 2^{-14}$
	3c	5c	3c	ad-	3c= $Z \cdot 2^{-14}$
	e06	D09	6c	mr	6c= $6A_i \cdot 2^{-7}$
	6c	4c	6c	mr-	6c= $\cdot Y \cdot 2^{-13}$
	1e06	D04	5c	ad	5c= $\theta \cdot 2^{-6}$
FA C20	D01	D01	D01	su	Clear tally
	5c	e06	7c	mr	7c= $X\theta \cdot 2^{-4}$
	5c	5c	8c	mr	8c= $\theta^2 \cdot 2^{-12}$
	7c	8c	7c	mr	7c= $X\theta^3 \cdot 2^{-23}$
	7c	D26	7c	sn	7c= " $\cdot 2^{-20}$
	6c	8c	9c	mr	9c= $Y\theta^2 \cdot 2^{-25}$
	9c	D07	9c	sn	9c= " $\cdot 2^{-20}$
	7c	9c	7c	su	7c= $(X\theta^3 - Y\theta^2)\ 2^{-20}$
	3c	5c	10c	mr	10c= $Z\ \theta \cdot 2^{-20}$

CONTROL COMBINATION					EXPLANATION
	7c	10c	7c	ad	$7c = (X\theta^3 - Y\theta^2 + Z\theta) \cdot 2^{-20}$
	7c	2c	7c	ad	$7c = f(\theta) \cdot 2^{-20}$
	5c	6c	10c	mr	$10c = 2Y\theta \cdot 2^{-20}$
	e06	D09	9c	mr	$9c = 3X \cdot 2^{-7}$
	9c	8c	9c	mr	$9c = 3X\theta^2 \cdot 2^{-19}$
	9c	D08	9c	sn	9c = " $\cdot 2^{-20}$
	9c	10c	9c	su	$9c = (3X\theta^2 - 2Y\theta) \cdot 2^{-20}$
	9c	D06	9c	sn	9c = " $\cdot 2^{-14}$
	9c	3c	9c	ad	$9c = f'(\theta) \cdot 2^{-14}$
	9c	7c	7c	dv	$7c = f(\theta)/f'(\theta) \cdot 2^{-6}$
	5c	7c	7c	su	$7c = \text{New } \theta^{(i+1)} \cdot 2^{-6}$
	7c	5c	9c	su	$9c = [\theta^{(i+1)} - \theta(i)] \cdot 2^{-6}$
	9c	D19	C21	Cm	Is $\lvert \Delta\theta \rvert < 2^{-17}$
	7c	D04	5c	ad	$5c = \theta^{(i+1)}$
	D08	D01	D01	ad	Cycle Tally
	D01	1D01	1C20	cm	Is tally ≥ 20
	D19	D19	D19	ad	$D19 = 2 \cdot 2^{-16}$
	001	9c	001	ro	Read out $(\Delta\theta) \cdot 2^{-6}$
	000	000	000	ex	
	512	001	C20	fi	Jump
FA C21	e06	7c	9c	mr	$9c = A_i\theta_{i+1} \cdot 2^{-10}$
	9c	7c	10c	mr	$10c = A_i\theta_{i+1}^2 \cdot 2^{-16}$
	4c	9c	9c	mr	$9c = A_i(\theta_i + \Delta y/C)\theta_{i+1} \cdot 2^{-16}$
	10c	9c	10c	su	$10c = [A_i\theta_{i+1}^2 - \text{"}] 2^{-16}$
	10c	9c	10c	su	$10c = [A_i\theta_{i+1}^2 - 2\text{"}] \cdot 2^{-16}$
	10c	1c	10c	ad	$10c = A_{i+1} \cdot 2^{-16}$
	10c	D18	6c	sn	$6c = A_{i+1} \cdot 2^{-4}$
FA C22	-e06	D04	-2e06	-ad	$A_{i+1} \rightarrow A_i$

CONTROL COMBINATION					EXPLANATION
	-6c	D04	-e06	-ad	$A_{i+2} \rightarrow A_{i+1}$
	-001	002	C22	ba	$\theta_{i+1} \rightarrow \theta_i, -\theta_{i+2} \rightarrow \theta_{i+1}$
	D04	D00	B00	cn	Jump
Constants					
FA D31					
DA 001	-000 000	000 09			D31
FA D05					
DA 001	-000 000	000 02			D05
FA D21					
DA 001	-000 000	000 03			D21
FA D03					
DA 001	-000 000	000 04			D03
FA D12					
DA 001	218 2A3	CF4 AC			D12= $\frac{h}{3} \cdot 2^2 = \frac{\pi}{96}$
FA D19					
DA 001	000 001				D19= 2^{-24}
FA D10					
DA 001	-000 000	000 05			D10
FA D02					
DA 001	-000 000	000 08			D02
FA D27					
DA 001	000 000	000 02			D27
FA D11					
DA 001	-000 000	000 06			D11
FA D36					
DA 001	-000 000	000 0A			D36
FA D37					
DA 001	-000 000	000 0C			D37

CONTROL COMBINATION					EXPLANATION
FA D20					
DA 001	000 4				D20
FA D00					
DA 001	000 000	000 04			D00
FA D09					
DA 001	C				D09
FA D04					
DA 001	-0				D04
FA D26					
DA 001	000 000	000 03			D26
FA D07					
DA 001	000 000	000 05			D07
FA D08					
DA 001	-000 000	000 01			D08
FA D06					
DA 001	000 000	000 06			D06
FA D18					
DA 001	000 000	000 0C			D18
FA D01					
DA 002	0				D01= Cycle tally
	000 000	000 14			1D01= Upper count

CONTROL COMBINATION				EXPLANATION
AC 136 B00				
FA E02				$\phi \cdot 2^{-6}$
AC 65E02				
FA E04				$\sin\phi \cdot 2^{-1}$
AC 65E04				
FA E05				$\cos\phi \cdot 2^{-1}$
AC 65E05				
FA E03				$u \cdot 2^{-3}$
AC 65E03				
FA E07				$(1+2Cu)\ 2^{-2}$
AC 65E07				
FA E06		SECTION A		$A_1 \cdot 2^{-4}, \theta_1 \cdot 2^{-6}, A_o \cdot 2^{-4}, \theta_o \cdot 2^{-6}$
AC 3E06				
FA E00		SECTION B		Parameters
AC 16E00				
FA C01		SECTION C		Temporaries
AC 9c01				
FA C05				Temporaries
AC 000				
FA C00				
BC 000				

CONTROL COMBINATION	TEMPORARIES			EXPLANATION
1c01	$2Cd \cdot 2^{-2}$			
2c01	$(\Delta y)^2 \quad \left[\frac{1+Cb}{\pi C}\right] \cdot 2^4$			
3c01	$2\Delta y/c \quad \left[1-d\ \Delta y\ (1+Cb)^2\right] 2^{-6}$			
4c01	$\left[(\Delta y)^2 \quad (b/C)\ (2+Cb) - 2\right] 2^{-12}$			
5c01	$\Delta y/C \cdot 2^0$			
6c01	Tally for A,θ Print out.			
7c01	Tally for ∅,u Print out.			
8c01	$y \cdot 2^{-4}$			
9c01	$\left(\frac{\Delta y}{1+Cb}\right) \quad \left[\omega_p/C\omega\right] 2 \cdot 2^{-4}$			
1c05				
2c05				
1c00				
2c00				
3c00				
4c00				
5c00				
6c00				
7c00				
8c00				
9c00				
10c00				
11c00				

CONTROL COMBINATION	PARAMETERS			EXPLANATION
1e00	$C \cdot 2^{0}$			
2e00	$b \cdot 2^{-4}$			
3e00	$d \cdot 2^{-2}$			
4e00	$\omega_p/\omega\ 2^{-4}$			
5e00	$\Delta y\ 2^{0}$			
6e00	$\Delta y\ 2^{4}$			
7e00	$\Delta y\ 2^{-4}$			
8e00	ϕ, u comparison constant 2^{-44}			
9e00	A, θ comparison "	2^{-44}		
10e00	$\Delta y\ 2^{-1}$			
11e00	$a_5 \cdot 2^{6}$			
12e00	$a_4\ 2^{4}$			
13e00	$a_3 \cdot 2^{2}$			
14e00	$a_2 \cdot 2^{0}$			
15e00	$a_1 \cdot 2^{-2}$			
16e00	$a_0 \cdot 2^{-4}$			

CONTROL COMBINATION	PARAMETER TAPE FOR TRAVELING-WAVE TUBE PROBLEM TRANSLATE BY INTERIM HEX ITP				EXPLANATION
					Program Tape No. 13M13
AC 473					
de 020 df					
				-4b	$A_1\ 2^{-4}$
				-6b	$\Theta_1\ 2^{-6}$
				-4b	$A_o\ 2^{-4}$
				-6b	$\Theta_o\ 2^{-6}$
				0b	$C\ 2^{0}$
				-4b	$b\ 2^{-4}$
				-2b	$d\ 2^{-2}$
				-4b	$\omega_p/\omega\ 2^{-4}$
	.25		-1d	0b	$\Delta y\ 2^{0}$
	.25		-1d	4b	$\Delta y\ 2^{4}$
	.25		-1d	-4b	$\Delta y\ 2^{-4}$
	.16		2d	-44b	ϕ, u comp. const. 2^{-44}
	.4		1d	-44b	A, Θ comp. const. 2^{-44}
	.25		-1d	-1b	$\Delta y\ 2^{-1}$
				6b	$a_5\ 2^{6}$
				4b	$a_4\ 2^{4}$
				2b	$a_3\ 2^{2}$
				0b	$a_2\ 2^{0}$
				-2b	$a_1\ 2^{-2}$
				-4b	$a_o\ 2^{-4}$
BC 013					

TRAVELING-WAVE TUBE: PROGRAM NO. 13M12m2

Operating Instructions for Run No. _____

1. Place tape 13M12m2 in the reader and insert and process the first word on halt.
2. With all switches on normal, push the start button; this will read in the remainder of the tape.
3. Read in the last word on halt.
4. Place the parameter tape in the reader and with the overflow switch on halt begin computing.
5. End of computation is signified by a print-out of the word fff.

CONTROL COMBINATION	CALCULATION OF POWER GAIN				EXPLANATION
	db=	20 $\log_{10}$	$\frac{A(y)_i}{A_o}$		Program Tape No. 13 M12m2
AC 006					
CD 022					
FA A00	E00	E00	E00	su	Clear E00
FA A02	002	001	D00	ri	Read in two words from Ferranti
FA A03	D00	1C00	A04	ex	
	D00	3C00	D00	sn	
	D00	2C00	A08	ex	
FA A04	000	001	D01	ri	Read in A_i's $.2^{-8}$
	000	000	000	ba	Clear C_b
FA A01	E00	4C00	E00	ad	$\Delta y + y \longrightarrow y$
	E00	C00	511	ad	$511 = y.2^{-4}$
	10C00	C00	510	ad	$510 = 4.2^{-44}$
	A06	001	1A06	fi	Print out y value
	1D00	-D01	511	-dv	$A_i/A_o.2^{-11}$
	A05	001	1A05	fi	Transfer control
	5C00	6C00	1E00	mr	$[11 \ln 2] 2^{-5}$
	511	1E00	1E00	ad	$[\ln A_i/A_o] .2^{-5}$
	7C00	8C00	2E00	mr	$[20 \log_{10} e] .2^{-5}$
	1E00	2E00	511	mr	$(db) .2^{-10}$
	9C00	C00	510	ad	$510 = 10.2^{-44}$
	A06	001	1A06	fi	Print out (db)
	-002	11C00	000	ro	Read out 2 C. R.'s
FA A08	-001	000	A01	ba	
	001	1C00	000	ro-	

CONTROL COMBINATION		EXPLANATION
FA A05		
dA 039	Subroutine 14d 9m3 for ln x	
FA A06		
dA 096	Subroutine 14d 18 m5	
FA C00		
dA 013	0	
	FFF	
	000 FFF	
	-000 000 000 0 C	12.2^{-44}
	019 999 999 99	$0.1.2^{-4}$
	B17217F7 DI0	ln2 = 0.693
	58	11.2^{-5}
	6F2DEC549B9	$\log_{10}e = 0.434 + ..$
	A0	20.2^{-5}
	000 000 000 0 A	10.2^{-44}
	000 000 000 0 4	4.2^{-44}
	d4	C. R.
	d4	C. R.

CONTROL COMBINATION	(PARAMETER TAPE) Translate Using Subroutine ITP				EXPLANATION
de 000df					
	(Number of Units to be Converted)			-12b	
	.225		-1d	3b	
	(List Numbers Beginning Here With			-8b	
	Proper Scale Factors.)				
bc					

BIBLIOGRAPHY

Small-Signal Theory

1. Brewer, G. R., and Birdsall, C. K., "Normalized Propagation Constants for a Traveling-Wave Tube for Finite Values of C", Technical Memorandum No. 331, Hughes Research and Development Laboratories, October, 1953

2. Chu, L. J., and Jackson, J. D., "Field Theory of Traveling Wave Tubes", Proc. IRE, 36, No. 7, 853-863 (July, 1948).

3. Fletcher, R. C., "Helix Parameters Used in Traveling-Wave-Tube Theory", Proc. IRE, 38, No. 4, 413-417 (April, 1950).

4. Hines, M. E., Unpublished Bell Telephone Laboratory curves of the small-signal propagation constants vs. b for several values of QC and C.

5. Kompfner, R., "The Traveling-Wave Tube as an Amplifier at Microwaves", Proc. IRE, 35, No. 2, 124-127 (February, 1947).

6. Kompfner, R., "Traveling-Wave Tube; Centimeter-Wave Amplifier", Wireless Engineering, 24, 255-266 (September, 1947).

7. Kompfner, R., "Traveling-Wave Tubes", Reports on Progress in Physics, 15, 278-328 (1952).

8. Pierce, J. R., Traveling-Wave Tubes, D. Van Nostrand, New York, 1950.

9. Sensiper, S., "Explicit Expressions for the Traveling-Wave-Tube Propagation Constants", Memorandum No. 53-16, Hughes Research and Development Laboratories, December, 1953.

10. Tien, Ping King, "Traveling-Wave Tube Helix Impedance", Proc. IRE, 41, 1617-1624 (November, 1953).

Large-Signal Theory

11. Brillouin, L., "The Traveling-Wave Tube (discussion of waves for large amplitudes)", Jour. App. Phys., 20, No. 12, 1196-1206 (December, 1949).

12. Nordsieck, A. T., "Theory of the Large-Signal Behavior of Traveling-Wave Amplifiers", Proc. IRE, 41, No. 5, 630-637 (May, 1953).

BIBLIOGRAPHY (cont.)

13. Poulter, H. C., "Large Signal Theory of the Traveling-Wave Tube", Technical Report No. 73, ONR Contract No. N6onr 251(07), Electronics Research Laboratory, Stanford University, January 28, 1954.

14. Tien, P. K., Walker, L. R., and Wolontis, V. M., "A Large Signal Theory of Traveling-Wave Amplifiers", Proc. IRE, 43, No. 3, 260-277 (March, 1955

15. Wang, C. C., "Solution of Partial Integral-Differential Equations of Electron Dynamics Using Analogue Computers with Storage Devices", Project Cyclone, Symposium II on Simulation and Computing Techniques, Part 2, Reeves Instrument Corporation, April 28 - May 2, 1952.

Space-Charge Wave Analysis and Electron Interaction

16. Bohm, D., and Pines, D., "A Collective Description of Electron Interactions: II. Collective vs. Individual Particle Aspects of the Interactions", Phys. Rev., 85, 338-353 (January 15, 1952).

17. Bohm, D., and Gross, E. P., "Theory of Plasma Oscillation: A. Origin of Medium-Like Behavior", Phys. Rev., 75, 1851-1864 (June 15, 1949).

18. Bohm, D., and Gross, E. P., "Theory of Plasma Oscillations: B. Excitation and Damping of Oscillations", Phys. Rev., 75, 1864-1876 (June 15, 1949).

19. Gabor, D., "Dynamics of Electron Beams", Proc. IRE, 33, No. 11, 792-805 (November, 1945).

20. Haeff, A. V., "Space-Charge Effects in Electron Beams", Proc. IRE, 27, No. 9, 586-602 (September, 1952).

21. Hahn, W. C., "Small Signal Theory of Velocity-Modulated Electron Beams", General Electric Review, 42, 258-270 (June, 1939).

22. Hahn, W. C., "Wave Energy and Trans-Conductance of Velocity-Modulated Electron Beams", General Electric Review, 42, 497-502 (November, 1939).

23. Kent, Gordon, "Space-Charge Waves in Inhomogeneous Electron Beams", Jour. App. Phys., 25, 32-41 (January, 1954).

24. Pierce, J. R., "Increasing Space-Charge Waves", Jour. App. Phys., 20, No. 11, 1060-1066 (November, 1949).

BIBLIOGRAPHY (cont.)

25. Pierce, J. R., "Note on Stability of Electron Flow in the Presence of Positive Ions", Jour. App. Phys., 21, No. 10, 1063 (October, 1950).

26. Pierce, J. R., "Possible Fluctuations in Electron Streams Due to Ions", Jour. App. Phys., 19, No. 3, 231-236 (March, 1948).

27. Ramo, Simon, "Currents Induced by Electron Motion", Proc. IRE, 27, No. 9, 584-586 (September, 1939).

28. Ramo, Simon, "Space Charge and Field Waves in an Electron Beam", Phys. Rev., 56, 276-283 (August, 1939).

29. Rigrod, W. W., and Lewis, J. A., "Wave Propagation along a Magnetically-Focused Cylindrical Electron Beam", Bell System Technical Journal, 33, No. 2, 399-416 (March, 1954).

30. Tonks, L., and Langmuir, I., "Oscillations in Ionized Gases", Phys. Rev., 33, 195 (February, 1929).

31. Wang, Chao-Chen, "Large-Signal High-Frequency Electronics of Thermionic Vacuum Tubes", Proc. IRE, 29, 200-214 (April, 1941).

32. Watkins, D. A., "The Effect of Velocity Distribution in a Modulated Electron Stream", Jour. App. Phys., 23, No. 5, 568-573 (May, 1952).

Numerical Analysis

33. Bellman, R., Stability Theory of Differential Equations, McGraw-Hill Book Co., Inc., New York, 1953.

34. Fort, Tomilson, Finite Differences and Difference Equations in the Real Domain, Oxford University Press, London, 1948.

35. Hartree, D. R., Numerical Analysis, Oxford University Press, London, 1952.

36. Householder, A. S., Principles of Numerical Analysis, McGraw-Hill Book Co., Inc., New York, 1953.

37. Milne, W. E., Numerical Calculus, Princeton University Press, Princeton, New Jersey, 1949.

BIBLIOGRAPHY (concl.)

38. Milne, W. E., Numerical Solution of Differential Equations, John Wiley and Sons, New York, 1953.

39. Wilks, Elementary Statistical Analysis, Princeton University Press, Princeton, New Jersey, 1949.

General Reference Books

40. Churchill, R. V., Fourier Series and Boundary Value Problems, McGraw-Hill, New York, 1941.

41. Churchill, R. V., Introduction to Complex Variables and Applications, McGraw-Hill, New York, 1948.

42. Dow, W. G., Fundamentals of Engineering Electronics, John Wiley and Sons, New York, 1952, Chapter 11.

43. Gray, A., Mathews, G. B., and MacRoberts, T. M., Bessel Functions and Their Applications to Physics, Macmillan and Company, London, 1931.

44. Jeans, J. H., The Mathematical Theory of Electricity and Magnetism, Cambridge University Press, London, 1951.

45. Pierce, J. R., Theory and Design of Electron Beams, D. Van Nostrand Inc., New York, 1949.

46. Slater, J. C., Microwave Electronics, D. Van Nostrand Inc., New York, 1950.

47. Stratton, J. A., Electromagnetic Theory, McGraw-Hill, New York, 1941.

48. Watson, G. N., A Treatise on the Theory of Bessel Functions, Macmillan and Company, New York, 1944.

49. Whittaker, E. T., and Watson, G. N., A Course of Modern Analysis, Cambridge University Press, London, 1952.

LIST OF SYMBOLS

A	Total transition loss suffered by the signal at the input and output ends, db
$A(y)$	Normalized amplitude of the r-f wave along the helix
A_i	Amplitude of the r-f wave at the ith row of the integration procedure
A_o	Normalized amplitude of the r-f wave impressed on the helix
a	$A/8.68$
a'	Mean radius of the helix, m
$a_1(y)$, $a_2(y)$	Vector components of the r-f voltage amplitude $A(y)$, defined by $A^2(y) = a_1^2(y) + a_2^2(y)$
B	$54.6\ x$
B	Large-signal space-charge range parameter, $\beta b'$
b	Relative injection velocity of the electron, $(u_o-v_o)/Cv_o$
b'	Radius of the electron stream, m
C	Gain parameter, defined by $C^3 = \eta Z I_o/2u_o^2$
C_o	Capacitance per section of the helical transmission line, farads/m
d	Loss factor, $0.01836\ \ell/C$
$\overline{E}(z,t)$	Longitudinal r-f electric field intensity at the stream, $-\partial\overline{V}(z,t)/\partial z$, volts/m
$\overline{E}_s(z,t)$	Space-charge field intensity in the stream, volts/m
$F(\phi-\phi')$	Space-charge weighting function
G_{db}	Small-signal gain, A + BCN, db
G_n	A guiding section of the electron stream
I	Instantaneous linear current density in the stream, amp/m
$I(z,t)$	Longitudinal r-f helix current, amp
I_n	Current in section n of the helical transmission line, amp

LIST OF SYMBOLS (cont.)

I_o	D-c stream current, amp
$I_o(\beta r)$	Zero-order modified Bessel function, first kind, of argument βr
$I_1(\beta r)$	First-order modified Bessel function, first kind, of argument βr
i	A-c convection current, amp
K	Large-signal space-charge amplitude parameter, $(\omega_p/\omega C)^2$
$K_o(\beta r)$	Zero-order modified Bessel function, second kind, of argument βr
$K_1(\beta r)$	First-order modified Bessel function, second kind, of argument βr
L_o	Self induction per section of the helical transmission line, henries/m
ℓ	Series loss per undisturbed wavelength along the helix, db/m
N	Length of the tube in electron wavelengths
P	Poynting vector, Wv_g, watts/m^2
P	Power output along the lossless helix, watts
P_i	Power input to the helix, watts
$P_o(y)$	Power output at any point y along the lossless helix, watts
$P_{oL}(y)$	Power output at any point y along the lossy helix, watts
QC	Small-signal space-charge parameter, E^2C/β^2P
Q_n	Charge on the capacitance of section n, coulombs
q_n	Charge brought on the capacitance of section n by the currents occurring in the line, coulombs
q_n'	Electric charge in the stream, in section n of the line, coulombs
R_o	Resistance per section of the helical transmission line, ohms/m
R_n	Electron-plasma-frequency reduction factor for axial symmetry
t	Clock time, sec
t_o	Electron entrance time, sec

LIST OF SYMBOLS (cont.)

$u(y,\phi_o)$	A-c velocity parameter
u_{ij}	Total a-c velocity of the jth electron in the ith row, m/sec
u_o	Average velocity of the electrons in the stream, m/sec
$u_t(y,\phi_o)$	Total a-c velocity of an electron relative to the electron stream, m/sec
$\overline{V}(z,t)$	R-f voltage along the line, volts
V_n	Potential on the capacitance of section n, volts
V_o	D-c stream voltage, volts
$\overline{V}_s(z,t)$	Space-charge voltage, volts
v	Velocity of propagation of the r-f wave on the helix, m/sec
$v(y,\phi_o)$	A-c velocity parameter
v_d	Difference between the stream velocity and the undisturbed phase velocity of the wave, m/sec
v_g	Group velocity, m/sec
v_o	Undisturbed axial phase velocity of the wave, $1/\sqrt{LC}$, m/sec
v_{oL}	Axial phase velocity for the lossy helix, m/sec
v_{pr}	Phase velocity of the wave relative to the stream velocity u_o, m/sec
v_{sg}	Propagation velocity of the slow-and-growing wave in the small-signal analysis, m/sec
$v_t(y,\phi_o)$	Total a-c velocity of an electron relative to the undisturbed velocity, m/sec
v_ϕ	Difference between the slow-and-growing wave velocity and the undisturbed velocity of the wave, m/sec
W	Stored energy per unit length, watts/m
x_n	Growth constant of the wave n in the small-signal solutions, nepers/m
y	Normalized distance variable, m
y_n	Propagation constant of the wave n in the small-signal solutions, radians/m

LIST OF SYMBOLS (cont.)

Z_o	Helix impedance, $\sqrt{L/C}$ or $E^2/2\beta^2P$, ohms
Z_{oL}	Characteristic impedance of the lossy helix, ohms
z	Distance along the tube, m
z_o	Entrance position of an electron, m
α, α_ϕ	Growth constant of the slow-and-growing wave in the small-signal analysis, nepers/m
α_i	Growth constant of any of the three waves in the small-signal analysis, nepers/m
β	Phase constant of the wave on the helix, ω/v, radians/m
β_e	Phase constant of the electron stream, ω/u_o, radians/m
β_i	Phase constant of any of the three waves in the small-signal analysis, radians/m
β_o	Free-space phase constant, ω/c, radians/m
Γ	Propagation constant describing propagation in the presence of an electron stream
Γ_1	Propagation constant describing propagation in the absence of an electron stream
Γ_n	$x_n + jy_n$, where n = 1,2,3,4
δ_i	Propagation constant, $\alpha_i + j\beta_i$
ϵ	Dielectric constant of vacuum, 8.854×10^{-12} farads/m
η	Ratio of charge to mass for an electron, q/m, coulombs/kg
η_s	Saturation efficiency, percent
$\theta(y)$	Phase lag across the tube relative to the electron stream, radians
θ_i	Phase lag of the wave at the ith row of the integration procedure, radians
λ_g	Wavelength along the helix axis, v_o/f, m
λ_s	Wavelength along the electron stream, u_o/f, m
ξ	Beam-to-circuit coupling coefficient

LIST OF SYMBOLS (concl.)

$\rho(z,t)$	Instantaneous linear space-charge density of the stream, coulombs/m
$\rho_{1c}(y,\phi_o)$	Fundamental cosine component of space-charge density, coulombs/m
$\rho_{1s}(y,\phi_o)$	Fundamental sine component of space-charge density, coulombs/m
$\rho_n(y,\phi_o)$	nth component of space-charge density, coulombs/m
$\Phi(y,\phi_o)$	Instantaneous phase of the fundamental r-f wave relative to v_o, radians
ϕ	Polar angle in cylindrical coordinates (used only in Appendix B)
$\phi(y,\phi_o)$	Instantaneous phase of the fundamental r-f wave relative to the stream, radians
ϕ_{ij}	Instantaneous r-f phase of the jth electron at the ith row, radians
ϕ_o	Entrance phase of an electron, radians
ψ	Input-signal level in db below CI_oV_o
ω	Angular frequency of the longitudinal r-f wave, radians/sec
ω_p	Electron-plasma frequency, defined by $\omega_p^2 = \eta I_o/\pi\epsilon b'^2 u_o$, radians/sec
ω_{qn}	Effective electron-plasma frequency, $\omega_p R_n$, radians/sec

DISTRIBUTION LIST

No. of Copies	Agency
35	Chief, Bureau of Ships Navy Department Washington 25, D. C. ATTENTION: Code 327
20	Director, Evans Signal Laboratory Belmar, New Jersey FOR: Chief, Thermionics Branch
10	Chief, Engineering and Technical Service Office of the Chief Signal Officer Washington 25, D. C.
10	Director, Air Materiel Command Wright-Patterson Air Force Base Ohio ATTENTION: Electron Tube Section
2	Mr. John Keto Director, Aircraft Radiation Laboratory Air Materiel Command Wright-Patterson Air Force Base Ohio
2	Document File Electronic Defense Group Engineering Research Institute University of Michigan Ann Arbor, Michigan
1	J. R. Black, Research Engineer Engineering Research Institute University of Michigan Ann Arbor, Michigan
1	W. G. Dow, Professor Department of Electrical Engineering University of Michigan Ann Arbor, Michigan
1	Engineering Research Institute File University of Michigan Ann Arbor, Michigan
1	Gunnar Hok, Professor Department of Electrical Engineering University of Michigan Ann Arbor, Michigan
1	J. S. Needle, Assistant Professor Department of Electrical Engineering University of Michigan Ann Arbor, Michigan
1	H. W. Welch, Jr., Project Supervisor Electronic Defense Group Engineering Research Institute University of Michigan Ann Arbor, Michigan
1	Air Force Cambridge Research Laboratories Library of Geophysics Directorate 230 Albany Street Cambridge, Massachusetts ATTENTION: Dr. E. W. Beth
1	Air Force Cambridge Research Laboratories Library of Radiophysics Directorate 230 Albany Street Cambridge, Massachusetts
1	Bell Telephone Laboratories Murray Hill Laboratory Murray Hill, New Jersey ATTENTION: S. Millman
1	Bell Telephone Laboratories Murray Hill Laboratory Murray Hill, New Jersey ATTENTION: Dr. J. P. Molnar
1	Bell Telephone Laboratories Murray Hill Laboratory Murray Hill, New Jersey ATTENTION: Dr. J. R. Pierce
1	Bell Telephone Laboratories Murray Hill Laboratory Murray Hill, New Jersey ATTENTION: Dr. P. K. Tien
1	Department of Electrical Engineering California Institute of Technology Pasadena, California ATTENTION: Professor L. M. Field
1	Collins Radio Company Cedar Rapids, Iowa ATTENTION: Robert M. Mitchell
1	Columbia Radiation Laboratory Columbia University Department of Physics New York 27, New York
1	Department of Physics Cornell University Ithaca, New York ATTENTION: Dr. L. P. Smith
1	Electronic Products Company 111 E. 3rd Street Mount Vernon, New York ATTENTION: Dr. J. H. Findlay
1	Vacuum Tube Department Federal Telecommunication Laboratories, Inc. 500 Washington Avenue Nutley 10, New Jersey ATTENTION: A. K. Wing, Jr.
1	General Electric Company General Engineering Laboratory Library Building 5, Room 130 1 River Road Schenectady 5, New York
1	Mr. A. C. Gable Ind. and Trans. Tube Dept. General Electric Co. (Bldg. 269) Schenectady, New York

DISTRIBUTION LIST (cont.)

No. of Copies	Agency
1	General Electric Research Laboratory Schenectady, New York ATTENTION: P. H. Peters
1	General Electric Research Laboratory Schenectady, New York ATTENTION: S. E. Webber
1	General Electric Research Laboratory Schenectady, New York ATTENTION: D. A. Wilbur
1	Mrs. Marjorie L. Cox, Librarian G-16, Littauer Center Harvard University Cambridge 38, Massachusetts
1	Cruft Laboratory Harvard University Cambridge 38, Massachusetts ATTENTION: Professor E. L. Chaffee
1	Electron Tube Laboratory Research and Development Laboratory Hughes Aircraft Company Culver City, California ATTENTION: Dr. C. K. Birdsall
1	Electron Tube Laboratory Research and Development Laboratory Hughes Aircraft Company Culver City, California ATTENTION: Dr. G. R. Brewer
1	Electron Tube Laboratory Research and Development Laboratory Hughes Aircraft Company Culver City, California ATTENTION: Dr. A. V. Haeff
1	Electron Tube Laboratory Research and Development Laboratory Hughes Aircraft Company Culver City, California ATTENTION: Dr. H. R. Johnson
1	Electronics Research Laboratory Electrical Engineering Department Illinois Institute of Technology Chicago 16, Illinois ATTENTION: Dr. George I. Cohn
1	Electron Tube Laboratory Department of Electrical Engineering University of Illinois Urbana, Illinois
1	Industry and Science Department Enoch Pratt Free Library Baltimore 1, Maryland
1	Mr. R. Konigsberg Radiation Laboratory Johns Hopkins University 1315 St. Paul's Street Baltimore, Maryland
1	Department of Electrical Engineering University of Kentucky Lexington, Kentucky ATTENTION: Professor H. Alexander Romanowit
1	Gift and Exchange Division University of Kentucky Libraries University of Kentucky Lexington, Kentucky
1	Document Office - Room 20B-221 Research Laboratory of Electronics Massachusetts Institute of Technology Cambridge 39, Massachusetts ATTENTION: John H. Hewitt
1	Electronic Defense Group Engineering Research Institute University of Michigan Ann Arbor, Michigan ATTENTION: Dr. J. A. Boyd
1	Mr. R. E. Harrell, Librarian West Engineering Library University of Michigan Ann Arbor, Michigan
1	Microwave Research Laboratory University of California Berkeley, California ATTENTION: Professor D. Sloan
1	Microwave Research Laboratory University of California Berkeley, California ATTENTION: Dr. J. Whinnery
1.	Department of Electrical Engineering University of Minnesota Minneapolis, Minnesota ATTENTION: Professor W. G. Shepherd
1	National Bureau of Standards Library Room 203, Northwest Building Washington 25, D. C.
1	Dr. D. L. Marton Chief, Electron Physics Section National Bureau of Standards Washington 25, D. C.
1	Mr. Stanley Ruthberg Electron Tube Laboratory Bldg. 83 National Bureau of Standards Washington 25, D. C.
1	National Research Council of Canada Radio and Electrical Engineering Division Ottawa, Ontario Canada
1	Department of Electrical Engineering Ohio State University Columbus, Ohio ATTENTION: Professor George E. Mueller

DISTRIBUTION LIST (concl.)

No. of Copies	Agency
1	Department of Electrical Engineering Pennsylvania State University State College, Pennsylvania ATTENTION: Professor A. H. Waynick
1	Dr. O. S. Duffendack, Director Phillips Laboratories, Inc. Irvington-on-Hudson, New York
1	Polytechnic Institute of Brooklyn 55 Johnson Street Brooklyn 1, New York ATTENTION: Dr. E. Webber
1	Radio Corporation of America RCA Laboratories Division Princeton, New Jersey ATTENTION: Fern Cloak, Librarian
1	Radio Corporation of America RCA Laboratories Division Princeton, New Jersey ATTENTION: Mr. J. S. Donal, Jr.
1	Radio Corporation of America RCA Victor Division 415 South 5th Street Harrison, New Jersey ATTENTION: W. J. Dodds
1	Radio Corporation of America RCA Victor Division 415 South 5th Street Harrison, New Jersey ATTENTION: Hans K. Jenny
1	Magnetron Development Laboratory Power Tube Division Raytheon Manufacturing Company Waltham 54, Massachusetts ATTENTION: W. C. Brown
1	Magnetron Development Laboratory Power Tube Division Raytheon Manufacturing Company Waltham 54, Massachusetts ATTENTION: Edward C. Dench
1	Raytheon Manufacturing Company Research Division Waltham 54, Massachusetts ATTENTION: W. M. Gottschalk
1	Sanders Associates, Inc. 135 Bacon Street Waltham 54, Massachusetts ATTENTION: Mr. James D. LeVan
1	Sperry Gyroscope Company Library Division Great Neck, Long Island, New York
1	Department of Electrical Engineering Stanford University Stanford, California ATTENTION: Dr. S. Kaisel
1	Department of Electrical Engineering Stanford University Stanford, California ATTENTION: Dr. D. A. Watkins
1	Sylvania Electric Products, Inc. 70 Forsyth Street Boston 15, Massachusetts ATTENTION: Mrs. Mary Timmins, Librarian
1	Sylvania Electric Products, Inc. Woburn, Massachusetts ATTENTION: Mr. Marshall C. Pease
1	Department of Physics Syracuse University 102 Steele Hall Syracuse 10, New York ATTENTION: Dr. E. P. Gross
1	Department of Electrical Engineering Yale University New Haven, Connecticut ATTENTION: Dr. L. P. Smith